High Precision Relative and Absolute Gravity in Britain

Kate Charles

PhD Thesis

University of Edinburgh

1995

For Ruth ,

in celebration of our life .....

Declaration

I declare that the work presented in this thesis is my own, unless otherwise stated in the text, and that the thesis was composed by me. Some of the results have been published elsewhere.

Acknowledgements

My supervisor, Roger Hipkin, has given me much of his valuable time, in discussion and in thought. He has also fulfilled the role of 'chief field assistant' with unending co-operation and diligence. It has been a privilege to work with one so patient and resourceful.

Bob Edge, Graham Jeffries, Trevor Baker, Hugh Hopewell and Martin Brown of the Proudman Oceanographic Laboratory have generously supplied data from FG5-103, and their comments discussions about the instrument have been very helpful. Bryan Kibble of the National Physical Laboratory (FG5-105), Bernd Richter of IfAG, Frankfurt, (FG5-101), Walter Spita of the Defense Mapping Agency (FG5-107) have also allowed me to use their data. Fred Klopping (NOAA) and Jacques Liard (Geological Survey of Canada) have both responded promptly and helpfully to my queries.

Nick Brookes and Alex Chapman have contributed much to the observation of the BPGN, and both performed beyond their call of duty during long and hard field campaigns. Jon Kirby has assisted with some of the local observations.

My parents have provided essential moral support and some financial assistance, for which I am very grateful.

This project was funded mainly by the Natural Environment Research Council.

Abstract

Tide gauge observations suggest current rates of uplift of the land with respect to mean sea level of a few millimetres per year ranging from +1.6 at Lerwick to -3.2 at Southend. The measurement of absolute heights separates the land movements from changes in mean sea level. 10 mm of uplift causes a change in gravity of about 2 μgal (1 μgal = 10^{-8} m s^{-2}) so a precision of 5 μgal detects a differential rate of 5 mm per year in about 10 years. The British Precise Gravity Network 1993 (BPGN93) was established by the author to provide a datum from which future reobservation could identify vertical crustal movements. It consists of 58 sites spaced about 100 km apart over mainland Britain. They were observed with three specially calibrated LaCoste & Romberg gravity meters and controlled by observations measured with FG5 absolute gravity meters at Edinburgh, Birkenhead, Teddington and Taunton.

Very high accuracy relative gravimetry depends on the calibration of the instrument and maintaining reproducible instrumental drift characteristics, correctly modelling environmental disturbances such as Earth tides and developing robust and appropriate statistical models. A search for periodic errors in the micrometer screw of the unique double-dial instrument D145 appeared to find a period of about 400 coarse dial turns, four times that expected from the gear ratios. The meter was balanced using the coarse screw at various settings of the fine screw. The sequence of readings every 10 minutes for up to 5 hours detected non-linear drift caused by changes in the direction of screw turning. Because a linear drift model was analysed using least-squares, this was initially interpreted as a periodic screw error. The 'spring hysteresis model' explains the anomalous result. Solid-Earth tides were calculated using the full Cartwright-Tayler-Edden expansion but other algorithms agree to better than 0.5 μgal. Inconsistent treatment of the static tide can create discrepancies of about 30 μgal for British latitudes. The ocean load tide is only important near the margins of continents, and in particular in SW England, but was implemented for all relative and absolute gravity data.

This thesis describes improved analysis techniques for absolute gravimetry, with a detailed study of three corrections, for vertical gradient, datum height and system response, which were incorrectly treated in the manufacturer's software. The vertical gradient of gravity was measured at the eight locations in the UK where absolute gravity has been observed, to correct the new data. The FG5 absolute gravity meter measures the position and time of a freely falling corner-cube reflector using fringes produced by laser interferometry, and estimates gravity by fitting them to an equation of motion. Ignoring the vertical gradient of

gravity in the equation of motion estimates gravity at the 'effective measurement height', but it is shown that theoretical predictions relating this position to the top of the drop are incorrect because of fringe counting errors. Thus the equation of motion used must include the vertical gradient of gravity, determined by relative gravimetry, in order to estimate gravity at a definite height for comparison with other instruments. Measured vertical gradients have been found to be non-linear, so the values needed for the equation of motion and for transferring the gravity estimate to the floor are different. Instrumental vibrations and imperfections with the release and catch of the falling mass constitute a 'system-response' to dropping which is manifested by non-random structure in the fringe residuals. It is shown that this structure causes an increase of up to 25 μgal in FG5's estimate of gravity when the drop length is decreased by one third: when the fringe positions are corrected with the whole of the stacked fringe residuals, the estimate no longer varies. Modelling the system-response by decaying sinusoids and using a least-squares search of the fringe residuals to identify the frequency and decay constant, allows the amplitude and phase of the response to be included as free parameters in the equation of motion. Systematic response corrections found for the normal 150-fringe drop length were commonly between 2 and 6 μgal. A detailed analysis of observations with the NERC absolute gravity meter FG5-103 at four sites between 1992 and 1994, and data from FG5-105 at Teddington, FG5-107 at Taunton and JILA4 at Edinburgh, have provided definitive values of absolute gravity to control BPGN93, as well as recording the effects of instrumental upgrades.

BPGN93 sites cover a gravity range of 900 mgal and have a mean standard error of 4.9 ± 1.2 μgal, in the range 3 to 8 μgal. This is an order of magnitude better than the existing National Gravity Reference Net 1973. The scale correction to the relative gravity meter G275 derived from FG5 absolute control is $1.000\,7565 \pm 0.000\,0210$ compared with $1.000\,622 \pm 0.000\,027$ with respect to IGSN71. The quality of the dataset and the relative importance of the drift parameters to the general solution has been investigated. By isolating regions of the network, and by simulating broken links, the uniformity of the net has been evaluated and a number of weaker areas identified, thus defining improved observation procedures, and a better adjustment model for the future reobservation program of BPGN.

Table of Contents

CHAPTER 1. Introduction

1.1 Introduction

The British Precise Gravity Network 1993 (BPGN93) has been established by the author specifically for monitoring vertical crustal movements in Great Britain. Previous precise gravimetry has been carried out for the purposes of improving the national geodetic levelling network (Masson Smith *et al.* 1974), and for studying deformation on local (e.g. mining subsidence (Lyness 1984)) and regional (e.g. uplift in central Scotland (Hipkin 1978)) scales. Vertical crustal movements on a regional scale are, at least partly, a response to deglaciation.

The study of glacial rebound and the accompanying variations in sea-level requires the examination of evidence from glaciology, rheology, geomorphology, oceanography and geodesy. A knowledge of the properties of the asthenosphere and lithosphere helps to constrain models of isostasy, and observations of postglacial rebound provide important constraints on the rheology of the crust and upper mantle. Relative sea levels can be determined from the study of past shorelines and from tide gauge data. Tide gauges around the world record local and regional vertical crustal movements, as well as the eustatic sea-level, but since they only record the height of the mean sea-level with respect to the land, it is important to separate the absolute land movements from sea-level changes. Relative land movements have been traditionally studied by spirit levelling, but for absolute studies on a nationwide or global scale, space geodetic methods are more appropriate. Gravimetry provides a ground based method of equivalent accuracy to space geodetic techniques, and makes a complementary contribution to the study of deformation and mantle flow processes.

The chapters of this thesis describe the realisation of the BPGN93, and other contributions to the advancement of high precision relative and absolute gravimetry.

1.2 Theory of Isostasy and Vertical Crustal Movements

1.2.1 Isostatic Rebound

The Airy and Pratt models of isostasy are both applications of Archimedes principle, whereby blocks of the crust, decoupled by fault planes achieve equilibrium by rising or

subsiding independently (Keary & Vine 1990). These models of local compensation imply unreasonable mechanical properties for the crust and upper mantle, because they suggest that independent movements would take place even for very small loads. The lithosphere is not as weak as this implies, since it is known to resist the stresses created over igneous intrusions, or under large ice sheets, for example, for thousands of years without breaking into the smaller pieces required for compensation by the Airy and Pratt models. An 'elastic-plate' model of the lithosphere allows it to support loads by flexing, enabling compensation to take place regionally. The region beneath the load subsides over a relatively wide area by displacing asthenospheric material, which forms peripheral bulges (Figure 1.1 a and b). Small loads, with a diameter of less than about 50 km, are supported by the elastic strength of the lithosphere. To support larger scale loads, with diameters more than 500 km, requires the attainment of isostatic equilibrium. The continuing readjustment of the crust to removal of a heavy ice sheet by 'isostatic rebound' is controlled by the viscosity of the asthenosphere. The expected flow of the asthenosphere and relative motions of plates during loading and unloading are shown schematically in Figure 1.1 b, c and d.

1.2.2 Properties of the Asthenosphere and Lithosphere

When the lithosphere is loaded by ice sheets, large sedimentary basins, mountain ranges (continental regions) or seamounts (oceanic regions), its flexural rigidity and thickness can be calculated from an estimate of the magnitude of the load and the distortion it produces. However, the complete explanation of the rebound observed on unloading requires a more sophisticated model than a uniformly high strength lithosphere overlying a weak, fluid asthenosphere. The upper 20-40 km of the lithosphere respond to stress by elastic deformation and transient creep. Beneath this is a layer which deforms by plastic flow, and its lowest part is continuous with the asthenosphere (Keary & Vine 1990). The comparison of observations of rebound on different scales indicates the rate of increase of the viscosity of the asthenosphere with depth. The form of the deformation also depends on the length of time for which the load was applied.

Most geophysical models of post glacial rebound assume a viscoelastic model for the Earth, so that it behaves as a purely elastic solid in the limit of short time and a purely viscous fluid in the limit of long time (Ekman and Mäkinen 1994). An alternative model, proposed principally by Mörner (1990), claims that the postglacial rebound is composed of two separate mechanisms: the glacial isostatic one which, according to him, has already faded out, and another one which is linear in time and can be observed today (*ibid.*). Mörner

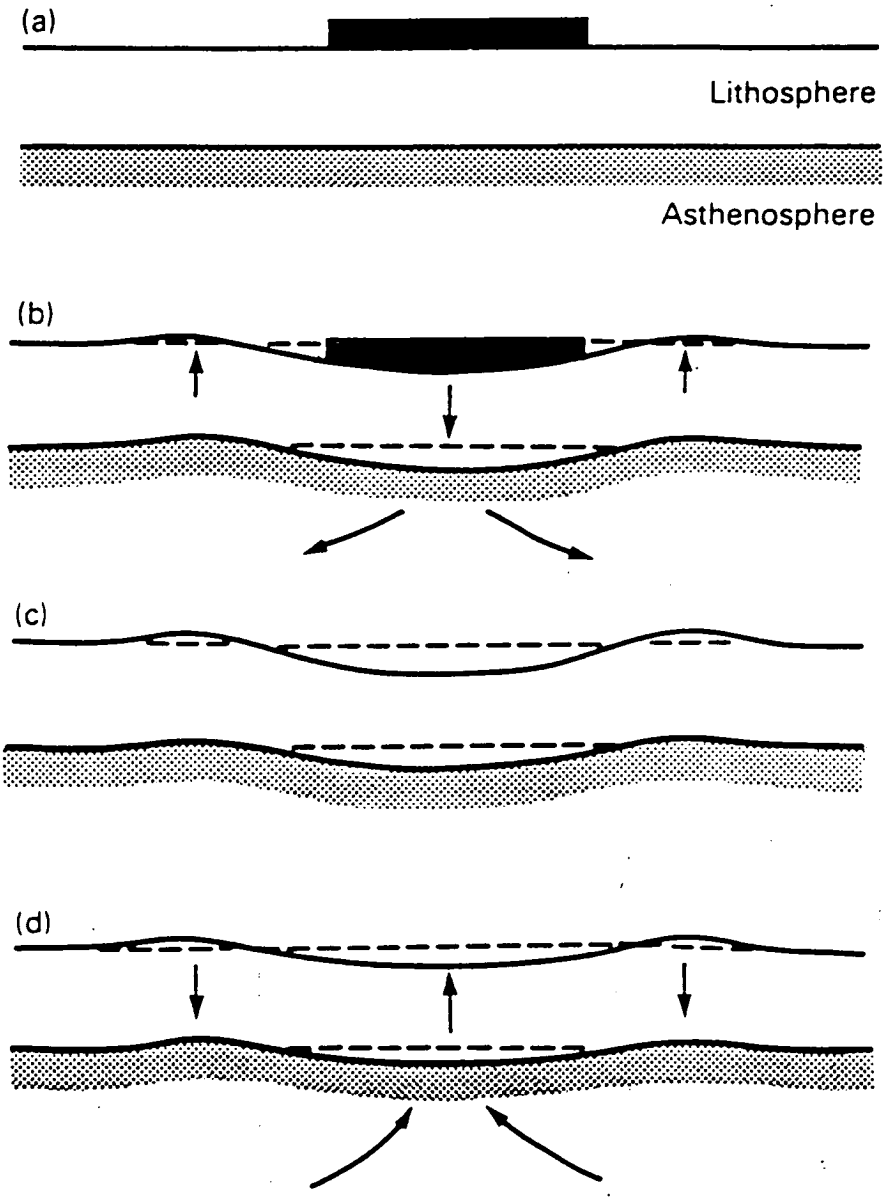

Fig. 2.32 Theory of isostatic rebound. (a) the load of an icecap on the lithosphere causes downbending accompanied by the elevation of the peripheral lithosphere and lateral flow in the asthenosphere (b). When the icecap melts (c), isostatic equilibrium is regained by reversed flow in the asthenosphere, sinking of the peripheral bulges and elevation of the central region (d).

Figure 1.1 Theory of isostatic rebound. (From Keary & Vine (1990)).

suggests that the linear component represents a phase boundary adjustment due to decompression, which involves no flow of mass (section 1.5.3).

1.2.3 Numerical Estimates from Postglacial Rebound Studies

The study of the post glacial rebound of Fennoscandia using precise levelling provides a maximum rate of uplift of about 10 mm per year. The ice sheet caused subsidence in the central area and the growth of peripheral bulges (Keary & Vine 1990). To determine the maximum load caused by the now melted ice sheets, reconstructions have to be done using isochron maps of the limits of the ice as the deglaciation proceeded. Gravity data summarised for Finland support a total uplift of 900 - 1000 m after the melting of an ice sheet 3.4 - 3.7 km thick, and the remaining potential uplift is about 100 - 150 m (Emery & Aubrey 1985). The viscosity of the asthenosphere is estimated to be between 2.4×10^{19} and 3.3×10^{20} Pa s from Fennoscandian levellings (Stacey 1992). Observations of the rate of rebound of northern Canada, as a result of the melting of the Laurentide ice sheet, provide an estimate for the viscosity of the upper mantle of 10^{21} Pa s (Keary & Vine 1990).

1.3 Post Glacial Rebound and Sea-level Change

1.3.1 Glaciation and Sea-level Change

Successive cycles of glaciation and deglaciation and their associated exchange of mass with the oceans cause major oscillations in sea-level which affect the deposition and erosion of coastal sediments around the world (Lambeck 1990). The extraction of water from the oceans to form an ice sheet leads to an overall lowering of the sea-level. The redistribution of mass on the Earth's outer crust changes the shape of the equipotential surface, so the prediction of the total relative sea-level change is not straightforward. As the ice sheet melts, the ocean volume increases and sea-level can rise by 100 - 150 m (Lambeck *et al.* 1990). The increased surface load produces small stresses which appear to be sufficient to produce a small tilting and upwarping of continental margins, observations of which permit estimates to be made of the mantle viscosity beneath. Sea levels predicted for the last ten to twenty thousand years are clearly a function of both ice and Earth response parameters, and only when these are understood can predictions for the future be made accurately .

1.3.2 Postglacial Rebound in Britain

The most recent period of major glaciation in Britain was during the Late Devensian. The ice sheet reached its maximum extent between 18 000 and 20 000 years BP (Boulton 1992), and at this time, there was a major ice dome over Scotland, a smaller ice cap over Wales, and ice streams flowing down the Irish Sea and the east coast of England (*ibid.*). The ice gradually retreated, as the temperature increased, until the beginning of the Loch Lomond stadial at about 11 000 BP. This was a time of strong regeneration of glaciers in Britain, where a major ice cap formed in western Scotland, and smaller corrie glaciers developed in Wales and the Lake District. This stadial was terminated by a rapid climatic amelioration in about 10 000 BP, marking the final retreat of British glaciers.

Lambeck *et al.* (1990) describe very high resolution models of the glacial rebound for Great Britain in response to the Late Devensian ice sheet, and use this relatively small load to examine the depth dependence of rheological parameters. The matching of the model predictions with sea-level observations indicates that the lithospheric thickness under Scotland is between 100 and 125 km, and the upper mantle viscosity is between 2 and 4×10^{20} Pa s, in agreement with values estimated previously from the Fennoscandian uplift. The rebound models attempt to explain the complex spatial and temporal pattern of sea-level change observed in Great Britain, and to place constraints on the ice sheet dimensions. The results suggest that this small ice sheet was unlikely to have been connected to the Fennoscandian ice sheet across the North Sea, and that the ice thickness over western and central Scotland was less than about 1.5 km.

Further investigations are needed to determine what proportion of the present day uplift and cumulative uplift seen in northern Britain is due to this small ice sheet, and what is due to the effect of being at the margins of the Fennoscandian ice sheet. Much more detailed information is needed about the regional variation of uplift and subsidence in Britain before such local ice sheet models can be improved. For example, parts of the crust which have been weakened due to faulting or sedimentary loading may behave more like the 'bobbing-up-and-down' plates of the Airy and Pratt models, than a 'strong and flexible' bending plate model. Tide gauge records hold important information about this regional variability, and in particular the data from all gauges (not just the 'A' class ones) should be used to provide maximum spatial coverage. Industrial activities such as mining and water extraction can contribute significantly to local subsidence, and local instability of the pier or harbour walls can create spurious apparent rises in sea level.

1.4 Observations of Relative Sea-level

1.4.1 Geomorphological Evidence

Shorelines

The study of present and former shorelines determines the effects of tectonic subsidence or uplift of the crust, and glacial rebound, since both processes have contributed to changes of relative sea-level during the past 10 000 years. The sedimentary record can indicate the presence and geographical position of former shorelines, and of the type and longevity of a particular coastal environment (estuarine, dune, shingle, etc.). Evidence for shoreline positions comes from varves (annual cycles), sedimentology, stratigraphy, pollen, lichen, archaeology, and radio carbon dating.

Observations at sites located near the centres of the Fennoscandia and Laurentide ice sheets show that the positions of past shorelines are well above present sea level as would be expected from a major rebound of the crust that has been depressed by an ice sheet several kilometres thick. The isochrons of the Fennoscandian ice sheet are generally well established, but the ice thickness is less certain (Lambeck 1990).

Crustal movements in Britain determined from geomorphology and geology

Using a large number of sea-level index points (mainly radiocarbon dates and shoreline markers), Shennan (1989) describes crustal movements and sea-level changes in Britain since 8800 BP. His analysis indicates that crustal downwarping has occurred throughout south and south east England, and most of Wales for at least 4000 years. The highest estimated rates (2 mm yr^{-1}) are for the Thames Estuary and Norfolk. The rates of uplift in north England and mainland Scotland are estimated to be 0 - 1 mm yr^{-1} in England and up to 2 mm yr^{-1} in central Scotland. Drowned topography on Orkney and Shetland suggests that these regions are sinking (Dunham 1972), but an analysis of the Lerwick tide gauge record from 1959-87 shows a mean sea-level fall of 1.61 ± 0.61 mm yr^{-1} (Woodworth *et al.* 1991). Clearly both uplift and subsidence have operated in this region during the last 10 000 years. The combined evidence suggests an arching of Great Britain, rather than a simple tilt (Dunham 1972). The map of Shennan (1989), showing current rates of crustal movement in Great Britain (in mm yr^{-1}) estimated from this geomorphological data, is reproduced in Figure 1.2. Except in the far north, the model is broadly consistent

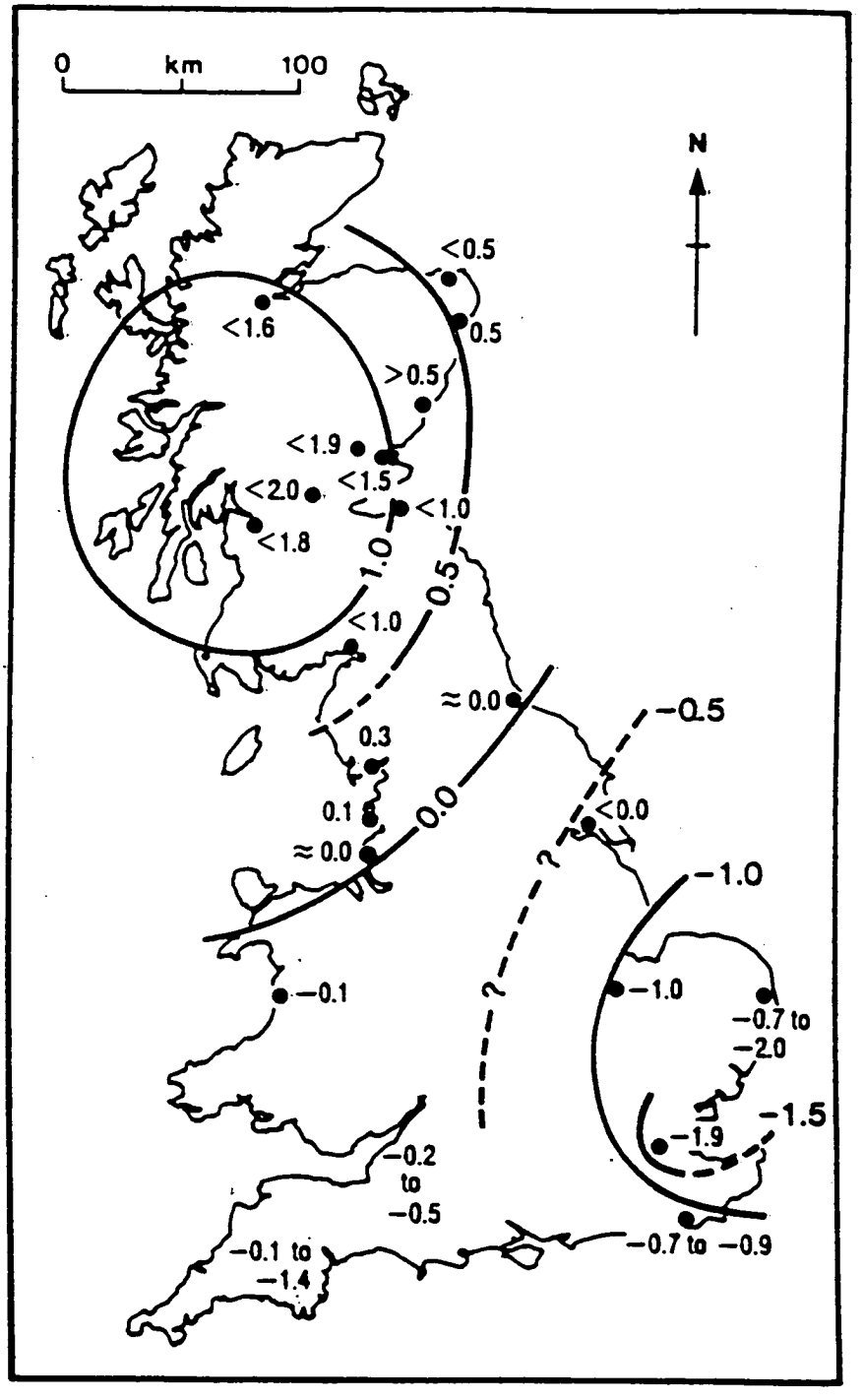

Figure 9 Map of estimated current rates (mm/yr) of crustal movement in Great Britain. Isolines cannot be drawn for much of southern England, point estimates are shown for guidance.

Figure 1.2 Shennan (1989)

with the tide gauge data of Woodworth (1987) and the previous analyses of Rossiter in the 1970's. Rossiter reckoned that the axis of zero mean sea-level change passed through central Britain at a latitude of Hull, and progressed eastwards through Denmark. The high rate of current sea-level rise derived from the tide gauge at North Shields, which is greater than the rate of rise in the Thames, is not supported by the Holocene data (Shennan 1989). This anomalous tide gauge record has been noted many times, and Rossiter (1972) attributes the effect to coal mining.

Shennan notes that the type of movement in south and eastern England is more complicated than simple linear subsidence. The Thames basin consists of 300 m of Mesozoic sediments (gault, greensand and chalk) resting on much older Devonian rocks. Evidence from the stratigraphy and lithology shows the continuing instability, with both uplift and subsidence occurring (Dunham 1972). The south east of England was south of the limit of the last glaciation, and there is no indication of isostatic uplift since. Emery & Aubrey (1985) suggest that a 'broad downwarp of at least 45m' occupies the North Sea, English Channel, and southern England, but the roles of basin sinking, peripheral bulge sinking and rejuvenation of graben faults caused by glacial loading and unloading cannot be clearly evaluated (*ibid.*). These features may well affect the Thames basin.

1.4.2 Tide Gauge Records

Nature of tide gauge data

Tide gauges give the height of the sea with respect to the land, so a rise in sea level cannot be distinguished from a subsidence of the crust at the tide gauge. The trends in sea-level observed from tide gauge data will arise from a combination of local land movements, global sea level rise, and any changes in oceanic or coastal circulation, or meteorological influences over the length of the tide gauge record (Woodworth 1987).

Interannual and decadal variations of 50 - 100 mm in the mean level of the sea require that at least 60 years data are necessary to get a reliable secular trend (Baker 1993). The oldest tide gauge record in Europe is at Amsterdam which started in 1700, and the oldest in Britain is Sheerness, starting in 1834. Figure 1.3 shows plots of annual mean sea levels from some of the other long tide gauge records in Europe, compiled by Woodworth *et al.* (1991). It can be seen that the mean sea levels are rising by 1.5-2.0 mm yr^{-1} which is typical of that found

in other parts of the world. However, at Stockholm (Sweden), the mean sea level is falling by about 4 mm yr^{-1}, due to the post glacial rebound of Scandinavia. At Aberdeen the trend is very small, and it appears that the rebound at Aberdeen is of a similar magnitude to the sea level rise (Baker 1993).

Tide gauge records in the UK

Four of the longest tide gauge records around the UK coast, which all span the epoch 1916-82, are described in Woodworth (1987). During this time, sea level at Aberdeen had risen at a rate of 1.29 ± 0.22 mm yr^{-1} slower than at Newlyn, which suggested a north-south tilting of the UK mainland. Sea level at Sheerness was found to have been rising even faster than at Newlyn (by 0.62 ± 0.2 mm yr^{-1}) supporting the idea of greater land subsidence in the south east. A large rise of 5 ± 0.5 mm yr^{-1} at Plymouth may be due to irregular sinking of the crust, which is associated by Emery and Aubrey (1985) with apparent sinking of western France. They suggest that the English Channel is part of the former peripheral bulge to the large areas of downwarped crust in Scandinavia and Scotland. A more recent analysis of Woodworth *et al.* (1991) gives the mean sea-level trends for these sites and others in the UK. The trend shown at Lerwick for the period 1959-87 is -3.37 ± 0.63 mm yr^{-1} with respect to Newlyn (*ibid.*), which might be expected in association with the post glacial rebound in north-west Europe. The values from Table 2b of the 1991 paper are plotted in Figure 1.4. The points show the observed trends, and the contours are drawn to indicate the approximate form of the apparent sea-level changes. The lack of data points in Scotland available for this analysis is unfortunate, since this is the region of greatest uplift. It also spoils the comparison of this map with Figure 1.2, which is compiled from geomorphological evidence, much of it from central Scotland.

Glacial rebound and other crustal motions from tide gauge data

The Baltic Sea tide gauges are important for monitoring the postglacial rebound of Scandinavia, and those in tectonically active areas record the dramatic and sudden changes in relative sea levels caused by earthquakes. Intensive study of areal patterns of sea level change in other regions having good tide gauge records have recorded the effect of crustal sinking in Japan, block faulting along the Atlantic coast of the US, and patterns of relative sea-level change consistent with long term sinking of continental shelf basins in the east Asian mainland.

Emery and Aubrey (1985) produced an analysis of tide gauge data from northern Europe which suggests maximum relative uplift centred near the northern Gulf of Bothnia at a

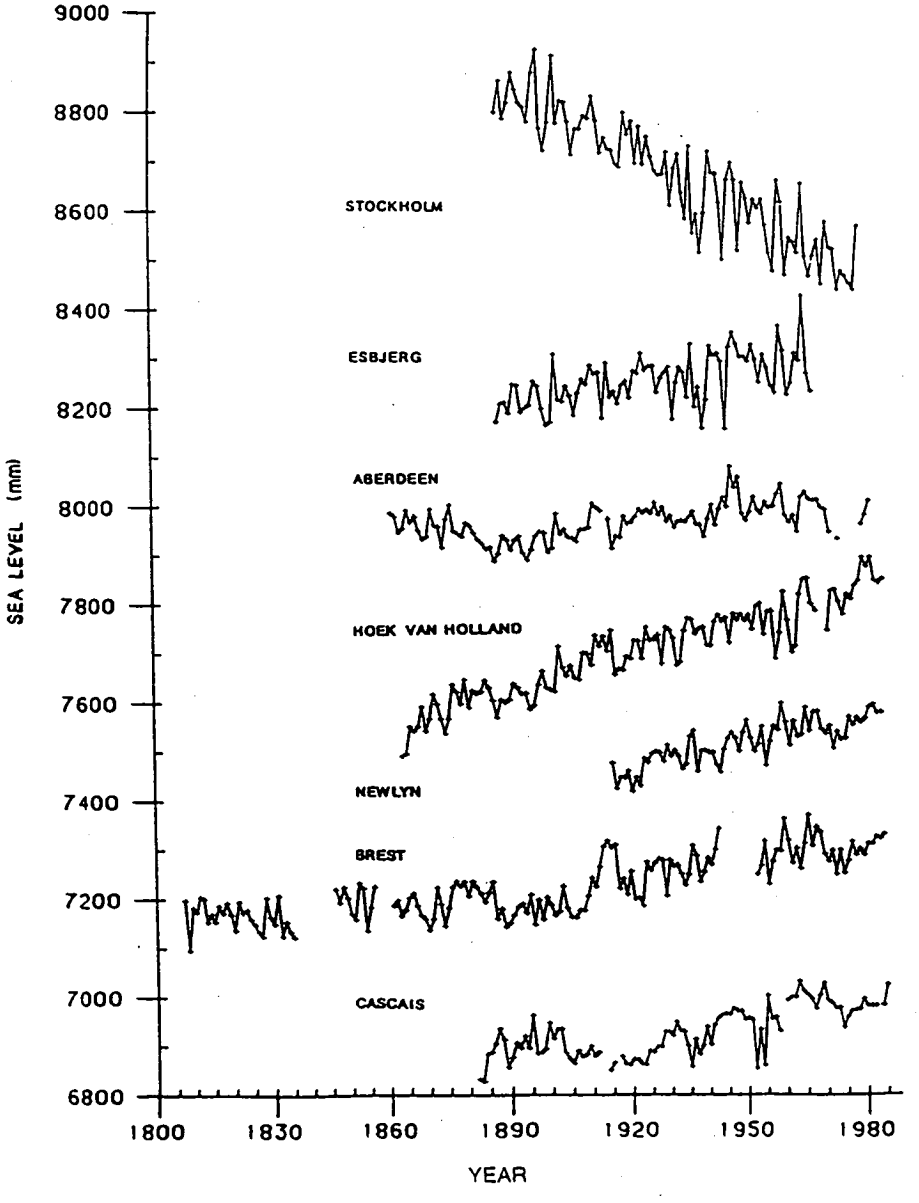

Figure 1.3 Some examples of long time series of European annual mean sea levels (offset arbitrarily for presentation purposes). (Figure from Baker 1993).

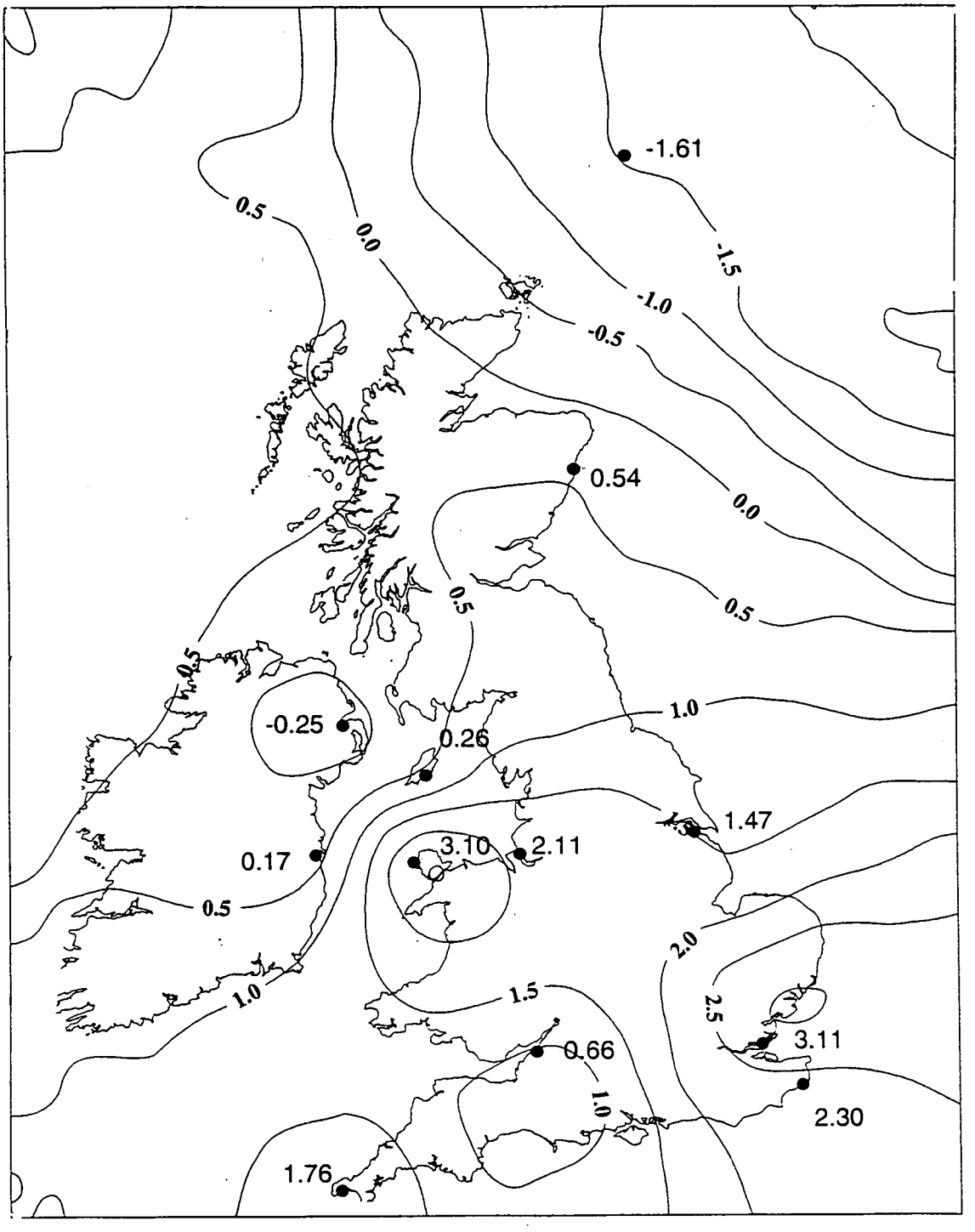

Figure 1.4 Contour map indicative of trends in UK mean sea level. The points are the secular trends in mean sea-level in mm yr^{-1}, given in Table 2b of Woodworth *et al.* (1991).

maximum rate of more than 8 mm yr^{-1}, and a smaller secondary maximum on Scotland, of 4 - 6 mm yr^{-1}. This rate for Scandinavia is smaller than the 10 mm yr^{-1} found elsewhere, and the value for Scotland is larger than expected. They failed to find evidence of the associated peripheral bulge from the tide gauge data, but note that the sinking of a former peripheral bulge of glacial origin in the North Sea is complicated by post-carboniferous basin deepening and sedimentary loading. They note that the areas presently uplifting are within shields of strong intrusive and metamorphic rock, whereas, for example, the region of apparently secondary uplift in the Gulf of Finland may be controlled by the block faulting in that area, which indicates a weaker region of crust. It is also suggested that the observed wide range of trends ($\pm$ 13 mm yr^{-1}) means that tectonic and isostatic controls exceed eustatic ones, but they record a general rising trend of mean sea level of about 3 mm yr^{-1}, which is a little higher than the value quoted by other observers.

Separation of absolute land movements from sea-level variations

The sea level at a tide gauge is measured with respect to a local tide gauge bench mark (TGBM). The estimation of global changes of mean sea level requires that vertical crustal movements at TGBMs be removed from the sea level records. This provides data for testing both models of glacial rebound and models of sea level variations due to climate change (Baker 1993).

The 'Woods Hole Report' on the geodetic fixing of tide gauge bench marks (Carter *et al.* 1989) recommends that 'all tide gauges used to monitor sea level must have a local network of 6-10 bench marks that are resurveyed by spirit levelling or GPS at least once a year'. It also recommends that TGBMs should be connected to the nearest primary SLR or VLBI site using GPS, and that absolute gravity measurements should be made at the SLR/VLBI stations, to give an independent check upon vertical crustal movements at both the tide gauge and position fixing sites.

1.5 Techniques for Measuring Vertical Crustal Movements

1.5.1 Spirit Levelling

The uplift in Scandinavia has been recorded successfully by repeated precise levellings, between about 1890 and 1960. This shows the usefulness of the technique where crustal

movements are relatively large (i.e. significant changes over about 100 km), and the traverses can be kept relatively short. The accuracy of geodetic levelling is assessed by circuit misclosures in the form of an error per kilometre of levelling. A first order network is defined as one with a tolerance of 2mm $\sqrt{km}$ (Kelsey 1972). Both the 2nd (1912 - 21, England & Wales, 1936 - 52, Scotland) and 3rd (1951 - 59) Ordnance Survey (OS) geodetic levellings reach this criterion, with total probable errors of 1.8 and 1.2 mm $\sqrt{km}$ respectively. However, the comparison of altitudes at fundamental bench marks (FBMs) derived from the two levellings shows differences of up to 80 mm in central England, and up to about 200 mm in the Scottish Highlands (Figure 5 of Kelsey 1972). These differences can lead to apparent slopes in mean sea level. Conventional levelling is also limited by atmospheric refraction which appears to cause significant systematic errors over distances of more than 100 km. The error accumulated in OS levelling to TGBMs along the east coast of England results in 'sea-level' at Immingham and Leith being 317 and 426 mm higher, respectively, than at Newlyn. Thompson (1980) describes this improbable result as the 'latitudinal slope of a geodetically determined mean sea level', and calculates that the effect of local winds and air pressure can only account for about 10 cm of the total apparent rise of 40 cm.

Height levelling measurements are usually made with respect to a TGBM, so any movement of the bench mark (at, for example, O.D Newlyn) with respect to the centre of the Earth must be monitored independently using, for example, GPS or gravity.

1.5.2 Space Geodetic Methods

The IERS, SLR and VLBI

The International Earth Rotation Service (IERS) defines and maintains conventional terrestrial and celestial reference systems. It co-ordinates very long baseline interferometry (VLBI), satellite laser ranging (SLR) and lunar laser ranging (LLR) observations.

Satellite Laser Ranging operates by measuring the time taken for a pulse of laser light to travel to a dedicated satellite reflector and back. Using a network of ground stations the vertical resolution is 2 - 4 cm. The Laser Geodynamics Satellite (LAGEOS) orbits at a height of nearly 6000 km (IERS 1988), and enabled Kolenciewicz *et al.* to determine the vertical motion of stations to within 1 mm yr^{-1} (Baker 1993). There is an SLR station at Hertsmonceux, near the south coast of England.

Networks of VLBI radio telescopes simultaneously track extragalactic radio sources. The signals are cross correlated and enable the horizontal positions of stations located thousands of km apart to be determined to a few cm in less than 24 hours of observations. Vertical positions are known to 2 or 3 cm. VLBI determines many other earth orientation parameters, including the pole co-ordinates needed for the polar motion correction to gravity observations. There is a VLBI site at Barry Buddon, near Dundee.

GPS

The U.S department of Defense has a constellation of 21 Global Positioning System (GPS) satellites at an altitude of 20 000 km (12 hour orbital period) arranged so that at any one time at least 4 satellites will be visible from any point on the Earth's surface (Baker 1993). The satellites transmit coded modulations at two carrier frequencies. The time delay required to match two signals, one generated by the satellite and one by the receiver, allows the position (pseudo-range) of a ground based receiver to be determined. The use of the phases of the two carrier frequencies rather than the codes, allows phase measurements to be made with a resolution of about 2 mm (Ashkenazi & Ffoulkes-Jones 1990).

A fiducial GPS network consists of a number of geodetic stations whose relative co-ordinates are known to a very high order of accuracy. The choice of reference framework is crucial to the accuracies which can be achieved by fiducial GPS (Ashkenazi *et al.* 1993), and for high accuracy deformation monitoring it is important to remember that the fiducial stations themselves may be moving with time. VLBI or SLR stations are often used as the fiducial sites, but a GPS network determined by a previous fiducial campaign is considered adequate. The measurement procedure involves taking phase measurements over a number of new points simultaneously at the fiducial and unknown sites, and solving for the co-ordinates of the new points and corrections to the satellite orbits. The errors on the vertical components from fiducial GPS are still one order of magnitude worse than for the horizontal components (Ashkenazi & Ffoulkes-Jones 1990), partly because the vertical component is three times more sensitive to errors in tropospheric calculations (Baker 1993). The best GPS results are obtained in dry and cloudless conditions.

A network aimed at monitoring the crustal dynamics around the San Andreas fault gave repeatabilities (rms) for the north, east and length components of 3, 6 and 4 mm respectively over baselines up to 500 km, but the height component has the largest scatter, of about 9mm (Ashkenazi & Ffoulkes-Jones 1990). The UK Tide Gauge fiducial GPS network includes 7 European GPS stations and 15 regional stations in the UK, of which 8 are tide gauge sites

(Ashkenazi *et al.* 1993). Mean height differences and corresponding errors are derived by fixing different subsets of fiducial stations, and using different global reference frameworks. These differences range between -22 ± 10 mm and -2 ± 1 mm, showing that not all of the fiducial stations are well defined, and suggesting that the only way to produce millimetric levels of consistency is to use a pure GPS based global reference frame (*ibid.*).

1.5.3 Gravity

Gravity and environmental effects

Gravity decreases with increasing distance from the centre of the Earth, so it potentially provides a way of monitoring uplift. However, microseismic noise interferes with gravity measurements, and is particularly large at the coast. It is recommended that gravity sites should be established between 1 and 10 km inland, and connected to TGBM by levelling or GPS. Having the sites inland avoids having to make corrections for the direct attraction of the sea, and simplifies the calculation of the ocean load tide. Another significant problem for attaining accurate gravity observations is the effect of the water table. Records made with continuously recording superconducting gravity meters show that gravity correlates with water table variations. The effect is difficult to model so it should be minimised by choosing stations on bedrock where possible (Lambert 1993).

Fennoscandian gravity uplift line

As well as being monitored using spirit levelling, the Fennoscandian uplift has been the subject of precise gravity surveys, whose results allow the computation of the relationship between gravity change and absolute land uplift, flow properties of the mantle, the geoid rise, and the remaining uplift. Ekman and Mäkinen (1994) describe such calculations, for data collected between 1966 and 1993, on the western and eastern parts of the land uplift gravity line which crosses Fennoscandia at about 63° N. The rates of gravity change are found to be -1.52 ± 0.20 μgal yr^{-1} and $+1.00 \pm 0.14$ μgal yr^{-1} on the western and eastern parts respectively. To find the relationship between gravity change and land uplift, tide gauge data from two long tide gauge records in Norway and Sweden (50 and 100 years of data respectively) were used as a measure of the uplift for the western part, and a readjustment of high precision levellings for the eastern part. These techniques gave the values 6.9 ± 0.5 mm yr^{-1} in the west and -4.7 ± 0.5 mm yr^{-1} in the east.

The relationship between gravity change and land uplift (dg/dh) was calculated by relating the Bouguer model (uplift plus addition of mass) and the free-air model (uplift only) through the 'mass flow parameter' of Ekman.

The Bouguer model for dg/dh is

$$\left(\frac{dg}{dh}\right)_B = \frac{2g}{R} + 2\pi G\rho \quad = \quad -0.17\ \mu gal\ mm^{-1} \qquad (1)$$

where the second term is the additional mass of the material assumed to flow into the space created by uplift, and the density ρ is that of the mantle (3.3 Mg m^{-3}).

The free-air model, corresponding to pure decompression, is simply

$$\left(\frac{dg}{dh}\right)_F = \frac{2g}{R} \quad = \quad -0.31\ \mu gal\ mm^{-1} \qquad (2)$$

The mass flow parameter, c, determines which of these two models best describes the data. For a Bouguer model, c =1 which corresponds to pure lateral viscous flow of the mantle; and for a free-air model c = 0, corresponding to pure decompression (section 1.2.2).

Ekman and Mäkinen (1994) compute the rate of uplift (dh/dt), the maximum rate of change of gravity with height $(dg/dh)_0$, the mass flow parameter (c) and the rate of geoid rise $(dN/dt)_0$ iteratively, and find the values

dh/dt	=	11.0 mm yr^{-1}
dg/dh_0	=	-0.204 ± 0.058 µgal mm^{-1}
c	=	0.76 ± 0.41
$(dN/dt)_0$	=	0.6 mm yr^{-1}

c is significantly different from zero, so that a viscous inflow of mass is a necessary part of the ongoing uplift process. The remaining uplift is calculated to be about 90 m.

Absolute gravity for determination of crustal movements in Canada

At its maximum, the Laurentide ice sheet spread over Canada, northward onto the southern Arctic Islands and southward into the northern United States (Lambert *et al.* 1991). The maximum thickness of this ice sheet is estimated at 3 - 4 km and present models of the

postglacial rebound predict rates of change of gravity between -1 and -2 μgal yr^{-1}. Since much of the uplift data is from tide gauges, and from the geomorphology of sites close to the present shorelines, much of the interior remains unsampled. The lack of roads in northern Canada hinders surveys with relative gravity meters, so that regular absolute gravity measurements at a small number of stations would improve the control of the relative observations. Lambert *et al.* have begun a program to study the rebound using the absolute gravity meter JILAG2. Because the accuracy of this instrument is estimated at about 3 μgal, observations would be required over a period of at least 5 years to determine a trend of about -1.5 μgal yr^{-1}.

Models of uplift and gravity change are sensitive to the presence of density discontinuities associated with phase transitions at 420 and 670 km depths, as well as to the assumed viscosity of the mantle, which is taken to be fairly uniform (Lambert *et al.* 1987). Using a model of Peltier, the rate of change of gravity with time is calculated to be about 2 μgal yr^{-1} for the central region of the Laurentide uplift (*ibid.*).

Absolute gravity measurements can assist the determination of global sea-level changes by confirming the vertical land velocities at tide gauges and to aid the verification of crustal deformation models at inland sites. Observations of surface displacements and surface gravity changes, in general, bear a different relationship to the subsurface displacement field, so gravity provides an extra constraint on the deformation process (Lambert 1993). The 'deformation gravity gradient' dg/dh is thought to be related to the opening and closing of cracks, pores or cavities, and the involvement of fluids in the deformation process (*ibid.*).

Other examples of using gravimetry to measure deformation

Lagios *et al.* (1988) measured vertical land movements in the Atalanti area of central Greece using precise relative gravimetry. A line of stations 20 km long, which crossed a number of active faults at approximately right angles, was surveyed every year between 1981 and 1985. The faulted blocks were observed to have positive and negative vertical movements, causing variations in the observed gravity differences of about 80 μgal, which corresponds to about 400 mm, during this period.

Becker (1989) describes a large scale geodynamic network in South America, designed to monitor the uplift which accompanies the subduction at the western margin of the continent. The survey covered a region 2000 km north-south and 800 km east-west, and the maximum gravity difference between sites was 2 gal (10^{-2} m s^{-2}) with a mean standard error on the

gravity values of 12 μgal. A more local survey by Becker measured the vertical displacement of the earth's surface due to the load of an artificial reservoir (Blue Lake) in Norway.

1.6 Precise Gravity in Britain

1.6.1 The Scottish Microgravimetric Net

A tentative conclusion of the early Scandinavian gravity levelling implied that the rheological properties of the asthenosphere, and its density structure, are regionally variable between the Caledonian fold belt and the Baltic Shield (Hipkin 1978). Secular gravity studies in northern Britain are necessary to confirm this hypothesis, and to provide quantitative information about the rates of uplift. Hipkin describes a 'small difference loop', consisting of 8 FBMs in central Scotland, which were to be measured by an 'equilibrium technique' with the relative gravity meter G275. Linking two sites using this technique involves two observers reading the meter alternately over a two-hour period at each gravity site, with each observer taking 10 readings. This long period was intended to allow the instrument drift to reach equilibrium, so as to minimise the large scatter potentially arising from the steep initial drift which occurs immediately after unclamping. The Edinburgh-Linlithgow gravity difference observed in this way was 556.5 $\pm$ 1.8 μgal, which is an improvement on the 552.6 $\pm$ 6.9 μgal observed in the conventional manner, by taking only two readings at each occupation.

Lyness (1984) describes reobservations of 6 FBMs on the Scottish microgravimetric net in 1980 and 1981. The largest observed gravity change (between the Tummel Bridge and Glenshee FBMs) was 24 μgal, which was more than double the estimated r.m.s. error of 10.5 μgal.

1.6.2 The National Gravity Reference Net 1973

The National Gravity Reference Net 1973 (NGRN) (Masson Smith *et al.* 1974) was established to provide gravity values along the primary geodetic levelling lines in Great Britain, so that the British values could be expressed in terms of the then-proposed Unified European Levelling Network.

The NGRN73 is composed of Ordnance Survey Fundamental Bench Marks (FBMs), measured initially with Worden gravity meters between 1964 and 1968. A more reliable Airport Net was established with 2 LaCoste & Romberg (LCR) meters, to provide a 'rigid primary net' to which the OS FBM network could be referred. The Airport Net was linked to IGSN71 sites in Europe. The formal standard errors on the definitive NGRN73 adjustment were between 20 and 70 μgal. Subsequent fragmentary re-observation of parts of the net with LCR meters demonstrated repeatability to a much better precision than this, but also revealed the presence of large errors of up to 200 μgal on the original values (Turnbull 1987). Many of the Airport sites and at least two FBMs have been destroyed, and another five FBMs are described as 'not found' in Turnbull. The lack of formal protection of FBMs makes them unsuitable as sites for a network designed to measure secular land deformation, and the gravity values of the NGRN73 are not precise enough to detect the small crustal movements that occur in Britain.

1.6.3 The British Precise Gravity Network 1993

The British Precise Gravity Network 1993 (BPGN93) has been established by the author to provide a baseline for future observations of crustal movements in Britain. It was considered that existing gravity sites did not meet the requirements for the program, which are that they must have a long (> 30 years) lifetime, be free from structural alterations and local subsidence during this time, and should be easily accessible. Most BPGN sites are on the doorsteps of churches which could be easily reached from the trunk roads so that the travel time between sites was minimised. In Scotland, where suitable buildings were less numerous, three OS FBMs were used. BPGN93 consists of 58 sites, which are fairly evenly spaced about 100 km apart, so that the distance between them could be driven in about 1 hour. The network includes two primary position fixing sites at Barry Buddon (VLBI) and Herstmonceux (SLR), and four absolute gravity sites at which observations have been made with FG5 instruments : Grant Institute, Edinburgh (103); Proudman Oceanographic Laboratory (POL), Birkenhead (103); National Physical Laboratory, Teddington (103, 105) and Hydrographic Office, Taunton (103, 107). The BPGN93 sites cover a range of 900 mgal and, with the network adjustment described in Chapter 6, have a mean standard error of 5 ± 1.3 μgal in the range 2 to 8 μgal. The differential rate of vertical land movement, as evidenced from tide gauge data, is about 5 mm per year over a baseline of 1000 km. Assuming that 10 mm of uplift is equivalent to 2 μgal, the precision obtained for the BPGN should enable crustal motions to be detected in less than a decade.

1.7 Scope of this Thesis

The BPGN93 has been established using three LaCoste & Romberg relative gravity meters. The design and calibration of these instruments is considered in Chapter 2, and experiments to correct the scaling factor and determine periodic errors are described. The preprocessing and adjustment of relative gravity data is the subject of Chapter 3. Part 1 reviews the methods of calculating the solid-Earth tide and describes the implementation of an ocean loading correction. Conventions regarding the Honkasalo Correction (static tide) are discussed in relation to the comparison of absolute gravity observations. The design, observation and adjustment of gravity networks is considered in Part 2 of Chapter 3. The robust statistical methods used in the Edinburgh adjustment program NETWORK, and modifications to the program for dealing with non - Gaussian populations are described.

The instrumentation and theory of modern rise-and-fall and free-fall absolute gravity meters are reviewed in Chapter 4, and the operation of the NERC absolute gravity meter FG5-103 is described in detail. The examination of the theory of free-fall gravity meters shows that the 'effective measurement height' concept fails to provide an accurate datum for the gravity estimate, so that the vertical gradient of gravity must be included in the equation of motion. The importance of consistent corrections to absolute gravity meter data is emphasised and the implementation of corrections for vertical gradient, datum height, speed of light, polar motion and atmospheric pressure in the FG5 software is described. Chapter 5 considers absolute gravity observations and the intercomparison of absolute gravity meters. The implementation of the vertical gradient and datum height corrections at UK sites is described. The variation of the FG5 gravity estimate with drop length is investigated and appropriate corrections are made. The instrument-floor response for FG5 are studied and the correction is estimated for the BPGN absolute sites. An extensive review of absolute gravity observations made in Britain since 1939 is undertaken, and comparisons of FG5-103 with other FG5s and different types of absolute instruments are made.

The British Precise Gravity Network 1993 combines over 2000 relative gravity measurements in an adjustment to find the relative gravity at 58 sites. The design, observation and testing of the Network is the subject of Chapter 6. The suitability of the daily linear drift model is assessed and alternative models are discussed. Novel methods for determining the reliability of the data and the final solution are described, and results are given for a 'free' adjustment, and for one constrained with FG5 absolute observations.

CHAPTER 2. The LaCoste & Romberg Gravimeter

2.1 The LCR Instrument

2.1.1 Introduction

The first LaCoste and Romberg gravity meter was built in 1937 at the University of Texas following the development of a long-period vertical seismometer incorporating a zero-length spring. The US patents (LaCoste and Romberg, 1942, 1945) describe the configurations of the spring and lever system whose basic design has changed little since. A simplified diagram indicating the main features of the meter is given in Figure 2.1. The sensing element is a mass on the end of a horizontal beam which is supported by a 'zero-length spring'. The meter is read by nulling the mass position. This is done by lifting up the top end of the spring with a series of levers. Tiny movements of the levers are made by turning the micrometer screw which is rotated by a gear box with a large reduction. The zero-length spring, beam suspension, and transmission system consisting of the gear box, micrometer screw and levers will be described in more detail in the sections below.

2.1.2 Theory

Astatisation

The simple vertical spring balance (mass on a spring) is an example of a *static* or *stable* gravity meter. Small changes in gravity move the mass against the restoring force of the spring and it performs vertical simple harmonic oscillations about the equilibrium position with a period given by

$$T_o = 2\pi\sqrt{\frac{\lambda - \lambda_o}{g}} \qquad \text{where } \lambda_o \text{ is the unloaded length of the spring.} \qquad (1)$$

The mechanical sensitivity $\frac{d\lambda}{dg} = \frac{T_o^2}{4\pi^2}$ is very small for realistic spring lengths.

Gravity meters which are *astatic* have an additional restoring force opposing gravity, leaving the restoring force of the spring to balance only the residual. This makes the

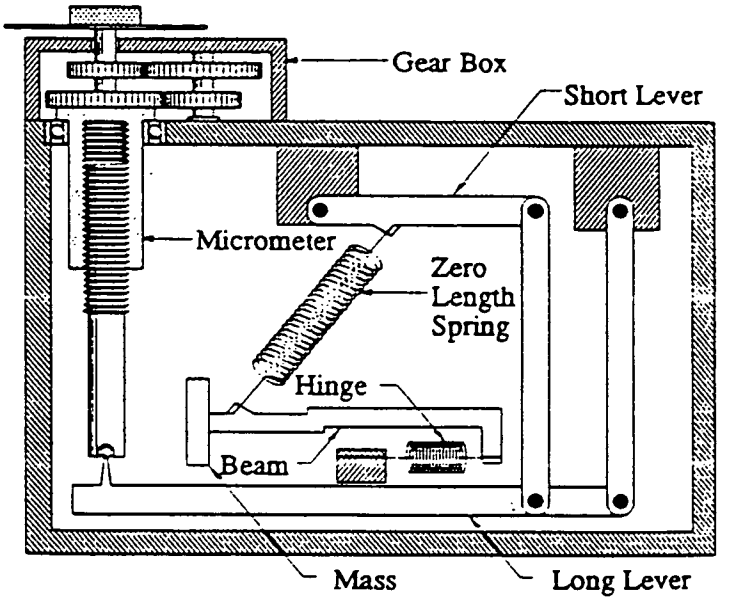

Figure 2.1 The main features of the LaCoste-Romberg gravity meter. (From the LCR manual, LaCoste & Romberg Gravity Meters Inc. 1989)

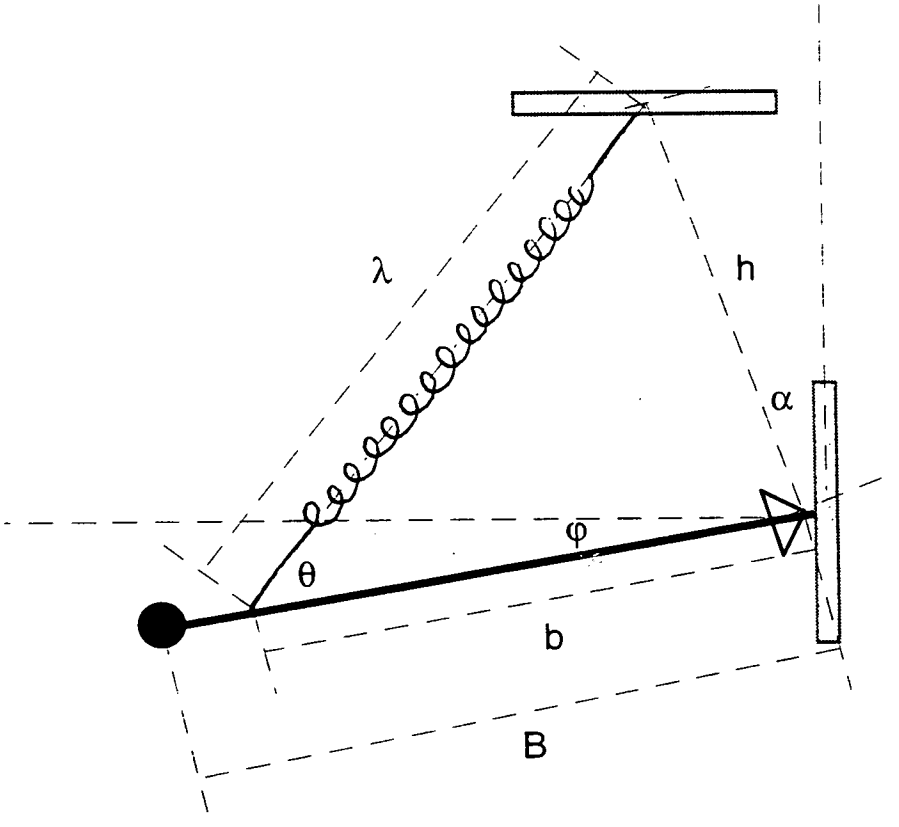

Figure 2.2 The geometry of the zero-length spring, beam, pivot and mass.

free period longer and gives greater sensitivity as the period is increased. The range for which readings vary linearly with gravity is smaller than for stable gravimeters, so astatic gravimeters are generally operated as null instruments. As an initial approximation, consider that the spring is made to support one particular weight (this particular value of gravity is 'backed off'). At this value, a zero-length spring supports the beam in any position. In practice the astatic condition is obtained by making the spring force oblique and balancing the torque that it exerts.

The torque is the product of the force and the perpendicular distance from the point of action of the force and the pivot. Referring to Figure 2.2, if the beam tilts upwards, the length of the spring decreases, so the tensional force it exerts is reduced, but its perpendicular distance from the pivot increases. If the beam tilts downwards the tension increases and the perpendicular distance decreases. This state of neutral equilibrium persists only at the 'backed off' value of gravity. A small increase in gravity causes an imbalance in the torques and the spring extends catastrophically. The meter is actually manufactured so that λ_o is very small rather than exactly zero, so that a very small restoring force remains. The theory of balance is given below.

The equilibrium balance condition

The torque τ_g on the mass due to the force of gravity acts in a direction perpendicular to the beam at a distance B from the pivot (Figure 2.2). The component of gravity in this direction is g cosφ where φ is the displacement of the beam from the horizontal, so

$$\tau_g = mgB\cos\varphi \ .$$

The torque τ_s upwards on the beam from the spring acts at the point of attachment of the spring to the beam which is a distance b form the pivot. The component of the spring force in a direction perpendicular to the beam is k (λ - λ_o) sin θ , where θ is the angle between the beam and the spring, and

$$\tau_s = k(\lambda - \lambda_o)b\sin\theta \qquad (2)$$

We can express θ in terms of α, the vertical angle between the pivot and the suspension point of the spring, and φ. Substituting for sinθ using the sine rule,

$$\sin\theta = \frac{h}{\lambda}\sin(\tfrac{\pi}{2} - \alpha + \varphi) \qquad (3)$$

where h is the distance of the suspension point of the spring to the pivot, gives

$$\tau_s = khb\left(\frac{\lambda - \lambda_o}{\lambda}\right)\cos(\varphi - \alpha) \tag{4}$$

The equilibrium condition for the moments generated by the gravity force and the spring force is

$$mgB\cos\varphi - khb\left(1 - \frac{\lambda_o}{\lambda}\right)\cos(\varphi - \alpha) = 0 \tag{5}$$

In the case where the suspension point of the spring is vertically above the pivot ($\alpha = 0$), the beam is horizontal ($\varphi = 0$) and the spring has zero natural length ($\lambda_o = 0$), we get

$$g = \frac{kb}{mB}h \qquad \text{i.e. there is a linear relationship between g and h.} \tag{6}$$

Sensitivity

The sensitivity describes how much the beam moves (rotates) for a given change in force. A high sensitivity ($d\varphi/dg$) means that a small change in gravity or a small displacement of the top of the spring produces a large movement of the beam. Rearranging the equilibrium condition (equation 5) for g we get

$$g = \frac{kbh}{mB}\,\frac{\cos(\varphi - \alpha)}{\cos\varphi}\left[1 - \frac{\lambda_o}{\lambda}\right]. \tag{7}$$

Using trigonometrical identities and noting that

$$\frac{d\lambda}{d\varphi} = \frac{hb}{\lambda}\cos(\varphi - \alpha)\,, \tag{8}$$

we can differentiate g with respect to the beam displacement angle φ to get

$$\frac{\partial g}{\partial \varphi} = \frac{kbh}{mB\cos^2\varphi}\left\{\sin\alpha - \frac{\lambda_o}{\lambda}\left[\sin\alpha - \frac{hb}{\lambda^2}\cos^2(\varphi - \alpha)\cos\varphi\right]\right\}$$

Since both α and λ_o/λ are very small and, at balance $\cos\varphi \approx 1$, this becomes

$$\frac{\partial g}{\partial \varphi} \approx \frac{kbh}{mB}\left\{\sin\alpha + \frac{\lambda_o}{\lambda}\frac{hb}{\lambda^2}\right\} \tag{9}$$

The sensitivity is the reciprocal of this quantity.

λ is the extended length of the spring and λ_o is determined during the manufacture. λ_o will be very small and either positive or negative. Thus the sensitivity can be altered by changing the angle α which is achieved by tilting the meter in the long axis. The sensitivity is increased by lowering the right side of the meter. The period of oscillation of the beam is proportional to the sensitivity, and by lowering the right side of the meter enough, the period becomes infinite : this is the neutral equilibrium state. Still more lowering of the right side of the meter and the beam becomes unstable and accelerates as it moves towards the upper or lower stops.

Dynamic balance conditions and stability

The equilibrium balance equation (equation 5) describes the condition when the gravity force is exactly equal to the spring restoring force, i.e. $\tau_g - \tau_s = 0$. If one of these torques suddenly changes, for example if either g increases or you change the position of the micrometer screw, there is a net torque and the beam accelerates. What happens then depends on the stability of the system and the presence of damping. If it is stable and there is some friction, the beam oscillates with gradually decreasing amplitude and comes to rest at the equilibrium position. If it is unstable, the beam accelerates away from the equilibrium position. The imbalance of the torques causes an angular acceleration $\partial^2\varphi / \partial t^2$ given by

$$mk^2\frac{\partial^2\varphi}{\partial t^2} = mgB\cos\varphi - kbh\left(1 - \frac{\lambda_o}{\lambda}\right)\cos(\varphi - \alpha) \tag{10}$$

where mk^2 is the moment of inertia and k is the radius of gyration. To examine the characteristics of the oscillation we need to express $\partial^2\varphi/\partial t^2$ in terms of φ. The length of the spring depends on φ i.e.

$$\lambda^2 = h^2 + b^2 + 2hb\sin(\varphi - \alpha) \tag{11}$$

We will substitute the equilibrium value for g (that is, equation (7) with $\varphi = 0$) into equation (10)

$$g = \frac{kbh}{mB}\cos\alpha\left[1 - \frac{\lambda_o}{\lambda^*}\right] \tag{12}$$

where λ^* is the value of λ when $\varphi = 0$, i.e. $\lambda^{*2} = h^2 + b^2 - 2hb\sin\alpha$. We then use the approximation (to first order in small quantities) that

$$\frac{\lambda^*}{\lambda} \approx \left(1 - \frac{hb}{\lambda^{*2}}\varphi + \ldots.\right) \tag{13}$$

to get

$$\frac{\partial^2\varphi}{\partial t^2} = -\frac{kbh}{m\kappa^2}\left\{\cos\varphi\cos\alpha\,\frac{\lambda_o}{\lambda^*}\frac{hb}{\lambda^{*2}}\varphi + \sin\varphi\sin\alpha\left(1 - \frac{\lambda_o}{\lambda^*}\left[1 - \frac{hb}{\lambda^{*2}}\varphi\right]\right)\right\} \tag{14}$$

Now, keeping only first order terms in the small quantities λ_o , α and φ we can write

$$\frac{\partial^2\varphi}{\partial t^2} = -\frac{kbh}{m\kappa^2}\left\{\sin\alpha + \frac{hb\lambda_o}{\lambda^{*3}}\right\}\varphi \tag{15}$$

If $\left(\sin\alpha + \frac{hb\lambda_o}{\lambda^{*3}}\right) > 0$, this describes simple harmonic motion, i.e. the beam is accelerated towards the equilibrium position.

2.1.3 Instrumental Details

Zero - length spring

Hooke's law for the force F exerted by a spring with spring constant k is

$$F = k\,(\lambda - \lambda_o)$$

where λ is the length of the spring and λ_o is the initial or unstretched length, i.e. the force is proportional to the extension $(\lambda - \lambda_o)$. For some springs, successive turns press against each other even when the spring is not supporting any weight, so λ_o cannot be determined by simply measuring the length of the unstretched spring. Instead, λ_o has to be determined by measuring the length of the spring for two different loads which separate the turns of the spring. 'If a spring has a length of 5 inches when supporting a load of 5 pounds and a length

of 6 inches when supporting a load of 6 pounds and these data are substituted into the equation (above) we find that $\lambda_0 = 0$. Such a spring will be called ..... a zero-length spring' (LaCoste and Romberg 1942). By similar argument, negative length springs also exist, and a negative length spring can be made into a zero-length spring by adding straight wire to it. Zero-length springs have the property that $F = k\lambda$, i.e. the force is proportional to the distance between the ends of the spring (λ).

Suspension of the beam

The horizontal beam carrying the mass (~10 g) is suspended at its centre of mass by the 'zero-length' spring. The spring has a physical length of about 35 mm and is at an angle of about 45 degrees to the horizontal. The end of the beam opposite to the mass is supported by a pair of fine wires and springs that act as a frictionless hinge. The springs are attached to posts fixed inside the meter housing (Patent 'Fig.1.' of Figure 2.3 illustrates this well). The line between the suspension points of these hinge springs represents the horizontal rotation axis (pivot) of the beam, and this is positioned almost vertically below the suspension point of the zero-length spring. The size of the vertical angle α (see Figure 2.2) between this point and the beam pivot controls the sensitivity of the beam (section 2.1.2). By virtue of this design, the beam is effectively 'floating' and is afforded considerable protection from impacts occurring to the meter. A number of screws set close to the beam limit its movement in three dimensions, and it is clamped securely for transport . When the beam is clamped it is pushed down against the bottom stops. This action stretches the spring a little so there is a mechanism which pushes the beam backwards at the same time by an amount necessary to shorten the spring to its unclamped length.

Levers and dimensions of movements

We have seen from equation (6) that when the suspension point of the spring is vertically above the pivot of the beam, and the beam is horizontal (balance position), the distance h between the top of the spring and the pivot is proportional to gravity g

$$g = \frac{kb}{mB}h \qquad \text{so} \qquad \frac{dg}{g} = \frac{dh}{h} . \tag{16}$$

The meters are built with $h \approx 25$ mm, so that the 7000 milligal range of a G meter requires moving the top of the spring by only 0.175 mm. A measurement precision of 10 µgal requires positioning to 0.25 nm. This is achieved via the gearbox reduction of 70.94 : 1 for a

G meter, a micrometer screw with a pitch of 184 t.p.i and a reduction ratio of 77.8 : 1 (Lyness 1984) in the lever system. D meters allow finer positioning of the beam than G meters by using a different lever system and different gear ratios.

How it works : Coarse and Fine lever systems

The lever and spring system for a single dial 'G' meter is described in the 1945 Patent (LaCoste & Romberg 1945). Figures 1 and 2 from the patent are reproduced in Figure 2.3 and figures 3, 4 and 5 in Figure 2.4. The numbers on the patent drawings will be referred to by italics in the following description.. The patent 'Fig. 5.' (in Figure 2.4) shows the detail of the attachment of the top of the main spring *4* to the block *35*. Vertical movement of the bottom of the micrometer screw is transmitted to the block *35* via the long horizontal lever *63* (Patent Fig.1 in Figure 2.3), the vertical lever *66* and the short horizontal lever *50* (Also indicated in Figure 2.1). The levers are connected by leaf springs. The lever *50* is attached to the plate *23* by a pair of spaced vertical leaf springs *51* which act as a fulcrum for the lever *50*. A second pair of leaf springs *53* attach the lever *50* to the block *35* so enabling the movement of block *35* with respect to the plate *23*. Fine adjustments of the top of the main spring are thus controlled by the micrometer screw. Coarse adjustments are achieved (in the Patent version) by the large screw *30* which moves the scored bar *23* with respect to the fixed plate *20*. The bar *35* and springs *51* and *53* - the 'fine adjust' - effectively act as a flexible tip of the scored bar - the 'coarse adjust'.

For D meters, the coarse adjust is also controlled by a micrometer screw, and the arrangement involves another set of levers (D for Double lever). The scored bar device of the original instruments is also replaced by a second pair of leaf springs. Figure 2.5 shows the bars F (fine adjust) and C (coarse adjust), which are *both* the equivalent of bar *35*. Bar C is attached to the fixed plate(P) by the horizontal leaf springs (B), and its movement is controlled by the coarse lever (CL) and vertical springs (A). Bar F is attached to bar C via springs D, and adjusted with respect to bar C by means of the fine lever (FL). The main spring is attached to the underside of bar F. In this way, the top of the spring can be moved independently by the fine and coarse adjust systems.

June 12, 1945. L. J. B. LA COSTE ET AL 2,377,889

FORCE MEASURING INSTRUMENT

Filed Aug. 12, 1939 2 Sheets-Sheet 1

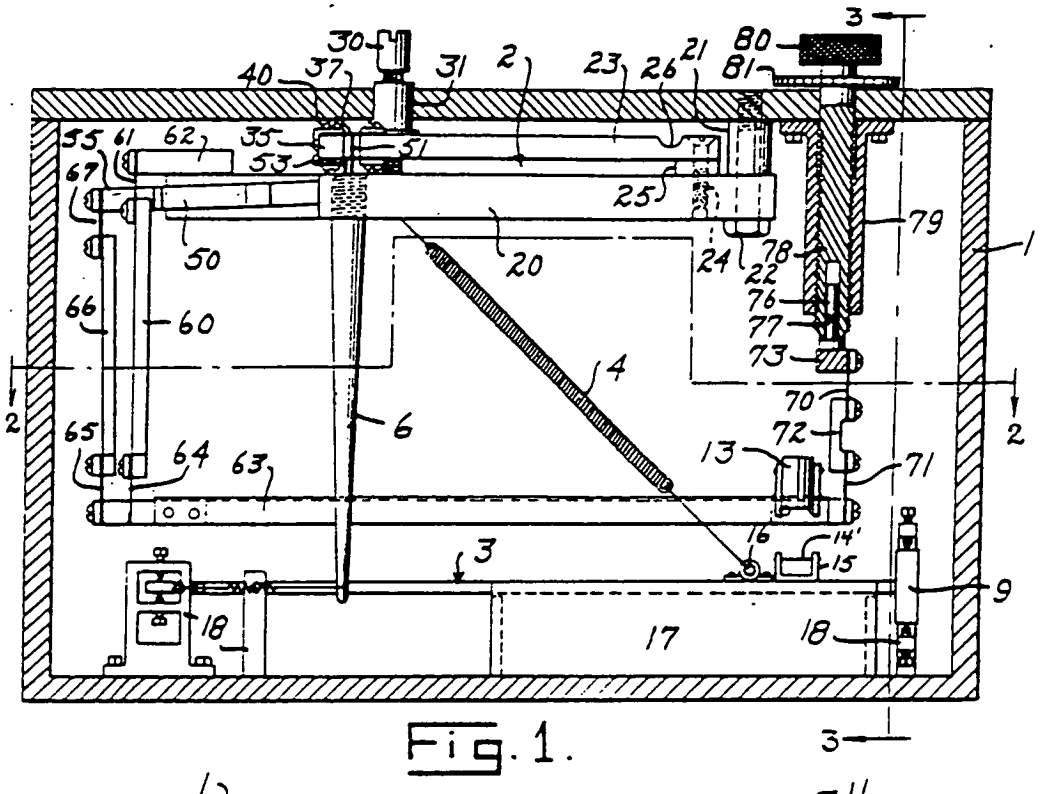

Fig. 1.

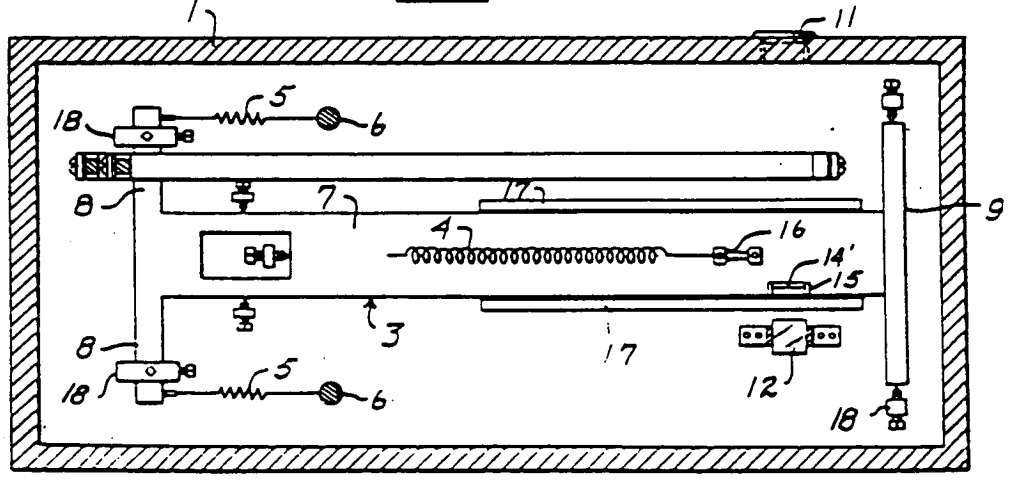

Fig. 2.

LUCIEN J. B. LACOSTE
ARNOLD ROMBERG
INVENTORS.

BY Jesse P. Stone
Lester B. Clark
ATTORNEYS.

Figure 2.3 US Patents for LCR meter. Patent figures 1 and 2, as viewed from the back of the meter (from LaCoste & Romberg 1945)

June 12, 1945. L. J. B. LA COSTE ET AL 2,377,889

FORCE MEASURING INSTRUMENT

Filed Aug. 12, 1939 2 Sheets-Sheet 2

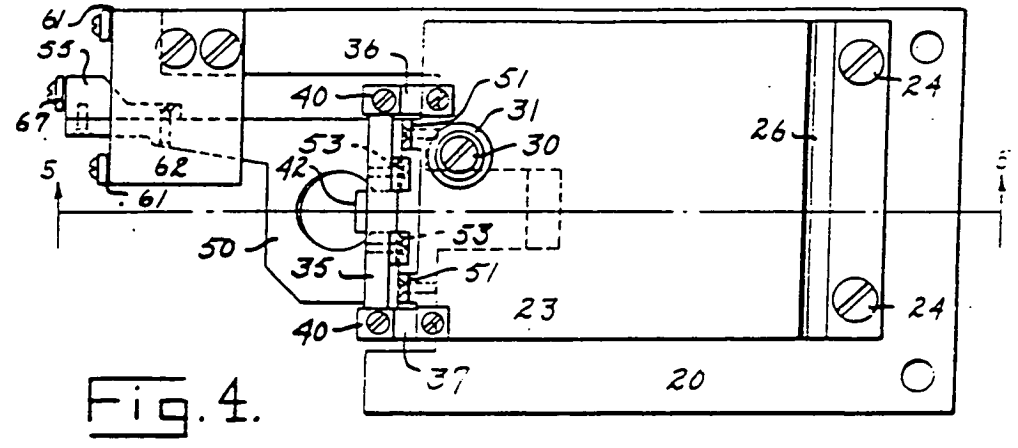

Fig. 4.

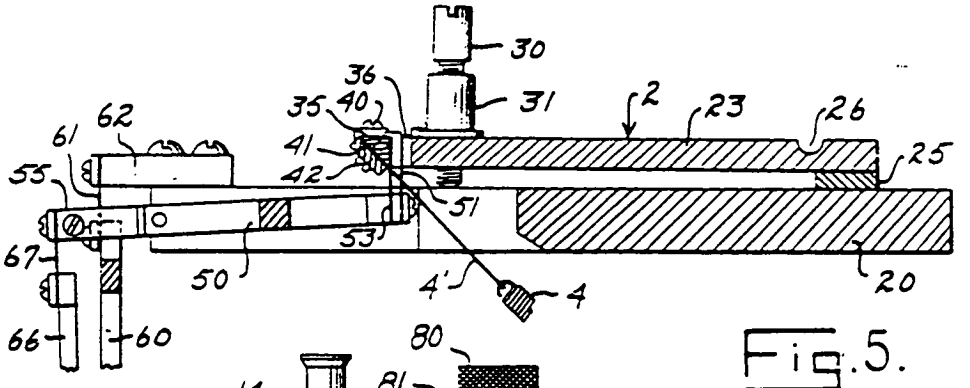

Fig. 5.

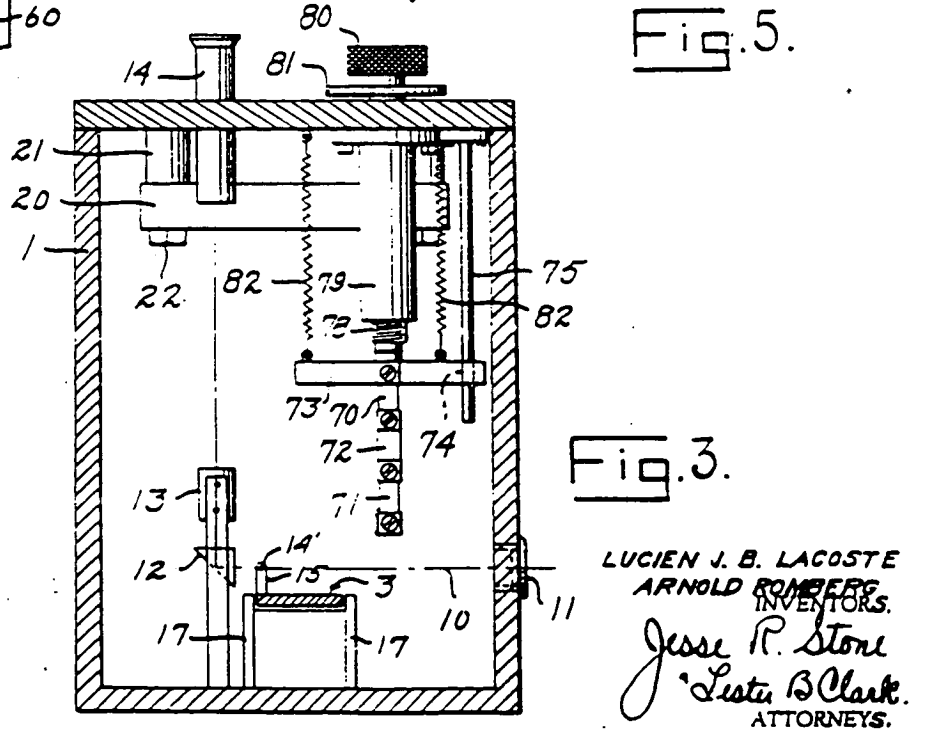

Fig. 3.

LUCIEN J. B. LACOSTE
ARNOLD ROMBERG
INVENTORS.
Jesse R. Stone
Lista B Clark.
ATTORNEYS.

Figure 2.4 US Patents for LCR meter. Patent figures 3,4 and 5, as viewed from the back of the meter (from LaCoste & Romberg 1945)

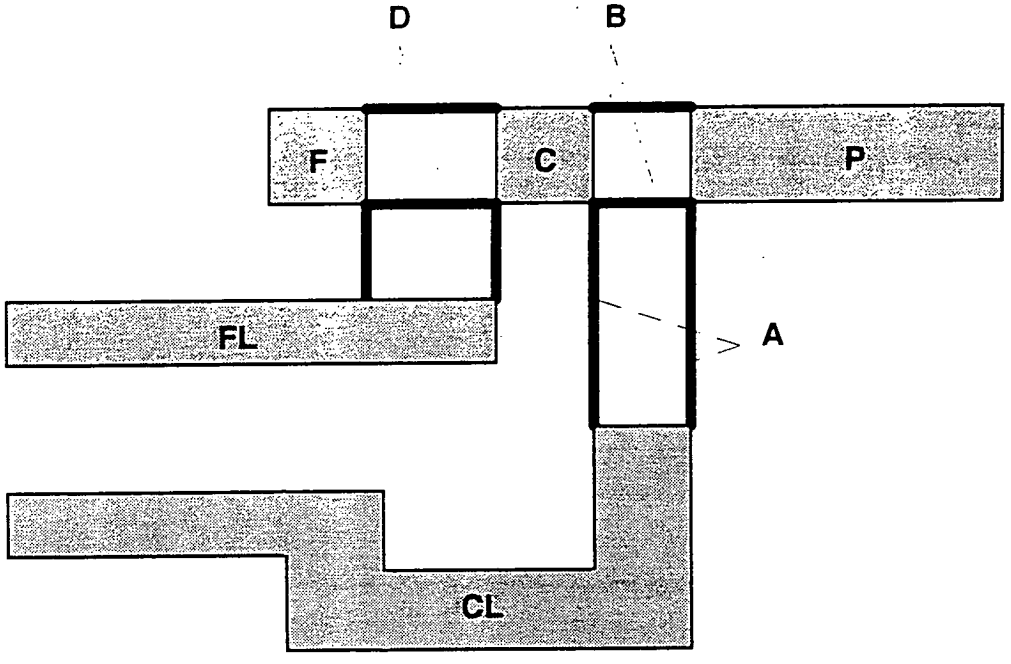

Figure 2.5 Diagram of the double lever system in a LCR D meter. Fine adjust (F) and coarse adjust (C) bars, fine lever (FL), coarse lever (CL), fixed plate (P), and pairs of leaf springs (A, B and D).

Gears

Every rotation of the dial on top of the meter causes a small rotation of the micrometer screw which moves the suspension point of the spring via the system of levers. The dial is connected to the micrometer screw by a gearbox with a large reduction attained by two sets of gears. For G meters up to G457 the reduction is 70.94:1, for G458 onwards it is 73.33 : 1. For a normal D meter with a fine calibrated screw and an uncalibrated coarse reset screw, the reduction on the fine screw is 32.5 : 1. For D meters with both screws calibrated (two dials on top of the meter), the fine screw has a ratio of 50 : 1 and the coarse has a 100 : 1 reduction. The component gears for G275 are (180/20).(134/17), and for D145 and D154 there are (180/18).(180/18) teeth for the coarse and (180/18).(150/30) for the fine screw. Imperfections in the micrometer screw and eccentricities in the gear wheels can cause periodic (or circular) errors (section 2.3) for which corrections to the manufacturers calibration table must be made. When making a reading it is important always to 'read from below', so that the final movement of the dials is in the increasing direction. This avoids 'backlash' by ensuring that the gear wheel teeth are in contact and the screw position is reproducible.

Readout

The position of the beam is monitored optically, and for more recent meters electronically as well. The image of a cross hair mounted on the beam is reflected up into a telescope through a graduated scale. The meter is balanced by turning the nulling dial until the beam image lies on the 'reading line', which is some position on the scale determined by the manufacturer. When the image of the crosshair lies on the reading line, the beam is horizontal. The 'Capacitance Position Indicator' (CPI) consists of a capacitance bridge sensing the position of the beam, with the beam acting as a movable capacitance plate between two fixed capacitance plates above and below it. The CPI electronics card connects to a galvanometer on the top of the meter and is also the means of providing electrostatic feedback for automatic nulling of the beam.

Electrostatic nulling

The force of gravity on the meter beam is mechanically balanced by adjusting the upward force of the main spring, but the CPI can also be used to null the instrument when mechanical balancing is incomplete. If a DC voltage is applied between the fixed plates and the moveable plate which is attached to the beam, an electrostatic force will act on the beam, in addition to the forces of gravity and the spring. The beam position voltage output

from the CPI circuit is used to generate a DC voltage which is applied to the capacitor plates in a negative feedback loop. This causes the voltage to stabilise at the value needed to keep the beam exactly at the null position (analogue feedback). An alternative but equivalent scheme keeps the voltage fixed but applies it as a square wave. The net force is then changed by varying the fraction of the cycle over which the voltage is applied (digital feedback). Harrison and Sato (1984) describe the original implementation of electrostatic feedback to a model G meter, and both analogue and digital systems are available from the manufacturers of LCR instruments.

A LCR analogue feedback device was fitted to D154 but tests carried out with it gave unacceptably erratic results. The adjustment procedures described in the manual did not improve its performance and the electronics failed completely after the initial tests. Nearly all the work for this project was done without electrostatic nulling.

Several successful feedback systems built by users of LCR instruments are in use. They differ mostly in their range of operation : the larger the range, the more useful is the system, as it reduces the need to adjust the micrometer screw and hence reduces the need for a screw calibration which may be inadequate for precise work. The most successful academic feedback device has been produced by the Institut für Erdmessung, Hannover, and has an extended range up to 140 mgal. The technique has now been developed commercially and is incorporated into the Zero-Length-Spring (ZLS) gravity meter developed by Valliant from the mechanical components of the LCR gravity meter. The same design is the primary operating principle for the Scintrex gravity meter, where electrostatic feedback provides a world-wide 7000 mgal range.

Oven, lights and batteries

The measurement system is made of metal parts and many design features help to eliminate possible disturbances due to external conditions. The measurement system is enclosed in an air-tight box which is shielded magnetically. The sealed box is filled with inert dry gas and thermostated at an optimum temperature which varies from meter to meter but is about 50°C. The meter is maintained at this operating temperature to ± 0.05° C, and the heater is powered by a 12 V DC supply provided by a charger/eliminator in the lab or battery when in the field. The maintenance of a steady 12 V supply in the field is of paramount importance because fluctuations in the voltage cause temperature variations. Changes in the ambient temperature of the spring lead to large and irregular drift which invalidate the readings. Care should be taken to allow the temperature to stabilise after swapping from a mains supply to

a battery (which may differ in voltage level by about 1 Volt) before reading. Although the heater takes most of the power, the battery also supplies the lights and electronics, and a dimming of the reading light is an early warning of a failing battery.

2.2 Calibration

2.2.1 Introduction

Determining the shape of the calibration curve is called 'relative calibration'. The relative calibration is made 'absolute' by measuring a single gravity interval on a national or international network such as the International Gravity Standardisation Net 1971 (IGSN71) (section 3.5), which provides the conversion factor to an 'absolute' scale. At LCR, the shape is found by adding small masses to the beam and determining the number of dial turns needed to rebalance (null) the meter. Other methods include changing the apparent gravity by tilting (e.g. Moore and Farrell 1970), calibration with electrostatic feedback systems (e.g. Schnüll *et al.* 1994) and on high precision calibration lines (e.g. Becker *et al.* 1987). Determining the calibration to a microgal level requires a knowledge of periodic errors resulting from imperfections in the measuring screw and gear wheels.

2.2.2 Calibration at LCR

At the LCR laboratory, small masses are added to the beam of the gravity meter and the response of the meter is observed. Figure 2.6 shows the calibration apparatus. The unit is attached to the side of the meter and two rods are temporarily attached to the beam mass. One rod is threaded to allow a range nut to be screwed along it, so the torque produced by the weight of the nut counterbalances the force provided by adjusting the dial, enabling the meter to be balanced at any point over the range of the micrometer screw. The other is the weighing rod, and has masses hanging from it. This arrangement allows a continuously adjustable torque to be applied to the beam. The weight of the test mass is equivalent to an acceleration of approximately 200 mgal for model G meters. Meters since D145 have been calibrated with a 20 mgal test weight. A detailed description of the process is given in the manual supplied with each instrument (LaCoste & Romberg Gravity Meters, Inc. 1989), but Valliant (1991) is a much more readable account with many explanatory comments.

The meter dial is set and the range nut is adjusted until the meter is balanced. The dial reading is recorded then the test mass is lowered onto the beam and the meter is rebalanced using the dial. The relative slope (or 'factor') for the interval is determined by the ratio of the difference in the two dial readings over the mgal equivalent of the test mass. The observed slope is the average slope over the interval and it is plotted against the median value of the dial turn interval. The test mass is now removed and the range nut adjusted so the meter is balanced at the new dial reading. In this way a series of factors for each interval over the complete range of the instrument (6800 dial turns for a G meter). The observations are at equal intervals of acceleration (200 mgal for G meters, 20 mgal for D meters), but generally not at equal intervals of dial turns. Values at 100 dial turn intervals are interpolated from a smooth curve drawn through the plotted values of 'factor' versus dial reading. Assuming that the meter can be read with a precision of 0.010 mgal (about 100th of a dial turn, equivalent to one of the smallest marked divisions), the slopes can be determined with a precision of one part in 20 000. Using a smaller test mass of 20 mgal for D meters over the 200 mgal range of the calibrated D meter screw reduces this precision to one part in 2000, but the width of the interpolation interval is reduced.

The calibration table, unique to each instrument, is provided by the manufacturers in the form of a conversion from dial turns to gravity at increments of 100 dial turns, and an 'interval factor' for interpolation within each of these intervals. 100 dial turns is equivalent to about 100 mgal for G275 and about 75 and 7.2 mgal for D145's coarse and fine screws respectively. The complete tables for the Edinburgh instruments G275, D145 and D154 are reproduced in Appendix 1. The interval factors are based on observations as described above, and the calibration curve is determined by integrating the interval factor curve. The overall shape of the interval calibration curve is a third order polynomial, determined by the geometry of the micrometer screw, lever system and suspension. The curve for G275, plotted in Lyness (1984), is shown in Figure 2.7. The interval factor curves for the coarse and fine dial of D145 are plotted in Figure 2.8a and 2.8b respectively. The manufacturers table should give a calibration accurate to 3 - 5 μgal over 10 mgal intervals (LaCoste 1991). However, the values in mgal given in the tables are rounded to 10 μgal for G275 and 1 μgal for D145 and D154. Gravity differences between sites with gravity values lying in different table intervals will be in error if the piece-wise linear approximation is not considered (Lyness 1984). A ninth order polynomial function has been fitted to the calibration data for G275 and both the calibrated screws on each of the D meters, and these are incorporated into the Edinburgh pre-processing program REDUCE (section 3.4).

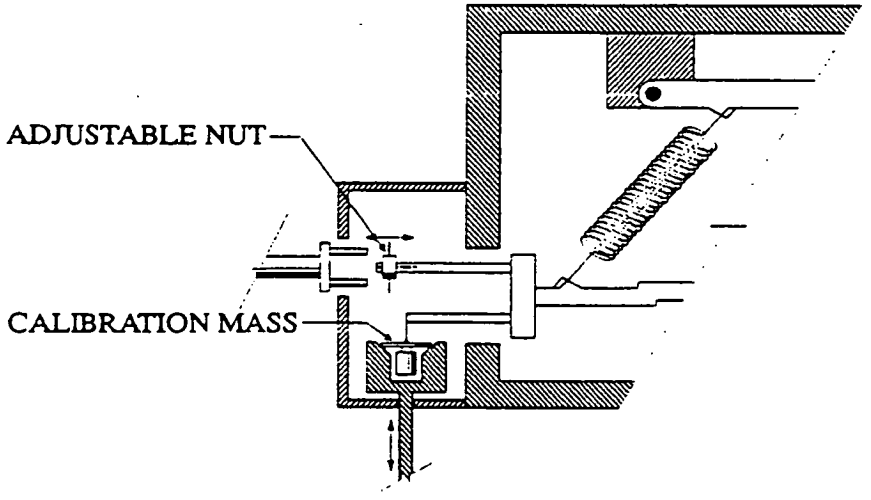

Figure 2.6 The LCR calibration apparatus. (From the Instruction Manual, LaCoste & Romberg Gravity Meters Inc. 1989)

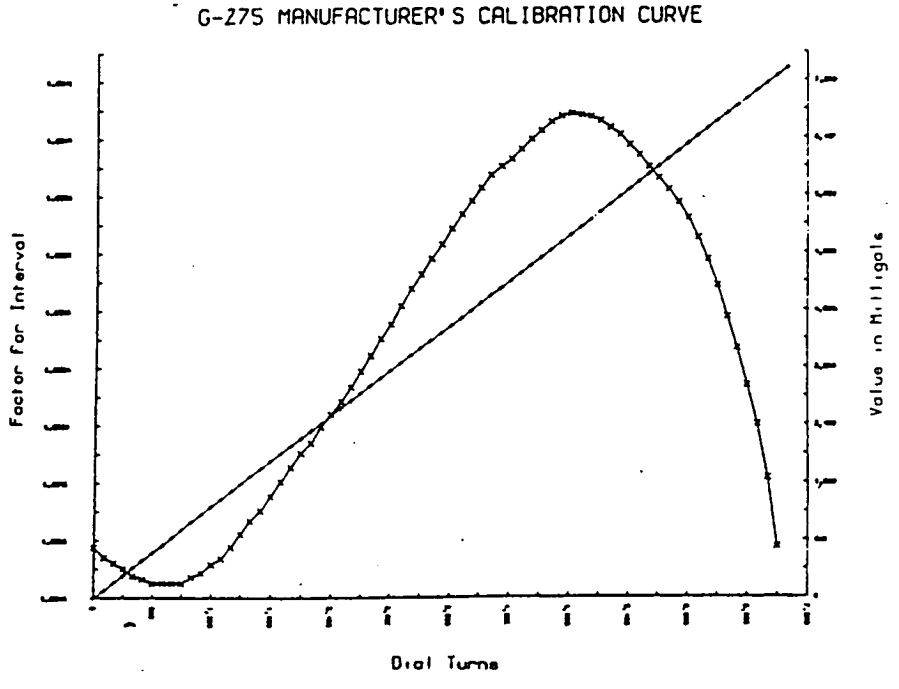

Figure 2.7 Factor interval curve and calibration curve for G275, taken from Lyness 1984

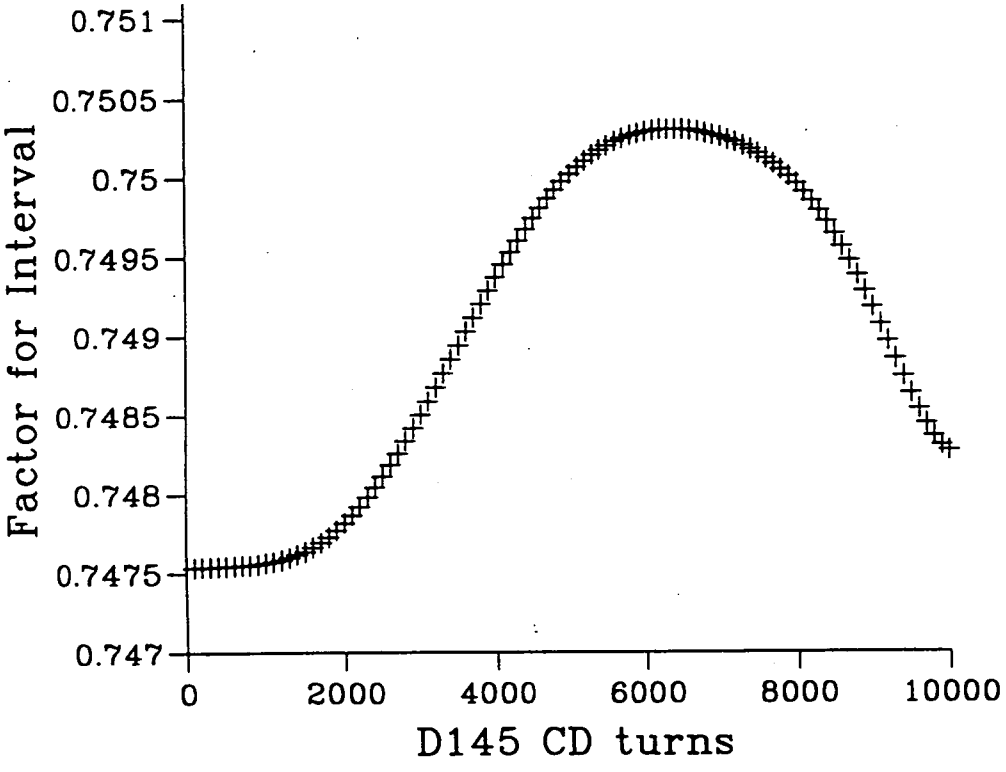

Figure 2.8a Factor interval curve for the coarse screw of D145.

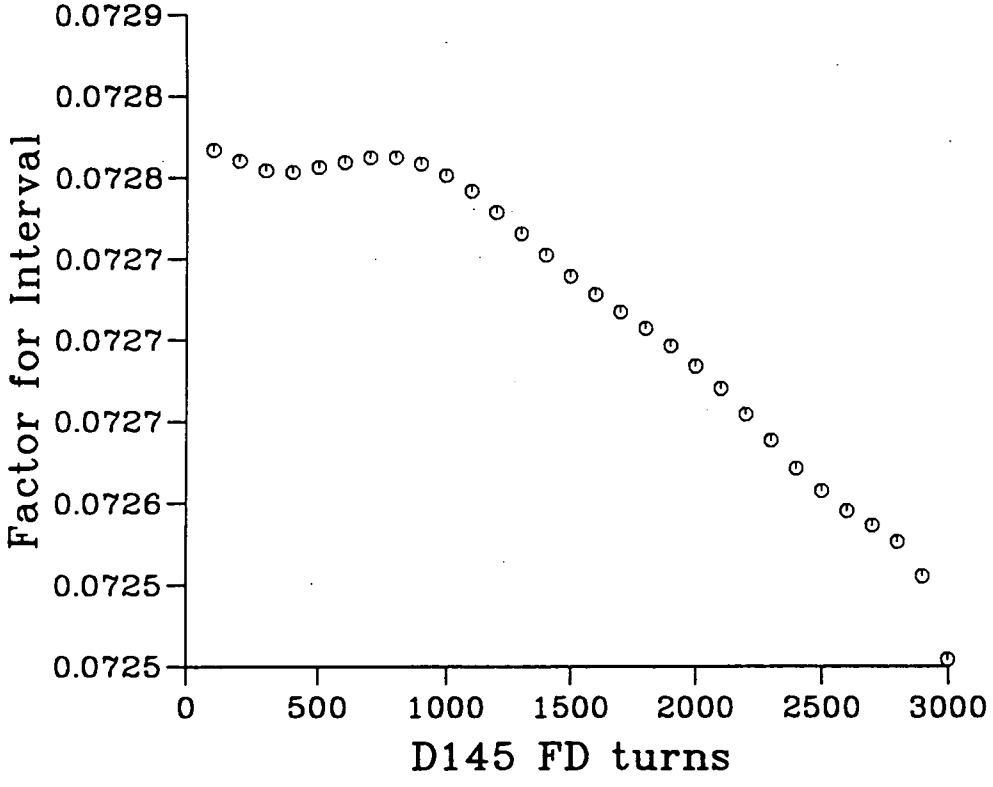

Figure 2.8b Factor interval curve for the fine screw of D145.

G meters

To convert the 'factor versus counter interval' curve resulting from the above procedure to an absolute one, the meter is read at two or more gravity stations of known gravity difference, and a single factor is determined. The gravity difference between these calibration stations should be as large as possible for the most accurate determination of the conversion factor. The closest large change in gravity is 1000 km from the LCR laboratory, at Cloudcroft where two stations with a difference of 241.9 mgal were established in about 1955 by LCR personnel using gravity meters which had been calibrated against existing pendulum measurements. Long range calibrations performed by Geological Survey Canada (GSC) suggest that the Cloudcroft value is too small by only 1 part in 2000 (R.K McConnell GSC in Valliant 1991). The calibration interval is equivalent to only a single interval-factor determination (200 mgal) and is thus a very small portion of the range of a G meter. This means that this small section of the calibration curve can be considered as a differential of the whole, and the scale factor can still be determined with an accuracy consistent with the relative calibration (1 part in 20 000). The Cloudcroft interval is observed by alternately reading the meter at one station then the other until at least four readings are taken at the top station and four at the bottom. The absolute calibration factor is the ratio of the average counter reading difference and the size of the gravity interval. This determines precisely the factor for the part of the screw covered by the 241.9 mgal of the Cloudcroft range, which falls at about 2500 dial turns. The interval-factors for the 7000 mgal covered by the rest of the screw are given by the ratio of the observed relative interval to the Cloudcroft interval. The counter reading differences are converted to gravity intervals by multiplying by the appropriate interval factor.

D Meters

The standard model D has a counter range of 200 mgals which covers only about 62% of the 330 mgal range of the lever and micrometer system (LCR manual 1989). This is closely equivalent to the central linear portion of the third order calibration curve. Meters D1 to D109 had calibration factors determined at on a local (Austin) field calibration range of 17 mgal by measuring at three points close to the ends and middle of the screw. Small changes in the shape of the calibration curve can be achieved by mechanical adjustments of the meter, and if this can be done so that values at 100, 500, 1000, 1500 and 1900 dial turns plot on a horizontal line then a single factor is used for the meter, otherwise a smooth curve through these points was used. Starting with meter D110, the shape of the curve was determined by the laboratory mass-calibration method using masses equivalent to about 100 mgal, and 5 points were measured to determine the calibration curve. The scale was

determined on the 240 mgal Cloudcroft range by using a temporary counter to allow the meters to be read a little above and below their normal 2000 dial turn range. This technique had the disadvantage that the 100 mgal calibration mass covered too large a portion of the range of the screw and could cause smoothing of the calibration curve. Also since the gravity interval at Cloudcroft encompasses the complete range, it cannot approximate a differential of the curve and therefore is not correct to match the slopes. Beginning with D145, a 20 mgal calibration mass was used, and a new intermediate field station was established at the Cloudcroft range, so that the problems mentioned above are addressed.

2.2.3 Calibration by tilting.

It is possible to simulate a variation in gravity by tilting the gravity meter. If the beam is assumed to be supported by a perfect pivot, so that it can only move up and down in the same plane, (i.e. has 1 degree of freedom), then the force g_{eff} experienced by the mass of a gravity meter tilted at θ to the horizontal is simply $g \cos \theta$. The maximum value of g_{eff} and hence the greatest downward deflection of the mass relative to the instrument case occurs when $\theta = 0$. This is the level condition and small tilts about this position give changes Δg in the effective g of

$$\Delta g = g(1-\cos \theta), \qquad \text{or} \qquad \Delta g \approx \frac{g\theta^2}{2} \text{ for small } \theta.$$

This is the equation of a parabola, symmetric about the vertical condition.

By re-zeroing the beam with the dial for different measured tilts, a relationship between Δg and dial turns is found. Measuring a tilt of, for example 1' with an accuracy of 1" gives $\Delta g = 41.5 \pm 1.4$ μgal. This calibration method can give an absolute calibration directly, rather than a relative one which needs an additional measurement on an absolute scale.

Moore and Farrell (1970) tilted an LCR instrument by a motor driven micrometer fixed to one corner of a triangular base plate. The number of rotations of the screw were measured by a metal film potentiometer coupled to the screw and the overall tilt accuracy was better than ± 0.5 %. The calibration constant was determined to a similar accuracy by using a linear electrostatic feedback of the beam position to null the meter. Lyness (1984) measured the tilt angle by using an interferometric arrangement for observing Newton's Rings to measure the displacement of the movable end of the tilting platform. Lyness tilted

separately in the long and cross level axes, and was able to determine a correction factor of 1.0039 ± 0.0099 to the scale of G275 from the long level results. Boedecker (1981) measured the tilt of the platform using two corner cube reflectors. The vertical displacement of one reflector was measured relative to the second which was fixed on the pivoting axis. Boedecker observed periodic errors with periods of about 6 mgal for G85.

2.2.4 Scale Factors determined by measuring on Calibration Lines

The simplest way to determine the scale factor for an instrument is to measure a 'known' gravity interval (as at the LCR Cloudcroft and Austin ranges). National calibration lines ensure that all the gravity meters in that country are at least converted to the same scale. The Short National Calibration Lines (Masson-Smith *et al.* 1974) in Britain were established mainly with Worden meters, but revisions in 1971 and 1983 suggest further significant discrepancies (Lyness 1984). The Airport Net of the NGRN73 (section 1.7) covers a range of 726 mgal with standard errors on the sites of between 11 and 30 μgal, but this is not sufficient for a microgal determination of the scale factors. The linear scale factor for G275 was determined with respect to the IGSN71 by measuring the large interval between IGSN71 stations at Edinburgh and Rome. It has the value 1.000 622 ± 0.000 027 (Hipkin *et al.* 1988). With the availability of new FG5 absolute observations in Britain since 1992, it has been possible to make an additional, independent calibration of G275 to the 'FG5 Absolute Scale'. This was done by constraining the gravity values at the British Precise Gravity Network (BPGN) absolute sites and fitting scaling factors for G275, D145 and D154 with respect to FG5. The scaling factor derived from this 'FG5 constrained' adjustment gave the value of 1.000 7565 ± 0.000 0210 for G275. This result will be derived in section 6.5. Corresponding scale factors for the D meters can be determined when all three instruments measure any large interval together.

Scale factors for D meters determined from BPGN

The BPGN has a range of 900 mgal and standard errors of 2 - 8 μgal, and was measured simultaneously with G275, D145 and D154. By processing the data for each meter separately the difference between the gravity values found by the instruments can be plotted. Figure 2.9 shows the difference between G275 and D145 plotted against the gravity values found by G275 for all the Network stations. The slope of the line found by least squares is 1.000 401 ± 0.000 052. These scaling factors are also fitted during the network adjustment, and by this method we find 1.000 4119 ± 0.000 0238 for D145 and 1.000 7291 ± 0.000 0321 for D154 to the scale of G275.

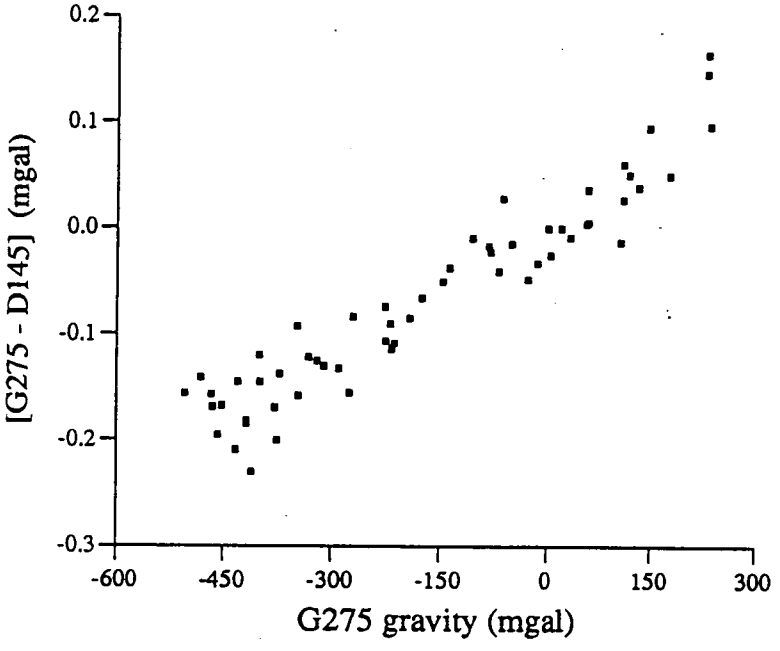

Figure 2.9 The difference between G275 and D145 plotted against the gravity values found by G275 for all BPGN stations. The slope of the line found by least squares is 1.000 401 ± 0.000 052.

2.3 Periodic Errors

2.3.1 Introduction

The process of cutting the micrometer screw (and the 'nut' through which it moves) introduces periodic errors whose periods are of the order of the fundamental and harmonics of a complete turn of the screw. Eccentricities of the gear wheels can also produce periodic errors. The maximum tolerable amplitude of error from the screw is 40 µgal for the G meter screw and 8 µgal for the fine screw on a standard D meter (Valliant 1991).

The gear ratio of a standard G meter is (180/20).(134/17) or 70.94118 : 1 which means that turning the dial 70.94 times turns the measuring screw once. The screw has a world-wide range of 7000 mgal, and commonly one turn of the dial on a G meter is equivalent to about 1 mgal. The literature reports periodic errors with a number of periods, and the most common for a G meters up to G 457 are

1206.0, 603.0, 70.94, 35.47, 7.88, 3.94 and 1.00 dial turns.

70.94 and 35.47 are one and one-half complete screw turns respectively. 7.88 and 3.94 are related to the second pair of gears (134/17), and 1206.0 and 603.0 come from a combination of the primary ratio 70.94 and an extra influence of the smallest gear wheel: 1206 (= 70.94 × 17), and half of this amount = 603. For G458 onwards, the most significant expected periods are 73.33, 36.67, 7.33 and 1.00 dial turns.

The gear ratio of a standard D meter is 32.5 : 1. A 'standard' D meter has two micrometer screws and lever systems. The coarse screw has a world-wide range of 7000 mgal like the G meter screw (in fact D meter coarse screws are often rejected G meter screws (Valliant *pers. comm.* 31 Oct. 94)), but is normally uncalibrated and used only as a 'reset' screw to bring the meter into the operating range of the fine screw. The fine screw normally has a range of 200 mgal and one turn of a D meter dial is equivalent to one-tenth of a G meter dial turn or 0.1 mgal. Periodic errors corresponding to one and one-half complete D meter (fine) screw turns have periods of 32.5 and 16.25 dial turns respectively. These are well documented in the literature (e.g. Becker *et al.* 1989, Liard 1989).

A few D meters have both coarse and fine screws calibrated, and these have two gearboxes, two counters and two nulling dials (section 2.1.3). The coarse screw gear box has a ratio of

100 : 1 produced by a (180/18).(180/18) gearbox. The effect of periodic errors in the coarse screw can be minimised by always setting it at integral turns of the micrometer screw. A D meter which was originally constructed with two calibrated screws has a gearbox on the fine screw with a ratio of 50 : 1 produced by a (180/18).(150/30) gearbox. The most significant periodic errors on the coarse screw would be expected at 100 and 50 coarse dial turns, and possibly 1800 and 900 following the reasoning above. The fine screw with a 50 : 1 gearbox should give periods at 50 and 25 fine dial turns. All the likely periods for G275 and D145 are summarised in Table 2.4 of section 2.4.3.

2.3.2 Methods of detecting Periodic Errors

Periodic errors at LCR

The test for periodic errors involves adding and removing force equivalent to a quarter of a turn of the measuring screw to the beam and proceeds in a manner similar to the relative calibration described above. For G meters, a mass equivalent to 18 mgal is applied to the beam, and for D meters, an electrostatic force equivalent to 0.8 mgal is applied. The new method is based on using electrostatic feedback to directly calibrate the portions of the screw lying between points which have been calibrated by the mass calibration method. LaCoste (1991) describes a proposed 'new calibration method' to find periodic errors in particular with much greater accuracy than the method described above.

Many authors have designed various experiments improving on the manufacturers' to measure the size of periodic errors in their LCR instruments. Some of these are discussed below.

Periodic error detection using electrostatic feedback

The principles of operation of electrostatic feedback have been discussed in section 2.1.3. Because the feedback force is completely independent of the screw and lever system it provides a stable reference for measuring periodic errors.

The Institut für Erdmessung (IFE), Hannover, have developed electrostatic feedback devices with an extended range of up to 140 mgal (Röder *et al.* 1987, Schnüll *et al.* 1994). The 1987 results show periodic errors in G298 of between 8 and 10 dial turns from a feedback with a linear range from -13 to +14 mgal. For G709 the 7.33 dial turn period is very well determined with a ± 34 mgal range. The measurements are made in the laboratory over

different portions of the screw. The 1994 results describe a normal feedback mode of 30 mgal and a 'booster' mode of 140 mgal. The periods and amplitudes found for G79 and G298 are reproduced in Table 2.1 below.

Period (dial turns)	Amplitude G79 (nm s^{-2})	s.e (nm s^{-2})	Amplitude G298(nm s^{-2})	s.e (nm s^{-2})
70.941	184	6	78	5
35.471	78	4	-	-
17.735	14	2	-	-
7.882	47	2	40	2
1.000	33	2	12	2

Table 2.1 Periods and amplitudes of periodic errors found with SRW booster feedback (after Schnüll *et al.* 1994). (1 nm s^{-2} = 0.1 μgal)

The linear calibration factor still had to be determined on a calibration line but long period non-linear terms, which may occasionally be statistically significant, can be found by using the reset screw to extend the feedback range over large gravity differences.

Staircase calibration lines

Staircases can make useful gravimeter calibration lines, and they have the advantages that there is a short time between readings, the gravimeter is not subject to adverse transport conditions, the observers are not subject to adverse weather conditions, the temperature should remain fairly constant, and more than one meter can be observed at each site simultaneously. Staircase lines rely on having a large number of measurements with many different instruments so that deviations from the mean are significant. The Hannover calibration line is in a 76m high building and has a range of 21 mgal in steps of 1 mgal known to ± 1 μgal and has been measured with a large number of instruments over many tens of years. The relatively large gravity intervals on this line make it more suitable for measuring the shape of the curve rather than determining periodic errors. The Darmstadt staircase line has a range of 7.5 mgal in steps of about 0.4 mgal with a standard error on each station of about 1 μgal. Larson *et al.* (1984) used the Washington Monument to determine periodic errors of D43 by 'making several runs from the top to the bottom'.

Part of the International D-Meter Campaign 1983 was the determination of periodic errors on the Darmstadt staircase line (Becker *et al.* 1987). For this exercise, 14 stations were chosen with eight spaced at about 0.4 mgal and five spaced at about 0.8 mgal with a

maximum gravity difference of 7.4 mgal. Each station gravity value is known to about 1.1 μgal. A typical sequence of observations starts in the middle, works up via each station to the top, then all the way down to the bottom and up to the middle again. The reset screw was adjusted by an amount chosen to maximise the changes in the observed gravity produced by the periodic errors, and the sequence was repeated (the following day). The data were analysed independently by three groups from separate institutions, and all groups found the one and one-half screw turns (32.5 and 16.25 D meter fine-dial turns respectively) to be present in all 14 instruments tested. Solving for the shorter periods of 7.2 and 3.6 fine-dial turns (about 0.7 and 0.4 mgal period respectively) was not considered valid by one group because these periods are less than twice the smallest gravity difference on the staircase line (because of the possibility of aliassing), nevertheless another group detected errors at these periods with amplitudes ranging between 0.4 and about 4.0 μgal.

Automatic laboratory technique (Liard) for D meters

Liard (1989) has calibrated the fine dial of a D meter against its own 'reset' screw using feedback to monitor the beam displacement. The 'sensitivity' of the instrument is changed so that a greater range of the dial will be covered at each 'reset' position, and the stop-to-stop range is increased to 4 mgal from its usual 1.4 mgal. Each sampled segment generates a set of residuals which overlaps the range of the next segment(s), so that noise can be reduced by averaging the residuals from consecutive sets (Figure 2.10). A Fourier transform of the combined residuals showed peaks at the 32.5 and 8.13 dial turns (corresponding to one and one-quarter turns of the micrometer screw respectively) for all four D meters tested (D28, D110, D6 and D27). The figures reproduced in Figure 2.11 represent the periodic errors as a function of one turn of the screw. The strength of the 8.13 dial turn (quarter micrometer screw turn) peak was unexpected, but may possibly be explained by imperfect alignment of one of the four pins which support the measuring screw inside the instrument (Liard *pers. comm.* 6 Dec. 1994).

Coarse dial - Fine dial (Edinburgh) method.

For a D meter with two calibrated screws but no feedback, periodic errors in the coarse screw can be detected by calibrating it against the fine screw, which is assumed to have much smaller periodic errors. This method is described fully in the next section (2.4).

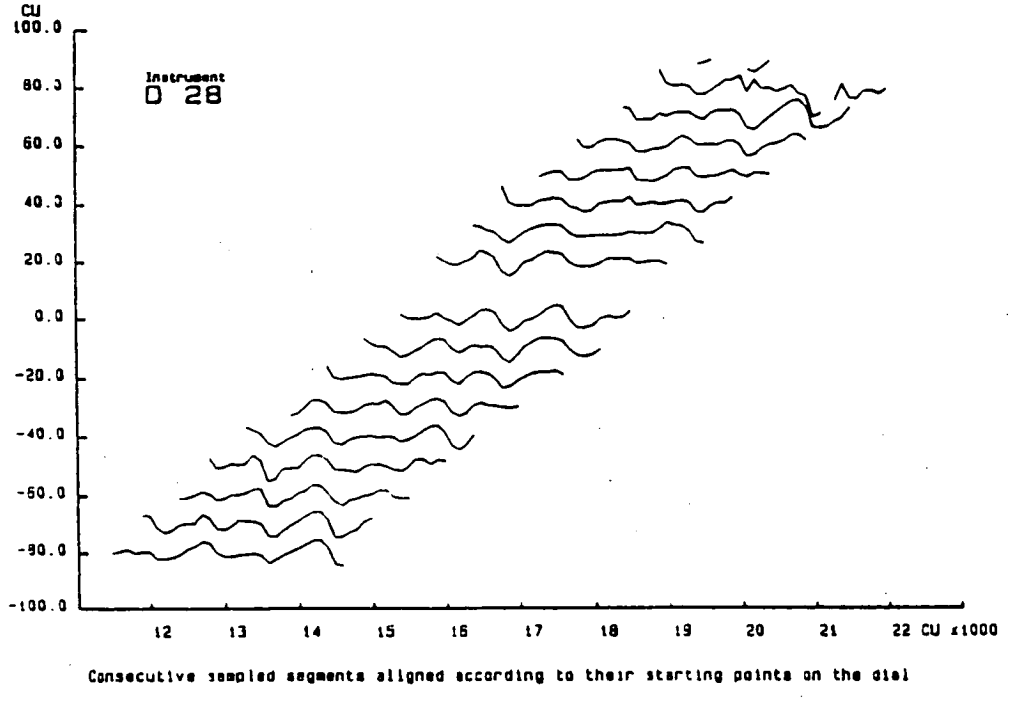

Figure 2.10 Sampled sets aligned according to their starting point on the dial. The noise can be reduced by averaging the residuals from consecutive sets. (From Liard 1989)

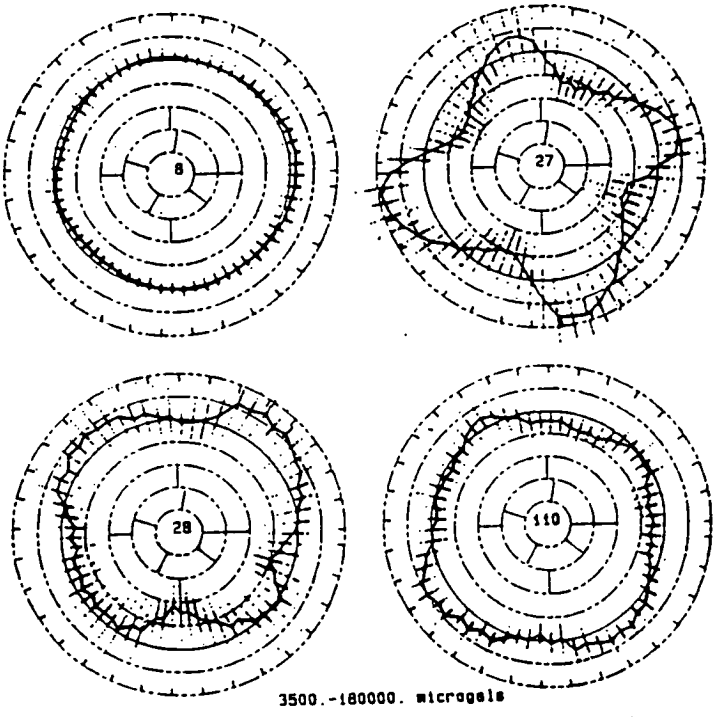

Figure 4

The residuals are plotted on circular diagrams where one full turn equals 3250 CU and the starting reference is at 0 CU on the dials of the instruments . Each concentric circle represents 5 CU and the third circle from the rim is the zero reference. The radial lines in the inner three circles show where the 812.5 and 722.2 CU would be. The outer radial lines indicate intervals of 100 CU.

Figure 2.11 Periodic errors represented as a function of one turn of the fine screw for the 'standard' D meters D28, D110, D6 and D27. Figure taken from Liard 1989

2.4 Investigating the Periodic Errors of D145

2.4.1 Introduction

The development of an instrument with two calibrated screws was motivated at least in part by the possibility of performing internal calibration experiments in the laboratory. This would provide another way of investigating the screw system, additional to the calibration lines and electrostatic feedback mentioned in section 2.3. Because the Edinburgh instruments D145 and D154 were the first to be manufactured with dials and gearboxes on both screws, the twin dial method of calibration presented the challenge of a previously untried technique. This section describes the extensive experiments carried out to establish the amplitude and phase of periodic errors and to verify the self-consistency of the calibration functions for both screws on D145.

Although these experiments seemed successful in that they did appear to identify systematic and periodic residuals for both the coarse and fine screws, it was eventually concluded that these results were spurious and they were not used to correct D145's contribution to the BPGN. This decision will be discussed in section 2.4.5 but an explanation for the calibration experiments is not yet entirely definitive. The experiments are described in detail so that their investigation can be continued in the future.

2.4.2 Experiments

Preliminary Experiments

The first experiment with D145 was to start with the fine dial at 3000 turns, balance with the coarse dial, then decrease the fine dial by 500 turns and rebalance with the coarse dial and so on, down to 0, back up to 3000 then repeat 1500 and 0. Figure 2.12 shows the adjusted values plotted against fine dial. The result of a similar experiment with D154 but at steps of 100 fine dial turns is shown in Figure 2.13. The error bars are much larger than for D145, so that a 'no structure' hypothesis would be valid. D154 is very difficult to read and the rms unweighted error for D154 in a common adjustment is often twice as large as that for D145. Subsequent calibration experiments have focused on D145, which is a much better instrument than D154. The experiments were done at different latitudes (see Table 2.2) so that the full range of the coarse screw needed for the BPGN was calibrated.

The coarse dial - fine dial (CD-FD) experiments

The next experiment with D145 was typical of almost all subsequent 'coarse dial - fine dial' (CD-FD) experiments, with an 'up and down ladder' sequence with steps of 200 fine dial (FD) turns, followed by an extra reading at the middle and the top to finish. The results, shown in Figure 2.14, were very similar to the preliminary experiment done at intervals of 500 FD turns shown in Figure 2.12. Most of the range (400 to 2200 FD turns) is consistent with a linear scale correction factor between the fine and coarse dials of about 9×10^{-4}.

With this interpretation, the 'hooks' at either end of the range would be defects at the ends of the fine screw and the shape of the curve shown in figures 2.12 and 2.14 would be generated by the *fine screw system*. Alternatively, the curve might be viewed as part of a sinusoid, representing a periodic error in the coarse screw system, with a peak and trough at the positions of the 'hooks' and a period of about 360 CD turns, or 270 mgal. (The conversion factors for D145 in this range are 0.073 and 0.750 mgal per dial turn for the fine and coarse dials respectively). Because the coarse screw is believed to be of lesser quality than the fine screw (see for example Valliant's (1991) remarks quoted in section 2.3), a coarse screw error was considered more likely.

A third possibility was considered in which the effect was a spurious consequence of irregular drift being modelled as if it was linear. The residuals from the linear drift model (Figure 2.15) have a non-linear deviation which is almost anti-symmetrical about the middle time. This is where the direction of dial turning changes, so the residuals are accidentally correlated with the part of the screw being used. The effect of non-linear drift on the CD-FD calibration experiments is discussed later in section 2.4.4. The remainder of this section describes experiments which were designed to identify a real property of the screw systems.

Testing whether the effect was a property of the coarse screw or the fine screw involved repeating the experiment at a site where gravity was different. If the slope was a property of the fine dial, the results from the different sites would superpose. If it was related to the coarse dial, the shape would not superpose, but would be shifted in phase by the number of coarse dial turns equivalent to the gravity difference between the sites. A calibration function equivalent to the whole of the BPGN could then be built up by doing CD-FD experiments in an overlapping sequence of gravity ranges.

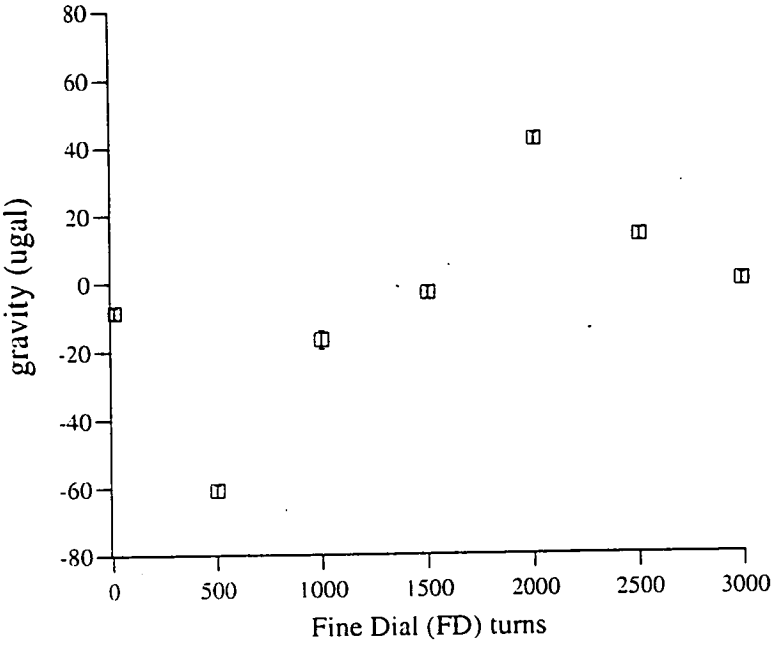

Figure 2.12 Gravity against FD for D145 at Edinburgh, with observations every 500 FD turns

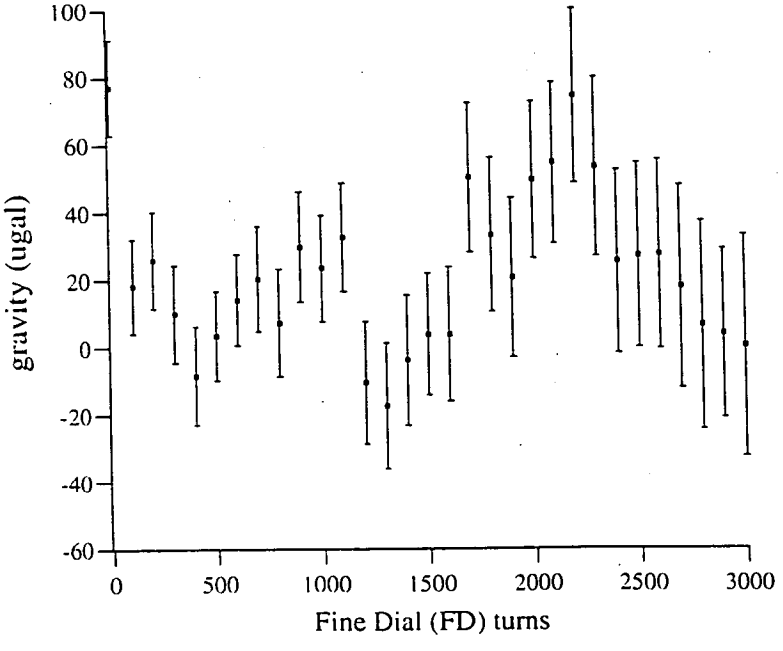

Figure 2.13 Gravity against fine dial for D154 at Edinburgh, with observations every 100 FD turns.

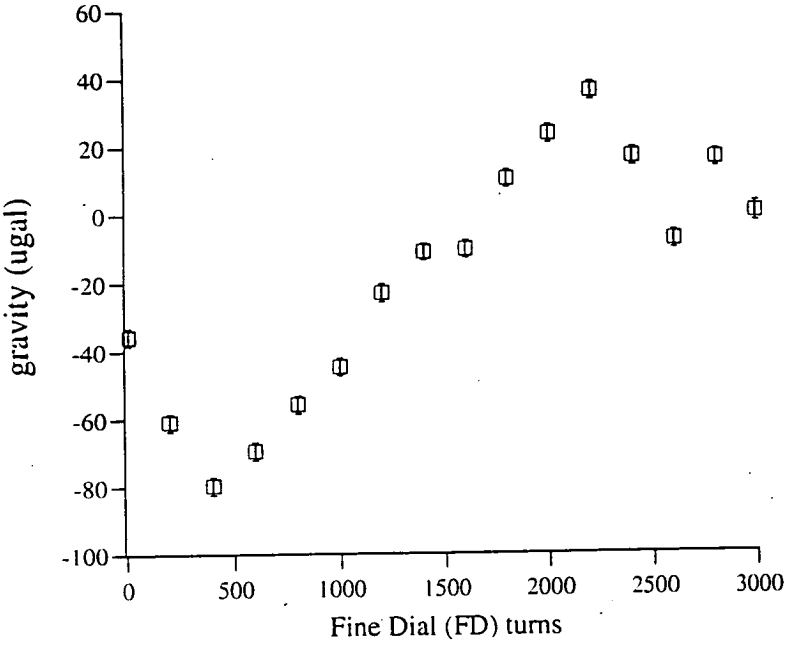

Figure 2.14 Gravity against FD for D145 at Edinburgh, with observations every 200 FD turns

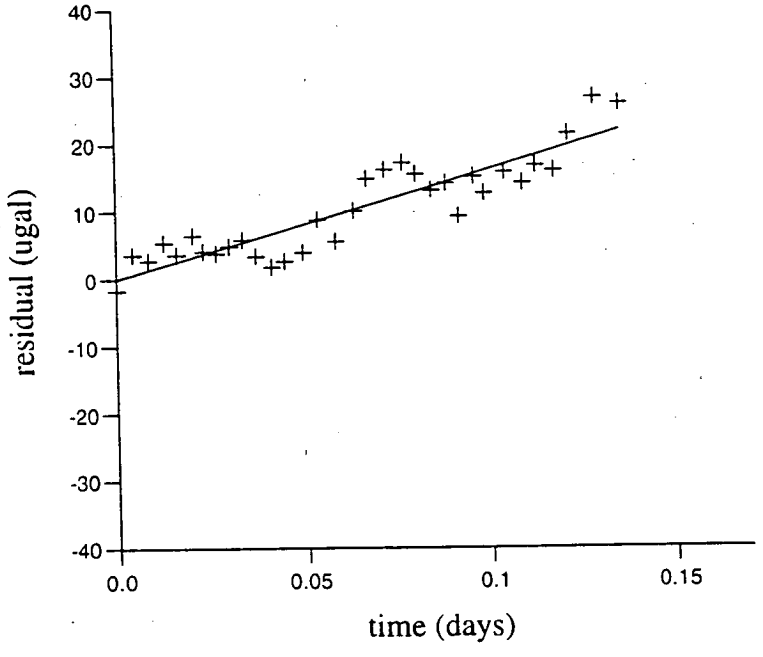

Figure 2.15 Drift Plot for D145 at Edinburgh, corresponding to the adjusted gravity values of Figure 2.14, with observations every 200 FD turns.

The second set of CD-FD observations were made by repeating the experiment at the Proudman Oceanographic Laboratory (POL) near Birkenhead (latitude 53.4°) to compare with those at Edinburgh (latitude 55.9°). This difference of latitude was enough to change the site gravity value by more than 200 mgal and extend the coverage of the coarse screw to more than 400 mgal. A further experiment at Hallsannery near Bideford in Devon (latitude 51.0°) extended the coverage to 600 mgal. However, with these gravity intervals, there was little or no overlap between the ends of the coarse screw range at the different sites. Since the data from the ends of the screw are associated with a change in direction of the dial turning, they tend to be more erratic than the central parts. A substantial overlap is desirable and two more experiments were done at Northampton and Penicuik to provide data at the joins. The five experiments are summarised in Table 2.2 below.

Location	Nominal relative gravity (mgal)	CD turn equivalent	Date	Sequence (FD turns)	Interval (FD turns)
Edinburgh	000.0	7000	18.2.93	0 - 3000 - 0	200
POL	-213.0	6720	23.3.93	0 - 3000 - 0	200
Hallsannery	-417.5	6470	9.10.93	1500-3000-0-1500	100
Northampton	-347.0	6560	17.8.94	0 - 3000 - 0	200
Penicuik	-039.1	6960	24.8.94	0 - 3000 - 0	200

Table 2.2 D145 coarse dial - fine dial experiments.

The POL experiment procedure was identical to the Edinburgh experiment, as were those at Northampton and Penicuik. The sinusoidal shape of the POL calibration curve (Figure 2.16) is generally similar to the Edinburgh result (Figure 2.14). The trough and peak appear at 800 and 2400 FD turns, compared with 400 and 2200 FD turns respectively for Edinburgh. When the two curves are superimposed (Figure 2.18a), it seems plausible that the FD screw is the cause of the structure. Although the overlap between the coarse dial range of the Edinburgh and POL experiments is only about 10 CD turns, the superposition of the curves according to CD (Figure 2.18b) could be fairly convincing evidence that a CD periodic error is the cause. Because the gravity difference between POL and Edinburgh of about 213 mgal is not inconsistent with the apparent period of about 240 mgal for the 'CD periodic error', the two curves would happen to superimpose when plotted against FD even if there were no error associated with it.

However, the POL drift plot (Figure 2.17) shows the same anti symmetry about the middle as did Figure 2.15 for Edinburgh. There is once again a correlation between drift residuals

and the shape of the adjusted calibration function. The magnitude of the drift residuals is about half the amplitude of the calibration function deviations.

This correlation between deviations in the observed calibration function and changes in the direction of dial turning stimulated the hypothesis of a hysteresis effect in the spring or lever system leading to systematic drift offsets. It should be noted, however, that the standard procedure to avoid 'backlash' was followed throughout, by always approaching the balance condition from below. Whether the sequence was going up or down the coarse dial range, the fine dial was wound down by typically 10 turns and the coarse dial by one or two turns before approaching balance. (The end points, nominally at 0 and 3000 FD turns, were actually at 10 and 2990 FD turns to permit this precaution. In any case, the screw stops prevent the very extremes being reached.)

The observation sequence at Hallsannery was different from the others in two ways. First, the number of dial turns between readings was halved (100 FD turns instead of 200). Secondly, the sequence was started in the middle (1500) instead of at the end (0 FD turns). The first change was so that periodic errors at frequencies which had previously been undetected due to aliassing could be identified. The second was so that the first few readings were taken at different part of the FD screw than usual, and that there would be two rather than one change in dial turning direction. This would associate possible effects due to non-linear or erratic drift, caused by the initial unclamping or by changing the direction of the screw turning, with different times in the sequence from usual.

The results of the Hallsannery experiment were more scattered than seen previously but a sinusoidal shape is still detectable (Figure 2.19). However, the pattern seems to be quite different from the others because it is upside down. The trough appears at about 2300 FD turns and the peak at about 800 FD turns, compared with the Edinburgh observations of 400 and 2200 FD turns for the trough and peak respectively.

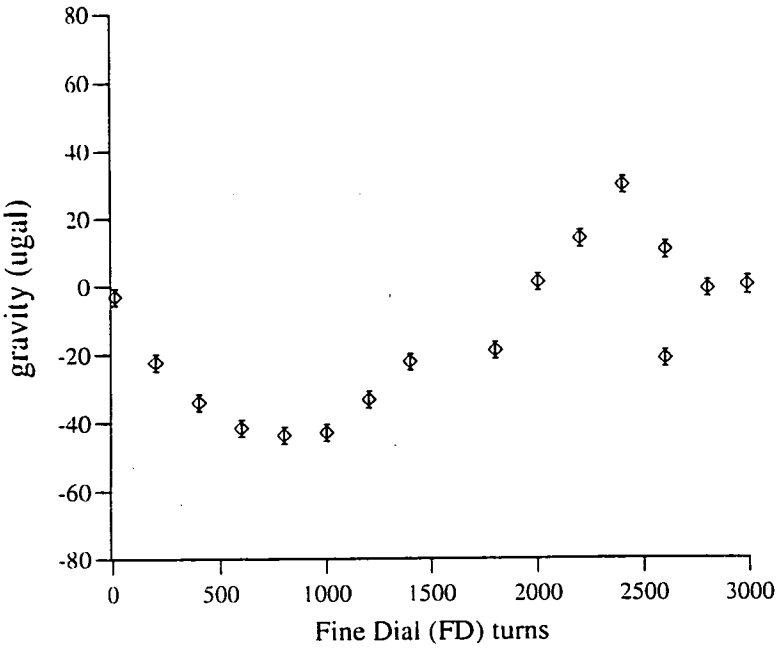

Figure 2.16 Gravity against FD for D145 at POL, with observations every 200 FD turns.

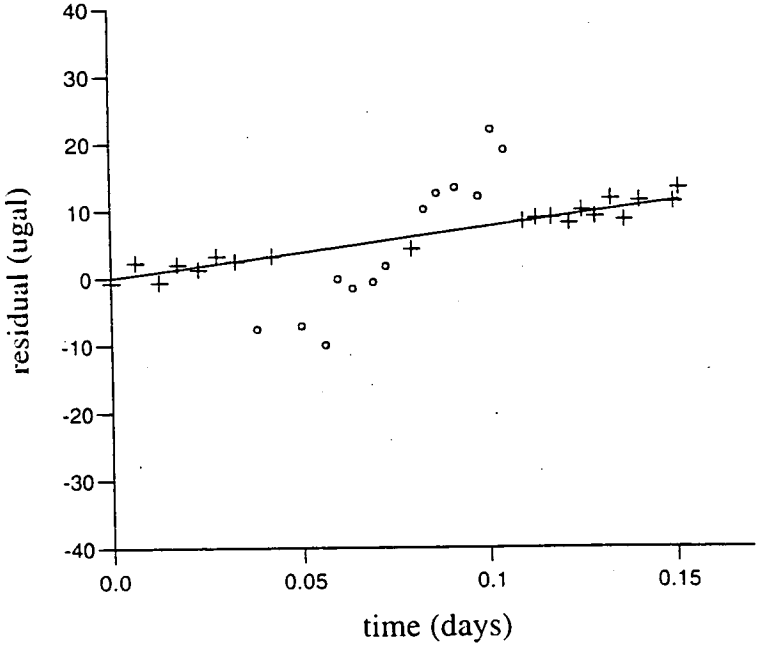

Figure 2.17 Drift Plot for D145 at POL, corresponding to the adjusted gravity values of Figure 2.16, with observations every 200 FD, in the sequence 0 - 3000 -0 FD turns. The circles show points with residuals larger than twice the rms error (section 6.4.1).

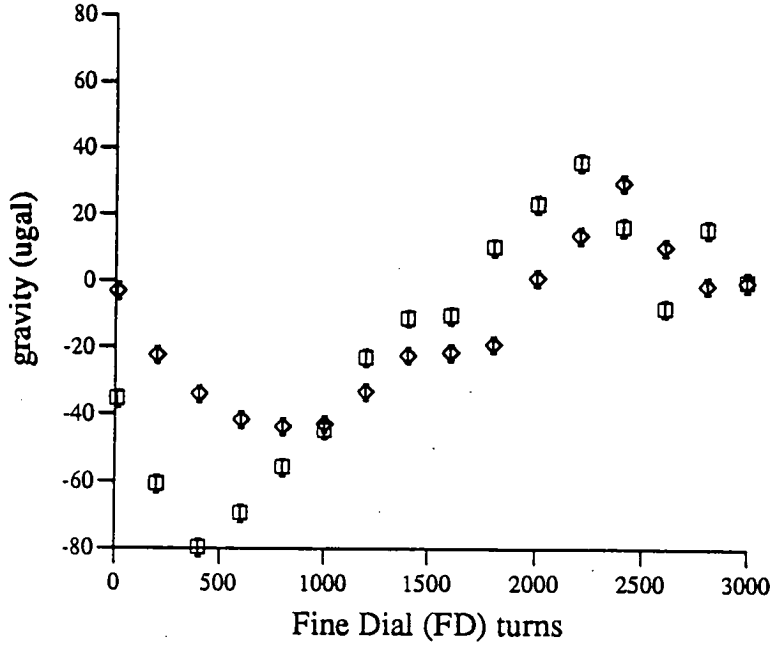

Figure 2.18a POL (rhombs) and Edinburgh (squares) adjusted gravity values superimposed according to fine dial.

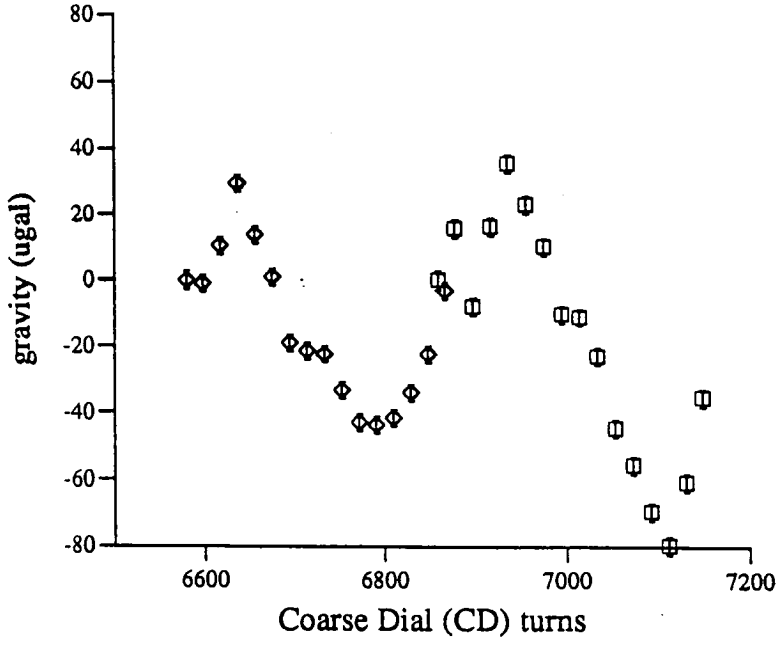

Figure 2.18b POL (rhombs) and Edinburgh (squares) adjusted gravity values superimposed according to coarse dial.

The Hallsannery drift plot (Figure 2.20) is again anti symmetrical about the middle, and shows 'mini tares' at the points where the dial turning changed direction. [Five additional readings were taken at the end of the sequence, in the order 1500-3000-1500-0-1500 to add drift control. However, the large amount of dial turning involved between these readings could easily disturb the instrument and invalidate the results (see Note† below), and they were not included in the drift adjustment. For further discussion of this point, see section 2.4.4 and Figure 2.29.]

The Hallsannery result had the positive effect of ruling out a purely fine dial cause because the phase shift with respect to the other sites meant that it was incompatible with this hypothesis.

The 'overlaps' in the combined adjusted-gravity versus CD plot for Edinburgh, POL and Hallsannery were strengthened by the Northampton and Penicuik experiments. The Northampton observations extended well into the POL and Hallsannery ranges and confirmed the validity of superimposing the segments according to CD value. Penicuik is rather close to Edinburgh to usefully extend readings into the POL range, but the experiment adequately reproduced the structure of the Edinburgh result.

Note†

Effect of high speed winding
Since the closure of these sequences involves reading at 0, 1500 and 2990 FD in succession, there is a large amount of dial turning involved. The time between these readings was about 10 minutes compared with about 6 minutes for readings separated by 200 FD turns. Our colleagues at POL offered us their 'high-speed cranks' which were used carefully for fear of disturbing the unclamped instrument too much. (The LCR manual makes the following salutary comment: 'We strongly urge the operator to use discretion in the rate of speed the dial is turned...'). In spite of this precaution, the last three readings in some sequences are widely scattered, demonstrating that in this sort of operation the instrument is particularly vulnerable to mechanical disturbance (e.g. spring hysteresis, uneven lever motion, beam sticking) and accidental small jolts caused by the observer. The hi-speed cranks were not used on any other occasion, but long periods of dial turning, even when done carefully by hand, still subject the instrument to disturbance. (See also the discussion of the 'spring hysteresis model' in section 2.4.4).

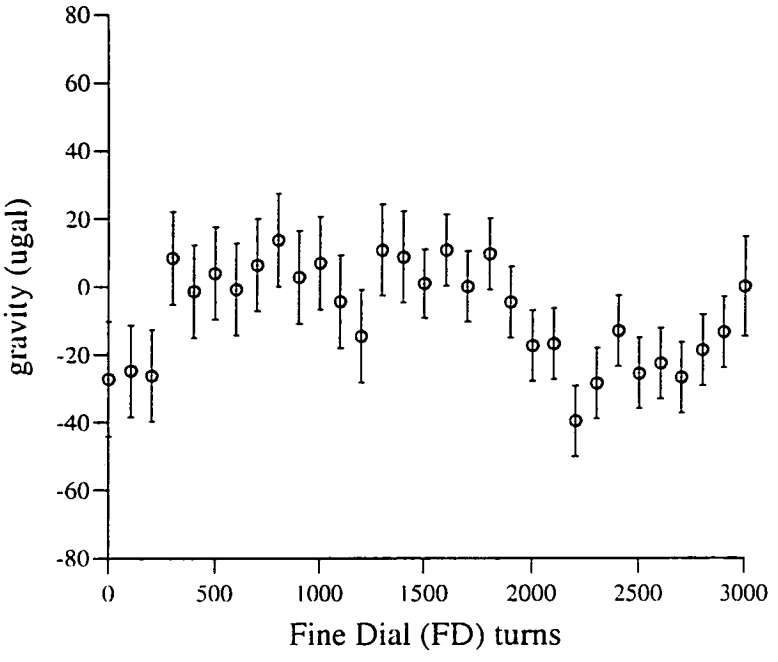

Figure 2.19 Gravity against FD for D145 at Hallsannery, with observations every 100 FD turns

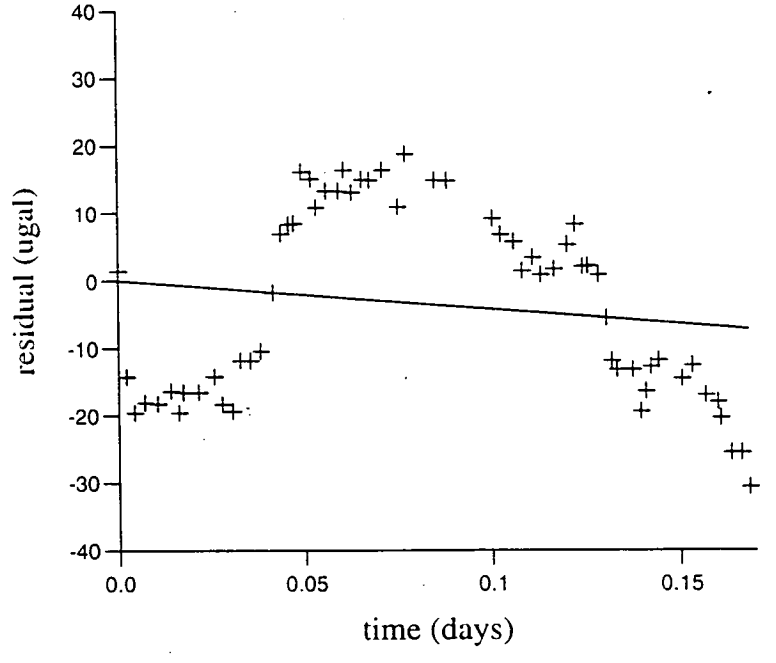

Figure 2.20 Drift Plot for D145 at Hallsannery, corresponding to the adjusted gravity values of Figure 2.19, with observations every 100 FD in the sequence 1500 - 3000 -0 - 1500 FD turns.

2.4.3 Coarse dial periodic errors : Results and Discussion

Combining the CD-FD calibration results

The results of the five experiments superimposed according to CD value and FD value are shown in Figures 21a and 21b respectively. The figures demonstrate that the dominant periodic error is in the CD, not the FD. The LCR rejection limits for the amplitude of periodic errors for a D meter with two calibrated screws are 10 μgal and 40 μgal for the fine and coarse screws respectively (Valliant *pers. comm.* 31 October 1994). The periodic errors on the fine screw of a D meter are expected to be smaller than those of the coarse screw (calibrated or uncalibrated) of a D meter or a G meter.

For the British Precise Gravity Network (BPGN) fieldwork, the fine dial was used in only a very small portion near the middle of its range to fine tune the instrument after it has been approximately balanced using the coarse dial. For BPGN purposes, small changes to the fine dial calibration would have made insignificant difference to the adjustment. The coarse dial calibration is therefore most important.

If the results are to be interpreted as a periodic error in the coarse screw system, then the results for each of the different experiments must be plotted against CD turn and a common sinusoid fitted to the composite graph. In addition, a datum shift for each segment and a linear scale correction between the fine and coarse screws may need to be included in the fit.

Fitting sinusoids

The program PERIODIC was used to join the result of the different CD-FD experiments by simultaneously finding the amplitude and phase of the sinusoid, the datum offset for each segment and the common slope due to a linear scale correction. Because determining the period of the sinusoid is a non linear process and cannot be solved by simple least squares, successive solutions were found by scanning a range of possible periods and the one with the minimum variance was chosen.

For the nth pair of gravity and CD values from the pth segment, we solve the equation

$$g_{(n)} = K_p + A\cos(x) + B\sin(x) + M \cdot CD_{(n)} + \varepsilon_{(n)} \qquad (17)$$

where $g_{(n)}$ and $CD_{(n)}$ are the gravity and coarse dial value for the nth pair respectively, K_p is a gravity offset for the pth segment, A and B are the amplitudes of the cosine and sine terms

respectively, $x = 2\pi f \cdot CD_{(n)}$, and the slope M is the linear scale correction. For a given trial frequency f, we minimise $\Sigma\varepsilon_{(n)}^2$ and find the offset for each segment, the amplitude of the sinusoid and the slope.

Figure 2.22a shows the five datasets plotted in different symbols and superimposed after correcting only for the datum offset for each segment. A small linear decrease and a very obvious sinusoidal term with a period of 300 - 400 CD turns are apparent. The sinusoid with the largest amplitude was removed first, then the residuals plotted and the largest remaining sinusoid was removed, and so on until the residuals showed no visible structure. This condition was reached after 3 sinusoids had been fitted. Their amplitudes and periods are shown in Table 2.3 below:

Period (CD turns)	Amplitude (μgal)	Slope (μgal/CD turn)
404	28.1	- 0.1219
101	8.7	+ 0.0066
50	4.5	+ 0.0029

Table 2.3 Periodic Errors on D145 Coarse Dial

After the fit, the calibration function for D145 was modified to include these terms and the small linear scale correction to the fine dial (equivalent to -0.1124 μgal /CD turn). The structure was then absent from the combined results of the CD-FD calibration experiments (Figure 2.22b).

Discussion of the periods found

Sinusoidal errors with periods of integral or half-integral numbers of a micrometer screw turn are most likely. Other periods are generated by the gear box connecting the dial to the micrometer screw (section 2.3). The expected periods (in dial turns) calculated using the gear ratios for G275 and the coarse and fine dials on D145 are summarised in Table 2.4 below.

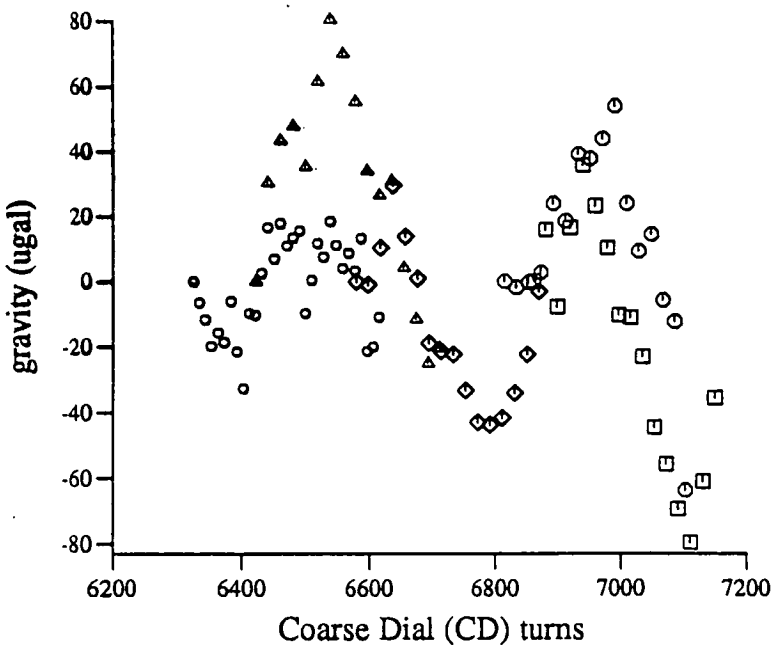

Figure 2.21a The five CD-FD experiments superimposed according to CD value, before correcting for offset. Hallsannery (circles), Northampton (triangles), POL (rhombs), Penicuik (octagons) and Edinburgh (squares).

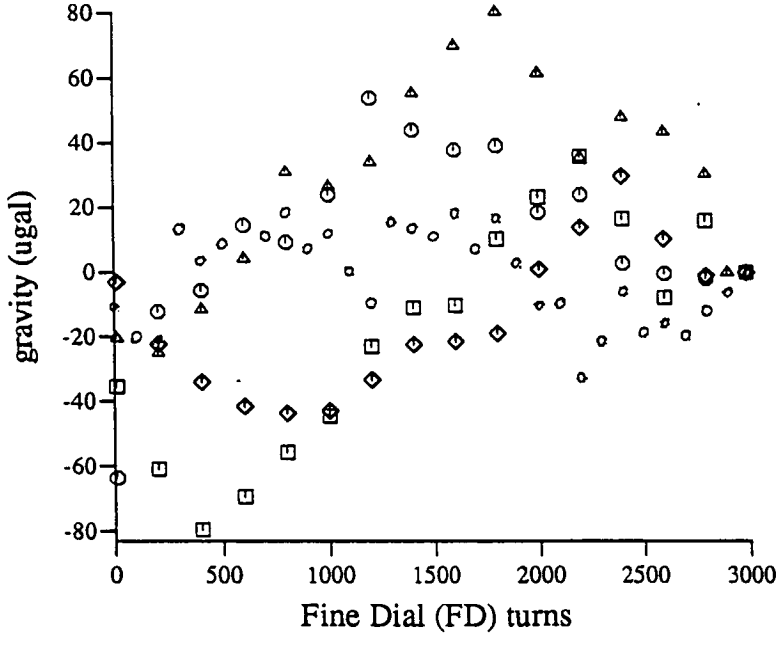

Figure 2.21b The five CD-FD experiments superimposed according to FD value, before correcting for offset. Hallsannery (circles), Northampton (triangles), POL (rhombs), Penicuik (octagons) and Edinburgh (squares).

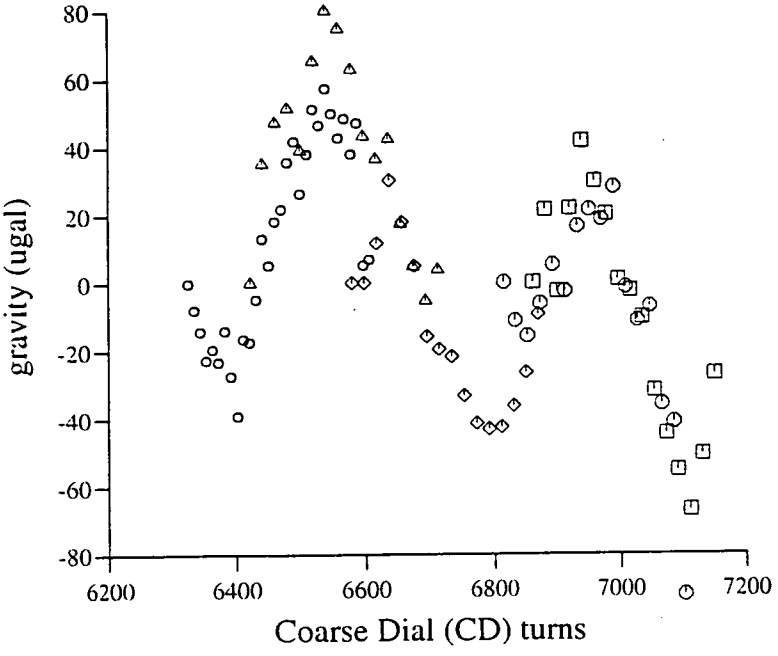

Figure 2.22a The five CD-FD datasets superimposed after correcting only for the datum offset for each segment. Hallsannery (circles), Northampton (triangles), POL (rhombs), Penicuik (octagons) and Edinburgh (squares).

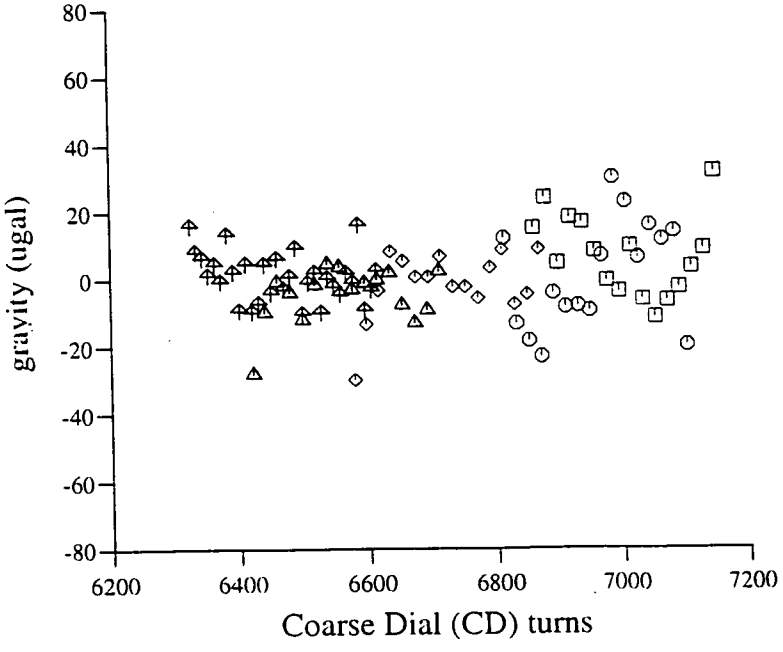

Figure 2.22b The data of Figure222a reprocessed after the calibration function for D145 had been modified to include periodic error terms and the small linear scale correction factor.

instrument	G275	D145 CD	D145 FD
gear I	(180/20)	(180/18)	(180/18)
gear II	(134/17)	(180/18)	(150/30)
	G275 dial turns	D145 CD dial turns	D145 FD dial turns
long period	1206.00	1800	1500
	(603.00)	(900)	(750)
primary ratio	**70.94**	**100**	**50**
	(35.47)	(50)	(25)
* see below		25*	12.5*
gear II	7.88	10	5
	(3.94)		
one turn	1.00	1	1

Table 2.4 Expected periods in dial turns for G275, and for the coarse and fine dials on D145. The figures in brackets are equal to half of the calculated periods.
* Liard (1989) shows that a quarter turn period may arise from the 4-sectioned nut that holds the micrometer screw inside the instrument.

Liard (*pers. comm.* 6 December 1994) suggests that periods at double the calculated ones would also be expected (200 CD and 100 FD turns). The large amplitude periodic error at about 400 CD turns is unexplained.

G275 periods from BPGN

The BPGN has been observed simultaneously with all three Edinburgh instruments, and as well as the final combined adjustment, the results from each instrument have been adjusted independently. One of the benefits expected from these calibration experiments was to improve the consistency between values assigned to BPGN stations by the three instruments G275, D145 and D154. A plot of the difference between the values from the separate adjustments of G275 data only and D145 data only before correcting for any periodic errors is given in Figure 2.23. The D145 values have been divided by the provisional scale factor of 1.000 4230 (section 2.2.4).

When the calibration function of D145 was modified so that the structure in the CD-FD experiments was removed, a sloping sinusoid was introduced into the plot of the difference between G275 data and D145. Assuming that the periods of 404, 101 and 50 CD turns found for D145 are correct, this new structure must be due to periodic errors in G275. After removing the slope, these periods were determined, and found to be about 248, 408 and 195 G275 dial turns with amplitudes of 32, 21 and 13 μgal respectively. These apparent periodic errors are compared in Table 2.5, where the periods have been converted to milligals using the interval factors from the manufacturers calibration table (Appendix 1, Table A1.1). For this part of the screw, the factors are 0.750 and 1.054 mgal per dial turn for D145 and G275 respectively.

D145 Period (CD turns)	D145 Period (mgal)	G275 Period (dial turns)	G275 Period (mgal)
404	303.0	408	430.0
101	75.8	248	261.4
50	37.5	195	205.5

Table 2.5 Apparent periods for G275 from BPGN after correcting for D145 periodic errors. Factors for interval (mgal per dial turn) : 0.750 for D145, 1.054 for G275, taken from the manufacturers' calibration tables.

Using the gear ratio of 70.94 : 1 for G275, these periods correspond to 3.5, 5.7 and 2.7 turns of the micrometer screw respectively, which are nothing like those expected for G275 (Table 2.4). The corrections for the apparent periodic errors were introduced into the calibration functions of D145 and G275, and have the effect shown in Figure 2.24. The difference between BPGN values found with D145 with and without the 'correction' is shown by the rhombs. The corresponding differences for G275 are shown by the site letter codes. The curves have been offset vertically for display. The phase of both datasets is very similar, which suggests that the apparent periodic errors in G275 are simply compensating for the introduction of incorrect periodic terms for D145.

Checking for aliassing

The possibility that the 400 turn period arises because of aliassing has been investigated. Most of the experiments were done with a sampling interval of 200 FD turns, which corresponds (using the LCR calibration table for D145) to about 19.4 CD turns. If the 25 CD turn period was present, then a 'sampling frequency' of less than 12.5 CD turns would be necessary to preserve it. Since the experiments were done at 19.4 CD turns, then only

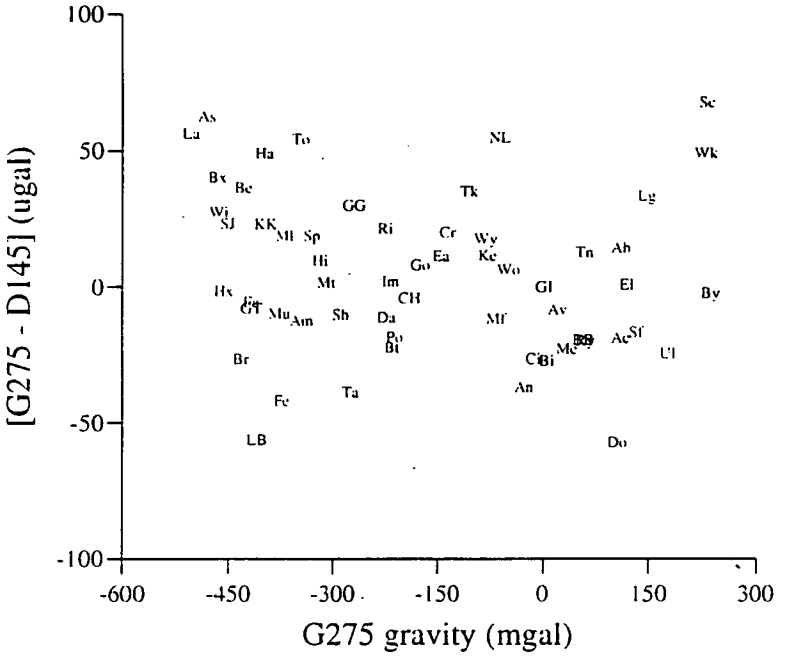

Figure 2.23 The difference between the values from the separate adjustments of G275 data only and D145 data only before correcting for any periodic errors. The D145 values have been divided by the scale factor 1.000 4230.

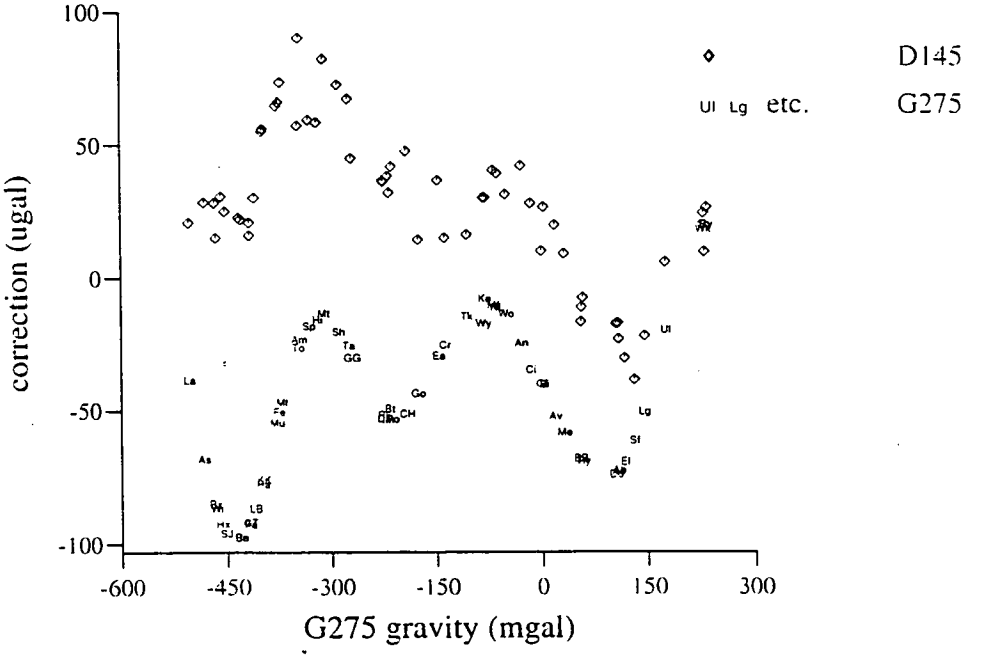

Figure 2.24 The difference between the original calibration fuctions of G275 and D145 and the fuction after 'correcting' for the apparent periods found from the D145 CD-FD experiments. The curves have a very similar phase which suggests that the apparent periodic errors in G275 are simply compensating for the introduction of incorrect periodic terms for D145.

periods greater than about 38 CD turns will be accurately identified. When sampling at a frequency close to a known period, that period may be aliassed to look like an apparent period at the wrong frequency.

For example, if there is a real periodic error of period Δ dial turns with an amplitude of k α then the movement of the micrometer screw is

$$z = k\left[\theta + \alpha \sin\left(\frac{2\pi\theta}{\Delta}\right)\right] \tag{18}$$

If the displacement is sampled at $\theta_n = n\Delta'$, i.e. every Δ' turns, then

$$z_n = kn\Delta' + k\alpha \sin\left(\frac{2\pi n\Delta'}{\Delta}\right) \tag{19}$$

Now $\Delta' = \Delta \pm \delta$, so

$$z_n = kn\Delta' \pm k\alpha \sin\frac{2\pi n\delta}{\Delta} \tag{20}$$

since $\sin(2\pi n) = 0$. The second term is the periodic error and repeats when n increases by

$$\frac{\Delta}{\delta} = \frac{\Delta}{\pm(\Delta' - \Delta)}$$

The apparent period would be $\frac{\Delta'\Delta}{\pm(\Delta' - \Delta)} = P$ dial turns. (21)

For example if the expected period at 25 CD turns is sampled at 19.4 CD turns, then an apparent period P of 86.6 turns would result. Alternatively, we can find which real periods (P) would appear as 404 turns for a sampling interval (Δ') of 19.4 turns using equation 21, which gives $\Delta_+ = 18.5$ and $\Delta_- = 20.4$ as the periods which might have been aliassed. Since neither of these are known periods, then it is unlikely that the 404 CD turn period is a result of aliassing.

2.4.4 Non-linear drift

Cubic spline functions

The standard adjustment of gravity observations is done in the program NETWORK. This program is described fully in Chapter 3, but it uses a least squares fit to a linear drift model. The residuals shown in the drift plots of Figures 2.15 and 2.17 show systematic departures from the linear model for central parts of the observation sequence. The hypothesis that the apparently consistent calibration function described in the previous section was a spurious consequence of non-linear drift was first investigated by fitting more complex forms of drift function. Least squares fitting was still used but the linear functions were replaced by cubic splines, whose complexity could be increased or decreased by choosing different numbers of nodal intervals. Because the CD-FD experiments consist of a large number of readings closely spaced in time over an interval of 3 to 4 hours, they are ideal for studying the drift characteristics of the instrument.

The observation equation (Chapter 3 equation 31) becomes

$$g_{obs}(t) = G_m + f(t) + \varepsilon \qquad (22)$$

where g_{obs} is the observed gravity and G_m the fitted value of gravity at station m, f(t) is the spline function for the drift and ε is the error. In this discussion a 'station' is really a fine-dial setting, for example 200 FD turns, 400 FD turns etc.

A program SPLINE, written by Hipkin and Lyness (Lyness 1984) was used to do the least squares adjustment of the observations to fit equation (22). An example of the effect of fitting the drift by a spline curve with 6 nodes is shown in the drift plot of Figure 2.25 for the D145 CD-FD dataset observed at POL. The equivalent plot for linear drift for the same data (Figure 2.17) is reproduced as Figure 2.26. The adjusted calibration function after the spline fit is insignificantly different to the result with linear drift which was shown in Figure 2.16. However, fitting an unrealistically complex curve with 16 nodes increases the amplitude of the adjusted value plot from about 40 μgal to about 100 μgal (although still maintaining the shape). A similar effect occurred with the Hallsannery data where a 16 node curve emphasised the sinusoidal structure which had been quite difficult to detect by fitting a linear drift. Using a spline drift for all datasets gave a peak to peak amplitude of the combined curve of about 140 μgal compared with about 110 μgal for a linear drift. Since the limit on the number of nodes would have to be arbitrarily chosen, and the spline fit gave a similar but amplified result, it was decided to maintain a simple linear drift equation for all processing.

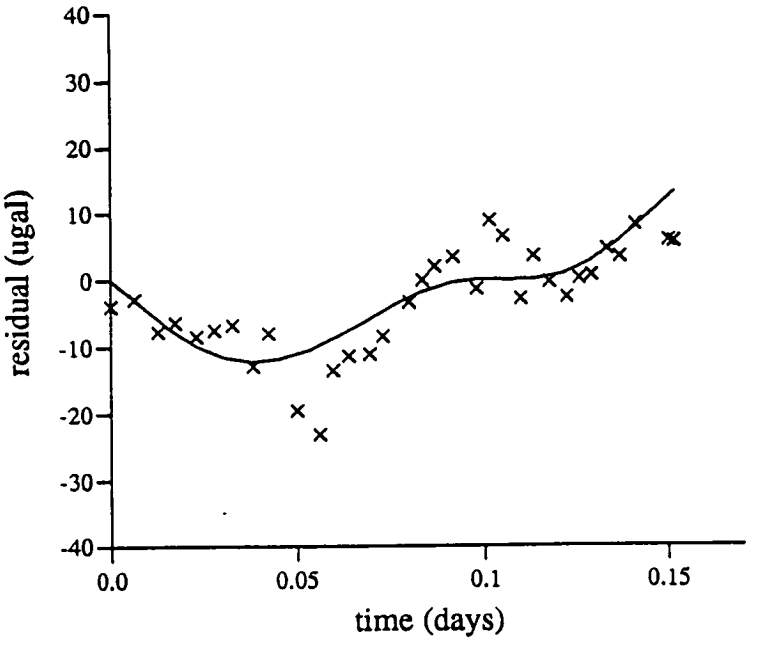

Figure 2.25 Drift plot for the D145 POL experiment using a cubic spline curve with 6 nodes to represent the drift function.

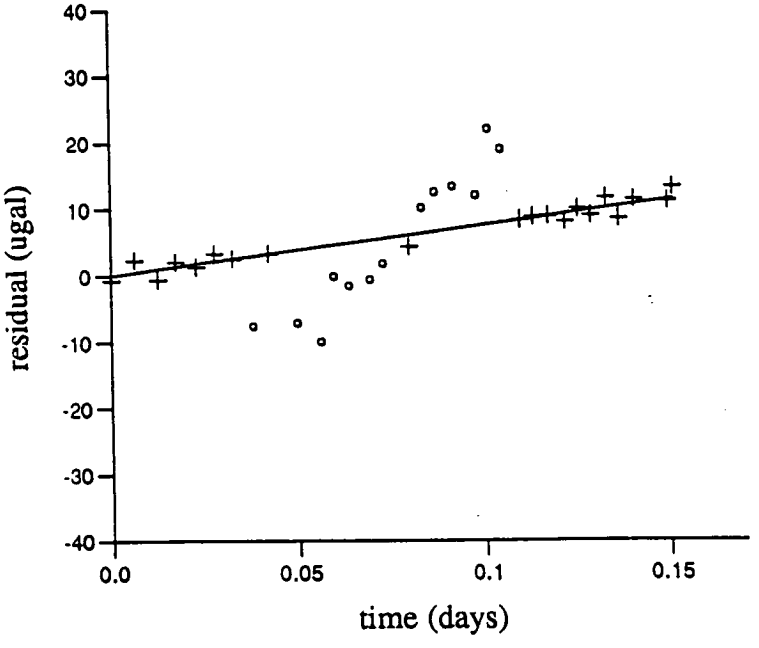

Figure 2.26 Drift plot for the D145 POL experiment using linear drift. (This figure is a copy of Figure 2.17)

The 'spring hysteresis' model and the effect of using least squares

The last section showed that increasing the complexity of the drift curve while continuing to fit it using least squares generated results which were qualitatively the same. If the deviations from linear drift are due to a causal event at a particular time then least squares fitting will always give a spurious result, no matter how complex a drift function is available. Unclamping the spring or changing the direction of dial turning are examples of events which may cause the spring to respond non-linearly.

Hipkin *et al.* (1988) document the anomalous drift of G275 at the beginning of an observation sequence. Figure 2.27 shows the response to unclamping, which is a rapid initial drift which flattens off to a much slower rate after about one hour. Harrison and Sato (1984) describe the response of the LCR spring to 'a steplike change in stress' as 'an immediate change in length followed by delayed, approximately exponential creep'. This behaviour has also been observed by the author with D145, but it is less marked with this instrument than with G275. A hypothesis to explain the CD-FD observations in terms of this type of drift will be called the 'spring hysteresis' model.

The apparent drift shown for example in Figure 2.26 can be converted to the actual drift if the 'spring hysteresis' model is adopted. The point marked by the circular symbol *below* the linear drift line at 0.05 days is FD position 1800 and successive points to the right are the *ascending* FD turn sequence 2000, 2200 and so on until the point shown by the cross at about 0.08 days, which is the single observation at 3000 FD turns. The following six points marked by circles, now lying *above* the linear drift line, are the *descending* sequence 2800, 2600, ..., 1800.

In a sequence like this one, each dial turn position (or equivalently each 'site') is observed only on two occasions, once going up and once coming down. The spring hysteresis model assumes that non-linear drift occurs at the start of the sequence (after unclamping), and again at the middle of the sequence (after the direction of dial turning is changed). Figure 2.28a shows the drift diagrammatically with time and the sequence of dial turn positions. The least squares fit to a linear drift model will distribute the residual generated at the time of the observation first *after* the disturbance equally between it and the corresponding observation made *before* the disturbance. In reality the residuals before the disturbance should be zero and those after should be twice as large. Figure 2.28b shows the apparent drift found by least squares for the sequence of Figure 2.28a. The first observation at site 5 is affected by the rapid drift caused by unclamping, but the second observation at

site 5 (occurring at the end of the sequence) is not. However because the real residual of the first observation is distributed between both observations, the first observation will have half its real residual, and the second will have an equal residual in the opposite direction. The two observations at site 25 can be treated similarly, but since the disturbance is actually associated with the second observation, rather than the first, the residuals are in the opposite direction. This model accounts adequately for the apparent drift shown in Figure 2.15 (Edinburgh) and Figure 2.17 (POL).

The different sequence observed in Hallsannery can also be interpreted using the model. The observation sequence started at 1500 FD turns and proceeded in steps of 100 FD turns through 3000 and 0 back to 1500, finishing with extra readings at 3000, 1500, 0 and 1500. The drift plot is reproduced in Figure 2.29 and the spring hysteresis model response is indicated on it. In particular the scatter of the apparent drift residuals of the four extra readings at the end can be explained by the frequent changes in direction, and the large amount of the dial turning. The arrows show the expected sign of the residual resulting from the disturbance according to the change in direction. These last four readings affect the drift assigned to the earlier observations at 1500, 3000 and 0, so they were omitted for the gravity adjustment (whose results were shown earlier in Figure 2.19).

2.4.5 Conclusions

The results of the CD-FD experiments with D145 suggest the presence of periodic errors in either, or both, of the coarse and fine screws of this instrument. The Hallsannery result in particular confirmed that these apparent errors were not a property of the FD. The amplitudes and frequencies of the CD periodic errors were determined by combining all the observations. When these sinusoidal terms were included in the calibration function for D145, the periodic structure seen in the original data was completely removed. Using the corrected calibration for D145 in the adjustment of the BPGN revealed apparent periodic errors for G275. The inclusion of periodic 'corrections' for both meters reduced the rms of the BPGN adjustment from 7.9 μgal to 6.8 μgal. However, the larger number of results which oppose this conclusion are summarised below.

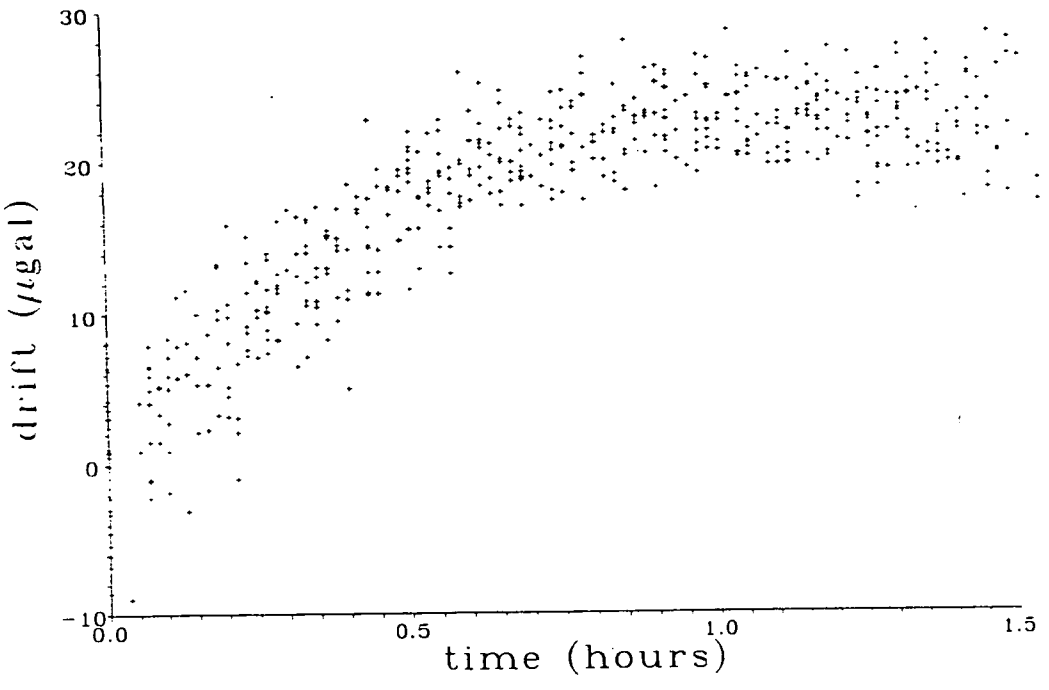

Figure 2.27 The characteristic response of G275 to unclamping, shown by superimposing 28 sequences observed in 1981. (Hipkin *et al.* 1988).

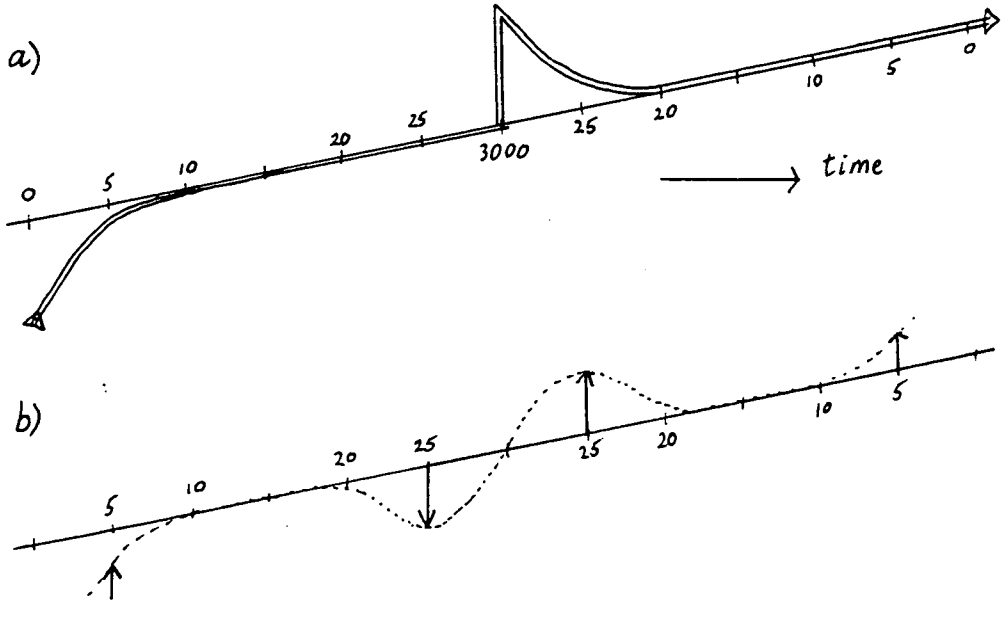

Figure 2.28a and b

a) The spring hysteresis model : sketch of the drift with time and the sequence of dial turn positions

b) The apparent drift found by least squares for the sequence of (a) demonstrating how the real residual due to a disturbance is distributed equally between observations before and after the disturbance.

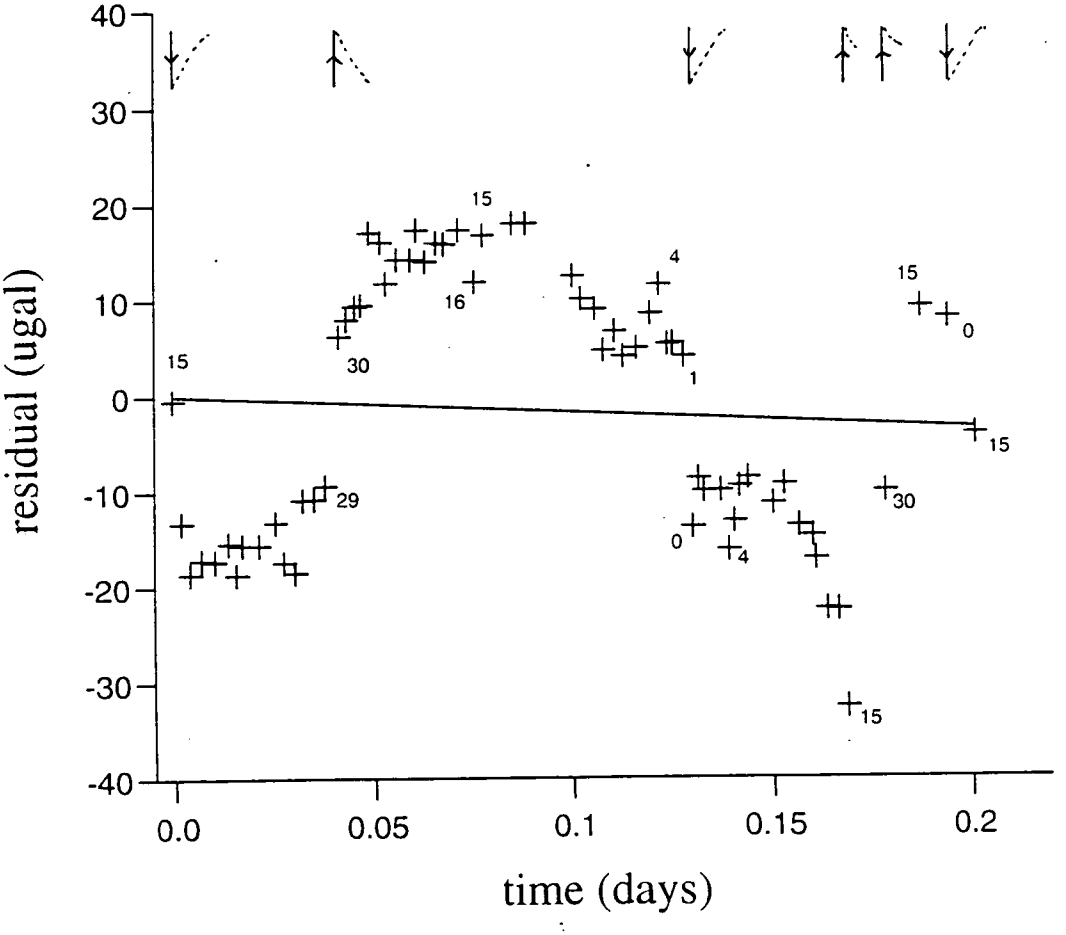

Figure 2.29 Hallsannery drift plot showing the sequence 1500-3000-0-1500, in steps of 100 FD turns, finishing with extra readings at 3000, 1500, 0 and 1500. The spring hysteresis model response is indicated on the figure : the arrows show the expected sign of the residual resulting from the disturbance according to the change in direction. These last four readings affect the drift assigned to the earlier observations at 1500, 3000 and 0, so they were omitted for the gravity adjustment (whose results were shown earlier in Figure 2.19).

The dominant period of 404 CD turns needed to correct the D145 CD-FD experiments, and periods found for G275, are both unexpected from the known gear ratios of the instruments. The phase of the correction term for G275 corresponds with that for D145 suggesting a dependence between the two results, and in any case, the coverage of the screw by the BPGN observations is probably not sufficient to use the network adjustment for precise calibration. A further result described in section 6.5 shows that *without* the calibration 'corrections' the agreement between the BPGN and the absolute gravity values from FG5 is improved.

The results of the Hallsannery experiment (section 2.4.3) were central to dismissing the 'FD periodic error' hypothesis. The spring hysteresis model, however, shows that the apparently 'upside down' result at Hallsannery was a consequence of the different observation sequence used. It was a coincidence that the difference in gravity at the five sites chosen for the CD-FD experiments was such as to demonstrate an apparent success for the CD periodic error hypothesis.

Further work is necessary to verify the periodic errors for D145. The risk of aliassing known periods could be reduced by re-designing the CD-FD experiments, or by using electrostatic feedback. A shorter sampling interval which was not an integer multiple of a known period, for example 75 instead of 200 FD turns, should be used. This would require many more observations to include the necessary range of the coarse screw. To look for the 25 CD period, samples at less than 12.5 CD turns (100 FD turns) would be necessary, although the total range could be reduced to 3 or 4 whole periods (100 CD turns).

The large number of readings made about every 10 minutes for periods of up to five hours have illuminated the drift characteristics of D145, and the spring hysteresis model explains well the behaviour observed in many of the sequences. Importantly, the discussion of the model has shown the limitations of using least squares for adjusting sequences which are symmetrical about the central time. A sequence designed to remove all ambiguities, for example by doubling it, or by forward looping, would take too long. The Hallsannery observations took about five hours and this is close to the maximum time that an observer can concentrate and obtain good readings.

The CD-FD experiments have not enabled the periodic errors of D145 to be determined unambiguously, but demonstrate the potential to do so with the suggested modifications to the observation procedures.

CHAPTER 3. Pre-processing and Network Adjustments

PART 1. Pre-processing

3.1 Tidal Corrections

3.1.1 Introduction

The tidal correction is made up of the direct tide, the elastic Earth response and ocean loading effects. The elastic Earth tide is a response to the tide generating potential of the sun and moon, which can be accurately calculated from astronomy. The elasticity of the Earth amplifies the direct tide due to the sun and moon by the gravimetric factor δ which has a value of about 1.16 for the predominant tidal component. The gravity effect of the tide is typically 50 - 100 μgal, which, at British latitudes, is mainly due to the semi-diurnal lunar tide. At mid-latitudes however, the diurnal tide is larger than the semi-diurnal tide. The ocean loading effect is part of the measured gravity signal from ground movement due to the surface loading of ocean tides. It is typically only a few percent of the elastic tide but is important near the coast.

3.1.2 The Tide Generating Potential

The tide-generating potential of the sun and the moon at a point on the Earth's surface can be expressed as a series of terms involving the positions of the sun and moon, and the latitude and longitude of the point on the Earth.

In Figure 3.1, the total potential at a point on the Earth's surface P due to the moon M, which is a distance R from the centre of the Earth O and a distance ρ from the moon, is U.

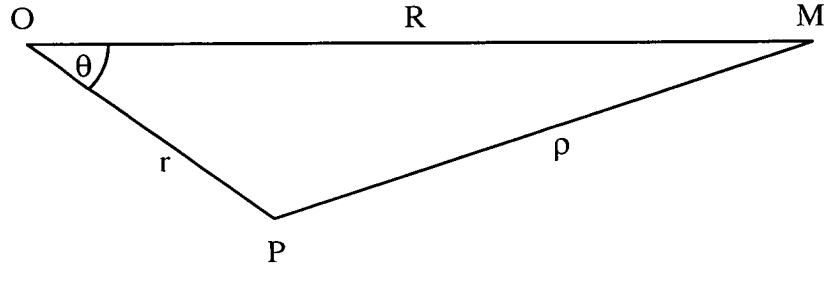

Figure 3.1 Potential at P due to the moon M.

If the moon has mass M, then the total potential due to the moon at P is

$$U = \frac{GM}{\rho} \tag{1}$$

$1/\rho$ can be expressed in terms of r, R and θ as

$$\frac{1}{R}\left(1+\left(\frac{r}{R}\right)^2 - 2\frac{r}{R}\cos\theta\right)^{-\frac{1}{2}} \tag{2}$$

and can be written as the series $\frac{1}{R}\sum_{n=0}^{\infty}\left(\frac{r}{R}\right)^n P_n(\cos\theta)$

where the P_n are Legendre polynomials of degree n.

Expanding the series gives

$$U = \frac{GM}{R}\left[P_0(\cos\theta)+\frac{r}{R}P_1(\cos\theta)+\left(\frac{r}{R}\right)^2 P_2(\cos\theta)+\left(\frac{r}{R}\right)^3 P_3(\cos\theta) + \ldots\right]$$

and substituting the expressions for P_n gives the total lunar potential:

$$U = \frac{GM}{R}\left(1+\frac{r}{R}\cos\theta+\left(\frac{r}{R}\right)^2\left(\tfrac{3}{2}\cos^2\theta-\tfrac{1}{2}\right)+\left(\frac{r}{R}\right)^3\left(\tfrac{5}{2}\cos^3\theta-\tfrac{3}{2}\cos\theta\right)+ \ldots..\right) \tag{3}$$

The first and second terms in this series do not form part of the tide generating potential. The first term is the constant amount by which the total potential of the Earth is raised due to the presence of the moon. The second term balances the centrifugal force acting along the line between the centres of the Earth and moon arising from their rotation about each other.
The rest of the potential causes the tides and this part is U_m :

$$U_m = \frac{GM}{R}\sum_{n=2}^{\infty}\left(\frac{r}{R}\right)^n P_n(\cos\theta) \tag{4}$$

(r/R) $\approx$ 1/60 for the moon (1/23 000 for the sun) so the second degree surface spherical harmonic P_2 (cos θ) is the dominant term. Keeping this harmonic only, gives

$$U_m = \frac{GM}{R}\left(\frac{r}{R}\right)^2 \left(\tfrac{3}{2}\cos^2\theta - \tfrac{1}{2}\right) \qquad (5)$$

A corresponding expression holds for the sun.

Because the Earth is rotating, it is convenient to express the position of the moon M (θ) in terms of it's declination (δ), the geocentric latitude of the point P (φ) and the moon's hour angle (t) (Figure 2). C is the pole of the celestial sphere and the hour angle increases in a clockwise direction about C. (The co-ordinate system is left handed so that the hour angle increases with time).

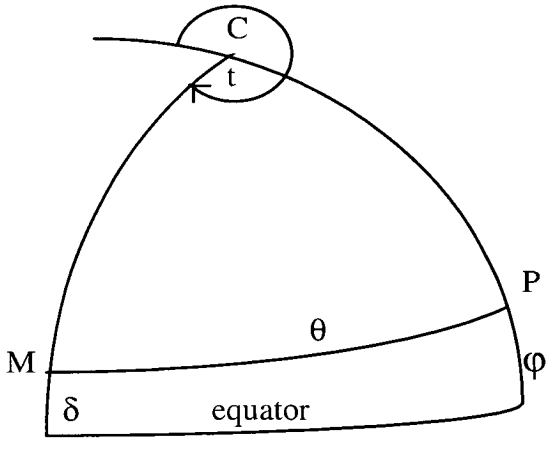

Figure 3.2 The cosine rule in astronomical co-ordinates.

From spherical trigonometry

$$\cos\theta = \sin\varphi \sin\delta + \cos\delta \cos\varphi \cos(t\text{-}180^\circ) \qquad (6)$$

Substituting for (6) in equation (5) gives

$$U_m = \frac{3}{4}GM\left(\frac{r^2}{R^3}\right)\left[3\left(\cos^2\delta - \tfrac{2}{3}\right)\left(\tfrac{1}{3} - \sin^2\varphi\right)\right.$$
$$- \sin 2\varphi \sin 2\delta \cos t \qquad (7)$$
$$\left. + \cos^2\varphi \cos^2\delta \cos 2t\right]$$

which shows that U_m gives rise to three groups of tides of different period and varying dependence on latitude, which can be represented by second degree spherical harmonics (illustrated in Figure 3.3)

$3(1/3 - \sin^2 \delta)(1/3 - \sin^2 \varphi)$ is independent of t and gives long period tides with periods of 14 days (moon) and 1/2 year (sun), which are represented by zonal surfaces.

$\sin 2\varphi \sin 2\delta \cos t$ has a period of 1 lunar day giving diurnal tides which are anti symmetric about the equator and represented by tesseral surfaces.

$\cos^2\varphi \cos^2\delta \cos 2t$ has a period of 1/2 lunar day. and gives rise to the familiar semi-diurnal tides which are sectorial.

3.1.3 Response of the Earth

Love's Numbers

The Earth responds elastically to the tide generating potential, and since the response is small, it can be treated linearly. The radial displacement δr caused by the tide-generating potential U is proportional to U, and the potential U_{def} created by the deformation associated with the displacement δr is also proportional to U:

$$\delta r \propto \frac{U}{g} \qquad \text{and} \qquad U_{def} \propto U \tag{8}$$

so that

$$\delta r = h \frac{U}{g} \qquad \text{and} \qquad U_{def} = k\, U\,. \tag{9}$$

The constants of proportionality h and k depend on the elasticity and density of the Earth and are called Love's numbers.

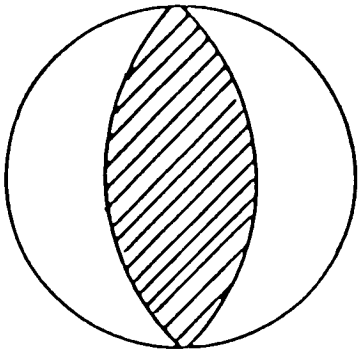

a) sectorial

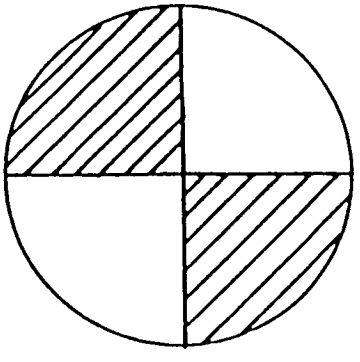

b) tesseral

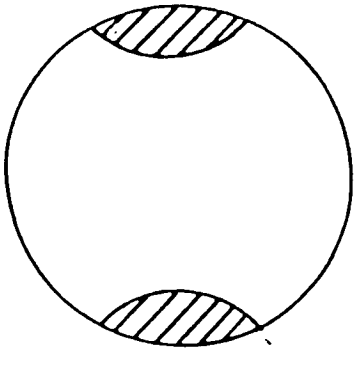

c) zonal

Figure 3.3 a) The familiar semi-diurnal tides are represented by a sectorial surface.
b) The diurnal tides, which are antisymmetric about the equator, are represented by a tesseral surface.
c) The long period tides with periods of 14 days (moon) and 1/2 year (sun), are represented by a zonal surface.

Variation of observed gravity

The presence of the moon causes gravity on the surface of the Earth to vary because of three effects. Firstly because of the direct gravitational attraction of the moon (g_m), secondly because the elastic distortion of the earth causes the surface to move through the Earth's 'free air' gravity gradient (g_{fa}), and thirdly because the new potential generated by the redistribution of the earth's mass has an associated gravity signal (g_{def}).

The second degree component of the potential due to the moon at a point P on the surface of the earth (Figure 3.1) is given by equation (5), which showed that

$$U(r) \propto \frac{r^2}{R^3}.$$

Gravity is the gradient of the potential so the gravity due to the presence of the moon is

$$g_m = \frac{\partial U}{\partial r} = \frac{2U}{r} \qquad (10)$$

Because the earth distorts, the surface on which the gravity meter is sitting moves a distance δr through the earth's potential field. The Earth's gravitational field is

$$g = -\frac{GM_e}{r^2} \quad \text{so} \quad \frac{\partial g}{\partial r} = \frac{2g}{r}$$

and the change in gravity experienced is

$$g_{fa} = \frac{\partial g}{\partial r}\,\delta r = \frac{2g}{r}\,\frac{hU}{g} = h\frac{2U}{r} \qquad (11)$$

The deformation potential has a source inside the earth, so from equation (8) it is of the form

$$U_{def}(r) = kU_{(r=r_0)}\left(\frac{r_o}{r}\right)^3$$

$$\text{So } g_{def} = \frac{\partial}{\partial r}\, k\,U(r_o)\left(\frac{r_o}{r}\right)^3 = -3k\,U(r_o)\frac{r_o^3}{r^4},$$

and at $r = r_o$,

$$g_{def} = -3k\,\frac{U}{r} \qquad (12)$$

The total variation in gravity is the sum of these three effects:

$$g = g_m + g_{fa} + g_{def}$$

$$g = \frac{2U}{r} + \frac{h\,2U}{r} - \frac{3k\,U}{r} = \frac{2U}{r}\left[1 + h - \frac{3}{2}k\right] \qquad (13)$$

The term in brackets is the gravimetric factor δ for the spherical harmonic degree 2, and it is the amount by which the elastic response of the Earth amplifies the potential due the gravitational attraction of the moon.

The gravimetric factor δ can be calculated for low degrees using the formula:

$$\delta_n = 1 + \left(\frac{2}{n}\right)h_n - \left(\frac{n+1}{n}\right)k_n \qquad (14a)$$

The h_n and k_n are Love's numbers for an elastic Earth.

Variation of the potential

The potential due to the presence of the moon is U. The surface moves towards the moon by a distance hU/g causing a potential change of -hU and the potential due to the new mass distribution is kU. The total disturbed potential is then

$$U - hU + kU = (1 - h + k)U = \phi U \qquad (14b)$$

Observed and theoretical values of Love's numbers

Kelvin obtained Love's numbers of degree 2 for his simple elastic Earth model in 1862. Love later described analytical solutions to degree n for the Kelvin model (Love 1927, section 177). Because each harmonic component of the tide generates a different physical response, Love's numbers vary with the degree of the spherical harmonic. Values of h and k can be computed for models of the Earth's density distribution and elasticity derived from seismology, and numerical solutions now exist for a variety of realistic models (e.g. Farrell 1972b).

Observations of the amplitude factor $\phi = 1 + k - h$ and the gravimetric factor $\delta = 1 + h - 3/2\,k$ by independent methods enable h and k to be found separately.

ϕ can be determined from the amplitude of very long period tides in the oceans or preferably large, enclosed bodies of water with symmetrical shape, or by horizontal pendulum experiments. Consequently ϕ is referred to as the 'amplitude factor' or 'horizontal pendulum factor'.

Long records of the Earth tide made with continuously recording gravity meters give observed values of δ which include a contribution from elastic Earth effects and from the deformation due to ocean loading.

The static tide

The 'static' part of the tide is an equatorial bulge caused by the gravitational potential of the sun and moon which does not vary with time. Honkasalo (1964) was the first to propose that this part of the tide should be excluded from the tidal correction of gravity data because gravity measurements made on the Earth's surface would not distinguish it from 'gravity' due to the general attraction of the Earth and it's rotation. Because contemporary methods of calculating the tidal correction used closed formulae, which implicitly include the static part, 'making the Honkasalo Correction' means excluding the static term from the tidal correction. This is achieved by calculating the static contribution using a formula and restoring this effect after the complete tide had been removed. This procedure was used for the International Gravity Standardisation Net 1971 (IGSN71) where the total tidal correction was computed from Longman's formulae. The static term was calculated using the formula

$$\text{static}_{\text{IGSN}} = -0.037\left(1-3\sin^2\varphi\right)\ \text{mGal} \qquad (15)$$

where φ is the station latitude. This is added to the total tidal correction, which is added to the observed gravity.

The static tide varies only with latitude, and has a value of about 30 μgal changing at a rate of about 2 μgal per degree at 51 degrees, and thus is an important consideration in any comparison of gravity values. Table 3.1 below shows the value of the static tide calculated using the above formula for a few latitudes representing the range in Britain.

latitude φ °	$static_{IGSN}$ (μgal)
58 (Wick)	42.83
56 (Edinburgh)	39.29
51 (London)	30.04
50 (Penzance)	28.14

Table 3.1 Values of the static tide for a range of British latitudes, calculated using equation (15). Making the Honkasalo Correction *increases* the observed gravity by this amount.

Other formulae may be used for this calculation, and two such are compared in section 3.2.3.

Conventions regarding the static term in tidal calculations (the Honkasalo Correction)

In the calculation of gravity anomalies, the 'normal gravity' is subtracted from the tidally corrected observations. 'Normal gravity' is the attraction of a simplified model Earth defined by observations of the real Earth's gravitational field made not on its surface but from space. The direct part of the static tide only appears to be part of the Earth's gravity field for an observer on its surface so observations from satellites (and hence 'normal gravity') do not include it. The 1989 Canberra meeting of the International Association of Geodesy (IAG) decided that the static tide *should be removed* from gravity observations along with the periodic part of the tidal correction. This reverses the procedure adopted for the IGSN71.

Although the direct attraction of the Sun and Moon do not form part of the Earth's gravity field as sensed by a satellite, the effect of the tidally redistributed mass *does*. Therefore normal gravity will include the gravitational attraction of the Earth tidal response, but not the direct tide. Multiplication of the static tide (the non time-varying component of the tidal correction) by the elastic gravimetric factor of 1.159 gives the sum of the direct tide and the tidal effect of the Earth's elastic deformation.

The 1983 Hamburg meeting of the IAG decided that surface observations should be consistent with satellite observations so that the *direct* tide should be removed from surface observations but not the elastic effect. This corresponds to the multiplication of the static tide by 1 rather than ($1 + h - 3/2\,k$).

3.1.4 Ocean Loading

The oceanic tides cause periodic loading which causes deformation of the solid Earth, generating a change in the observed gravity. In addition to this change, there is also the direct gravitational attraction of the ocean tide. The ocean tide loading signal is in general only a few percent of the solid Earth tide signal. For the duration of the BPGN fieldwork, the solid Earth tide and ocean load corrections had typical amplitudes of 90 and 6 μgal respectively. The effect is regionally variable with an amplitude range of 1 to 12 μgal in Britain (Figure 3.4), and its importance increases near the coast. Although the elastic Earth tide can be calculated with an accuracy of better than 0.1 μgal anywhere, the determination of the ocean loading effect is not so easy. The effect at a particular location can be measured from Earth tide meter observations by separating the known elastic tide from the observed signal using harmonic analysis. This allows the determination of the amplitude and phase of the load tide.

The spatial variation of the tidal loading can be investigated by modelling. The ocean can be considered as a thin surface layer on the Earth expanded into spherical harmonics. The effect of each harmonic on the gravitational potential can be described by load Love numbers for various Earth models (Farrell 1972a). Alternatively, the loading can be computed by convolving a Green's function with a model of the ocean and shelf tide distribution. Green's functions are a sort of weighting function for describing the effect at a particular location due to the load at another. Global ocean tide distribution models exist for M_2 and O_1 tides e.g. Schwiderski (1980) and more detailed local tide models are available. Baker *et al.* (1991) described modifications to a shelf tide model of Flather for NW Europe which agrees well with tide gauge observations. Figure 3.4 (from Baker 1980) is derived from a model of the M2 tidal gravity loading in Britain.

Ocean loading observations are important for testing and improving models of the ocean tides and Earth response functions.

The ocean load correction

Because the ocean load effect can be an important factor for precise gravity surveys, some effort was made to develop a practical method of making the correction, with an accuracy appropriate to the particular relative and absolute gravity measurements described in this thesis.

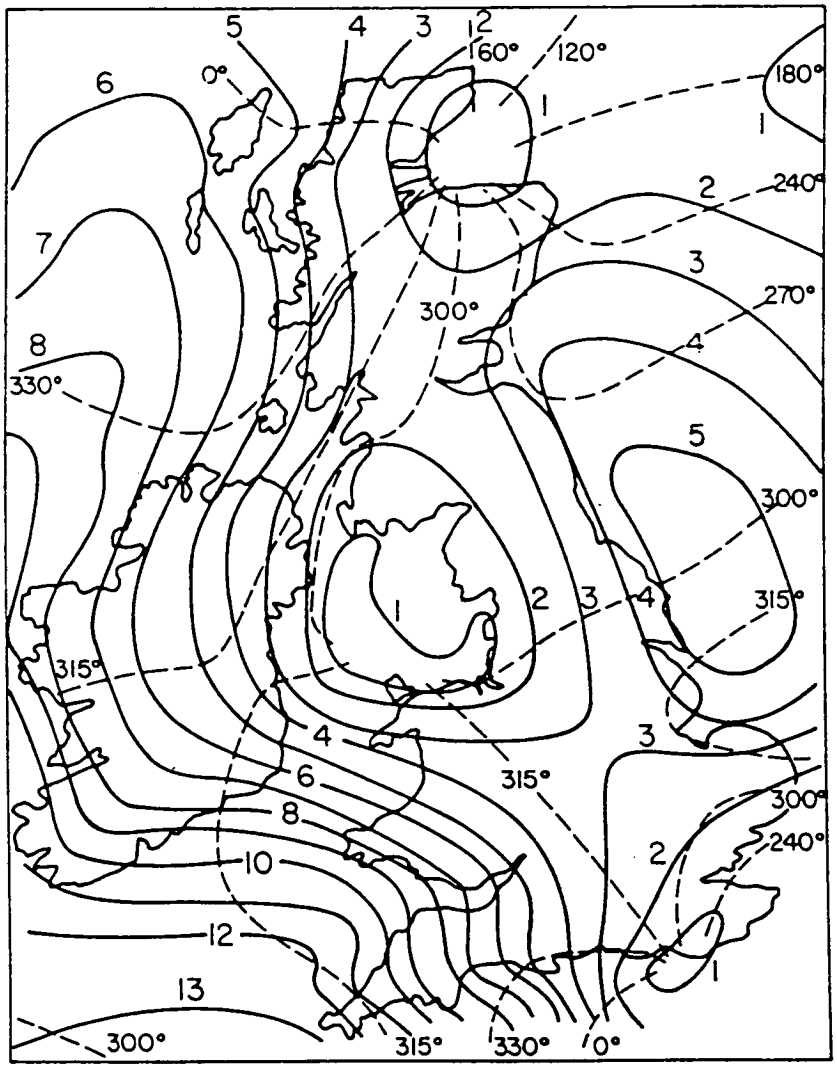

Figure 3.4 The M_2 tidal gravity loading in Britain. The full lines are the contours of the calculated loading amplitude in μgal and the the dashed lines are contours of the phase lag of the loading with respect to the tidal potential in the Greenwich meridian. (From Baker 1980)

The relationship between the load tide and the elastic tide can be represented on a phasor plot, as shown in Figure 3.5.

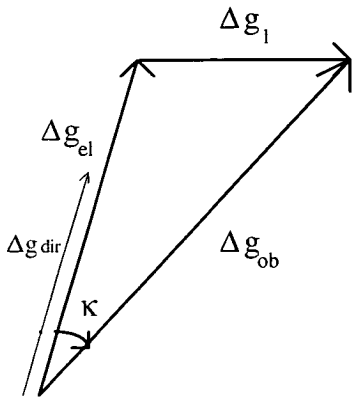

Figure 3.5 The relationship between the elastic tide Δg_{el} , the direct tide Δg_{dir} , the observed tide Δg_{ob} , and the load tide Δg_l .

Δg_{el} is the elastic tide, Δg_{ob} is the observed tide and Δg_l is the load tide. Δg_{dir} is the direct tide, which is the tide that would be observed on a rigid Earth. Multiplying the direct tide by the elastic gravimetric factor $\delta_{el} = (1 + h - 3/2\, k)$ gives the elastic tide: $\Delta g_{el} = \delta_{el}\, \Delta g_{dir}$. A similar relationship describes the 'observed gravimetric factor' δ_{ob} which is that $\Delta g_{ob} = \delta_{ob}\, \Delta g_{dir}$. Using this notation, we can write the cosine rule for κ :

$$\Delta g_l^{\,2} = \Delta g_{ob}^{\,2} + \Delta g_{el}^{\,2} - 2\, \Delta g_{ob}\, \Delta g_{el}\, \cos\kappa \qquad (16)$$

κ is the phase lag of the observed tide with respect to the tidal potential in the local meridian (phase leads positive).

If there were no load tide ($\Delta g_l = 0$), then the observed tide would simply be the elastic tide. The load tide modifies the amplitude and phase of the observed tide with respect to the predictable elastic tide. Harmonic analysis of continuous Earth tide observations allows the determination of δ_{ob} and κ .

The amplitude of the load tide can be expressed by writing Δg_{ob} and Δg_{el} in terms of Δg_{dir} and substituting into equation (16)

$$\Delta g_l^{\,2} = \Delta g_{dir}^{\,2}\left(\delta_{ob}^{\,2} + \delta_{el}^{\,2} - 2\, \delta_{ob}\, \delta_{el} \cos\kappa\right) \qquad (17)$$

The direct tide is that which is can be calculated by, for example, the harmonic expansion computation described in section 3.2.2.

Table 3.2 shows observed gravimetric factors δ_{ob} and phases κ in degrees for the major tidal constituents determined from Earth tide observations at absolute gravity sites (as at 1994) in Britain.

station	M_2		N_2		S_2		O_1		K_1	
	δ_{ob}	(κ)	δ_{ob}	(κ)	δ_{ob}	(κ)	δ_{ob}	(κ)	δ_{ob}	(κ)
Taunton	1.132	(6.13)	1.264	(7.5)	1.304	(-0.05)	1.134	(-0.23)	1.138	(0.24)
s.e	0.002	(0.07)	0.009	(0.4)	0.003	(0.1)	0.002	(0.09)	0.002	(0.08)
London	1.186	(3.08)	1.159	(3.3)	1.196	(0.9)	1.140	(-0.2)	1.136	(0.41)
s.e	0.002	(0.08)	0.008	(0.4)	0.005	(0.2)	0.002	(0.1)	0.001	(0.06)
Bidston	1.147	(0.77)	1.140	(0.7)	1.165	(0.86)	1.132	(0.13)	1.144	(0.50)
s.e	0.0009	(0.04)	0.005	(0.2)	0.002	(0.09)	0.001	(0.06)	0.0008	(0.04)
Edinburgh	1.186	(5.88)	1.1174	(7.66)	1.243	(2.59)	1.136	(0.28)	1.149	(-0.01)
s.e	0.0015	(0.07)	0.0100	(0.051)	0.002	(0.11)	0.003	(0.15)	0.003	(0.15)

Table 3.2 Observed gravimetric factors δ_{ob} and phases κ in degrees determined from Earth tide observations. The standard errors are given underneath their appropriate number. The values for Taunton, London and Bidston are from Baker (1980) and the value for Edinburgh is from Baker (*pers. comm.* 18 March 1992).

The gravimetric factor (δ_{ob}) is the observed amplitude (Δg_{ob}) of the constituent normalised by dividing by the amplitude that would be observed on a rigid Earth (Δg_{dir}). The errors are the standard errors from the harmonic analysis.

It is usually more convenient for tidal loading to work directly with the amplitudes rather than the gravimetric factors and the usual convention for ocean tide maps is to express phase lags with respect to the tidal potential in the Greenwich meridian (zero longitude) rather than the local meridian. The conversion for the semi-diurnal tide from local phase κ to Greenwich phase G is

$$\kappa = - G - (2 \, . \, \text{longitude}) \qquad \text{with east longitudes positive.} \qquad (18)$$

Ocean loading at Taunton

The large gravimetric factors and phase leads for the semi-diurnal (M_2 , S_2 and N_2) constituents at Taunton (Figure 3.4) show that the tidal loading is particularly large in SW England. In September 1993, the absolute gravity meter FG5-107 observed in Taunton at the

end of an East-European measurement campaign. This instrument belongs to the Defence Mapping Agency (DMA) of the United States. The on-line gravity is normally corrected for the elastic Earth tide, but not for the ocean load. At the continental sites, the ocean load signal was too small to be immediately obvious in the on-line gravity. The record of the Taunton occupation in Figure 3.6a shows consecutive hourly values for 54 hours and clearly shows the ocean load signal, which is not usually directly visible. The maximum amplitude of the signal during the recording period is about 7.5 μgal, but the length of record is too short to determine the true maximum amplitude. The data was generously supplied to Edinburgh University by the DMA, and an ocean loading correction was implemented using the values in Table 3.2 for Taunton from Baker (1980). Figure 3.6b shows the corrected gravity record.

It is fortunate that Baker *et al.* chose to make continuous Earth tide observations at sites where, almost 20 years later, FG5 absolute gravity meters were to observe (Taunton, London, Bidston and Edinburgh). This enabled the author to make ocean loading corrections to the FG5 observations with particularly reliable values for the amplitude and phase, at a time when this correction was not implemented in the on-line code. The computation is described in section 3.2.2.

The effect of making the correction at sites other than Taunton is far less spectacular. Table 3.3 below compares the result with and without the correction for Taunton and NPL (London) absolute observations. The values given are the overall mean of the occupation.

Site (Instrument)	drops	without oload corr (μgal)	with oload corr (μgal)
Taunton (FG5-107)	5300	981 168 867.84 ± 4.77	981 168 868.37 ± 1.52
NPL (FG5-103)	6000	981 181 340.58 ± 3.22	981 181 340.63 ± 2.36

Table 3.3 Absolute gravity value (occupation mean) and rms residual with and without the ocean loading (oload) correction, for Taunton and NPL (London) observations. The Taunton values are corrected to the top of the drop (using a vertical gradient of 3.080 μgal cm^{-1}), without speed of light correction and with the atmospheric pressure correction. NPL values corrected to the top of the drop (using a gradient of 2.991 μgal cm^{-1}), with speed of light correction and without pressure correction.

The plot of set means for the London values (NPL0307A) with and without the ocean load correction are given in Figures 3.7a and 3.7b respectively.

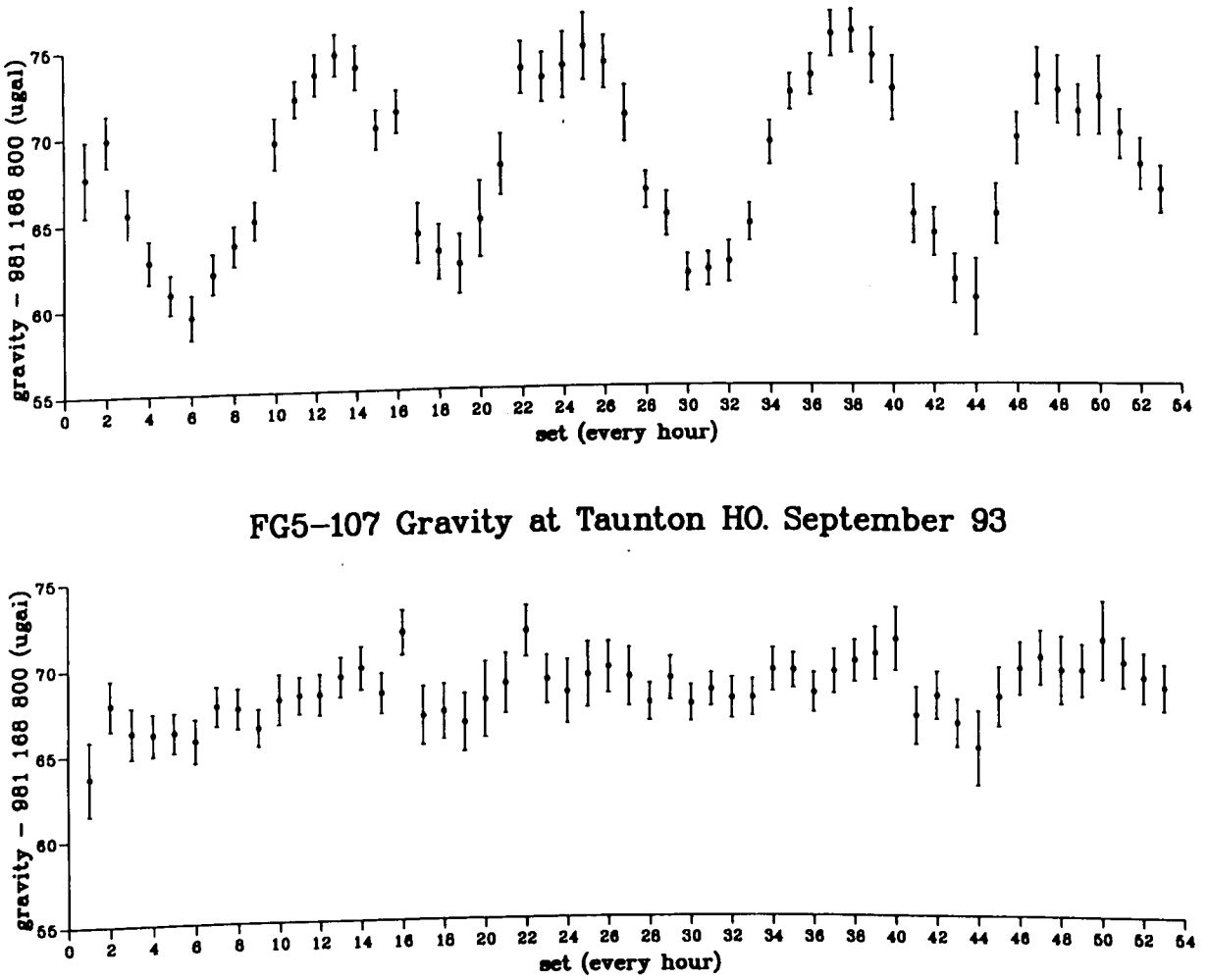

Figure 3.6 Data from FG5-107 at Taunton, without (a) and with (b) the ocean loading correction. The correction was implemented by the author in the program DDT.

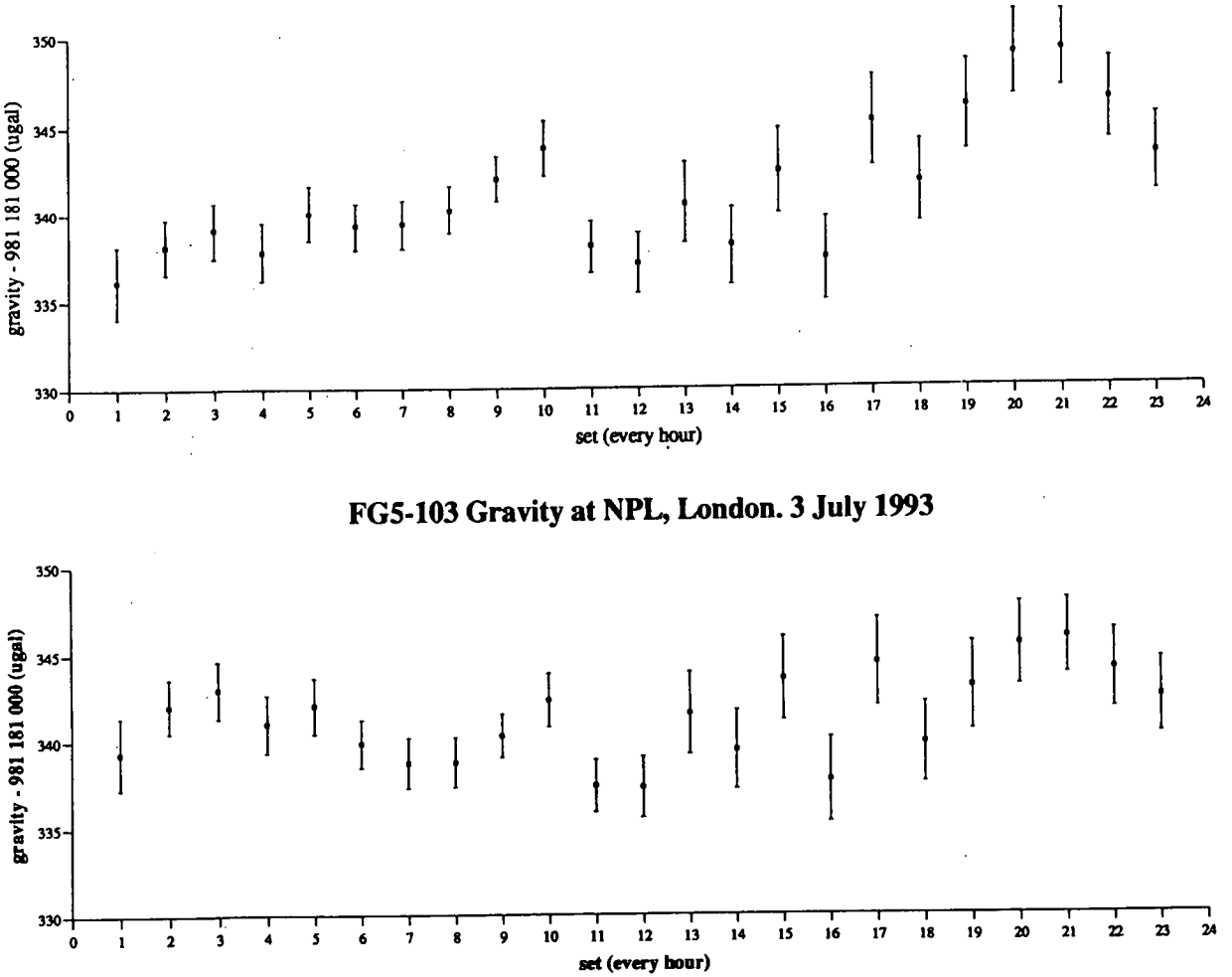

Figure 3.7 Data from FG5-103 at NPL (London), without (a) and with (b) the ocean loading correction. The correction was implemented by the author in the program DDT. Making the ocean load correction to the NPL data increases the gravity values of the first 5 sets and decreases the values of the last 7 sets, so reducing the overall scatter.

3.2 Tidal Computations

3.2.1 Computations of the tide-generating potential

The calculation of the tide-generating potential may be done using a closed expression or a series expansion. Commonly used examples are the closed form of Longman (1959) and the series expansion of Cartwright & Tayler (1971).

The series expansion makes use of the fact that the variation of δ, φ and t, in equation (7), for example, can be formulated as harmonic functions of time which depend on five astronomical quantities. This approach was first developed by Darwin in 1883. The improved lunar theory of Brown (1905) was used by Doodson for his classic expansion (Doodson 1921). Cartwright, Tayler & Edden made use of 1964 I.A.U astronomical constants and new calculations of Ephemeris Time and Brown's coefficients to produce a new harmonic expansion and revised tables of coefficients for 484 partial tides (Cartwright & Tayler 1971, Cartwright & Edden 1973). The potential is calculated up to degree 3 for the moon and 2 for the sun and includes all tidal components whose relative amplitudes are greater than 10^{-5}.

The closed form calculates the ephemeris (position with time) for the tide generating body, then computes the tide at the place of observation by inserting values for δ, φ and t in the expression for U_m (equation (7)) This method does not need tables of coefficients and its accuracy depends on the sophistication of the ephemeris calculation.

3.2.2 An example of a harmonic expansion calculation - the subroutine TIDAL

The tidal corrections to observations of relative gravity made by Edinburgh University are made by the subroutine TIDAL in a program called REDUCE. The solid Earth tide and the ocean load tide are calculated using a Cartwright-Tayler-Edden (CTE) harmonic expansion.

TIDAL requires the latitude, longitude, height, and ocean load tide coefficients of the station, and the time of observation. It also requires a separate tidal data file containing coefficients and argument numbers for 484 harmonic terms taken from CTE tables (Cartwright & Tayler 1971, Cartwright & Edden 1973).

Fundamental arguments

Doodson used six independent variables to describe the shape and orientation of the orbits of Moon and Sun with respect to a position on the Earth. These are τ, the time angle in lunar days; s and h, the mean longitude of Moon and Sun respectively; p and p', the longitude of the mean perigee (point of closest approach) of the Moon and Sun respectively and N, the negative longitude of the Moon's mean node. The node is where the moon's orbit crosses the plane of the Earth's orbit.

The six fundamental arguments k_r, corresponding to Doodson's τ, s, h, p, N and p', (k_1 to k_6 respectively) describe how the position of the moon and sun vary with time. The expression

$$k_r = 2\pi f_r t + \varphi_r \qquad (19)$$

can be evaluated using the periods ($1/f_r$) and phases (φ_r), which are given in Table 3.4 below for the epoch 1951 to 1969.

Doodson	r	f_r	φ_r
τ	1	0.96613 6807	217°.89822
s	2	0.03660 11023	022°.22101
h	3	0.00273 79092	060°.11923
p	4	0.00030 94548	271°.56503
N	5	0.00014 70940	188°.82048
p'	6	0.00000 01308	282°.25919

Table 3.4 Values of f_r and φ_r for the CTE epoch 1951-1969. The fundamental arguments (k_r) are evaluated using equation (19) above.

Argument numbers

The CTE harmonic expansion series includes 385 second degree components (orders 0, 1 and 2 for the moon and sun and 99 third degree components (orders 0, 1, 2 and 3 for the moon).

For example, the calculation of the second degree semi-diurnal tides is

$$\sum_{i=267}^{385}\left[\cos(c_{1i}k_1 + c_{2i}k_2 + c_{3i}k_3 + c_{4i}k_4 + c_{5i}k_5 + c_{6i}k_6)\cdot c_7\right] \qquad (20)$$

and the modified Doodson coefficients c_{ji}. (In CTE, these coefficients may be positive or negative; Doodson added 5 to make them positive.

The coefficients c_{ji} from the CTE tables for the two largest tidal components are given in Table 3.5 below. Both are second degree semi-diurnal tides - the M_2 and S_2 components corresponding to i=326 and i=353 respectively.

tide	k_1	k_2	k_3	k_4	k_5	k_6	amplitude (c_7)
M_2	2	0	0	0	0	0	63192
S_2	2	2	-2	0	0	0	29400

Table 3.5 The coefficients c_{ji} from the CTE tables for the M_2 and S_2 tides, for substitution in equation (20).

Latitude factors

The latitude dependence varies according to the tidal group and degree of the spherical harmonic. The latitude weighting function and the normalisation factors for the spherical harmonic tidal components are given in Table 3.6 below

	degree n	order m	normalisation	latitude function
long period	2	0	$\sqrt{(5/4\pi)}$	$3/2\ \cos^2\theta - 1/2$
diurnal	2	1	$-\sqrt{(5/24\pi)}$	$3\ \sin\theta\ \cos\theta$
semi diurnal	2	2	$\sqrt{(5/96\pi)}$	$3\ \sin^2\theta$
long period	3	0	$\sqrt{(7/4\pi)}$	$5/2\ \cos^3\theta - 3/2\ \cos\theta$
diurnal	3	1	$-\sqrt{(7/48\pi)}$	$3/2\ \sin\theta\ (5\ \cos^2\theta - 1)$
semi diurnal	3	2	$\sqrt{(7/480\pi)}$	$15\ \sin^2\theta\ \cos\theta$
ter diurnal	3	3	$-\sqrt{(7/2880\pi)}$	$15\ \sin^3\theta$

Table 3.6 Latitude dependence and normalisation for 2nd and 3rd degree spherical harmonics. θ is co-latitude. (From Cartwright & Taylor 1971).

The geodetic latitude and longitude from the station information file are converted to geocentric values and the radius of the Earth at each site is calculated using the Geodetic Reference System 1967 (International Association of Geodesy 1971).

The gravimetric factor δ has the value 1.159 for the second degree tides and 1.042 for the third degree tides.

Ocean load calculation

For the correction of the relative gravity data for the British Precise Gravity Network (BPGN) (Chapter 6), only the M_2 ocean load tide was calculated. The amplitude of the ocean

load correction rarely exceeded 6 μgal. M_2 forms about half of the total tide in Britain and is the only component for which reliable models exist. The amplitudes and phases for the M_2 ocean load tides for all the BPGN sites are held in the station location file and were supplied by Baker (*pers. comm.* 4 May 1994) who calculated them using the loading models described in Baker, Edge and Jeffries (1991). These values are shown in Table 3.7. The phases are Greenwich phase lags G (with lags positive), which were converted to local phases κ using equation (18). The amplitudes α_o are in μgal, and have been computed for zero altitude (h in Table 3.7).

The M_2 ocean load tide is calculated explicitly:

$$\text{oload}_{M2} = [\cos(2 \cdot k_1 - \kappa)]\alpha_o \qquad (21)$$

k_1 is the first fundamental argument, calculated using the values given in Table 3.4

For the absolute gravity data, all five main constituents M_2, S_2, N_2, O_1 and K_1 were included in the correction, using values of the observed gravimetric factor δ_{ob} and local phase κ from Earth tide meter observations (Table 3.2). Early versions of the Axis FG5 software (REPLAY) did not include an ocean loading calculation so a routine was written to make this correction in the Edinburgh FG5 processing program DDT. The most recent version of REPLAY (version 3.1) does include an ocean loading calculation.

The calculation in DDT was different to that of equation (21), which uses the amplitudes and Greenwich phases from the M_2 loading model data. In DDT, δ_{ob} and κ are used directly to calculate the theoretical elastic tide (TITH) and the observed tide (TIOB) vectors (Figure 3.5) separately for each component. The load tide is the difference of these vectors.

For example for the M_2 component, the theoretical elastic tide is

$$\text{TITH}_{M2} = [\cos\ (2k_1)] \cdot \alpha \cdot \delta_{el} \qquad (22)$$

where k_1 is the first fundamental argument and α is the CTE amplitude. δ_{el} is the elastic gravimetric factor.

ref	name	lat	long	h(m)		α(μgal)	G(°)
140	GI140Floor	55.90000	-3.17700	75.00	GI	2.970	-69.689
11	Abd StMach	57.17000	-2.10100	19.00	Ab	2.410	-95.425
13	Bishopton	55.90460	-4.51979	31.00	Bi	2.954	-50.187
15	Moffat TH	55.19000	-3.24000	120.00	Mf	2.423	-70.976
17	Crooklands	54.24500	-2.71100	91.00	Cr	1.886	-77.126
18	Goosnargh	53.82333	-2.66666	61.00	Go	1.798	-71.218
19	Daresbury	53.34000	-2.63000	60.00	Da	2.360	-57.952
20	POL Abs1	53.40333	-3.07166	46.00	Pl	1.218	-70.668
24	POL SPorch	53.40333	-3.07166	50.00	Po	1.218	-70.668
201	Wooler	55.54600	-2.01100	67.00	Wo	3.662	-77.198
202	Wylam	54.97700	-1.82200	34.00	Wy	3.635	-71.474
203	Easby	54.39800	-1.71400	92.00	Ea	3.254	-65.685
204	Chpl Hadd	53.72700	-1.11700	6.00	CH	3.448	-57.567
205	Gt Gonerb	52.93200	-0.66400	94.00	GG	3.333	-52.926
206	Histon	52.25500	0.10400	12.00	Hi	2.655	-58.168
207	Sproughton	52.06300	1.00000	13.00	Sp	1.843	-76.988
208	Farningham	51.37900	0.22300	28.00	Fa	1.608	-79.361
209	StJ Comma	51.15100	1.19200	149.00	SJ	1.962	-161.443
210	Hstmnceux	50.86700	0.33400	24.00	Hx	0.806	-140.854
211	Boxgrove	50.86000	-0.71000	29.00	Bx	1.950	-45.160
212	Wimborne	50.79855	-1.98723	29.00	Wi	4.388	-35.934
213	Broadway	50.93900	-2.95400	46.00	Br	6.026	-38.580
50	Taunt Abs	51.02506	-3.07866	15.00	Tu	6.156	-38.431
52	Ldg Bay	51.02506	-3.07866	15.00	LB	6.156	-38.431
53	Wtr Tan	51.02506	-3.07866	15.00	WT	6.156	-38.431
214	Ashburton	50.51400	-3.75600	75.00	As	8.238	-40.941
215	Lanivet	50.44400	-4.76200	78.00	La	10.226	-45.965
216	Gt Torgtn	50.95200	-4.14300	94.00	GT	8.885	-39.283
217	Mounton	51.63300	-2.70400	23.00	Mu	4.927	-38.867
218	Malvern	52.11200	-2.34600	244.00	Ml	3.873	-46.393
219	Shareshill	52.65700	-2.08300	136.00	Sh	3.311	-51.155

.....continued overleaf

Table 3.7 British Precise Gravity Network site listing. The columns (left to right) are: reference number, site name, latitude, longitude, height above sea level, code, and the amplitude (α) and Greenwich phase (G) of the M_2 ocean load tide. α and G were supplied by Baker (*pers. comm.* 4 May 1994).

ref	name	lat(°)	long(°)	h(m)		α(μgal)	G(°)
220	Beedon	51.49900	-1.30500	170.00	Be	3.228	-48.852
222	Hmptn Chch	51.41300	-0.36000	19.00	Ha	2.235	-58.916
33	NPL1 Bldg1	51.41970	-0.33774	10.00	KK	2.218	-59.343
223	Towcester	52.14300	-1.02200	119.00	To	3.091	-53.142
224	Montgomery	52.56000	-3.14600	160.00	Mt	3.686	-45.281
225	Talybont	52.48900	-3.97900	64.00	Ta	4.253	-34.001
226	Talkin	54.90800	-2.70300	165.00	Tk	2.598	-71.482
230	Immingham	53.56000	-0.33200	20.00	Im	4.142	-51.829
231	Rishworth	53.65800	-1.95200	190.00	Ri	2.815	-59.609
232	Felindre	51.70600	-3.97100	85.00	Fe	7.391	-32.079
233	Ambleston	51.89400	-4.90600	134.00	Am	7.631	-34.601
234	Betws	53.09100	-3.80200	18.00	Bt	2.334	-44.647
240	Methven	56.41600	-3.57900	70.00	Me	2.842	-60.470
241	Tannadice	56.71100	-2.85770	65.00	Tn	2.934	-80.247
242	BBudn VLBI	56.47800	-2.78100	7.00	BB	3.377	-85.599
243	Elgin Sth	57.64600	-3.31400	18.00	El	1.290	-48.977
244	Strthpefr	57.58900	-4.53800	76.00	Sf	2.977	-25.521
245	Lairg	58.02500	-4.39900	110.00	Lg	2.790	-15.082
246	Wick	58.44400	-3.09400	3.00	Wk	1.081	16.789
247	Btyhil FBM	58.48600	-4.21400	61.00	By	2.923	0.688
248	Scourie	58.34800	-5.15900	6.00	Sc	4.507	-2.411
249	Ullapl Mus	57.89600	-5.16100	12.00	Ul	3.988	-13.861
250	Acnshn FBM	57.57900	-5.08000	156.00	Ac	3.694	-21.353
251	Dornie	57.27800	-5.51000	12.00	Do	4.207	-24.081
252	Roybridge	56.89200	-4.83900	97.00	Ry	3.433	-34.625
253	Alvie	57.16100	-3.87800	216.00	Av	2.556	-43.117
254	Crnlar FBM	56.39700	-4.57100	166.00	Ci	3.214	-43.513
255	Annbank	55.48600	-4.52100	53.00	An	2.359	-61.579
256	New Luce	54.94200	-4.85000	55.00	NL	1.641	-72.274
257	Kelton	54.92100	-3.93700	67.00	Ke	1.460	-125.368

Table 3.7 continued...
British Precise Gravity Network site listing. The columns (left to right) are: reference number, site name, latitude, longitude, height above sea level, code, and the amplitude (α) and Greenwich phase (G) of the M_2 ocean load tide. α and G were supplied by Baker (*pers. comm.* 4 May 1994).

The observed tide is

$$TIOB_{M2} = [\cos\ (2k_1 - \kappa)] \cdot \alpha \cdot \delta_{ob} \qquad (23)$$

where κ is the phase and δ_{ob} the 'observed gravimetric factor' for the M_2 tide given in Table 3.2.

The load tide is given by (TIOB-TITH) which is multiplied by the appropriate latitude factor from Table 3.6.

3.2.3 Comparison of Tidal Calculations

The processing software written by Axis Instruments for FG5 absolute gravimeter performs tidal calculations in a subroutine called GRAVTIDE. GRAVTIDE provide an example of a closed form of calculation (for example Longman 1959).

Elastic tide

A comparison of the elastic tidal corrections from REDUCE and GRAVTIDE for 24 hour periods on three different dates show that they differ by less than 0.5 μgal (Table 3.8 below). Figure 3.8a shows the total tide correction and 3.8b the difference between the two calculations for 07.05.92 at Bidston. Note the very different vertical scales.

date	site	range of correction (μgal)	difference (μgal) (REDUCE - GRAVTIDE)
07.05.93	Bidston POL	200	< 0.5
12.05.93	Bidston POL	104	< 0.25
03.07.93	London NPL	296	< 0.5

Table 3.7 Comparison of the elastic tide calculated by the programs REDUCE and GRAVTIDE for the 24 hour periods shown.

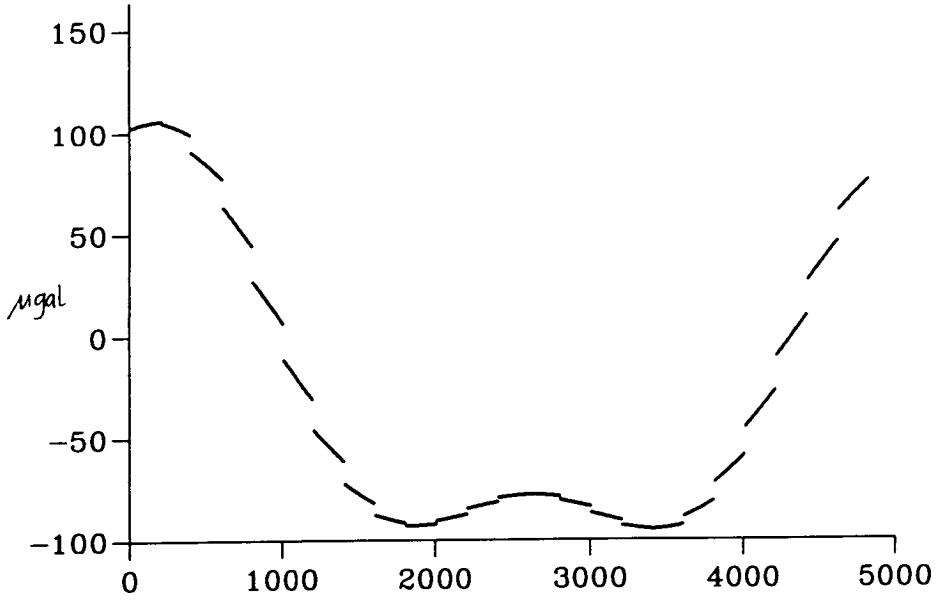

Figure 3.8a Total tide correction (μgal) calculated by REDUCE for 07.05.93 at POL.

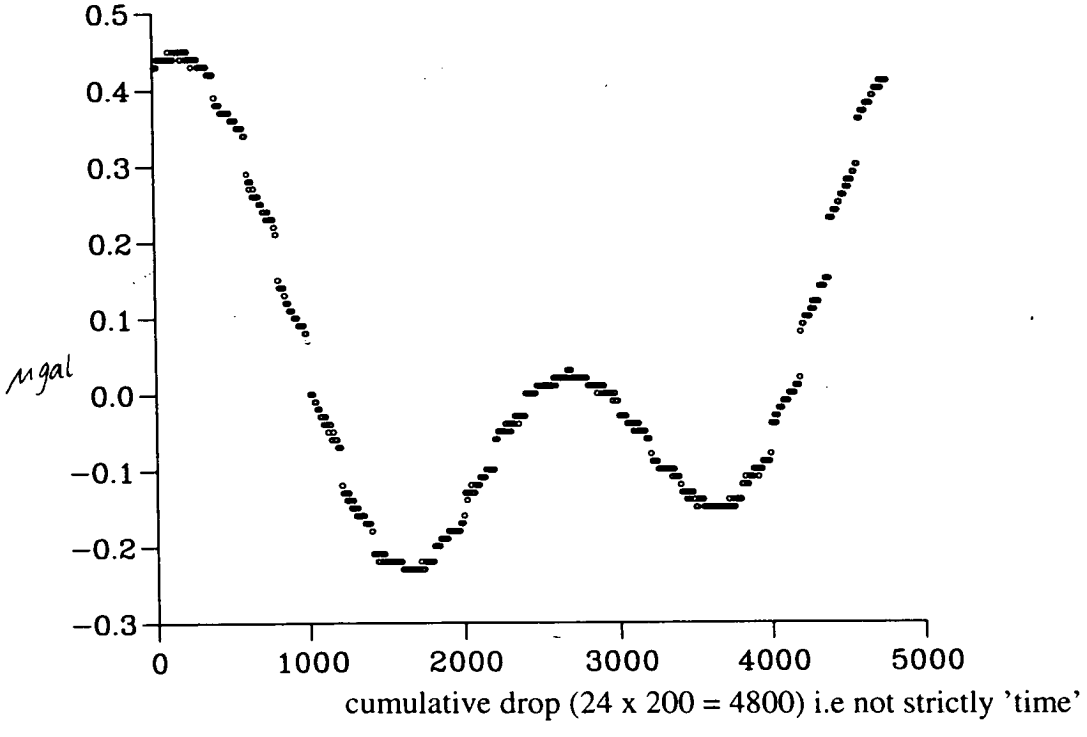

Figure 3.8b The difference (in μgal) between the tidal calculations of REDUCE and GRAVTIDE for 07.05.92 at POL. Note the very different vertical scale.

Static tide

In GRAVTIDE the static tide for an elastic Earth is calculated explicitly using the formula

$$\text{static}_{\text{grvtd}} = -0.030481(3\cos^2\varphi_{gc} - 1)\delta\, r_{gc} \text{ mgal} \tag{24}$$

where δ is the gravimetric factor, r_{gc} is the conversion to geocentric radius given by

$$r_{gc} = 1 - f\cos^2\varphi_{gc}\left(1 + \tfrac{3}{2} f \sin^2\varphi_{gc}\right) \tag{25}$$

and f is the flattening of the Earth.

An explicit formula was also used for the Honkasalo Correction (section 3.1.3) in the IGSN71 adjustment :

$$\text{static}_{\text{IGSN}} = -0.037(1 - 3\sin^2\varphi) \text{ mgal} \tag{26}$$

where φ is the station latitude.

In a harmonic expansion type of tidal calculation such as TIDAL, the static part is simply one of the harmonics, so it is easy to identify.

$$\text{static}_{\text{TDL}} = \left[\frac{1}{2}\cdot\sqrt{\frac{5}{4\pi}}\cdot C_g \cdot {r_{gc}}^2 \cdot \alpha\right](3\sin^2\varphi_{gc} - 1)\,\delta \text{ mgal} \tag{27a}$$

The terms in square brackets are defined as follows: $\sqrt{(5/4)}$ is the normalisation factor for the spherical harmonic of degree 2, order 0; C_g is the factor $2GM_e/r_e^3$ for conversion from potential to gravity in mgal; r_{gc} is the conversion to geocentric radius as defined by the International Spheroid 1967 and α is the amplitude of the static term (= -31455 in CTE tables). φ_{gc} is the geocentric latitude. Evaluating some of these terms gives

$$\text{static}_{\text{TDL}} \approx -0.0304806(3\sin^2\varphi_{gc} - 1)\,\delta \text{ mgal.} \tag{27b}$$

Table 3.9 below compares the value for the static tide computed with the three formulae, for a range of British latitudes.

latitude	static tide (μgal)		
(φ°)	GRAVTIDE	IGSN71	TIDAL
58.0	40.38	42.83	40.41
56.0	37.00	39.29	37.04
51.0	28.20	30.04	28.23
50.0	26.39	28.14	26.47

Table 3.9 Comparison of values of the static tide as computed by three different formulae (equations 24, 26 and 27) at a range of British latitudes.

3.3 Non-Tidal Corrections

3.3.1 Polar Motion

Polar Motion is the movement of the Earth's rotation axis with respect the 'Conventional International Origin', which is the average pole position for the time interval 1900.0 - 1906.0. The position of the Earth's rotation axis moves relative to stations fixed to the crust causing changes in latitude (polar motion) and in angular velocity (corresponding to changes of the length of day) cause a gravimetric effect which can be computed by

$$\delta g_{pol} = \delta_{pol}\, \omega^2 R \sin 2\theta\, (x \cos\lambda + y \sin\lambda) \qquad (28)$$

(Niebauer & Faller 1992), where θ is the colatitude and λ is the east longitude of the station and the instantaneous pole co-ordinates x and y can be obtained from published tables. The evaluation of the polar motion correction is described in section 4.4.8.

3.3.2 Atmospheric Pressure

The main effect of the local atmosphere on gravity is due to the direct attraction of the atmosphere. Warburton and Goodkind (1977) showed that the change in gravity due to the elastic deformation of the Earth by the load of the atmosphere is much smaller and of opposite sign to the effect of direct attraction.

The gravity effect of an infinite plate model for the atmosphere gives $-2\pi G/g$ or -0.427 μgal mbar^{-1}.

The admittance between gravity and local air pressure can be found by correlating a continuous gravity dataset which has been corrected for tides, ocean load and polar motion to the barometric record at the gravimeter site over the same period. Simple fits like this give values around -0.36 ± 0.02 (Niebauer & Faller 1992) and -0.34 μgal mbar^{-1} (Merriam 1992). This value varies from station to station and from time to time probably due to the effect of large scale weather systems. Using an infinite slab model, with a scale height for the atmosphere of about 12 km, Merriam finds that 90 percent of the gravity signal of a regional system 1000 km in diameter comes from the area within 50 km of the gravimeter, almost no signal arises from the area between 50 and 250 km of the instrument, and about 10 percent comes from the zone between 250 and 500 km away. In the local (<50 km) zone, loading effects calculated using Green's functions are only about 1 percent of the Newtonian attraction. The local admittance calculated from this model is -0.356 μgal mbar^{-1} (Merriam 1992).

The inclusion of global air pressure corrections tends to increase the magnitude of the admittance, for example from -0.36 to -0.41 μgal mbar^{-1} and to reduce the hourly rms residuals from continuous gravity datasets (Niebauer & Faller 1992). Since by far the most significant contribution comes from the very local zone, a single barometer with precision of about 1 millibar can enable adequate pressure corrections to be made to most gravity observations. For comparisons over periods longer than a few days the global corrections can be up to a few microgals, but better models of the oceanic response to the atmosphere are needed.

Gravity readings should be corrected to the standard pressure at the station height h using a standard atmosphere:

$$\text{Standard Pressure} = 1013.2\,(1 - 2.2557\,.10^{-5}\,h)^{5.2613}\ \text{mbar}. \qquad (29)$$

A correction of -0.3 μgal per millibar of the difference between the observed pressure and the standard pressure is generally applied if no information about the local admittance is available.

3.3.3 Groundwater

The gravitational effects of groundwater have been studied on time scales ranging from hours to years, for example Delcourt-Honorez (1990b) and Mäkinen & Tattari (1990). Generalisation of results is not usually possible due to the often complex hydrogeological situation and insufficient hydrological data. The effect of groundwater level and soil moisture can both be calculated by a Bouguer slab approximation.

For a change in groundwater level of δH, the change in gravity is

$$\delta g = 2\pi G\rho\, P\delta H \qquad (30a)$$

where ρ =water density and P = % porosity.

For a change in soil moisture,

$$\delta g = 2\pi G\rho\, H\delta P \qquad (30b)$$

where H = thickness of the layer and δP is the change in % porosity due to the change in moisture content of the soil.

The gravity effect for an infinite sheet of water (porosity = 100 %) is 0.042 μgal mm^{-1}. The porosity has to be determined experimentally and is typically 5 to 30 %. In sandy formations with simple structure, the above formulae can predict gravity changes values which are close to those observed. Mäkinen & Tattari (1990) measured a porosity of 26.5% in sandy soil at a Finnish site, which means that a 100 mm change in groundwater level corresponds to 1.1 μgal in gravity. They observed a maximum peak-peak gravity variation of 13 μgal of which about 6 μgal was the contribution from groundwater and 8 μgal from soil moisture variations. More spectacular variations in the gravity signal from ground water variations have been observed with a superconducting gravimeter at a site in a geothermal field (Goodkind 1986). The signatures of the dry and rainy season are very well observed. A rainy season which had 1.8 m of rain caused a 60 μgal signal which persisted until about 10 days

after the rain stopped. Clearly in conditions like this, the groundwater effects on gravity are important, but in general they are less than a few μgal.

The indirect effect due to deformation of the ground has been shown to be negligible in most cases, unless there is some known large scale pumping or extraction in the region (Delcourt-Honorez 1990b).

Because of the difficulty in obtaining groundwater data, it is a sensible precaution to choose gravity sites where this effect will be minimised, such as on impervious bedrock. Obviously this is not always possible but areas where the geology is known to be water-carrying (some sandstone basins, and some chalk formations) should be avoided. Sites close to rivers, canals, drains, water tanks etc. are also undesirable.

3.4 The Edinburgh pre-processing program REDUCE

The necessary corrections to observations of relative gravity made by Edinburgh University are made by a program called REDUCE. This program first converts the dial readings from the field observations to gravity using the calibration functions described in Chapter 2. The solid Earth tide and the ocean load tide are calculated by subroutines which use a Cartwright-Tayler-Edden (CTE) harmonic expansion. The effect of the atmosphere is removed by correcting all values to the standard pressure for the station height. REDUCE does not include polar motion or groundwater calculations.

REDUCE requires information from three files. The observation data file contains the gravimeter dial readings, with times, site codes, air pressure and temperature observations. The station location file contains site codes, station names, longitude, latitude and height for each station, and the amplitudes and phases of the M_2 ocean load tide for each station. The tidal data file 'cartride.dat' containing the Doodson coefficients is needed for the subroutine TIDAL (section 3.2.2).

There are two forms of output from REDUCE. Examples are given in Tables 3.10a and 3.10b (section 3.7.1). The form of Table 3.10b is a file containing the time, corrected relative gravity value, instrument code, traverse number and site code and a list of stations and traverse start times. A traverse is a sequence of observations made with the same instrument in the same day (usually). A value of zero (plus pressure correction) is assigned to the first reading of each traverse. This forms the input to the network adjustment program described in section 3.7.

3.5 Networks

Introduction

Gravity networks are established for a variety of applications, from studying continental geodynamics, supporting national geodetic and gravimetric activities, and monitoring local and regional deformation to very high precision comparisons of relative and absolute observations. The spatial separation of stations ranges from thousands of kilometres to a few metres, and precisions from milligal (1 part in 10^6) to microgal (1 part in 10^9 of gravity).

Historical

The first international gravity system was adopted in 1900. It was known as the Vienna Gravity System and had an estimated relative accuracy of ± 10 mGal. Between 1898 and 1904, Kühnen and Furtwängler measured absolute gravity at Potsdam, and these observations provided the absolute datum for the Potsdam Gravity System which was introduced in 1909. The Potsdam datum became integrated into a global net, called the 'International First Order Gravity Net (Potsdam System)' which was established in 1958 (Coron & Monnet 1959) and became the accepted global reference net. A gravity value of 9.81274 ± 0.000 03 ms^{-2} was assigned to the Potsdam station.

The International Gravity Standardisation Net (IGSN71)

In 1962 the International Gravity Commission began to create some order over the many new long range measurements with relative gravimeters and pendulums being made, and to direct the activity towards three International Calibration Lines. These were the American (Ushuaia to Point Barrow), Euro-African (Capetown to Hammerfest) and West Pacific (Christchurch to Sapporo) Calibration Lines. During the 1960's, the accuracy of the gravimeter measurements (± 0.05 mgal) and improved pendulum apparatus (± 0.3 mgal) led to a world network of high *relative* accuracy. The evolution of Cook's apparatus (± 0.1 mgal), Faller's transportable apparatus (± 0.05 mgal) and Sakuma's apparatus (± 0.03 mgal) gave a high *absolute* accuracy . Development of the software to deal with large numbers of gravity observations and to make use of increasingly powerful computers led to a new, definitive adjustment - the International Gravity Standardisation Net (IGSN71) (Morelli *et al.* 1974). The IGSN71 constitutes about 24 000 gravity measurements of which 1 200 were new, relative pendulum observations and 10 were absolute observations. The rest of the IGSN71 observations were made with relative instruments, particularly LCR meters. This new

adjustment superseded the Potsdam Gravity System, which was by then known to have a error of +12 to +16 mgal in the Potsdam datum.

National First Order Nets

Numerous national networks have been established to densify the coverage provided by IGSN71 sites. A 'first order' network is generally the most accurate net available, and lower orders are established later, holding the higher order values fixed. A first order network will usually have fewer sites at larger spacings of about 100 km, and a third order one should provide dense coverage with site spacing of tens of km. One of the best-observed first order national base nets is the German Gravity Base Network (DGSN76). The DGSN76 consists of 21 stations about 150 km apart. Three security excenters have been established at all these stations, and 4 of them have been surveyed with the absolute meter of the Istituto di Metrologia 'G.Colonnetti' (IMGC), Torino. The network was measured independently by two observing teams each with two LCR meters, providing a total of 656 gravity differences. The adjustment gives standard deviations of ± 6 - 11 μgal on station gravity values, and the maximum gravity difference of 800 mgal is determined to ± 15 μgal. In Britain, the National Gravity Reference Net (NGRN73) (section 1.6.2) has provided first order gravity stations with standard errors of between 20 and 70 μgal. The NGRN73 has been superseded by the British Precise Gravity Network (BPGN93), which consists of 58 sites spaced about 100 km apart. It includes 4 absolute gravity sites, a Satellite Laser Ranging site and a Very Long Baseline Interferometry site. Standard errors on the gravity differences are about 4 μgal, with 8 μgal on the largest difference of 500 mgal. The BPGN93 is the subject of Chapter 6.

With increasing availability of absolute measurements, many new adjustments are possible. The Unified European Gravity Network 1994 (UEGN94) includes data from 11 European countries at nearly 500 stations at various spacings, observed mainly with LCR meters. The adjustment by Boedecker *et al.* (1994) gives standard deviations on the gravity values at the relative stations mostly between 5 and 20 μgal. Base nets composed entirely of absolute measurements are also being established, for example in the US and Germany.

Calibration Lines

Calibration lines are effectively 'linear networks' which make use of changes in gravity with latitude or height, or both. A particularly well-determined example is the Cuxhaven - Hannover - Harz line (described in Torge 1989) which covers a range of 310 mgal in subdivisions of 10 mgal. Measurement on stations of known gravity enables the

determination of overall 'scale factors' of relative gravimeters (section 2.2.4). Staircase calibration lines are used to determine periodic errors in LCR meters (section 2.3.2).

Micro-nets

The most precise networks are those measured (usually indoors) particularly in association with absolute observations. An example of a 'micro-net' is that at the Bureau International des Poids et Mesures (BIPM), Sèvres, where relative gravity is observed between the sites of different absolute gravity meters in the same group of buildings. The BIPM net has a range of about 1 mgal with site values determined to 0.2 μgal and is measured approximately every 4 years by groups involved in intercomparison campaigns (section 5.1).

3.6 Network Adjustments

3.6.1 The Model

The starting point of an adjustment is the observation equation, which relates the observed gravity value g_i at a site, the adjusted gravity value G_m, error ε_i, instrument drift $(a_k + b_k t)$ and scale correction factor C_f for meter f. For example

$$(1 + C_f)g_i = G_m + (a_k + b_k t) + \varepsilon_i \qquad (31)$$

Some authors use the difference between successive equations like (31) to give an expression for the gravity difference $(G_i - G_j)$ between two sites, for example

$$G_i - G_j - C(\Delta R_{ij}) - d(\Delta t_{ij}) = \varepsilon_{ij} \qquad (32)$$

where G_i and G_j are the unknown gravity values at stations i and j respectively, ΔR and Δt are the observed quantities of dial reading and time between stations. ε_{ij} is the error on the gravity interval between stations i and j. The drift d is usually considered linear but sometimes higher order factors are sought (section 2.4.4).

The g_i in equation (31) and the G_i in equation (32) have been converted from dial turns to relative gravity values using a provisional calibration function such as the one provided by the manufacturers (section 2.2.2). The adjustment model requires the assumption that the

shape of this calibration function is correct and it needs only a linear scaling correction. The methods used by the manufacturer to establish the shape and the scale of the calibration were described in section 2.2.1.

Finding the solution for the gravity values and other unknowns such as drift and scaling factors from a network is a redundant problem in that there are always more observations than unknowns, and it is solved by least squares.

Least squares estimates are 'notoriously lacking in robustness' (Chave *et al.* 1987) which means that the solution may be strongly influenced by a small number of outlying observations. For this reason it is usual to employ some form of weighting scheme, so that the observational equation [(31) or (32)] is multiplied by a term w_i which may be composed from instrument weight, observation weight, or both.

3.6.2 Robust Weighting Schemes

The nature of gravimetric field observations means that some measurements will lead to observations that will be far away from the mean. Many of these are due to events which are essentially non-random, and cannot be adequately modelled. Examples of such events are the occasional and unpredictable bad behaviour of instrument or observer, poor environmental conditions (high wind, high levels of ground noise) or unhelpful site conditions such as wobbly floors.

The simplest weighting scheme is to weight each observation with the reciprocal of its variance, but robust weighting schemes generally imply that observations far from the mean are more severely downweighted. The extreme of this is to use a 'box-car' filter, so that such observations have a weight of zero outside and one inside a chosen limit (3σ in the program DDT (section 4.4)). There are almost as many different weighting schemes as there are adjustments, so only a few methods are described here. A typical example of Huber estimation is discussed below, and another approach to dealing with outliers, as used in the Edinburgh adjustment program NETWORK, is described in detail in section 3.7.3.

Robust-M-Estimation

A form of weighting, proposed by Huber, and often used for least squares, is based on a probability density function with a Gaussian centre and Laplacian tails. Huber's 'Maximum-Likelihood' (M-) estimators minimise an arbitrary function ρ of the residuals,

rather than minimising the sum of the squared residuals. Becker (1989) describes a comparison of a 'robust-M-estimation' method to a standard least squares solution for high precision networks on a variety of scales. Depending on the form of ρ we get different estimators, for example, $\rho(z) = z^2$ gives the least squares estimator; $\rho(z) = |z|$ gives the average absolute deviation estimator. In order to minimize the effect of outlying observations, $\rho(z)$ is chosen so that

$$\rho(z) = \begin{cases} \frac{1}{2}z^2 & , \ |z| \le c \\ c|z| - \frac{1}{2}c^2 & , \ |z| > c \end{cases} \tag{33}$$

To minimise $\rho(z)$ we differentiate:

$$\varphi(z) = \frac{\partial \rho(z)}{\partial z} \quad \text{where} \quad \varphi(z) = \begin{cases} z & , \ |z| \le c \\ c \bullet \text{sign}(z), & |z| > c \end{cases} \tag{34}$$

$\varphi(z)$ is called the influence function, which shows that compared to least squares, the robust Huber estimator has a constant value outside the interval determined by the value of c. In practice, this means that the residuals greater than $\pm$ c have the same effect on the solution as those which are equal to $\pm$ c exactly (Becker 1989). The weight function of the Huber estimator is

$$\omega(z) = \begin{cases} 1 & , \ |z| \le c \\ \sqrt{\left(\frac{2c}{|z|} - \frac{c^2}{z^2}\right)} & , \ |z| > c \end{cases} \tag{35}$$

where a value of c = 1.5 gives better than 95% efficiency for outlier-free normal data (Chave *et al.* 1987). This function is plotted in Figure 3.9a.

The different filter used in the Edinburgh program NETWORK is given here for comparison with the Huber estimator, and is plotted in Figure 3.9b.

$$w_{bi} = \begin{cases} 1 & , \ \varepsilon_i^2 < 4(\sigma_f)^2 \\ \dfrac{1}{1+4\left(\dfrac{\varepsilon_i^2}{\sigma_f^2}-4\right)^2} & , \ \varepsilon_i^2 > 4(\sigma_f)^2 \end{cases}$$

ε_i is the residual and $(\sigma_f)^2$ is the instrument variance. This choice of function is discussed in section 3.7.3.

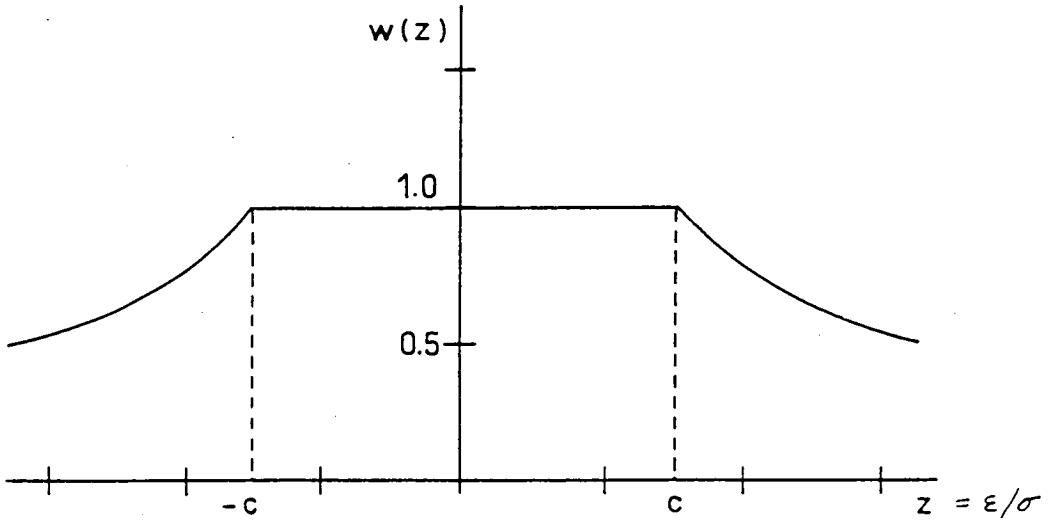

Figure 3.9a The weight function of the Huber estimator (from Becker 1989).

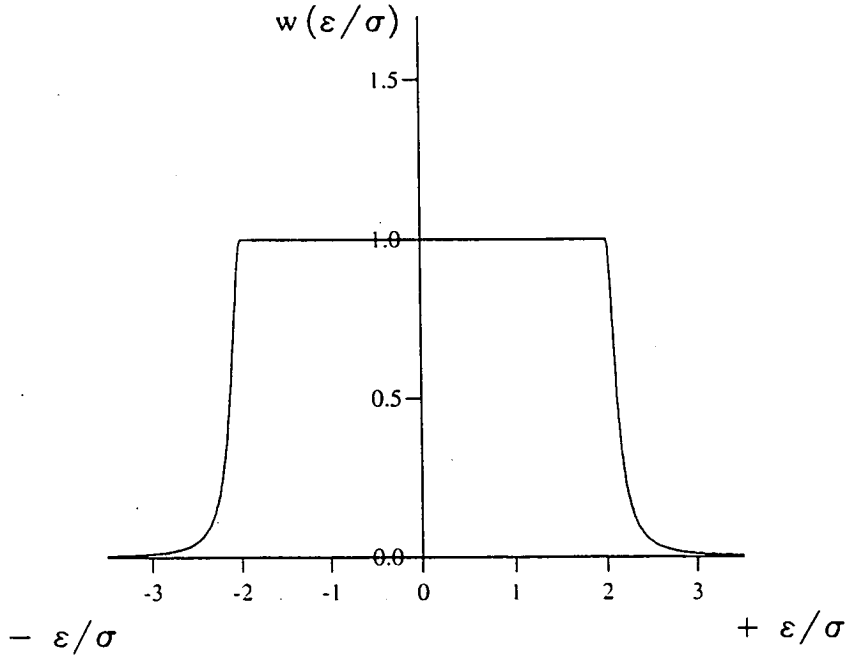

Figure 3.9b The blunder weight function used in the Edinburgh program NETWORK.

3.7 The Edinburgh Adjustment Program - NETWORK

3.7.1 Introduction

The program NETWORK and variations of it have been used for processing gravity networks of many sizes and complexity by Edinburgh University since the first version was written by Hipkin in 1973. An overview of early versions is given in Lagios (1979) and Hipkin & Lagios (1986), but here a thorough description of the philosophy of the model and of the weighting and iterative procedures will be attempted.

Before input to NETWORK, the pre-processing program REDUCE (section 3.4) converts the raw dial readings to gravity intervals using the manufacturers calibration tables, and makes earth tide, ocean loading and atmospheric pressure corrections. Two forms of output are produced : the first shows the decimal day, local time, gravity value and tidal correction, and the second forms the input to NETWORK. Tables 3.10 a and b show a sample of these files for the Teddington vertical gradient observations. Table 3.10a shows the pattern of making two or three readings at each site, and the time taken over the observations. Only the first few observations from each traverse are shown. The 'Initial gravity value' is the number assigned from the calibration function to the first (tidally corrected) gravity value of each traverse. It is then subtracted from all readings in the traverse, so making the first value zero. The atmospheric pressure correction is then added. Table 3.10b shows the arrangement of the data into nine traverses. The first line of the file gives the total number of observations (N), the number of sites (M), the site which is assigned zero gravity (M_0), the total number of traverses (K) and the number of gravity meters (F). A list of the sites follows, and then the data. The columns 'coarsedial' and 'finedial' give the actual dial readings, which are useful for identifying the individual observations.

NETWORK is designed to estimate gravity values and their uncertainty at sites connected by relative gravity meter observations. A typical example of the result of a NETWORK adjustment is given in Table 3.11. The various types of information will be discussed in the sections that follow.

Station	Decday	d	m	year	h	m	s	grav(ugal)	tide(ugal)
Jan19Tue G-275 Tedd.A VGrad1				Initial gravity value 47920.832					
30 Teddingto	33986.40694	19	1	1993	9	46	0	01.6763	-46.3570
30 Teddingto	33986.40972	19	1	1993	9	50	0	02.9277	-46.2076
30 Teddingto	33986.41250	19	1	1993	9	54	0	07.3256	-46.0720
31 Tripod Te	33986.41944	19	1	1993	10	4	0	-322.2143	-45.7962
31 Tripod Te	33986.42708	19	1	1993	10	15	0	-318.7548	-45.6003
Jan19Tue G-275 KK1-Tedd.A				Initial gravity value 47920.263					
33 KKitchen1	33986.57847	19	1	1993	13	53	0	00.4454	-54.8024
33 KKitchen1	33986.57986	19	1	1993	13	55	0	-00.6411	-54.7982
30 Teddingto	33986.58611	19	1	1993	14	4	0	83.6171	-54.6988
30 Teddingto	33986.58819	19	1	1993	14	7	0	80.4621	-54.6358
Jan19Tue G-275 KK1 V.Grad				Initial gravity value 47920.299					
33 KKitchen1	33986.70208	19	1	1993	16	51	0	-02.1363	-19.5479
33 KKitchen1	33986.70556	19	1	1993	16	56	0	-09.4990	-17.4008
34 Tripod KK	33986.70972	19	1	1993	17	2	0	-334.6815	-14.7467
34 Tripod KK	33986.71319	19	1	1993	17	7	0	-331.3674	-12.4719
Jan20Wed G-275 Tedd.A V.Grad2				Initial gravity value 47921.187					
30 Teddingto	33987.75903	20	1	1993	18	13	0	-02.2180	-03.4357
30 Teddingto	33987.76111	20	1	1993	18	16	0	-03.7669	-01.8228
32 Tripod Te	33987.76597	20	1	1993	18	23	0	-346.7154	02.0093
32 Tripod Te	33987.76875	20	1	1993	18	27	0	-345.5317	04.2400
Jan21Thur G-275 KK1-KK2-V.GradKK2				Initial gravity value 47920.004					
35 KKitchen2	33988.40625	21	1	1993	9	45	0	-00.0058	-42.7045
35 KKitchen2	33988.41042	21	1	1993	9	51	0	17.8202	-41.8557
35 KKitchen2	33988.41250	21	1	1993	9	54	0	16.1839	-41.4399
35 KKitchen2	33988.41458	21	1	1993	9	57	0	15.5951	-41.0305
33 KKitchen1	33988.41875	21	1	1993	10	3	0	17.5583	-40.2327
33 KKitchen1	33988.42153	21	1	1993	10	7	0	17.0927	-39.7180
36 Tripod KK	33988.42708	21	1	1993	10	15	0	-305.3753	-38.7346
Jan19Tue D-145 Tedd.Atri-KK1				Initial gravity value 49574.436					
31 Tripod Te	33986.57500	19	1	1993	13	48	0	00.5368	-54.7852
31 Tripod Te	33986.57708	19	1	1993	13	51	0	-01.7129	-54.7995
33 KKitchen1	33986.58403	19	1	1993	14	1	0	266.4086	-54.7474
33 KKitchen1	33986.58611	19	1	1993	14	4	0	264.9466	-54.6998
Jan19Tue D-145 KK1 V.Grad				Initial gravity value 49573.907					
34 Tripod KK	33986.70069	19	1	1993	16	49	0	-02.1259	-20.3899
34 Tripod KK	33986.70347	19	1	1993	16	53	0	-04.8142	-18.6962
34 Tripod KK	33986.70486	19	1	1993	16	55	0	-07.5970	-17.8350
33 KKitchen1	33986.70903	19	1	1993	17	1	0	332.3361	-15.1948
33 KKitchen1	33986.71042	19	1	1993	17	3	0	326.6853	-14.2962
33 KKitchen1	33986.71319	19	1	1993	17	7	0	329.9521	-12.4719
Jan20Wed D-145 Tedd.A V.Grad2				Initial gravity value 49574.884					
32 Tripod Te	33987.75903	20	1	1993	18	13	0	-02.2180	-03.4357
32 Tripod Te	33987.76111	20	1	1993	18	16	0	00.8493	-01.8228
30 Teddingto	33987.76597	20	1	1993	18	23	0	350.7274	02.0093
30 Teddingto	33987.76806	20	1	1993	18	26	0	345.8600	03.6796
Jan21Thur D-145 KK1-V.GradKK2-KK2				Initial gravity value 49577.319					
33 KKitchen1	33988.40625	21	1	1993	9	45	0	-00.0058	-42.7045
33 KKitchen1	33988.40833	21	1	1993	9	48	0	-00.9766	-42.2774
36 Tripod KK	33988.41319	21	1	1993	9	55	0	-319.7401	-41.3027
36 Tripod KK	33988.41736	21	1	1993	10	1	0	-318.8212	-40.4953
35 KKitchen2	33988.42361	21	1	1993	10	10	0	16.1797	-39.3417
Station	Decday	d	m	year	h	m	s	grav(ugal)	tide(ugal)

Table 3.10a Example of output from REDUCE showing the decimal day, local time, and the gravity value, which includes the tidal correction shown in the last column. Only the first few readings of each traverse are shown.

```
  N     M    Mo  K    F
 177    7    1   9    2
NPL,Teddington Vertical Gradients (19-21 Jan 93)
   0.0
 30   Teddington A Bld 3    TA
 31   Tripod TeddA 1158     TA
 32   Tripod TeddA 1167     TA
 33   KKitchen1 BH Bld 1    K1
 34   Tripod KK1    1103    K1
 35   KKitchen2 BH Bld 1    K2
 36   Tripod KK2    1121    K2
 Decday        grav(ugal)   m   k   f   coarsedial      finedial
 33986.40694      01.676    30  1   1   4554.70800       0.00000
 33986.40972      02.928    30  1   1   4554.70900       0.00000
 33986.41250      07.326    30  1   1   4554.71300       0.00000
 33986.41944    -322.214    31  1   1   4554.40000       0.00000
 33986.42708    -318.755    31  1   1   4554.40300       0.00000

 33986.57847      00.445    33  2   1   4554.66200       0.00000
 33986.57986     -00.641    33  2   1   4554.66100       0.00000
 33986.58611      83.617    30  2   1   4554.74100       0.00000
 33986.58819      80.462    30  2   1   4554.73800       0.00000

 33986.70208     -02.136    33  3   1   4554.63200       0.00000
 33986.70556     -09.499    33  3   1   4554.62300       0.00000
 33986.70972    -334.681    34  3   1   4554.31200       0.00000
 33986.71319    -331.367    34  3   1   4554.31300       0.00000

 33987.75903     -02.218    30  4   1   4554.70100       0.00000
 33987.76111     -03.767    30  4   1   4554.69800       0.00000
 33987.76597    -346.715    32  4   1   4554.36900       0.00000
 33987.76875    -345.532    32  4   1   4554.36800       0.00000

 33988.40625     -00.006    35  5   1   4554.62600       0.00000
 33988.41042      17.820    35  5   1   4554.64200       0.00000
 33988.41250      16.184    35  5   1   4554.64000       0.00000
 33988.41458      15.595    35  5   1   4554.63900       0.00000
 33988.41875      17.558    33  5   1   4554.64000       0.00000
 33988.42153      17.093    33  5   1   4554.63900       0.00000
 33988.42708    -305.375    36  5   1   4554.33200       0.00000

 33986.57500      00.537    31  6   2   6437.40000    1884.41000
 33986.57708     -01.713    31  6   2   6437.40000    1884.38000
 33986.58403     266.409    33  6   2   6437.40000    1888.07000
 33986.58611     264.947    33  6   2   6437.40000    1888.05000

 33986.70069     -02.126    34  7   2   6437.40000    1883.21000
 33986.70347     -04.814    34  7   2   6437.40000    1883.15000
 33986.70486     -07.597    34  7   2   6437.40000    1883.10000
 33986.70903     332.336    33  7   2   6437.40000    1887.74000
 33986.71042     326.685    33  7   2   6437.40000    1887.65000
 33986.71319     329.952    33  7   2   6437.40000    1887.67000

 33987.75903     -02.218    32  8   2   6437.40000    1884.32000
 33987.76111      00.849    32  8   2   6437.40000    1884.34000
 33987.76597     350.727    30  8   2   6437.40000    1889.10000
 33987.76806     345.860    30  8   2   6437.40000    1889.01000

 33988.40625     -00.006    33  9   2   6437.40000    1888.21000
 33988.40833     -00.977    33  9   2   6437.40000    1888.19000
 33988.41319    -319.740    36  9   2   6437.40000    1883.79000
 33988.41736    -318.821    36  9   2   6437.40000    1883.79000
 33988.42361      16.180    35  9   2   6437.40000    1888.38000
```

Table 3.10b Example of the output from REDUCE which forms the input to NETWORK. Only the first few readings of each traverse are shown (see text).

Iteration 11 χ^2 = 7.946 with 14 degrees of freedom

RMS weighted error of the adjustment = 3.85 µgal
RMS error for meter 1 unweighted = 3.11 µgal, weighted = 3.84 µgal
RMS error for meter 2 unweighted = 6.42 µgal, weighted = 3.85 µgal

Scale factor used for meter 2 = 1.0004230

Base	Gravity (µgal)	s.e (µgal)	Weight	Observations
30 Teddington A Bld	000.0	0.6	36.085	32
31 Tripod TeddA 1158	-343.5	1.7	19.847	20
32 Tripod TeddA 1167	-348.0	1.9	7.718	12
33 KKitchen1 NPL1	- 83.7	1.3	54.609	57
34 Tripod NPL1 1103	-412.4	1.8	17.743	20
35 KKitchen2 NPL2	- 83.1	1.9	17.023	19
36 Tripod NPL2 1121	-414.5	1.9	13.638	17
				Total 177

Traverse	Estimated drift function a_k (µgal)	+/- s.e(a_k) (µgal)	b_k (µgal day^{-1})	+/- s.e(b_k) (µgal day^{-1})
1	024.2	2.8	166.275	026.913) * days
2	083.3	1.5	079.432	026.751) * days
3	077.4	2.0	266.736	041.300) * days
4	-000.3	1.8	028.493	061.008) * days
5	102.1	2.0	215.973	020.612) * days
6	345.6	3.1	368.112	059.959) * days
7	408.4	3.0	272.863	072.520) * days
8	344.5	3.3	262.179	109.375) * days
9	098.5	3.2	157.948	044.629) * days

20 residuals greater than 2 standard errors

Time (days)	Error (µgal)	Station	Traverse	Meter
33986.407	-22.5	30	1	1
33986.410	-21.7	30	1	1
33986.412	-17.8	30	1	1
33988.406	-19.0	35	5	1
33988.508	-10.4	36	5	1
33988.512	- 8.5	36	5	1
33986.596	-10.0	31	6	2
33986.658	- 9.2	33	6	2
33986.720	-11.2	34	7	2
33986.723	- 9.3	34	7	2
33986.726	12.4	33	7	2
33986.742	9.1	33	7	2
33986.744	10.5	33	7	2
33986.751	- 9.1	34	7	2
33986.753	- 8.4	34	7	2
33987.781	-12.3	32	8	2
33987.801	8.6	32	8	2
33988.406	-14.8	33	9	2
33988.408	-16.1	33	9	2
33988.465	8.4	33	9	2

Table 3.11 Example of output from NETWORK (with fixed scaling factor), for the vertical gradient sequences at NPL, Teddington, showing the a_k and b_k values.

3.7.2 Observational and Normal Equations

The observational equation has the basic form:

$$(1+C_f)g_i = G_m + (a_k + b_k t) + \varepsilon_i \qquad (36)$$

where g_i is the observed gravity, G_m is the adjusted gravity value at the site m, a_k and b_k are the constant and linear terms describing the drift during the k^{th} traverse and $(1 + C_f)$ is the multiplying correction to the provisional scale factor for gravity meter f with respect to the primary instrument. The whole equation is multiplied by a weight w_i and the arrays α, β, and γ as follows.

$$w_i g_i = \sum_m (\alpha_{im} w_i) G_m + \sum_k (\beta_{ik} w_i)\, a_k + \sum_k (\beta_{ik} w_i t_i)\, b_k - \sum_f (\gamma_{if} w_i g_i)\, C_f + w_i \varepsilon_i \qquad (37)$$

where

w_i = weight for observation i

α_{im} = 1 if i^{th} observation is at site m

β_{ik} = 1 if i^{th} observation is on traverse k

γ_{if} = 1 if i^{th} observation is with meter f ($\gamma_{if} = 0$ for f=1)

otherwise the α, β, and $\gamma = 0$

The set of observational equations (42) can be represented in matrix form as

$$\mathbf{y} = \mathbf{G}\mathbf{x} + \boldsymbol{\varepsilon}.$$

where $\mathbf{y}$ is a vector of n observations, $\mathbf{x}$ is a vector of u unknowns (the G_m, a_k, b_k, and C_f) and $\mathbf{G}$ is an $n \times u$ matrix which relates the observations to the unknowns. $\mathbf{G}$ is sometimes called the model matrix, or the design matrix in the case where the optimal design of a network is sought before any observations are made.

The variance follows from the sum of the $\Sigma(\omega_i \varepsilon_i)^2$:

$$\sum_i (\omega_i \varepsilon_i)^2 = \sum_i \left(\omega_i g_i - \sum_m \omega_i \alpha_{im} G_m - \sum_k \omega_i \beta_{ik} a_k - \sum_k \omega_i \beta_{ik} b_k t_i + \sum_f \omega_i \gamma_{if} C_f g_i \right)^2 \qquad (38)$$

The least squares principle requires $\Sigma(\omega_i \varepsilon_i)^2$ to be minimised, so the normal equations are found by differentiating $\Sigma \varepsilon_i^2$ with respect to each of the unknowns in turn:

$$\frac{\partial}{\partial G_{m'}}\sum_i(\omega_i\varepsilon_i)^2=0$$ so there are *M* equations (m' = 1, 2, ..., M) of the form

$$\sum_i\left(\omega_i g_i-\sum_m\omega_i\alpha_{im}G_m-\sum_k\omega_i\beta_{ik}a_k-\sum_k\omega_i\beta_{ik}b_kt_i+\sum_f\omega_i\gamma_{if}C_fg_i\right)\omega_i\alpha_{im'}=0 \qquad (39)$$

$$\frac{\partial}{\partial a_{k'}}\sum_i(\omega_i\varepsilon_i)^2=0$$ so there are *K* equations (k' = 1, 2, ..., K) of the form

$$\sum_i\left(\omega_i g_i-\sum_m\omega_i\alpha_{im}G_m-\sum_k\omega_i\beta_{ik}a_k-\sum_k\omega_i\beta_{ik}b_kt_i+\sum_f\omega_i\gamma_{if}C_fg_i\right)\omega_i\beta_{ik'}=0 \qquad (40)$$

$$\frac{\partial}{\partial b_k}\sum_i(\omega_i\varepsilon_i)^2=0$$ so there are another *K* equations of the form

$$\sum_i\left(\omega_i g_i-\sum_m\omega_i\alpha_{im}G_m-\sum_k\omega_i\beta_{ik}a_k-\sum_k\omega_i\beta_{ik}b_kt_i+\sum_f\omega_i\gamma_{if}C_fg_i\right)\omega_i\beta_{ik'}t_i=0 \qquad (41)$$

and

$$\frac{\partial}{\partial C_f}\sum_i(\omega_i\varepsilon_i)^2=0$$ so there are (*F* - *1*) equations (f' = 1, 2, ..., F - 1) of the form

$$\sum_i\left(\omega_i g_i-\sum_m\omega_i\alpha_{im}G_m-\sum_k\omega_i\beta_{ik}a_k-\sum_k\omega_i\beta_{ik}b_kt_i+\sum_f\omega_i\gamma_{if}C_fg_i\right)\omega_i\gamma_{if'}g_i=0 \qquad (42)$$

Note that the m' (k' and f') terms define which $G_{m'}$ ($a_{k'}$, $b_{k'}$, and $C_{f'}$) the differentiation is with respect to. The unprimed m, k and f within the brackets are the indices which are being summed over. There are M + 2K + F - 1 normal equations for the M + 2K + F - 1 unknowns, where M is the number of sites, K the number of traverses, and F is the number of gravity meters. Because the sum of the first M normal equations is equal to the sum of the next K equations, the 'M + K' th equation can be determined from the difference between the sum of the first M equations and the sum of the next K - 1 equations. Therefore there are only M + 2K + F - 2 independent equations and one more condition is required to enable the problem to be properly determined. The constant drift term for the first traverse is set equal to zero i.e $a_1 = 0$, so that there are now M + 2K + F - 1 independent equations.

The set of normal equation (39) to (42) can be written as

$$\mathbf{Ax = B} \qquad (43)$$

The unknowns (G_m, a_k, b_k, and C_f) in the vector **x** are now related by the normal equation matrix **A**, which implicitly contains the conditions that arise from the differentiations, and the vector **B**.

The diagonal elements of the matrix **A** contain the 'squared' terms like $\sum(\omega_i\alpha_i)^2$, etc and the off-diagonal elements contain the 'cross' terms like $\sum(\omega_i\alpha_i\beta_i t)^2$ etc.

The effect of the arrays α, β, and γ (equation 37) mean that there are lots of zeros in the matrix **A**, and since **A** is symmetric, each observation affects only 10 elements of the matrix. Figure 3.10 illustrates the form of the matrix **A** and indicates the values of the 10 elements updated for observation i, at base m, on traverse k, with meter f. The program NETWORK computes only these 10 necessary additions, rather than carry out the full summations of equations (39 - 42), greatly increasing the efficiency compared with a general least squares algorithm.

The constraint $a_1 = 0$ is acheived by overwriting the m + 1 th row and column [$\mathbf{A}_{(i,m+1)}$ and $\mathbf{A}_{(m+1,i)}$] with zeros, overwriting $\mathbf{B}_{(m+1)}$ with zero and then reassigning the diagonal element $\mathbf{A}_{(m+1,m+1)}$ to enforce $a_1 = 0$.

The vector **B** contains the observations of gravity and time, weighted as appropriate. The solution (i.e the elements of **x**) is found by inversion of **A** since

$$\mathbf{x}=\mathbf{A}^{-1}\mathbf{B} \qquad (44)$$

The errors on the adjusted quantities are the product of the elements of $\mathbf{A}^{-1}$ with the root mean square error (σ) of the adjustment (section 3.7.4).

Residuals

The drift equation ($a_k + b_k t_i$) can be solved for each traverse to correct the observed gravity g_i for drift. The residual ε_i is the difference between the drift-corrected observed g_i and the solution for G_m for site m, i.e

$\varepsilon = \mathbf{y} - \mathbf{G}\mathbf{x}$ and the variance is $\sum(\omega_i\varepsilon_i)^2$.

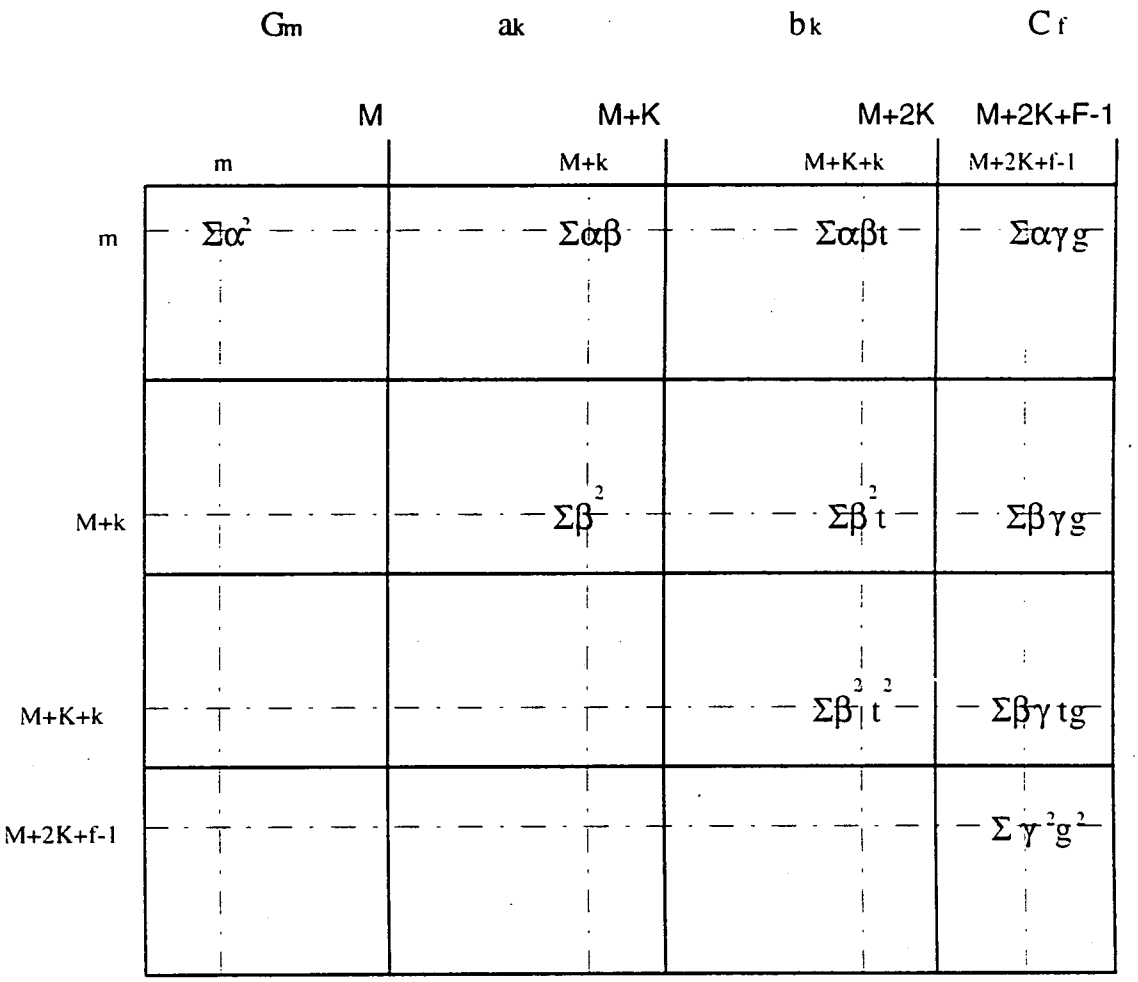

Figure 3.10 The normal equation matrix **A**, showing the 10 elements updated for an observation at base m, on traverse k, with meter f. Columns 0 to M contain the site gravity values G_m, columns M to M+K contain the drift constants a_k, columns M+K to M+2K contain the linear drift coefficients b_k and the columns M+2K to M+2K+F-1 contain the scale correction factors C_f. All the elements should be multiplied by ω^2, but these are omitted from the diagram for clarity.

3.7.3 Weighting

The weights w_i are chosen with two objectives in mind and are the product of two factors i.e $w_i = w_f\, w_{bi}$ where w_f is a 'meter weight' which normalizes observations made with different instruments and w_{bi} is a 'blunder weight' which suppresses outliers. The two will be treated separately to start with, so the discussion of the 'meter weight' assumes no blunders.

Meter weight w_f

If there are N_f observations with meter f, and the residual of observation i made with meter f is $(\varepsilon_i)_f$ then the unweighted standard deviation is σ_f and the unweighted variance is given by

unweighted variance for meter f

$$(\sigma_f)^2 = \frac{1}{N_f} \sum_{i=1}^{N_f} (\varepsilon_i{}^2)_f \qquad (45)$$

If each residual f is weighted with $1/\sigma_f$, the weighted standard deviation is σ_{wf} and the weighted variance is given by

weighted variance for meter f

$$(\sigma_{wf})^2 = \frac{1}{N_f} \sum_{i=1}^{N_f} \left(\frac{(\varepsilon_i)_f}{\sigma_f} \right)^2 \qquad (46)$$

When N_f is large, the sum over all the $\Sigma\varepsilon_i{}^2$ tends to $N_f\, \sigma_f{}^2$ and the weighted variance tends to one. i.e

$$\sum_{i=1}^{N_f} \left(\frac{(\varepsilon_i)_f}{\sigma_f} \right)^2 \rightarrow \frac{N_f\, \sigma_f{}^2}{\sigma_f{}^2} \qquad \text{and} \qquad (\sigma_{wf})^2 \rightarrow 1 \qquad \text{for large } N_f .$$

Using the weight $w_f = 1/\sigma_f$ for each meter will ensure that the residuals from each meter belong to the same population since they all have a weighted standard deviation equal to one. However, the sum of the w_f is not equal to the sum of all the observations. If we use a weight $w_f = c/\sigma_f$ where c is a constant, then the standard deviation of residuals from all the meters will still be equal, and we can choose the value of c so that the sum of weights *is* equal to the total number of observations, N, i.e

$$N = \sum_{f=1}^{F} \left(\sum_{i=1}^{N_f} \frac{c}{(\sigma_f)^2} \right)_f \qquad \text{and the constant c has the value} \qquad c = \frac{N}{\sum_{f=1}^{F} \left(\sum_{i=1}^{N_f} \frac{1}{\sigma_f{}^2} \right)_f} \qquad (47)$$

For the case when all meters have equal numbers of observations and equal σ_f ,every observation has a weight of one and $c = (\sigma_f)^2$.

Blunder weight w_{bi}

If all the residuals arose from entirely random errors, they would have a normal distribution. In practice, some errors are due to instrumental tares or observer carelessness, and these are not normally distributed. Blunders are assumed to be rare, so that the part of the combined distribution within $\pm 2\sigma$ of the mean should be dominated by random errors. The blunder distribution is assumed to be flat (all sizes of blunders have equal probability) so this dominates in the region $> \pm 2\sigma$ where the normal distribution is small. The weighting system is designed to suppress the contribution by blunders to the mean and variance of the population. A possible solution would be to set the w_{bi} equal to 0 in the region outside $\pm 2\sigma$, and this would eliminate the blunders completely. A disadvantage of this approach is that during subsequent iterations, an observation labelled as a blunder with a zero weight cannot be 'brought back into play' with full weight if the mean of the distribution changes so that the 'blunder limits' move. The solution will then be erratic. A more flexible condition is to use a smoother filter, so that blunders have a much reduced rather than zero weight. For the assignment of initial weights, the total observation weight, w_i is reduced from the value 1 if $(\varepsilon_i^2/\ \sigma^2)$ is greater than 4. The use of a quartic decay (equation 49) gives a smoothly tapering function for the blunderweight, which makes the convergence of the solution less erratic than with a step function. The w_{bi} function was plotted in Figure 3.10b.

$$w_{bi} = \frac{1}{1 + 4\left(\frac{\varepsilon_i^2}{\sigma_f^2} - 4\right)^2} \qquad \text{for } \varepsilon i2 > 4\,(\sigma f)2 \tag{49}$$

$$w_{bi} = 1 \qquad \text{for } \varepsilon_i^2 < 4\,(\sigma_f)^2$$

Combined meter weight and blunder weight

Now that we know how many blunders there are for each meter f we can produce an expression for the combined weight $w_i = w_f\ w_{bi}$ for the general case where there will be some blunders.

If we assign blunderweights w_{bi} (observation weights), but not a meter weight, the sum of the blunder weights with meter f is:

$$N_{bf} = \sum_{i=1}^{N_f} (w_{bi})_f \tag{50}$$

and the expression for the unweighted variance for meter f (equation 45),

$$(\sigma_f)^2 = \frac{1}{N_f} \sum_{i=1}^{N_f} (\varepsilon_i^2)_f \quad \text{becomes} \quad (\sigma_f)^2 = \frac{1}{N_{bf}} \sum_{i=1}^{N_{bf}} (w_{bi}\varepsilon_i^2)_f \tag{51}$$

unweighted variance for meter f with blunderweights

If we assign blunderweights *and* a meter weight $w_f = c/(\sigma_f)^2$ as defined earlier,

$$(\sigma_{wf})^2 = \frac{1}{N_f} \sum_{i=1}^{N_f} \left(\frac{(\varepsilon_i^2)_f}{\sigma_f^2} \right) \quad \text{becomes} \quad (\sigma_{wf})^2 = \frac{1}{N_{bf}} \sum_{i=1}^{N_{bf}} \left(\frac{(c\, w_{bi}\varepsilon_i^2)_f}{\sigma_f^2} \right) \tag{52}$$

weighted variance for meter f with blunderweights

The *total* weight for observation i is given by $w_i = (c\, w_{bi})/\sigma_f^2$, where c is redefined so that the sum of the weights of all observations equals N_b (the sum of all the blunderweights) rather than N (the total number of observations).

$$c = \frac{N_b}{\sum_{f=1}^{F} \left(\sum_{i=1}^{N_f} \frac{w_b}{\sigma_f^2} \right)} \tag{53}$$

or

$$c = \frac{N_b}{\sum_{f=1}^{F} \left(\frac{N_{bf}}{\sigma_f^2} \right)} \quad \text{since} \quad N_b = \sum_{i=1}^{N} w_{bi} .$$

Effect of blunderweighting on the BPGN adjustment

The adjustment of the 2175 observations of the British Precise Gravity Network (Chapter 6) with and without allowing blunderweighting is shown in Table 3.12.

description	iter'n no	χ^2	rmsadj µgal	rms G275	rms D145	rms D154
With Bweight	11	10.39	7.9	5.1	12.1	17.7
No Bweight	7	14.83	12.2	8.5	16.5	20.5

Table 3.12 Network adjustment of BPGN with and without blunderweighting.

The method of blunderweighting improves the rms of the solution from 12.2 to 7.9 µgal. solution. Without blunderweighting, the solution converged after 7 iterations.

3.7.4 The RMS error

The root mean square error is also called the standard error of unit weight. The mean square error is the mean of the sum of the squared errors or the variance:

$$\sigma^2 = \frac{\sum \varepsilon_i^2}{N} \qquad (54)$$

If the errors have been weighted and the weighting also normalises the effect of the different instruments, we have seen that the weight w_i can take the form $w_i = (c\, w_{bi})/(\sigma_f)^2$. Because the total distribution of residuals is made up of a normal population of random errors and a flat but 'thin' distribution of blunders, calculating the variance s^2 from the total distribution will not give a very good estimate of the true variance σ^2 of the population of random errors. In calculating the rms error, we need to minimise the contamination by blunders. We can make an estimate of the root mean square residual from

$$s^2 = \sum_{i=1}^{N} \frac{w_i\, \varepsilon_i^2}{N_b} \qquad \text{with} \qquad w_i = \frac{c\, w_{bi}}{\sigma_f^2} \,. \qquad (55)$$

N_b is the total sum of blunderweights for all meters: $N_b = \sum_{i=1}^{N} w_{bi}$.

Testing the first estimate of σ^2 *by fitting the population of residuals to a normal distribution*
The goodness of this estimate is found by dividing the residuals into 16 classes having equal width of $\sigma/4$ in the range where $w_{bi} = 1$, that is $|\varepsilon_i| \leq 2s$, and comparing the distribution of these residuals with those predicted by a normal distribution. Because the standard deviation is being estimated from a 'trimmed' population ($-2s \rightarrow +2s$), the total number of observations in this range must be multiplied by a factor (greater than one) to give the total size of an

equivalent normal population and make an unbiased prediction of the normal distribution frequencies. The value of this factor is derived as follows:

For the normal distribution, the probability distribution $p(x - \mu)$ is given by

$$p(x-\mu) = \frac{1}{\sqrt{(2\pi\sigma^2)}} \exp\left\{-\frac{(x-\mu)^2}{2\sigma^2}\right\} \tag{56}$$

and the probability that x lies within $\pm 2\sigma$ of the mean is given by

$$\int_{-2\sigma}^{2\sigma} p(x-\mu)\, dx \tag{57}$$

which can be found from tables of the Normal distribution, and has the value 0.954 499. This means that about 95% of the residuals lie in this range for the theoretical distribution. The number of observations expected in each quarter sigma class of a normal distribution can also be worked out from tables of $p(x- \mu)$. The values for the two largest and two smallest classes are given in Table 3.13.

class	probability
$\mu + 0.00$ to $\mu + 0.25\sigma$	0.098705
$\mu + 0.25\sigma$ to $\mu + 0.50\sigma$	0.092755
⋮	⋮
$\mu + 1.50\sigma$ to $\mu + 1.75\sigma$	0.026335
$\mu + 1.75\sigma$ to $\mu + 2.00\sigma$	0.017720

Table 3.13 Probabilities that residuals fall into each of the classes of width $\sigma/4$ for a theoretical normal distribution. Only the two largest and two smallest classes in the range μ to $\mu + 2\sigma$ are shown.

To find the number in each class these probabilities are multiplied by the total number of observations in the theoretical Normal distribution. The number of real observations lying within the whole of Normal curve is not known, but can be predicted because 95% of them lie within $\pm 2\sigma$. The total number of observations in this range is divided by 0.954 499 (equation 57) to give the total size of the equivalent normal population. We can now compute the theoretical number in each class and compare it with the actual number. We use χ^2 to measure the correspondence between the theoretical and actual distributions.

Finding the best fit using χ^2

The criterion χ^2 is used to measure the misfit of the actual distribution of the residuals to a theoretical normal distribution:

$$\chi^2 = \sum \frac{(\text{actual} - \text{theory})^2}{\text{theory}} \qquad (58)$$

The most probable value of χ^2 is equal to the number of degrees of freedom , i.e the number of independent variables. For 16 classes ($\pm 2\sigma$ divided in to width $\sigma/4$) there would be 15 degrees of freedom, since we know the mean. We have also assigned the standard deviation, so in this case the remaining number of degrees of freedom is 14. In defining 'acceptable' values of χ^2, the author has followed the reasoning of Fisher (1954) :

'If (the probability that χ^2 exceeds a specified value) is between .1 and .9 there is certainly no reason to suspect the hypothesis tested. If it is below .02 it is strongly indicated that the hypothesis fails to account for the whole of the facts. We shall not often be astray if we draw a conventional line at .05 , and consider that higher values of χ^2 indicate a real discrepancy.'

The ranges of P between 0.90 to 0.10 and 0.95 to 0.05 probability points are the 80% and 90% Confidence Intervals (C.I), respectively, for the value of χ^2. An alternative criterion often used for χ^2 is that it should lie between $n \pm \sqrt{n}$ (where n is the number of degrees of freedom). These (rather tighter) limits are shown, for comparison, with the 80% and 90% C.I, for n=14 in Table 3.14 for 14 degrees of freedom.

P	χ^2	χ^2 for $n \pm \sqrt{n}$
0.95	6.57	
0.90	**7.79**	10.26
0.10	**21.06**	17.74
0.05	23.69	

Table 3.14 Probability points of the χ^2 distribution for the 80% and 90% C.I for n= 14 degrees of freedom, and an alternative criterion for 'acceptable' χ^2 using $n \pm \sqrt{n}$.

Condition for convergence and choice of iteration

The condition for convergence of the weighting scheme in the program NETWORK is that the new rms (σ) is almost equal to the rms of the previous iteration (σ_0):

$$\left| \left(1 - \frac{\sigma_0}{\sigma} \right) \right| < 0.001 \qquad (59)$$

In any case, the adjustment is stopped after twelve iterations. The 'best' iteration is the one having the smallest σ of those with acceptable χ^2. In the case of equal σ, the χ^2 closest to the number of degrees of freedom is chosen. An acceptable χ^2 is one in the 80% C.I.

An alternative test was that the weighted rms error (equation 52) for all the meters should be equal. Although this is no longer used as a convergence condition, the values are still monitored, and are usually insignificantly different at the final iteration.

Improving the test to allow for the Blunder population (IR FACTOR)

It was found that iterative adjustments tended to converge with quite unsatisfactory values of χ^2 (Hipkin & Lagios 1986). A large sample of about 2000 observations from the British Precise Gravity Net (Chapter 6) will be used to illustrate this test. The convergence of an adjustment (with fixed scaling factor) is shown in Figure 3.11a. The value of the rms weighted error of the adjustment (σ) (top figure) and the value of χ^2 (lower figure) are plotted against iteration number. Only iterations 2, 3 and 4 have acceptable values of χ^2, i.e values which lie between 7.79 and 21.1 (the 80% confidence interval). These are marked with squares. Iteration 11 has a χ^2 of 48.1.

Because the estimate s of the variance may be contaminated by the presence of blunders, which in the first iteration have not been downweighted, a search was made after each iteration for the value of s which gave the best fit of the true normal distribution to the residuals. This is a reasonable method because most of the residuals within $\pm 2\sigma$ of the true mean *will* be normally distributed. The search covers a range of 50% either side of the starting point, and χ^2 is calculated for each new estimate of σ. A minimum χ^2 is sought for values of the factor $\phi = \sigma / s$ in the range $0.5 < \phi < 1.5$. After the best estimate of σ is found, blunderweights are assigned to all residuals with $\varepsilon_i^2 > 4(\phi\sigma_f)$. The convergence of the adjustment of the same dataset as above, with this extra condition, is shown in Figure 3.11b. Now all but the last iteration have acceptable values of χ^2.

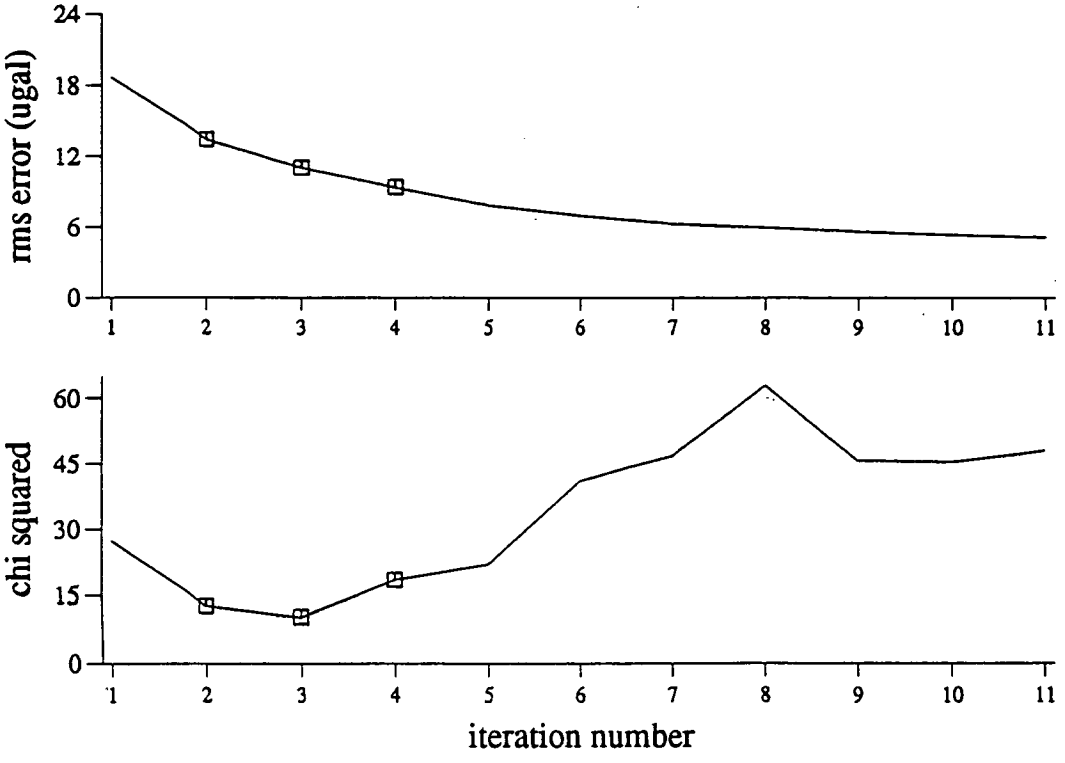

Figure 3.11a The convergence of an adjustment (with fixed scaling factor) of about 2000 observations produces unsatisfactory values of χ^2, demonstrating that the population of residuals is far from normally distributed.

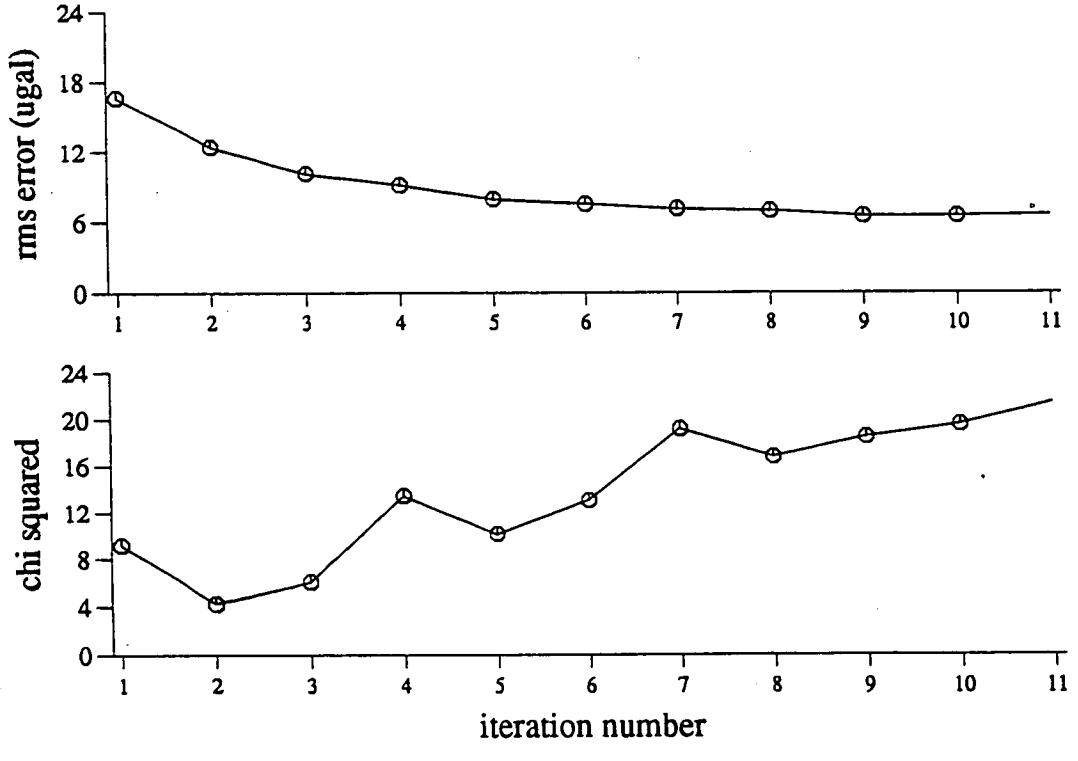

Figure 3.11b Convergence of the same data after search for a σ between 0.5 and 1.5 times the original estimate s of the standard deviation, with a minimum χ^2.

3.7.5 Modifications to NETWORK for small datasets

Introduction

When adjusting small datasets (less than about 150 observations), the convergence using the sophisticated procedure above was often unsatisfactory. Having only a small population means that the number of blunders may be proportionally higher than that for a large population, so the distribution of residuals is particularly 'un-normal'. There is also the possibility of fitting too many unknowns (scaling factors etc) to not enough data points.

Caution : The datasets discussed here are used only to illustrate the effect of modifications to the adjustment procedure of the program NETWORK. Where results, given in this section, for gravity ex-centres and vertical gradients, differ from those in Chapter 5, the Chapter 5 version should be taken as definitive. Reasons for the (usually only marginally significant) differences are various, for example different scaling factors, typos, data excluded, different combinations of data run in the same adjustment etc..

Fixing the scaling factor C_f

The instrument scaling factors for all instruments with respect to the primary instrument are usually determined during the network adjustment. However, many small datasets, for example a set of vertical gradient or ex-centre observations cover only a small range of gravity (about 400 and 1000 µgal respectively). As well as the possibility of 'overfitting' the data, there is the more significant problem that the instrument scaling factor cannot be well determined from a group of observations covering such a small range of gravity. In order to avoid the possibility of the gravity values determined by these small adjustments being undesirably influenced by incorrect solutions for C_f, this factor was held fixed for all 'small' (vertical gradient and ex-centre) adjustments, at the value determined by the adjustment of the whole of the BPGN (range about 900 mgal).

This condition was arranged by overwriting the appropriate elements of the normal equation matrix **A** with zeroes (section 3.7.2) before the inversion, and specifying the fixed predetermined value to be used instead.

The effect of fitting the scaling factor or holding it fixed for two ex-centre adjustments are described below. The Taunton ex-centre dataset consists of only 61 observations, and has a relatively small maximum gravity difference of 218 µgal. The Kings Buildings dataset has 151 observations and has a maximum gravity difference of 1085 µgal.

When the scaling factor is fitted as a free parameter to the Taunton observations, convergence is complete after only 7 iterations but the χ^2 value is lower than the 80% confidence interval (Table 3.14). With a fixed scaling factor, the χ^2 is generally more acceptable, and the rmse of the 'best' iteration is smaller (Table 3.15a). This is achieved by downweighting 31 observations compared with only 1 from the free solution, out of a total of 61. The 'fixed' solution would be preferable on the grounds of having a more acceptable χ^2 and a lower rms.(Table 3.15b)

	Fixed C_f			Free C_f		
iter	χ^2	rms µgal	n > 2σ	χ^2	rms µgal	n > 2σ
1	4.82	3.1	20	5.08	5.7	1
2	2.36	4.0	14	5.59	5.8	1
3	4.23	2.8	22	5.66	6.1	1
4	9.61	4.2	13	4.87	6.1	1
5	9.51	4.6	8	**6.07**	**5.7**	**1**
6	4.73	3.4	18	4.87	5.7	1
7	4.57	2.6	21	4.87	5.7	1
8	9.99	4.0	15	-	-	-
9	5.50	3.4	18	-	-	-
10	13.00	1.6	36	-	-	-
11	**11.68**	**1.5**	**31**	-	-	-

Table 3.15a Comparison of the convergence of the Taunton ex-centre observations with a fixed and free scaling factor for D145. There are a total of 61 observations.

	Iteration **11**		Iteration **5**			
Scale factor C_f for D145	1.000 4230 (fixed)		1.030 3269 ± 0.016 6402		Difference (fixed - free)	
	g(µgal)	se	g(µgal)	se	(µgal)	se
Taunton Abs	0.0	1.1	0.0	2.6	0.0	2.8
Loading Bay	218.5	1.1	222.5	2.7	-4.0	2.9
Water Tank	121.0	1.2	126.6	2.5	-5.6	2.8

Table 3.15b Comparison of the solution from the 'best' iterations of the fixed and free adjustments in Table 3.13a. The 'fixed' solution has a more acceptable χ^2 and a lower rms.

For the KB ex-centre data, both the fixed and free solutions produce acceptable χ^2 showing that the residuals can be successfully fitted to a normal distribution. The KB example has a 151 observations compared with Taunton which has only 61, and it also includes

observations from a third LCR meter. The proportion of downweighted observations is similar for the fixed and free solutions of the KB data (38 and 23 observations respectively). The final rmse is smaller for the fixed solution, but it has a less optimal χ^2 than the free solution. The difference between the resulting gravity values is barely significant. The convergence of the KB ex-centre adjustments is shown in Table 3.16a, and the 'best' solution (shown in bold) is given in Table 3.16b.

	Fixed C_f			Free C_f		
iter	χ^2	rms μgal	n > 2σ	χ^2	rms μgal	n > 2σ
1	11.28	7.9	12	10.46	9.0	8
2	15.29	7.5	12	13.11	7.2	13
3	14.66	6.9	13	7.30	5.2	25
4	14.92	6.9	12	**13.90**	**5.0**	**23**
5	14.82	2.9	60	7.75	4.7	24
6	14.56	3.9	44	6.65	4.5	25
7	13.28	3.1	53	7.59	4.6	25
8	8.03	4.1	40	6.42	4.6	25
9	9.85	4.3	36	6.33	4.6	25
10	**9.75**	**4.1**	**38**	5.75	4.6	25
11	7.69	4.9	25	-	-	-

Table 3.16a Comparison of the convergence of the King's Buildings ex-centre observations with a fixed and free scaling factors for D145 and D154. There are a total of 151 observations.

	Iteration **10**		Iteration **5**			
Scale factor C_f for D145	1.000 4230 (fixed)		1.015 8787 ± 0.002 9244		Difference (fixed - free)	
Scale factor C_f for D154	1.000 6751 (fixed)		1.009 1374 ± 0.004 0185		Difference (fixed - free)	
	g(μgal)	se	g(μgal)	se	(μgal)	se
GI 140	0.0	2.7	0.0	2.6	0.0	3.7
JCMB	-804.5	3.1	-807.6	2.7	3.1	4.1
Car Park	-1084.2	2.6	-1088.5	2.4	4.3	3.5
BGS Abs	-534.3	2.5	-535.3	2.3	1.0	3.4

Table 3.16b The best iterations of the fixed and free adjustments (Table 3.16a) have insignificantly different solutions.

Convergence for small populations

The methods of section 3.7.4 for determining the rms error generally work satisfactorily for datasets with at least 150 observations. For smaller populations, the adjustment scheme may fail either because the division of the residuals into sixteen 'quarter-sigma' classes is too many classes for the small number of observations, or because the search for a better fit to a normal distribution is inappropriate for a small population. Two alternative models were tried for small datasets. The first was to reduce the number of classes by half, so there were 8 classes of width half-sigma. and 6 degrees of freedom. The second was to exclude the search, so that $\phi = 1$ always (see *'Improving the test to allow for the Blunder population'* in 3.7.6 above). The probability points of the χ^2 distribution for 6 and 14 degrees of freedom for the 80% and 90% confidence limits are given in Table 3.17.

n	0.95	**0.90**	**0.10**	0.05
6	1.64	2.20	10.65	12.59
14	6.57	7.79	21.06	23.69

Table 3.17 Probability points of the χ^2 distribution for the 80% and 90% C.I. for 6 and 14 degrees of freedom.

The two methods described above were tested on some small (ex-centre and vertical gradient) datasets. The vertical gradient data for Edinburgh GI is discussed as an example.

The original vertical gradient observations at Edinburgh GI140 form a 'small' dataset with a relatively large number of blunders (about 50 from a total of 118 observations). The convergence of the four possible adjustments for this dataset is shown in Figure 3.12.

Figure 3.12a shows the effect of reducing the number of degrees of freedom for the χ^2 test of the fit of the population of residuals to a normal distribution. The top plot shows the convergence of the rms error of the adjutment, and the bottom plot shows the variation of χ^2. The solid line is for the 'original' configuration, keeping 14 degrees of freedom, with classes of width 'quarter-sigma' (solution A). This scheme produces only three iterations with an acceptable χ^2. The dotted line shows the convergence for the solution with 6 degrees of freedom (solution B). The iterations with values of χ^2 which fall in the 80% confidence interval for the respective degrees of freedom (Table 3.17 above) are indicated with a symbol on the plot (octagons and squares for the solutions with 14 and 6 degrees of freedom respectively). The 'best' iteration is the one having the smallest rms error with a χ^2 within the 80% C.I. The 'best' iterations are shown with a solid (black) symbol.

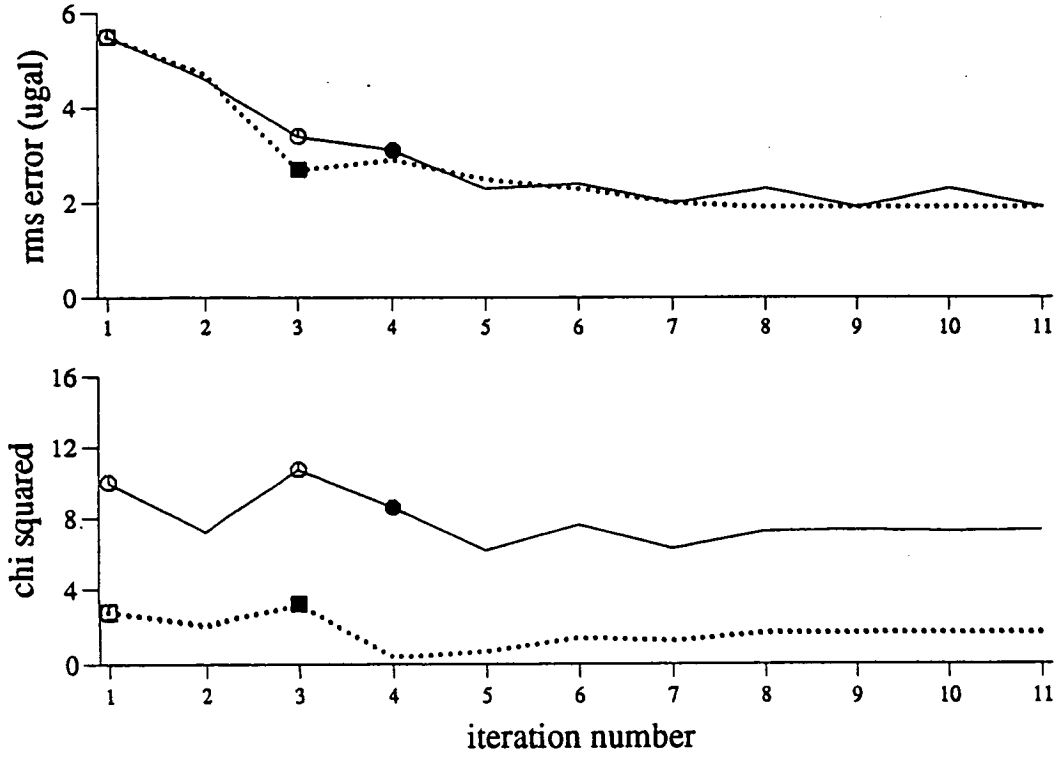

Figure 3.12a Solutions retaining the search. A (—) (14 d.f) and B (·····) (6 d.f). Acceptable χ^2 shown in symbols, 'best' iteration in black.

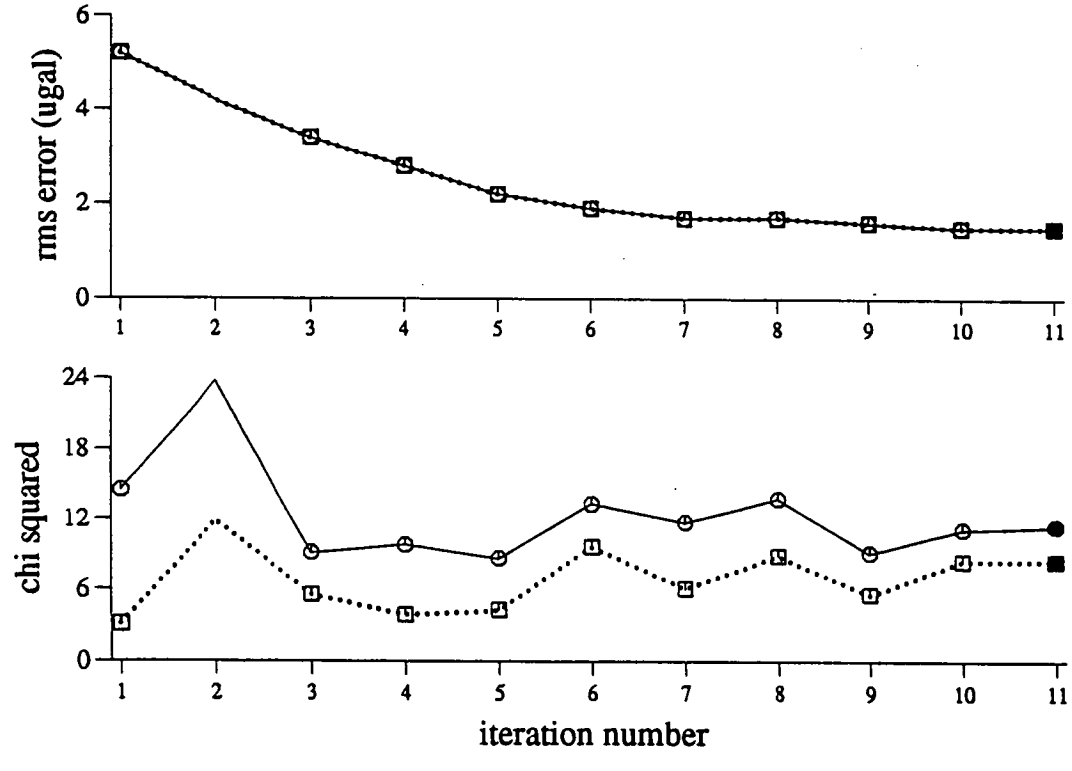

Figure 3.12b Solutions excluding the search. C (·····) (6 d.f)and D (—) (14 d.f). Acceptable χ^2 shown in symbols, 'best' iteration in black.

Figure 3.14b shows the effect of excluding the search for a best fit of the residuals to a normal distribution. Since σ is therefore the same at each iteration, the convergence of the rms error is identical for the 14 (solid line) and 6 (dotted line) degrees of freedom cases. The solutions (C and D respectively) are identical apart from the value of χ^2 . Forcing the rms weighted error of the adjustment to stay equal to the estimate of equation (55) produces many more iterations with 'acceptable' χ^2. The convergence of χ^2 is not quite identical because there is more freedom in distributing the residuals amongst a larger number of classes. In both cases, the solution with the smallest rms error (iteration 11) also has an 'acceptable' χ^2 (black symbols). 54 of the 118 residuals are larger than twice the rms of 1.5 μgal.

The gravity results of the best iteration in each case are shown in Table 3.18. The solutions are insignificantly different except for the value at Tripod 1512 where the difference between solutions A and C is 2.5 ± 1.7 μgal. The convergence of C and D, however, is better (Figure 3.12b), showing that forcing a population with a high proportion of blunders to fit a normal distribution is inappropriate.

μgal	GI Floor	GI Abs	Table 0755	Tripod 1135	Tripod 1512
A 14 deg. free.	0.0 ±1.1	1.4 ±1.1	-220.4 ±1.6	-334.0 ±1.0	-447.9 ±1.5
B 6 deg. free.	0.0 ±0.9	0.6 ±1.0	-221.6 ±1.4	-334.4 ±0.9	-448.2 ±1.3
C/D no search	0.0 ±0.5	1.4 ±0.5	-220.9 ±0.8	-334.3 ±0.5	-450.4 ±0.8

Table 3.18 Gravity solutions for the alternative adjustments for the small dataset of the Edinburgh GI vertical gradient results. Solutions A and B retain the search for a best fit to a normal distribution, but the residuals are divided into 16 classes of width $\sigma/4$ for A, and eight classes of width $\sigma/2$ for B. Solutions C and D result from excluding the search so that the rms weighted error is equal in both cases, and the gravity solutions are therefore identical.

Conclusions for small datasets

It is unwise to use an over-sophisticated adjustment procedure for small datasets. In general there is a risk of 'over-fitting' i.e squeezing too much information from a small and therefore un-representative population. In particular, the 'search for a best fit to a normal distribution' is not appropriate for data which does not adequately approximate a normal distribution, either because there are not enough observations, or because the proportion of blunders is too large. For datasets with a large proportion of blunders (> 1/3), some of the modified schemes described above produce significantly better convergence.

3.8 Summary and Conclusions

The Earth resides in a potential field which is due to the combined effects of the moon, the sun, its own mass and its rotation. Because it is not solid, it responds to the forces generated by the potential by changing shape. This causes gravity on the surface of the Earth to vary in a complex but predictable way with time. Different methods of calculation of the tide-generating potential give small differences in the tidal correction of generally less than 0.5 μgal. Various formulae for the magnitude of the static tide give answers differing by a few μgal, but different conventions regarding the correction of gravity for it lead to confusion and error.

The fluid oceans respond in a more complicated way to the influences of the tide-generating potential and the shape of the ocean basins. Mathematical models give estimates of the loading effect of the ocean tides on the continents, but more accurate values can be obtained by analysing long records obtained by Earth tide gravity meters. The ocean load tide varies spatially but is important at the margins of continents. In Britain it is particularly large in SW England where up to 12 μgal of the tidal signal is due to the load tide. The ocean load correction has been implemented for relative and absolute gravity observations.

The free nutation of the Earth's axis ("polar motion") causes a small gravity effect which varies only slowly over several months, but is important when comparing values of absolute gravity from different epochs. The Newtonian attraction of the mass of the atmosphere has a small effect on gravity observations and the effect of the atmospheric pressure over the local zone (within a 50 km radius of the site) is generally about -0.3 μgal per millibar. The regional and global direct and loading effects can be modelled but are much smaller and are not usually considered.

Groundwater variations can cause significant variations in gravity (up to a few tens of μgal) at the surface, due to the direct attraction of the water and displacement of the ground surface. The effect is difficult to monitor without borehole information, so sites where it is likely to be large, for example on porous rocks, in regions where there are aquifers or significant extraction, or near rivers, tanks and lakes, are best avoided.

Once the raw observations have been reduced to equivalent quantities of gravity, some form of statistics is needed to find the best solution and some indication of its validity. The common use of a portable mass on a spring for measuring gravity differences means that the effects of the instrument and of the structure imposed by the sequence of field observations must be modelled. The observation equation which relates the observed quantity, the instrumental effects (drift and calibration), and the true gravity at a particular site forms the

basis for the model. By travelling backwards and forwards between the same two sites and repeating the observations, the values of the difference in gravity observed between successive visits can be used to monitor the drift of the instrument. The repetition of observations also provides some redundancy so that a useful estimate of the statistical reliability of the solution can be obtained.

Because the model does not exactly describe the reality, each observation has an error associated with it, and the solution which minimises the sum of the squares of all these errors (the least-squares method) is sought. The condition of least-squares allows the construction of the normal equation matrix. The solution for gravity, the drift and the calibration is found by inverting the normal equation matrix. The residuals of the solution show which observations gave values far from the mean and they can be downweighted before repeating the adjustment. The nature of gravity observations requires the use of robust methods which reduce the contamination of the solution by these outlying observations.

The quality of the solution is measured by the root mean square (rms) error of the adjustment. This is influenced by the combination of the populations of residuals from the different insruments and constraints on the model such as fitting the instrumental scale calibration factors and assigning initial parameters. The use of 'normal' or 'Gaussian' statistics on data which contains non-normal observations (blunders) gives unsatisfactory results. In this case it is necessary to modify the standard procedure for finding the rms error.

Small datasets are inherently less normal than large ones, especially if they also have a large blunder population. The sophisticated modifications, which improve the solution for a large population, increase the risk of overfitting when the population is small. The adjustment should be simplified for small datasets.

Reliable adjustments of high quality relative observations are important for the densification of national and international First Order networks. The International Gravity Standardisation Network (IGSN71) is a global adjustment which includes early absolute observations and approximately 20 000 relative observations. It improved on the previous standard of the Potsdam System (adopted in 1909 with a relative accuracy estimated at ± 3 mgal) by assigning gravity values globally with an accuracy of about ± 0.1 mgal. The increasing quantity of precise absolute gravity measurements is leading to new adjustments requiring equally reliable adjustment procedures and relative observations.

CHAPTER 4. Absolute Gravimetry - Instrumentation and Theory

4.1 Historical Development

4.1.1 Introduction

The earliest observations of absolute gravity were made with pendulum instruments. This type of measurement is obsolete and absolute gravimetry is based on measuring the acceleration of freely falling masses. Figure 4.1 shows how the accuracy of absolute gravity measurement has increased by more than four orders of magnitude during the last 300 years. The FG5-103 absolute gravity meter is operated by the Natural Environment Research Council of the UK. The author has studied data from this instrument in depth (Chapter 5) and used absolute values from it to control relative gravity observations in Britain (Chapter 6). The aim here is review its origins and to briefly describe the other types of absolute gravimeters which currently contribute to international gravity measurement programmes. The emphasis is on the particular benefits and limitations of each type and the accuracy and precision achieved in normal use.

4.1.2 Ruler-Dropping Experiments

In 1952, Volet was probably the first to measure absolute gravity precisely by dropping a graduated bar. The bar was observed through a reference graticule in an optical system. Flashes of light, equally spaced in time, generated images of the graticule and the graduations which were recorded on photographic film. The rods were usually about 1 metre long and fell through a few metres. Some details of similar experiments are given in Torge (1989). The largest error source was in the measurement of distance which was badly affected by inclinations and rotations of the ruler during the fall. Although performed at reduced pressures (10^2 Nm^{-2}), the early experiments were significantly degraded by the effect of air resistance. To overcome this, some experiment were designed so that the rulers fell inside another falling body, or by dropping in various degrees of vacuum (10^{-2} to $<10^{-3}$ Nm^{-2}). In general, estimated precisions of these experiments (c. 1951 - 1969) were between 1 and 2 milligals, but the actual values obtained were later found to be up to about 6 milligal larger than the true value.

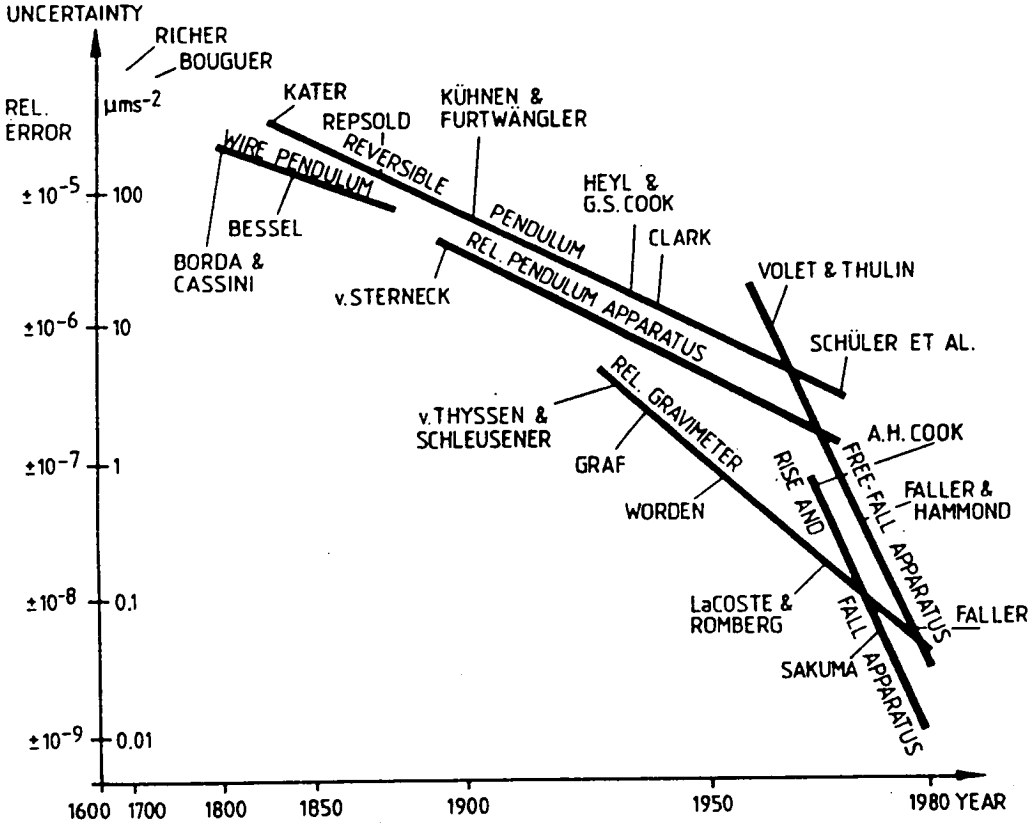

Figure 4.1 Increase in the accuracy of terrestrial gravimetry, 1600 - 1980. (Figure 1.1 of Torge (1989))

4.1.3 Rise and Fall Instruments

Introduction

The rise-and-fall method is in principle the best way to minimise the relatively large effects of air resistance and reduces possible systematic effects in timing, but is technically more difficult to achieve than free fall.

The equation for determining g from these experiments is

$$g = \frac{8H}{T_2^2 - T_1^2} \qquad (1)$$

where H is the vertical distance between the measurement stations, T_2 and T_1 are the times between the passage of the body through the bottom and top stations respectively in its upward and downward flight (Figure 4.2).

Cook

Cook (1967) successfully produced a rise-and-fall apparatus whose 'test mass' was a glass ball. The ball passed through the gaps in two glass blocks arranged vertically above one another (Figure 4.3). Light produced at a slit on one side of the gap was focused by the ball onto a detector on the other side. The separation of the blocks was measured by arranging their horizontal surfaces to form part of a Fabry-Perot interferometer. The throwing chamber was evacuated to 0.15 Nm^{-2}. The ball could be fired at intervals of 2 - 3 minutes, and by averaging about 100 experiments the error of the result was reduced to 130 μgal, and the accuracy estimated at 100 μgal.

NSL, Sydney

The National Standards Laboratory in Australia (Gibbings *et al.* 1971) launched a corner cube reflector by pneumatic means in a rise-and-fall instrument to measure the time and position simultaneously in a white light interferometer. Rays of light from the moving corner cube were reflected at the top and bottom of a length standard bar in the form of a cylindrical tube of fused silica. When the optical path of the rays from either end of the bar was equal to the optical path through the corner reflector, the recombined rays formed an interference pattern. 51 determinations made over a period of three days gave a value of gravity with a standard deviation of 190 μgal.

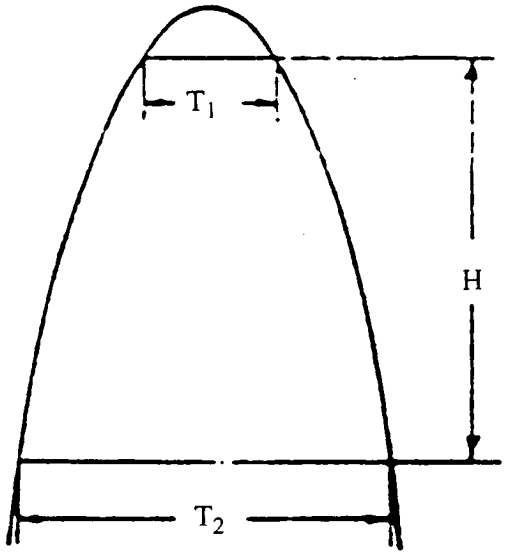

$$g = \frac{8H}{T_2^2 - T_1^2}$$

Figure 4.2 Rise and fall trajectory. H is the vertical distance between the measurement stations. T_2 and T_1 is the time between the passage of the body through the bottom and top stations respectively in its upward and downward flight

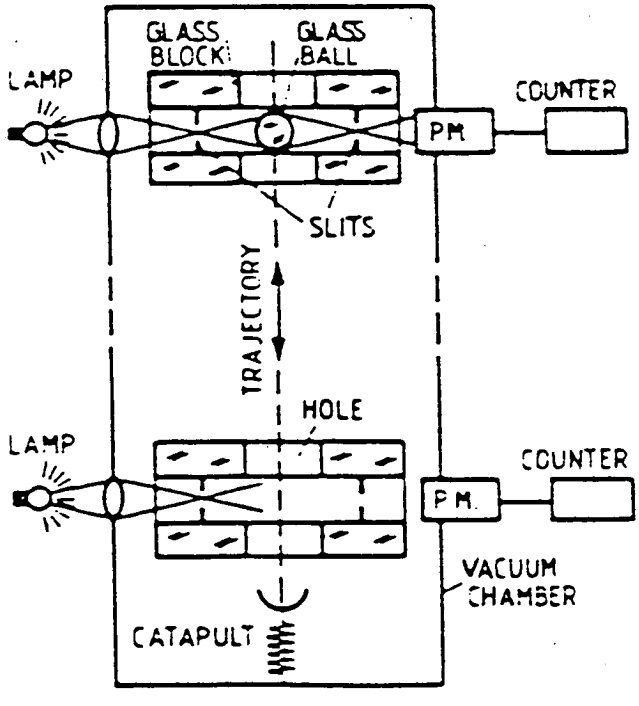

Figure 4.3 Schematic diagram of Cook's rise-and-fall apparatus. (Figure 5.8 of Torge (1989))

Sakuma (BIPM)

Sakuma first developed an instrument with very high precision (1 - 10 μgal) in 1963. His original design has undergone continuous improvement and has resulted in a remarkably continuous record of precise absolute gravity observations at the Bureau International des Poids et Mésures (BIPM) Sèvres ever since. A cornercube reflector forms one mirror of a Michelson type interferometer, and it is thrown upwards by means of an 'elastic band' catapult in a vacuum of ~ 10^{-5} Nm^{-2}. The distance between the two fringe-producing devices in the trajectory is measured with the interferometer, by comparing the distance with an iodine-stabilised He-Ne laser length standard. The microseismic noise is damped by a long-period seismometer, and the reference reflector is suspended by a similar seismometer.

IMGC

The Istituto di Metrologia "G.Colonnetti" (IMGC), Torino, developed a transportable rise-and-fall instrument which was constructed in co-operation with BIPM. It has been used since 1976 on many stations world-wide (Alasia *et al.* 1982). Gravity is measured by means of a technique for bi-directional counting of the interference fringes. Two photomultipliers detect the fringes produced in the interferometer with a He-Ne laser. The fixed corner cube of the interferometer is attached to a long-period seismometer to isolate it from ground noise. The instrument was converted from a two-position instrument to a multi-position instrument in about 1987. Currently (1994) the IMGC meter achieves precisions of about 1 μgal and reoccupation accuracies of < 5 μgal (Marson 1994). A new IMGC instrument is under development.

Jaeger GA60

The Jaeger / GA60 was the first commercially available rise-and-fall instrument. It was developed from the IMGC prototype and manufactured by the French company Jaeger S.A. The corner cube reflector is projected vertically about 40 cm, and its position is observed continuously by means of an iodine-stabilised laser interferometer using a sub-nanosecond time digitiser (Sakuma 1983). A total of about 1300 relative position-time measurements are used for a least-squares fit of the best trajectory for each throw. All the data recording and processing is controlled by a microprocessor. The microprocessor calculates the value of gravity at a well-defined height, the value of the vertical gradient of gravity throughout the trajectory and a proportional factor which relates the air resistance to the velocity of the reflector. During operation 20 measurements of g can be made by a semi-automatic

procedure in 1 hour. Normally about 8 -10 sets of 12 measurements each are sufficient to give a standard deviation of less than 1 part in 10^8 of g. The GA60 No.2 was used to establish six absolute gravity stations in the French gravity network. Another GA60 is operated by the Geographical Survey Institute in Japan. GA60 type instruments participated in the first (1981) and fourth (1994) Inter Comparisons of Absolute Gravimeters (ICAG) at Sèvres (section 5.1).

4.1.4 Free-Fall (Dropping only) Instruments

Hammond-Faller

The Hammond-Faller instrument (Hammond and Faller 1967) was the first transportable free-fall absolute gravimeter and it measured on eight stations of the World Gravity Network in 1968/69. The falling corner cube forms the movable arm of a Michelson type interferometer and generates fringes at a range of 4 to 20 MHz during a drop of 1 metre. By counting the number of fringes that have been produced at two points in the trajectory, the initial velocity as well as the value of gravity can be determined. The mass is transported up the evacuated dropping tube by a carriage, and held by a magnetic field immediately prior to being dropped. An accuracy of better than 5 parts in 10^8 could be achieved from 100 drops made in about 1 hour. In field operations at NPL (Teddington) and BIPM (Sèvres), the residual systematic errors for an occupation (timing, non-verticality of laser beam, atmospheric drag, electrostatic and magnetic forces) amounted to about ± 50 μgal (Torge 1989). An occupation consisted of 20 to 30 sets, with 50 drops per set.

GABL

The GABL free-fall gravimeter was built by the Institute of Automation and Electrometry, USSR Academy of Sciences. It has been operated extensively in USSR and Europe since 1976 and has participated in a number of ICAGs at Sèvres (section 5.1). The falling body is a corner cube with a ferrite element with which it is held by a magnetic field before the drop. Because of a uniform distribution of electromagnetic force in the dropping region, rotations of the corner cube can be minimised during the fall. The dropping chamber is made of non-magnetic stainless steel, and the corner cube is returned to the top of the drop by an electromagnet outside the chamber. An iodine-stabilised HeNe laser is used as the length standard and interference fringes are measured at three stages of the fall. The reference corner cube is isolated by a 4 s period seismograph. A set of 100 drops take about 25 minutes. The effects of random errors can be reduced to about 4 μgal (Table 4.1), and the

systematic errors are of similar magnitude. The accuracy of the gravity value is ± 10 μgal (Torge 1989).

NAOM and GSI

Two institutes in Japan, the National Astronomical Observatory, Mizusawa (NAOM) (formerly the International Latitude Observatory (ILO)), and the Geographical Survey Institute (GSI) have independently developed absolute gravimeters (Tsubokawa 1991).

NAOM have an original Sakuma type (Jager) gravimeter and a small number of their own transportable free-fall type, of which NAOM2 participated in the 1989 (third) Sèvres Intercomparison. The falling body is a reflector and the interferometer uses an iodine-stabilised He-Ne laser. The reflector falls through a high vacuum for a relatively short distance of 30 cm and its rotation is sensed by a two-dimensional position sensor. The interferometer is separated from the vacuum chamber to avoid mechanical coupling and a seismometer is attached to the interferometer. The NAOM have improved on this basic design by using a corner cube prism and a new dropping mechanism. A rotating vacuum pipe absolute gravimeter developed by NAOM achieved a drop-to-drop scatter of 19 μgal in 1989. This instrument measured with the NAOM2 in Antarctica (Syowa) in early 1993 (Okubo and Fukuda 1994).

The GSI instrument is a modified GA60 (Jaeger). A comparison of the GSI instrument and NAOM1 showed a discrepancy of about 60 μgal. GSI measured at Sèvres with the GA60 and FG5-104 in March 1994 as part of the fourth ICAG.

NIM

The National Institute of Metrology in Beijing, China have produced their own absolute gravimeters. NIM-I was a free-fall instrument which monitored the position of the falling mass at 3 points during its fall. It lacks an antivibration system, but showed an agreement of 20 μgal in the BIPM comparisons in 1980 and 1985 (Torge 1989). A second generation instrument, NIM-II, has measured in co-operation with the German JILA3 and the Finnish JILA5 (Houtse 1991), and obtained a standard deviation of between ± 5 and 13 μgal.

JILAG

In 1980 the Joint Institute for Laboratory Astrophysics (JILA), Colorado developed a portable free-fall instrument of which six are now in use by research institutes world-wide (section 5.1). A schematic diagram of the apparatus is shown in Figure 4.4. The wavelength of a stabilised laser provides the length standard and interference fringes are produced in a Michelson-type interferometer by a falling corner cube. Many of the features of JILA are retained in the new generation FG5, and are described fully in section 4.2. The random error on one drop of a JILAG meter is ± 30 - 300 μgal depending on the microseismic noise, and ± 10 - 20 μgal for a set of 50 to 150 drops. A site occupation of 10 - 20 sets leads to a precision of ± 1 - 5 μgal, and an accuracy of the absolute value of about 10 μgal (Torge 1989).

IGPP

The Institute of Geophysics and Planetary Physics (IGPP), Scripps Institute of Oceanography, California, developed a free fall gravimeter based on the JILAG prototype. It was designed to measure temporal gravity changes, and is more transportable than the JILA instruments. During gravity surveys of 15 sites in California in 1984/85, standard deviations of 8 - 23 μgal were obtained (Torge 1989). The IGPP team are working towards vehicle based absolute gravity meters and have tested an ocean bottom instrument (Zumberge *et al.* 1986) .

FG5

The FG5 is a new generation of JILA-type instrument which is now commercially available from Axis Instruments in Colorado. Eight FG5s are currently (1994) in operation worldwide, and data from four of these is discussed in Chapter 5. The FG5 development was steered by the JILA workers with the objective of making it easier to use by a wider scientific community, and with significant improvements in design, precision and accuracy over the JILA series. A fuller description of FG5 is given in section 4.2.

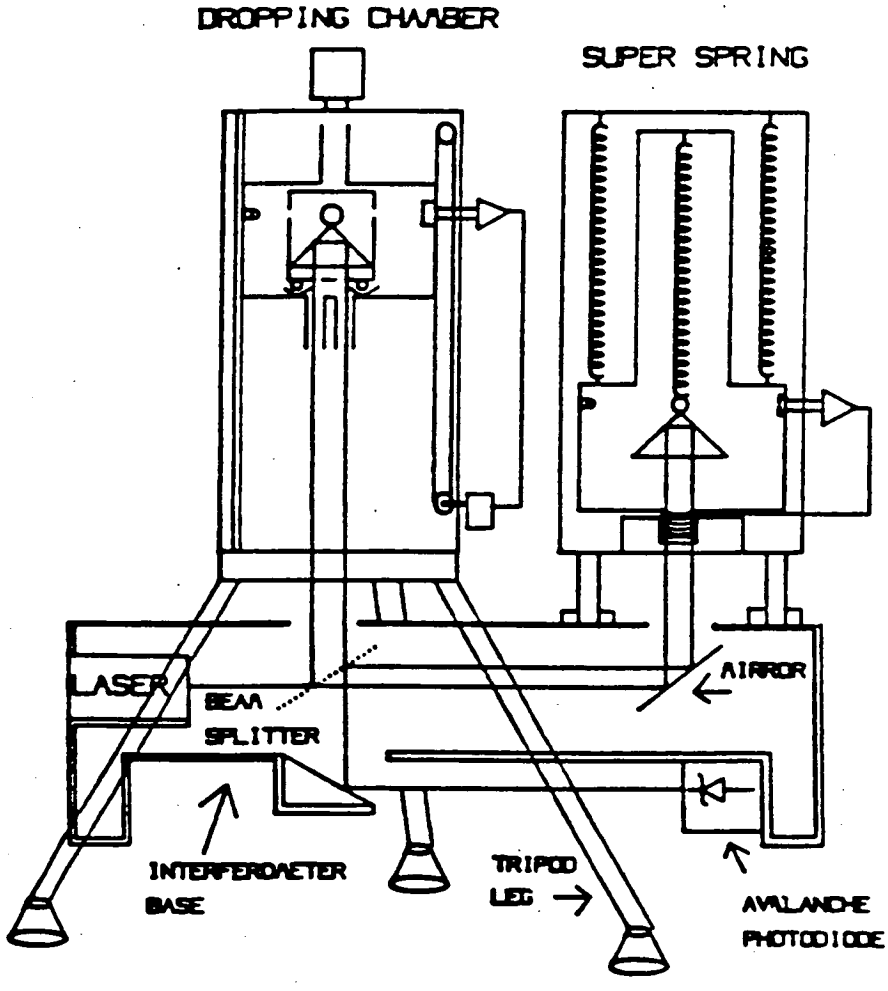

Figure 4.4 Block diagram of the JILA absolute gravity meter. (From Niebauer 1987).

4.2 FG5 - The Instrument

4.2.1 Introduction

The FG5 is an 'inline' version of the JILA design, achieved by placing the superspring directly underneath the interferometer (Figure 4.5) instead of deflecting the beam out sideways and then upwards as in the JILA (Figure 4.4). The FG5 superspring has much smaller dimensions, and the drop is also shorter. The laser is a polarisation stabilised He-Ne and can be operated in 'red' and 'blue' modes (as for the JILA laser). Most FG5 users have now replaced the original polarisation stabilised lasers with an Iodine stabilised one recently developed for field use (Chartier *et al.* 1993).

4.2.2 Test Mass and Cart

The test mass (dropped object) is a retroflective corner cube surrounded by a metal cylinder about 8 cm high and 3 cm diameter. It has an annular trim weight which can be adjusted to make the centre of mass coincide with the optical centre of the corner cube. It is enclosed in a cart which reduces the residual air drag inside the evacuated test chamber. A glass sphere is attached to the top of the cylinder and focuses light from a source on one side of the cart onto an array of photocells at the other (Figure 4.6) which serves to sense the position of the test mass with respect to the cart. The cart is attached to a stainless steel belt driven by a servo controlled motor, and travels up and down guide rods which prevent any horizontal or vertical rotation. The photocell signal is fed back to the motor so that the cart is kept in a constant position with respect to the mass during its free-fall. The cart has two holes at the bottom for the entry and exit of the laser beam, and a single hole at the top which enables the position and rotation of the mass to be monitored.

Three tungsten (very hard, non magnetic) balls on the mass sit in three radial grooves in the cart so providing a kinematic support to assist in a perfectly vertical (i.e. no rotations) 'lift-off' of the mass. The mass is 'dropped' by making the cart accelerate downwards faster than g so that the mass is 'left behind' and begins to fall freely. When the separation of the mass and the cart reaches 3 mm, the cart begins to track the mass, and this separation is maintained to ±10 μm during the drop. When a signal is sent to 'catch', the cart slows down

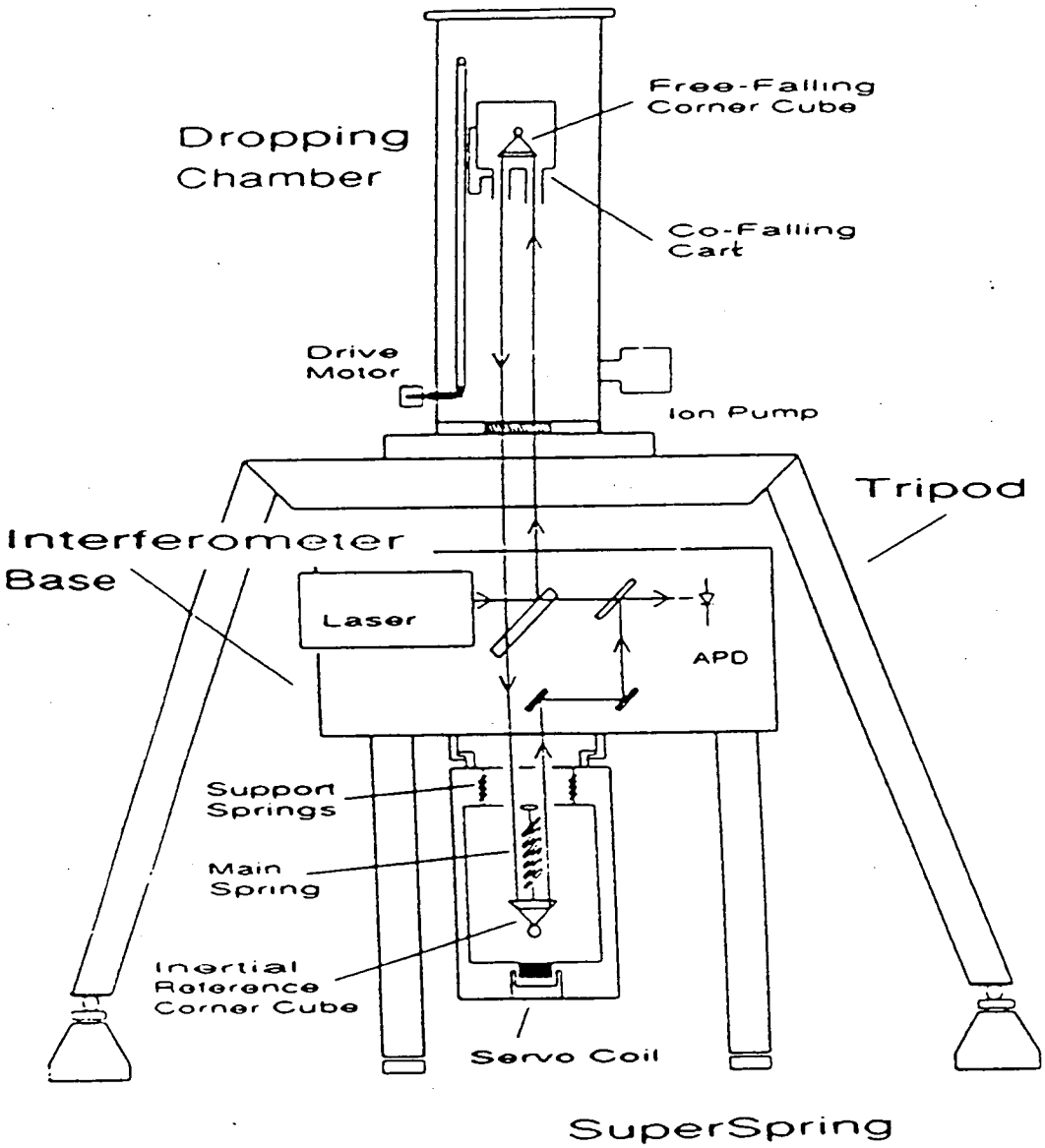

Figure 4.5 Schematic of the FG5 absolute gravity meter (redrawn from a diagram supplied by Axis Instruments, Colorado).

gradually until the mass has caught up with it and then the cart and mass decelerate together. The cart carries the mass back up to the top ready for the next drop.

The cart is attached to a stainless steel belt which is driven by a pulley at the bottom of the dropping chamber (Figure 4.5). The pulley is coupled to a motor via a ferrofluidic feedthrough. The motor has a rotary shaft encoder which counts the number of rotations of the shaft, and this is the means by which the position of the 'top of the drop' is controlled. In the JILA meters, the top of the drop is fixed by a linear position detector. In FG5, this critical parameter relies on there being no slippage of the drive belt on the pulleys, and there is no independent monitoring of the position of the mass at the top of the drop.

4.2.3 Superspring

The FG5 superspring

The super spring was developed by Rinker and Faller (Niebauer 1987) to prevent changes in the path length of the test beam due to seismic motions of the Earth. These motions, which have periods of between 3 and 6 seconds, are transmitted to reference corner cube in the interferometer via the interferometer base. A simple mass on a spring is mechanically isolated for all frequencies higher than the natural period of the mass-spring combination. A simple spring with a natural period of about 60 seconds would need to have a length of nearly 1 km! The 'super' property of the spring in the absolute gravimeters is that it can behave as if it has natural periods of between 30 and 60 seconds while being only about 20 cm long. These characteristics are achieved by the use of electronic feedback.

The super spring is essentially a mass on a spring on a mass on a spring. This configuration is sketched in Figure 4.7a. The aim is to apply a variable force to the mass m_1 which exactly cancels the inertial forces of the ground vibrations and so keeps it in a state of zero acceleration. The distance y between m_1 and m_2 will be constant if m_1 is not accelerating, so the relative position of m_1 and m_2 is sensed and fed back as a force which drives m1. In this way, m_1 tracks m_2. In practice, the reference corner cube is the bottom mass m_2, and the mass m_1 is the support housing. The main spring is contained in the support housing and connects m_2 to m_1 (Figure 4.7b). The support springs connect the housing to the interferometer base and the housing tracks the corner cube.

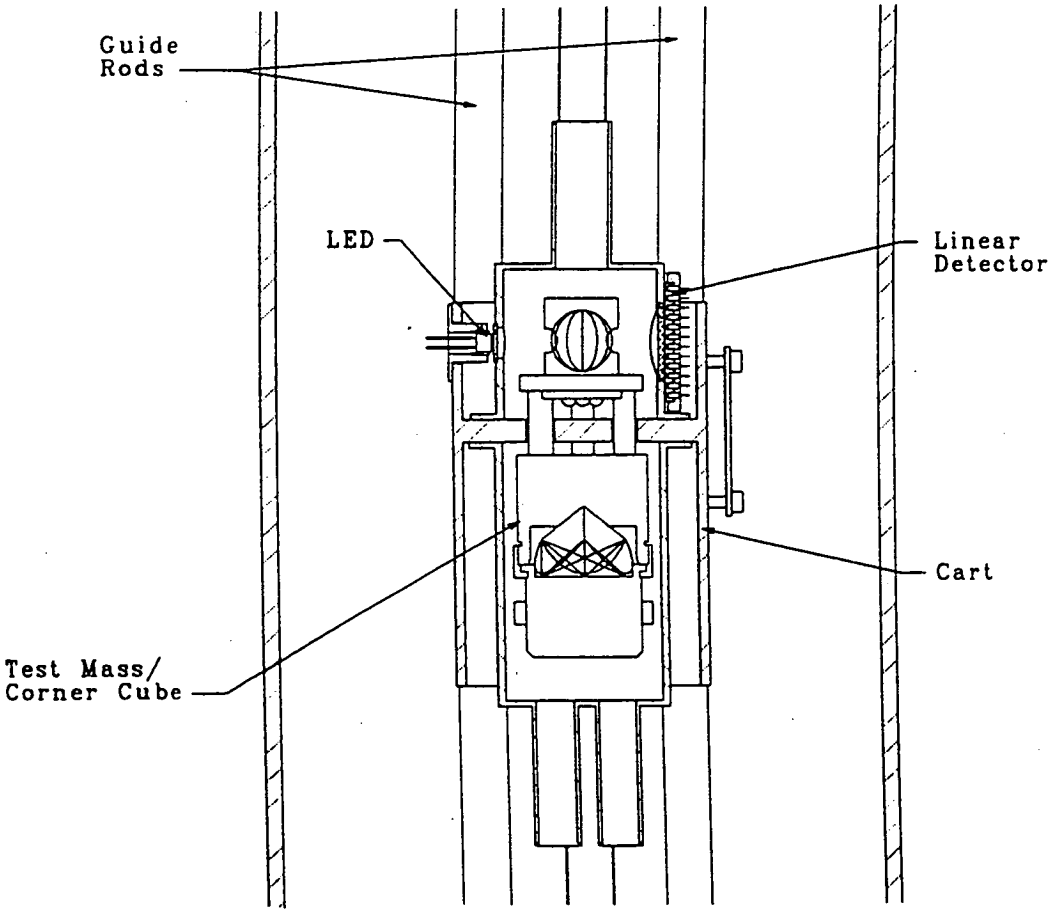

Figure 4.6 Front view of the test mass and drag-free cart assembly. The glass sphere, attached to the mass, focuses light from the LED, on one side of the cart, onto an array of photocells (Linear Detector) on the other. The cart travels up and down guide rods which prevent any horizontal or vertical rotation. The two pipes at the bottom allow entry an exit of the laser beam (Figure 2.3 of the FG5 Manual (Axis Instruments Company 1992)).

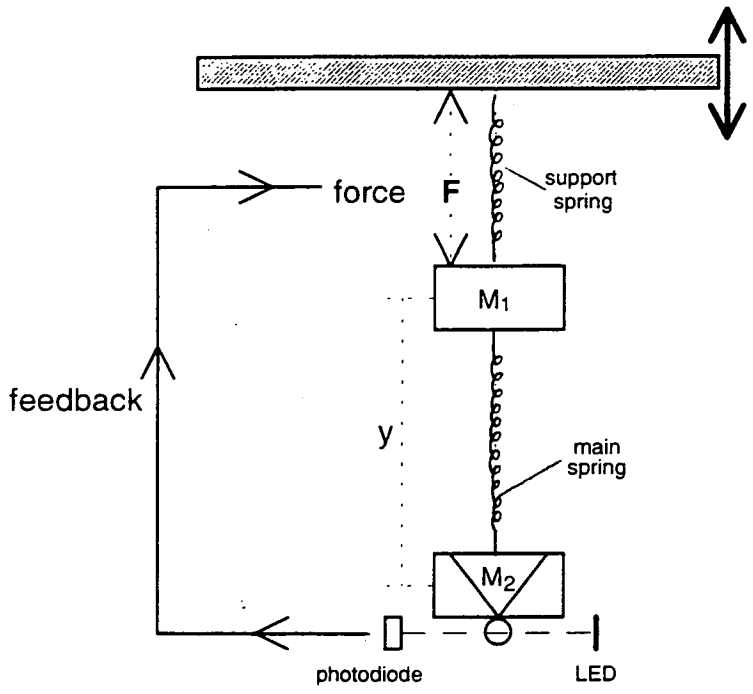

Figure 4.7a The 'mass on a spring on a mass on a spring' configuration for the FG5 superspring. The distance y is sensed and fed back as a force F which drives m_1, so that m_1 tracks m_2.

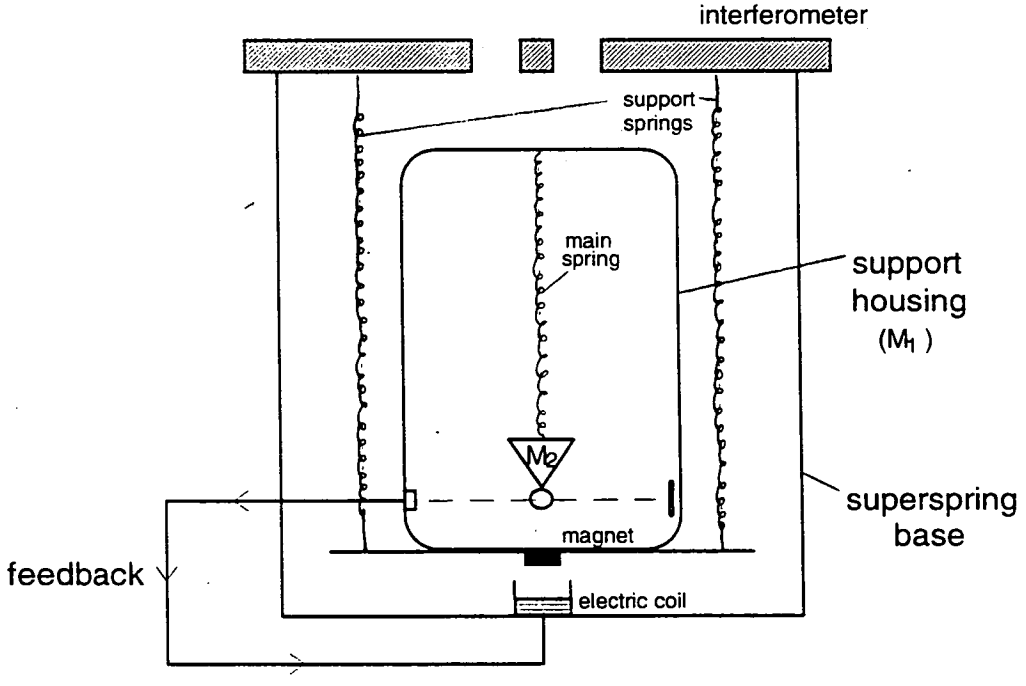

Figure 4.7b The bottom mass m_2 is the reference corner cube, and the mass m_1 is the support housing. The position of m_2 with respect to the housing is sensed and the housing is driven to cancel these motions using the magnet and electric coil.

To detect motions of the corner cube relative to the support housing, an LED located onto the support housing directs light through a glass sphere attached to the corner cube. The sphere focuses the light onto a photo diode which is also mounted on the support housing. The housing itself is driven to cancel these motions using a magnet and an electric coil mounted on the housing and the superspring base respectively. Coarse adjustments to the position of the superspring corner cube m_2 ('setting the superspring zero') can be made with a motor attached to the top of the mainspring. This is necessary to ensure that the light from the LED is focused onto the responsive part of the diode.

Performance of the FG5-103 superspring at the POL absolute gravity site

During the very first observations by FG5-103 at the Proudman Oceanographic Laboratory (POL) in August 1992, the author made a qualitative comparison of the scatter on the gravity set means with the amplitude of the contemporary seismic noise.

The seismic noise was recorded by the LCR Earth Tide meter ET13 at POL. The amplitude (in millivolts) of the trace of the chart recording the oscillations of the instrument's measuring beam was plotted against the set standard deviation for 6 days of absolute gravity measurements (POL TST01 to POL TST10). A linear relationship between the seismic noise and the standard deviation on the gravity sets was found. Without a conversion from 'chart recorder millivolts' to amplitude of seismic noise in μgal, this relationship remains qualitative. However, it shows the inability of the super spring to isolate the falling mass from ground noise such as is experienced only a mile or two from the sea. Section 5.4 describes the POL gravity data in more detail and discusses the subsequent upgrades of the FG5-103 superspring.

Noise characteristics at the Edinburgh GI absolute gravity site

The superspring is designed to eliminate seismic noise in the 0.1 - 0.3 Hertz frequency band. These frequencies are low enough not to contribute to the scatter of the parabolic fit of the time-distance data (measured by the interferometer (section 4.2.3)) over a single drop, but a leakage of electrical or mechanical noise at higher frequencies may do so. A typical ground acceleration spectrum was constructed for the GI site using a Guralp CMG-3 broad band vertical seismometer and a Reftek data acquisition system.

The microseismic noise at GI is characterised by accelerations in the frequency range 0.15 - 0.28 Hertz, having a peak amplitude of about 44 mgal at about 0.2 Hz. There is a band of noise, probably mechanically related, at 10 - 20 Hz with a peak amplitude also about 44 mgal. The 50 Hertz peak is relatively large, as would be expected of the campus environment. There is also an *un*expectedly large peak at 60 Hertz. The amplitudes of these peaks correspond to about 290 mgal in terms of ground acceleration (Charles 1994).

A qualitative estimate of the ground noise can be obtained from either the absolute or relative gravity observations. The superspring of the FG5 is designed to have a period which is long enough to damp out the microseismic frequencies, but will never do so perfectly. The drop-drop scatter of FG5 drops gives some indication of the relative magnitude of the microseismic noise (see above), and is typically between about 0.05 and 0.1 mgal.

The beam of an LCR relative gravity meter is attached to a spring (section 2.1) so it also acts as a long period seismometer. (The concept of the zero-length spring, which is now at the heart of all LCR gravity meters, was originally developed for applications to long period vertical seismometers.) As will be familiar to anyone who has measured gravity with an LCR meter, the beam oscillates at the periods close to the microseismic noise, with an amplitude which may be up to 0.8 mgal.

Both these estimates are influenced by the respective qualities of the spring-mass systems concerned, and do not indicate the unfiltered magnitude of the noise. The accelerations caused by natural and artificial seismic noise can be predicted from measurements of the ground displacement, using a simple harmonic model for the oscillations of the earth's surface. Torge (1989) suggests that for periods of about 0.2 and 5 seconds, the maximum accelerations would be about 10 and 0.15 mgal respectively. The value of 44 mgal obtained from the seismic measurements at Edinburgh is perhaps unrealistically large. The agreement between the maximum peaks in both the microseismic (0.2 Hz) and 'machinery' (10-20 Hz) bands may be an artefact of the resolution of the spectrum. The seismometer used for the measurements was actually designed to operate in the DC to 10 Hertz range, and the records obtained in the higher frequency band (10 to 20 Hertz) were amplified according to the 'roll-off' of the instrument's transfer function. The estimates of acceleration at frequencies above 10 Hertz are therefore less reliable than the ones below.

4.2.4 Interferometer

The arrangement of the optics for splitting and recombining the beam is shown in Figures 4.8 and 4.9. The laser emits a beam of 0.8 mm diameter which passes through a spatial filter to produce a more uniform beam. The spatial filter consists of a microscope and a 30 μm diameter pinhole to block out stray light (Figure 4.8). After emerging from the pinhole, the beam is collimated at 7 mm diameter and is divided at the first beamsplitter (BS1) into a reflected test beam and a transmitted reference beam of equal intensity (Figure 4.9).

The test beam is reflected vertically up through a compensator plate into the dropping chamber, where it is translated and reflected back down by the corner cube in the test mass (CC_1). It returns through the compensator plate and BS1 to the superspring corner cube (CC_2). The beam returning from the superspring is deflected by a mirror to miss BS1 and then passes through a translator plate to the second beamsplitter BS2, where it is recombined at the top surface with the reference beam. The translator plate is used to align the test beam so that it recombines properly with the reference beam.

The reference beam is transmitted through BS1 and travels straight to BS2. At BS2, half of the recombined beam is reflected off the top surface to the fringe detector. The other half of the recombined beam is transmitted through BS2 to the attenuator plate where some is directed into a periscope (Figure 4.8). This allows the fringes to be monitored by the user. The rest passes out of the interferometer base and into a collimating telescope so that the alignment of the reference and test beams can be checked.

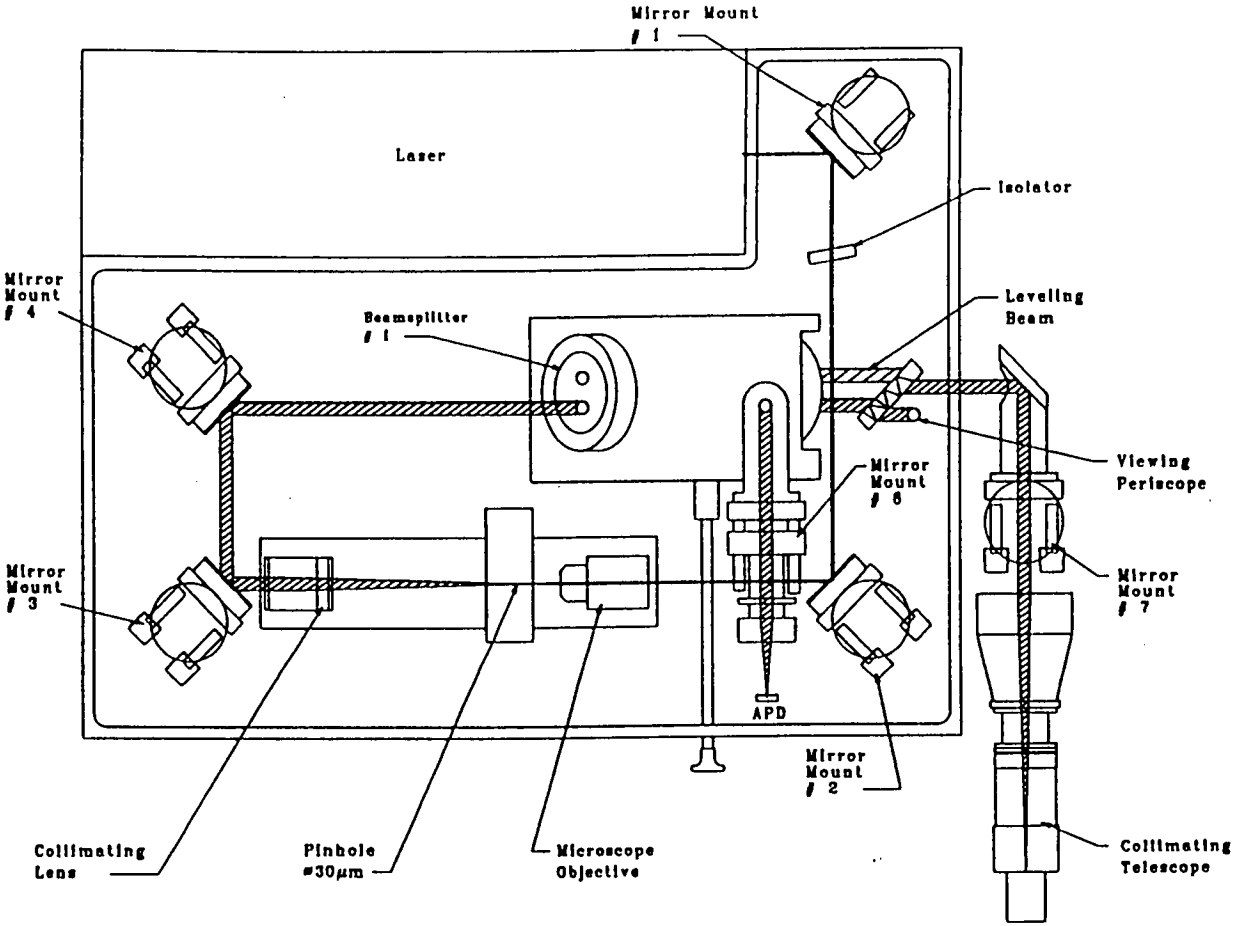

Figure 4.8 Path of the laser beam through the interferometer optics (Figure 2.7 of the FG5 manual (Axis Instruments Company 1992)). The laser emits a beam of 0.8 mm diameter which passes through a spatial filter (the microscope and the pinhole). The path of the collimated beam after reaching Beamsplitter 1 is shown schematically in Figure 4.9.

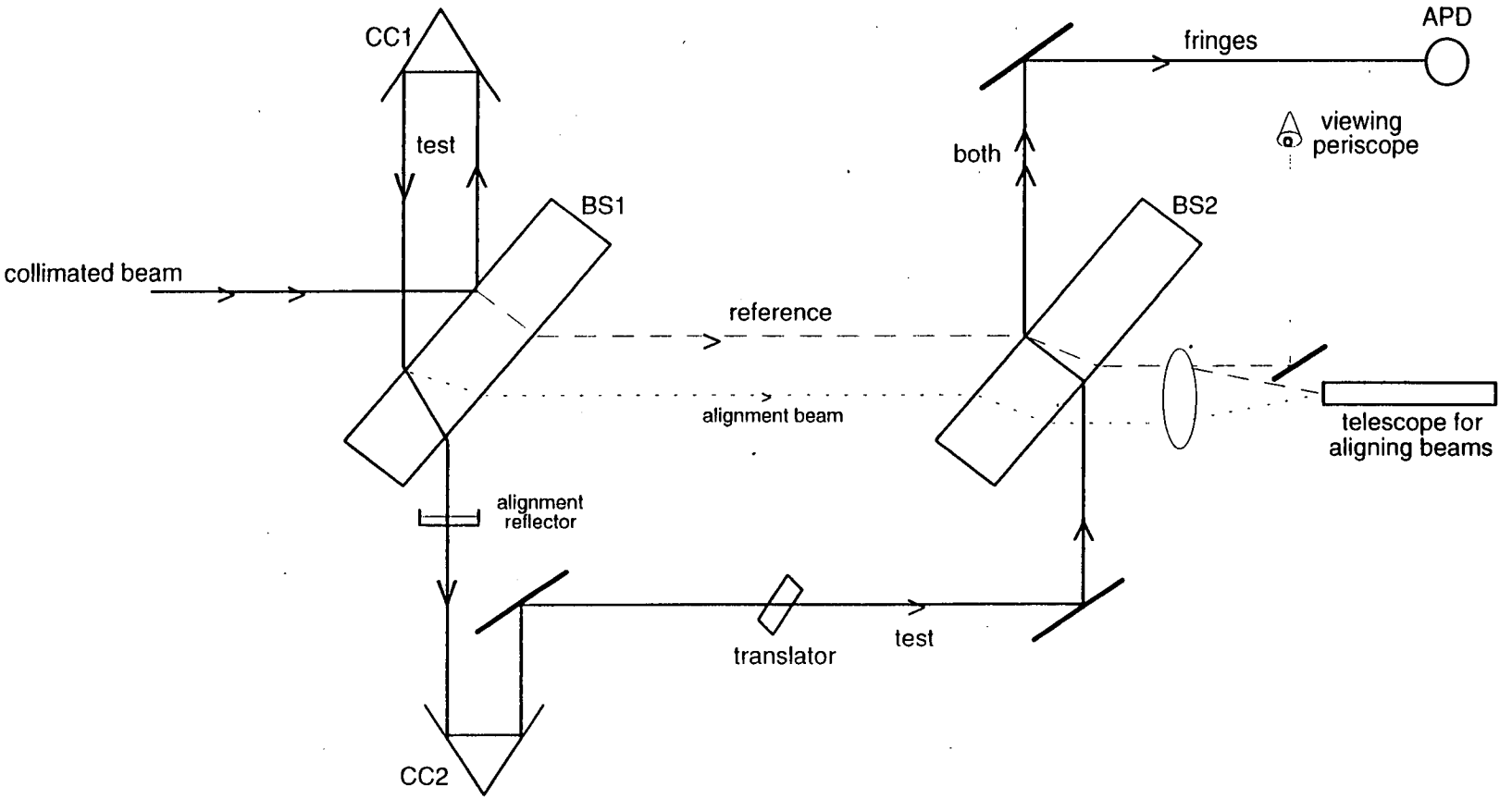

Figure 4.9 Schematic diagram of the light paths in the interferometer. CC1 is the falling corner cube, CC2 is the 'stationary' corner cube in the superspring. The alignment beam is only present when the superspring is not in place, and the temporary reflector is used to reflect to test beam into the telescope, where its alignment with the reference beam can be checked. The fringes are detected by an avalanche photo diode (APD). Figure redrawn after sketch by W. Hollander (*pers. comm.* 8 June 1992).

The verticality of the path of the test beam in the dropping chamber is checked before the superspring is in place. The alignment reflector (a pool of alcohol) is used in place of CC2 to direct the test beam (now the 'alignment beam' in Figure 4.9) into the telescope. The legs of the dropping chamber (Figure 4.5) are adjusted until the images of the reference and test beams in the telescope are coincident.

4.2.5 Lasers

The absolute accuracy of the measurement of gravity depends heavily on the accuracy to which the wavelength of the laser light is known. A frequency difference of 1 MHz corresponds to about 2 μgal in gravity. Two types of frequency-stabilised He-Ne lasers have been used in FG5 instruments: polarisation-stabilised and iodine-stabilised types. The polarisation-stabilised He-Ne is relatively simple, rugged and cheap, and was used in most JILA meters and early FG5s. The iodine-stabilised He-Ne laser has long been used as a laboratory frequency standard as it has a number of very precisely defined wavelengths which do not vary appreciably with time. Until recently, this type of laser was not considered suitable for general use as it usually employed rather sophisticated servo-systems which were too delicate for field use. The iodine-stabilised laser (ISL) has always been an option for FG5, and now (Dec. 1994) most FG5 users have an operational ISL developed by themselves (Institute für Angewandte Geodäsie (IfAG)- the operators of FG5-101) and/or in collaboration with BIPM and Axis Instruments (Chartier *et al.* 1993).

Polarisation stabilised lasers

These stabilised laser systems are constructed using HeNe lasers with internal mirrors. Each longitudinal mode is orthogonally polarised to the adjacent mode. The frequency difference between longitudinal modes ($\Delta f = c/2L$) of the laser tube used in JILA and FG5 gravimeters is about 720 MHz. The Doppler width of the neon emission line (f= 474 THz (1 THz = 10^{12} Hz)) is about 1500 MHz, so only two modes can be supported.

The frequency stability is obtained by keeping the ratio of the intensities of the modes constant. Balhorn *et al.* (1972) achieved this by regulating the voltage supplied to the discharge tube. In the JILA and FG5 lasers, the length of the cavity is tuned to a particular mode by heating the tube (Niebauer 1987). The two modes are separated by polarising beam-splitters and detected by two identical photo cells. Only one polarisation is selected for the interferometry (Figure 4.10).

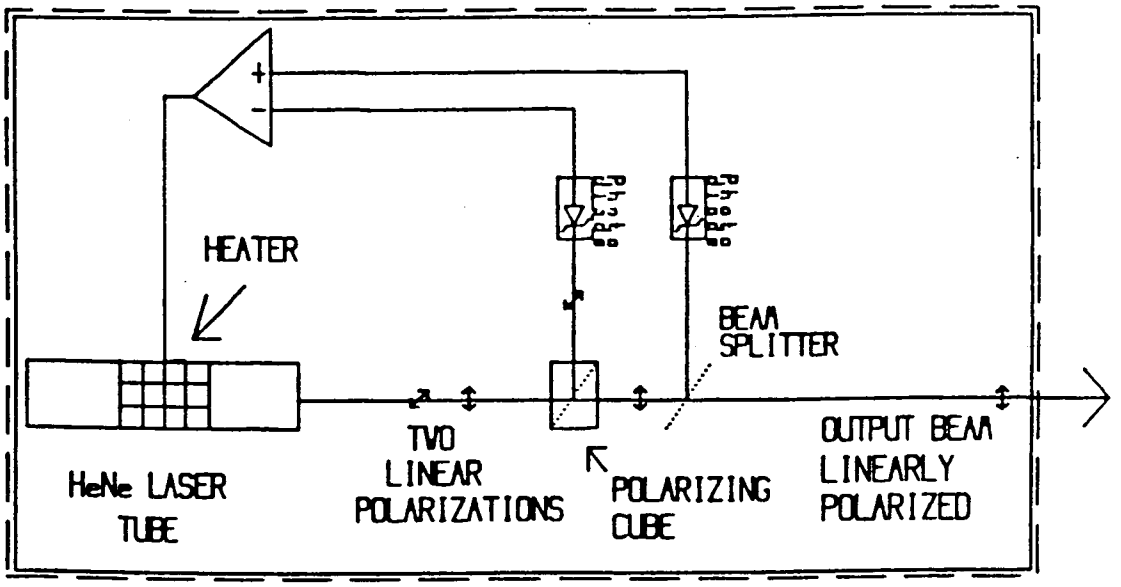

Figure 4.10 Schematic of a polarisation stabilised HeNe laser, showing the separation of the orthogonally polarised beams, and the feedback loops which keeps the ratio of the intensities of the two modes constant. (From Niebauer 1987).

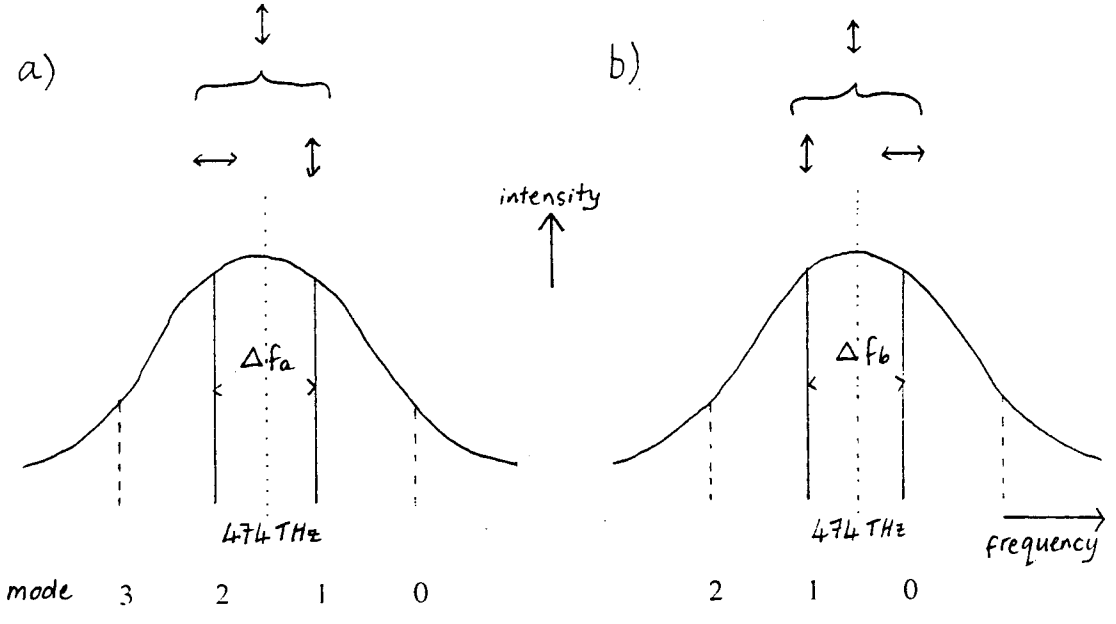

Figure 4.11 The longitudinal cavity modes (0, 1, 2, 3 etc.) of the HeNe laser pass successively through the Doppler broadened neon emission line as the length of the cavity is varied. Alternate modes are orthogonally polarised, but the beam selected for the interferometry always has the same polarisation (shown by a vertical arrow in the figures). The laser locks when the intensity of the two modes are equal. In (a), modes 1 and 2 have equal intensity, and the selected mode (1) has a higher frequency than the central neon line ('blue side'). In (b) the length of the cavity has changed so that modes 0 and 1 have equal intensity, and the selected mode (vertical arrow) has a lower frequency than the central neon line ('red side').

Changing the length of the cavity causes successive modes to pass through the Doppler broadened emission line. There are two possible lock points where the intensity ratio of the modes is constant, corresponding to the selected beam having a higher frequency than the central neon line (Figure 4.11a), or a lower frequency (Figure 4.11b). These frequencies are known as the 'blue' and 'red' modes respectively.

Mode leakage in polarisation stabilised lasers

The monochromaticity of the laser beam used for the interferometry depends on the ability of the polarisers to isolate the two modes. Only when the mode purity is 100% is the wavelength known precisely. If there is some leakage of say the red mode into the blue mode, then the intensity of the resulting beam is the sum of the two amplitudes, and the 'zero crossings' or points of minimum intensity of the interference fringes no longer occur at regularly spaced intervals of distance fallen by the corner cube. This phenomenon is well known amongst JILA and FG5 users, and was first documented by Liard and Courtier (1991) who called it the 'Beat-mode effect'. They discovered that by increasing the path length of the test beam by raising the dropping chamber away from the interferometer, the magnitude of the red-blue shift goes through a maximum and minimum.

As well as the mode-leakage effect, the wavelength of both modes changes as the laser 'ages', and with external effects such as temperature and magnetic field. These effects act in opposite directions on the red and blue wavelengths, adding weight to the argument for measuring gravity by alternating modes. Liard and Courtier found that the temperature effect was not exactly symmetric, so that taking the 'average' value of gravity from both modes does not give the 'true' value. The magnetic field of the gravity meter has a much more significant effect on the mean frequency. In the JILA meter, the magnetic field of the super spring changed the mean frequency of the laser by about 0.5 MHz (*ibid.*). In the FG5 design, it is the large electromagnet in the ion pump which has the greatest effect. In any case it is widely agreed that for accurate wavelength observations, the lasers should be calibrated under the same conditions experienced during operation i.e. whilst in place on the instrument.

Iodine stabilised lasers (ISL)

He-Ne lasers can be stabilised to produce a single mode output on any one of the peaks *d*, *e*, *f* or *g* of the hyperfine components of $^{127}I_2$ vapour. The absolute frequencies of these absorption peaks are known to a few parts in 10^{11} for a saturated vapour cell (Chartier *et al.* 1993). The length of the laser is tuned using piezoelectric elements to lock onto the chosen peak (iodine *f* is commonly used). The piezoelectric elements are set to vibrate at a high frequency ('dither') at about 1170 Hz to help maintain the lock. Unfortunately, this 'dither' frequency is transferred to the laser output and a correction term is needed in the software for the ISL. This is a sort of 'beat mode effect', but the beats come from a mechanical fluctuation of the length of the tube rather than from leakage of a laser mode having a different frequency (see previous section on 'Mode leakage').

4.2.6 Fringe Counting

One interference fringe is generated when the falling corner cube moves half a wavelength. During the fall, fringes are generated which results in a sine-wave of frequency, increasing from 0 to 6 MHz, in proportion to the velocity of the mass. The conversion of this signal into fringe count-time pairs is illustrated in Figure 4.12. Zero-crossings of the sine wave are detected by a comparator and transformed into a series of square-wave (or Transistor-Transistor-Logic ('TTL')) pulses. A scaler-counter counts the number of zero-crossing signals and divides the total number by a preset factor (typically 4000). It also scales down the 10 MHz clock pulses from a rubidium oscillator (divides by 2000). The time between the occurrence of each scaled fringe and the next scaled clock pulse is measured with a Universal Time Interval Counter (UTIC) and these fringe count - time pairs are accumulated by the computer. They may be processed in real time to give an immediate estimate of gravity, or stored in a compressed binary form as a 'Densified Data' file for post-processing and analysis.

A drop takes typically 170 ms during which time about 160 scaled fringes are accumulated. In general the first 5 scaled fringes are ignored and a parabola is fitted to 150 scaled fringes. The number of scaled fringes counted varies with instrument from 100 to 180, but the number fitted for gravity can be chosen by the user. All subsequent reference to 'fringe' means 'scaled fringe'.

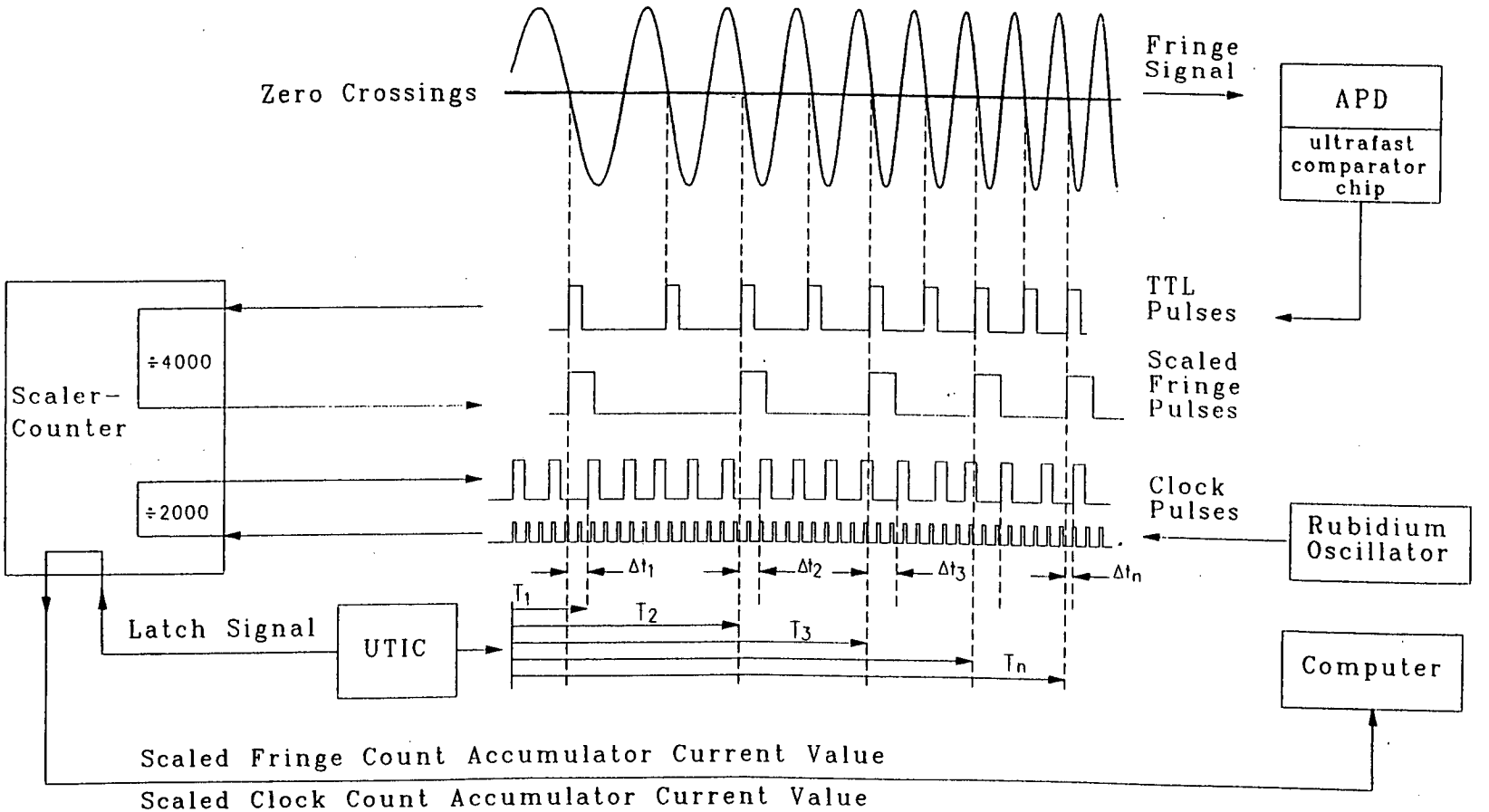

Figure 4.12 Zero-crossings of the sinusoidal fringe signals are detected by a comparator and transformed into a series of square-wave ('TTL') pulses. A scaler-counter counts the number of zero-crossing signals and clock pulses, and divides by typically 4000 and 2000 respectively. Figure 2.10 of the FG5 Manual (Axis Instruments Company 1992).

4.2.7 Instrumental Error Budgets

The various parts of the FG5 have been described in the previous sections. It must be appreciated that there are many possible sources of error in such a complex instrument, and that many of these sources are common to other types of gravimeter. Table 4.1 compares the 'error budget' of five types of apparatus, as displayed in the advertising literature for FG5 (Axis Instruments). All these instruments have been described briefly in section 4.1.

Instrument Researcher	IGPP [1] Zumberge	Faller[2]	IMGC Marson[3]	JILAG Niebauer[4]	FG5 AXIS[5]
Year	1981	1981, 85	1985	1987	1992
Error Source (errors in μgal)					
Differential pressure	1.0	2.0	2.0	1.0	0.3
Differential temperature	1.5	1.0	1.0	1.0	0.3
Magnetic field gradients	0.5	0.5	0.5	0.5	0.3
Electrostatics	1.1	0.5	0.5	1.0	0.3
Attraction of apparatus	0.5	0.5	0.5	0.5	0.1
Verticality	0.8	1.0	1.0	0.5	0.1
Air gap	No data	1.0	0.0	0.7	0.2
Laser wavelength	1.0	1.0	1.0	1.0	0.3
Rotation of corner cube	1.0	0.5	1.0	1.0	0.3
Translation (coriolis)	1.0	No data	No data	1.0	0.3
Floor recoil and tilt	1.0	1.5	1.5	0.5	0.2
Electronic phase shift	1.0	1.5	0.0	0.6	0.6
Frequency standard	0.5	No data	No data	0.5	0.1
Glass wedges	2.8	No data	No data	1.0	0.1
Uncorrelated Error μgal	**4.2**	**3.7**	**3.3**	**3.0**	**1.1**

Table 4.1 Error budgets (in μgal) of five absolute gravimeters compared (retabulated from Axis Instruments advertising literature).

References and Notes

1. Zumberge (1981).
2. Faller & Marson (1988).
3. Faller & Marson (1988).
4. Niebauer (1987).
5. Preliminary estimates from AXIS Instruments FG5 Absolute Gravimeter.

Error budgets for some other of the instruments in section 4.1, which measured at the second Intercomparison of Absolute Gravimeters (ICAG) (section 5.1), are given in Boulanger *et al.* (1986). Some of the errors can be calculated theoretically (examples are given in Niebauer (1987), but many are determined in a manner which Boulanger (*ibid.*) describes as 'the engineering-physical basis'. This presumably means that they are estimated based on specific instrumental tests and/or operational experience.

4.3 FG5 Theory

4.3.1 Introduction

Gravity varies with height by about 300 μgal m^{-1}, so, in order to make comparisons with other absolute or relative gravity observations, it is important to know the precise height at which an observation was made. If an equation of motion based on constant gravity is used, the value obtained will be some average over the drop length. In this case the appropriate height is known as the 'Effective Measurement Height'. If the equation of motion incorporates a variation of gravity with height, the solution corresponds to a particular point in the trajectory, which is more well determined than the 'Effective Measurement Height', but depends on the exact form of the equation. Because the collection of absolute gravity data is now so highly automated, it is particularly important that the chosen equation is identified and understood, and that the appropriate corrections are applied.

4.3.2 Equations of Motion

Constant gravity

The acceleration of a mass falling under constant gravity g_o (no vertical gradient) is

$$\ddot{z}_o = g_o$$

The notation adopted is that the subscript $_o$ signifies quantities applicable where constant gravity is assumed. Integrating twice with respect to time t gives the equation of motion

$$z_o(t) = z_o(0) + v_o(0)t + \tfrac{1}{2} g_o t^2 \qquad (1)$$

where z_o is the distance fallen at a particular time, $z_o(0)$ the initial position, and $v_o(0)$ is the initial velocity. The 'initial' position and velocity correspond to the point where t = 0, chosen to be the first fitted fringe (start fringe), which is usually fringe 5.

Linear gradient of gravity

When sub milligal precision is sought, it is necessary to consider the variation of gravity with height. We look for a solution as a linear perturbation of the case with constant gravity. The advantage of including the gradient in the fit is that the solution for gravity applies to the top of the drop, which is at a known height. As shown below, there are two interpretations of where the 'top of the drop' should be defined. The first is at the point where *distance* equals zero, which is at fringe 'zero', or the point where the mass begins to fall (section 4.2.2). This datum is known precisely from the dimensions of the instrument and distances which can can be measured easily when the instrument is set up. The second uses the position where *time* equals zero, which corresponds to the start fringe (usually fringe 5). This position is about 5 mm lower than the mechanically defined 'top' of the first derivation. This distinction is emphasised because it has been a lively discussion point among JILA and FG5 users, and in particular because the Edinburgh software DDT (section 4.4) uses the 'zero *position*' definition but the Axis software REPLAY follows the 'zero *time*' definition .

i) Gravity at zero position - g_{oz}

Assuming a linear gradient of gravity, the acceleration of the mass is

$$\ddot{z} = g_{oz} + \gamma z \qquad (2)$$

where γ is the vertical gradient of gravity and g_{oz} is g when z = 0.

The solution of a linear perturbation z_1 is sought so that

$$z(t) = z_o(t) + z_1(t) \quad \text{and} \quad \ddot{z} = \ddot{z}_o + \ddot{z}_1 \qquad (3)$$

Substituting (1) into (2) gives

$$\ddot{z} = g_{oz} + \gamma\left[z_0(0) + v_0(0)t + \tfrac{1}{2}g_{oz}t^2 + z_1(t)\right] \tag{4}$$

So, by comparing (3) and (4)

$$\ddot{z}_1 = \gamma\left[z_0(0) + v_0(0)t + \tfrac{1}{2}g_{oz}t^2 + z_1(t)\right] \tag{5}$$

Neglecting the second order term $\gamma z_1(t)$ and then integrating twice gives

$$z_1 = \gamma\left[\tfrac{1}{2}z_0(0)t^2 + \tfrac{1}{6}v_0(0)t^3 + \tfrac{1}{24}g_{oz}t^4\right] + v_1(0)t + z_1(0) \tag{6}$$

Neglecting the seond order terms $\frac{1}{6}\gamma v_1(0)t^3$ and $\frac{1}{2}\gamma z_1(0)t^2$, and substituting (6) and (1) into (3) :

$$\boxed{z(t) = z(0)\left[1 + \tfrac{1}{2}\gamma t^2\right] + v(0)t\left[1 + \tfrac{1}{6}\gamma t^2\right] + \tfrac{1}{2}g_{oz}t^2\left[1 + \tfrac{1}{12}\gamma t^2\right]} \tag{7}$$

ii) Gravity at zero time - g_{ot}

Beginning with the definition

$$\ddot{z} = g_{ot} + \gamma(z - z(0)) \tag{8}$$

for the acceleration of a mass through a linear gravity gradient γ, z(0) is the position at time t = 0 and g_{ot} is g at t = 0. (Note the different definition of g_{oz} in (2)).

As before, $\ddot{z}_0 = g_{ot}$ and equation (1) applies.

Again, the linear perturbation $z_1(t)$ is sought. This time

$$\ddot{z}_1 = \gamma[z - z(0)] \tag{9}$$

Expanding z and z(0) using (3)

$$\ddot{z}_1 = \gamma[z_0(t) + z_1(t) - z_0(0) - z_1(0)] \tag{10}$$

Substituting from (1) for $z_o(t)$, we find that the $z_o(0)$ cancel to give

$$\ddot{z}_1 = \gamma\left[v_o(0)t + \tfrac{1}{2}g_{ot}t^2 + z_1(t) - z_1(0)\right] \tag{11}$$

Because the small terms in $z_1(0)$and $z_1(t)$ are factored by the small quantity γ, they can be neglected.

Integrating the two remaining terms of (11) twice with respect to time, gives

$$z_1 = \gamma\left[\tfrac{1}{6}v_o(0)t^3 + \tfrac{1}{24}g_{ot}t^4\right] + v_1(0)t + z_1(0) \tag{12}$$

Now we can substitute for z_o (equation 1) and z_1 (equation 12) into the expression (3) for z

$$z(t) = z_o(0) + v_o(0)t + \tfrac{1}{2}g_{ot}t^2 + \gamma\left[\tfrac{1}{6}v_o(0)t^3 + \tfrac{1}{24}g_{ot}t^4\right] + v_1(0)t + z_1(0)$$

Neglecting $\gamma\, v_1(0)t^2$ gives

$$\boxed{z(t) = z(0) + v_o(0)t\left[1 + \tfrac{1}{6}\gamma t^2\right] + \tfrac{1}{2}g_{ot}t^2\left[1 + \tfrac{1}{12}\gamma t^2\right]} \tag{13}$$

iii) Consistency of the solutions (7) and (13)

From (2) we have the definition of gravity as

$$g = g_{oz} + \gamma z \tag{14}$$

from which equation (7) is derived.

From (8), the alternative definition of gravity is

$$g = g_{ot} + \gamma(z - z(0)) \tag{15}$$

from which equation (13) is derived.

Setting z = 0 in (14) and (15) gives

$$g = g_{oz} \qquad \text{and} \qquad g = g_{ot} - \gamma\, z(0)$$

where g_{oz} is the solution to the first derivation and g_{ot} the solution to the second and the two solutions are related by

$$g_{ot} = g_{oz} + \gamma\, z(0) \tag{16}$$

Substituting (16) into (13) gives

$$z(t) = z(0) + v_o(0)t\left[1 + \tfrac{1}{6}\gamma\, t^2\right] + \tfrac{1}{2}\{g_{oz} + \gamma\, z(0)\}t^2\left[1 + \tfrac{1}{12}\gamma\, t^2\right]$$

and on expanding gives

$$z(t) = z(0)\left[1 + \tfrac{1}{2}\gamma\, t^2 + \tfrac{1}{24}\gamma^2\, t^4\right] + v_o(0)t\left[1 + \tfrac{1}{6}\gamma\, t^2\right] + \tfrac{1}{2}g_{oz}t^2\left[1 + \tfrac{1}{12}\gamma\, t^2\right] \tag{17}$$

Comparing this with (7) shows that the two solutions are consistent except for the second order term $\frac{1}{24}z(0)\gamma^2 t^4$. The vertical gradient γ is $\sim 3\times10^{-6}$ s^{-2} and t is less than about 0.2 s, so γt^2 is less than 10^{-7}. The derivations above have been to first order in γt^2 so this discrepancy is certainly negligible here and the solutions are consistent.

Defining g_o at z = 0, rather than at t = 0, gives an extra term in the equation of motion when the vertical gradient is included. The Edinburgh program DDT (section 4.4.1) uses the equation:

$$z = z(0)\left[1 + \tfrac{1}{2}\gamma\, t^2\right] + v(0)t\left[1 + \tfrac{1}{6}\gamma\, t^2\right] + \tfrac{1}{2}g_{oz}t^2\left[1 + \tfrac{1}{12}\gamma\, t^2\right]$$

where z(0) and v(0) are the position and velocity at zero time, but g_{oz} is gravity at zero position. The extra term is the factor $1/2\,\gamma t^2$ multiplying z(0), which alters the value of gravity by about 1.5 μgal.

Consequence of approximating gravity as a constant

Early data from free-fall absolute gravity meters did not incorporate an equation of motion derived with gravity varying with height.

When the full equation (7) is approximated by the simple equation (1),

$$z_o(t) = z_o(0) + v_o(0)t + \tfrac{1}{2} g^* t^2 \qquad (18)$$

the presence of a vertical gradient means that the value of gravity changes by about 60 μgal over the distance between the top and bottom of a 20 cm drop, so that the solution g^* obtained is some average value over this region, typically 20 - 30 μgal larger than g_0. The estimate of gravity g^* corresponds to the actual gravity at some distance down the drop, h_{eff} - the 'Effective Measurement Height' referred to by Niebauer (1989). If a theory existed which correctly predicted h_{eff}, the early data could be reliably compared with more modern ones based on equation (7). The next section reviews attempts to find such theories.

4.3.3 The Effective Measurement Height

Theory

The effective measurement height for an object dropped a distance Δz has been estimated by different authors (see Niebauer 1989). For data which is equally spaced in time, h_{eff} has been shown to be located about $2\,\Delta z / 7$ (for a small initial velocity) below the initial dropping point (*ibid.*). However, the FG5 generates data which are equally spaced in distance, and for this case, an estimate based on the time-averaged acceleration predicts h_{eff} to be approximately $\Delta z / 3$ for small initial velocities. This rule of thumb which says that h_{eff} is about 1/3 of the way down the drop can be theoretically in error by several centimetres. In practice, it is in error because missed fringes (see later this section) cause the drop length to be underestimated. Some better predictions are compared below, but it is shown that the ratio $h_{eff} / \Delta z$ for FG5 is in practice closer to 1/2.

Niebauer (1989) describes various theoretical ways of calculating h_{eff}. The least-squares solution (**LSS**) for z(0), v(0) and g_0 and linear gradient γ with data equally spaced in *time*, gives the time-averaged acceleration as

$$\langle \ddot{z} \rangle = g_o + \gamma\, v_o \langle t \rangle + \tfrac{1}{2} \gamma\, g_o \langle t^2 \rangle \approx g_o + \gamma\, h_{eff} \qquad (19)$$

where

$$h_{eff} = \frac{1}{3}\Delta z + \frac{1}{6} v_o \Delta t. \qquad (20)$$

Δz and Δt are the total dropping distance and time, and for small initial velocities, $h_{eff} \approx \frac{1}{3}\Delta z$.

Niebauer also describes a Continuous-Least-Squares (**CLS**) method which approximates the least-squares equations by integrals. The method is more straightforward for data equally spaced in time, but can be accomplished for data equally spaced in distance by including the velocity as a weighting function for the time integrand. In this way, Niebauer derives the result

$$h_{eff} \approx \frac{3}{14} v_o \Delta t + \frac{2}{7}\Delta z \qquad \text{for data equally spaced in time, and}$$

$$h_{eff} = \frac{5}{14}\Delta z \qquad \text{for data equally spaced in distance}$$

when the initial velocity is small. When the velocity is not small, the weighting function mentioned above is no longer appropriate and Niebauer gives a general formula for a set of data points equally spaced in distance :

$$\frac{h_{eff}}{\Delta z} = f - \frac{3\, g_o (\Delta t)^2}{28\, \Delta z} \qquad (21)$$

f depends on the velocity, varying 'from about 0.57 to 0.52 for initial velocities of 0 to 100 cm s^{-1} (asymptotically approaching 0.50)'. Since the initial velocity for FG5 drops is 0.2 - 0.3 m s^{-1} then the appropriate value of f would seem to be about 0.56.

Observations

The ratio $h_{eff}/\Delta z$ can be measured in practice by solving equations (18) (no vertical gradient) and (7) (including vertical gradient) and calculating

$$\frac{h_{eff}}{\Delta z} = \frac{g^* - g_o}{\gamma \Delta z} \qquad (22)$$

In practice, this consistently gives a value of about 0.43. The value does not apparently vary with the total number of fringes counted, or with the vertical gradient used. It does vary systematically with starting fringe, but this probably a symptom of the drop characteristics of each instrument (see Chapter 5), rather than an error in the theory.

Instrument	Dropset	LSS	CLS	observed
FG5-**101**	ON193221	0.37	0.38	0.43
FG5-**107**	TAU93270	0.38	0.40	0.43
FG5-**103**	POL0912A	0.38	0.39	0.43

Table 4.2a Comparison of h_{eff} / Δz resulting from the three methods described above for specimen drops (set 1, drop 2) from FG5-101, FG5-107 and FG5-103 observations. The details of the drops are given in Table 4.2b.

name	g_0	v(0)	T	Δz	fringes
on1 s1d2	9.81 716 231 75	0.226 481 2978	0.183 990 312	0.20256	180/160/5
tau s1d2	9.81 168 870 46	0.324 322 7417	0.177 727 624	0.20256	180/160/5
pl9 s1d2	9.81 367 386 23	0.285 058 2593	0.174 300 207	0.18990	170/150/5

Table 4.2b Details of drop used for Table 4.2a.g_0 is the value at the top of the drop and v(0) the initial velocity. T and Δz are the total drop time and distance respectively. 180/160/5 means that a total of 180 fringes were counted and 160 were fitted, starting at fringe 5 (i.e fringes 5 to 165 were fitted).

The above demonstrates that the use of the effective measurement height concept is not adequate for precise comparisons so in order to assign a precise height for the value of g, the vertical gradient must be included in the equation of motion.

Missed fringes

The problem of missed fringes was first detected when the parameters z_0 and v_0 (initial position and velocity) were printed out for each drop. The initial velocity is expected to be relatively variable because at the moment when the mass is released from the cart it is not isolated from ground motions. Typical solutions range from 0.26 to 0.31 ms^{-1}.

The initial position should be the constant distance equivalent to the 'start fringe', (specified in REPARAM.DAT or interactively for DDT), which usually has the value 5. The 'initial position' is the distance travelled by the mass when the fifth scaled fringe is

estimates, z_0 *is* very close to -5.064 mm. for about 10 % it is estimated at about -3.798 mm (three scaled fringes) and for less than 1 % of the drops, the estimate is -6.330 mm (five scaled fringes).

DDT provides an option to print out each time-distance pair for a drop, and this list gives a continuous serial index of the pair, the time value in seconds, the number of the scaled fringe this corresponds to and the time and distance residuals of the fit of the point to the curve. If no fringes were missed, the first time (zero) would be fringe 5 and the last (with 150 fitted fringes) would be 154. The sequence of fringe numbers would have no gaps.

In fact, the last fringe used in the fit was typically 15 greater than 154, and 15 gaps appeared in the sequence of fringe numbers. Because the fringe residuals did not systematically change sign at the gaps, it seems that the correct fringe number was being associated with the correct time, so that no error is introduced into the least squares solution by missing out a time-distance pair. Although one fringe may be missed at the beginning of the drop, the number missed increases rapidly towards the bottom of the drop, where the mass is falling fastest. Figure 4.13 illustrates this effect. The vertical axis shows the frequency with which each fringe is counted for the 24 sets of POL0705. Each set has 200 drops, so each fringe number should be counted 4800 times. The figure shows that fringe numbers up to about 110 are counted almost 100 % of the time, and thereafter, more and more are missed. Fringe 172 is counted only about 2800 times. The effect of missed fringes is to extend the part of the drop used for the least squares fit to slightly different lengths.

The failure of the observed value of the ratio $h_{eff}/\Delta z$ to agree with the theoretical predictions is due to missed fringes. Although 150 are fitted, and time and distance are always correctly associated, an average of 16 fringes are missed, which is about 10 % of the total number. This increases the actual length (Δz) by 10 % and then the agreement between the observed fraction and the CLS estimate of Niebauer (equation 21) for data equally spaced in distance is improved.

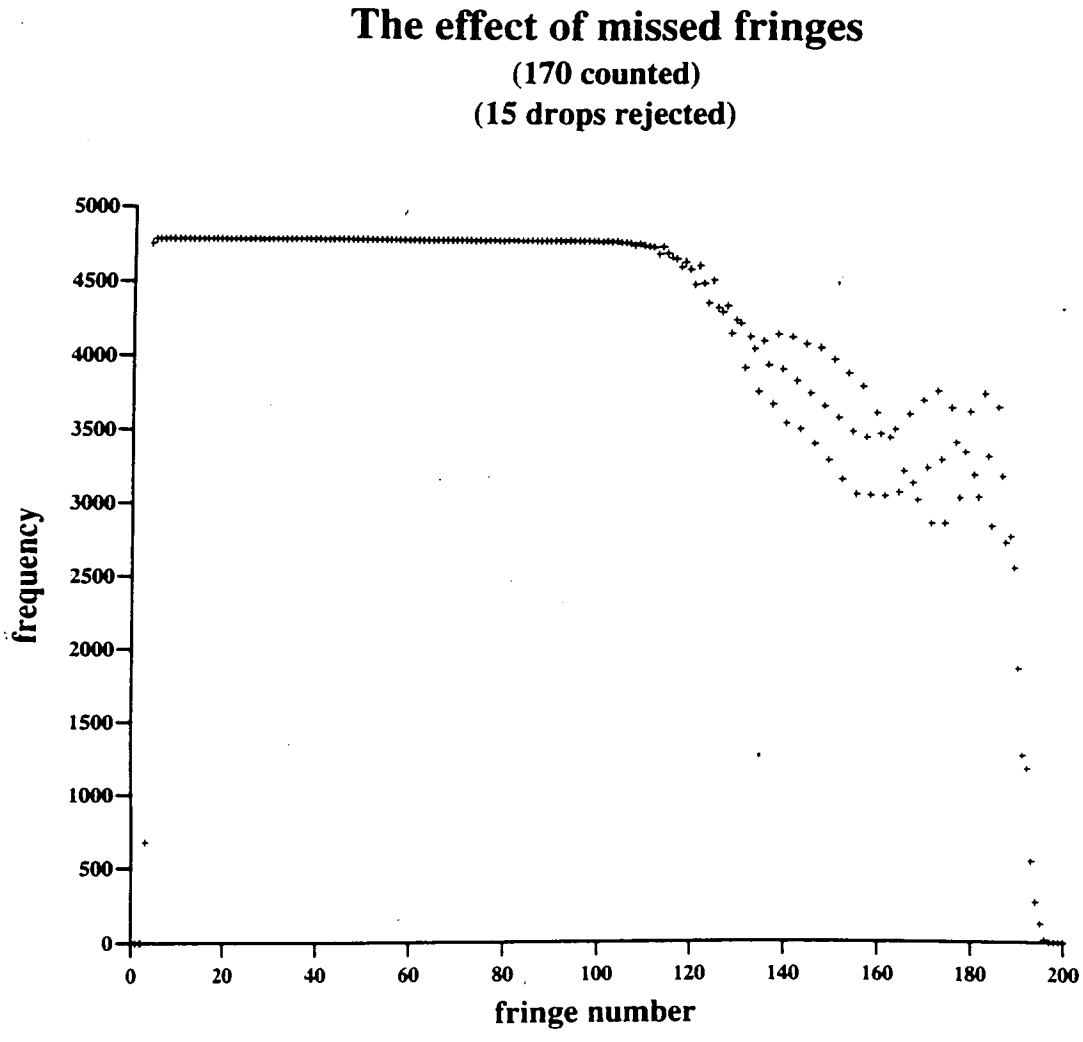

Figure 4.13 The vertical axis shows the frequency with which each fringe is counted for the 24 sets of POL0705. Each set has 200 drops, so each fringe number should be counted 4800 times. The number of fringes missed increases rapidly after about fringe 110.

4.4 FG5 Software

4.4.1 The Programs DDT and REPLAY

The real-time Axis processing software OLIVIA produces 'densified data files' which can be reprocessed subsequently, allowing the application of different or new corrections, and further analysis. The binary densified data ('ddt') files can be read by the post-processing programs REPLAY or DDT.

REPLAY was written in a DOS-based version of FORTRAN mainly by K. Buxton at Axis (control software) and G. Sasagawa at NIST/NOAA (gravity data processing). A thorough examination of these programs was necessary to fully interpret the absolute observations. The program DDT was adapted from early versions of REPLAY supplied with the first commercially available Axis FG5 instruments. DDT was written in FORTRAN77 by R.G Hipkin (Edinburgh University) and it was designed to enable greater data analysis than afforded by the Axis programs. The REPLAY subroutines which decode the compressed binary times, fringe numbers and sensor data are incorporated into DDT without modification except that necessary to compile with a standard FORTRAN77 compiler. The REPLAY subroutines SOLVER and SOLVDROP which determine a value of gravity from a single drop have been replaced by the DDT version SOLVE. In the Edinburgh software, the rejection of outliers and averaging of single drop gravity estimates to give set means is done by a separate program MEAN. These procedures are included in the Axis program REPLAY.

The program DDT enables a thorough analysis of the data by producing detailed drop information including the initial velocity and initial position which are not output by REPLAY. The REPLAY parameter files REPARAM.DAT and RECOMND.DAT are not needed by DDT. The necessary information about corrections and number of fringes to count is written into the program or requested interactively at the start of each run.

A diagram showing the relationship of the programs and files described here is given in Figure 4.14.

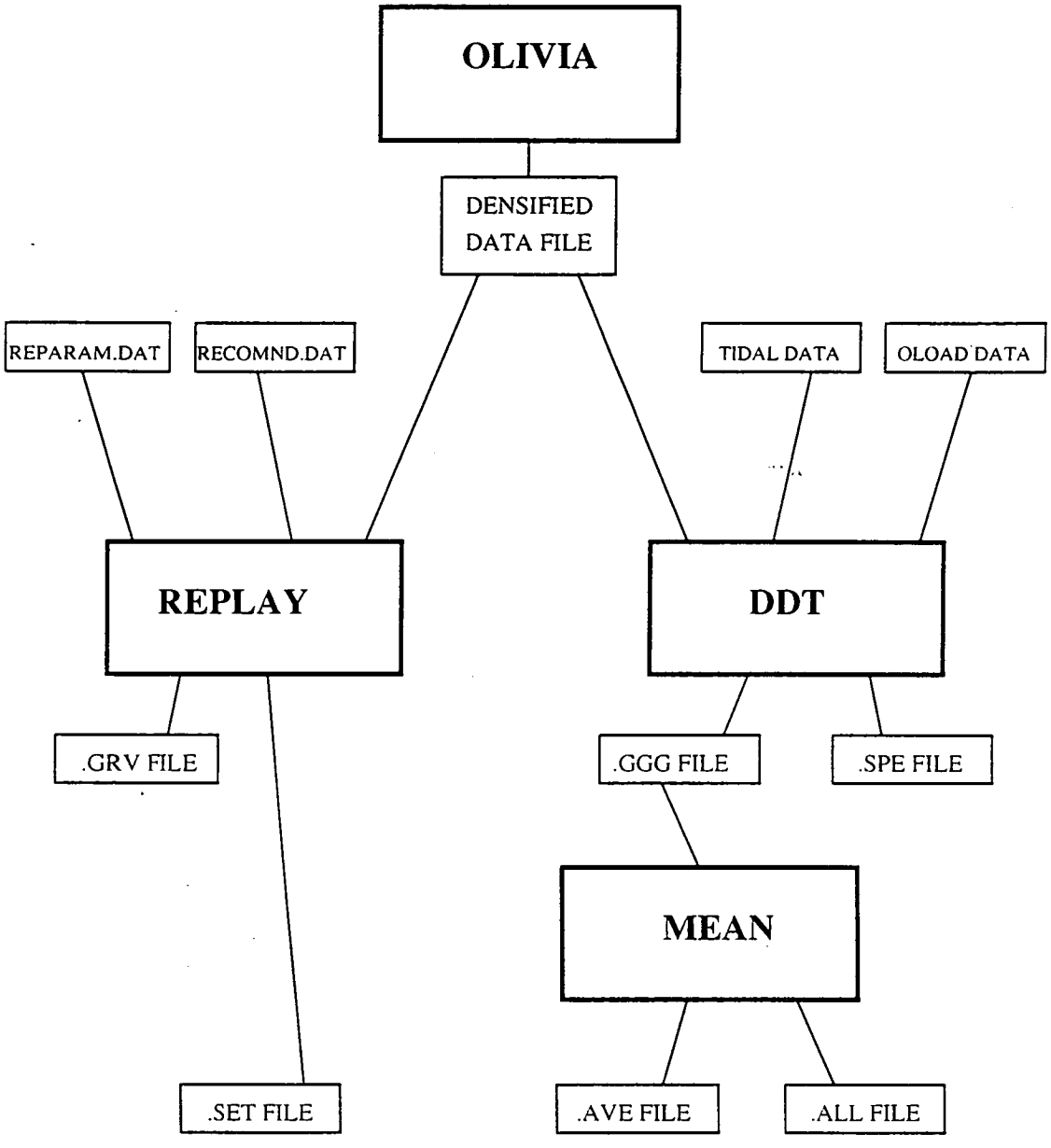

Figure 4.14 The relationship between the programs (large boxes) and files used for processing FG5 data. OLIVIA and REPLAY are the programs supplied with FG5, written by Axis Instruments. DDT and MEAN were written by R.G. Hipkin and were used for all the absolute gravity data processing described in this thesis.

The initial analysis of the Axis code at Edinburgh was done by R.G Hipkin and the programming errors noted below were detected by him. The author continued the work by exploring the differences in gravity estimates and corrections between the apparently accurate versions of DDT and REPLAY, and extending the program to identify and correct biases due to systematic structure in the residuals (section 5.3). Most of the errors found in the original version of REPLAY (v1.0) have been corrected and some of the more fundamental modifications (including a different equation of motion) employed by DDT are incorporated into recent versions of REPLAY (now at version 3.01 Dec 1994). The main differences between versions 1.0 and 3.01 are that the errors (described in section 4.4.3) have been rectified; polar motion, ocean loading and laser modulation corrections are included; and the static tide is removed from the gravity estimates. In version 1.0, the Honkasalo Correction (section 3.1.3) is made, which means that the estimates of gravity include the static tide. In versions 2.0 onwards, this convention is reversed, so that the calculation of the tidal *correction* includes the static term, and its effect is removed from the gravity data along with the rest of the elastic tide.

H. Hopewell (*pers. comm.* 7 June 1994) draws attention to the particular differences between versions 2.0 and 3.0 of REPLAY. He notes a change in some set means of up to 1.5 μgal as a result of subtle differences in the use of box-car and 3σ filters in the subroutines SETSTATS (v 2.0) and FILTSORT (v 3.0). When set on alternate lock mode for the polarisation stabilised laser (section 4.2.5), version 2.0 started on red lock, but version 3.0 started on blue. This will causes the wrong wavelength to be used for the gravity estimate if the hardware is set to always start on red.

The discussion that follows is relevant to versions 1.0 and 2.0 of REPLAY which were available during the main development of DDT (1993).

4.4.2 DDT Program Structure

The program begins interactively so the user can choose to change the number of fringes fitted, print out x-t pairs for a particular drop and make corrections for vertical gradient, speed of light, elastic tide, static tide, ocean loading, and atmospheric pressure. The appropriate information is then immediately written to the header of the output file (the .ggg file of Figure 4.14), so it is easy to see which corrections have been applied to the numeric data which follows. The main loop processes one drop at a time, beginning by unpacking

the densified data file using the subroutines GETDENSE, PARSEDATA, CONVERT, and GETABTIME to create arrays containing the fringe times and associated distances for the drop. These arrays are passed to the subroutine SOLVE which constructs the observational equation matrices to calculate gravity, initial velocity, initial position and residuals along with the appropriate corrections. On returning to the main program, the distance, time, fringe data and residuals are written to a special file if requested, the number of missed fringes are calculated, and the tidal and atmospheric pressure corrections are made. Detailed information is written to the screen and to an output file as shown in Table 4.3 below:

```
                Source file:                              npl0307a.ddt

                Number of fringes counted                          170
                Start fitting at fringe                              5
                Number of fringes fitted                           150

                Gradient correction applied with       0.2955  ugal m-1

                Finite speed of light correction applied

                CTE tidal corrections applied
                Latitude:    51.41970;   Longitude:     -0.33774
                The static tide on an elastic Earth has been removed
                Ocean loading correction made

                Pressure corrections made using      -0.3  ugal mbar m-1
                Station height  10.0 m;  Standard pressure 1012.00 mbar

set drp year day  h  m  s      gravity    s.d   velocity    s.d   position   s.d
amplit s.d phas s.d tide    light  vgrad baro  oload   n   temp  press  tlaser  vac  ssz

  1   1 1993 184 20 21 40  981181361.82 17.58 265769038.2 18.6  3797946.21  .89
 6.75  .23 105. 2.  89.83  12.26  24.89 -2.79 -2.68  17   22.82 1021.3 -.096 6.541  50.2

  1   2 1993 184 20 21 53  981181320.97 17.58 287169295.5 18.5  5063921.74  .88
 6.97  .24 179. 2.  89.82  12.54  26.21 -2.79 -2.68  24   22.84 1021.3 -.075 4.448  51.1

  1   3 1993 184 20 22  6  981181348.21 17.08 271383795.5 18.2  3797937.05  .88
 6.82  .23-145. 2.  89.81  12.47  25.70 -2.79 -2.69  23   22.86 1021.3 -.043 1.311  49.5

  1   4 1993 184 20 22 19  981181352.23 17.73 276236473.9 18.7  5063937.99  .90
 6.75  .24  -8. 2.   89.80 12.45  25.96 -2.79 -2.69  23   22.87 1021.3 -.044 1.398  51.7

  1   5 1993 184 20 22 32  981181409.37 19.03 296403838.5 19.9  5063935.89  .94
 6.96  .26  41. 2.   89.78 12.53  26.08 -2.79 -2.70  23   22.87 1021.3 -.035 1.170  54.0
```

Table 4.3 Example of a .ggg file output from DDT. Information for the first 5 drops is shown as follows.

Top line:
set number, drop number, year, day number, hour, minute, second, gravity (μgal), standard deviation (μgal), initial velocity (nm s^{-1}), s.d (nm s^{-1}), initial position (nm), s.d (nm).

Bottom line:
amplitude (nm), s.d (nm), and cosine phase (°), s.d (°) of the fringe displacement due to ISL frequency modulation, elastic tide correction (μgal) speed of light correction (μgal), vertical gradient correction (μgal), pressure correction (μgal), ocean load tide (μgal), number of missed fringes, room temperature (° C), atmospheric pressure (mbar), laser temperature (° C), dropping chamber vacuum (μtorr), superspring zero (mV).

4.4.3 The Subroutine SOLVE

SOLVE is the heart of the program and solves the arrays of observation equations for gravity, initial velocity, initial position and laser term corrections. The vertical gradient and speed of light corrections are calculated using appropriately modified equations of motion.

The equation of motion (equation (18)) for an object falling freely under constant gravity is

$$z = z_o + v_o t + \tfrac{1}{2} g^* t^2$$

where the unknowns are the initial position (z_0), initial velocity (v_0), and gravity (g^*) which is some average value of gravity over the drop region. In an FG5 drop, the number of distance-time pairs fitted to the parabola varies with the particular instrument, from 90 to 170, so the least-squares problem is overdetermined. The matrix **a** contains the terms in time, **b** is the vector of distances and **x** contains the unknowns. For m distance-time (z-t) pairs and n unknowns, we solve $\mathbf{a}_{mn}\,\mathbf{x}_n = \mathbf{b}_m$ with the matrices as follows:

$$\begin{pmatrix} \frac{1}{2}t_1^2 & t_1 & 1 \\ \frac{1}{2}t_2^2 & t_2 & 1 \\ \frac{1}{2}t_3^2 & t_3 & 1 \\ \vdots & \vdots & \vdots \end{pmatrix} \begin{pmatrix} g \\ v_o \\ z_o \end{pmatrix} = \begin{pmatrix} z_1 + \varepsilon_1 \\ z_2 + \varepsilon_2 \\ z_3 + \varepsilon_3 \\ \vdots \end{pmatrix} \qquad (23)$$

The equations are solved by least-squares using QR reduction in the subroutine DQR, which converts **a** into upper triangular form using successive Householder rotations, and solves the system by backsubstitution. The covariance matrix is calculated by the subsequent routine DQRCOV.

Using the resulting values of g, z_0 and v_0, the distance and time residuals are calculated.

Errors in SOLVDROP

Most of the REPLAY subroutine SOLVDROP (where gravity is estimated) appears to contain an error whereby the index counting the time-distance pairs, already incremented outside the subroutine so that the time is zero at the fifth scaled fringe, is again incremented by this amount within the subroutine (Hipkin 1993a). This double displacement at the start of the drop means that REPLAY fits fringes 10 to 160 instead of the intended 5 to 155. This has the

effect of giving a significantly smaller number of bad gravity estimates (about 0.5% compared with about 9.1%), but the mean over 24 sets was not significantly different (...369.97 ± 0.56 μgal compared with ...371.12 ± 0.68 μgal). This feature is retained in SOLVE.

Considerable confusion occured because of *different sign conventions* within early versions of Axis programs (*ibid.*). In SOLVDROP, where the real analysis is, there is a consistent choice of the z-axis being positive up. Consequently gravity, the position at zero time and the initial velocity are all negative numbers. In order to give a positive value for gravity, the estimated quantity is simply multiplied by -1 outside the subroutine. With this convention, there is *no sign error* for the gravity gradient in the program. In the newer version (REPLAY v 2.0), the gravity gradient is explicitly multiplied by -1 which generates an error which was not there previously. The confusion arises because the RECOMND.DAT file has a default value for the gradient of -3.086 μgal cm^{-1}.

Other errors occurred in calculating the vertical gradient correction (section 4.4.4) and speed of light correction (section 4.4.5).

4.4.4 Vertical Gradient Correction

The equation of motion (equation 7) for free-fall where gravity varies linearly with height is

$$z = z(0)\left[1+\tfrac{1}{2}\gamma t^2\right] + v_o(0)t\left[1+\tfrac{1}{6}\gamma t^2\right] + \tfrac{1}{2} g_{oz}\, t^2\left[1+\tfrac{1}{12}\gamma t^2\right]$$

to first order in the vertical gravity gradient γ. g_{oz} is the value of gravity at the top of the drop ($z = 0$). This is the equation used in DDT. The program REPLAY uses equation (13) which lacks the term $1/2\ \gamma t^2$ multiplying z(0), so the values of gravity from REPLAY will be too high by about 1.5 μgal.

The matrix a_{mn} is modified to

$$\mathbf{a}_{mn} = \begin{pmatrix} \frac{1}{2}t_1^2+\frac{1}{24}\gamma t_1^4 & t_1+\frac{1}{6}\gamma t_1^3 & 1+\frac{1}{2}\gamma t_1^2 \\ \frac{1}{2}t_2^2+\frac{1}{24}\gamma t_2^4 & t_2+\frac{1}{6}\gamma t_2^3 & 1+\frac{1}{2}\gamma t_2^2 \\ \frac{1}{2}t_3^2+\frac{1}{24}\gamma t_3^4 & t_3+\frac{1}{6}\gamma t_3^3 & 1+\frac{1}{2}\gamma t_3^2 \\ \vdots & \vdots & \vdots \end{pmatrix} \qquad (24)$$

In the first version of REPLAY, an array index is taken beyond its declared bounds during calculation of the vertical gradient correction. This does not, in fact, affect the corrected value of gravity (which is computed with a different equation of motion), but the size of the *gravity gradient correction* overflows the available space and asterisks are output in the REPLAY .grv file. This error was corrected in the second version of REPLAY.

Reference Height Correction

The reference height correction is an option to correct all the gravity values to a chosen datum height (for example 1 meter or floor level). It simply calculates the gravity difference between the top of the drop and the reference height using the constant vertical gradient given in the RECOMND.DAT file. As discussed in section 5.2, this correction should only be used with caution, because large errors can accumulate by transferring the absolute gravity value to a datum using a vertical gradient which may not be appropriate over the region of transfer. Consequently, DDT does not include this correction.

4.4.5 Speed of Light Correction

Because light reflected from the falling reflector in the upper part of the drop takes longer to reach the interferometer than when the reflector is close to the bottom of the drop, all the fringe times have to be corrected according to their distance down the drop. To make the correction, each time is delayed by $2\,z\,/\,c$, where c is the speed of light. One fringe is produced every time the total (up and down) path length of the test beam changes by one wavelength λ, which occurs when the reflector falls $\lambda/2$. Fringe times from the bottom of a drop are given a bigger delay than times from the top to compensate for the fact that they have travelled a shorter distance. All the times t_n become $(t_n - n\,2\,\lambda\,/\,c)$, where n is the fringe number.

REPLAY uses a formula of Kuroda & Mio (1991) to calculate the speed of light correction which does not give exactly the same answer as solving the equation of motion with retarded times. REPLAY estimates gravity using retarded times but lists the *correction* given by the formula. For example, for 150 fringes starting at fringe 5, the solution using retarded times gives -12.54 μgal, but the formula gives -10.79 μgal.

4.4.6 Laser Correction

As discussed in section 4.2.5, two sorts of stabilised Helium-Neon laser have been used in FG5 : they involve polarisation stabilisation and Iodine vapour absorption stabilisation.

Mode leakage correction for polarisation stabilised laser

The polarisation stabilised laser relies on matching the intensities of two orthogonally polarised modes (section 4.2.5). A 'beat-mode' correction for the leakage of these modes is described in Liard and Courtier (1991) and what follows is a summary of their derivation.

The light amplitude of the laser with weak mode leakage can be approximated as the sum of two components:

$$I = \cos(kx) + \varepsilon \cos((k+\theta)x) \tag{25}$$

where $k = \frac{2\pi}{\lambda}$, $\theta = \frac{2\pi\delta}{c}$, λ is the wavelength of the predominant mode, c the speed of light, and δ the inter-mode frequency. x is the fringe position and ε is the leakage ratio with respect to the predominant mode intensity.

The fringe counters detect 'zero-crossings' so the positions x_i where the intensity, I is zero are calculated. As a first approximation,

$$x_i = \frac{2\pi i}{k} = \lambda i \tag{26}$$

and the zeroes of the cos (kx) term occur for

$$x_i = (2i-1)\frac{\pi}{2} \quad . \tag{27}$$

Liard and Courtier derive

$$x_i = \lambda\left\{ i + \phi - \frac{\varepsilon}{2\pi} \sin\left(\frac{2\pi\lambda\delta i}{c} \right) \right\} \tag{28}$$

for the zero crossings, where i is the i^{th} scaled fringe. The phase of the beats is a function of the difference in path lengths of the reference and test beams which depends on the separation of the dropping chamber and the interferometer. The fringe equivalent ϕ of this distance must be added to the equation (*ibid.*). ϕ is equal to zero only when the two path lengths are equal. It follows that the size of the 'red-blue shift' varies according to this distance ϕ, and can be minimised in theory by setting up the dropping chamber and interferometer with an optimum separation. Niebauer (*pers. comm.* 2 Feb 1994) describes experiments to determine this separation with FG5-109, and found that the 'red/blue shift ...can be changed from a maximum to null in 5.2 cm by increasing/decreasing the path length.' The dropping chamber was raised 3 cm in increments of 1 cm and the red-blue shift was minimised for a raise of 1 cm. In practice it is easier to apply a correction in the software. The red-blue shift can also by reduced by increasing the effectiveness of the polarisation by rotating the laser tube, or realigning and/or improving the polarisers. These mechanical adjustments can be spoiled by vibration or careless handling of the interferometer.

Iodine Stabilised Laser (ISL) Correction

The 'dither' frequency (section 4.5.4) of the ISL is about 1170 Hz. This mechanically generated signal modulates the fringe signal, so must be filtered out before solving the distance-time pairs. The phase is found by solving for sine and cosine waves at the known frequency. This adds an extra two columns to the matrix $\mathbf{a}_{mn}$ (equation 23). For the set POL0705, the amplitude of this correction was found to be steady at about 7nm, but with random phase. An investigation of the gravity effect of this correction was made with another set POL1205, and it was found that the correction to a single drop ranges randomly between about ± 100 μgal (Figure 4.15), which affects the set (200 drops) means by about ± 5 μgal, and the overall mean of an occupation (24 sets) by less than ± 1.5 μgal. The most significant effect of including this correction is to reduce the standard error on a single drop (and hence on the set mean) by a factor of typically two or three, and to reduce the drop to drop scatter by a similar amount. Figure 4.16 shows the fringe residuals of a single drop before and after applying the modulation correction.

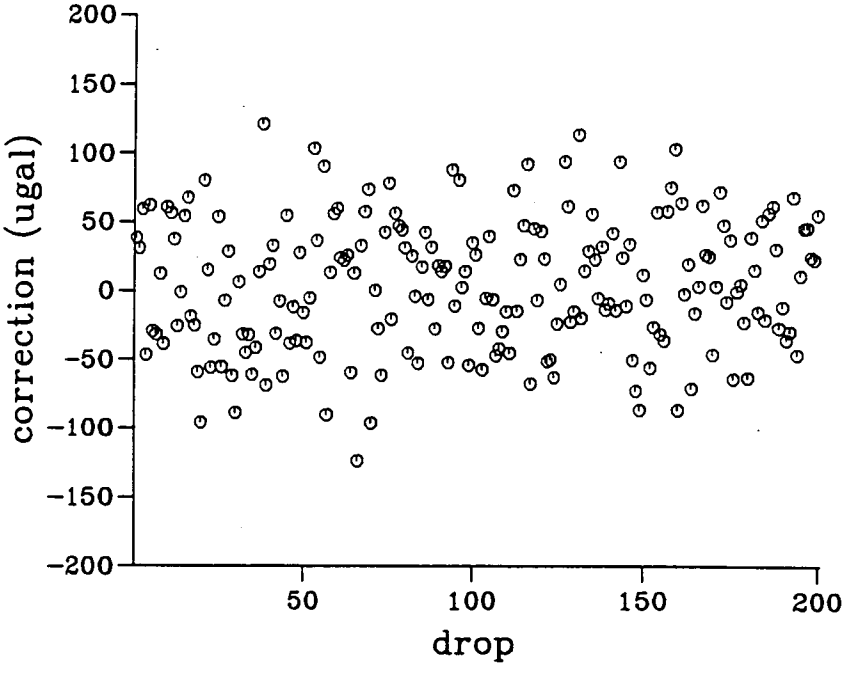

Figure 4.15 The gravity effect of the Iodine Stabilised Laser correction on the set POL1205 varies randomly with drop number. The correction affects the set (200 drop) means by about ± 5 μgal, and the overall mean of an occupation (24 sets) by less than ± 1.5 μgal.

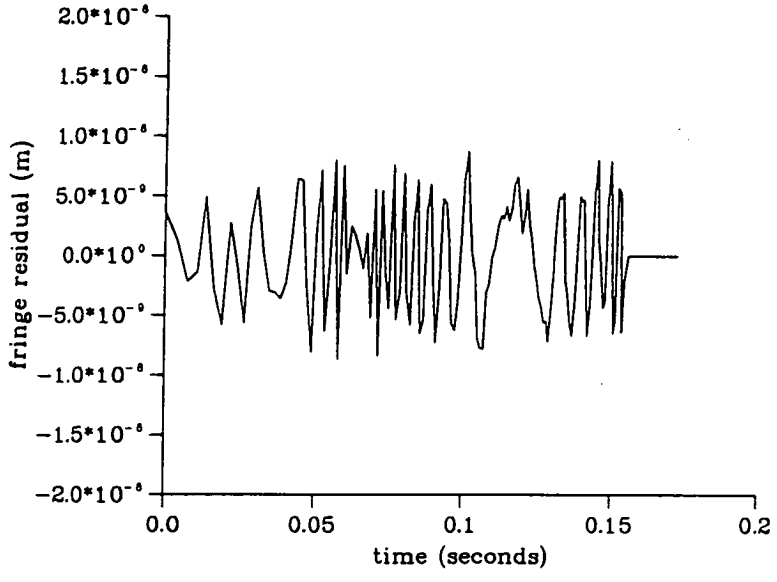

Figure 4.16a Line graph of the amplitude of the fringe residuals for the single drop (drop 3, set 1) of POL0705 *without* the ISL modulation correction.

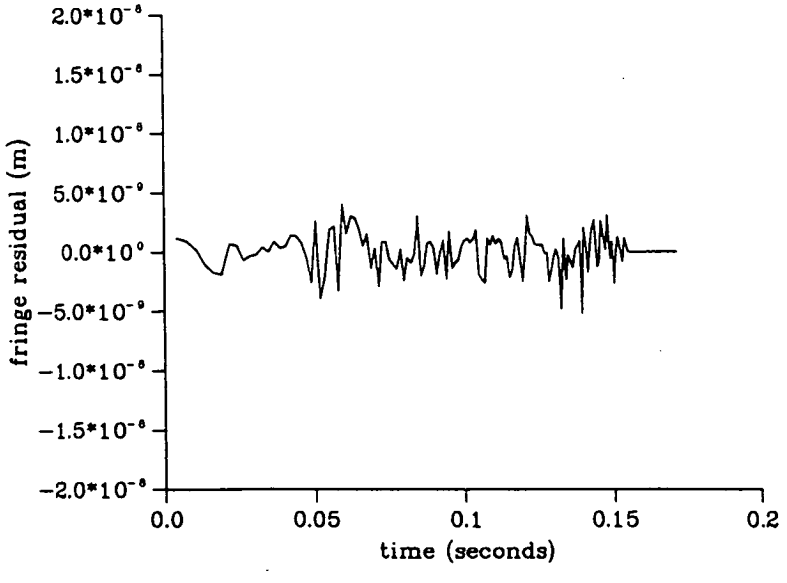

Figure 4.16b Line graph of the fringe residuals for drop 3, set 1 of POL0705 *with* the ISL modulation correction applied.

4.4.7 Atmospheric Pressure Correction

If pressure observations are included in the densified data file, this correction can be made. All values are corrected to the standard atmospheric pressure p_{sa} at the station height *h*, calculated using the International Civil Aviation Authority Standard Atmosphere:

$$p_{sa} = 1013.2\ (1 - 0.000022557\ h)^{5.2613}\ \text{mbar} \qquad (29)$$

The difference between the observed pressure p_{obs} and the standard pressure p_{st} is multiplied by -0.3 mgal mbar $^{-1}$, so that

$$\text{pressure correction} = -0.3\ (p_{obs} - p_{st})\ \mu\text{gal}. \qquad (30)$$

4.4.8 Polar Motion

The polar motion correction in REPLAY is given as

$$g_{pomo} = -0.039 \sin(2\varphi')[x \cdot \cos\lambda - y \cdot \sin\lambda]\ m.s^{-2} \qquad (31)$$

where φ' is the colatitude and λ the east longitude of the station, and x and y are the pole coordinates in radians.

The values of x and y were obtained from the International Radio Interferometric Surveying (IRIS) Earth Orientation Bulletin service by electronic file transfer (ftp) from ray.grdl.noaa.gov. The login is 'anonymous', and an email address is required as the password. The file 'iris.93' is in the directory dist/vlbi. Table 4.4 below shows some example data and the value of the correction at the National Physical Laboratory (NPL) (latitude 51.419°, longitude -0.342°). The x and y coordinates are from the 'iris.93' file with the header 'earth orientation determinations, series 29/ 3/94 23:17:51'.

date time	x	se	y	se	g_{pomo}
yy/mm/d h:m	milliarcseconds		milliarcseconds		μgal
92/08/03 19:17	-83.951	0.202	452.268	0.228	1.50
92/08/31 19:43	-12.604	0.182	502.367	0.197	0.18
92/10/01 21:32	58.620	0.185	502.977	0.192	-1.14
92/11/02 19:24	132.261	0.175	477.536	0.178	-2.49
92/11/30 20:15	175.048	0.137	431.052	0.138	-3.27
93/01/04 21:13	209.374	0.168	347.843	0.158	-3.90
93/02/01 21:23	205.810	0.151	276.507	0.160	-3.82
93/03/01 20:32	175.130	0.157	213.568	0.159	-3.25
93/04/05 20:48	102.183	0.183	167.782	0.195	-1.90
93/05/06 05:39	29.446	0.142	166.926	0.146	-0.56
93/06/02 05:47	-16.628	0.137	181.116	0.141	0.29
93/07/07 06:17	-67.686	0.128	217.304	0.131	1.22
93/08/04 01:17	-85.951	0.134	260.125	0.140	1.55

Table 4.4 Pole coordinates (x, y) and polar motion gravity correction (g_{pomo}) for Aug 92 - Aug 93 at London (NPL) ($\varphi = 51.419°$, $\lambda = -0.342°$).

The largest value of this correction for the location of London during the period August 1992 to August 1993 was -3.9 μgal. The polar motion calculation is not included in DDT, but the correction can easily be added later for any time and place.

A summary of the corrections discussed in sections 4.4.4 - 8, and the tidal corrections from Chapter 3, with their approximate effect on the gravity estimate is given in Table 4.5.

4.4.9 Comparison of drop-drop data from DDT and REPLAY

The differences in some of the corrections have been highlighted above, but a comparison of the drop to drop data from DDT and REPLAY, with no corrections at all, shows the values are identical at the 0.1 μgal level. (The DDT and REPLAY values are rounded off at 0.01 and 0.1 μgal respectively). Table 4.6 shows a sample of a .ggg file (DDT output) and a .grv file (REPLAY output) from NPL0307A.

correction	varies with	comments	range (µgal)
Vertical Gradient (4.4.4 and 5.2)	drop length (fringes) (at 2.925 ± 0.633 µgal cm^{-1})	130 to 160	-22.0 to -28.0 *
	vertical gradient value (µgal cm^{-1}) (at 150 fringes)	2.151 ± 0.066 to 3.168 ± 0.611	-19.1 to -28.1 *
Datum Height (4.4.4 and 5.2)	height (mm) (at 2.151 ± 0.066 µgal cm^{-1})	-300 to -1300	64.5 to 279.6 *
	vertical gradient value (µgal cm^{-1}) (at 1190 mm)	2.151 ± 0.066 to 3.168 ± 0.611	256.0 to 377.0 *
Speed of Light (4.4.5)	drop length (fringes)	130 to 160	-11.4 to -12.9
Static Tide (3.2.4)	latitude	50° to 80° N	-26.5 to -40.4
Elastic Tide (3.2.2)	latitude, longitude and time (periods from 0.5 day to > 10^5 years)	1990 - 1994 inclusive (at locations in Britain)	± ~ 150
Ocean Load (3.1.4)	"	"	± ~ 10
Polar Motion (4.4.8)	latitude, longitude and time		± ~ 4
Atmospheric Pressure (4.4.7)	time	-0.3 µgal $mbar^{-1}$ max range 70 mbar	typically ± 4 (for 24 hour set)

Table 4.5 Summary of corrections to absolute gravity meter data, and the sections where they are discussed.
* Error linear in value of vertical gradient.

Source file: npl0307a.ddt

Number of fringes counted 170
Start fitting at fringe 5
Number of fringes fitted 150

No gradient correction applied

No speed of light correction made

No tidal corrections made

No pressure corrections made

NP03NOTI.GGG (Edinburgh DDT)

```
1  1 1993 184 20 21 40 981181483.34 17.55 265769021.4 18.5 3797946.62  .89
6.75  .23 105. 2.  .00  .00  .00  .00  17  .00 22.82 1021.3 -.096 6.541  50.2
1  2 1993 184 20 21 53 981181444.06 17.50 287169278.1 18.4 5063922.17  .88
6.97  .24 179. 2.  .00  .00  .00  .00  24  .00 22.84 1021.3 -.075 4.448  51.1
1  3 1993 184 20 22  6 981181470.70 17.08 271383778.0 18.2 3797937.49  .88
6.81  .23-145. 2.  .00  .00  .00  .00  23  .00 22.86 1021.3 -.043 1.311  49.5
1  4 1993 184 20 22 19 981181474.95 17.68 276236456.6 18.6 5063938.42  .89
6.74  .24  -8. 2.  .00  .00  .00  .00  23  .00 22.87 1021.3 -.044 1.398  51.7
1  5 1993 184 20 22 32 981181532.28 19.04 296403821.6 19.9 5063936.30  .94
6.95  .26  41. 2.  .00  .00  .00  .00  23  .00 22.87 1021.3 -.035 1.170  54.0
1  6 1993 184 20 22 45 981181462.70 16.92 295950629.8 17.7 5063923.81  .84
6.81  .23-174. 2.  .00  .00  .00  .00  22  .00 22.92 1021.3 -.117 8.141  52.7
1  7 1993 184 20 22 58 981181452.60 16.91 295045962.8 17.5 5063927.43  .83
6.92  .23 108. 2.  .00  .00  .00  .00  20  .00 22.89 1021.3 -.125 9.420  52.3
1  8 1993 184 20 23 11 981181447.59 18.12 302691173.5 19.0 5064239.68  .90
6.68  .25 140. 2.  .00  .00  .00  .00  25  .00 22.91 1021.3 -.040 1.406  53.4
1  9 1993 184 20 23 24 981181513.89 16.50 278461970.3 17.4 5063923.17  .83
6.72  .22 151. 2.  .00  .00  .00  .00  23  .00 22.90 1021.3 -.132 9.720  52.7
1 10 1993 184 20 23 37 981181489.81 18.09 273035321.9 19.0 5063938.82  .91
6.91  .24 -39. 2.  .00  .00  .00  .00  20  .00 22.91 1021.3 -.045 1.416  52.4
```

NP03NOTI.GRV (Axis REPLAY)

```
 1   1  1993:185      20:21:40      9.811814833     .00  .00IF
 1   2  1993:185      20:21:53      9.811814441     .00  .00IF
 1   3  1993:185      20:22: 6      9.811814707     .00  .00IF
 1   4  1993:185      20:22:19      9.811814749     .00  .00IF
 1   5  1993:185      20:22:32      9.811815323     .00  .00IF
 1   6  1993:185      20:22:45      9.811814627     .00  .00IF
 1   7  1993:185      20:22:58      9.811814526     .00  .00IF
 1   8  1993:185      20:23:11      9.811814476     .00  .00IF
 1   9  1993:185      20:23:24      9.811815139     .00  .00IF
 1  10  1993:185      20:23:37      9.811814898     .00  .00IF
```

Table 4.6 Comparison of drop-drop data for the set NPL0307A.with no corrections at all, showing that the DDT and REPLAY gravity values are identical.

4.4.10 Statistics - The Edinburgh program MEAN

MEAN was written by R.G Hipkin to calculate the gravity value and standard error for each drop in the .ggg files generated by DDT. MEAN produces two output files (Figure 4.14). The main one is the .ave file which is similar the the Axis .zzg file (called the .set file in version 3), and contains set means and standard deviations, as well as an overall weighted mean and standard deviation. The second output file .all gives details of the iterative statistics, showing which drops have been assigned reduced weights by the program. An example of the .all (rejected drops) file is given in Table 4.7 for EDI2007A. The .ave (set means) file for NPL0307A is shown in Table 4.8 with the .zzg set means file from REPLAY.

The gravity value estimated for each drop is initially assigned unit weight and the mean and standard deviation for the set (200 drops) is calculated. In subsequent passes over the data, each gravity value is given a new weight according to how different it is from the previous mean. A new weighted mean and standard deviation is calculated, and weights reassigned until no significant change in weight occurs between iterations.

The weights are determined by the parameters ONE and ZERO, which are set by a parameter statement in the program. Data with residuals less than ONE standard deviation are assigned unit weight, values with residuals greater then ZERO standard deviations are given zero weight. In between these limits, the weights are decreased from one to zero with a cosine taper. The weight w_z for values of gravity g with deviations $(g-\bar{g})$ between ONE and ZERO σ is

$$w_z = \frac{1}{2}\left[1+\cos\left(\frac{\pi}{\text{ZERO}-\text{ONE}}\cdot\left(\frac{(g-\bar{g})}{\sigma}-\text{ONE}\right)\right)\right] \qquad (32)$$

Choosing both parameters to be 3 reproduces the 3σ trimmed mean statistics used by Axis, except that their code allows only two passes over the data and sometimes does not converge.

REPLAY uses a different method of suppressing outliers based on two successive box-car filters. The first is a box-car filter about the median. The second is another box-car filter about the resulting mean with a width $n\,\sigma$. The width of the first filter and the value of n are specified in the RECOMND.DAT file and usually have the values 100 μgal and 3, respectively.

The different statistics result in different numbers of drops being rejected, and this is the predominant cause of variation between set means from DDT and REPLAY. This variation, however, does not cause the weighted mean of the 24 sets to be significantly different.

Comparison of set means

Table 4.8 gives the set means and the number of drops included for the 24 sets of NPL0307A, from MEAN and REPLAY. The effect of the different statistics is shown by the sets where different numbers of drops are counted (shown with an asterisk in the table). The sets where the same number of drops are counted differ only by the tidal correction. Note that the MEAN values are in μgal (to 0.01 μgal), and the REPLAY values are in $m\ s^{-2}$ (to 0.1 μgal).

The differences are most noticeable when the data is noisy, i.e there are relatively large numbers of 'bad' drops. In this case, MEAN tends to reject more drops than REPLAY.

EDI2007A.ALL

Source file: edi2007a.ddt

Drop set 1; weight 200.00
Simple mean 981579**192.26**
Standard deviation **16.56**

No change

Drop set **2**; weight 200.00
Simple mean 981579206.51
Standard deviation 291.05

Down weighted residuals

index	residual	weight
25	3856.81	.00
197	-1409.72	.00

Drop set **2**; weight 198.00
Weighted Mean 981579**194.15**
Standard deviation **15.84**

Down weighted residuals

index	residual	weight
25	3869.17	.00
197	-1397.36	.00

No change

Drop set **3**; weight 200.00
Simple mean 981579188.40
Standard deviation 89.20

Down weighted residuals

index	residual	weight
149	-1235.89	.00

Drop set **3**; weight 199.00
Weighted Mean 981579194.61
Standard deviation 16.83

Down weighted residuals

index	residual	weight
54	-60.03	.00
78	-92.61	.00
149	-1242.10	.00

Drop set **3**; weight 197.00
Weighted Mean 981579195.39
Standard deviation 14.96

Down weighted residuals

index	residual	weight
30	47.60	.00
54	-60.81	.00
78	-93.39	.00
149	-1242.88	.00

Drop set **3**; weight 196.00
Weighted Mean 981579**195.15**
Standard deviation **14.60**

Down weighted residuals

index	residual	weight
30	47.84	.00
54	-60.57	.00
78	-93.15	.00
149	-1242.64	.00

No change

Drop set **4**; weight 200.00
Simple mean 981579178.91
Standard deviation 163.99

Down weighted residuals

index	residual	weight
22	-1875.61	.00
156	-1324.62	.00

Drop set **4**; weight 198.00
Weighted Mean 981579195.07
Standard deviation 16.55

Down weighted residuals

index	residual	weight
22	-1891.77	.00
97	59.78	.00
156	-1340.78	.00

Drop set **4**; weight 197.00
Weighted Mean 981579**194.76**
Standard deviation **16.03**

Down weighted residuals

index	residual	weight
22	-1891.46	.00
97	60.09	.00
156	-1340.47	.00

No change

Table 4.7 Example of a .all file (for the FG5-103 EDI2007A dataset taken on (20.07.94)) produced by the Edinburgh program mean, showing the progressive elimination of bad drops. (First 4 sets only).

Set means from **DDT & MEAN** NPL0307A.AVE

decimal day	set	gravity (ugal)	error	weight	
34151.86730	1	981181**374.48**	32.68	242.00	
34151.90887	2	981181**376.51**	24.99	245.00	
34151.95049	3	981181**377.43**	25.89	247.00	
34151.99204	4	981181**376.18**	26.37	243.00	
34152.03370	5	981181**378.41**	25.77	239.00	*
34152.07556	6	981181**377.67**	21.76	241.00	*
34152.11714	7	981181**377.75**	22.85	247.00	
34152.15885	8	981181**378.59**	22.57	239.00	
34152.20048	9	981181**380.36**	19.85	240.00	*
34152.24184	10	981181**382.19**	24.30	245.00	
34152.28382	11	981181**376.40**	23.66	243.00	
34152.32543	12	981181**375.46**	27.29	245.00	*
34152.36721	13	981181**378.89**	37.38	241.00	
34152.40889	14	981181**376.50**	35.67	244.00	
34152.45039	15	981181**380.77**	37.98	245.00	*
34152.49209	16	981181**375.70**	38.52	241.00	*
34152.53394	17	981181**383.55**	39.93	241.00	
34152.57556	18	981181**380.17**	36.31	246.00	
34152.61706	19	981181**384.35**	38.55	244.00	
34152.65880	20	981181**387.13**	36.81	242.00	
34152.70035	21	981181**387.36**	33.33	245.00	
34152.74214	22	981181**384.55**	35.37	246.00	
34152.78381	23	981181**381.56**	33.80	245.00	*
34152.82559	24	981181**382.94**	33.91	246.00	*

Weighted average (ugal) 981181**379.19** st dev **3.20**

Set means from **REPLAY** NPL0307A.ZZG

julian hour	gravity (ms^{-2})	error	weight		laser wavelength
819644.81069	9.81181**374 5**	.32745E-06	242		.6329912127E-06
819645.81069	9.81181**376 5**	.25038E-06	245		.6329912127E-06
819646.81069	9.81181**377 4**	.25959E-06	247		.6329912127E-06
819647.81069	9.81181**376 1**	.26428E-06	243		.6329912127E-06
819648.81069	9.81181**378 0**	.26290E-06	240	*	.6329912127E-06
819649.81069	9.81181**378 0**	.22196E-06	242	*	.6329912127E-06
819650.81069	9.81181**377 8**	.22886E-06	247		.6329912127E-06
819651.81069	9.81181**378 7**	.22623E-06	239		.6329912127E-06
819652.81069	9.81181**380 3**	.20968E-06	243	*	.6329912127E-06
819653.81069	9.81181**382 3**	.24350E-06	245		.6329912127E-06
819654.81069	9.81181**376 5**	.23722E-06	243		.6329912127E-06
819655.81069	9.81181**375 1**	.27817E-06	246	*	.6329912127E-06
819656.81069	9.81181**378 7**	.37463E-06	241		.6329912127E-06
819657.81069	9.81181**376 2**	.35748E-06	244		.6329912127E-06
819658.81069	9.81181**380 3**	.36865E-06	243	*	.6329912127E-06
819659.81069	9.81181**375 2**	.37400E-06	239	*	.6329912127E-06
819660.81069	9.81181**383 1**	.38699E-06	239		.6329912127E-06
819661.81069	9.81181**379 8**	.36383E-06	246		.6329912127E-06
819662.81069	9.81181**384 1**	.39641E-06	244		.6329912127E-06
819663.81069	9.81181**387 0**	.36884E-06	242		.6329912127E-06
819664.81069	9.81181**387 4**	.33396E-06	245		.6329912127E-06
819665.81069	9.81181**384 7**	.35445E-06	246		.6329912127E-06
819666.81069	9.81181**382 1**	.33323E-06	244	*	.6329912127E-06
819667.81069	9.81181**383 1**	.33982E-06	246	*	.6329912127E-06

Weighted average (ugal) 981181**379.7** st dev **3.8**

Table 4.8 The set means for NPL0307A, with no corrections except tidal. Note the different units for gravity, except for the weighted means, which are both given in μgal.

4.5 Conclusions

The FG5 is a commercially available absolute gravity meter which is operated in free-fall mode. The trajectory of a falling mass is recorded using laser interferometry. At the 1994 Intercomparison of Absolute Gravimeters at Sèvres, 5 out of the 12 participateing instruments were FG5s, and 4 were JILAG meters, from which FG5 was developed. The proper comparison of the absolute gravity estimates from these instruments, and with observations made with different types of instrument in the past and future, requires all the observations to be referred to a precise height.

It has been shown that the 'Effective Measurement Height' for absolute gravity estimates, made without including the vertical gradient of gravity in the equation of motion, is incorrectly predicted by the theory. The failure is partly due to the fact that about 10 % of the interference fringes are missed by the counting mechanism, which increases the actual length of the drop by about 10 %. This means that the concept of an 'Effective Measurement Height' is inadequate for precise comparisons, and the full equation of motion *with* the vertical gradient terms must be used. This equation gives an estimate for gravity at the top of the drop. The two common interpretations of the 'top of the drop' are the points where distance equals zero, and time equals zero respectively, and this leads to estimates of gravity which differ by about 1.5 μgal. The consequences of the particular equation used must be appreciated when intercomparing.

The programs DDT and REPLAY, used for processing the raw absolute gravity data, give identical estimates of the drop-to-drop gravity values from FG5. The set means may vary due to the different filtering procedures and tidal corrections. DDT performs a superior filtering routine in which a weighted mean and standard deviation are calculated, and weights are applied, iteratively, until no significant change in weight occurs between iterations. The REPLAY routine passes over the data at most twice. The tidal correction in DDT uses a full Cartwright-Tayler-Edden expansion, which is more precise than the closed approximation used in REPLAY.

The appreciation of the effects of software corrections, for example the speed of light and datum corrections, and systematic instrumental effects, in particular those arising from the laser, is essential for the intercomparisons which are described in the next chapter.

CHAPTER 5. Absolute Measurements and Intercomparisons

Introduction

The first part of this chapter reviews the results of international comparisons of some of the types of gravimeters described in Chapter 4, and then considers how the gravity estimate from a single instrument can vary according to the equation of motion used, the drop length and the characteristics of the site. In the second part of the chapter, the techniques described for attaining the most accurate value of gravity are applied to the observations of FG5 instruments at seven absolute sites in Britain. Comparisons between FG5-103 and 105 andFG5-103 and 107 are made at Teddington and Taunton respectively, and the comparison between FG5-103 and JILA4 is made at Edinburgh.

Part 1. Intercomparisons and important considerations for comparing free fall observations

5.1 Intercomparisons of Absolute Gravimeters

5.1.1 Sèvres

Since Volet's early free-fall experiments in 1951, the Bureau International des Poids et Mésures (BIPM) at Sèvres in France has been an important centre for the measurement of absolute gravity. Stationary rise-and-fall apparatus developed by Sakuma (section 4.1.3), which first measured gravity there in about 1963, is now the standard to which other instruments are compared. The Istituto di Metrologia 'G. Colonnetti' (IMGC) transportable instrument made regular observations at BIPM throughout its development and as part of the first European absolute gravity programme during 1976 - 77 (Cannizzo *et al.* 1978).

The development of different absolute gravimeters has been reviewed in Chapter 4 (section 4.1). On the recommendation of the International Association of Geodesy the first observational campaign to compare absolute gravimeters was held at BIPM in 1981. Further comparisons followed in 1985, 1989 and 1994. The instruments participating at each event are shown in Table 5.1. Six institutions took part in the first comparison and the exercise confirmed the existence of 'certain previously suspected systematic errors' (Boulanger *et al.* 1986). The Second International Comparison of Absolute Gravimeters (ICAG) was held in 1985 and again six instruments (of which three were the same as in the

1981 comparison) participated. The absolute instruments measured at different pillars at the BIPM and the gravity values were reduced to the surface height of the pillars. Vertical gradients and the differences in gravity between the pillars were observed by 14 LCR relative gravity meters during the campaign. The absolute observations were transferred to Sèvres A using the relative observations for comparison.

A detailed study of the vertical gradients on and around some of the pillars used for the ICAG was made in 1985 and 1986 (Röder & Wenzel 1986). Some significant changes in the vertical gradients were observed between the 1981 and 1985 ICAG campaigns. (Table 5.2).

Station	Gradient 1981 (μgal m^{-1})	Gradient 1985 (μgal m^{-1})	Discrepancy (μgal m^{-1})
A1	not observed	311.8 ± 0.6	
A3	283.6 ± 1.6	295.3 ± 1.2	+ 11.7
A4	253.5 ± 1.3	255.3 ± 1.0	+ 1.8
A5	250.8 ± 1.1	252.4 ± 0.7	+ 1.6
A6	251.8 ± 1.2	258.9 ± 0.9	+ 7.1
A7	not observed	259.0 ± 0.5	

Table 5.2 Comparison of gravity gradients from 1981 (1st) and 1985 (2nd) ICAG at Sèvres (from Röder & Wenzel 1986).

Röder & Wenzel attribute the changes to four possible causes: i) different evaluation methods (causing discrepancies of 1 - 3 μgal), ii) measuring at ex-centres (for example 0.8 m from the pillar instead of on top of the pillar), iii) systematic errors arising from the use of different relative instruments and iv) real changes in the gravity field due to the construction of a new building. The non-linearity of the gravity field in the vertical direction was investigated by observing at 0.0 m, 0.4 m, 0.6 m, 0.8 m, 1.0 m and 1.2 m elevation, and was found to be 3 μgal at maximum.

The atmospheric pressure correction was applied and all the tidal corrections were made using tables supplied by Sakuma. The polar motion and the Honkasalo corrections were not introduced. Systematic differences of about 40 μgal were detected, some of which were due to the relative transfers. The average value determined at Sèvres A was 18.8 ± 3.0 μgal higher than in 1981. This difference was attributed to 'local causes' (Boulanger *et al.* 1986). Table 5.3 shows the absolute values measured at the various pillars and the values transferred to pillar A. The column giving the difference between the BIPM instrument and the others shows that IMGC, GABL and JILA give a value about 22 μgal higher than the BIPM instrument, and NIM and IGPP give a value about 38 μgal higher. This suggests that

1981 - 1st	**1985** - 2nd	**1989** - 3rd	**1994** - 4th
BIPM	BIPM	BIPM	BIPM
IMGC	IMGC	IMGC	IMGC
Jaeger	GABL	NIM	Jaeger
GABL	NIM	GABL	JILAG-2
Hammond	JILA	NAOM	JILAG-3
Faller	IGPP	JILAG-2	JILAG-5
		JILAG-3	JILAG-6
		JILAG-4	FG5-101
		JILAG-5	FG5-102
		JILAG-6	FG5-104
			FG5-107
			FG5-108

Table 5.1 Instruments measuring at the Four International Comparisons of Absolute Gravimeters (ICAG) at Sèvres 1981, 1985, 1991 and 1994.

BIPM Bureau International des Poids et Mesure, Sèvres. Stationary rise-and-fall instrument built by Sakuma.

IMGC Istituto di Metrologia 'G. Colonnetti', Torino. Transportable rise-and-fall instrument.

Jaeger Jaeger S.A Manufacturers, France. Commercially available rise-and-fall developed by BIPM and IMGC.

GABL Institute of Automatics and Electrometry, Siberian Branch of Academy of Sciences of the USSR, Novosibirsk. Free fall instrument.

Hammond USA. Free fall instrument built by Hammond and Faller in about 1965.

Faller Predecessor of JILAG free-fall instrument.

NIM National Institute of Metrology, Beijing, China. Free fall instrument.

IGPP Institute of Geophysics and Planetary Physics, Scripps Institute of Oceanography, USA. Free fall instrument built by Zumberge, based on JILAG.

NAOM National Astronomical Observatory, Mizusawa, Japan. Free fall instrument.

JILAG Joint Institute for Laboratory Astrophysics (JILA) Gravimeter, Boulder USA. Free fall instrument developed from Faller's prototype.
2 - Geological Survey of Canada. 3 - Institut für Erdmessung, Hannover.
4 - National Geodetic Survey, USA. 5 - Finnish Geodetic Institute.
6 - Institute for Metrology and Geophysics, Austria.

FG5 Commercial free fall instrument built by Axis Instruments, Boulder USA, developed from JILAG.
101 - Institut für Angewandte Geodäsie, Frankfurt.
102 - National Institute for Standards and Technology (NIST) / NOAA, USA.
104 - Geographical Survey Institute, Japan.
107 - Defence Mapping Agency, USA.
108 - BIPM, Sèvres.

Instrum (error)[1]	Site	H_{eff} [2] (mm)	grad [3]	g(H_{eff})[4] - 980 920 000	D.C [5]	transfer[6] to A	g(A)[7] - 980 920 000	diff [8]
BIPM (0)	A	1120	311.4 (0.7)	**5 627.5 (5.6)**	348.8	-	5 976.3 (5.6)	**0.0 (5.6)**
IMGC (4.7)	A3	851	295.2 (1.1)	**5 673.4 (2.2)**	251.2	+70.7 (0.4)	5 995.4 (5.3)	**19.1 (7.7)**
GABL (4.5)	A3	980	295.2 (1.1)	**5 642.5 (3.2)**	289.3	+70.7 (0.4)	6 002.5 (5.6)	**26.2 (7.9)**
GABL (4.4)	A6	971	259.0 (0.8)	**6 359.7 (4.0)**	251.5	-609.2 (0.4)	6 002.0 (6.0)	**25.7 (8.2)**
NIM (8.1)	A4	1120	255.9 (1.0)	**6 313 (11.2)**	286.6	-583.2 (0.5)	*6 016.4 (13.9)	**40.1 (15.0)**
JILA (7.7)	A5	830	252.5 (0.7)	**6 368.5 (2.0)**	209.6	-578.7 (0.4)	5 999.4 *(8.0)	**23.1 (9.8)**
IGPP (5.7)	A7	1090	259.1 (0.5)	**6 391.1 (3.6)**	282.4	-660.1 (0.4)	6 013.4 (6.8)	**37.1 (8.8)**

Table 5.3 Comparison of absolute gravity observations from the second ICAG, compiled by the author from Tables 1, 2a, 3, 4 and 5 of Boulanger *et al.* (1986). All numerical values (except H_{eff}) are in μgal.

Notes

1 Estimated instrumental error budget Table 3 of Boulanger *et al.* (1986).
2 H_{eff} is the effective measurement height (section 4.3.3)
3 Vertical Gradient values are the mean of all observations with 12 LCR instruments (Table1 *ibid.*).
4 Statistical error on the mean of all the observations of the particular occupation (Table 3 *ibid.*).
5 The error on the reduction to the pillar surface (Table 3 *ibid.*) was assumed to be equal to that on the vertical gradient in the original calculations.
6 Error on the transfer from the combined adjustment of all the relative gravity measurements made between the pillars (Table 2a *ibid.*).
7 Error calculated by the rms sum of errors 1,3,4 and 6.
8 Difference between value transferred to Sèvres A and the BIPM value.
* Transcription and rounding errors (amounting to 0.2 μgal) noted in the original paper (*ibid.*) have been corrected here.

the BIPM value is too low. Since the other rise-and-fall instrument (IMGC) agrees with the GABL and JILA values then a systematic difference between the rise-and-fall and free-fall types is not evident from this intercomparison.

The Third ICAG duly took place four years later in 1989 with ten instruments which included five JILA meters (Boulanger *et al.* 1991). The possibility of non-linear gradients above measurement pillars had been acknowledged, and the relative observations were designed to minimise any errors associated with this phenomenon. Since most of the instruments have measurement heights between 0.6 and 1.2 metres, careful observations were made at points between 0.85 and 1.25 metres with a group of relative gravity meters. This enabled the absolute observations to be transferred reliably to a datum of 0.85 metres. Relative ties were made directly between 0.85 metres above the various pillars and the comparison datum at 0.05 metres above the pillar A. Table 5.4 shows the results from this comparison.

The observations took place in two groups from 16 to 20 November and 28 November to 7 December. There was a systematic difference between the average values of these two groups of 10.3 ± 2.5 μgal. The cause of this short-term change was attributed to unstable weather or hydrogeological changes (BIPM is rather close to the Seine river) and it was suggested that these gravity variations should be recorded with a cryogenic gravimeter during future intercomparisons. The participation of a large number of JILA instruments provided the opportunity to investigate sytematic differences between this type and other absolute gravimeters. The difference of 1.7 ± 3.9 μgal between these groupings was not significant. Corrections were made as for the second ICAG, but this time polar motion was included. The overall results (Boulanger *et al.* 1991) concluded that a single absolute gravimeter could operate with an accuracy of ± 7 - 8 μgal, but recommended that groups of four of five instruments be used for global first order networks if accuracies of ± 3 - 4 μgal were to be achieved.

The Fourth ICAG was in June 1994. It included a workshop on Gravimetry at which the author gave a paper, but unfortunately the NERC FG5 absolute meter did not participate in the measurements. Of the twelve instruments present there were five FG5s, four JILAs and three rise-and-fall instruments. The relative gravity measurements were made by twenty relative gravity meters (17 LCR, 2 Scintrex, 1 ZLS) (Becker 1994). The absolute results are expected soon (Metrologia Special Issue on Gravimetry, 1995 in press).

Results of the Third ICAG at Sèvres 1989

Instrument (error)[1]	Site	H_{eff} [2] (mm)	grad [3]	$g(H_{eff})$[4] - 980 920 000	D.C [5]	transfer [6] to A	g(A)[7] - 980 925 900	difference from IMGC
IMGC (5)	A3	926	290.5	**5 631.0 (1.8)**	+22.1	+310.2 (2.2)	63.8 (5.8)	**0.0 (5.8)**
GABL (3.3)	A	984	302.2	**5 697.5 (2.8)**	+40.5	+248.9 (1.2)	86.9 (4.4)	**23.1 (7.3)**
	A3	986	290.5	**5 636.1 (2.8)**	+37.8	310.2 (1.2)	84.1 (4.7)	**20.3 (7.5)**
NIM	A1	1178	300.5	**5 611.8 (5.9)**	+37.8	+257.4 (1.2)	67.8 (6.4)	**4.0 (8.6)**
(3.9)	A5	1177	252.8	**6 267.6 (5.9)**	297.5	-596.8 (1.2)	68.3 (8.0)	**4.5 (9.9)**
NAOM	A2	581	308.5	**5 819.8 (15.)**	-83.0	+242.4 (1.2)	70.0(17.9)	**6.2 (18.8)**
(5.5)	A8	581	242.8	**6 397.1 (15.)**	-65.3	-354.2 (1.2)	77.6(14.1)	**13.8 (15.2)**
JILAG2	A	910	302.2	**5 714.5 (0.6)**	+18.1	+248.9 (1.0)	81.5 (1.8)	**17.7 (6.1)**
(1.4)	A1	910	300.5	**5 706.5 (0.6)**	+18.0	+257.4 (1.0)	82.0 (1.8)	**18.2 (6.1)**
	A3	910	290.5	**5 651.3 (0.6)**	+17.4	+310.2 (1.0)	78.9 (1.9)	**15.1 (6.1)**
JILAG3	A1	795	300.5	**5 729.0 (3.4)**	-16.5	+257.4 (1.2)	69.9 (4.8)	**6.1 (7.5)**
(3.3)	A3	801	290.5	**5 688.5 (3.4)**	-14.2	+310.2 (1.2)	84.5 (4.8)	**20.7 (7.5)**
JILAG4(2.8)	A2	907	308.5	**5 780.7 (0.4)**	+17.6	+242.4 (1.2)	80.7 (3.0)	**16.9 (6.5)**
JILAG5	A1	834	300.5	**5 717.5 (0.7)**	-4.8	+257.4 (1.2)	70.1 (3.2)	**6.3 (6.6)**
(3.0)	A2	834	308.5	**5 729.7 (0.7)**	-4.9	+242.4 (1.2)	67.2 (3.3)	**3.4 (6.7)**
	A8	833	242.8	**6 326.2 (0.7)**	-4.1	-354.2 (1.2)	67.9 (3.3)	**4.1 (6.7)**
JILAG6	A2	840	308.5	**5 746.1 (1.2)**	-3.1	+242.4 (1.2)	85.4 (4.3)	**21.6 (7.3)**
(3.9)	A8	840	242.8	**6 337.2 (1.2)**	-2.4	-354.2 (1.2)	80.6 (4.3)	**16.8 (7.3)**

Table 5.4 Comparison of absolute gravity observations from the third ICAG, compiled by the author from Tables 3 and 4 of Boulanger *et al.* (1991). All numerical values (except H_{eff}) are in μgal.

Notes: 1 Total instrumental error from Table 3 of Boulanger *et al.* (1991).
2 H_{eff} is the effective measurement height (section 4.3.3).
3 and 5 as for Table 5.3.
4 The error is the column 'accidental errors' in Table 3 (*ibid.*).
6 The error on the transfer to A is the column 'Error reductions to pillarA' in Table 3 (*ibid.*).
7 The error on gravity at A is from the column 'M_A' of Table 4 (*ibid.*). Where it is not equal to the sum of the squared errors 1, 4 and 6, the discrepancy is due to a rounding error in the calculations of the original which cannot be identified from the information available.

5.1.2 Table Mountain Intracomparison

The NOAA Table Mountain Gravity Observatory at Boulder, USA is another site at which many absolute gravity meters have measured simultaneously or within periods of days or weeks. The short-term repeatability of individual FG5 instruments and the results of simultaneous observations of pairs of FG5s have been tested over 6 months in 1993 at Table Mountain, where JILA4 was also in operation (Carter *et al.* 1994). The term 'Intracomparison' was adopted by Sasagawa to distinguish this sort of comparison of many instruments of one type from the Intercomparisons described above. The 28 gravity values of this 'Intracomparison' have a standard deviation of 1.1 μgal (each 'gravity value' is a mean of typically 24 sets of 200 gravity observations). Sasagawa *et al.* (1994) gives an estimated standard deviation of 7 - 8 μgal on individual sets of 100 - 250 observations. Neither of these results include atmospheric or groundwater corrections.

5.1.3 Other Comparisons

'Mini comparisons' of two or three absolute gravity meters are easier to organise and always of value, for example JILA3, JILA5 and the superconducting meter TT30 (Ducarme *et al.* 1990), FG5-101 and FG5-102 at Onsala (Klopping *pers. comm.*). The comparisons of FG5-103 observations with a JILA4 observation at Edinburgh, with FG5-105 at London and with FG5-107 at Taunton are made in sections 5.5, 5.6 and 5.7 respectively. As a forerunner to the comparisons, the detailed work which was done with respect to the vertical gradient determinations (section 5.2) and systematic instrumental effects (section 5.3) is discussed. The whole of this chapter describes, what is in effect, a 'large scale intercomparison', where the differences between sites are a few hundred milligals rather than a few hundred microgals. The relative transfers and vertical gradient corrections for this comparison have been made, not using tens of thousands of observations collected by an international team using about 15 LCR instruments, but with hundreds of observations made by three observers with one LCR each. The differences betwen the sites constitute the British Precise Gravity Network, which is the subject of Chapter 6. Raw data for FG5-101, 103, 105 and 107, supplied by their respective owners, has been reprocessed extensively by the author to determine the optimum values for the comparison.

5.2 Vertical Gradients

5.2.1 Introduction

The importance of measuring the vertical gradient at absolute stations precisely has been discussed in Chapter 4. It is needed for the Vertical Gradient Correction and for the Datum Height Correction. Because of the non-uniform mass distribution, the vertical gradient can vary significantly from the free-air value of 308.6 μgal m^{-1}, especially inside buildings or underground. Many of the most suitable gravity sites are in basements to minimise the effects of building sway or bouncy floors. In addition, absolute sites are often on pillars which have a different density from the surrounding floor. In the discussion of intercomparisons of absolute gravimeters in Boulanger *et al.* (1991), Boulanger notes that 'In laboratory, ..., concentrations of exciting masses are often located in immediate vicinity to a pillar'. As well as being non-linear, the value of the vertical gradient varies considerably. Gradients measured at the National Geodetic Survey (NGS) Absolute Gravity Network (NGS 1990) at sites all over North America range from 220.7 to 449.6 μgal m^{-1}.

This section describes the observation of the vertical gradient at seven absolute gravity sites in Britain. Two sites are at the Proudman Oceanographic Laboratory (POL1 and POL2); two are in Edinburgh, at the Grant Institute of Edinburgh University (GI) and at Murchison House of the British Geological Survey (BGS); three are at the National Physical Laboratory, Teddington (NPL1, NPL2 and TEDA) and one site is at the Hydrographic Office, Taunton. These observations show that some of these gradients are non-linear.

The variation of gravity with height was estimated by supporting one LCR base plate (dish) with a tripod or table and measuring with the gravity meter alternately on this elevated dish and on another dish sitting vertically below on the floor. On some occasions, the observation sequence involved three dishes, two elevated at different heights and the third on the floor. Three of four loops were observed with two gravity meters simultaneously. All three dishes were the same size and shape and were adequately levelled, so the relative heights of the gravity meters were found by measuring from the floor to the bottom of the feet of the upper dishes. The study of Röder & Wenzel (1986) on, around and above the pillars used for the ICAG campaigns at Sèvres indicated that it is important that the gradients are estimated from observations in the same vertical line. The non-uniform mass distribution, which is the cause of non-linearity in the vertical gradient, will also cause lateral variations in gravity. Their results were summarised in section 5.1.

The data analysis leading to estimates for the vertical gradient and datum height corrections will be described in detail for the sites at the Proudman Oceanographic Laboratory. Corresponding analysis for the other sites will only be given where the procedure or interpretation differs but the results for all sites are given in Table 5.5 (vertical gradient data), Table 5.6 (polynomial coefficients for non-linear fits), Table 5.7 (average gradient over the drop) and Table 5.8 (datum corrections).

5.2.2 POL Basement Observations

The Proudman Oceanographic Laboratory at Bidston, Birkenhead, is the 'home base station' for FG5-103. The gravity site is in the sub-basement of the old observatory which is at the top of a steep sided hill. Two sites POL1 and POL2 are at opposite ends of the basement and about 12 metres apart (Figure 5.1). In 1992 the vertical gradient was measured at both sites between the floor and one elevated dish (the sites labelled 'old tripod' in Table 5.5 at 1.062 and 1.050 m for POL1 and POL2 respectively). The vertical gradient at POL1 was measured with LCR meters G275 and D154. The gradient at POL2 was measured with G275 and D145 in a sequence which included the tie between POL1 and POL2. The two sites were connected via the top of the tripod at POL2, i.e they were not linked directly at floor level. Figure 5.2 shows the 1992 observation sequence. The adjustment of the 1992 observations alone gave gradients which were unexpectedly low and apparently different: 231.5 ± 4.0 μgal m^{-1} (POL1) and 240.1 ± 4.4 μgal m^{-1} (POL2).

In 1994 the gradients were remeasured using two elevated dishes - one on a tall tripod, the other on a table underneath the tripod - and on a baseplate on the floor underneath the table. (The FG5 'party tray' was conveniently used as the 'table'.) The sequence for the 1994 vertical gradient observations consisted of 4 measurements at each station with G275 and D145. With the addition of the 1992 observations, we have four pairs of gravity-height values at each site. Table 5.5 gives the values for POL1 and POL2 and the corresponding data for the other absolute sites. Reobservation of the vertical gradients also took place at Edinburgh GI and BGS, and at Taunton.

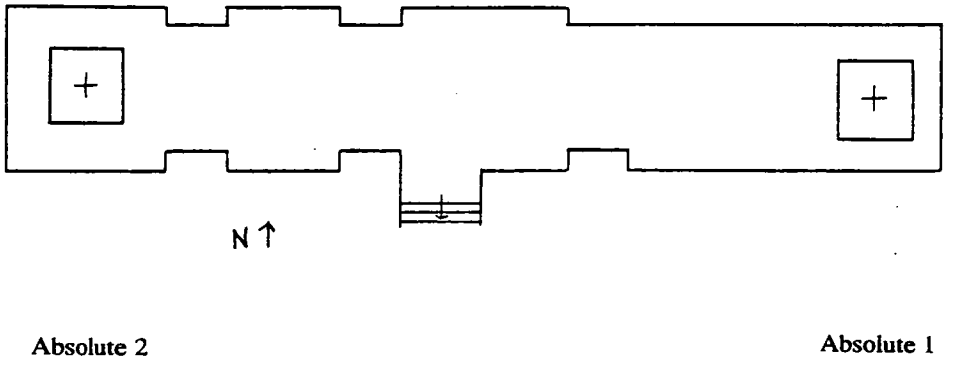

Figure 5.1 Plan of the observatory basement at the Proudman Oceanographic Laboratory (POL). The centres of the sites POL1 and POL2 are about 12 m apart.

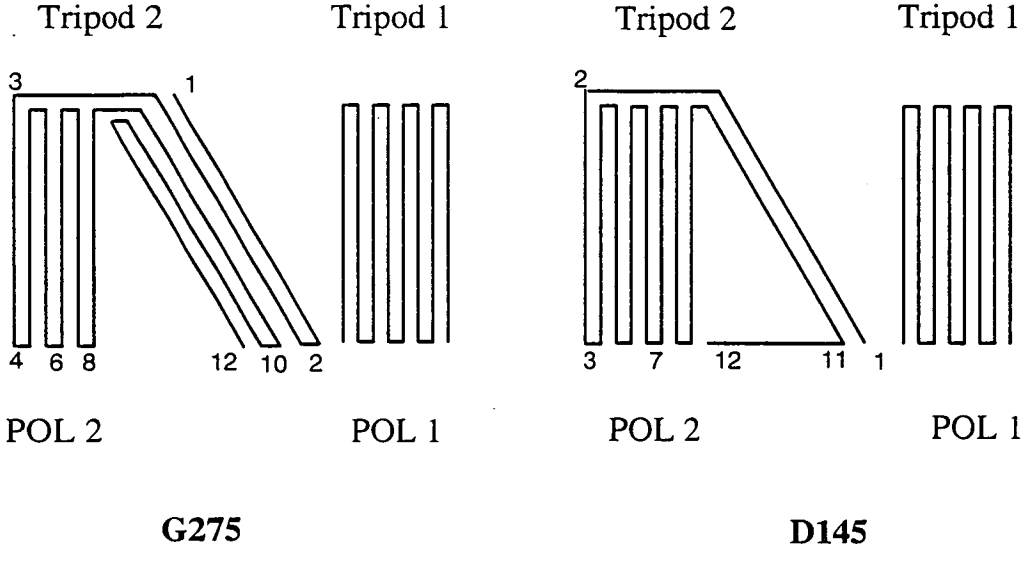

Figure 5.2 Observation sequence made in 1992 for measuring the vertical gradients at POL1 and POL2, and for connecting the two sites.

Site	h ± 3 (mm)	Δg (μgal)	s.e (μgal)
POL1			
New Tripod 1	1605	-364.6	2.7
Old Tripod 1	1062	-248.3	3.6
Party Tray 1	0873	-214.2	2.5
Floor 1	0000	000.0	2.7
POL2			
New Tripod 2	1584	-370.6	4.5
Old Tripod 2	1050	-253.5	3.9
Party Tray 2	0873	-213.4	4.6
Floor 2	0000	000.0	4.1
BGS			
New Tripod	1342	-393.6	6.0
Old Tripod	1141	-335.3	5.9
Tripod A	1030	-289.4	6.5
Table	0764	-209.0	6.0
Floor	0000	000.0	5.7
GI			
New Tripod	1512	-452.9	0.9
Old Tripod	1135	-335.5	0.6
Table	0755	-223.6	1.0
Floor	0000	000.0	0.6
TEDA			
Tripod A1	1167	-348.0	3.5
Tripod A2	1158	-343.0	1.9
Floor NPLA	0000	000.0	2.9
NPL1			
Tripod NPL1	1103	-328.7	3.2
Floor NPL1	0000	000.0	3.0
NPL2			
Tripod NPL2	1121	-331.3	3.3
Floor NPL2	0000	000.0	3.3
TAU			
New Tripod	1373	-409.4	1.4
Old Tripod	1128	-347.7	1.0
Table	0754	-226.2	1.3
Floor	0000	000.0	0.9

Table 5.5 Results of relative observations to measure the vertical gradient at British Absolute sites.

5.2.3 Non-linear Gradients

For the purposes of the Vertical Gradient and Datum Corrections to absolute gravity measurements, the non-linearity of the gradient needs to be investigated. It is important to use the value of the gradient averaged over the drop length for fitting the full equation of motion (equation (7) of Chapter 4). For the transfer of the absolute value to some other height ('Datum Correction'), for example to 1 metre above floor level, it is not sufficiently accurate to multiply the height difference by the same average vertical gradient. The actual gravity difference between the two heights must be used. If this gravity difference between the two heights has not been measured directly, then the variation of gravity with height may be determined by fitting the available gravity-height data with low order polynomials.

In general, one would fit polynomials of increasing order until the fit did not change significantly between orders. There were usually 4 pairs of gravity-height observations which limited the complexity of the fit to a cubic. A comparison of linear gradients calculated in the regions between the actual observations showed that they were usually inconsistent with the gradient being linear over the height range (about 1.5 m) of the observations (section 5.2.6). The next simplest hypothesis to a linear gradient is a quadratic one. A least squares fitting routine QUAD was used to find the linear, cubic and quadratic coefficients for each set of observations of relative gravity and height, by fitting the equations

$$\Delta g(h) = a_1 + b_1 h \qquad (1)$$

$$\Delta g(h) = a_2 + b_2 h + c_2 h^2 \qquad (2)$$

$$\Delta g(h) = a_3 + b_3 h + c_3 h^2 + d_3 h^3 \qquad (3)$$

(h = Height - 120 mm, as discussed below).

The errors on the quadratic fits (Table 5.6) are often more than twice as large as the errors on the linear gradients calculated more simply using two pairs of gravity-height observations and their associated error from the adjustment of the observations. Although cubic terms would be necessary to 'straighten out' an unrealistic quadratic curve, it was felt unsatisfactory to place any weight on the cubic fits. The likelihood of them being distorted by observational errors in the data was significant because there are no degrees of freedom left.

The coefficients for the linear, quadratic and cubic fits are given in Table 5.6. The errors on the linear (a_1, b_1) and quadratic (a_2, b_2, c_2) coefficients are given in brackets. Since there are only four points, the cubic passes through all these points so there are no errors.

5.2.4 Vertical Gradient over the Drop

The absolute value of gravity obtained when the vertical gradient is included in the fit to free-fall distance-time data is assigned to the 'top of the drop'. For FG5-103, this position is known from the dimensions of the instrument, and is at about 1309 mm above the floor. FG5-103 is set up to start counting at fringe 5 and to fit 150 fringes. One fringe corresponds to a distance of $4000\ \lambda/2 \approx 1.266$ mm, so that fringe 5 occurs at a height of 1304 mm and fringe 150 at 1114 mm. The vertical gradient required for the equation of motion is therefore that between 1114 and 1304 mm above the floor.

The zero of gravity in Table 5.5 corresponds to the meter sitting on the baseplate on the floor; the sensing element (the mass of the beam) of the LCR meter is then 120 mm above the floor. The zero of h in equations (1) to (3) above corresponds to the position where relative gravity is zero, i.e 120 mm above the floor.

The value of gravity at 1114 mm above the floor (the bottom of the drop) therefore corresponds to h = (1114-120), i.e $\Delta g(h = 994)$. Similarly the first fitted fringe (fringe 5) occurs at $\Delta g(h = 1184)$. The average gradient over the drop as predicted from the fit is found by calculating the slopes

$$g'(h) = b_1 \tag{4}$$

$$g'(h) = b_2 + 2c_2h \tag{5}$$

$$g'(h) = b_3 + 2c_3h + 3d_3h^2 \tag{6}$$

of each curve at the first and last fitted fringe (5 and 150 respectively) and taking the average.

Calculation of the error in the slope ($b_2 + 2c_2h$) from the quadratic coefficients uses components of the variance-covariance matrix of the least squares fit. The variables a, b and

c all result from the same fit, so they are not independent. The variance V in the function (b + 2ch) at some particular value, h_k, of h is

$$V(b+2ch_k) = V(b) + 4h_k\, cov(bc) + 4h_k^2\, V(c) \qquad (7)$$

The standard error on the slope is the square root of the variance, and is calculated by the program QUAD.

The variances and covariances are found by multiplying the normal equation inverse matrix by the mean square error of the fit (σ^2).

The results of this procedure are given in Table5.7. POL1 data give the value -215.3 ± 31.1 μgal m^{-1} for the quadratic fit.

5.2.5 Datum Correction

Datum correction or height transfer of the measured absolute value is necessary for comparisons between different instruments and sites. The error on the transferred value is greater than on the original absolute measurement because of the uncertainty in the relative observations, and will be in proportion to the size of the correction. For these reasons, the datum for comparison should be made as close to the original measurement height as possible, for example a datum of 1.0 m is preferred to floor level.

One of the aims of the work described in this thesis is to compare relative and absolute gravity observations over distances of many hundreds of kilometres (equivalently hundreds of mgal in gravity) in Britain. In this case, the absolute observations (referred to the 'top of the drop' at about 1300 mm above the floor) have to be transferred to the height of the relative observations (about 120 mm above the floor). These points will be referred to as the 'absolute datum' and 'relative datum' respectively.

As discussed above, the height of the sensing element of an LCR meter sitting on a base plate is about 12 cm above the floor. This point corresponds to the zero of h in equations (1) to (3). The value of relative gravity *at* the floor would be $\Delta g\,(h = -120)$. If the LCR meter is standing directly on the floor, its sensor is at about 65 mm and the corresponding value of gravity is $\Delta g\,(h = -55)$.

	POL1 (4)	POL2 (4)	BGS (5)	GI (4)	TAU (4)	TAU (3)†
a_1 (μgal)	-0.005 032 (0.008 429)	-0.003 353 (0.005 491)	0.005 458 (0.009 036)	0.001 201 (0.002 025)	-0.000 549 (0.005 845)	-0.000 411 (0.001 041)
b_1 (μgal mm^{-1})	-0.227 958 (0.007 978)	-0.234 984 (0.005 251)	-0.294 036 (0.009 272)	-0.297 884 (0.001 989)	-0.301 415 (0.006 056)	-0.298 244 (0.001 509)
a_2 (μgal)	-0.288 080 (5.349 879)	-0.015 349 (0.313 944)	0.122 220 (4.916 349)	-0.050 205 (0.523 144)	0.582 056 (8.300 455)	
b_2 (μgal mm^{-1})	-0.258 125 (0.014 377)	-0.256 783 (0.000 856)	-0.243 807 (0.016 920)	-0.288 951 (0.001 585)	-0.311 968 (0.029 172)	
c_2 (μgal mm^{-2})	1.966 320 10^{-5} (0.886 977 10^{-5})	1.442 738 10^{-5} (0.053 610 10^{-5})	-3.963 198 10^{-5} (1.281 957 10^{-5})	-0.612 609 10^{-5} (0.103 786 10^{-5})	0.800 479 10^{-5} (2.127 690 10^{-5})	
a_3 (μgal)	0.000 000	0.000 000	-0.036 371 (0.213 648)	0.000 000	0.000 000	
b_3 (μgal mm^{-1})	-0.360 702	-0.263 266	-0.213 648 (0.095 703)	-0.310 798	-0.196 639	
c_3 (μgal mm^{-2})	1.904 633 10^{-4}	0.253 184 10^{-4}	-0.967 097 10^{-4} (1.767 749 10^{-4})	0.313 002 10^{-4}	-2.139 795 10^{-4}	
d_3 (μgal mm^{-3})	-6.683 041 10^{-8}	-0.430 562 10^{-8}	2.624 087 10^{-8} (8.088 414 10^{-8})	-1.577 532 10^{-8}	10.198 451 10^{-8}	

Table 5.6 Coefficients for the linear, quadratic and cubic fits to the vertical gradient observations of Table 5.5.The standard errors are given in brackets under their appropriate values. The number of points used for fit in brackets is given after the site name.
† see section 5.2.6

	fringe	Height (mm)	h (mm)	b_1 µgal mm^{-1}	$b_2 + 2c_2h$ µgal mm^{-1}	$b_3+2c_3h+3d_3h^2$ µgal mm^{-1}
POL1						
Top	0	1309	1189		-0.2114	-0.1912
start	5	1304	1184		-0.2116	-0.1907
bottom	155	1114	994		-0.2190	-0.1802
Average over fitted drop (start to bottom)				-0.2280 ± 0.0080	**-0.2153 ± 0.0311**	-0.1855
POL2						
Top	0	1309	1189		-0.2225	-0.2213
start	5	1304	1184		-0.2226	-0.2214
bottom	155	1114	994		-0.2281	-0.2257
Average over fitted drop (start to bottom)				-0.2350 ± 0.0053	**-0.2254 ± 0.0020**	-0.2236
TAU (FG5-103)						
Top	0	1315	1195		-0.2928	-0.2711
start	5	1310	1190		-0.2929	-0.2726
bottom	155	1125	1000		-0.2960	-0.3186
Average over fitted drop				-0.3014 ± 0.0061	-0.2945 ± 0.0059	-0.2956
Linear solution from 3 points				**-0.2982 ± 0.0015**		
TAU (FG5-107)						
Top	0	1291	1171		-0.2932	-0.2782
start	5	1286	1166		-0.2933	-0.2797
bottom	165	1084	964		-0.2965	-0.3249
Average over fitted drop				-0.3014 ± 0.0061	-0.2949 ± 0.0578	-0.3023
Linear solution from 3 points				**-0.2982 ± 0.0015**		

Continued over.....

Table 5.7 Showing the linear, cubic and quadratic fits to the gravity vs. height data of Table 5.5 using the coefficients given in Table 5.6. The range of different drop lengths for different instrument configurations require different values of the vertical gradient to be used in the equation of motion. The gradient used for fit in each case is shown in bold type (section 5.2.6).

	fringe	Height (mm)	h (mm)	b_1 µgal mm^{-1}	$b_2 + 2c_2h$ µgal mm^{-1}	$b_3+2c_3h+3d_3h^2$ µgal mm^{-1}
GI						
Top	0	1309	1189		-0.3035	-0.3033
start	5	1304	1184		-0.3035	-0.3030
bottom	155	1114	994		-0.3011	-0.2953
Average over fitted drop (150 fringes total)				-0.2987 ± 0.0023	**-0.3023 ± 0.0035**	-0.2992
bottom	95	1192	1072		-0.3021	
Average over fitted drop (90 fringes total)				-0.2987 ± 0.0023	**-0.3028 ± 0.0035**	
BGS						
Top	0	1310	1190		-0.3381	-0.3323
start	5	1305	1185		-0.3377	-0.3323
bottom	95	1191	1071		-0.3287	-0.3075
Average over fitted drop (start to bottom)				-0.2940 ± 0.0093	**-0.3332 ± 0.0377**	-0.3199
TEDA						
gradient from TripodA1				-0.2982 ± 0.0039		
gradient from TripodA2				-0.2962 ± 0.0299		
Simple average used for fit				**-0.2972 ± 0.0024**		
NPL1 (FG5-105)						
Linear gradient assumed				**-0.2980 ± 0.0040**		
NPL2 (FG5-103)						
Linear gradient assumed				**-0.2955 ± 0.0042**		

Table 5.7 continued...

Showing the linear, cubic and quadratic fits to the gravity vs. height data of Table 5.5 using the coefficients given in Table 5.6. The range of different drop lengths for different instrument configurations require different values of the vertical gradient to be used in the equation of motion. The gradient used for fit in each case is shown in bold type (section 5.2.6).

We now consider the transfer from the absolute datum to the relative datum using the vertical gradient observations described above for POL1. Equations (1) to (3) for $\Delta g(h)$ are used to calculate the gravity difference directly, which avoids the need to estimate an average vertical gradient which may not be appropriate for the region of the datum correction. For example the datum correction using the quadratic equation is calculated as follows:

At the Absolute Datum Height = 1309 mm $\quad h = 1189$
At the Relative Datum Height = 120 mm $\quad h = 0$

From $\Delta g(h) = a_2 + b_2\, h + c_2\, h^2$, $\quad \Delta g(1189) =$ -279.4 ± 3.4 μgal
$\Delta g(0) =$ 0 μgal

so Datum Correction = **-279.4 ± 3.4** μgal

The datum correction used for the other absolute sites are given in Table 5.8.

The error (± 3.4 μgal) on this value is the formal error from the error on the function $a + bh + ch^2$ is calculated in a similar manner as the error on the slope described in section 5.2.4. For a particular value of h, (h_k), the value of $\Delta g\ (h_k)$ is

$$\Delta g(h_k) = a_2 + b_2\, h_k + c_2\, h_k^2$$

The variance of $\Delta g\ (h_k)$ is

$$V(\Delta g(h_k)) = \begin{pmatrix} 1 & h_k & h_k^2 \end{pmatrix} \begin{pmatrix} V(a) & cov(ab) & cov(ac) \\ cov(ab) & V(b) & cov(bc) \\ cov(ac) & cov(bc) & V(c) \end{pmatrix} \begin{pmatrix} 1 \\ h_k \\ h_k^2 \end{pmatrix} \qquad (8)$$

where the variance and covariance terms of a, b and c are the elements of the inverse of the normal equation matrix multiplied by σ^2. The standard error on $\Delta g\ (h_k)$ is the square root of $V[\Delta g\ (h_k)]$.

Site	h (mm)	$a_1 + b_1$ (μgal)	$a_2+b_2h+c_2h_2$ (μgal)	$a_3+b_3h+c_3h^2+d_3h^3$ (μgal)
POL1	1189	276.1 (5.2)	**279.4 (3.4)**	271.9
POL2	1189	282.7 (3.4)	**284.9 (0.2)**	284.5
BGS	1190	344.4 (5.3)	**346.1 (2.8)**	347.0
GI	1189	353.0 (1.3)	**352.3 (0.3)**	351.8
TAU (103)	1195	**356.8 (0.9)**† 360.7 (3.9)	360.8 (5.2)	366.5
TAU (107)	1171	**349.6 (0.8)**† 353.5 (3.8)	353.8 (5.1)	359.9
NPL1 (105)	1193	**355.5 (4.8)**	-	-
NPL2 (103)	1192	**352.2 (5.0)**	-	-
TEDA	0677*	201.2 (1.6)	-	-

Table 5.8 Datum Corrections in μgal from the absolute datum at the 'top of the drop' to the relative datum at 120 mm. (h=Height-120 mm). The coefficients a_i etc are given in Table 5.6.

† The Taunton values for linear gradient in bold are those calculated from a linear fit to the three points from the 1994 observations only (section 5.2.6)

* h=677 mm for the IMGC instrument which measured at a Height of 797 mm at Teddington A (TEDA).

5.2.6 Choosing the Best Fit

To decide whether a linear or quadratic gradient is the best representation of the true gradient at each of the sites, the rms error (σ) of the fit was used. For one of the sites (Taunton), the original height observation appeared to be inconsistent with the more recent 'triple height' observations, therefore a least squares linear fit was also made to the most recent three points. This test was done at each site, so there were three fits to choose from: a linear fit to the most recent three points, a linear fit to four points and a quadratic fit to four points. For BGS, where there were 5 points, there were two further possibilities. The results of this test are shown in Table5.9.

fit (no. of points)	POL1	POL2	BGS	GI	TAU
linear (3)	13.0	7.5	10.5	2.7	**1.1**
linear (4)	9.2	6.0	9.6	2.2	6.3
quadratic (4)	**5.4**	**0.3**	7.4	**0.5**	8.3
linear (5)			9.7		
quadratic (5)			**4.9**		

Table 5.9 The rms (σ) in μgal of the fit of linear and quadratic curves to various combinations of vertical gradient data points. The fit with the smallest σ (shown in bold type) was used in each case. For the NPL sites, a linear fit to 2 points was used.

The table shows that in all cases except Taunton, a quadratic fit to all the points has the smallest rms error. Figures 5.3 a - d show the deviation of the quadratic fit from the linear fit (to four points for POL1, POL2, and GI, to five points for BGS).

The effect of the choice of fit on the vertical gradient and the datum height corrections is not very significant. Table 5.10 shows the variation in these corrections resulting from linear and quadratic fits to data from POL1 and GI. The values of the gradient are the average over the fitted drop (150 fringes) are from Table 5.7, and the datum correction is from the top of the drop (1309 mm) to the relative datum (120 mm) are from Table 5.8.

	vertical gradient correction (μgal)		datum correction (μgal)	
	POL1	**GI**	**POL1**	**GI**
linear (4)	19.4 ± 0.7 (at 222.8 ± 8.0 μgal m^{-1})	26.6 ± 0.2 (at 297.9 ± 2.0 μgal m^{-1})	276.1 ± 5.2	353.0 ± 1.3
quadratic (4)	18.7 ± 2.7 (at 215.3 ± 31.1 μgal m^{-1})	27.0 ± 0.3 (at 302.3 ± 3.5 μgal m^{-1})	279.4 ± 3.4	352.3 ± 0.3
difference (lin-quad)	**0.7**	**-0.4**	**-3.3**	**0.7**

Table 5.10 Comparing the vertical gradient and datum corrections resulting from linear and quadratic fits to POL1 and GI data. The gradient used for the vertical gradient correction is shown in brackets. The datum correction is from 1309 mm to 120 mm.

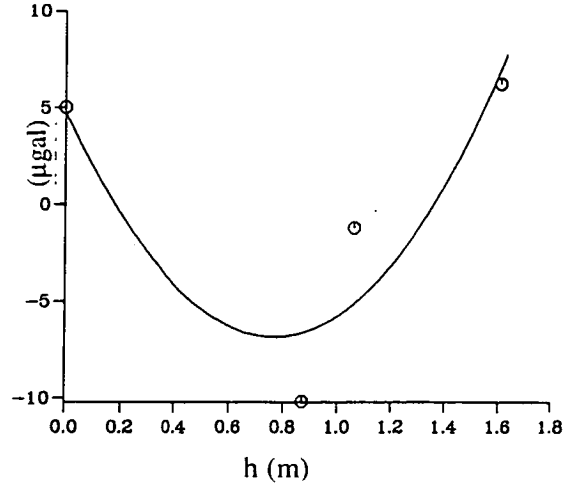

a) POL1

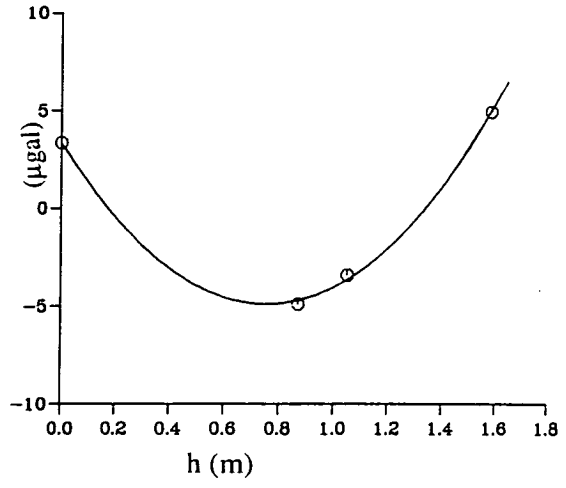

b) POL2

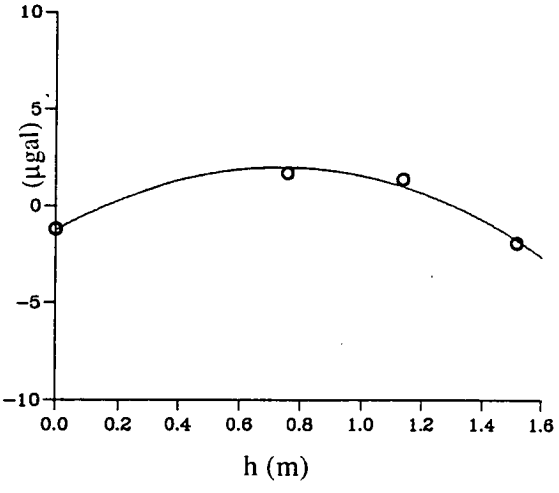

c) GI

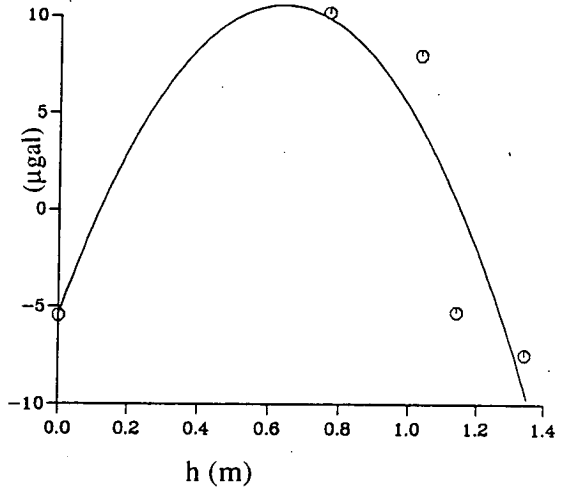

d) BGS

Figure 5.3 Figures a - d show the deviation (in µgal) of the quadratic fit from the linear fit to the variation of gravity versus height. The zero of h is the point where relative gravity as measured by the LCR instrument equals zero, and is at 120 mm above the floor (see text).

5.3 Variation of Gravity with Drop Length

Introduction

As discussed in Chapter 4 (section 4.3), the full equation of motion which includes the vertical gradient of gravity (Equation 7 of Chapter 4) should estimate gravity at the top of the drop, which is at a fixed height. The results should therefore be constant no matter which part of the drop is fitted to the equation of motion. However, it is found that the gravity estimate varies when the length of the drop is changed, which contradicts this theory. The following sections describe work done to understand and correct this defect.

5.3.1 Variation of Gravity Estimate with Drop Length

Varying the end fringe ('cut-off tests')

When FG5-103 was first delivered in August 1992, it was set to count a total of 100 fringes and fit 90, starting at fringe 5. Since its first upgrade in February 1993, the instrument has been set to count 170 fringes and fit 150. When the number of fringes fitted is varied between 90 and 160 fringes for the first set (200 drops) of POL0705 (observed in May 1993), the solution to the full equation of motion varies. The triangles of Figure 5.4a show the variation. The continuation of this test from drop lengths of 95 to 50 fringes (squares) is the result from POLTST01, which was the very first set observed at POL in August 1992. A similar variation is seen for the single set NPL0307A (observed at NPL in July 1993) shown in Figure 5.4b. The squares show the solution to the full equation of motion which includes the vertical gradient.

The minimum estimate of gravity occurs when 150 fringes are fitted, and the difference between the estinates at 150 and 90 fringes is about 24 μgal in Figure 5.4a and about 30 μgal in 5.4b. The same effect is seen in the sets POL1808A (August 94) and EDI1907A (July 94), with the shorter drop giving a value which is higher by about 24 μgal. This demonstrates that, with all other conditions being constant, simply increasing the number of fringes counted for FG5-103 decreases the estimate of gravity.

The variation of the solutions to the equation of motion with and without the vertical gradient terms for other FG5 instruments is shown in Figures 5.5 a and b. The FG5-107 data is from Taunton and the 101 data from Onsala, Sweden. The results are from the first set mean (100 or 200 drops). Of the three examples shown in Figures 5.4b, 5.5a and 5.5b,

FG5-107 alone shows the expected constant behaviour for the solution of the full equation (squares), but only in the region between about 90 and 150 fringes fitted (Figure 5.5a). The solution to the simple equation (circles) should increase linearly with drop length. FG5-107 and 101 show this behaviour more or less between 100 and 170 fringes fitted. The FG5-103 results show the gravity estimate apparently decreasing for longer drops, which is totally contrary to expectation.

Varying the start fringe

When the total number of fringes fitted is kept constant but the starting fringe is varied, a similarly large (20 - 40 μgal) change in the estimate of gravity is observed, particularly for shorter drops. An example for FG5-103 at POL is shown in Figure5.6a from POL2211B. Both the variation in starting fringe (from 5 to 20) and the total number of fringes fitted is shown (100 to 160). Gravity should be the same no matter which fringe you start at. The figure shows that the solution having the behaviour closest to that expected (i.e no variation with fringes fitted) is, in this case, that for starting at fringe 15. Another example, showing a similar structure for FG5-103 data from NPL is shown in Figure 5.6b (NPL0307A). Data from FG5-105 Figure 5.6c has less systematic structure but still demonstrates a variation in gravity with start fringe.

The 'drop length correction'

Different FG5s leave the manufacturer with a 'standard' drop length which varies between instruments : FG5-103 now counts 150, but in 1992 it had a much shorter drop length of 90 fringes. FG5-105 counts 130 fringes, and FG5-101 and 107 both count 160 fringes. Since the estimate of gravity has been shown to depend on the drop length, a 'drop-length correction' should be applied when comparing the absolute values obtained with the same instrument with different drop lengths, or different instruments. The comparison of FG5-103 values made with a drop length of 90 fringes in 1992 and subsequent values made with a drop length of 150 fringes requires a correction of -23 ± 7 μgal, since the gravity estimates from the shorter drop are too high. This correction has been calculated from the values at 90 (POLTST1) and 150 (POL0705) fringes shown in Figure 5.4a. Comparisons between different instruments are made in section 5.6 (103 and 105 at NPL) and section 5.7 (103 and 107 at Taunton). Using the cut-off test data shown in Figure 5.5a for FG5-107 and Figure 5.6c for FG5-103, a 'drop length correction has been calculated. The difference between the FG5-107 estimates at 150 and 160 fringes gives a drop length correction to 150

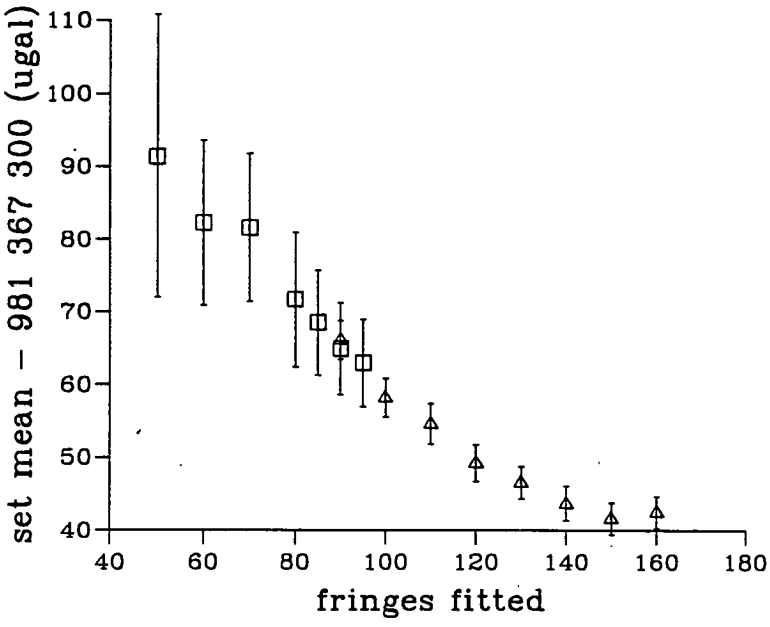

Figure 5.4a Cut-off test for POL0705 (triangles), varying the drop length between 90 and 160 fringes, and for POLTST01 (squares), varying between 95 and 50 fringes.

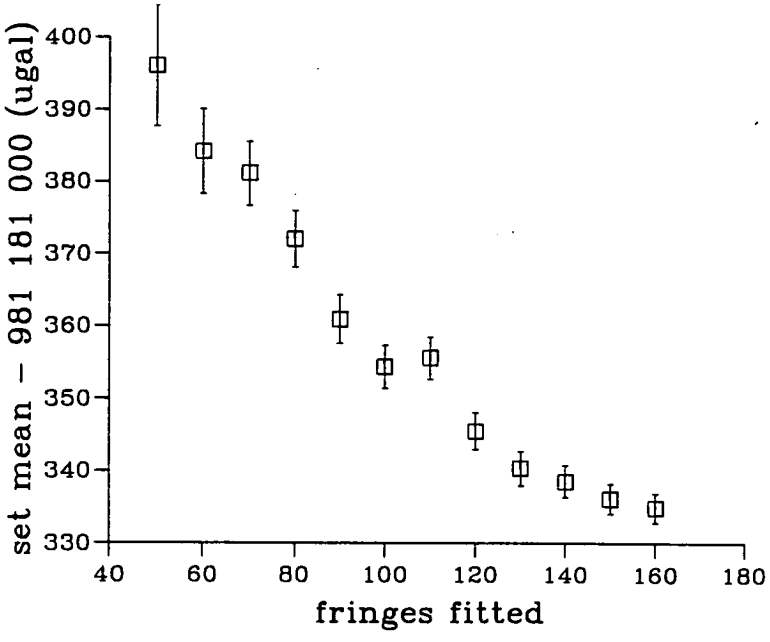

Figure 5.4b Cut-off test for the dataset NPL0307A, taken with FG5-103 at NPL in July 1993. The squares show the solution to the full equation of motion, which includes the vertical gradient terms, when the drop length is varied from 50 to 160 fringes.

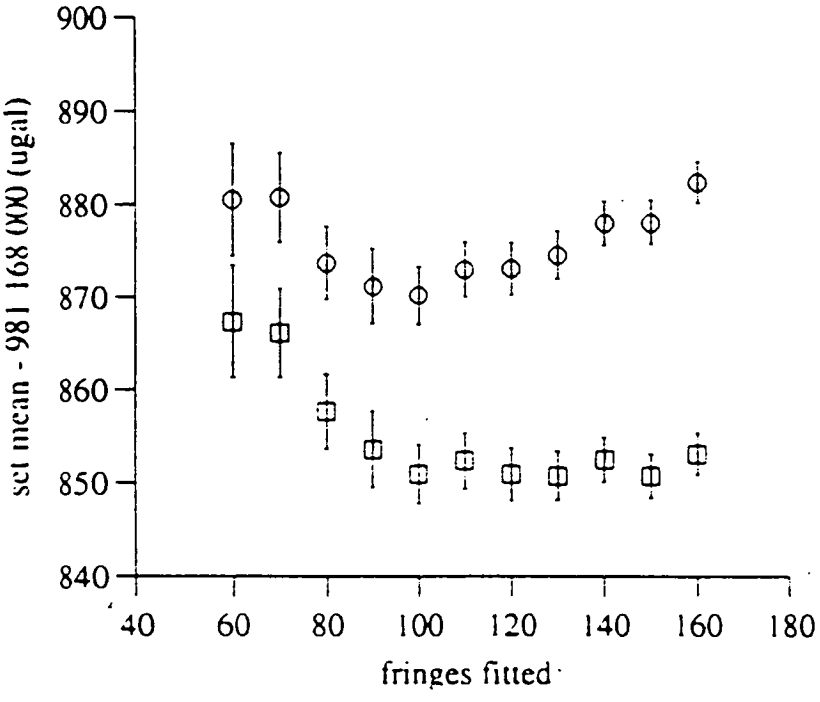

Figure 5.5a Cut-off test for FG5-107 at Taunton 107, showing the expected theoretical behaviour. The solution to the full equation of motion (squares), is constant in the region between about 90 and 150 fringes. (29.09.93). The circles show the solution to the simple equation of motion which assumes no vertical gradient.

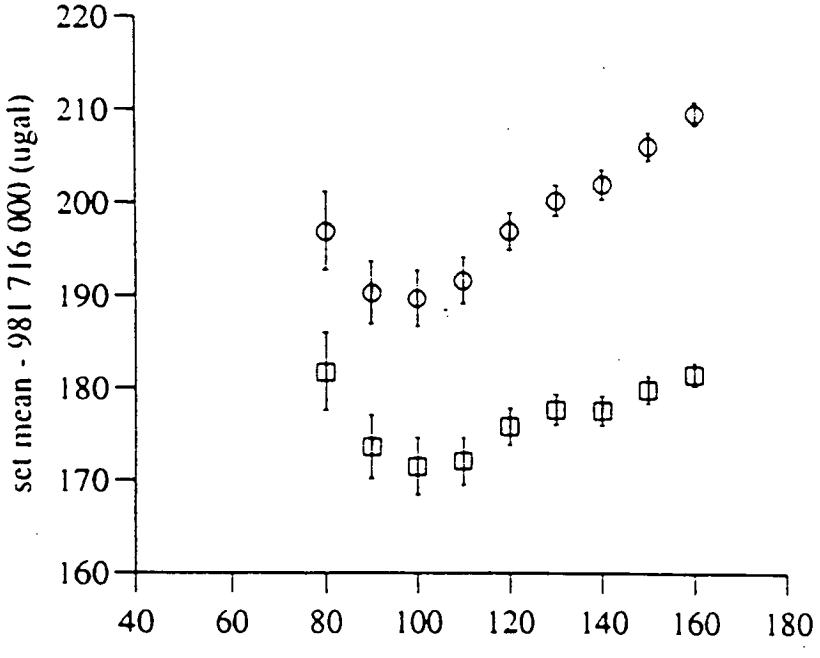

Figure 5.5b Cut-off test for FG5-101 at Onsala, Sweden (09.08.93). The squares show the solution to the full equation of motion, and the circles show the solution to the simple equation of motion which assumes no vertical gradient.

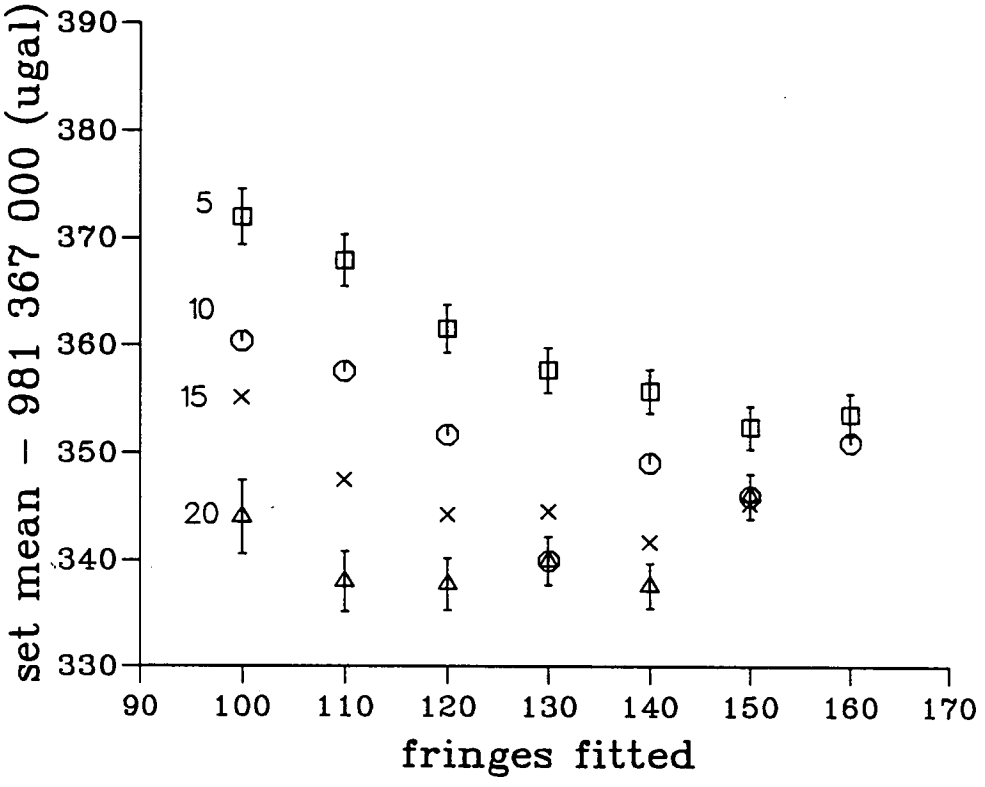

Figure 5.6a Variation of the gravity estimate when the starting fringe is varied for POL2211B.The start fringe values from 5 to 20 are shown in different symbols (labelled on the figure). The total number of fringes fitted is shown on the horizontal axis (100 to 160). The most constant solution is that for starting at fringe 15.

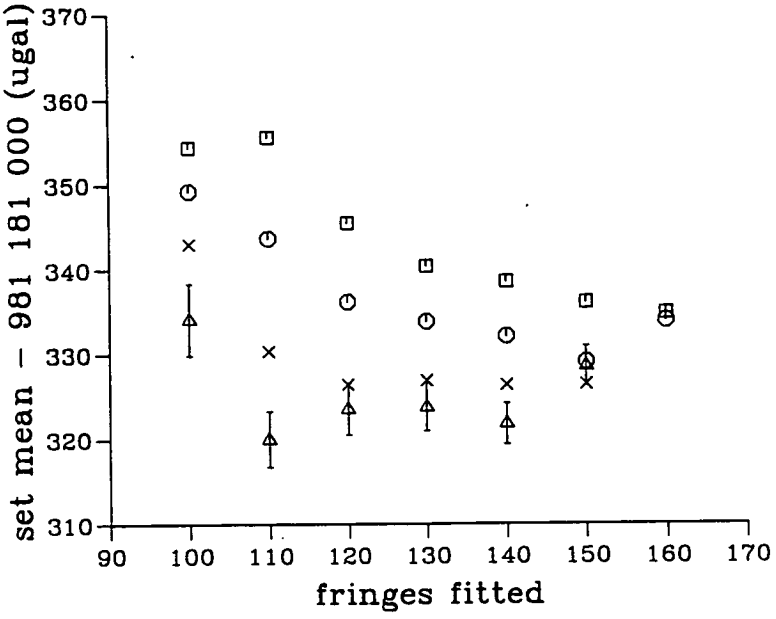

Figure 5.6b Effect of varying the start fringe for FG5-103 at NPL (NPL0307A). Key for start fringe number : squares (5), octagons (10), crosses (15) and triangles (20). The total number of fringes fitted is shown on the horizontal axis. The error bars for all the values are of similar size to the ones shown shown for the solution starting at fringe 20.

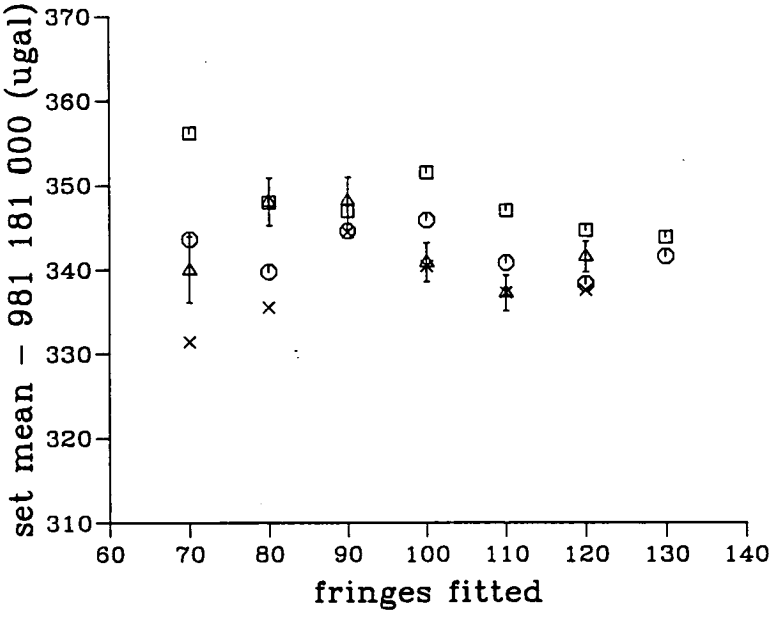

Figure 5.6c Effect of varying the start fringe for FG5-105 at NPL (N030793C). Key for start fringe number : squares (5), octagons (10), crosses (15) and triangles (20). FG5-105 was set to count a total of 130 fringes compared with 150 counted by FG5-103.

fringes for this instrument of -2.4 ± 3.2 μgal. The estimate at 110 fringes for FG5-105 is 3.2 ± 2.4 μgal higher than for 130 fringes. Since FG5-105 counts a maximum of 140 fringes, the value at 150 fringes cannot be measured directly and is estimated by extrapolation of this decreasing trend. The drop length correction to 150 fringes for FG5-103 is therefore estimated to be -3.2 ± 2.4 μgal.

5.3.2 Cumulative Residual Plots

Introduction

Gravity is found by fitting a parabola to pairs of distance-time observations. A good solution will result if the residuals are randomly scattered for all parts of the drop. Structured residuals may mean that the mass is not falling freely, or that the tracking mechanism which monitors the relative motion of the mass and cart (section 4.2.1) is not working properly. Since the estimate of gravity was apparently dependent on which portion of the parabola was fitted, the residuals were examined to determine how smoothly the mass was falling.

The time and distance residuals are calculated by the program DDT (section 4.4). The distance residual of each fringe is the difference between the measured distance fallen by the mass at a particular time and the distance predicted for that time by the parabolic fit to the distance-time pairs for the drop. DDT stores the distance residuals of a particular single drop, the average distance residuals of a set (200 drops) and the cumulative average distance residuals of all the drops processed. Figures 5.7 a b and c show examples of the residuals from one drop, 200 drops and 3000 drops, respectively plotted against time, for POL0912A. Plots like Figures 5.7 for other data sets show structure which varies with instrument and site, and is best seen in the residuals accumulated over 3000 drops.

Chebychev polynomial fits

Chebychev polynomials were used to convert the cumulative residual data, which is equally spaced in distance, to data equally spaced in time for frequency analysis (section 5.3.4). Plotting the polynomial instead of the residuals also helps to make clear the structure. The program CHEBT determines a least squares polynomial approximation in Chebychev series form and produces values of the Chebychev coefficients. CHEBT reads in stored residual data in the format of a '.spe' file (an example is given in Table 5.11), which has the fringe index, time of the fringe, time residual and distance residual.

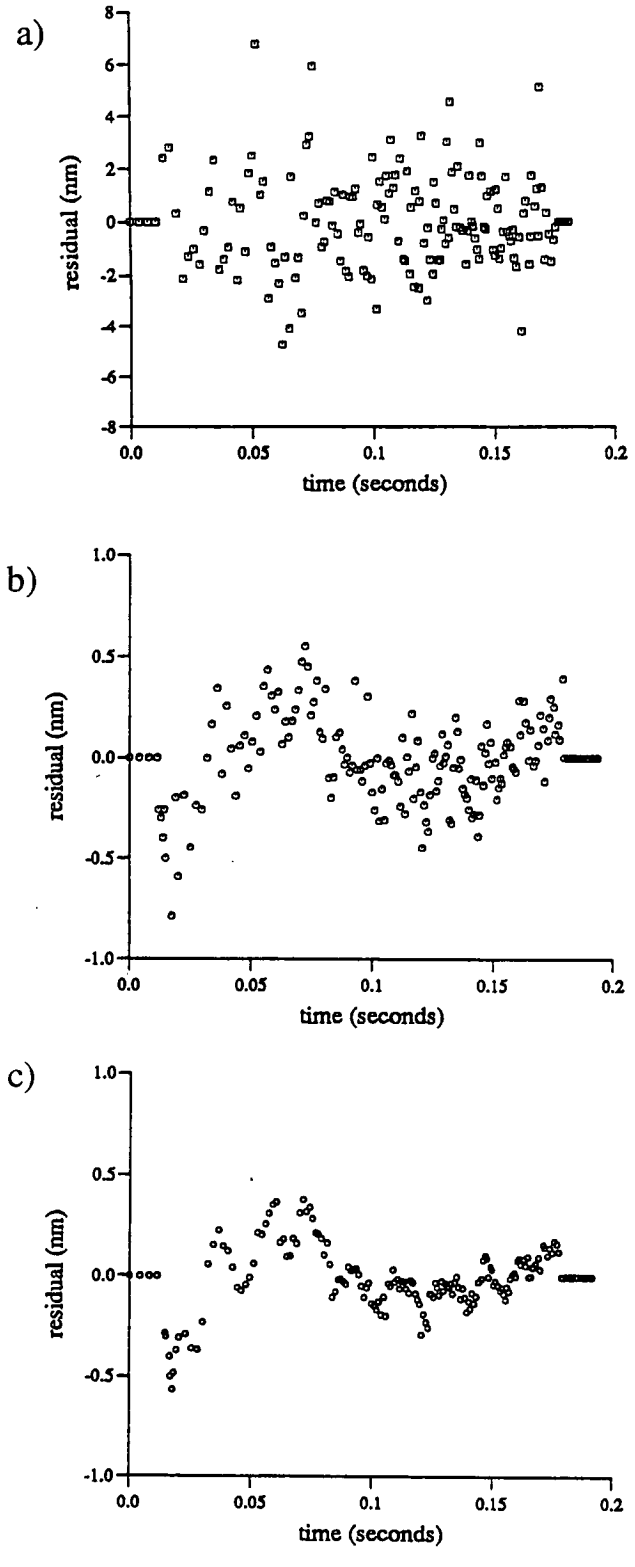

Figure 5.7 Figures 5.7 a, b and c show the distance residuals in nanometres (nm) from the fit of the equation of motion for a) single drop, b) the average over one set (200 drops) and c) the average over 3000 drops. Note the very different vertical scale for the single drop residuals shown in (a).

The NAG routine E02ADF is used to find the polynomial approximation to a set of data points [(x, y)] which are the columns headed 'time' and 'dist resid' respectively in Table 5.11. The rms misfit for a solution up to different degrees of polynomial up to the exact fit (where the degree equals the number of data points) is calculated. The user then chooses which degree of polynomial to evaluate.

The variation of the rms of the fit with the number of terms included in the series for two sets POL0912A and EDI1907A is shown in Figure 5.8. The fit improves with increasing numbers of terms between 1 and about 25, then remains at about the same level between 25 and 130, where it begins to get worse as the fit 'chases the scatter' of the data. The result of fitting 10, 20 and 40 terms to the POL0912A data is shown in Figures 5.9 a, b and c respectively. In general, 40 terms were sufficient to fit the structure without chasing the scatter. All subsequent reference to 'chebychev fit' or 'polynomial fit' means the 40 degree fit unless otherwise stated.

By fitting a polynomial to the cumulative residual data which was originally equally spaced in distance, and then evaluating this polynomial at points equally spaced in time, the data is converted to the form needed for spectral analysis.

index	x time (s)	time resid (s)	y dist resid (m)
1	.000000000000E+00	.000000000000E+00	.000000000000E+00
2	.433651421984E-02	.000000000000E+00	.000000000000E+00
3	.815132845595E-02	.000000000000E+00	.000000000000E+00
4	.115963450629E-01	.000000000000E+00	.000000000000E+00
5	.147619348009E-01	-.665797278172E-09	-.286477843730E-09
6	.177067406304E-01	-.124111456958E-08	-.564339755452E-09
7	.204713893745E-01	-.640748607467E-09	-.308332395886E-09
8	.230853772108E-01	-.566466211766E-09	-.287383139944E-09
9	.255709531657E-01	-.673577870771E-09	-.358459016800E-09
10	.279453548448E-01	-.662522037169E-09	-.366168569084E-09
11	.302222847331E-01	-.402064408410E-09	-.230529756034E-09
12	.324128503418E-01	.947953822457E-10	.577978546076E-10
13	.345261943007E-01	.248599663586E-09	.154218484334E-09
14	.365699475640E-01	.355519048289E-09	.226370649659E-09
15	.385505520725E-01	.225709278012E-09	.147941927217E-09

Table 5.11 An example of a '.spe' file, showing the first 15 lines only. The data continues to index 154, which corresponds to the 150th fitted fringe. The columns headed 'time' and 'dist resid' (distance residual) are the x and y variables for the Chebychev polynomial fit.

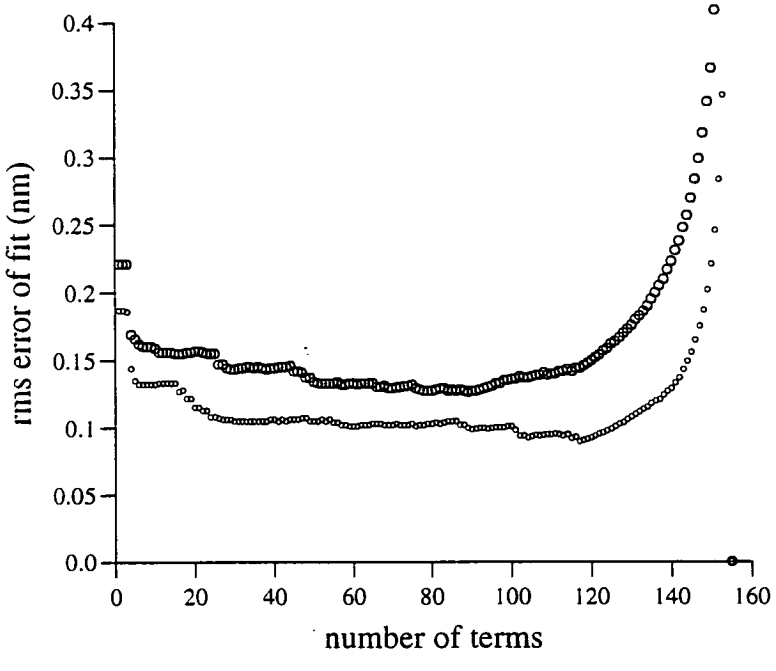

Figure 5.8 Variation of the rms error of the polynomial fit to the stacked residuals, when different numbers of terms are included in the series, for two sets POL0912A (small circles) and EDI1907A (large circles).

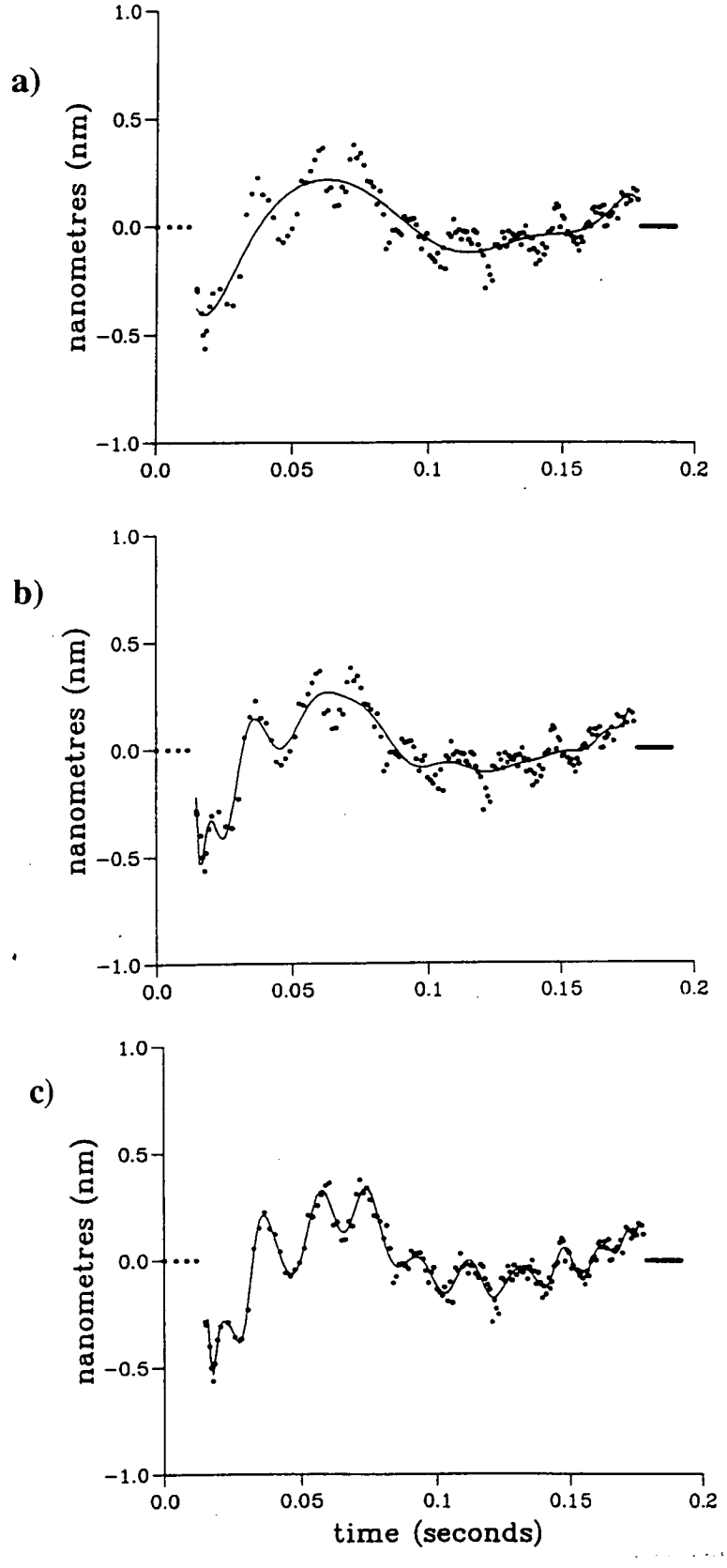

Figure 5.9 Effect of fitting a Chebychev polynomial with a) 10, b) 20 and c) 40 terms to the POL0912A data.

Examining the cumulative residuals

The cumulative residual plots for about 3000 drops from a simultaneous occupation at the National Physical Laboratory (NPL) by FG5-103 and FG5-105 are given in Figure 5.10. The structure in Figure 5.10a (103, 02.07.93) is extremely marked compared to 5.10b (105, 02.07.93), demonstrating that the effect has *instrument dependence* since both meters were standing on the same floor, about 6 metres apart. FG5-103 has a longer drop (150 fringes) than FG5-105 (130 fringes). Figures 5.10 c and d are for 03.07.93. The structure remains very similar for 105, but has become less sinusoidal for 103, perhaps because of a realignment.

The structure in the distance residuals from the FG5-107 and FG5-101 datasets is shown in Figure 5.11a and 5.11b respectively for comparison with the examples from FG5-103 and FG5-105. The 'cut-off tests' for the 107 and 101 data were shown in Figure 5.5.

The Chebychev polynomial fits to two sets taken at POL with FG5-103 are superimposed in Figure 5.12a. The sets are from POL0912A (09.12.93), and POL1808A (18.08.94) and the figure shows that the structure seen at POL is fairly *constant with time* i.e it does not seem to depend on the particular setup.

Polynomial fits to the figures of 5.10 a and c (FG5-103 at NPL on 02.07.93 and 03.07.93) have been superimposed in 5.12b. The structure found with FG5-103 at NPL (5.12b) is different to that found with the same instrument at POL (5.12a), demonstrating *site dependence*.

Further comparison of the Figures 5.12 a, b and c suggests that the low frequency component, which is identified by the 10-degree Chebychev polynomial of Figure 5.9a, is a constant feature of FG5-103 data. The characteristics of the oscillations superimposed on this curve are site dependent, being of a higher frequency and smaller amplitude at POL (Figure 5.12a) than at NPL (Figure 5.12b). If the low frequency component 'leaks' into the quadratic fit to the distance-time pairs, it may significantly bias the estimate of gravity. The higher frequency terms are less likely to interfere with the fit because they have a much smaller quadratic component.

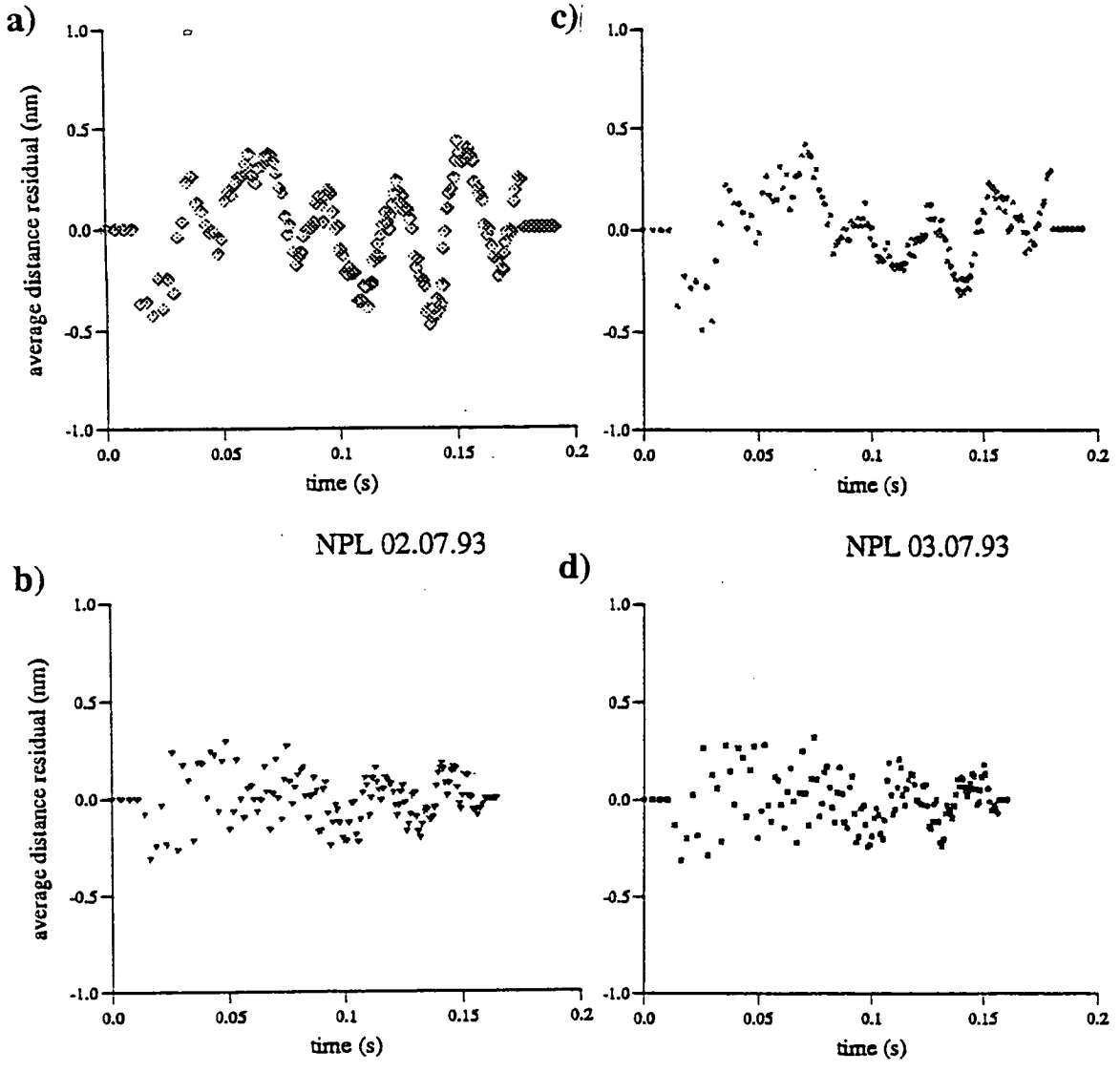

Figure 5.10 Cumulative residual plots for FG5-103 and FG5-105, averaged over 3000 drops, for the simultaneous occupation of NPL on 2 and 3 July 1993.
a) and b) for FG5-103 and FG5-105 on 02.07.93 respectively;
c) and d) similarly on 03.07.93.

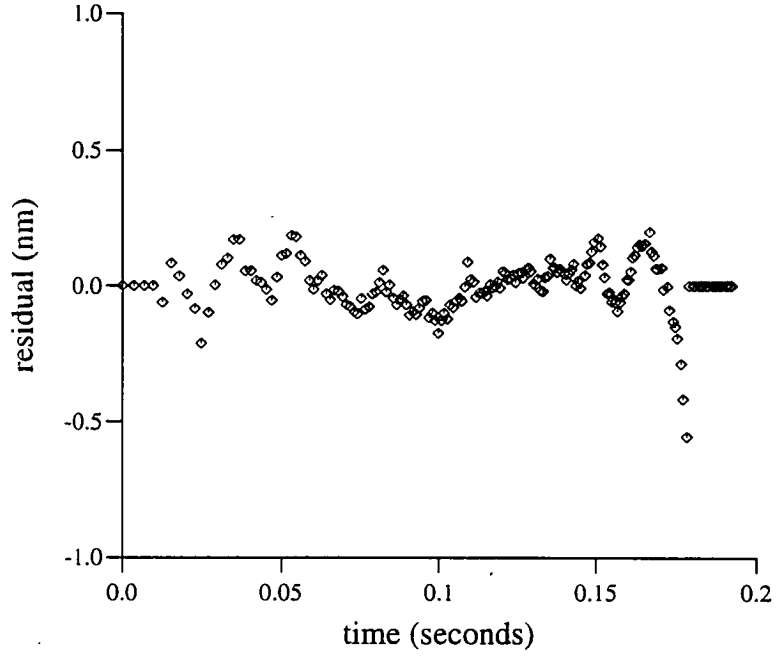

Figure 5.11a Cumulative residual plot for FG5-107 at Taunton (29.09.93), averaged over 2500 drops. The cut-off test for this dataset was given in Figure 5.5a.

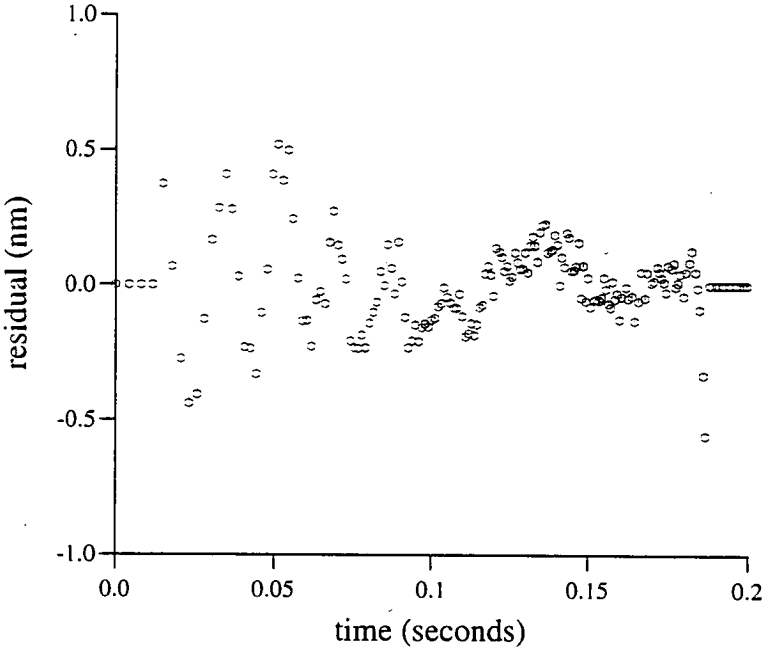

Figure 5.11b Cumulative residual plot for FG5-101 at Onsala (09.08.93), averaged over 2000 drops. The cut-off test for this dataset was given in Figure 5.5b.

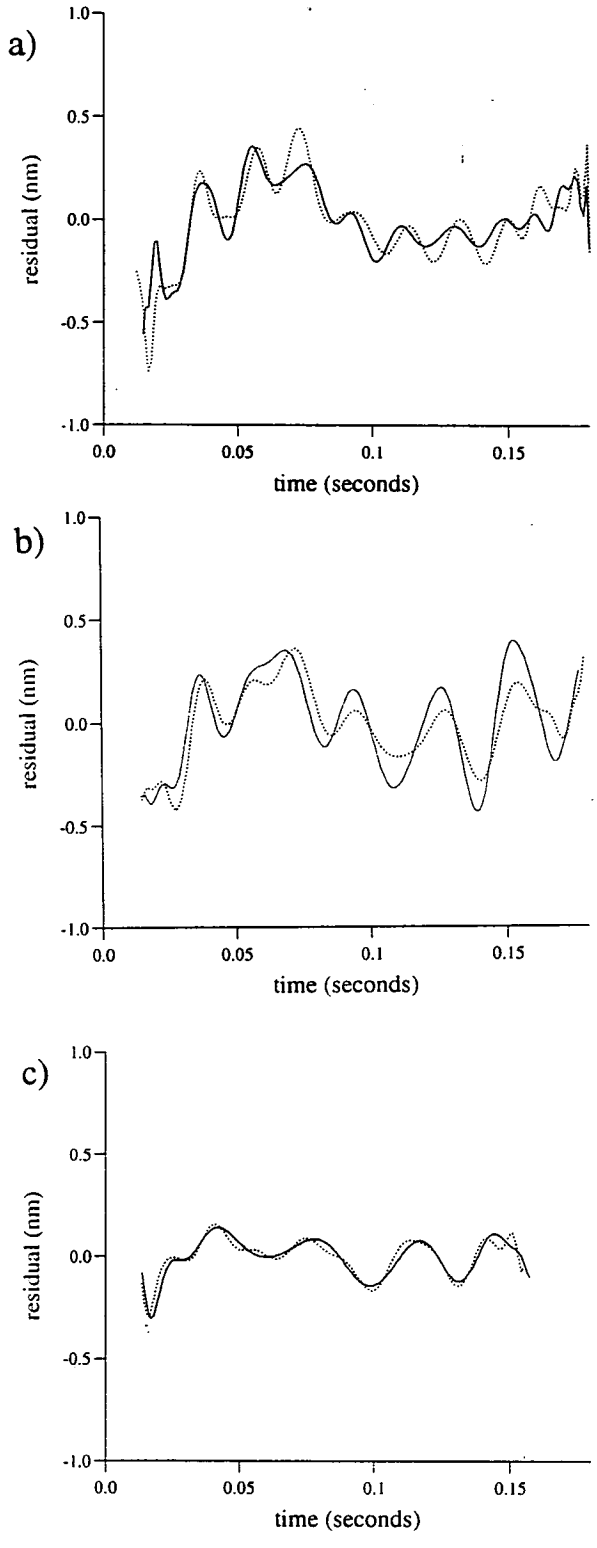

Figure 5.12 Chebychev fits: **a)** two sets from FG5-103 at POL on 09.12.93(·····) and 18.08.94(——), showing that the structure is fairly *constant with time*; **b)** the FG5-103 sets at NPL on 02(——) and 03.07.93(·····); and **c)** the FG5-105 sets from the same timesat NPL, showing that the structure is *site* and *instrument* dependent.

Although some of the structure at the beginning and end of the drop may be due to a poor 'drop' and 'catch' of the mass (instrument dependent), most of it is probably caused by vibrations set up in the instrument-floor system when the mass is dropped (site dependent). The presence of any structure in the residuals will cause the estimate of gravity to vary with the number of fringes fitted ('cut-off tests'). The removal of the variation of gravity with drop length can be achieved by subtracting the whole of the averaged stacked residual from each drop.

5.3.3 Correcting with the Stacked Residuals

The program DDTSPE sums the residuals of all the drops (after checking and rejecting 'bad' drops, i.e those which have any fringes with distance residuals larger than 10 nanometres), and at the end of each set (200 drops) it calculates the average distance and time residual for each fringe. The residuals are summed according to their fringe index (1 to 150). The average residuals from each set are stored in the '.sto' file, and the cumulative residuals from all drops so far are stored in the '.cum' file. No account is taken of missed fringes, so, because different fringes are missed in each drop, the fringes included in the sum for a particular index will not all have occurred at exactly the same distance (or time) down the drop. The times associated with each average residual in the fringe residual file (.sto or .cum) are those from the most recent drop. Since the actual fringes missed for each drop are random (except that most are missed during the last 40 fringes of the drop) (section 4.3.3, Figure 4.13), the sum is insignificantly affected.

After accumulating the average residuals, the program DDTDIST subtracts them from each fringe positon before solving for gravity. The first set was corrected with the residuals from the first set, etc (from the .sto file). The solution no longer varied with drop length. Figures 5.13 a and b show the cut-off tests for POL2211B before and after correcting the first set with the residuals from the first set. A similar result was obtained using the average of the residuals stacked cumulatively over all sets (from the .cum file) to correct each set. The solution of the equation of motion including the vertical gradient (squares) after correction (Figure 5.13b) does not vary with drop length. The solution of the simple equation (circles) varies linearly with drop length as expected. Figures 5.14 a and b show the corrected FG5-107 and FG5-101 datasets for comparison with their uncorrected cut-off tests which were shown in Figure 5.5.

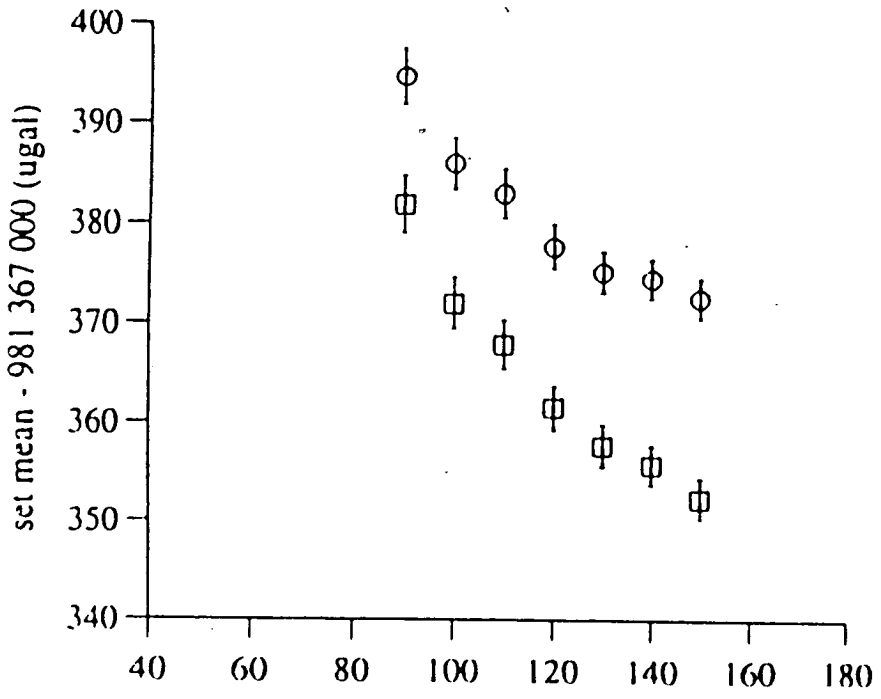

Figure 5.13a Cut-off tests for POL2211B before correcting with the stacked residuals. The squares show the solution of the equation of motion including the vertical gradient, the circles show the solution without.

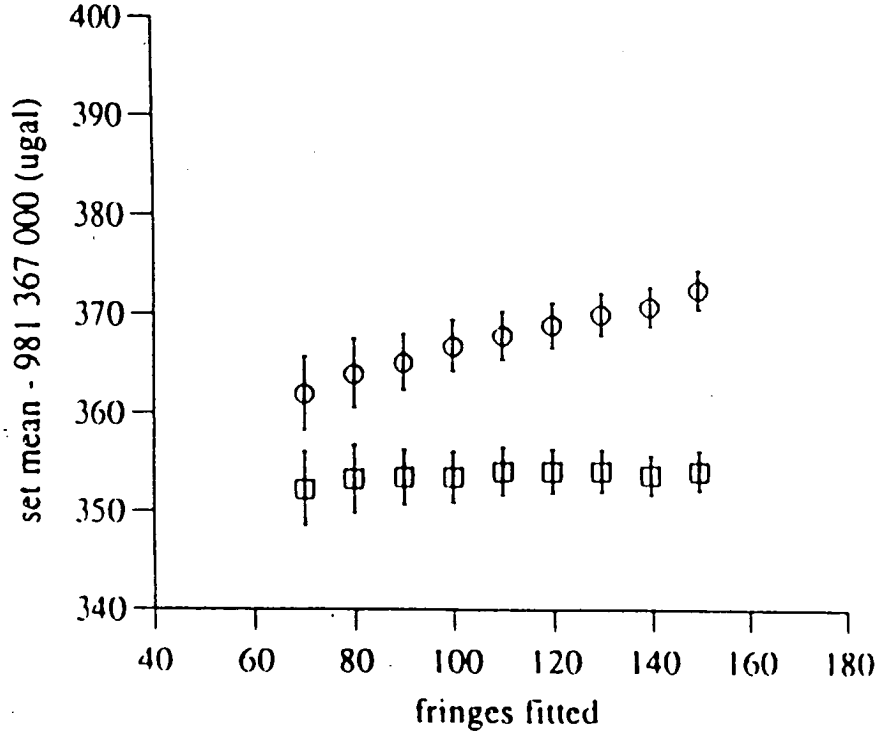

Figure 5.13b Cut-off tests for POL2211B after correcting with the stacked residuals. The squares show the solution of the equation of motion including the vertical gradient, and this solution no longer varies with drop length. The circles show the solution without the vertical gradient, and the solution varies linearly with drop length as expected.

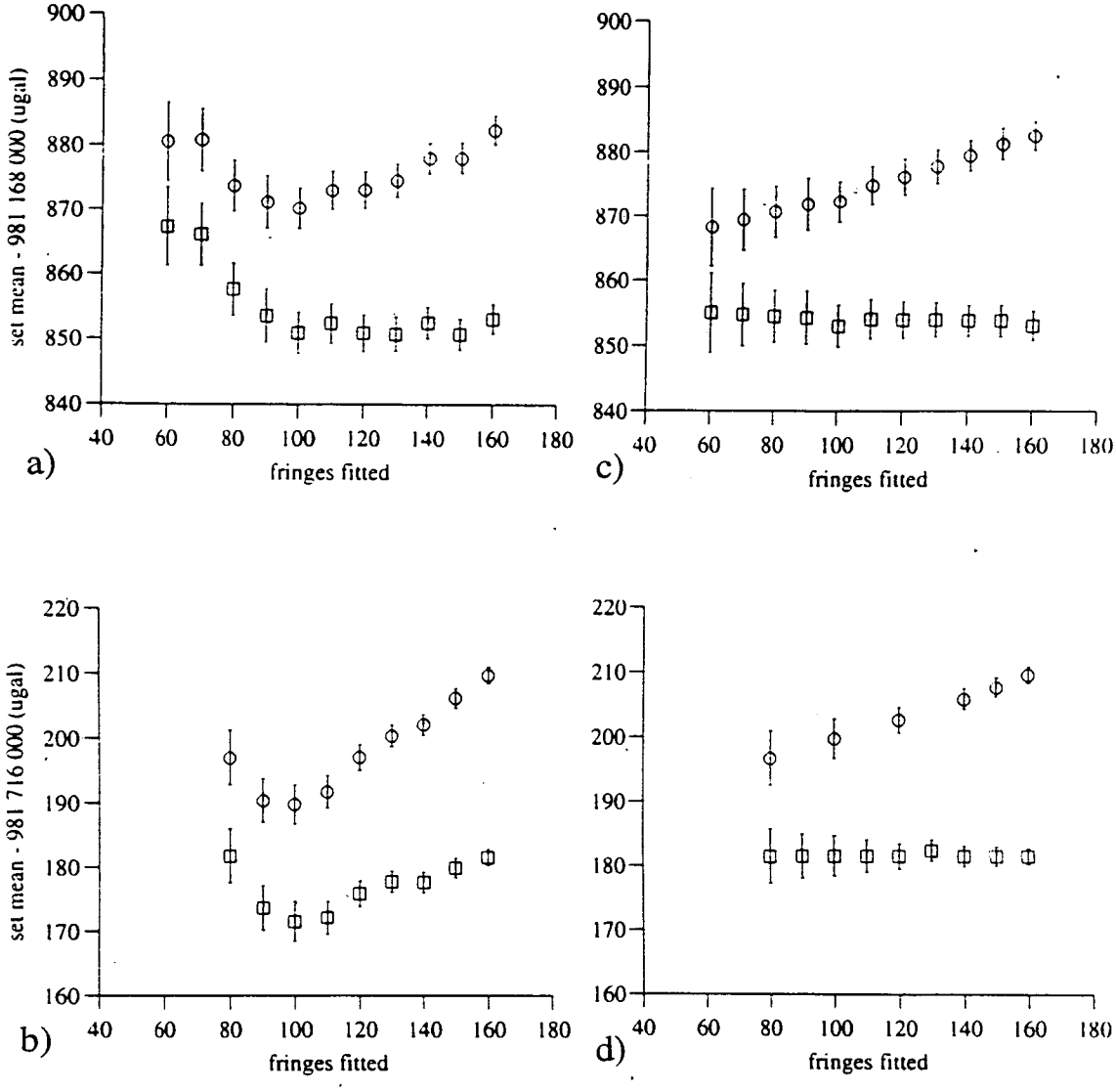

Figure 5.14 Effect of correcting the fringe times with the stacked residuals for FG5-107 and 101. Figures a and b show the uncorrected cut-off tests for 107 and 101 respectively, and Figures c and d the solution after correction

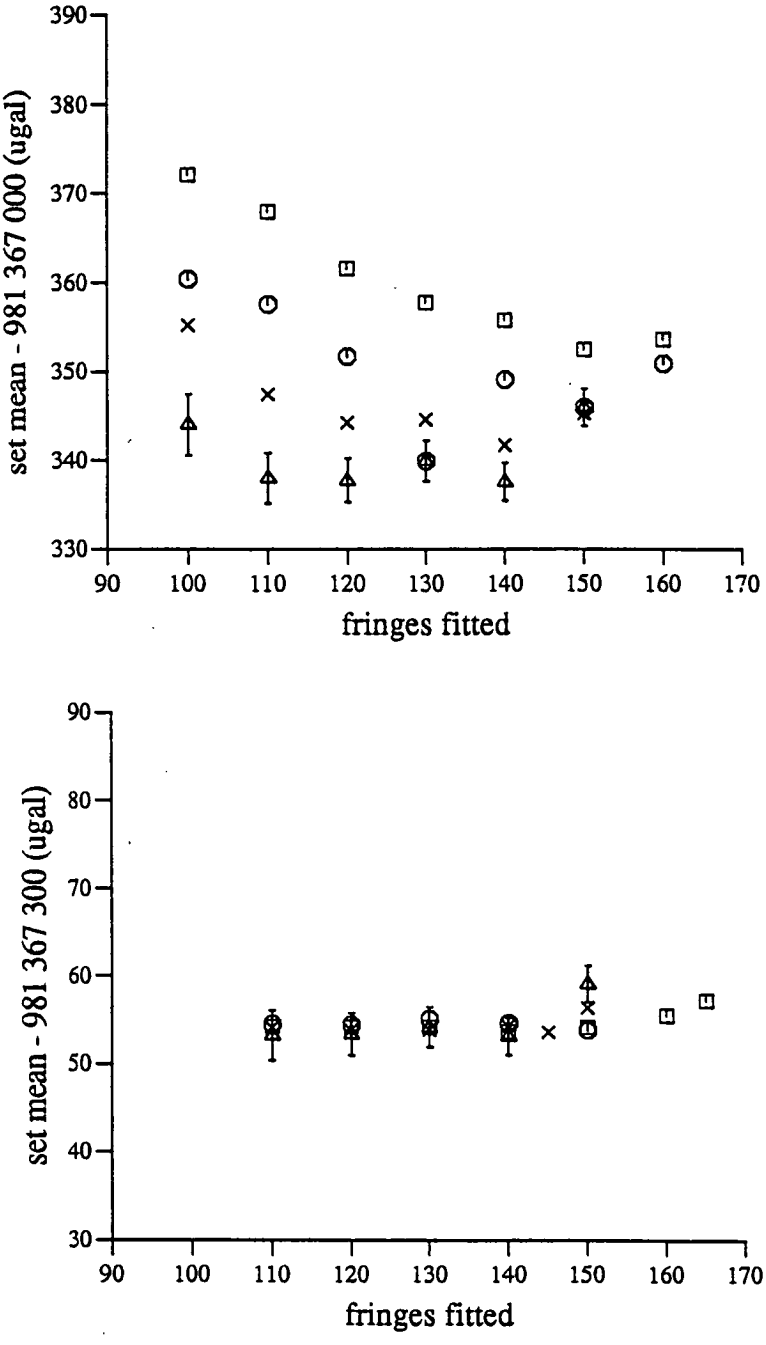

Figure 5.15 The variation of gravity with start fringe is prevented by subtracting the stacked residual from each fringe positon before solving for gravity. Figure 5.15 a and b shows the result before and after correction respectively.

The variation of gravity with start fringe (Figure 5.6a) is also prevented by the above procedure. Figure 5.15 shows the results before and after correction.

These results establish that structure in the fringe residuals is the cause of the variation of the estimate of gravity with drop length.

Although the method of correcting with the whole of the stacked residuals stops the variation of gravity with drop length, it does not indicate the value of the gravity offset caused by the structured residuals. The constant value of gravity obtained is that for the original number of fringes counted when making the stack. A different constant value would result if the original number of fringes counted was, for example, 150 instead of 160 for FG5-103. This gravity offset or 'system response correction' can be found by identifying and removing the largest of the sinusoidal vibrations seen in the residuals.

5.3.4 Modelling of the Residual Structure by Damped Sinusoids

Introduction

An alternative to simply taking away the whole of the stacked residual from the data is to model the effect as a set of damped sinusoids which represent the instrument-floor system response. This method should allow the gravity effect of the structure to be calculated. Klopping *et al.* (1991) describes corrections of typically 2 - 7 μgal resulting from filtering out the sinusoidal terms from the gravity signal of JILA4 data. In the analysis of Klopping *et al.*, an algorithm for computing the power spectral density of unevenly spaced data was used to identify the frequency components in the residual data set. The decay constants were estimated by comparing the amplitudes of the frquency in the first and second halves of the residual data. With the frequency and decay constant known, the amplitude and phase of each component was found from a least squares fit to the original time-distance data. The damped sinusoids were removed one at a time until no more were found above the noise level. Klopping *et al.* present results from JILA type gravity meters, from which FG5 were developed. The potential effect of the floor - instrument response for JILA instruments is larger than for FG5. Klopping *et al.* describe amplitudes of up to 3 or 4 nm for some sites observed with JILA4 and an analysis by Timmen *et al.* (1993) of JILA3 data using software supplied by Klopping finds amplitudes of similar magnitude. The maximum amplitude seen in the residuals of this analysis of data mainly from FG5-103 is about 0.6 nm.

Identifying the frequency and decay constant

A two stage method was used to identify sinusoids in the residuals from FG5 data, like those shown for example in Figures 5.10 and 5.11. The approximate frequencies and decay constants were determined firstly from the Fourier transform ('spectrum') of the data. This was followed by a higher resolution search, made by least squares, for the best fitting decaying sinusoids having parameters close to the 'first guess' values found from the spectrum.

Klopping's software used a special algorithm designed for computing the power spectrum of unevenly spaced data. Since this algorithm was not available to the author, another technique for converting the original data which is evenly spaced in distance, to data which is evenly spaced in time was developed. A 40 degree Chebychev polynomial (section 5.3.2) was fitted to the residual data. The polynomial was then evaluated at about 150 equal time intervals of about 0.001 second. The program SPEC was used to calculate the Fourier transform of the evenly-spaced-in-time data. Given that an FG5 drop is only about 0.17 seconds in length, the resolution of the spectrum was poor (about 6 Hz) but it typically showed maximum peaks at about 8 Hz and 50 Hz.

The method of estimating the decay constant is after Klopping *et. al.* (1991). The equally-spaced-in-time data were divided into two 'halves', both having a duration of about 0.09 seconds. The total drop time (t_d) is about 0.18 seconds for 150 fringes. The spectrum of each half was taken and the amplitude of the frequency in question was estimated from these.

If the amplitudes for the first and second halves are B_F and B_S respectively, the decay constant k is given by

$$k = \frac{1}{t_{1/2}} ln \frac{B_S}{B_F} \qquad (9)$$

The spectra from the first and second halves of POL0912A with no sinusoids removed are shown in Figure 5.16. The amplitudes B_F and B_S for the peak at about 8 Hz were estimated and k was calculated using equation (9). The terms B_F , B_S and k for the next largest sinusoid were found by processing the residuals remaining after the largest sinusoid had been removed from the gravity data. This procedure continued until there were no large spikes in the spectrum i.e until all the spikes had amplitudes below about 0.05 nm. In this way, between two and four sinusoids were found for each dataset. The estimates for the frequency and decay constants calculated as above are given in Table 5.12.

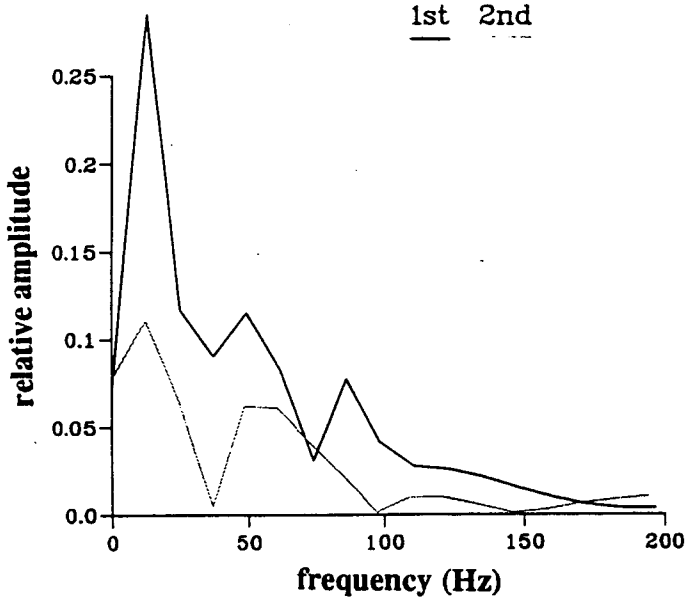

Figure 5.16 Spectra from the first and second halves of POL0912A with no sinusoids removed. The decay constant k was calculated with B_F (amplitude in the first half) and B_S (amplitude in the second half) using equation (9).

f (Hz)	8.7	32.2	50.0
B_F (nm)	0.2850	0.0830	0.1070
B_S (nm)	0.1110	0.0405	0.0499
k	-10.5	-8.0	-8.5

Table 5.12 First estimates of the frequencies and decay constants for POL0912, made by examining the spectrum of the data. The decay constants were estimated after the method of Klopping *et al.* (1991) by comparing the amplitude of the sinusoids in the first and second half of the drop.

These values were used as a starting point for the least squares search by the program PERIOD3, which enabled the parameters to be determined with much greater precision. The final frequency and decay values found by period three after successively higher resolution searches, and the amplitude A of the terms in the residual data set, are given in Table 5.13.

f (Hz)	8.711	31.185	50.949
k	-10.407	-21.186	-7.084
A (nm)	0.5427	0.2695	0.1473

Table 5.13.Final frequency (f) and decay constant (k) found by least squares with the program PERIOD3 for POL0912A. The amplitude (A) is that occuring in the residual dataset.

A comparison of Tables 5.12 and 5.13 shows that the rough method using the spectrum is adequate for finding the approximate frequencies, but less successful at determining the decay.

5.3.5 Correcting for Damped Sinusoids

DDTDIST method

The program DDTDIST was used to subtract the sum of the three largest sinusoids, rather than the value of the whole of the residuals, from the fringe times before solving for gravity (section 5.3.3). The sinusoids had the amplitude and phase as they occured in the residual dataset found by PERIOD3, and were therefore not allowed to vary with each drop. Although subtracting the whole of the residuals flattens the cut-off tests, taking away only the three largest sinusoids is not so effective. In theory, if *all* the sinusoids could be identifed then the sum of them would completely describe the residual data set, and the subtraction of the sum

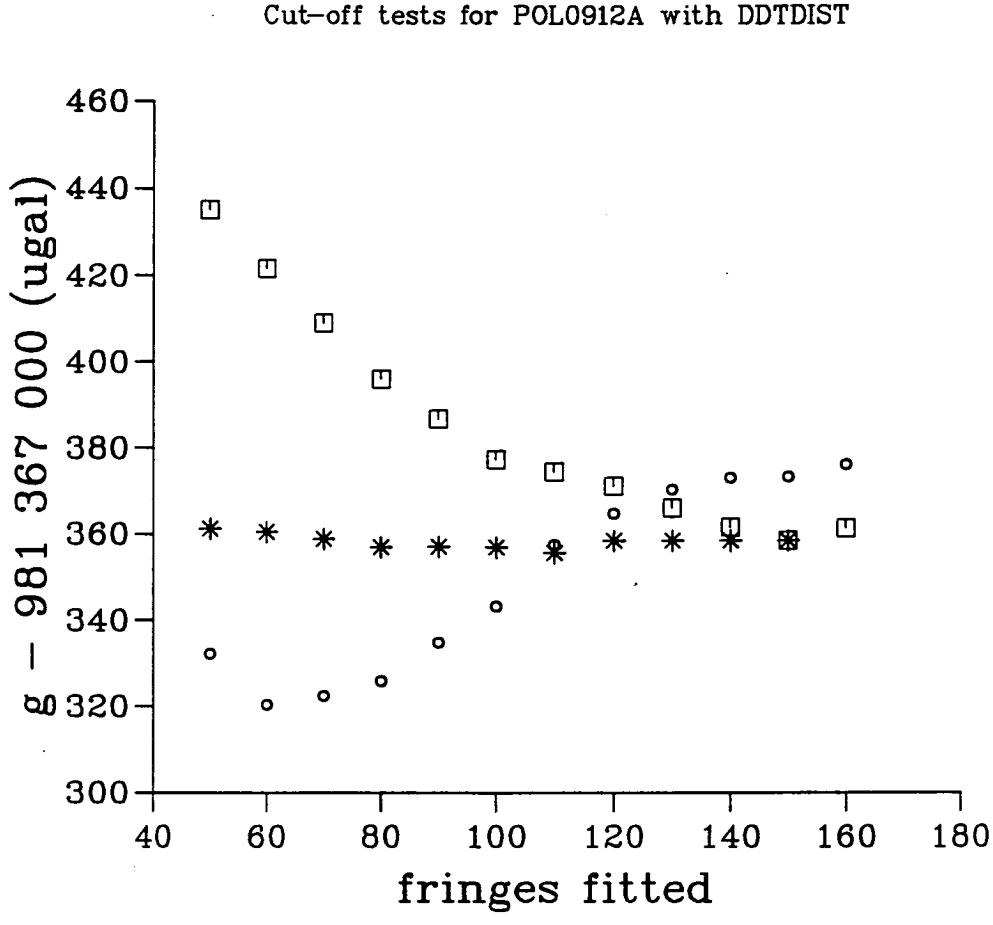

Figure 5.17a Cut-off tests using DDTDIST for the raw data (squares), for the raw data corrected with the whole residuals (stars) and for the raw data corrected with the first three sinusoids only (circles). ddtdist corrects each drop with sinusoids having the same fixed amplitude and phase. Correcting with only the the three largest sinusoids does not flatten the cut-off test, but appears to give a system response correction of about 8 μgal at 150 fringes.

of these sinusoids would then be exactly the same as taking away the whole residual data set. Figure 5.17a (previous page) shows cut-off tests, for the first set of POL0912A, for the raw data (squares), for the raw data corrected with the whole residuals (stars) and for the raw data corrected with the first three sinusoids only (circles). It has been noted that taking away the whole of the residuals does not give the value of the system response correction, since the value of gravity at 150 fringes does not change when the cut-off tests are flattened. When only the three largest sinusoids are removed, however, there is apparently a gravity offset of about 8 μgal at 150 fringes.

The spectrum after correcting the residuals for these sinusoids with DDTDIST (Figure 5.17b) shows that the spikes have increased amplitude. The phase of each sinusoid varies with each drop, and the original residual data set probably preserves the average or most likely phase, so only those drops having 'average' phase will be corrected properly by the method of DDTDIST. Correcting the other drops with sinusoids of the 'wrong' phase simply introduces a spike rather than removing it.

Since correcting the data with only a few sinusoids having *fixed* amplitude and phase is not effective at flattening the cut-off tests *or* the spectrum, then the apparent system response correction found by this method is questionable.

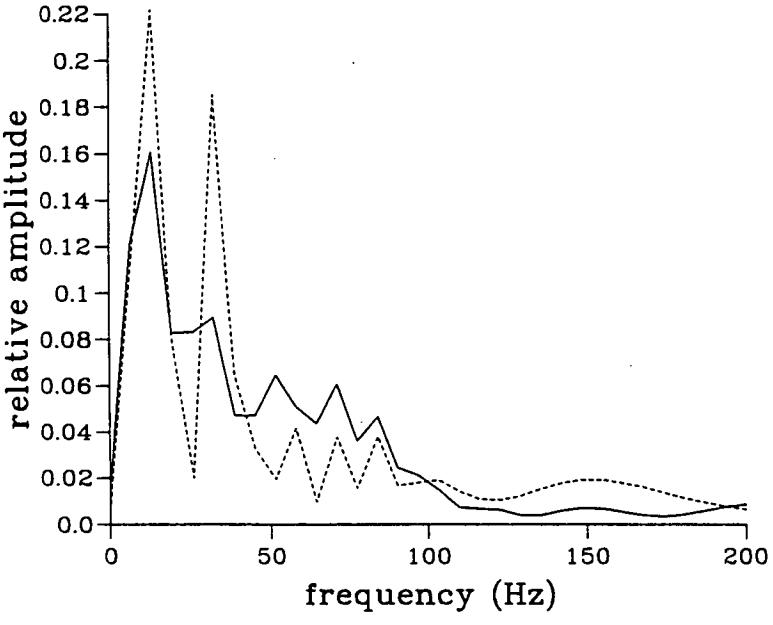

Figure 5.17b Spectrum of the residuals of the first set of POL0912A before (——) and after (-----) correcting for sinusoids at 8, 31 and 51 Hz with DDTDIST. The spikes at 8 and 31 Hz are increased.

DDTSIN method

By fitting the original time-distance data set to an equation of motion including sinusoidal terms, the amplitude and phase are allowed to vary with each drop. The modified equation including one sinusoid:

$$z(t) = z(0)\left[1+\tfrac{1}{2}\gamma t^2\right] + v_o(0)t\left[1+\tfrac{1}{6}\gamma t^2\right] + \tfrac{1}{2}g_o t^2\left[1+\tfrac{1}{12}\gamma t^2\right] + exp(-kt)(a\,cos\,\omega t + b\,sin\,\omega t) \tag{10}$$

is solved for a and b as well as z(0), v(0), and g_o.

The amplitude (A) and phase (θ) of the sinusoid are then given by

$$A = \left(a^2 + b^2\right)^{1/2} \qquad \text{and} \qquad tan\,\theta = \frac{b}{a} \; . \tag{11}$$

The values of the cosine and sine amplitudes a and b found by the fit, the total amplitude A and phase θ calculated as above for the largest sinusoid, with a frequency of 8.7 Hz and decay constant equal to -10.5, for the first five drops of POL0912A are given in Table 5.14.

drop	a (nm)	b (nm)	A (nm)	θ (°)
1	-2.058	0.680	2.167	-18.28
2	-0.097	-1.170	1.174	85.26
3	-0.252	0.647	0.694	-68.72
4	-0.224	-1.509	1.526	81.56
5	-0.390	-0.772	0.865	63.20

Table 5.14 Cosine (a) and sine (b) amplitudes found by the fitting equation (10) to the original distance-time data, with the total amplitude (A) and phase (θ), for the first five single drops of POL0912A.

When three sinusoids are included, the equation of motion is modified to

$$z(t) = z(0)\left[1+\tfrac{1}{2}\gamma t^2\right] + v_o(0)t\left[1+\tfrac{1}{6}\gamma t^2\right] + \tfrac{1}{2}g_o t^2\left[1+\tfrac{1}{12}\gamma t^2\right] + \sum_3 exp(-kt)(a\,cos\,\omega t + b\,sin\,\omega t) \tag{12}$$

The values of a and b for each of the 200 drops of the first set of POL0912A are plotted in Figure 5.18. The average value of each stacked set is printed on the figure. Although it appears at first that the amplitudes for 31 Hz are larger than for 8 Hz, the 31 Hz residuals are randomly scattered about zero (offset 6 and 10 nm for the cosine and sine terms

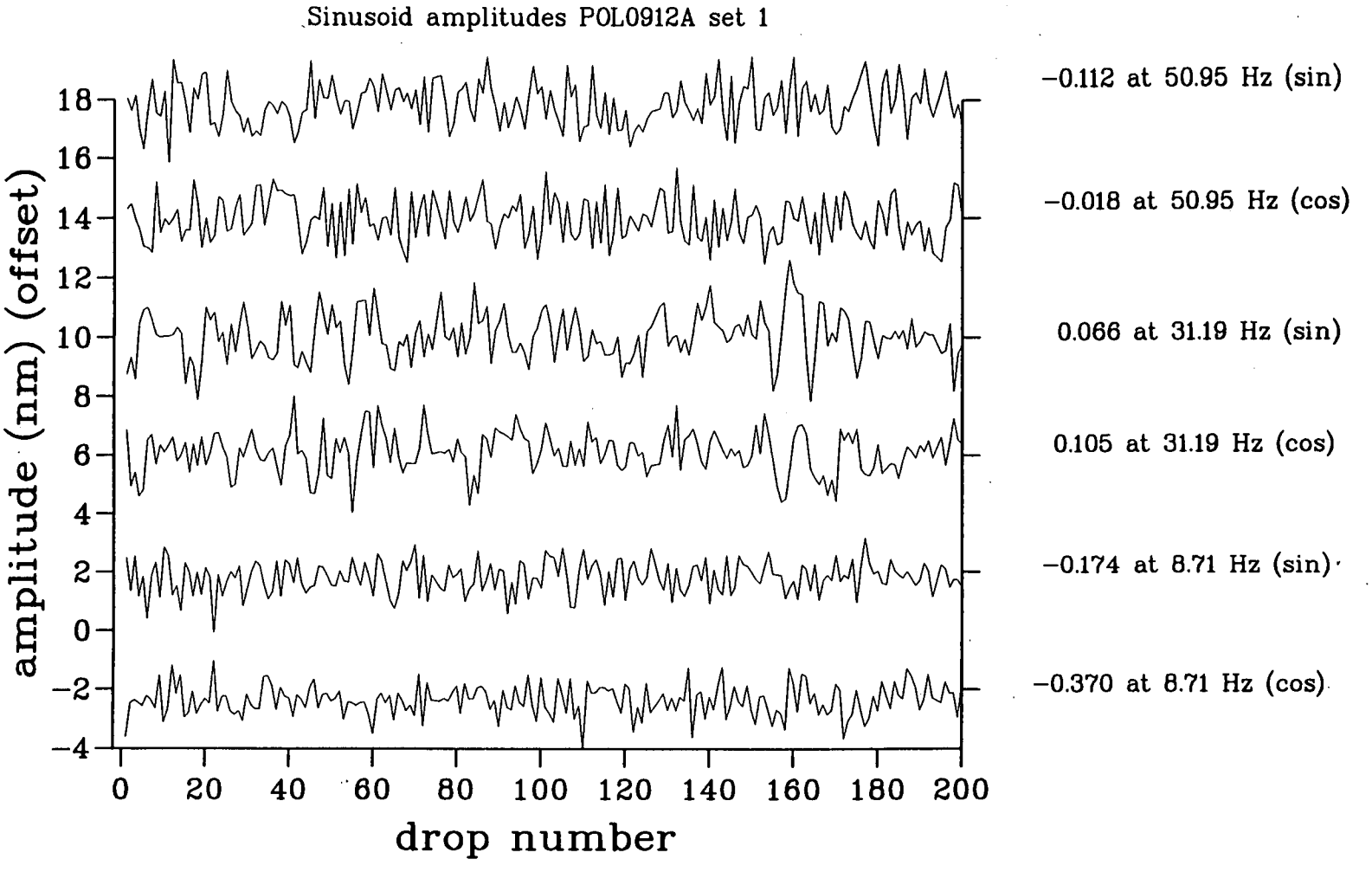

Figure 5.18 Variation of sine and cosine amplitudes with drop number for the first set of POL0912A. The graphs are offset at 4 nanometre (nm) intervals, beginning at -2 nm for the cosine term at 8.71 Hz.

respectively), but systematically negative for the 8 Hz (zero at offset -2 and +2 nm for cosine and sine respectively). It is this systematic character which causes the 8 Hz to dominate the appearance of the stacked residuals from the original data as shown in Figure 5.7b (200 drops) and 5.7c (1500 drops).

The amplitude A and phase θ for each of these three sinusoids are given in Table 5.15 for the first five drops. Note that the (A, θ) values for the 8.7 Hz term are similar Table 5.14 (8.71 Hz only) and Table 5.15 (8.71, 31.19 and 50.95 Hz).

f(k)	8.711 (-10.407)		31.185 (-21.186)		50.949 (-7.084)	
drop	A (nm)	θ (°)	A (nm)	θ (°)	A (nm)	θ (°)
1	1.682	-16.40	1.528	-55.02	0.309	13.45
2	0.797	54.60	1.259	32.58	0.579	-37.56
3	0.659	-55.29	1.525	67.77	0.175	-73.74
4	0.936	61.27	1.470	-17.13	1.005	70.11
5	0.587	14.20	1.510	-37.19	1.932	60.91

Table 5.15 Total amplitude (A) and phase (θ), for the first five single drops of POL0912A, resulting from including three damped sinusoids in the equation of motion (equation 12).

The spectrum of the cumulative residuals for one set resulting from the inclusion of these three damped sinusoids in the equation of motion is shown in Figure 5.19, with the original spectrum for comparison. The figure shows that these sinusoids have been effectively removed from the residuals.

The cutoff tests for the raw data, with a single sinusoid (8.71 Hz) only and with three sinusoids (8.71, 31.19 and 50.95) included in the equation of motion are shown in Figure 5.20. The squares show the raw data, where the gravity estimate varies by 60 μgal for the range of fringes fitted between 160 and 60. The crosses show the solution when one sinusoid is included, and the circles for three sinusoids. The addition of two more sinusoids to the 8.71 Hz does little to improve the 'flatness' of the cut-off tests.

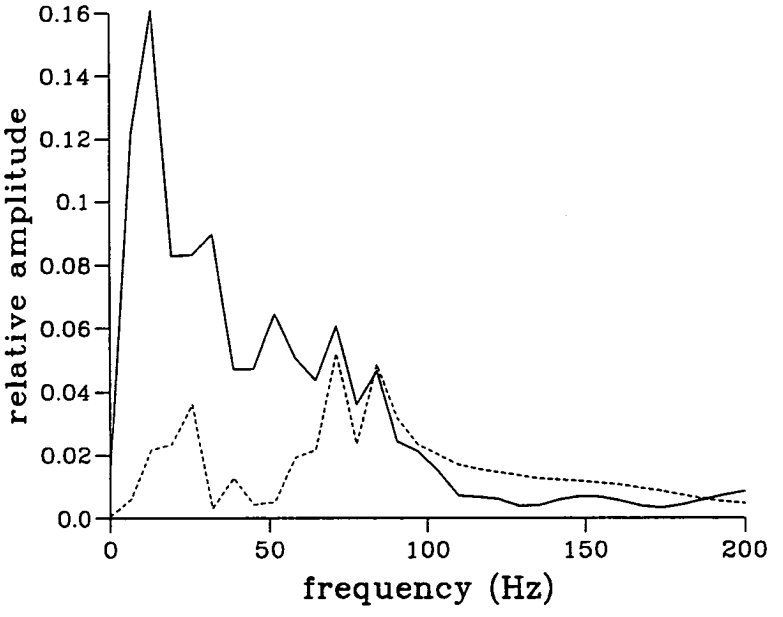

Figure 5.19 Spectrum of the distance residuals for set 1 of POL0912A before (——) and after (------) including three damped sinusoids in the equation of motion using the program SINE.

Estimation of the system response correction

The estimate of gravity at 150 fringes is increased by 1.6 μgal when three sinusoids are included in the fit. However, because the choice of 150 fringes as the 'best drop length' is somewhat arbitrary, a more representative estimate of the true value of gravity is the mean of the corrected values at *all* different drop lengths. The weighted mean of the gravity estimates, for a drop length between 60 and 160 fringes, made by including three sinusoids in the fit for POL0912A is 981 367 364.93 ± 5.26 μgal. The value of the single estimate at 150 drops for the raw data is 981 367 358.55 ± 6.56 μgal, so the system response correction is 6.38 ± 8.41 μgal. Since the structure in the residuals from all 24 sets of POL0912A are similar, this estimate is applicable to the 24 set mean from POL0912A.

Corrections to FG5-103 values used in BPGN

The above procedure has been carried out for FG5-103 data at Edinburgh GI, POL, NPL and Taunton for the datasets whose values were used in the BPGN adjustment (section 6.5). The frequencies, decay constants and stacked amplitudes for the 3 largest sinusoids for each set are summarised in Table 5.16.

Set	f (Hz)	decay	average cosine amplitude (nm)	average sine amplitude (nm)
EDI1907A	8.8	-10.9	-0.4075	-0.2467
	52.3	-8.4	0.1717	-0.0763
	33.5	-4.0	0.0732	0.0381
POL1306A	8.7	-10.4	-0.3503	-0.0573
	31.2	-21.2	0.0098	0.0228
	50.9	-7.1	-0.0379	0.0004
NPL0207	8.8	-11.4	-0.1929	-0.0468
	56.6	-4.9	0.0038	0.0695
	37.1	0.0	-0.0244	-0.1103
TAU0607A	9.33	-10.3	-0.3768	-0.3632
	6.0	-2.2	-0.0936	0.1709
	45.5	-12.7	0.1814	-0.0945

Table 5.16 Summary of frequencies (f), decay constants (k) and stacked amplitudes for the 3 largest sinusoids for representative FG5-103 sets at the four BPGN absolute sites.

The cut-off tests for the sets EDI1907A, POL1306A, NPL0207 and TAU0607A referred to in the table are given in Figure 5.21 a, b, c and d, and the weighted means of the corrected values and the system response corrections are given in Table 5.17.

μgal (se)	EDI1907A g - 981 579 000	POL1306A g - 981 367 000	NPL0207 g - 981 181 000	TAU0607A g - 981 168 000
uncorrected g at 150 fringes	199.03 (1.03)	359.75 (0.94)	337.47 (3.08)	838.64 (1.18)
wtd mean for 60-160 fringes	204.47 (1.95)	363.55 (2.40)	348.22 (5.45)	837.24 (2.58)
System Response correction	**+5.4 (2.2)**	**+3.8 (2.6)**	**+10.8 (6.3)**	**-1.4 (2.8)**

Table 5.17 System response corrections for the BPGN absolute sites at Edinburgh, POL, NPL and Taunton. The corrections are calculated by taking the difference between the single uncorrected value at 150 drops, and the weighted mean of all the values for drop lengths between 60 and 160 fringes.

The values for 'uncorrected g at 150 fringes' given in Table 5.17 differ from those shown in sections 5.4 to 5.7 (giving details of the absolute observations) only by the atmospheric pressure and ocean load corrections.

The fully corrected, representative mean values from all the observations at the BPGN absolute sites include the system response from Table 5.17.

5.3.6 Conclusions

The variation with drop length documented for JILA instruments in, for example Klopping *et al.* (1991), was expected to have been diminished to an insignificant level in FG5. The results of this section show that this variation is indeed reduced, but only to a level which is of the same order as the enhanced precision of 2 - 3 μgal. FG5 has many improvements in design over the JILA instruments, but they serve to identify the system response as a problem still to be solved. FG5-103 seems to have the largest and most systematic variation with drop length of all the data studied, but this may be due in part to the limited availability (to the author) of data from the other instruments. Because the drop length of FG5-103 was changed from 90 to 150 fringes during its first upgrade, a correction of about 23 μgal is needed to reconcile pre and post upgrade observations, which seems rather absurd for an instrument with a specified accuracy of 2 - 3 μgal. Most FG5s have a drop length of between 130 and 160 fringes, so the 'drop length correction' is reduced to less than 4 μgal. It would be much more satisfactory if all FG5s counted exactly the same number of fringes all of the time.

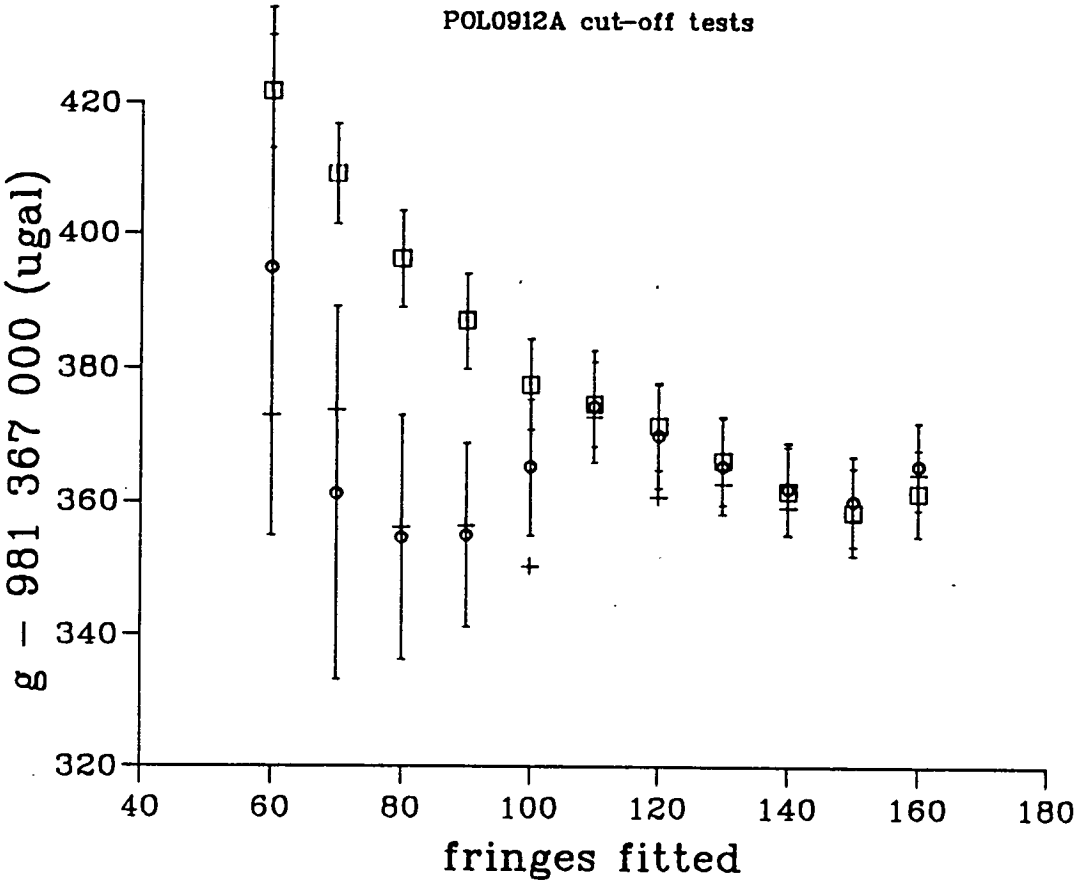

Figure 5.20 The cutoff tests for the raw data (squares), with a single sinusoid (8.71 Hz) only (crosses) and with three sinusoids (8.71, 31.19 and 50.95) (circles) included in the equation of motion. The error bars shown on the 3-sinusoid solution are of similar size for the single sinusoid solution, and are representative of most of the datasets mentioned here.

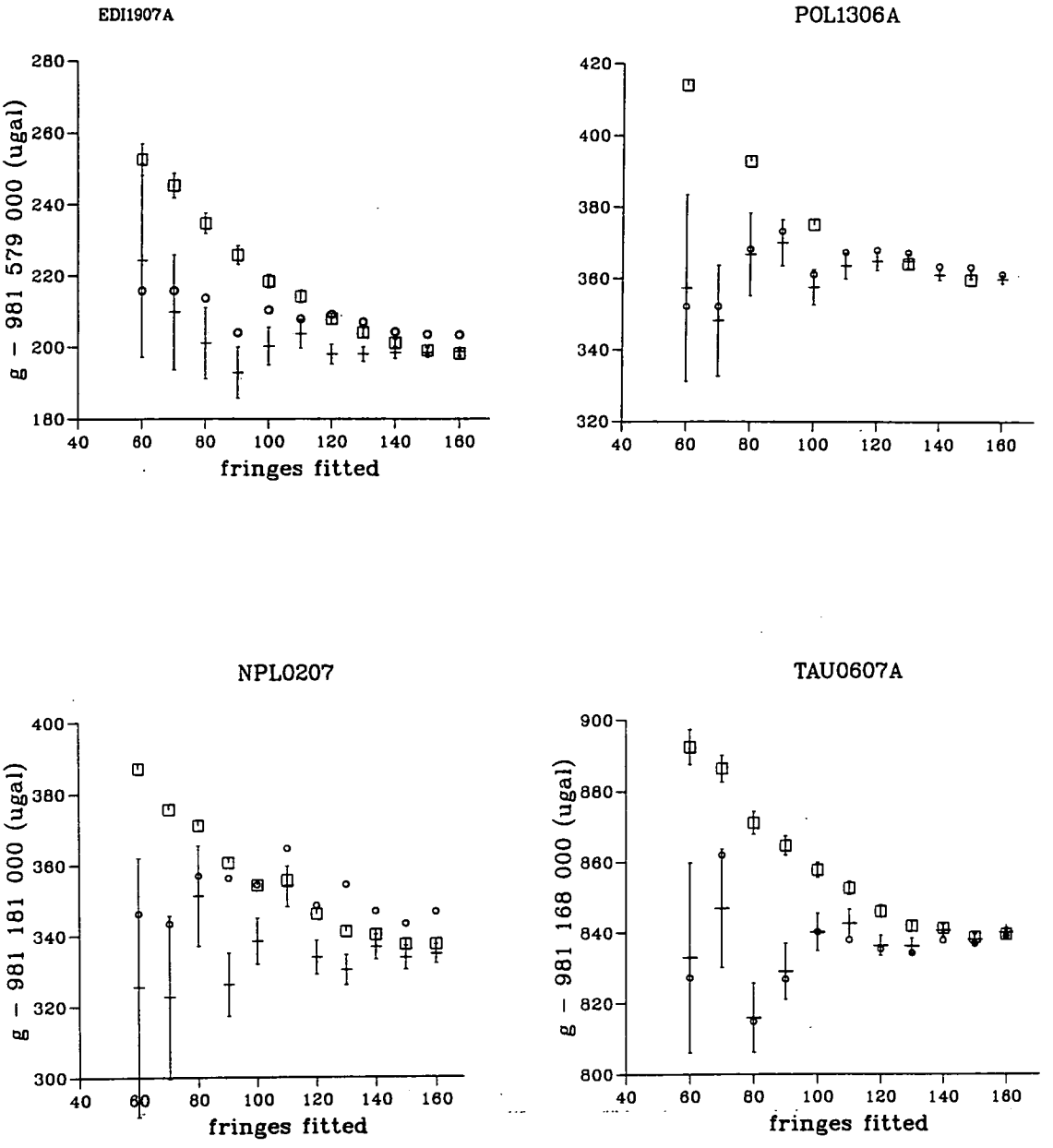

Figure 5.21 Cut-off tests for the sets EDI1907A, POL1306A, NPL0207 and TAU0607A, after correcting with one and three sinusoids. Some error bars are omitted for clarity, but are adequately represented by those shown on Figure 5.20. The weighted means of the corrected values at all the drop lengths and the system response corrections are given in Table 5.17. See Figure 5.20 for key.

The variation in gravity estimate with drop length is related to structure in the fringe residuals, which has an amplitude of up to 0.6 nm for FG5. If the fringe times are corrected with the average residuals, the gravity estimate becomes constant. When the residuals are stacked over a large number of drops, the structure is seen to depend on the particular instrument and the site. Klopping *et al.* (1991) modelled the structure in the stacked residuals from JILA meters with a series of damped sinusoids, and by including these in the fit for gravity were able to reduce the amplitude of their residuals from 3 or 4 nm to less than 0.5 nm. Attempts to do this with FG5 data have been less overwhelmingly convincing, but demonstrate that the method can be used to determine a 'system response' correction.

The frequencies of the sinusoids can be found from the Fourier transform of the residuals. By definition, the 'residuals' are the bits which have not been included in the solution, so to rid the gravity estimate of the influence of the sinusoids, they have to fitted at the same time as gravity. The amplitude and phase vary with each drop, so simply correcting with two or three sinusoids having an average, but fixed, amplitude and phase is not successful. The amplitude and phase have to be included as unknowns in the equation of motion. Because the fit to the distance time pairs is parabolic, it is the lower frequency sinusoids which have the greatest influence on the estimate of gravity.

The largest sinusoidal component in FG5-103 residuals typically has a frequency of about 8 Hz, but because it *is* the largest, it can be more easily identified and removed. This results in a change between 2 and 6 μgal in the estimate of gravity, depending on the instrument and site. The remaining residuals have smaller sinusoids at about 50 and 30 Hz, but these have only a barely significant effect.

5.4 FG5 observations at the Proudman Oceanographic Laboratory (POL)

5.4.1 Introduction

The Proudman Oceanographic Laboratory at Bidston, Birkenhead, is the 'home base station' for FG5-103. FG5-103 began observations at POL in August 1992. These have continued somewhat intermittently until the present. Those between August 1992 and November 1994 are divided into four phases for discussion.

5.4.2 Relative Gravity Observations at POL

In March 1992, in anticipation of FG5's delivery later that year, the vertical gradients at two sites were measured, and two ex-centres were established. One of the ex-centres was linked to the British Precise Gravity Network site at Daresbury. In March 1994, the gradients at the absolute sites were re-measured at three heights, and the POL-Daresbury link was strengthened. The main absolute gravity site at POL is POL1 which is in the sub-basement of the former Bidston Observatory building at the POL site. POL2 is at the other end of the same room. Two other ex-centres were established outside the building, at the Current Meter site and the South Porch (Figure 5.22). The Current Meter site is a concrete platform, of convenient size for measuring gravity with an LCR meter, set into the lawn in front of the Proudman Building. The South Porch site is on the doorstep of the south door of the old observatory which houses the absolute sites. The South Porch site has been connected to the British Precise Gravity Network (BPGN93) site at Daresbury.

The links between the Current Meter and POL1, and South Porch and POL1 were made in two separate sequences on 18 March 1992. Each sequence consisted of four occupations of each site with both of the LCR meters, G275 and D145. The results of the network adjustment of the ex-centre observations is given in Table 5.18.

site	gravity (μgal)	se (μgal)
POL1	000.0	3.9
POL2	6.1	4.1
South Porch	-1 281.5	4.3
Current Meter	-70.7	3.7

Table 5.18 Gravity values of POL ex-centres relative to POL1, on the scale of FG5.

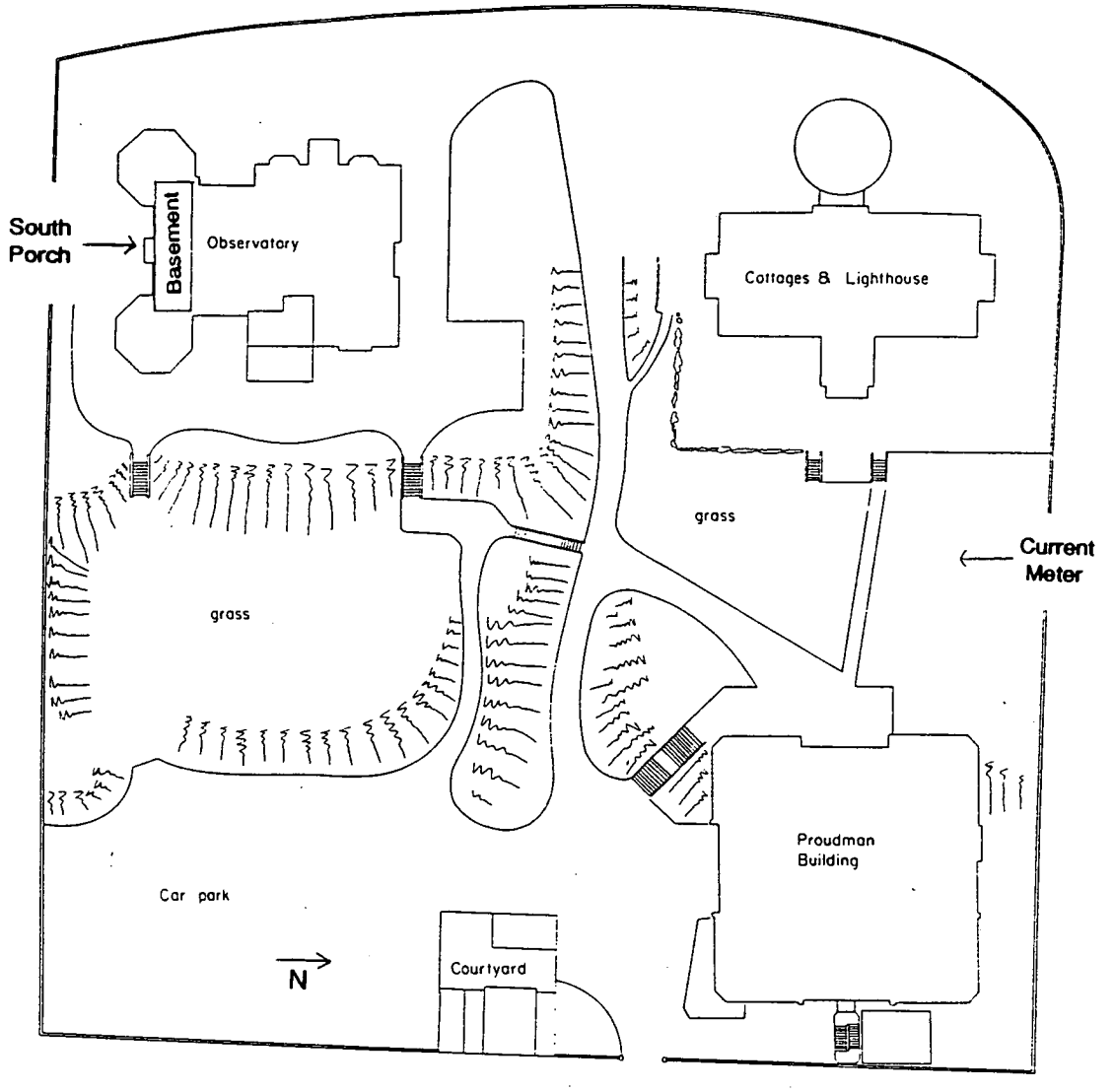

Figure 5.22 Gravity ex-centres at POL : the Current Meter site and the South Porch of the observatory. The absolute sites POL1 and POL2 are in the basement of the observatory.

The South Porch - Daresbury link was included in the main BPGN adjustment. Gravity at Daresbury is 11 863.7 ± 10.1 μgal lower than at South Porch on the scale of FG5 (section 6.5.4).

Vertical gradient observations and analysis were given in section 5.2, with results in Tables 5.5 and 5.7.

5.4.3 FG5-103 at POL

Introduction

FG5-103 was purchased by the Proudman Oceanographic Laboratory, which is an institute of the Natural Environment Research Council (NERC). The instrument was delivered in August 1992 and the first observations were made at POL2 site. All observations since October 1992 have been made at the primary POL1 site. The FG5 data acquired at POL is divided, for this discussion, into four phases which mainly coincide with the use of different lasers as the wavelength standard.

From August 92 to December 92, a Newport polarisation stablised He-Ne laser (NL1) was used, with version 1.0 of the processing software. This phase included, but ended with, the Edinburgh 1992 data after which the instrument was returned to the manufacturer for repairs and upgrading. POL Phase 2 began in April 93, with a new Iodine stabilised laser, environmental sensors and version 2.0 software. The power of the Iodine laser gradually faded and after the NPL (Teddington) observations in July 1993, it became unusable. A new Axis polarisation-stabilised He-Ne (AL1) laser was acquired in September 1993 and was used for Phase 3. Because of the poor performance of the instrument after the AL1 was installed, the interferometer was adjusted (by Niebauer) in November 1993. Poor alignment of the optics can reduce the intensity of the laser beam, and degrade the coincidence of the reference and test beams. It can also increase mode leakage (section 4.4.6). Values since 15 November 1993 are currently accepted as 'valid' estimates of absolute gravity at POL. Phase 4 ends in May 94 when a new 'Winters' Iodine stabilised laser replaced the AL1. A sample of values since then have been used for control of the BPGN93. The instrument returned to Boulder in November 1994 for a routine service during which the laser tube was renewed and the controlling hardware was upgraded. The Rubidium clock was recalibrated and found to be running at a frequency which caused gravity to be low by 1.9 μgal (*pers. comm.* R. Edge 17 Jan 1995).

The means of most of the 24 hour runs have been supplied to the author for Phases 1, 2 and 3, and for Phase 4 up until April 1994. The values supplied by POL result from processing the original data with the Axis programs OLIVIA and REPLAY, and in many cases the values are not fully corrected. Only a few .ddt files have been available to the author, but with these, the agreement of the results from the program REPLAY and the Edinburgh program DDT has been verified. The important vertical gradient and datum height corrections could be calculated for the few POL .ddt files, which enabled the rest of the lists of set means to be similarly corrected with an accuracy of about 1 μgal. Many sets observed since the beginning of Phase 2 have since been reprocessed at POL and corrected for atmospheric pressure and vertical gradient. The current online software (version 3.01) includes corrections for the ocean loading and polar motion. The set means given here are as supplied to the author by POL, except for the sets POL1306A and POL1808A in Phase 4, where the values have been recalculated by the author from the original .ddt file. Where additional corrections have been made, the values may not agree precisely with those which may have been subsequently released by POL.

Because the value of gravity at POL estimated by FG5-103 changed by up to 10 μgal after each upgrade or laser replacement, there has been a tendency of the instrument operators at POL to ignore all previous values and take the most recent as 'best'. The author believes that there is still some value in analysing *all* the data, especially to illustrate how the instrument has behaved with time, and to examine the effect of the different components installed.

Phase 1. Early He-Ne : August to December 1992

The set means of 18 runs of Phase 1 are given in Table 5.19. The values are those from version 1.0 of REPLAY, corrected for the elastic tide only, as they were recorded in the FG5 log book at POL at run-time.

The first 8 sets were observed at POL2, then all subsequent sets at POL1. Observations were suspended between 26.09 and 07.10 because of the high noise level caused by stormy weather. Between sets POLTST 12A and 12B, the transformer on the power supply to the instrument failed and was replaced. Immediately after POL1 2711, the instrument was taken to Edinburgh where it began observing on 02.12.92.

The only correction which has been applied to the values in Table 5.19 is for the elastic tide. The mean of the POL2 sets is 981 367 418.8 ± 1.8 μgal. The POL1 sets show a very large

range of 63 μgal, whose origin is unknown. The mean of the 14 POL1 sets in Phase 1 is 981 367 426.9 ± 17.7 μgal.

It is possible to estimate the vertical gradient correction for Phase 1 with an accuracy of better than 1 μgal by processing the .ddt file for POLTST01 which was the only example available from this phase. The vertical gradient correction, which enables the values at the 'effective measurement height' to be transferred to the top of the drop (section 4.3.3), is -12.5 μgal for POL2 and -12.0 μgal for POL1 (using gradients of 215.3 ± 32.9 μgal m^{-1} and 225.4 ± 2.0 μgal m^{-1} respectively). The speed of light correction for a 90 fringe drop is -9.9 μgal. Phase 1 values were derived from OLIVIA version 1.0, which makes the Honkasalo Correction, i.e the estimates of gravity include the static tide. To make the version 1.0 values consistent with later data, the static tide must be removed from the data which means subtracting the contribution of the static tide (32.04 μgal at POL). Because the estimate of gravity varies with drop length (section 5.3.1) a correction of 23 ± 7 μgal should be applied to the Phase 1 values (made with a drop length of 90 fringes), to make them consistent with later values which were all made with a drop length of 150 fringes. These corrections are shown in Table 5.20.

	end date	sets	g (μgal) - 981 367 000.0	s.d (μgal)
POL 2				
POL TST01	19.08.92	20	410.0	5.7
POL TST02	20.08.92	15	414.0	7.3
POL TST04	21.08.92	16	415.0	6.8
POL TST05	22.08.92	20	408.0	4.7
POL TST07A	25.08.92	3	413.0	1.7
POL TST07B	26.08.92	2	416.3	1.1
POL TST08	27.08.92	4	414.6	1.5
POL TST12A	04.09.92	20	413.1	20.0
weighted mean **POL2**		(8 sets)	**981 367 414.8**	**1.8**
POL 1				
POL TST12B	17.09.92	20	404.6	8.6
POL TST13	26.09.92	20	418.3	12.2
POL TST16	07.10.92	17	385.6	3.7
POL TST17	08.10.92	20	384.8	4.6
POL TST18	09.10.92	20	389.2	4.0
POL1 2010	21.10.92	20	404.9	8.0
POL1 2910	30.10.92	20	392.1	6.7
POL1 0511	06.11.92	20	419.0	7.5
POL1 0911	09.11.92	20	443.2	9.2
POL1 1311	14.11.92	20	443.2	5.7
POL1 1811	19.11.92	20	448.0	14.1
POL1 2011	21.11.92	20	444.1	6.9
POL1 2611	27.11.92	5	430.0	20.0
POL1 2711	28.11.92	2	434.4	1.0
weighted mean **POL1**		(14sets)	**981 367 426.9**	**17.7**

Table 5.19 Means for early sets at POL1 and POL2 using the NL1 He-Ne laser. No corrections have been made except for the elastic tide.

	μgal	s.e
POL2 (Phase 1)		
g at measurement height (inc. elastic tide)	981 367 414.8	1.8
vertical gradient correction (at 225.4 ± 2.0 μgal m^{-1})	-12.5	†0.1
speed of light (90 fringes)	-9.9	
static tide	-32.04	
drop length correction	+23	7
corrected g at ~ 1300 mm **POL2**	**981 367 383.4**	**7.2**
POL1 (Phase 1)		
g at measurement height (inc. elastic tide)	981 367 426.9	17.7
vertical gradient correction (at 215.3 ± 32.9 μgal m^{-1})	-12.0	†1.8
speed of light (90 fringes)	-9.9	
static tide	-32.04	
drop length correction	+23	7
corrected g at ~ 1300 mm **POL1**	**981 367 396.0**	**25.2**

Table 5.20 Means of gravity values and summary of corrections for Phase 1 at POL1 and POL2.
† Error is linear in vertical gradient.

Phase 2. First values with Iodine stabilised laser (ISL1) : April to July 1993

While FG5-103 was being repaired, it was also considerably upgraded. An iodine stabilised laser was fitted, environmental (atmospheric pressure, temperature and humidity) and instrument (chamber pressure and laser temperature) sensors were attached, new software (version 2.0) was installed, and the drop length was increased from 100 fringes to 170. The data obtained in Phase 2 were much better than Phase 1, with a scatter of about 13 μgal and average set s.d of about 4.5 μgal compared with 63 and 7.5 μgal respectively for Phase 1. The values given in Table 5.21 were supplied to the author by R.J Edge of POL (*pers. comm.* 11 March 1994), and they had been corrected for the elastic tide (static tide removed from the data), atmospheric pressure and speed of light. The iodine laser modulation correction (section 4.4.6) has not been applied, but it is a random rather than systematic effect which results in a correction to the set means which is expected to be less than ± 1.5 μgal. The main significance of the correction is that it reduces the standard deviation of a drop, and hence of the set mean, by a factor of about three. (These estimates result from an investigation of only one of the sets below - POL 1205 (section 4.4.6), whose ddt file was available to the author.)

name	end date	sets	g (μgal) - 981367000.0	s.d (μgal)
POL 2104	22.04.93	20	374.8	18.7
POL 2204	23.04.93	20	373.7	5.2
POL 2304	24.04.93	20	372.6	8.9
POL 2704	28.04.93	20	370.6	3.0
POL 2804	29.04.93	20	369.1	6.6
POL 2904	30.04.93	24	368.9	4.8
POL 0605A	07.05.93	20	365.0	6.4
POL 0705	08.05.93	24	370.0	2.2
POL 1005	11.05.93	24	365.5	3.8
POL 1205	13.05.93	24	364.7	3.7
POL 2605	27.05.93	24	367.3	3.4
POL 0906	10.06.93	24	368.8	10.0
POL 1006	11.06.93	24	361.7	1.3
POL 1406	15.06.93	24	363.0	1.5
POL 1706	18.06.93	24	361.3	4.6
POL 2106	22.06.93	24	363.0	2.1
POL 2306	24.06.93	24	364.6	2.1
POL 2406	25.06.93	24	364.1	1.7
POL 2806	29.06.93	20	373.7	3.3
weighted mean POL1 (19 sets)			**981 367 364.8**	**3.4**
vertical gradient correction (at 215.3 ± 32.9 μgal)			-12.0	1.8
correction from 990 mb to 1006.7 mb †			-5.0	
corrected g at ~ 1300mm POL1			**981 367 347.8**	**3.8**

Table 5.21 Set means from Phase2 (ISL1) corrected for elastic tide, atmospheric pressure and speed of light.
† See note on atmospheric pressure correction under Phase 4.

The vertical gradient correction for POL1 is -12.0 ± 1.8 μgal, and the correction for the incorrect nominal pressure (see Table 5.21) is -5.0 μgal. The mean value of gravity at the top of the drop (about 1300 mm) for Phase 2 data is 981 367 347.8 ± 3.8 μgal. The corrections for ocean loading and polar motion are not made. Their effect ranges between about ± 2 and ± 4 μgal at POL.

Some of the improvement in the Phase 2 data will be due to the atmospheric pressure correction (-0.3 μgal $mbar^{-1}$), but most is attributed to the superior laser. The super spring and its controlling electronics had also been upgraded and the performance of the ground-noise isolation system was therefore improved. Phase 1 took place during August to December, and was therefore more prone to high microseismic noise than Phase 2, which lasted through the summer months (April to July).

Phase 3. AL1 'Optics not focused' : September to November 93

This short (two month) phase consists of data obtained with the Axis polarisation stabilised He-Ne laser (AL1) from its installation up until the interferometer was adjusted by Niebauer at POL on 15 November. Most of the sets (13.10 to 8.11) consisted of 50 sets of 90 drops, with sets made every hour, presumably to allow the laser to 'lock' properly between sets. The values, shown in Table 5.22, are very scattered and have a standard deviation on the set means which is an order of magnitude larger than the Phase 2 sets. The poor quality of this data emphasises the importance of correct adjustment of the interferometer optics, since this is the only difference between Phase 3 and the much better Phase 4 data.

name	end date	sets × drops	g (μgal) - 981367000.0	s.d (μgal)
POL 2009A	21.09.93	24 × 250	316.0	26.7
POL 2109A	22.09.93	24 × 250	319.4	2.8
POL 2309A	24.09.93	24 × 250	339.0	1.8
POL 2409A	25.09.93	24 × 250	335.7	2.4
POL 1310A	14.10.93	50 × 90	327.2	3.1
POL 1410A	15.10.93	50 × 90	326.9	3.2
POL 1810A	19.10.93	50 × 90	304.6	22.6
POL 1910A	20.10.93	50 × 90	294.4	22.6
POL 2010A	21.10.93	50 × 90	242.3	17.9
POL 2110A	22.10.93	50 × 90	242.6	15.6
POL 2510A	26.10.93	50 × 90	238.3	13.7
POL 2710A	28.10.93	50 × 90	239.4	19.4
POL 0111A	02.11.93	50 × 90	314.5	36.1
POL 0211A	03.11.93	50 × 90	300.8	26.9
POL 0411A	05.11.93	50 × 90	393.5	4.2
POL 0811A	09.11.93	50 × 90	391.4	6.9
weighted mean (16 sets)			**981 367 335.1**	**21.6**
vertical gradient correction (at 215.3 ± 32.9 μgal)			-12.0	1.8
correction from 990 mb to 1006.7 mb †			-5.0	
corrected g at ~ 1300 mm POL1			**981 367 318.1**	**21.7**

Table 5.22 Values from Phase 3 (September to November 1993) using AL1 laser, corrected for speed of light at atmospheric pressure.
† see note on atmospheric pressure correction under Phase 4.

Phase 4. Good data with AL1 : November 93 to May 94

Since 15 November 1993, FG5-103 has given consistent values at POL1 at around 981 367 360 ± 5 μgal at 1309 mm with standard deviation on a set of about 4 μgal Phase 4 includes values from the AL1 laser between 15 November 93 and May 94. Twenty values of set means from 15.11.93 to 15.04.94, corrected for elastic tide, speed of light and atmospheric pressure to a reference pressure of 990 mbar, using the program REPLAY were supplied to the author by H. Hopewell of POL (*pers. comm.* 2 September 1994). The 990 mbar is the value of the nominal air pressure at Boulder (which is about 1000 m above sea level). This value should have been updated in the REPLAY command file to the standard pressure for POL which is only 54 m above sea level. Correcting to the standard pressure of 1006.7 mbar at 54 m changes the POL estimates by (1006.7 - 990) mbar multiplied by -0.3 μgal $mbar^{-1}$, which is a correction of -5.0 μgal. It is assumed that this error was present during Phase 2 and Phase 3 data. so the same correction has been applied..

The twenty values from H. Hopewell have been additionally corrected by the author for the vertical gradient and polar motion. The polar motion values are exactly those printed on the REPLAY screen output as the 'polar motion correction'. The .ddt file for POL 2511A was processed using the program DDT and the estimated gravity was found to agree with the corrected value from REPLAY. These corrected values are now consistent with the values at NPL, Edinburgh 1994, Taunton and with the most recent POL sets, except for the ocean loading correction. The values supplied by POL and the corrections made by the author are given in Table 5.24. The convention followed is that all corrections are added, so that vertical gradient corrections are negative, datum height are positive, speed of light are negative.

Recent sets - POL 1306A and POL 1808A

These are two representative sets from the period May to November 1994 when the Winters ISL was used. The .ddt files were processed with the program DDT with corrections for vertical gradient (at 215.3 ± 32.9 μgal), speed of light, atmospheric pressure (to 1007.7 mbar) and ocean loading. The polar motion correction was calculated using the program REPLAY, and added to the set mean. The final representative value for absolute gravity at 1309 mm at POL1 is taken to be the weighted mean of these two sets POL 1306A and POL 1808A, since these are the only ones which have been corrected for ocean loading. This makes them consistent with the representative values for FG5 at NPL, Edinburgh and Taunton. The corrected values are shown in Table 5.25.

name	end date	sets × drops	g (μgal) - 981 367 000	polar motion	g. inc po. mo	s.d
POL 1511A	16.11.93	15 × 200	388.6	0.4	389.0	4.7
POL 1611B	17.11.93	16 × 200	384.3	0.4	384.7	3.7
POL 1711B	18.11.93	18 × 200	382.8	0.4	383.4	3.9
POL 2211B	23.11.93	20 × 200	381.3	0.3	381.6	1.9
POL 2311A	24.11.93	13 × 200	383.8	0.3	384.1	2.5
POL 2411B	25.11.93	24 × 200	381.4	0.3	381.7	3.8
POL 2511A	26.11.93	18 × 200	380.3	0.3	380.6	2.1
POL 0612A	07.12.93	18 × 200	379.0	0.0	379.0	5.0
POL 0712A	08.12.93	24 × 200	381.5	0.0	381.5	4.7
POL 0912A	10.12.93	24 × 200	380.2	0.0	380.2	5.1
POL 1312A	14.12.93	24 × 200	384.1	0.0	384.1	4.8
POL 0601B	07.01.94	24 × 200	388.4	-0.8	387.6	3.9
POL 1101B	12.01.94	24 × 200	388.4	-1.2	387.2	5.4
POL 3101A	01.01.94	20 × 200	379.8	-2.0	377.8	22.9
POL 0103B	02.03.94	21 × 200	378.7	-3.1	375.6	9.2
POL 2103A	22.03.94	24 × 200	384.6	-3.4	381.2	12.6
POL 2203A	23.03.94	21 × 200	384.6	-3.4	381.2	12.8
POL 2803B	29.03.94	24 × 200	384.9	-3.4	381.5	11.6
POL 1404B	15.04.94	24 × 200	389.6	-3.7	385.9	6.1
POL 1504A	16.04.94	24 × 200	390.1	-3.7	386.4	5.9
weighted mean (20 sets) including polar motion correction				**981 367 382.8**		**2.6**
vertical gradient correction (at 215.3 ± 32.9 μgal)				-12.0		1.8
correction from 990 mb to 1006.7 mb				-5.0		
corrected g at ~ 1300 mm POL1				**981 367 365.8**		**3.2**

Table 5.24 Phase 4 values from November 93 to May 94, with the AL1, corrected for elastic tide, speed of light and atmospheric pressure to the standard pressure at POL.

name	end date	sets × drops	g (μgal) - 981367000.0	polar motion	g. inc po. mo	s.d (μgal)
POL 1306A	14.06.94	18 × 200	364.2	-3.1	361.1	1.3
POL 1808A	19.08.94	24 × 200	361.8	-0.9	360.9	4.1
weighted mean at 1309 mm POL1					981 367 **361.1**	**0.2**
datum correction to 120mm					+ 279.4	3.4
system response correction					+ 3.8	2.6
weighted mean at 120 mm POL1					**981 367 644.3**	**4.3**

Table 5.25 Representative value for POL1, corrected for atmospheric pressure (to the standard pressure at 46 m), vertical gradient (at 215.3 ± 32.9μgal m^{-1}), speed of light, polar motion and ocean loading. The system response correction is described in section 5.3.2.

5.4.4 Summary of FG5 observations at POL August 1992 to June 1994.

The set means from POL between August 1992 and June 1994 are plotted in Figure 5.23. All values have been corrected for speed of light and to the top of the drop, and the static tide has been removed from the data. Other corrections have been made where possible, and they have been discussed in the previous sections. Figure 5.23a shows all the values, including the invalid data from Phase 3 (vertical scale = 300 μgal). Figure 5.23b shows the data without Phase 3 (vertical scale = 100 μgal) its relative quality can be more easily compared.

The weighted means of the phases are shown in Table 5.26. The instrument was significantly upgraded before Phase 2, which resulted in a much reduced scatter. However, the absolute value of the Phase 2 mean is about 12 μgal lower than all later means (excepting Phase 3). Because of its extended 'settling down' time (15 months), FG5-103 did not give consistent values at POL with a repeatability close to specification until November 1993. However, observations made at NPL in June 1993 agreed with FG5-105 to within one standard deviation (section 5.6). Observations made during the 'Recent' era at Edinburgh give a good agreement with a JILA4 observation made there in 1989 (section 5.5).

Phase (site) (N sets)	dates	weighted mean	laser
Phase 1 (POL2) (8)	19.08.92 - 04.09.92	367 383.4± 7.2	NL1
Phase 1 (POL1) (14)	17.09.92 - 18.11.92	367 396.0 ± 25.2	NL1
Phase 2 (POL1) (19)	21.04.93 - 28.06.93	367 347.8 ± 3.8	ISL1
Phase 3 (POL1) (16)	20.09.93 - 08.11.93	367 318.1 ± 21.7	AL1 out of focus
Phase 4 (POL1) (20)	15.11.93 - 15.04.94	367 365.8 ± 3.2	AL1, Winters ISL
Recent (POL1) (2)	14.06.94 & 18.08.94	367 361.1 ± 0.2	Winters ISL

Table 5.26 Weighted means of phases (- 981 000 000 μgal), corrected to ~ 1300 mm.

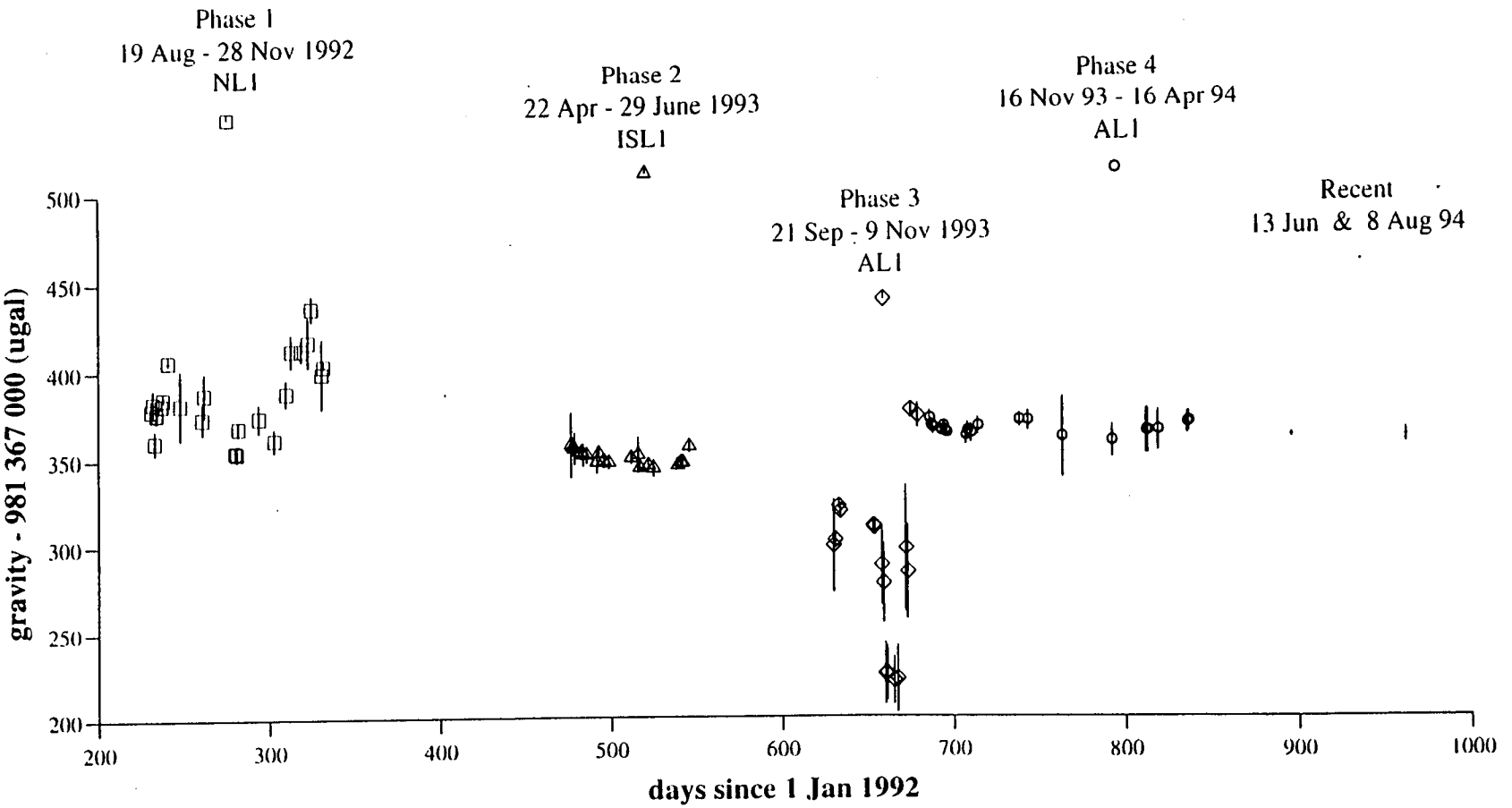

Figure 5.23a Plot of all the FG5-103 values at POL between August 1992 and July 1994. The data have been corrected as much as possible (see text) to give equivalent values at the top of the drop at POL1. The same data is shown, but without the poor quality Phase 3 data, in Figure 5.23b.

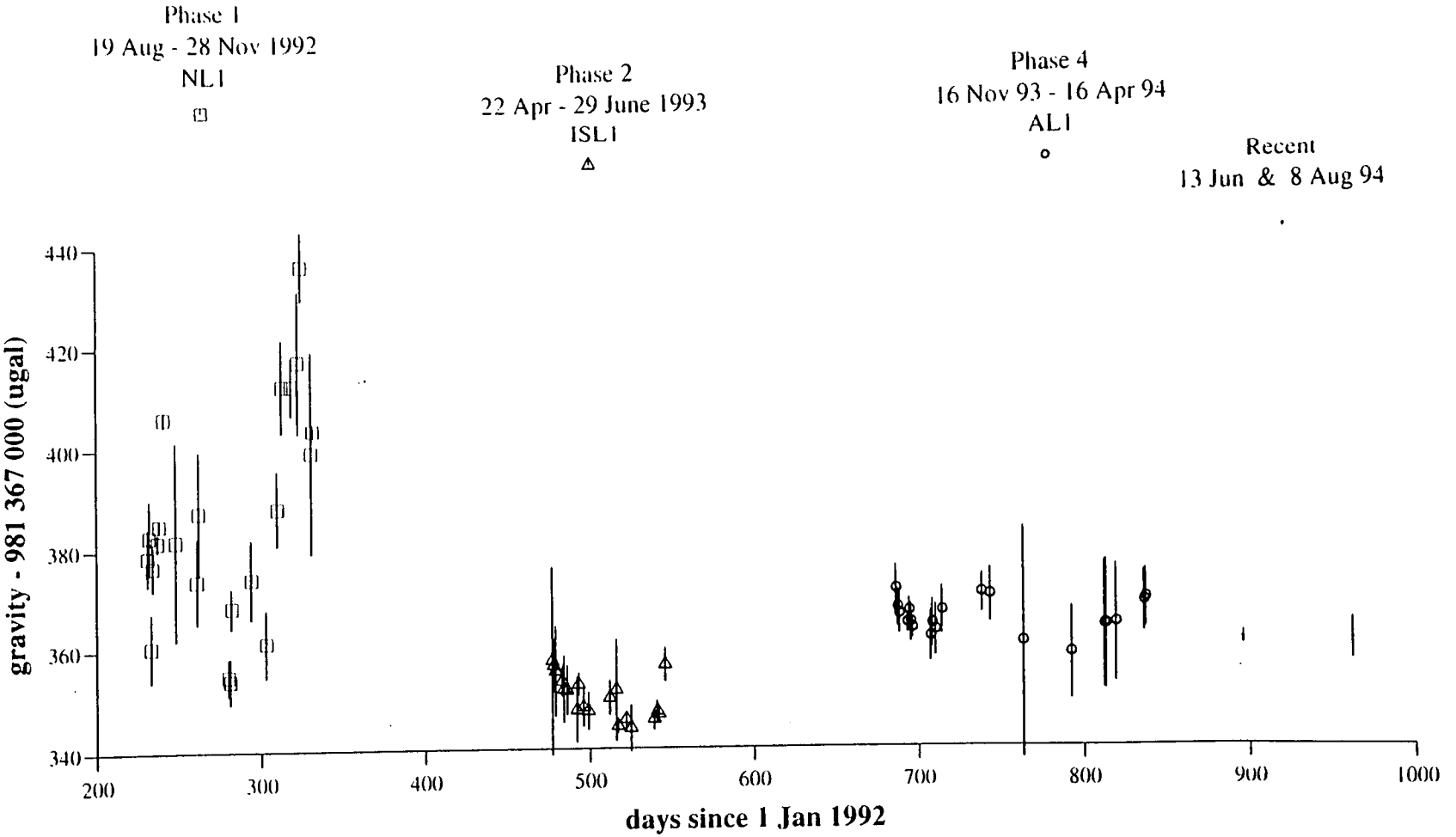

Figure 5.23b Plot of all the FG5-103 values at POL between August 1992 and July 1994., excluding the poor quality Phase 3 data, The data have been corrected as much as possible see text) to give equivalent values at the top of the drop at POL1.

5.5 Absolute Gravity Observations at Edinburgh

5.5.1 Introduction

Edinburgh A is one of two principle IGSN71 sites in Britain, the other being Teddington A. Other IGSN71 sites are either ex-centres or of lesser quality. The Edinburgh A site in the Royal Observatory is now inaccessible, but it was connected to the Edinburgh Fundamental Bench Mark (FBM) and the Edinburgh University JCMB site by Hipkin *et al.* (1988). Edinburgh FBM is part of the National Gravity Reference Net 1973 (NGRN73) (Masson Smith *et al.* 1974) and Edinburgh JCMB was an important base for precise gravimetry in Northern Britain until 1992 when the gravimetrists moved to a new building - the Grant Institute (GI).

In December 1989, the absolute gravity meter JILA4 observed at the British Geological Survey (BGS) Murchison House, Edinburgh. The instrument was operated by the US National Geodetic Survey (NGS) and the National Oceanic and Atmospheric Administration (NOAA), and relative observations of the vertical gradient at BGS and a transfer to Edinburgh JCMB were made by the No.2 Doppler Section of the 512 Specialist Team Royal Engineers (STRE). The sites are described in the STRE internal report (CollierJackson 1990) which gives no results, but suggests that observations at Edinburgh with a Sakuma instrument and at Proudman Oceanographic Laboratory (POL), Birkenhead, with a Hammond meter might be forthcoming. Neither of these proposals were realised so the only absolute observations in Edinburgh have been with JILA4 and FG5-103. In December 1992, FG5-103 observed at the BGS site and at the Grant Institute (GI), which is the new Edinburgh University base station. These observations were the first to be made with FG5-103 outside its 'home base' at POL since its delivery from the manufacturers (Axis Instruments, Boulder, Colorado). The instrument has since returned to Colorado twice and has been significantly upgraded. FG5-103 remeasured at GI in July 1994 (after the first upgrade).

Hundreds of relative observations at and between these sites (which are all on the King's Buildings (KB) campus of the University of Edinburgh) have been made by the author with LCR meters G275, D145 and D154. The Royal Engineers observed the gradient at BGS and the connection from BGS to JCMB during the JILA4 occupation in December 1989 and repeated the relative observations in the autumn of 1993.

5.5.2 Relative Gravity Observations at King's Buildings, Edinburgh

KB Gravity Sites

The two absolute gravity sites at King's Buildings (KB) are at the British Geological Survey (BGS) and the Grant Institute (GI). The BGS site is in Room 44 of the basement of the building at a 25 mm brass disk sunk into the floor. This site is in a particularly awkwardly shaped corner of the room which is barely large enough to take a JILA or FG5 meter. An accessible ex-centre for the BGS site was established in the stairwell of an adjacent car park (Figure 5.24). The GI site is in the basement of a new wing of the Grant Institute built in 1990 to house the geophysicists when they moved from JCMB. It is evident (from multiple large cracks in the plaster all over the building) that the new wing is still settling into its foundations. The Edinburgh JCMB site which was the base station for the University gravity surveys until 1991 is in the main entrance hall of the James Clerk Maxwell Building, and was monumented by a 100mm diameter circular disk mounted on the wall at ground level by the Royal Engineers.

Observations

For all the relative observation sequences, four occupations were made at each site with each meter, and usually two or more readings were taken at each occupation. In December 1991, the link between BGS and its ex-centre at the Car Park, and the link between the Car Park and JCMB were measured with G275 and D145. In January 1992, the Car Park - JCMB link was remeasured as part of a closed loop which also included the newly established site at GI. Each link was observed separately (i.e forward and back between two sites, rather than a repeated triangular sequence) with each of three meters G275, D145 and D154. FG5-103 made absolute observations at GI and BGS in December 1992, and in order to make a comparison of the difference between these two sites as measured by relative and absolute instruments, the link between GI and BGS was measured directly with G275 and D145 in December 1993. When all this data is adjusted together, the results are as shown in Table 5.27.

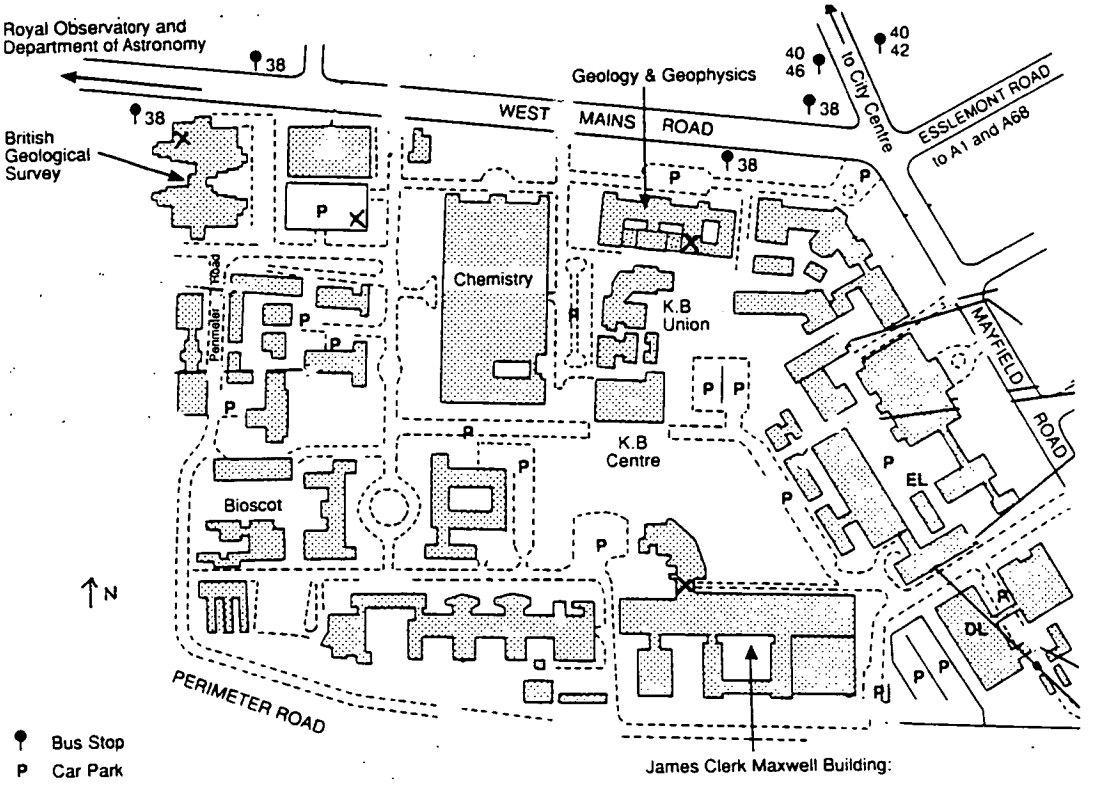

Figure 5.24 Gravity sites at King's Buildings, University of Edinburgh. The Grant Institute (GI) is the Geology and Geophysics building. The Car Park site is between the British Geological Survey (BGS) and the Chemistry Building. The James Clerk Maxwell Building (JCMB) is on the south of the campus. The approximate location of the sites is shown with a cross.

site	gravity (μgal)	se (μgal)
Grant Institute (GI)	000.0	3.0
BGS	-534.8	2.7
Car Park	-1085.5	2.9
JCMB	-804.5	3.4

Table 5.27 Relative gravity values at King's Buildings absolute sites and ex-centres.

The relative gravity site GI is about 1 metre north of the absolute site GI. The gravity difference was measured as part of the vertical gradient observations and found to be $GI_{abs} - GI_{rel} = 1.6 \pm 0.6$ μgal. The vertical gradient data and analysis are given in Tables 5.5 and 5.7.

5.5.3 The JILA4 Observation

JILA4 occupied the BGS site in Edinburgh on 18 - 20 December 1989. 24 sets of 250 drops were observed, with 2 hours between sets. The red and blue modes of the laser were used on alternate sets. The initial results were sent to Edinburgh University via Capt. Thurgate of the MOD (*pers. comm.* 25 May 1990). The value given was corrected for the elastic tide, ocean load, local atmosphere, polar motion, laser drift and laser temperature. The vertical gradient value was not available at the time of the absolute observations so the value of absolute gravity is referred to the 'operating height' of 82.62 cm. One set was rejected (set 14) 'due to its large anomaly' and a value of 981 578 805.2 s.d 3.4 μgal is given for 826.2 mm above the floor at BGS (*pers. comm.* I. Thurgate 25 May 1990). The author suspects that the value of 826.2 mm is calculated using some rule of thumb for the 'effective measurement height' (section 4.3.3), which would make it a somewhat unreliable datum.

The Edinburgh JILA4 occupation is mentioned in Klopping *et al.* (1991) with reference to the 'system response correction' (section 5.3.2), and the reprocessed observations were supplied to the author by Klopping (*pers. comm.* 4 Nov 1994). These new results were corrected as listed above (apart from laser drift) and also for the 'system response correction' and vertical gradient using 301.0 ± 3.0 μgal m^{-1} to give a weighted mean of 24 sets of 981 578 752.7 se 2.0 μgal corrected to 1 meter. An 'occupation RMS error' which is the combination of the uncertainties from known error sources is shown in Table 5.28 amounts to 3.4 μgal.

ERROR SOURCES	μgal
instrument error budget	3.0
environmental models	1.5
vertical transfer	0.3
occupation RMS error	**3.4**

Table 5.28 Error sources for JILA4 data, after Klopping (*pers. comm.* 4 Nov 1994))

Klopping (*ibid.*) however recommends an additional correction of 5 μgal due to an error in the 'center of mass computation' of the dropped corner cube. He also describes laser mode errors of 3.65 μgal which is combined with the occuption rms error to give 'a more reasonable uncertainty of 5.0 μgal'. These additional corrections result in the value **981 578 757.7 ± 5.0** μgal quoted at 1 metre over the marker in BGS. The static tide (-36.9 μgal at BGS) has been included in the tidal correction, so is removed from the data.

5.5.4 FG5-103 at BGS and GI in December 1992

FG5-103 observed at the Edinburgh BGS and GI sites between 3 and 21 December 1992. This was its first excursion into the field after 'bedding down' tests at the Proudman Oceanographic Laboratory (POL). Both FG5-101 and -102 had been in operation in Boulder for some months, but only in the hands of 'experts' who had either helped build it and/or had experience with the previous generation (JILA) instruments. FG5 was designed and is sold for field use, but a transatlantic flight and a few months in the hands of capable but inexperienced users was the first real test of its ruggedness. The principle aim of the Edinburgh visit was to perform 're-occupation tests' to check that the instrument could be moved between sites and would give the same value of gravity on its return. The early Edinburgh runs were plagued by printer paper jams which caused the computer to hang up, resulting in short datasets (5 or 10 sets of 200 drops instead of 24 sets). The sphere position of the super spring (section 4.2.2) showed unexpectedly large drifts, and the whole instrument appeared to be sliding down the sloping floor in BGS. With frequent attention, 17 datasets were obtained over 14 days, of which 12 were taken during 2 occupations at BGS. A disconcerting buzzing noise from the lifting motor was first noticed on 8 December, which was later interpreted as slippage of the drive belt. The Edinburgh occupation came to an abrupt end rather sooner than anticipated when the drive belt finally snapped on 22 December. In spite of these incidents, the 're-occupation' test was fairly successful, with

end date	dataset	N (sets)	g (μgal) - 981570000	s.d μgal
03.12.92	GI14002	24	9 251.6	6.0
04.12.92	GI14003	18	9 246.9	8.8
Mean of GI occupation #1			**981 579 249.3**	**5.3**
12.12.92	GI0020	20	9 249.8	5.0
13.12.92	GI0021	20	9 249.7	3.8
14.12.92	GI0022	8	9 247.3	3.8
15.12.92	GI0023	12	9 251.3	8.9
Mean of GI occupation #2			**981 579 249.5**	**2.9**
Mean of both GI occupations (at 'measurement height')			**981 579 249.4**	**3.0**
Difference between occupations (#2 minus #1)			0.2	6.0

Table 5.29a GI original values at measurement height, corrected for elastic tide and atmospheric pressure only.

end date	dataset	N (sets)	g (μgal) - 981570000	s.d μgal
07.12.92	BGS006	5	8 706.6	5.4
08.12.92	BGS007	15	8 703.7	5.5
08.12.92	BGS008	5	8 704.1	4.9
09.12.92	BGS009	10	8 704.7	3.5
09.12.92	BGS010	10	8 703.1	4.3
10.12.92	BGS011	5	8 701.5	6.9
10.12.92	BGS012	5	8 702.4	5.1
Mean of BGS occupation #1			**981 578 703.7**	**2.0**
18.12.92	BGS020	20	8 697.9*	8.6
18.12.92	BGS021	12	8 703.5	6.8
19.12.92	BGS022	5	8 698.2	4.8
20.12.92	BGS023	15	8 698.3	6.0
21.12.92	BGS024	20	8 694.8	6.1
Mean of BGS occupation #2			**981 578 698.6**	**2.9**
Mean of both BGS occupations (at 'measurement height')			**981 578 701.2**	**1.8**
Difference between occupations (#2 minus #1)			5.1	3.5

Table 5.29b BGS original values at the measurement height, corrected for elastic tide and atmospheric pressure only.

* value corrected at -0.42 μgal $mbar^{-1}$ (others at -0.3 μgal $mbar^{-1}$)

the two occupations of BGS differing by 5.1 ± 3.5 μgal (later occupation lower) and the occupations of GI by 0.2 ± 6.0 μgal. Table 5.29 shows the dates of the observations and initial values corrected only for the elastic tide and atmospheric pressure. The drive belt snapped at the beginning of the third sequence at GI (so no values were obtained).

Processing the data

Both .grv and .ddt files were saved during the Edinburgh occupation, but, due to problems with recovering data from the backup tapes, only two of the .ddt files (BGS011 and GI14003) were able to be reprocessed in the usual way with the program DDT (section 4.4). All the other datasets in Table 5.29 were processed using .grv files with a program MEAN4W (a predecessor of the program MEAN described in section 4.4.10) which was designed to make pressure corrections, modify tidal corrections, perform a 3σ filter and calculate set means.

Atmospheric pressure correction

In 1992, FG5-103 was not equipped with environmental sensors, so the corrections for atmospheric pressure were calculated from the barograph recorded by the Meteorology Department at KB, which was digitised for the purpose. The occupation coincided with extreme variations of the local atmospheric pressure (from 967 to 1045 mb), so it was particularly important to make this correction. The digitised pressure file has values every 30 minutes, which are interpolated by the program MEAN4W to provide a value at the time of each drop (drops occur every 10 seconds). MEAN4W calculates the standard pressure for the elevation of the site, and corrects the observed gravity for the difference between the observed pressure and the standard pressure at -0.3 μgal $mbar^{-1}$.

Tidal correction

The tidal correction calculated by the FG5 online software (OLIVIA version 1) is replaced by values from the subroutine TIDAL (section 3.2.2). The static tide is included in the calculation of the tidal correction, so that its effect is removed from the gravity values. No ocean loading correction was made to the 1992 values.

The mean of the gravity values corrected for the tide and atmospheric pressure was calculated, and any values greater than 3σ from the current mean were rejected. The mean of each set (250 drops) was calculated and the overall weighted mean of the run (a 'run' is a

group of between 5 and 20 consecutive sets) are the values shown in Table 5.29. We can now calculate a single mean value for each site appropriate to the measurement height, since the remaining corrections (vertical gradient, speed of light, polar motion) are identical for all the values at the same site.

Vertical gradient and datum height corrections

The vertical gradient correction enables the observed value of gravity to be assigned to a specific height above the ground, and the datum correction allows this value to be transferred to other heights (for comparison between instruments) such as floor level. These corrections are described fully in section 5.2, and the values of the vertical gradient over the drop and the datum correction to 120 mm are given in Tables 5.7 and 5.8 respectively. The value of the correction depends on the vertical gradient and the total length of the drop and it can only be calculated accurately if the original distance-time data (.ddt file) is available. (section 4.3.3). The .ddt files for BGS011 and GI14003 were processed using the program called DDT (section 4.4) which enabled the corrections to be evaluated for both sites.

Other corrections

The correction for the finite speed of light (section 4.4.5) varies only with the drop length, and the value for a drop counting 90 fringes (section 4.2.5) is -9.9 μgal. The polar motion correction (section 4.4.8) for Edinburgh on 14.12.92 was -3.73 μgal. The drop length correction (section 5.3.1) from 90 fringes to 150 fringes for comparison with later FG5-103 values is -23 ± 7 μgal. The occupation means for GI and BGS and the corrections are given in Table 5.30. The values of the Table 5.29, after correcting as shown in Table 5.30, are plotted in Figure 5.25.

GI	μgal	s.e (μgal)
g at measurement height inc. tidal and atmospheric corrections	981 579 249.4	3.0
vertical gradient correction (at 302.8 ± 3.6 μgal m^{-1})	-16.6	†0.2
speed of light (90 fringes)	-9.9	
polar motion	-3.7	
drop length correction	-23	7
corrected g at 1309 mm	**981 579 196.2**	**7.6**

BGS	μgal	s.e (μgal)
g at measurement height inc. tidal and atmospheric corrections	981 578 701.2	1.8
vertical gradient correction (at 333.2 ± 39.1 μgal m^{-1})	-18.3	†2.2
speed of light (90 fringes)	-9.9	
polar motion	-3.7	
drop length correction	-23	7
corrected g at 1309 mm	**981 578 646.3**	**7.6**

Table 5.30 Mean values at Edinburgh GI and BGS from FG5-103 in 1992, showing the corrections which were added to the occupation means.
† see note on error below

† *Estimating the error on the vertical gradient correction*
The actual value of the effective measurement height (section 4.3.3) is not known to better than 2 cm. Making the vertical gradient correction (VGC), means including the vertical gradient terms in the equation of motion. This does not change the error on the mean gravity because that is an estimate of the scatter of the results. However, the uncertainty in the observed or fitted gradient (section 5.2) must contribute in some way to the uncertainty in the gravity estimate (which is now at a precise height, but has a bigger error). The error on the VGC is an estimate based on a simple hypothesis that the VGC is linear in the vertical gradient. For the GI data in Table 5.30 above, a correction of 300 μgal has an error of about 4 μgal, so for a correction of 17 μgal the error is 0.2 μgal. The corresponding estimate for BGS is made similarly.

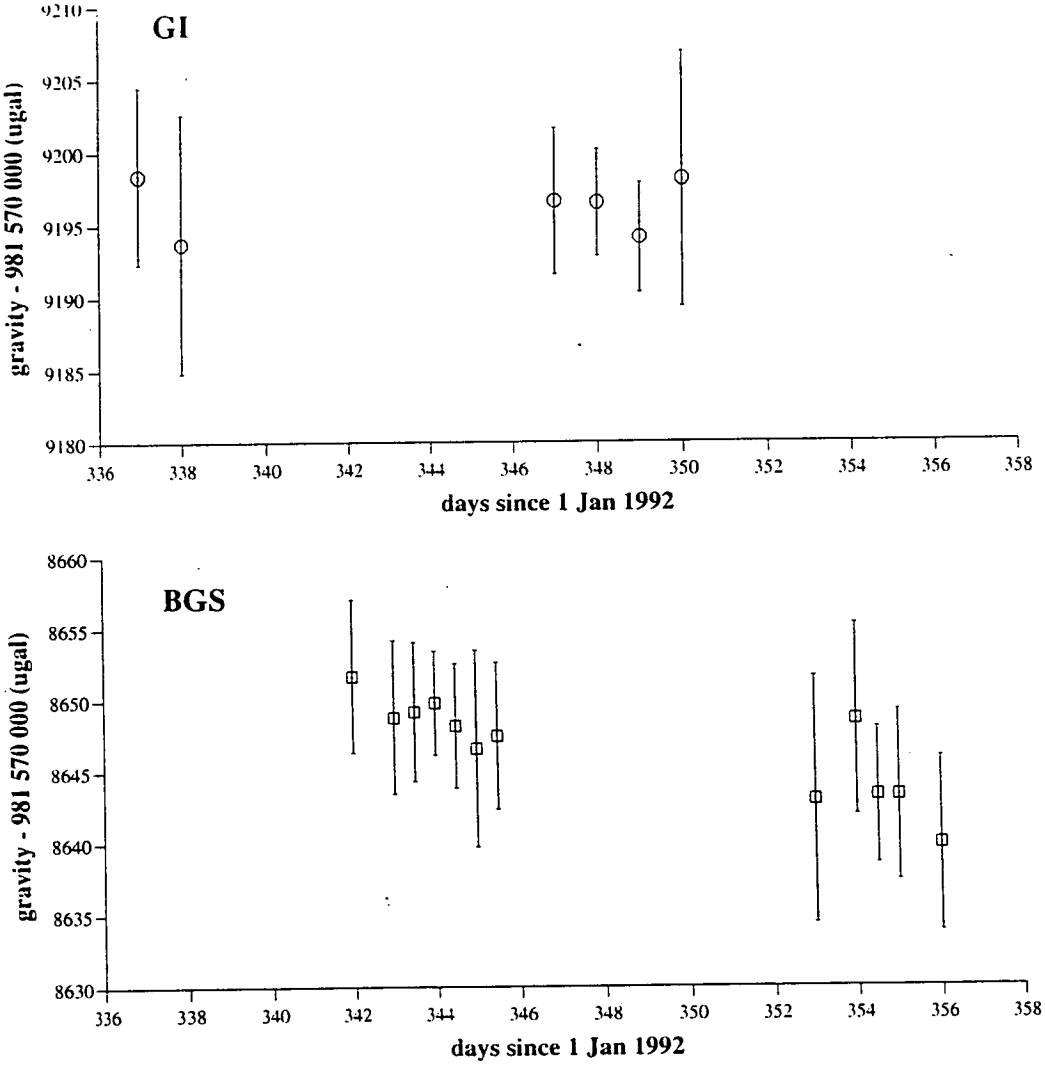

Figure 5.25 Edinburgh 1992 values at GI (top figure) and BGS (lower figure) showing 'reoccupation tests'. The BGS values show a decreasing trend (particularly during the second occupation), which could have been caused by the instrument sliding down the sloping floor, or by slippage of the lift motor (see text).

5.5.5 FG5-103 at GI in July 1994

FG5-103 repeated observations at Edinburgh GI in July 1994. The instrument was now significantly improved compared to its 1992 condition, with some new hardware and upgraded software. The hardware and software differences in the FG5-103 system between the 1992 and 1994 occupations of GI are described below:

i) New Laser : A Newport polarisation stabilised He-Ne was used in 1992 and a Winters Iodine stabilised He-Ne in 1994. The iodine stabilised lasers are generally much superior for absolute gravity measurements particularly as they have a stable wavelength (section 4.2.4).
ii) Increased Fringe Count : In 1992, FG5-103 fitted only 90 fringes to a parabola for the estimate of gravity, rather than 150 which has been the norm since the first upgrade (i.e all observations after February 1993). In theory the estimate of gravity should not depend on the length of the drop, provided that the estimate is referred to the same height above the ground, but section 5.3 shows that this is not the case for FG5. In addition, the data from the beginning and end of the drop are more susceptible to error (especially for FG5-103), so a longer drop would increase the proportion of 'good' data, and this may be one of the reasons for the discrepancy between 1992 and 1994 FG5-103 observations.
iii) Environmental Sensors : Pressure, temperature, humidity and the position of the 'super-spring zero' (section 4.2.2) are now monitored automatically. The atmospheric pressure correction is also made on-line.
iv) Software : The online processing software (OLIVIA) was at version 1.0 in 1992 and version 3.1 in 1994. Most of the absolute gravity values given in this thesis have been derived by processing which is largely independent of the Axis programs OLIVIA and REPLAY, but the main differences between versions 1.0 and 3.1 of OLIVIA have been described in section 4.4.

The occupation took place between 17 and 20 July 1994 and two runs were completed, each with 24 sets of 200 drops per set. All the data was processed using the program DDT. The results from the two sets EDI1907A and EDI2007A are given in Table 5.31 and include corrections for the vertical gradient, speed of light, laser modulation, elastic tide (the static tide is removed from the gravity estimate), ocean loading, and atmospheric pressure. The polar motion correction has been calculated separately and has the value -2.0 for 19.07.94 at Edinburgh. The corrected mean at 120 mm is used as the representative value for Edinburgh in the adjustment of the British Precise Gravity Network in Chapter 6.

Dataset	γ (drop) (μgal m^{-1})	value at top (1309 mm) μgal
EDI1907A	302.3 ± 3.6	981 579 187.3 ± 1.1
EDI2007A	302.3 ± 3.6	981 579 186.9 ± 0.7
Mean at 1309 mm		981 **579 187.1 ± 0.7**
correction to 120 mm		+352.3 ± 0.3
system response correction		+5.4 ± 2.2
corrected mean at 120 mm		981 **579 544.8 ± 2.3**

Table 5.31 Corrected mean values for the 1994 occupation of Edinburgh GI by FG5-103.

5.5.6 Comparison of Absolute values at Edinburgh

The comparison of FG5-103 with JILA4 is made using the 1994 FG5 values, because the data obtained in 1992 is much less reliable for the reasons discussed in section 5.5.4 above. Further evidence for the relatively poor quality of 1992 data comes from the review of FG5-103 absolute values obtained at POL between August 1992 and June 1994 in section 5.4. The 1994 observations were made at Edinburgh GI, so they are transferred to the site of the JILA4 occupation at Edinburgh BGS using the relative gravity data discussed in section 5.5.2. The FG5 1992 value at BGS is compared with the 1994 value transferred from GI, and the 1992 and 1994 FG5 values at GI are compared.

The transfer from GI at 1309 mm to BGS at 1309 mm uses the datum corrections in Table 5.8, and the ex-centre observations from Table 5.27. The transfer of the JILA4 value from 1000 mm to 1309 mm at BGS is calculated as described in section 5.2.5 (the estimate of the error assumes that it is linear in the size of the correction). These values are summarised in Table 5.32 below.

	μgal (s.e)
DC from 1309 to 120 mm at GI	352.3 (0.3)
Transfer from 120 mm at GI to 120 mm at BGS	-534.1 (4.9)
DC from 120 mm to 1309 mm at BGS	-346.1 (2.8)
Total transfer from 1309 mm GI to 1309 mm BGS	**-527.9 (5.7)**
DC from 1000 mm to 1309 mm at BGS	-101.0 (4.4)

Table 5.32 The datum corrections (DC) are from Table5.8 and the transfer from GI to BGS from Table 5.27.

Comparison 1. FG5 94 observation at GI with JILA4 89 observation at BGS

The mean of the JILA4 1989 observations at BGS, as supplied by Klopping (*pers.comm.* 4 Nov 1994) from section 5.5.3 is corrected to 1309 mm for comparison with the FG5-103 1994 observation transferred from GI.

	gravity (μgal)	DC (μgal)	g at BGS 1309mm (μgal)
JILA4 at BGS 1000 mm	981 578 757.7 (5.0)	-101.0 (4.4)	981 578 656.7 (6.7)
FG5 (94) at 1309 mm GI	981 579 187.1 (0.7)	-527.9 (5.7)	981 578 659.2 (5.7)
JILA4 minus FG5 (94)			**-2.5 (8.8)**

Table 5.33 FG5-103 and JILA4 observations and the datum correction (DC) to BGS 1309 mm for comparison. (The standard errors are given in brackets).

JILA4 89 is lower than FG5 94 by 2.5 ± 8.8 μgal when compared at 1309 mm at BGS. Table 5.33 shows that in 1994, FG5-103 gave values consistent with JILA4 in 1989, which corresponds with the statement by Klopping (*pers. comm.* 4 Nov 1994) that JILA4 'currently shows excellent agreement with FG5 systems'. The transfer by relative observations has been made with adequate precision and accuracy for a good comparison of absolute instruments which observed at different sites.

Data from JILA4 and six FG5 instruments (including 103) at the Table Mountain Gravity Observatory (Carter *et al.* 1994) and Klopping (*ibid.*) dispute the existence of a systematic offset between JILA4 and FG5 systems. However, Klopping suggests that the results from the 1994 BIPM intercomparison (section 5.1), at which there were five FG5s and four JILAs, show a 10 to 15 μgal offset between the two types (JILA type lower). The results of this intercomparison are in press (Metrologia 1995 Special Issue on Gravimetry).

Comparison 2. FG5 92 observation in BGS with FG5 94 observation in GI

The corrected observation made at BGS in 1992 with FG5 (Table 5.30) is compared with the 1994 FG5 observation transferred from GI (Table 5.33) in Table 5.34 below.

	gravity in μgal (s.e)
FG5 (94) tranferred to at 1309 mm BGS	981 578 659.2(5.7)
FG5 (92) at 1309 mm BGS	981 578 646.3(7.6)
FG5 GI (94) minus FG5 BGS (92)	**+12.9(9.5)**

Table 5.34 FG5 1992 observation at BGS compared with FG5 1994 observation transferred from GI.

Comparison 3. FG5-103 at GI in 1992 and 1994

The 1994 value (without the system response correction) from Table 5.31 is compared with the corrected 1992 value from Table 5.30, at the top of the drop (1309 mm), in Table 5.35.

	gravity in μgal (s.e)
FG5 (94) at 1309 mm GI	981 579 187.1 (0.7)
FG5 (92) at 1309 mm GI	981 579 196.2 (7.6)
FG5 GI (94) minus FG5 GI (92)	**-9.1 (7.6)**

Table 5.35 Comparison of 1992 and 1994 FG5 values at 1309 mm at GI.

Comparisons 2 and 3 show that FG5 92 at BGS is lower than FG5 94 by 12.9 ± 9.5 μgal when compared at 1309mm at BGS, and that FG5 92 GI is higher than FG5 94 by 9.1 ± 7.6 μgal when compared at 1309 mm at GI. The large number of changes in the hardware and software of FG5-103 between 1992 and 1994 were described in section 5.5.5. Some of these changes, for example the different drop length, have been corrected for, but the results of the comparsion show that some discrepancies remain. Given the difficulties of the 1992 occupations at BGS (section 5.5.4) and the large number of corrections applied by means less automated and less precise than those to the 1994 values, the comparison is still, however, remarkably successful.

5.5.7 Summary and discussion of gravity observations at Edinburgh

1) JILA4 89 is lower than FG5 94 by 2.5 ± 8.8 μgal when compared at 1309 mm at BGS.
2) FG5 92 BGS is lower than FG5 94 by 12.9 ± 9.5 μgal when compared at 1309mm BGS.
3) FG5 92 GI is higher than FG5 94 by 9.1 ± 7.6 μgal when compared at 1309 mm at GI.

Although there are undoubtable arguments for preferring the accuracy of the absolute values given by FG5-103 in 1994, the 're-occupation' tests of 1992 *should* give an adequate estimate of the gravity *difference* between the sites. Comparisons 2 and 3 show that there is an inconsistency of 22 μgal in the difference in gravity between the 1309 mm datum at BGS and GI, as measured by relative observations and by the 1992 're-occupation' tests with FG5-103. Although the 're-occupation' tests (section 5.5.4) were successful in that the same value of gravity was observed on returning to each site after a few days at another, there must be systematic effects having different consequences for the measurement of gravity at GI and BGS.

The success of the FG5 (1994) and JILA (1989) comparison shows that the transfer by relative observations of 527.9 ± 5.7 μgal has been made with adequate precision and accuracy for a good comparison of absolute instruments which observed at different sites. Transfers of similar magnitude are a vital part of the international comparisons discussed in section 5.1. Boulanger *et al.* (1991) make a comparison of the differences between sites at the BIPM measured by relative and absolute instruments, and show that for JILA observations, the methods give generally consistent results. There is a 'chicken and egg' problem with this sort of comparison, because absolute gravimetrists would rather not rely on the apparantly crude relative observations to test their instruments. Relative gravimetrists, for their part, are reluctant to place too much credibility on the thousands of numbers which come out of absolute gravimeters with apparantly little effort and discomfort to the observer, but may be wrong by tens of microgals because of an overlooked systematic error. Both methods are essential, and improvements in one must encourage corresponding development in the other.

5.6 National Physical Laboratory (NPL) - Teddington

5.6.1 Historical

The British National Gravity Base was for many years housed at the Royal Greenwich Observatory (RGO). Pendulum observations by Putnam in 1900 and Miller in 1928 transferred the Potsdam value to Greenwich (Coron & Monnet 1959). Bullard and Jolly made a connection in about 1935, from the RGO to the National Physical Laboratory (NPL) in Teddington. The first independent absolute determination at NPL was made by Clark (1939) with a reversible pendulum in Room 11 of the Metrology Department (now called Building 3). The RGO was transferred from Greenwich to Herstmonceux in about 1950 and the site of Clark's determination at NPL was adopted as the British Fundamental Gravity Station (Anon 1954). Cook (1967) made new absolute determination of gravity with his rise and fall instrument in 'a basement room (15) of Bushy House, one of the buildings of the NPL' (Cook 1967). The free-fall Hammond-Faller instrument observed at NPL and Hammond & Faller (1971) gives a value at 'Room B-17, Bushy House (BH)'. The only subsequent absolute observation at NPL prior to the 1993 FG5 series was made with the tranportable rise-and-fall 'Istituto di Metrologia "G. Colonnetti" ' (IMGC) instrument (Cannizzo *et al.* 1978).

5.6.2 Relative Gravity Observations made by Edinburgh University at NPL

Introduction

Due to the impending destruction of Building 3 which housed the British Fundamental Gravity Station at Clark's pillar, Edinburgh University made relative gravity observations with primary objective of transferring this important datum to a new fundamental site (BFGS93) in Bushy House. Other objectives of the survey were i) to redetermine the vertical gradient at Teddington A before the site was destroyed, ii) to measure the vertical gradient at the two new sites in Room 16 of Bushy House in preparation for the FG5 observations iii) to provide security out stations (ex-centres) for the new fundamental site and iv) to connect it to the nearby British Precise Gravity Network 1993 site at Hampton Church. The observations were made with the LCR meters G275 and D145 during 19 - 21 January 1993.

Sites

The BFGS93 is monumented by a square stainless steel plate fixed directly to the concrete floor of Room 16 in Bushy House. The current 'Room 16' is at ground level, *not* in the basement described by Cook (1967). It appears from the site diagrams shown in Figure 5.26 (from Cook 1967) and Figure 5.27 that the new BFGS93 is one floor above and within 10 metres horizontally of Cook's laboratory (basement room (15) of Bushy House). The complete outline of Bushy House is shown in Figure 5.28, which helps to orient the two previous diagrams. BFGS93 is the site referred to here as NPL1, and NPL2 is 1.3 metres along the centre line of the room from NPL1 in a westerly direction. During the simultaneous occupation by FG5 absolute gravity meters in July 1993, FG5-105 observed at NPL1 and FG5-103 at NPL2.

Four out-stations were established to provide insurance against damage to or destruction of the new BFGS93 and to connect it to the British Precise Gravity Network 1993. The sites were i) at the 40mm Ordnance Survey marker on the north side of the entrance hall to Bushy House (Site C in Figure 5.28), ii) at the 300mm square stainless steel marker plate next to the smallest force balance in Building 17 (Site A in Figure 5.28) iii) at the 300mm square stainless steel marker plate on the south side of the porch of Building 31 (Site D in Figure 5.28) and iv) at the centre of the door step of the north door of Hampton Parish Church, which is a British Precise Gravity Network site. Site A at the force balance was primarily designed to transfer a precise value of gravity for metrological purposes and is unsuitable for external connections. Site D at Building 31 is particularly convenient for external connections but the doorstep on which it is located is loose which makes it unusuable when people are entering or leaving the building. Site C in Bushy House is as quiet and stable as NPL1 (the BFGS93), and readily accessible.

The level of vibration and microseismic noise at the former British Fundamental Station in Building 3 (Teddington A) was found to be particularly high and unusually irregular. This noise so disrupted a vertical gradient measurement sequence with D145 that it had to be abandoned until after working hours. Previously there have been many comments about the level of noise at this site. Coron & Monnet (1959) mention disturbance 'due to nearby building work and heavy machinery', an observation which Anon (1954) attributes to both Clark and Cook, who measured gravity there in 1939 and 1965 respectively. The IMGC measured at seventeen European sites during 1976 and 1977 and Cannizzo *et al.* (1978) reports very high microseismic noise at only Teddington and Naples. The new BFGS93 is much less prone to high frequency irregular noise than Teddington A.

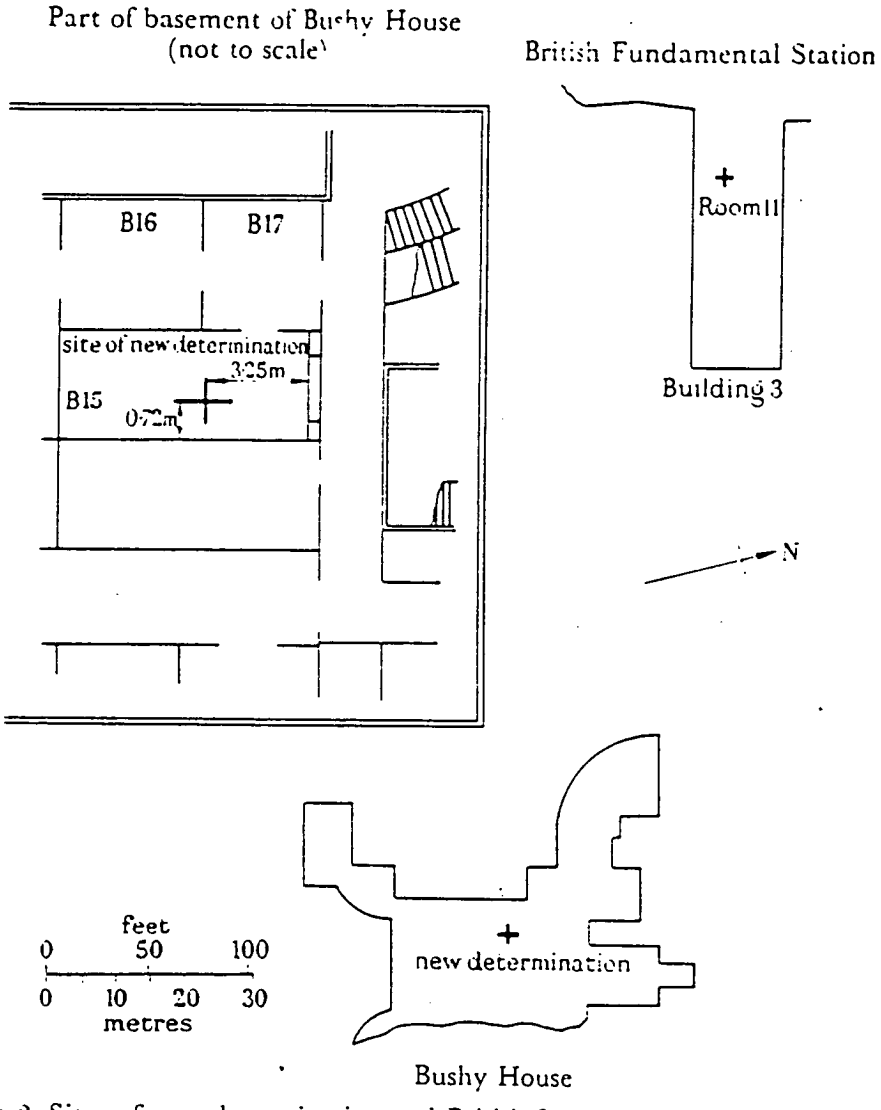

FIGURE 2. Sites of new determination and British fundamental gravity station.

Figure 5.26 Figure 2 of Cook (1967), showing the basement room B15 in Bushy House at the National Physical Laboratory, and the relative location of Teddington A within Building 3. See also Figure 5.28.

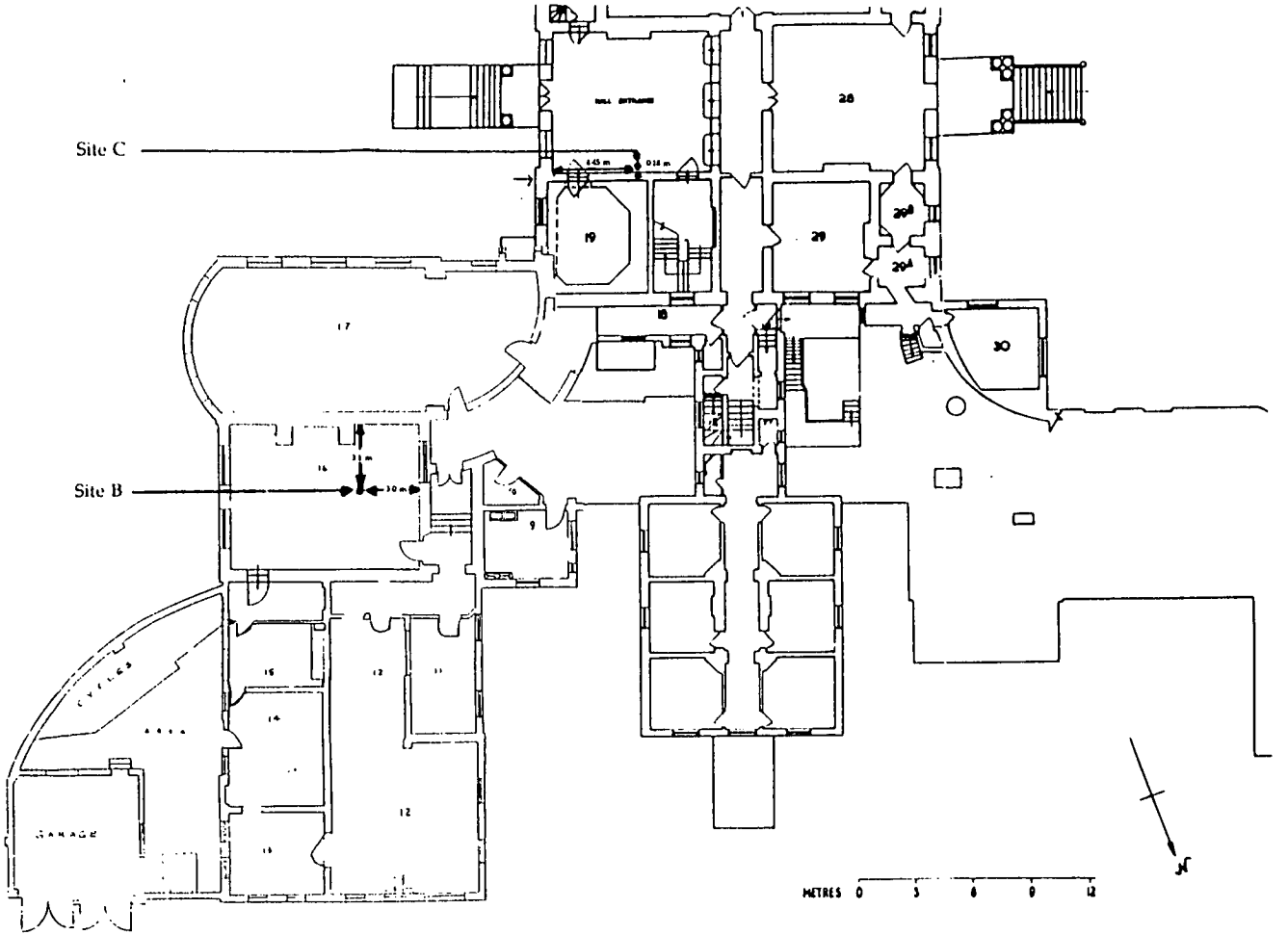

Figure 5.27 Plan of Bushy House (Building 1 at NPL), showing the BFGS93 (NPL1) (Site B) and the entrance hall ex-centre (Site C).

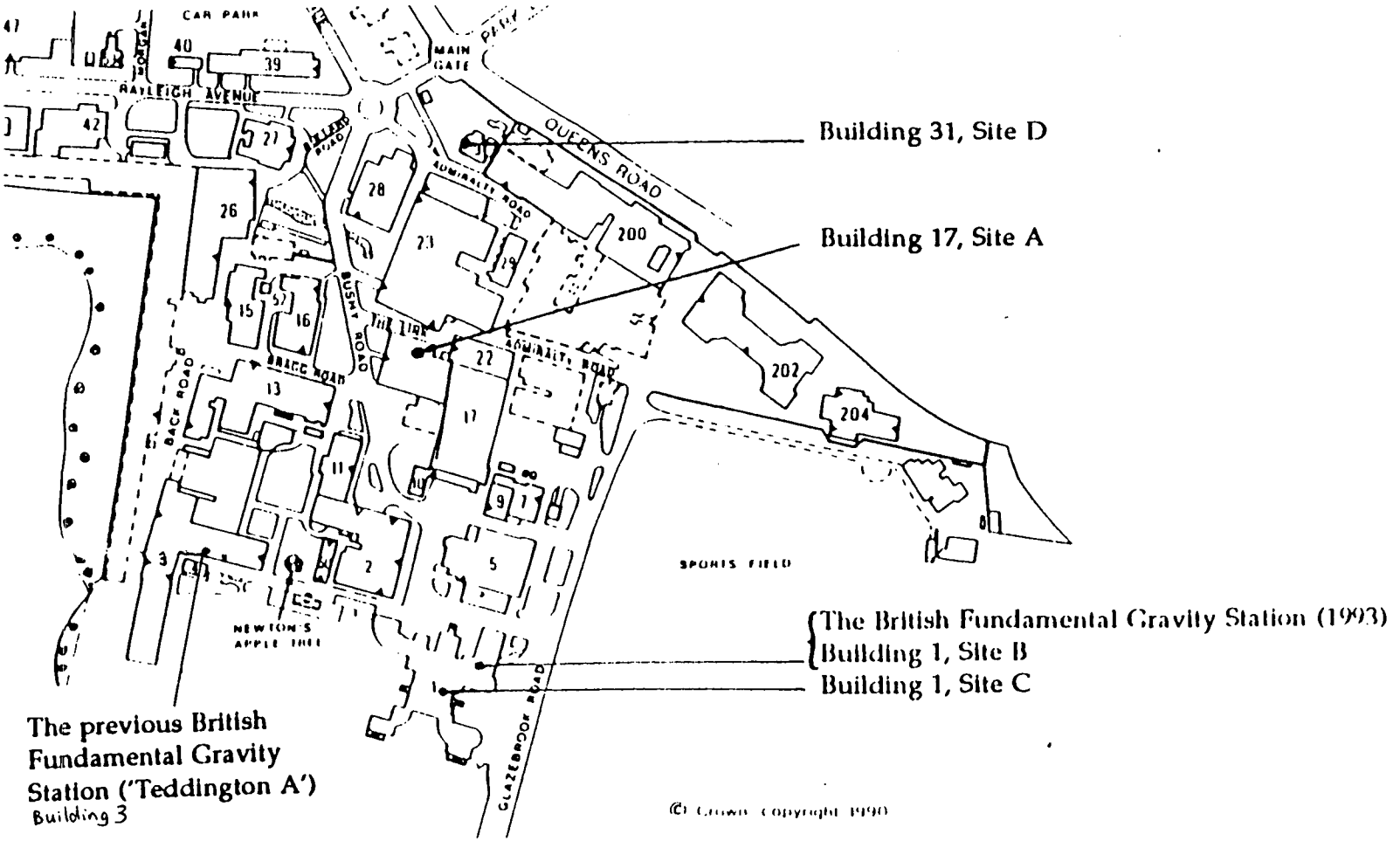

Figure 5.28 Plan of the NPL site showing the ex-centres at Building 31 (Site D), the force balance in Building 17 (Site A), the Bushy House (Building 1) entrance hall (Site C) and the British Fundamental Gravity Station (1993) at Site B (NPL1). The location of Teddington A (in Building 3) is also shown.

Observations

Repeated observations were made with both gravity meters on identical base plates on Clark's pillar at Teddington A and the floor at BFGS93. The pillar at Teddington A is a 2m concrete block set into the floor and isolated from it. Its upper surface is about 1.8 m by 0.9 m in size and level with the surrounding floor. Each site was occupied four times with each gravity meter and typically two independent readings were observed during each occupation. The difference (Teddington A minus BFGS93) is +83.8 ± 1.7 μgal (BFGS93 has a lower g) (Table 5.36).

The connection from NPL1 to Site C in the Entrance Hall of Bushy House was made with four occupations at each site with both meters. The Force Balance (Site A) and Building 31 (Site D) were connected to NPL1 via three loops around these sites with both meters. Table 5.36 shows the results of the network adjustment of the ex-centres observations.

Site	μgal	s.e
BFGS93 (NPL1) (Site B)	000.0	1.1
'Teddington A'	83.8	1.3
Entrance Hall BH (Site C)	-575.1	1.6
Force Balance (Site A)	358.0	1.9
Building 31 (Site D)	261.4	1.7

Table 5.36 Gravity difference and s.e (μgal) between BFGS93 and the ex-centres at National Physical Laboratory.

The tie to the British Precise Gravity Network (BPGN) was made with four occupations at NPL1 alternating with three at Hampton Parish Church. The observations were included in the BPGN adjustment (section 6.5). Gravity at Hampton Church is 1587.5 ± 8.0 μgal lower than at NPL1.

Vertical gradient observations and analysis were given in Tables 5.5 and 5.7, and in section 5.2. The measurement of the gradient at NPL2 was combined with the measurement of the difference between NPL1 and NPL2 in a sequence which consisted of three repeated loops with both meters around the sites NPL1 (floor), NPL2 (tripod) and NPL2 (floor). The link between the two sites was adjusted along with the other vertical gradient observations, and the difference between NPL1 and NPL2 was found to be 0.6 ± 4.5 μgal (Table 5.5). The gradients at NPL1, NPL2 and Teddington A were measured at only one tripod height rather than two or three different heights as for sites elsewhere in Britain. The very similar vertical gradients found at all three NPL sites (Table 5.7) suggest that it is linear.

5.6.3 FG5 Observations at NPL

On 2-3 July 1993, two FG5 absolute gravity meters, FG5-103 (NERC) and FG5-105 (NPL) observed simultaneously at sites NPL1 and NPL2. Both instruments observed two 24-hour sets and the results are summarised in Table 5.37.

FG5-103 at NPL2	gravity (μgal)
NPL0207	981 181 340.8 ± 3.3
NPL0307A	981 181 344.1 ± 2.2
Weighted mean at 1312 mm	981 181 343.1 ± 1.5
Datum correction to 120 mm	352.2 ± 5.0
Weighted mean at 120 mm	981 181 **695.3 ± 5.2**
FG5-105 at NPL1	
N020793D	981 181 355.5 ± 4.4
N030793C	981 181 349.2 ± 2.7
Weighted mean at 1313 mm	981 181 350.9 ± 2.8
Datum correction to 120 mm	355.5 ± 4.8
Weighted mean at 120 mm	981 181 706.4 ± 5.6
*Drop length correction from 130 to 150 fringes for FG5-105	-3.2 ± 2.4
Weighted mean (including drop length correction) at 120 mm	981 181 **703.2 ± 6.1**
Weighted mean of FG5-103 and FG5-105 values at 120 mm	981 181 698.6 ± 3.9
Polar motion correction	+1.14
Weighted mean including polar motion correction	981 181 699.7 ± 3.9
†System response correction	+10.8 ± 6.3
Weighted mean for NPL including system response correction	**981 181 710.5 ± 7.4**

Table 5.37 Values of the 24-set means (NPL0207 etc) for FG5-103 and FG5-105 on 02 and 03.07.93. The vertical gradients are given in Table 5.5, and the datum corrections in Table 5.8.

* The drop length correction is described in section 5.3.1

† The system response correction is described in section 5.3.5.

The 24-set means for NPL0207, NPL0307A, N020793D and N030793C given in Table 5.37 have been obtained using a full equation of motion which includes vertical gradient terms so the solution is for the top of the drop. They include the speed of light correction, made using retarded times, and the atmospheric pressure correction using the pressure observations made by the FG5-103 sensor. The elastic tide was calculated using the subroutine TIDAL (section 3.2.2). The static tide is one of the harmonic terms included in the tidal calculation so it has been removed from the data. An ocean load correction was applied using the routine described in section 3.1.4. The same vertical gradient was used in the equation of motion as for the datum correction (section 5.2).

The difference in gravity between NPL1 and NPL2 at 120 mm above the floor as measured by the relative meters is 0.6 ± 4.5 μgal. This result indicates no significant difference between the sites at the level of precision of the relative measurements. The difference between the weighted means of the FG5-103 and FG5-105 results at 120 mm is 7.9 ± 8.0 μgal which again is not significant, but the standard error is much larger than the specified accuracy of 2 μgal for FG5. Some of the 8 μgal arises from the error on the various corrections, but it does, however, represent the precision with which absolute measurements can be transferred by relative instruments. The weighted mean of the corrected values at 120 mm is 981 181 710.5 ± 7.4 μgal, and is taken as the representative absolute value at NPL.

Transfer to Teddington A

This value transferred to the same height above the floor at Teddington A, using the gravity difference from the relative observations of 83.8 ± 1.7 μgal (Teddington A is higher), gives a value of 981 181 794.3 ± 7.6 μgal for FG5 observations at 120 mm above the floor at Teddington A. Using the vertical gradient of 297.2 ± 2.4 μgal m^{-1} (Table 5.7) gives a correction of 35.7 ± 0.3 μgal from 120 mm to the floor. The value of the FG5 observations made at NPL1 transferred to floor level at Teddington A is therefore 981 181 830.0 ± 7.6 μgal, where the formal standard error (7.6 μgal) is probably an underestimate of the real error incurred by the combination of vertical gradient and ex-centre relative gravity results, and the estimates of the drop length and system response corrections for FG5 data. The optimum transfer of the FG5 absolute value to Teddington A would be to measure the relative gravity difference between the measurement height (1313 mm) at NPL1 to 120 mm at Teddington A directly, rather than via the vertical gradient observations and the difference between the sites at 120 mm. Given that the Cook and Hammond-Faller observations have also been transferred from Bushy House (using a

value of 0.07 s.d 0.02 mgal) one cannot now improve on the accuracy of that transfer (especially with the ambiguity of the location of 'Teddington E', see Note†† below).

5.6.4 Comparison of 1939 - 1993 absolute determinations at NPL

Clark (1939) gives a value of 981 181.5 ± 1.6 mgal referred 'specifically to the position occupied by the pendulum apparatus in Room 11 of the Metrology Department' (Teddington A), but gives no information on the precise height of the observation. Anon (1954) gives a plan of Room 11 and the pillar which Clark used and states that the 'mean height of the centre of gravity of Clark's pendulum was 95 cm. above floor-level', so that it would be 'subjected to a mean acceleration of gravity 0.29 mgal. less than at floor level'. (This correction is obtained by using a gradient of approximately 0.305 mgal m^{-1}). Using these estimates, Clark's value transferred to floor level in Room 11 is 981 181.79 ± 1.6 mgal. It is interesting to note that this value is only 0.04 mgal different from the 1993 FG5 value, whereas the value assigned to the datum of the Potsdam Gravity System in 1958 (section 3.4) was later found to be in error by about 14 mgal. Cook (1967) gives a value for Clark's determination 'made in the room containing the British Fundamental Station' and '*reduced to the fundamental station*' of 981 183.2 ± 0.7 mgal, without explanation of the 'reduction'. Cook, however, quotes vertical gradient observations made with a spring balance gravity meter at the site where his own rise-and-fall measurements were made and gives a value for the difference 'Gravity at floor level - gravity at fundamental station' as + 0.07 mgal, s.d 0.02 mgal. Cook's (1967) rise-and-fall values (as revised in Cook & Hammond 1969) are 981 181.88 mgal at the floor of the laboratory in Bushy House, and 981 181.81 mgal at the British Fundamental Station with a standard deviation on each value of 0.13 mgal. [The revision was due to an error in the reduction to the floor level given in Cook (1967), and the original correction of 0.20 mgal was revised to 0.26 mgal.] A plaque on the wall in Room 11 (the Fundamental Station) describes a 'GRAVITY DETERMINATION 1937', and gives a value of 981.183 cm/s^2 at a point 95 cm above floor level, which obviously refers to Clark's observation, but gives Cook's revision of Clark's result.

Note†† The IGSN71 nomenclature for 'Teddington E' is consistent with the Faller-Hammond (1971) paper, but some confusion arises because Cook refers to room 15 of Bushy House, and Figure 2 of Cook (1967) is a plan of the basement showing rooms B15, B16 and B17 which clearly indicates that his observation was in B15 (*not* B17). Hipkin suggests that B17 is wrongly labelled as B15 in the figure (Hipkin & Charles 1993), but the author thinks it unlikely that the same error would be repeated in the text. The main listing of IGSN71 absolute gravity values gives results for 'Teddington A' and outstations J, K, M, N and O, but not for Teddington E.

Hammond and Faller correct their observed free fall value to the 'zero-velocity position' using an equation of motion which includes a measured vertical gradient. Their determination includes a speed of light correction, and Hammond & Faller (1971) gives a value corrected to floor level (using this measured gradient) of 981 181.930 ± 0.042 mgal at Room B-17, Bushy House (BH). An adjusted value at the 'British Fundamental Station, Building 3' is given as 981 181.86 ± 0.05. The difference between these two values is the + 0.07 mgal given in Cook (1967).

The International Gravity Standardisation Net 1971 (IGSN71) (Morelli *et al.* 1974) adjustment included absolute measurements made by only three instruments - those of Cook, Hammond-Faller and Sakuma. Values quoted at 'B.H. Rm B.17 Teddington E' for the Cook and Hammond-Faller observations are given in Table 5.38.

B.H Rm B. 17 Teddington E	Cook, 1967	981 181.82 ± 0.13
B.H Rm B. 17 Teddington E	Cook, Hammond 1969 *(Cook, 1967 Revised)*	981 181.88 ± 0.13
B.H Rm B. 17 Teddington E	Hammond, Faller 1971	981 181.930 ± 0.042

Table 5.38 Values at Teddington E used in the IGSN71, reproduced from page 98 of Morelli *et al.* 1974. The values include the Honkasalo correction, and are corrected to floor level.

The IGSN71 adjusted value for Teddington A is 981 181.78 ± 0.015 mgal. Teddington A is the British Fundamental Gravity Station in Room 11, Building 3.

In 1976, the IMGC rise-and-fall measured at Teddington A, which was by then monumented as IGSN71 Ref. 18110 A. (Cannizzo *et al.* 1978). The IMGC value at the measurement height of 797 mm was 981 181.580 with a standard deviation of 0.026 mgal. This was corrected to floor level using a gradient of 0.300 mgal m^{-1} attributed to a measurement by Sakuma with an LCR G meter. The final IMGC value quoted in Cannizzo *et al.* (1978) includes the addition of + 0.031 mgal for the Honkasalo Correction (which is the value obtained using the explicit formula given in Morelli *et al.* 1974 (section 3.2.4)), and is 981 181.850 ± 0.026 mgal at floor level.

'Making the Honkasalo Correction' means that the static tide is *not* removed from the observations. It is not clear whether the Cook (1967) and Hammond-Faller (1971) observations include the Honkasalo Correction, but since the values corrected to Teddington A by their respective authors are consistent with those for IGSN71 Teddington E values (Table 5.38), it is assumed that they did. The IMGC value in Table 5.39 below includes the Honkasalo Correction made in Cannizzo *et al.* (1978). The FG5 values given throughout this thesis have the static tide removed from the gravity estimate as part of the tidal correction, which means that they do not include the Honkasalo Correction. For this comparison, the FG5 value at NPL has been made consistent with the others in the table by adding 0.031 mgal to the value transferred to Teddington A (section 5.6.3). The absolute values, corrected to floor level at Teddington A by the various authors, are summarised in Table 5.39.

Reference	Transfer by / comments	g (mgal) - 981 000	quoted error	type of error
Clark (1939)	Anon (1954)	181.79	1.6 †	mean residual
Clark (1939)	Cook (1967)	183.2	0.7	
Cook (1967)	from BH Rm 15	181.81	0.13	s.d
Hammond-Faller (1971)	from BH Rm B17	181.86	0.05	estimated error
IGSN71 (Morelli *et al* 1974)	(adjusted value)	181.78	0.015	s.e
IMGC (Cannizzo *et al* 1987)	to floor	181.850	0.026 (s.d)	0.0022 (s.e)
FG5 103 and 105	from BFGS93 BH	181.8610	0.0076	s.e

Table 5.39 Comparison of values transferred to floor level at Teddington A. The gravity values include the Honkasalo Correction.
† see note on 'Error on Clark's result' below

† *Error on Clark's result*
Clark (1939) quotes a 'probable error' of ± 0.34 mgal on the mean of eighteen determinations, having a 'mean residual' of ± 1.6 mgal. He estimates an uncertainty of ± 1.4 mgal due to the corrections required by the pendulum apparatus and suggests that 'the most likely value of g is 981.181$_5$ cm./sec. sq with a possible range of about ± 1.5 mgal.' Given that Clark's value agrees rather better than this with the more recent absolute values, then it may be more appropriate to consider the 'probable error' of ± 0.34 mgal. This is, after all, a statistical error determined from the scatter of the observations, and is therefore comparable with the standard errors quoted for most of the other instruments. Only the Hammond-Faller observation includes an estimate of sytematic instrumental effects in its quoted error.

The values in Table 5.39 are plotted in Figure 5.29. Since Cook's revision of Clark's result is nowhere explained, and seems to create an inconsistency of about 1.4 mgal with all the other determinations, only Clark's original value is included in the plot. In order that the vertical scale allows the more recent determinations to be displayed more clearly, the error bar shown on Clark's value is reduced to about half of the 'probable error' of 0.34 mgal.

5.6.5 Gravity observations at NPL - Conclusions

The imminent destruction of the historical gravity station at Teddington A prompted repeat observations of vertical gradients and ties to excentres.The similarity of the vertical gradients measured at Teddington A, NPL1 and NPL2 suggests that they are also likely to be linear at these sites. A new British Fundamental Gravity Site (BFGS93) has been established at NPL, and two FG5 instruments observed there simultaneously in July 1993.

The difference between the weighted means of the FG5-103 and FG5-105 results at 120 mm at the BFGS93 is just insignificant at 7.9 ± 8.0 µgal, although the individual occupation means at the respective measurement heights at NPL1 and NPL2 suggest that there may be a systematic difference between the instruments. This could be due to deteriorating quality of the ISL1 laser mounted on FG5-103 which lost power completely at the end of the occupation. A drop length correction of -3.2 ± 2.4 µgal has been applied to the gravity estimate of FG5-105 because of its shorter drop length (130 fringes compared to 150 for FG5-103). The system response correction for FG5-103 at NPL2 has been estimated to be $+10.8 \pm 6.3$ µgal, but since this correction has not been determined for FG5-105, it is not included in the comparison of the two instruments.

The 1993 FG5 observations have enabled absolute values made at various sites at NPL since 1939 to be a compared with this high precision determination. The comparison, made at Teddington A, shows a remarkable agreement of 70 µgal between the pendulum observations of Clark (1939) and the FG5 observations, which is more than adequately covered by Clark's error estimate of 1.6 mgal. Figure 5.29 shows that the Cook (1967), Hammond-Faller (1971) and IMGC (1987) determinations agree with the FG5 value within their stated errors, but the value assigned to Teddington A in the IGSN71 adjustment is too low by about 60 µgal.

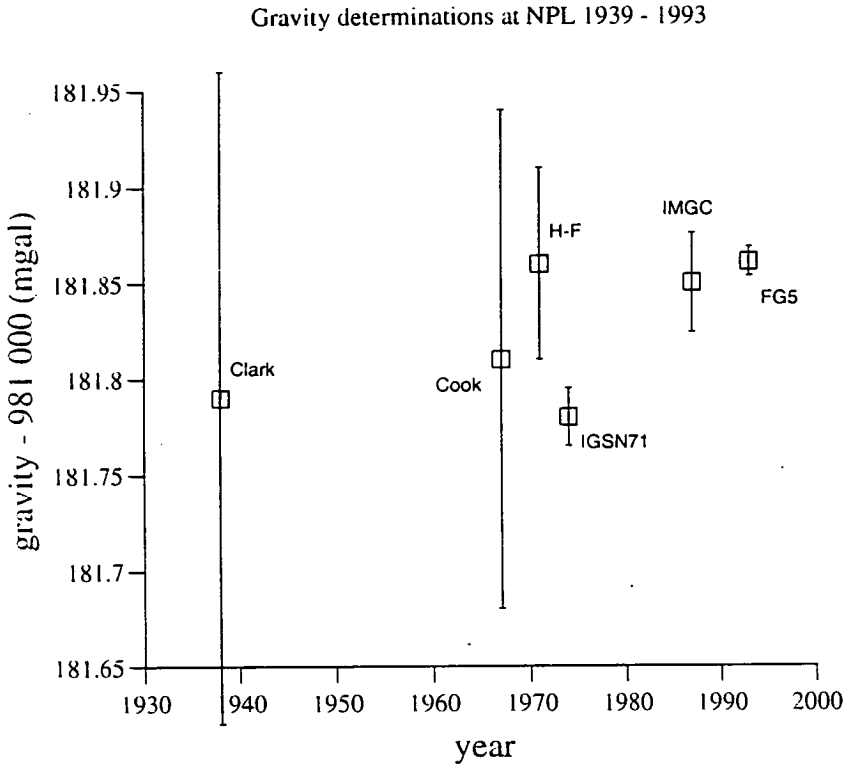

Figure 5.29 Clark's original value is included in the plot. In order that the vertical scale allows the more recent determinations to be displayed clearly, the error bar shown on Clark's value is reduced to about half of the 'probable error' of 0.34 mgal (see note†† above). The values include the Honkasalo Correction.

5.7 Absolute Gravity at the Hydrographic Office, Taunton

5.7.1 Introduction

The Challenger gravity site at the Hydrographic Office (HO) of the Ministry of Defence in Taunton, is an important base station for gravity measurements in the south of Britain. The relative gravity differences between this site and other Primary base stations in south-west England have been measured and documented by the Geophysics and Survey Analysis Branch (now Marine Science Branch 6) of the HO. In September 1993, the FG5-107 Absolute Gravity Meter occupied the Challenger site for three days. This instrument belongs to the Defence Mapping Agency (DMA) of the USA, and Taunton was the last of the sites to be visited during its East European observation campaign. Immediately following the FG5-107 occupation, Edinburgh University established two ex-centres for the absolute site with their LaCoste and Romberg instruments G275, D145 and D154. The vertical gravity gradient at the Challenger absolute site was also measured in September 1993, and a connection was made to a nearby station of the British Precise Gravity Net 1993 (BPGN93) at Broadway Church. In July 1994, FG5-103 observed at Challenger, and in August 1994, the vertical gradient was remeasured at three heights with G275 and D145. The connection to Broadway, which had been hampered by bad weather and instrument problems in 1993 was also re-observed in August 1994.

5.7.2 Relative Gravity Observations

The Challenger gravity site is on a stone plinth approximately 1 metre square in Room E2c of the Challenger block at the HO site. Two ex-centres outside the Challenger Block were established: one in the loading bay on the west side of the building, and the other next to the water tank on the east side (see Figure 5.30). The nearest BPGN93 site is about 10 miles from the HO at Broadway, and this was connected to the Loading Bay site.

The Loading Bay, Water Tank and Challenger absolute sites were observed with G275 and D145 in a triangular sequence in which both meters occupied each site four times. The relative values for the ex-centres are given in Table 5.40.

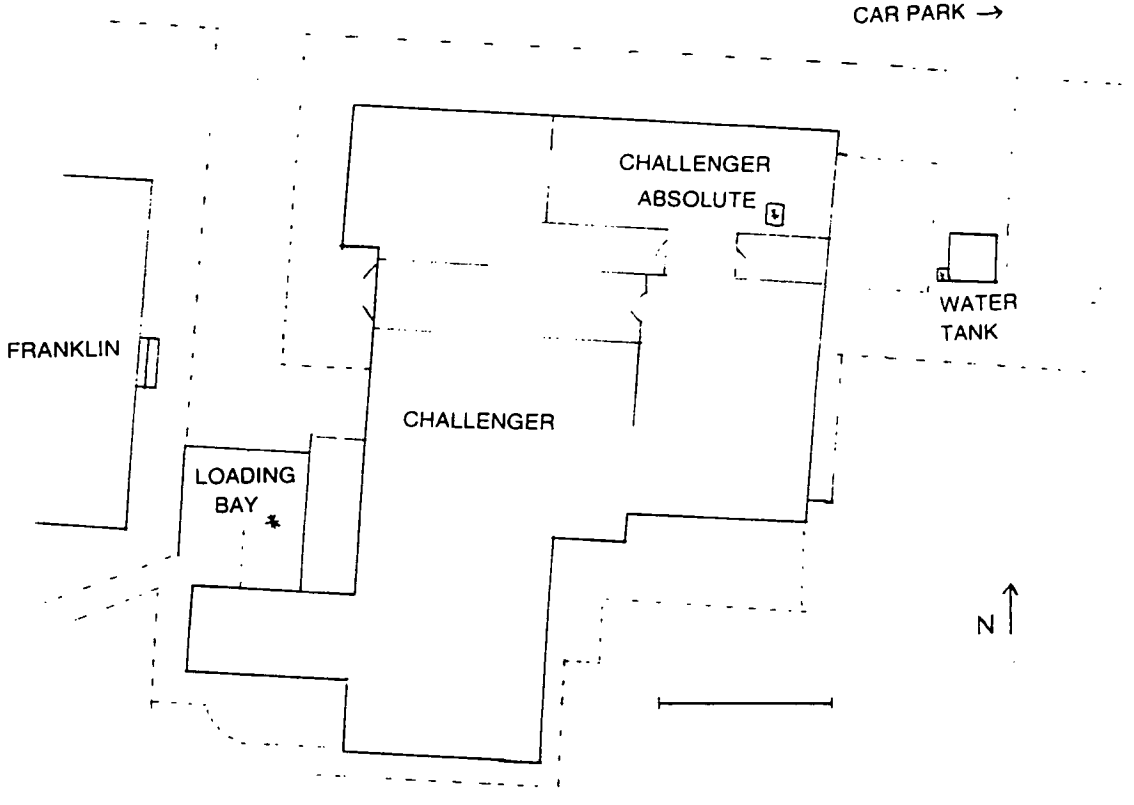

Figure 5.30 Absolute gravity site in the Challenger Block of the Hydrographic Office at Taunton. The ex-centres at the Loading Bay and Water Tank are shown.

site	gravity (μgal)	se (μgal)
Challenger	000.0	2.3
Loading Bay	218.4	2.3
Water Tank	124.2	2.3

Table 5.40 Gravity values at the Taunton ex-centres in μgal relative to the Challenger site.

For the Loading Bay - Broadway link, each site was occupied four times with each meter. This data was included in the main BPGN adjustment (section 6.5). Gravity at Broadway is 22 481.2 ± 5.4 μgal lower than at Loading Bay on the scale of FG5.

The results of the vertical gradient observations were given in section 5.2, Table 5.7 and Table 5.8.

5.7.3 Absolute Observations with FG5-107 and FG5-103

FG5-107 made 53 sets of 100 drops starting at about 16h on 27 September 1993, with one set every hour. The raw FG5 data was kindly supplied to Edinburgh University by the DMA and it showed a large ocean loading signal. FG5-103 made 24 sets of 200 drops on both of 5 July and 6 July 1994. All the data were reprocessed with the Edinburgh program DDT (section 4.4) and the ocean loading correction (section 3.1.4) was made. A plot of the FG5-107 set means with and without the ocean loading correction was shown in Figure 3.6. The set means given in Table 5.41 below include corrections for the vertical gradient (at -298.2 ± 1.5 μgal m^{-1}), elastic tide (static tide removed from the data), ocean loading, speed of light and atmospheric pressure to the standard pressure of 1011.40 mbar for the station height of 15 m. The polar motion correction was calculated using the Axis program REPLAY. The drop length correction to the FG5-107 value is described in section 5.3.1. The system response correction for FG5-103 was calculated as described in section 5.3.5 for the purposes of comparing FG5-103 values at other sites in Britain.

	g (μgal) - 981 168 000.0	s.d (μgal)
FG5-107		
TAU93270 set mean at 1291 mm	856.3	1.4
polar motion	1.4	
g. including. polar motion	857.7	1.4
datum correction to 1315 mm	-7.2	0.1
drop length correction from 160 to 150 fringes	-2.4	3.2
corrected g at 1315 mm FG5-107	**981 168 848.1**	**3.4**
FG5-103		
TAU0507B set mean	834.6	1.8
TAU0607A set mean	836.9	1.8
weighted mean at1315 mm	835.8	1.3
polar motion	-2.8	
corrected g at 1315 mm FG5-103	**981 168 833.0**	**1.3**
datum correction to 120 mm	+356.8	0.9
system response for FG5-103	-1.4	2.8
corrected g at 120 mm FG5-103	**981 169 188.4**	**3.2**

Table 5.41 FG5 103 and 107 absolute values at Taunton Challenger with polar motion, datum height, drop length and system response corrections applied as appropriate.

Comparison of FG5-107 and FG5-103 at Taunton Challenger

FG5-107 and FG5-103 have slightly different operating heights, so the FG5-107 value has been corrected to the FG5-103 height for comparison. The occupation means are compared in Table 5.42 at 1315 mm above the stone plinth at Challenger.

Instrument and date	occupation mean
FG5-107 27-29.09.93	981 168 848.1 ± 3.4
FG5-103 05.07.94 & 06.07.94	981 168 833.0 ± 1.3
FG5-107 minus FG5-103	**15.1 ± 3.6**

Table 5.41 Comparison of FG5-107 and FG5-103 at 1.315m at Taunton Challenger. The system response corrections are not included.

The difference of 15.1 μgal is incompatible with the precision expected from FG5 instruments, but it is consistent with the rumour (*pers. comm.* R.J.Edge 17 January 1995, and T.M Niebauer 15 September 1994) that FG5-107 has an incorrect 'instrument height term' in the REPARAM.DAT file (section 4.3), and that the height of the top of the drop has

been mechanically adjusted so the value given by FG5-107 agrees with a previously established absolute value at one of the DMA sites in the US. The result of this adjustment is that FG5-107 now gives values 'about 17 μgal' higher than other FG5 instruments.

5.8 Summary of Chapter 5

The methods of high precision intercomparisons of absolute gravity meters have been developed and improved through the experience gained at the International Comparisons of Absolute Gravimeters at Sèvres. An awareness of the implications of non-linear gradients for correcting absolute observations and making relative transfers is essential. Gradients at British absolute sites have been carefully observed by the author and techniques for optimising the accuracy of vertical gradient and datum corrections have been developed.

Before a comparison of different instruments at different sites can be made, the individual gravity estimates have to be made equivalent. The unique characteristics of each FG5 instrument may cause the estimate of gravity to vary with the length of its drop. The variation is caused by structure in the fringe residuals and can be prevented by including damped sinusoids in the equation of motion for gravity.

Data from FG5-103 at POL during the period August 1992 to August 1994 is wide-ranging in quality and repeatability. It is possible to correct for some of the different configurations of FG5-103 between upgrades, but comparisons with JILA4 and other FG5 instruments demonstrate that FG5-103 did not perform according to its specification until November 1993.

A new British Fundamental Gravity Station (BFGS93) has been established at the National Physical Laboratory (NPL). A comparison of absolute observations made at NPL since 1939 shows that determinations by Cook (1967), Hammond-Faller (1971) and IMGC (1987) agree with the FG5 value within their stated errors, but the value assigned to Teddington A in the IGSN71 adjustment is too low by about 60 μgal. The pendulum observation made by Clark in 1939 is different from FG5 by only 70 μgal.

CHAPTER 6. The British Precise Gravity Network 1993

6.1 Background

6.1.1 Introduction

The British Precise Gravity Network 1993 (BPGN93) was designed to measure small vertical movements of the crust using precise gravimetry. Current rates of uplift in Britain are of the order of a few millimetres per year ranging from +1.6 at Lerwick to -3.2 at Southend. The measurement of absolute heights is important to separate land movement from changes in mean sea level determined by tide gauge observations (section 1.4.2). 10 millimetres of uplift is equivalent to about 2 μgal (1 μgal = 0.01 g.u = 10^{-8} ms^{-2}), so in order to detect a differential rate of 5 mm per year in about 10 years the target precision of the network was 5 μgal.

Existing gravity sites, for example, those the National Gravity Reference Net (section 1.6.2), did not meet the particular requirements for monitoring vertical crustal movements so new sites, which were carefully chosen, have been established. The LCR instruments used for the observation program, and the methods used for their calibration were described in Chapter 2. The program REDUCE (section 3.4) was used to convert the field readings into equivalent gravity observations. The adjustment program NETWORK has been described in section 3.7, but further examples of its characteristics and additional modifications to the drift model are discussed in this chapter.

New techniques which both help to identify errors in the dataset and to establish the reliability of the final solution are described. The solution from a free adjustment of the 2171 observations constituting the main BPGN is compared with an adjustment constrained by absolute observations from FG5-103, which were derived in Chapter 5.

6.1.2 Selection of Sites

The requirements for BPGN sites were that they must have a long (> 30 years) lifetime, be free from structural alterations and local subsidence during this time, and should be easily accessible. In order to provide adequate drift control by 'double forward looping' sequences (section 6.2.1), seven site occupations must be completed in a day. Consequently, most

BPGN sites are on the doorsteps of churches which could be easily reached from trunk roads so that the travel time between sites was minimised. In Scotland, where suitable buildings were less numerous, three Ordnance Survey Fundamental Bench Marks (FBM) were used. Elsewhere, FBMs were avoided because the Ordnance Survey no longer maintain them, and they are prone to destruction. Figure 6.1 shows the distribution of the 58 sites, which are fairly evenly spaced about 100 km apart. Table 6.1 gives the name, location and code for the sites. The network includes two primary position fixing sites at Barry Buddon (VLBI) and Herstmonceux (SLR), and four absolute gravity sites. FG5 absolute gravity meters (section 4.2) have observed at the Grant Institute, Edinburgh (FG5-103); the Proudman Oceanographic Laboratory (POL), Birkenhead (FG5-103); the National Physical Laboratory, Teddington (FG5-103 and 105) and the Hydrographic Office, Taunton (FG5-103 and 107). The observations and their links to the BPGN have been discussed in sections 5.4 to 5.7.

6.1.3 Instruments

Edinburgh University has three LaCoste & Romberg (LCR) relative gravity meters (section 2.1) - G275, D145 and D154. G275 is a small case instrument with optical readout and has been on heat continuously and in use regularly since 1970. It is very stable and reliable. D145 and D154 differ from the majority of D meters in that both the coarse and fine screws are calibrated (section 2.2). Both are equipped with CPI cards (section 2.1.3) and a beam position galvanometer on top of the meter. The author's tests have shown that equivalent accuracy can be obtained by reading optically or using the galvanometer, but the physical strain on the observer is much reduced when the galvanometer is used.

D145 and D154 have been in use since 1989, but neither has produced such consistent results as G275. Because of the CPI facility, D145 is easier to read than G275. Results from D145 are generally reproducible but not quite as good as G275. D154 has never performed well and it is often difficult to obtain two or more readings within 8 μgal during an occupation. The root mean square (rms) errors from any combined adjustment (section 3.7) of data from these three instruments confirms the subjective judgements made above about their relative quality. The rms unweighted errors for G275 and D145 results are always smaller than for D154. The error for G275 is smaller than D145 except for a very few vertical gradient or ex-centre sequences (sections 5.2 and 5.4 - 5.7).

British Precise Gravity Net 1993

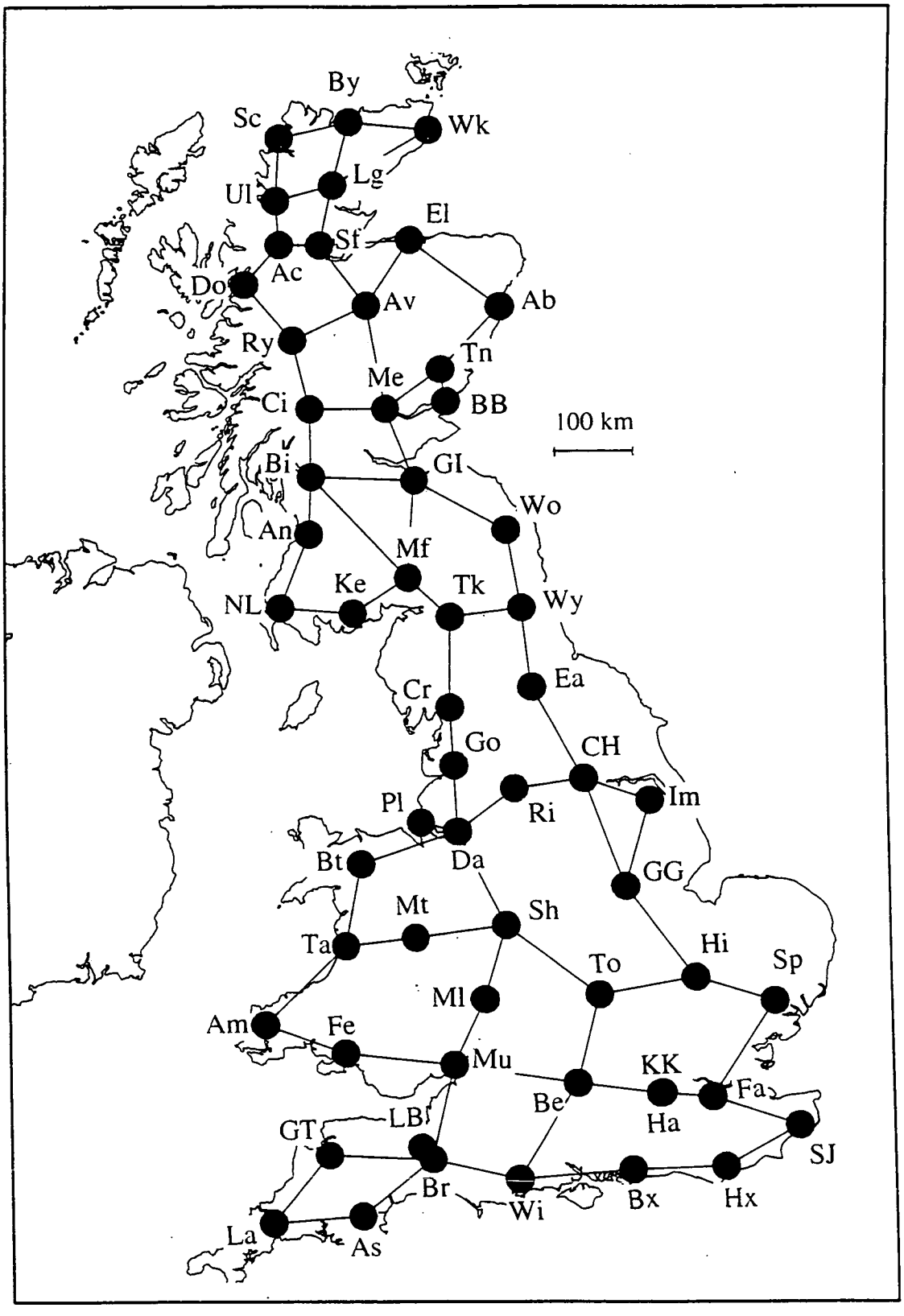

Figure 6.1 BPGN 93 site locations and links. The codes are identified in Table 6.1

CODE	SITE	LAT	LONG	EASTING	NORTHING
GI	Edinburgh GI140	55.90000	-3.17700	326413.	668053.
Ab	Aberdeen St. Mach	57.16974	-2.10138	393870.	808750.
Bi	Bishopton	55.90460	-4.51979	242493.	670808.
Mf	Moffat TH	55.19000	-3.24000	321064.	589120.
Cr	Crooklands	54.24500	-2.71100	353673.	483508.
Go	Goosnargh	53.82333	-2.66666	356120.	436569.
Da	Daresbury	53.34000	-2.63000	358058.	382781.
Po	POL South Porch	53.40333	-3.07166	328761.	390176.
Wo	Wooler	55.54600	-2.01100	399306.	628033.
Wy	Wylam	54.97700	-1.82200	411392.	564733.
Ea	Easby	54.39800	-1.71400	418566.	500335.
CH	Chapel Haddlesey	53.72700	-1.11700	458252.	426009.
GG	Great Gonerby	52.93200	-0.66400	489789.	338048.
Hi	Histon	52.25500	0.10400	543597.	263999.
Sp	Sproughton	52.06300	1.00000	605620.	244808.
Fa	Farningham	51.37900	0.22300	554689.	166839.
SJ	St John Commandery	51.15100	1.19200	623208.	143985.
Hx	Herstmonceux	50.86700	0.33400	564219.	110157.
Bx	Boxgrove	50.86000	-0.71000	490781.	107576.
Wi	Wimborne	50.79855	-1.98723	400900.	99950.
Br	Broadway	50.93900	-2.95400	332978.	116001.
LB	Taunton LBay	51.02506	-3.07866	324360.	125690.
As	Ashburton	50.51400	-3.75600	275515.	69784.
La	Lanivet	50.44400	-4.76200	203918.	64174.
GT	Gt Torrington	50.95200	-4.14300	249493.	119199.
Mu	Mounton	51.63300	-2.70400	351281.	192974.
Ml	Malvern	52.11200	-2.34600	376309.	246066.
Sh	Shareshill	52.65700	-2.08300	394386.	306628.
Be	Beedon	51.49900	-1.30500	448238.	178067.

.....continued over

Table 6.1 BPGN93 sites, name, locations and codes

CODE	SITE	LAT	LONG	EASTING	NORTHING
To	Towcester	52.14300	-1.02200	466919.	249908.
Mt	Montgomery	52.56000	-3.14600	322321.	296453.
Ta	Talybont	52.48900	-3.97900	265646.	289780.
Tk	Talkin	54.90800	-2.70300	354932.	557267.
TA	Teddington A Bld 3	51.42043	-0.33915	515470.	170410.
HA	Hampton Church	51.41300	-0.36000	514039.	169551.
KK	KK Bld 1 NPL1	51.41970	-0.33774	515570.	170331.
Im	Immingham	53.56000	-0.33200	510471.	408363.
Ri	Rishworth	53.65800	-1.95200	403172.	417972.
Fe	Felindre	51.70600	-3.97100	263824.	202696.
Am	Ambleston	51.89400	-4.90600	200070.	225756.
Bt	Betws	53.09100	-3.80200	279339.	356416.
Me	Methven	56.41670	-3.57945	302570.	726050.
Tn	Tannadice	56.71177	-2.85770	347500.	758100.
BB	Barry Buddon VLBI	56.47800	-2.78100	351900.	732050.
El	Elgin South C of S	57.64601	-3.31360	321600.	862520.
Sf	Strathpeffer Epis	57.58855	-4.53766	248320.	858200.
Lg	Lairg	58.02512	-4.39948	258300.	906480.
Wk	Wick C of S	58.44386	-3.09408	336140.	951100.
By	Bettyhill FBM	58.48639	-4.21363	270960.	957440.
Sc	Scourie C of S	58.34848	-5.15852	215180.	944300.
Ul	Ullapool Museum	57.89628	-5.16143	212650.	894000.
Ac	Achnasheen FBM	57.57872	-5.08027	215850.	858450.
Do	Dornie RC	57.27826	-5.51041	188420.	826280.
Ry	Roybridge RC	56.89216	-4.83939	227060.	781440.
Av	Alvie C of S	57.16076	-3.87779	286440.	809310.
Ci	Crianlarich FBM	56.39732	-4.57128	241320.	725740.
An	Annbank	55.48600	-4.52100	240750.	624250.
NL	New Luce	54.94200	-4.85000	217450.	564500.
Ke	Kelton	54.92100	-3.93700	275900.	560250.

Table 6.1 continued.....BPGN93 sites, name, locations and codes

The network adjustment program (section 3.7) determines corrections to the scale factors of the instruments with respect to a designated primary instrument. Because of its superior quality and relative age (LCR meters generally become more stable with use), G275 is considered the primary instrument. The D meters are more than 10 years younger than G275 and were not used regularly (indeed hardly used at all) before 1992.

6.2 Fieldwork

6.2.1 Observation Sequence and Planning

The observation sequences were designed to provide optimum drift control, so that 'double forward looping' sequences were completed in a single day wherever possible. An example of such a sequence to link for example, Edinburgh, Methven and Tannadice would proceed as follows: Measure at Edinburgh, drive to Methven, measure at Methven, drive back to Edinburgh, measure at Edinburgh, drive to Methven, measure again at Methven, drive on to Tannadice, measure at Tannadice, drive back to Methven, measure at Methven, drive to Tannadice and measure at Tannadice. The distance between sites was chosen to be about one hour driving time, which was a suitable compromise between getting as many repeat observations as possible and covering the country in a reasonable time. In fact most links took between 70 and 100 minutes, with the sites about 100 km apart. A complete sequence as above would achieve seven occupations and involve six 'drives' in one day. Because of the larger distances between some sites, it was more usual to achieve only six occupations and five 'drives'.

Each fieldwork campaign was planned in advance by estimating the time needed for the driving and gravity readings. In England and Wales, most sites were at churches and could be located from suitable maps. Scotland has both fewer churches and fewer roads. In particular the condition of the roads is very variable and a three day reconnaissance trip was completed before the main Scotland fieldwork.

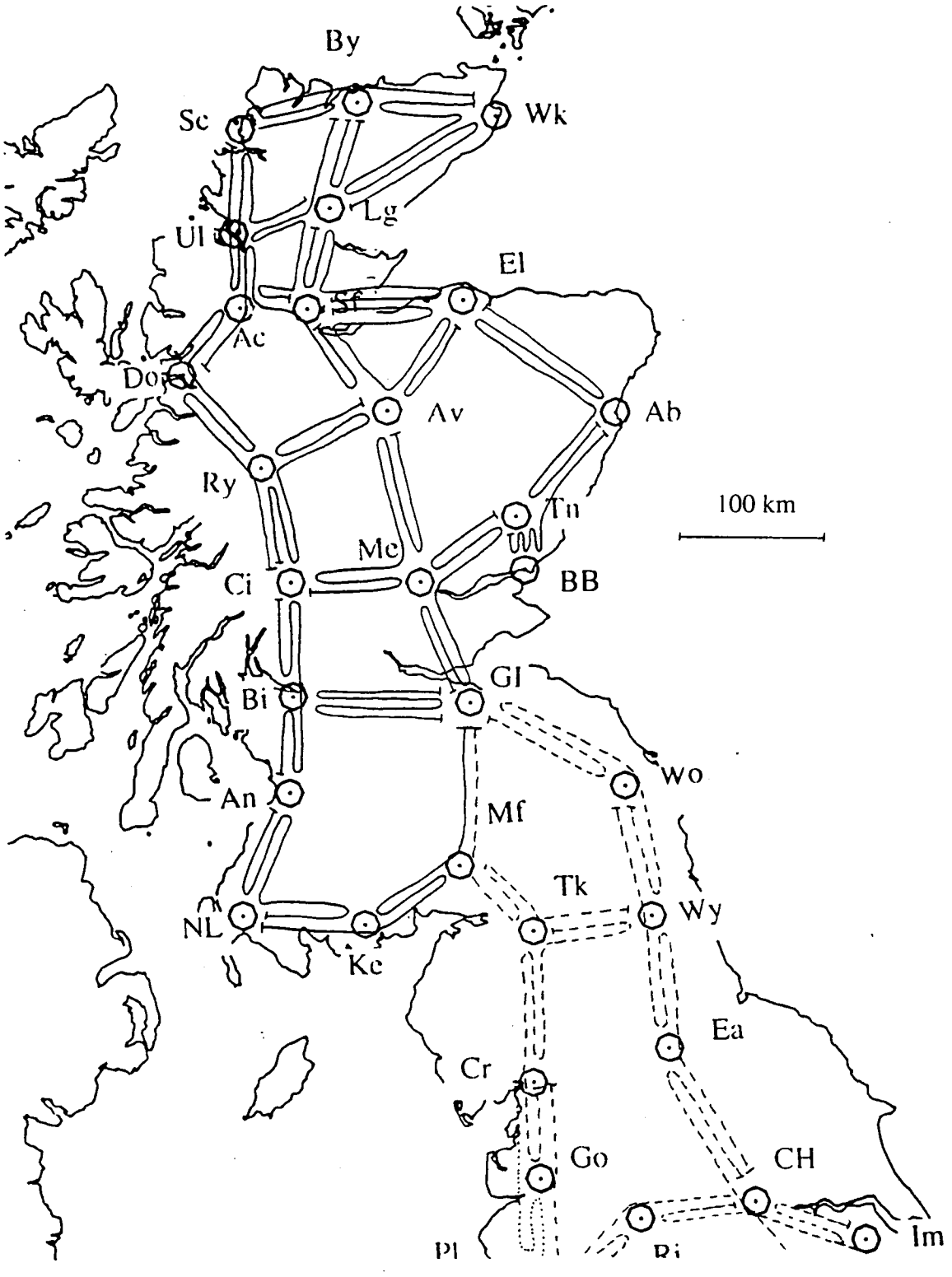

Figure 6.2a BPGN (North) Daily observation sequences for the survey. Each link was measured simultaneously with three instruments. The solid lines show the links observed on the July 93 campaign, and the dashed lines show the September 92 observations (Figure 6.2b)

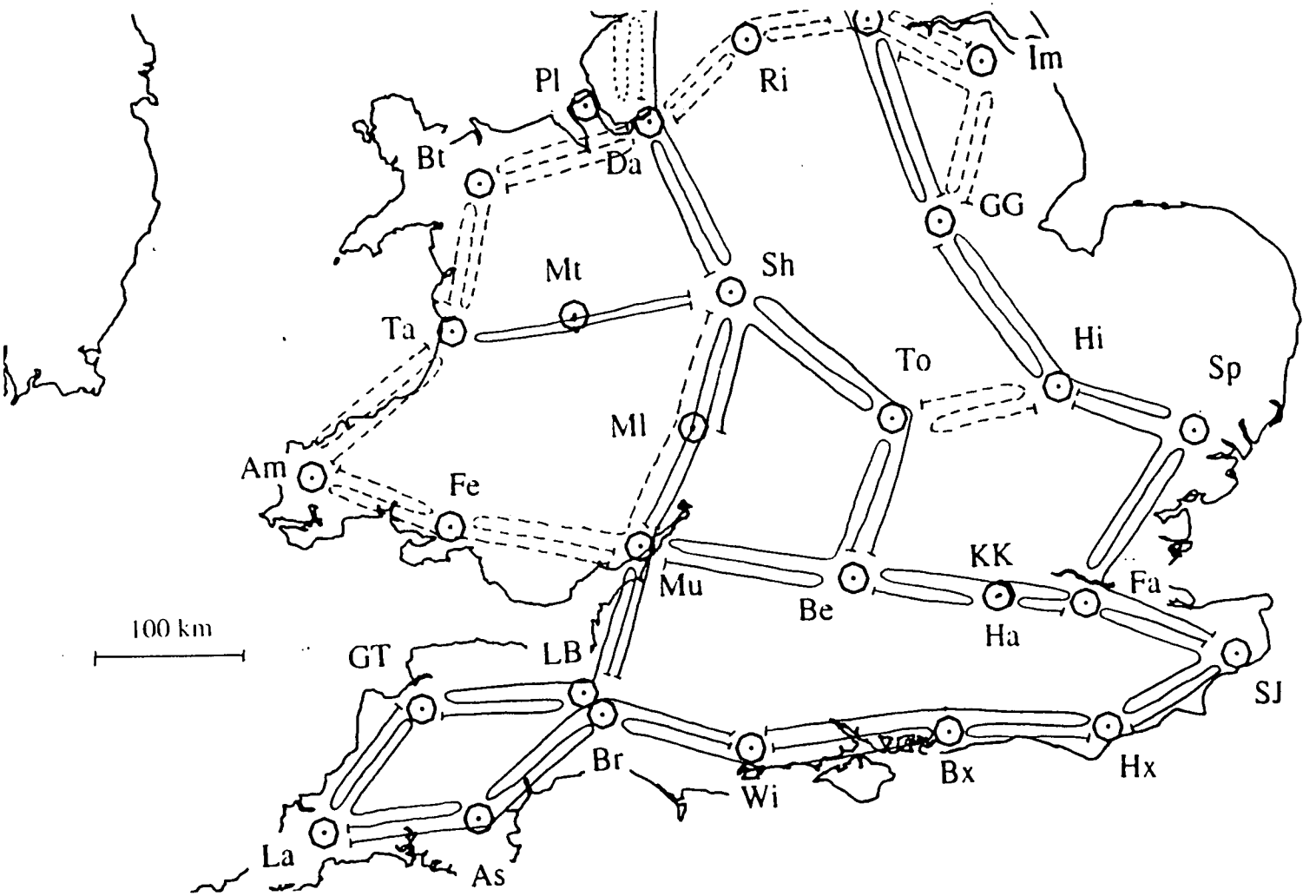

Figure 6.2b BPGN (South) Daily observation sequences for the survey. Each link was measured simultaneously with three instruments. The solid lines show the links observed on the September 92 campaign, and the dashed lines show the March 93 observations. (The dotted line shows a single sequence observed in March 92)

Because of the geometry of the network, which was affected by the locations of suitable sites and the availability of good roads, 'double forward looping' sequences were not always possible. The task of completing the network without duplication, in the minimum time and driving distance, while still maintaining adequate drift control meant that on many days the sequence was more complicated. The actual sequences for the survey of Britain are shown in Figures 6.2a (North) and 6.2b (South). Local links, for instrumental tests and strengthening, between Edinburgh, Moffat and Bishopton are not shown. Over 17,000 miles were driven during the 60 days of fieldwork and each link was measured simultaneously with three instruments. Table 6.2 shows the dates when the BPGN was observed.

inclusive dates	sites observed
05.08.92	Edinburgh-Bishopton
05. - 27.09.92	ENGLAND
14. - 26.03.93	WALES
03. - 22.07.93	SCOTLAND
23.08.93	Edinburgh-Moffat
06.06.94	Moffat-Bishopton

Table 6.2 The dates when the BPGN was observed. (The links to absolute sites were observed at other times (see below)).

6.2.2 Links to Absolute Sites

The BPGN sites at Broadway, Daresbury and Hampton Church were chosen because of their proximity to the absolute sites at Taunton, POL and NPL respectively. Broadway was linked to the Taunton ex-centre called Loading Bay, and Daresbury to the POL ex-centre, South Porch. Hampton Church was linked directly to the absolute site at NPL1. These important links were made with G275 and D145 during the respective vertical gradient and ex-centre campaigns (sections 5.4 - 5.7). A minimum of four occupations of the absolute ex-centre and three of the BPGN sites were made for each sequence, and the results are given in Chapter 5. Because the interval between readings was generally between 20 and 40 minutes. these links were included in the main BPGN adjustment rather than the ex-centre adjustments.

6.2.3 Gravity Observation Control

At each site, gravity readings were made consecutively with all 3 instruments - G275, D145 and D154. Each instrument was observed until two readings within about 3, 4 and 8 μgal

were obtained for G275, D145 and D154 respectively. To reach these standards, generally two or three readings were sufficient for G275 and D145, but up to five for D154. Because of the differing characteristics of each instrument and the day to day performance of them and their observers, the total number of measurements made during one occupation of a site varied between six and fifteen. The time taken therefore varied considerably, although on a good day - with each observer achieving the required repeatability with only two readings, the occupation could be completed in under thirty minutes.

6.2.4 Transport of Gravity Meters

The instruments were transported in their aluminium carrying cases and their original shipping containers. These containers are strong cardboard boxes lined with foam rubber. During the England and Scotland Fieldwork, two of the instruments travelled in these boxes on the back seat of a Ford Escort estate car. The third was cradled on the knees of the back seat passenger. For the Wales fieldwork, all three instruments were transported in the boxes which were secured behind the seats of a Citroen D-15 van. On this occasion, the non-driving observer read both the D meters and thus made two sets of observations at each site.

6.2.5 Batteries and Charging

During the first main campaign in September 1992, four of the standard 12 Volt, 6.5 Amp-hour gel type rechargeable batteries (supplied by LCR with the two D meters) were used. These would be used continuously during the day and recharged at night. Occasionally one of the batteries ran down towards the end of a field day, causing the meter to 'lose heat'. This was noticed when the observer switched on the lights at the start of the next site occupation, and the battery was replaced. It was not always possible to get a good reading in these circumstances (about 15 observations from a total of over 2000 were lost due to battery failure during the fieldwork (section 6.5.6)). Because three meters were used all the time the disruption to the adjustment was very small.

In November 1992 a larger 12 Volt, 24 Amp-hour battery was acquired so that the meters ran off that during transport and were transferred to the smaller (12 Volt, 6.5 Amp-hour) batteries 10 minutes before readings commenced. This procedure avoided failure of the smaller batteries especially on long field days. All batteries were recharged at night. Three

new 9.5 Amp-hour batteries were purchased in March 1993 before the Wales fieldwork to replace the original 6.5 Amp-hour batteries, which were then about 5 years old. The system of 'large' battery for transport and 'small' batteries for reading worked well.

6.3 The Adjustment

6.3.1 Overview

The pre-processing of the instrument readings is done with the program REDUCE (section 3.4). REDUCE applies the calibration (section 2.2), earth tide and ocean load corrections (sections 3.2.2) and atmospheric pressure corrections (section 3.3.2).

The adjustment of the corrected gravity values is based on the observation equation

$$g_{obs}(1+C_f) = G_m + (a_k + b_k t) + \varepsilon_{obs} \qquad (1)$$

where g_{obs} is the observed gravity, G_m is the adjusted gravity value at the site m, a_k and b_k are the constant and linear terms describing the drift during the k^{th} traverse and $1+ C_f$ is the multiplying correction to the provisional scale factor for gravity meter f with respect to the primary instrument. A traverse is usually equivalent to one field day.

The program NETWORK (section 3.7) finds a least squares solution based on the model of equation (1). The influence of this particular model on the BPGN adjustment is discussed here using specific numerical examples. Representations of the daily drift and the cumulative drift during extended periods of fieldwork help to define the suitability of the linear drift model. Alternative representations of the drift are investigated in section 6.3.

Tests for consistency between small portions of the net ('loops') and the complete net help to identify weak areas and bad observations (section 6.5.3). The resilience of the result to breaking an individual link demonstrates the effect of the particular structure of the net and the sequence in which it was observed (section 6.4.5). Singular value decomposition is used to verify the uniqueness and reliability of the final solution (section 6.5.4). These and the other methods described here help to identify errors in the data.

The relative effect of each of the three instruments on the adjustment is investigated in section 6.6. Absolute gravity values from FG5 (sections 5.4 - 5.7) are used to control the adjustment. The scaling factor for the relative instruments, previously defined on the IGSN71 (section 3.5), can now be replaced with a conversion to the absolute scale of FG5.

6.3.2 The Program LOOPDIF

The effect of many of these tests is displayed in the form of a plot showing the difference between the 'before and after' solutions, for example the difference between gravity values resulting from the adjustment of a small loop and the values from the adjustment of the complete net. The difference between the solutions is calculated by the program LOOPDIF which reads the output from NETWORK. LOOPDIF calculates the differences between the gravity values at all the sites and the standard deviation of the differences. The differences in the solutions (in microgals (μgal)) are plotted against the relative gravity of the sites (in milligals (mgal)) with respect to a reference site. The origin (zero gravity, zero difference) corresponds to the Edinburgh GI site unless otherwise indicated in the figure caption. The points are labelled with the site codes, which are defined in Table 6.1. No error bars are shown, but the tables accompanying some of the figures give this information. Note that different vertical scales are used according to the particular test, but figures shown on the same page usually have the same scale.

The values shown in the LOOPDIF plots result from doing the sum

'*test*' minus '*normal*'

so that positive differences mean that the adjusted solution from the 'test' (a network with a broken link, for example) for that particular site had a more positive value than the normal (unbroken) solution.

6.4 Drift Model

6.4.1 Drift Plots

'Drift Plots' show how well the observations on a traverse fit the equation (1). Examples of drift plots showing typical sequences of observations from the BPGN are given in Figure 6.3. Figures 6.3a, b, d and e have the same vertical scale of 120 μgal. Figures 6.3 c and f have extended vertical axes of 180 and 140 μgal respectively. The line shows the drift and the points show the difference between the recalibrated observed gravity ($[1 + C_f]\ g_{obs}$) and the assigned gravity (G_m) at each site. The gravity values on the plots are offset by the drift constant a_k, and the time axis starts at the first observation of the traverse (i.e. the drift line always passes through the origin). Observations which have been downweighted during the adjustment (blunders) (section 3.7.3) are shown by circles. A 'blunder' is an observation with a residual larger than twice the rms unweighted standard error for the appropriate instrument.

Figures 6.3 a, b and c are examples of drift plots from the day-long 'double forward looping' sequences (section 6.2.1) from the September 1992 field campaign. Figure 6.3a shows a 'good' traverse, with all the observations lying close to the line. The closeness of the pairs of observations made at each site occupation demonstrates the excellent repeatability achieved by G275 on this day. The sites Mounton (Mu), Beedon (Be) and Towcester (To) were observed in the sequence Mu-Be-Mu-Be-To-Be, which can be identified on Figure 6.2b. Figure 6.3b shows the link between Herstmonceux (Hx) and Wimborne (Wi) via Boxgrove (Bx) (Figure 6.2b), observed with D145. Although there is only one blunder, at least three readings were necessary at each occupation to achieve repeatability standard of 7 μgal (section 6.2.3).

Figure 6.3c is an example of a 'bad' traverse measured with D145 in the sequence GG-Hi-GG-Hi-Sp-Hi (Great Gonerby, Histon, Sproughton) - note the expanded vertical scale (180 μgal instead of 120 μgal). The figure shows how the solution for the linear drift term b_k is anomalously large, so that the both the observations at GG and the last two observations at Hi lie on the line. Perhaps if the first observations at GG had been slightly lower, they would have been downweighted, causing a less steep b_k and more weight to the Sproughton (Sp) observations. The single observation at Sproughton on this day demonstrates the importance of making consistent observations there on subsequent (or previous) days.

Figures 6.3 d, e and f are examples of drift plots from 'local' i.e. vertical gradient and ex-centre sequences, which provide information about the drift over a much shorter time scale (3 hours instead of 12). In contrast to the field-days, the high frequency of observations during these 'local' sequences mean that the drift can be very well determined (section 2.4). Figure 6.3d shows the Taunton ex-centre observations with D145. Although all the observations lie very close to the drift line, some are designated as blunders because the rms unweighted error for the meter is only 2.3 μgal. The rms weighted error of the Taunton excentre adjustment, which consisted of only this traverse and the corresponding one for G275, was 2.2 μgal, which is typical of the formal standard error resulting from the adjustment of a small number (61) of consistent observations in isolation. (Modifications to the standard adjustment of small datasets such as this are discussed in section 3.7.5).

Figure 6.3e shows the initially steep and non-linear drift characteristic of G275 (the 'early morning curve' (section 6.4.4)), for G275, recorded in the very first vertical gradient sequence of the National Physical Laboratory observations (Table 6.3). The instruments had not been used for at least a month, and had been transported by train from Edinburgh on the previous day. This behaviour was absent from all subsequent sequences at the NPL.

Figure 6.3f is a classic example of a tare. The observations before *and* after the event are reasonably consistent, demonstrating the apparently immediate (and therefore remarkably good) recovery of G275, but fitting a single drift curve to them is clearly inappropriate. Fortunately, the tare occurred at the middle of the sequence (Taunton vertical gradient re-observation (17.8.94)) so that the two halves could be treated as separate traverses without significant loss of drift control. A tare in a field sequence, where the observations are an hour or more apart in time, is much more difficult to identify than a tare occurring, like this one, in a vertical gradient or ex-centre sequence.

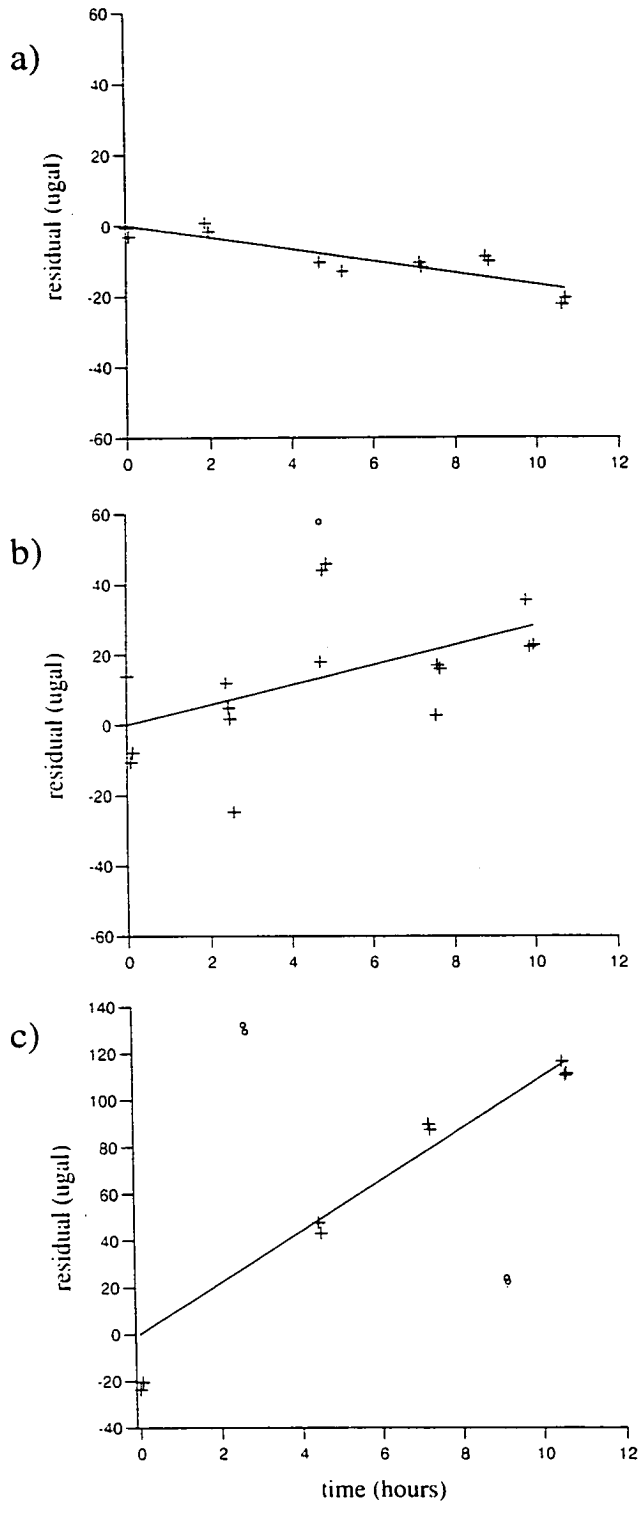

Figures 6.3 a, b and c. Examples of field sequences from the September 1992 observation campaign. a) A 'good' traverse with G275, all points lying close to the line, and both observations at each occupation are consistent. b) A more scattered sequence with D145, where at least 3 readings were needed at each occupation to achieve the repeatability standard of 7 µgal for D145. c) A 'bad' traverse (note the different vertical scale) showing how the linear drift parameter b_k can vary considerably in order to fit even very scattered data.

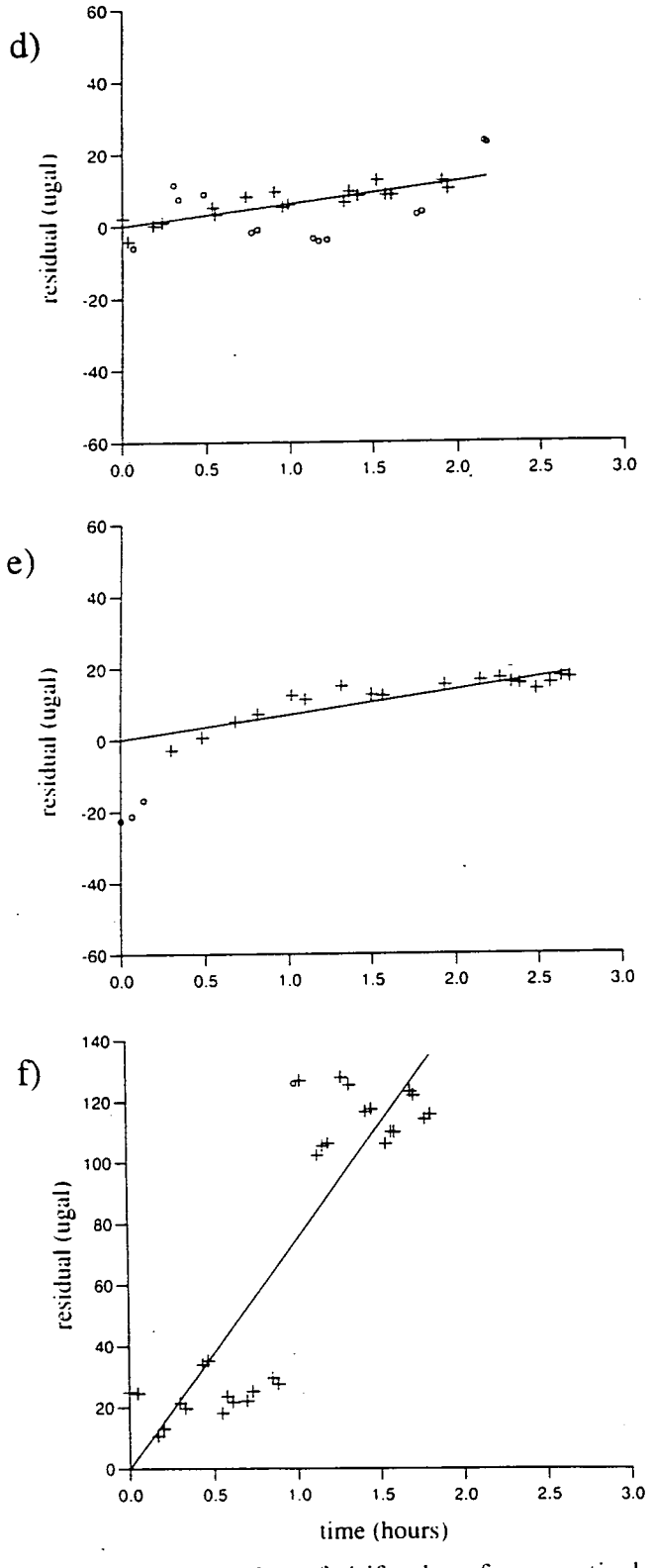

Figure 6.3 d. e and f. Examples of drift plots from vertical gradient and ex-centre sequences. d) Observations around the three Taunton ex-centres with D145. Even though the points all lie close to the drift line, some (shown by circles) are downweighted because the rms error of the adjustment is so small (see text). e) Characteristic initial drift for G275. f) Classic example of a tare, occurring in a vertical gradient sequence. Note the different vertical scale.

These few examples illustrate the usefulness of drift plots for quickly identifying which traverses were 'good' (small drift, all points lying close to the line) and which were not. Blunders can be easily detected and the data files and field notes checked for transcription errors and notes of potential causes (low battery, accidental impact, etc.).

6.4.2 Comparison of Day to Day Drift on Fieldwork

The day to day variation of b_k during the twenty consecutive days of the Scotland field campaign are shown in Figures 6.4 a, b and c, for G275, D145 and D154 respectively. A visual inspection suggests that on average the drift is positive for all three meters, and this is borne out by numerically averaging all the b_k values. When this is done for the 157 traverses of the whole network (England, Scotland and Wales), the 'average daily value' of the drift for each meter is 10 μgal per day for G275 and 20 μgal per day for both D meters. It is also apparent from Figures 6.4 that the D meters drift more 'steeply' (whether positively or negatively) than G275. The 'average daily magnitude' of b_k is 50, 80 and 110 μgal per day for G275, D145 and D154 respectively. Table 6.3 is an example of the output from NETWORK for a small dataset (Teddington vertical gradient observations), showing the b_k values from which these averages may be calculated.

6.4.3 Varying the Drift Model

In order to investigate the validity of the chosen drift model, which is to fit a different linear drift rate b_k and constant a_k to each instrument on each day, two alternatives were tried. The first was to fit a single drift line to the whole of a particular field campaign, i.e. to treat the twenty days of observations with each instrument as a single traverse. The second was to constrain b_k to be zero for all traverses.

Effect of fitting one drift line to the whole of a field campaign

When this is done for the Scotland data, the drift plots in Figure 6.5 a, b and c are obtained. The values of b_k for these 20-day-long single traverses represent the net drift over the 20 days and are given in Table 6.4

Iteration 11 χ^2 = 7.946 with 14 degrees of freedom

RMS weighted error of the adjustment = 3.85 µgal
RMS error for meter 1 unweighted = 3.11 µgal, weighted = 3.84 µgal
RMS error for meter 2 unweighted = 6.42 µgal, weighted = 3.85 µgal

Scale factor used for meter 2 = 1.0004230

Base	Gravity (µgal)	s.e (µgal)	Weight	Observations
30 Teddington A Bld	000.0	0.6	36.085	32
31 Tripod TeddA 1158	-343.5	1.7	19.847	20
32 Tripod TeddA 1167	-348.0	1.9	7.718	12
33 KKitchen1 NPL1	- 83.7	1.3	54.609	57
34 Tripod NPL1 1103	-412.4	1.8	17.743	20
35 KKitchen2 NPL2	- 83.1	1.9	17.023	19
36 Tripod NPL2 1121	-414.5	1.9	13.638	17
			Total	177

Traverse — Estimated drift function

	a_k (µgal)	+/-	s.e(a_k) (µgal)		b_k (µgal day^{-1})	+/-	s.e(b_k) (µgal day^{-1})	
1	024.2	+/-	2.8	+ (	166.275	+/-	026.913)	* days
2	083.3	+/-	1.5	+ (	079.432	+/-	026.751)	* days
3	077.4	+/-	2.0	+ (	266.736	+/-	041.300)	* days
4	-000.3	+/-	1.8	+ (	028.493	+/-	061.008)	* days
5	102.1	+/-	2.0	+ (	215.973	+/-	020.612)	* days
6	345.6	+/-	3.1	+ (	368.112	+/-	059.959)	* days
7	408.4	+/-	3.0	+ (	272.863	+/-	072.520)	* days
8	344.5	+/-	3.3	+ (	262.179	+/-	109.375)	* days
9	098.5	+/-	3.2	+ (	157.948	+/-	044.629)	* days

20 residuals greater than 2 standard errors

Time (days)	Error (µgal)	Station	Traverse	Meter
33986.407	-22.5	30	1	1
33986.410	-21.7	30	1	1
33986.412	-17.8	30	1	1
33988.406	-19.0	35	5	1
33988.508	-10.4	36	5	1
33988.512	- 8.5	36	5	1
33986.596	-10.0	31	6	2
33986.658	- 9.2	33	6	2
33986.720	-11.2	34	7	2
33986.723	- 9.3	34	7	2
33986.726	12.4	33	7	2
33986.742	9.1	33	7	2
33986.744	10.5	33	7	2
33986.751	- 9.1	34	7	2
33986.753	- 8.4	34	7	2
33987.781	-12.3	32	8	2
33987.801	8.6	32	8	2
33988.406	-14.8	33	9	2
33988.408	-16.1	33	9	2
33988.465	8.4	33	9	2

Table 6.3 Example of output from NETWORK (with fixed scaling factor), for the vertical gradient sequences at NPL, Teddington, showing the a_k and b_k values.

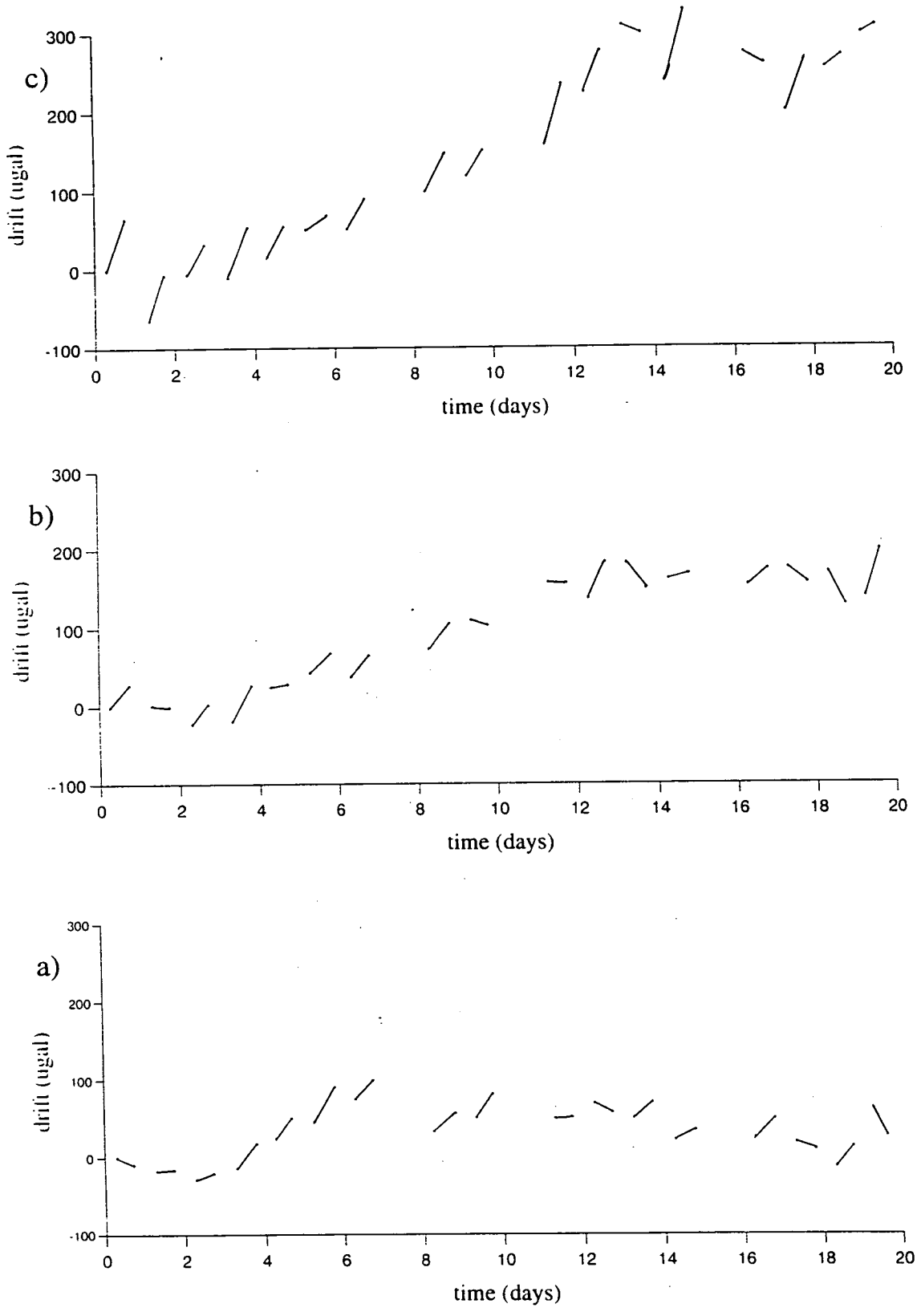

Figure 6.4 a, b and c. The day to day variation of b_k during the twenty consecutive days of the Scotland field campaign for G275, D145 and D154 respectively. On average the drift is positive for all three meters.

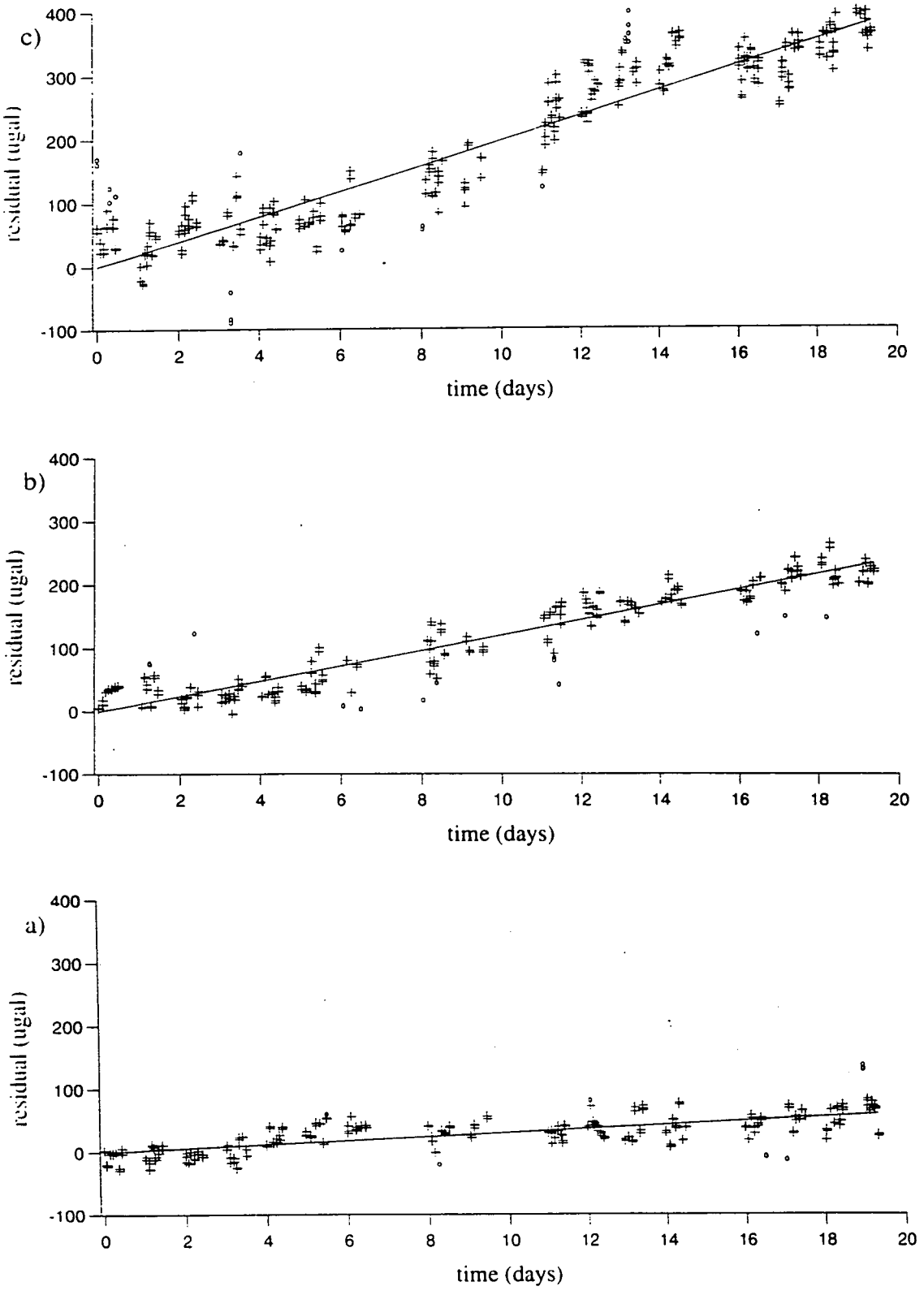

Figure 6.5 a, b and c showing the 'single traverse' drift model for G275, D145 and D154 respectively. The drift line and residuals resulting from treating the whole of the 20 day sequence of the Scotland campaign as a single traverse.

Instrument	b_k for 20-day traverse (μgal per day)
G275	3.08 ± 0.32
D145	12.06 ± 0.36
D154	19.66 ± 0.48

Table 6.4 Drift rates calculated by NETWORK when the whole of the Scotland data is treated as if each instrument made only a single traverse.

The effect of this approximation on the adjustment is shown in Table 6.5, and the change in the gravity solution in Figure 6.6. A slope has been introduced into the gravity values, which means that the scaling factor and the b_k values are related.

traverses	χ^2	rmse (μgal) adjustment	rmse G275	rmse D145	rmse D154
59	9.6	10.29	6.14	15.58	22.56
3	17.4	24.93	19.16	24.08	41.65

Table 6.5 Effect on the adjustment of treating all data as a single traverse.

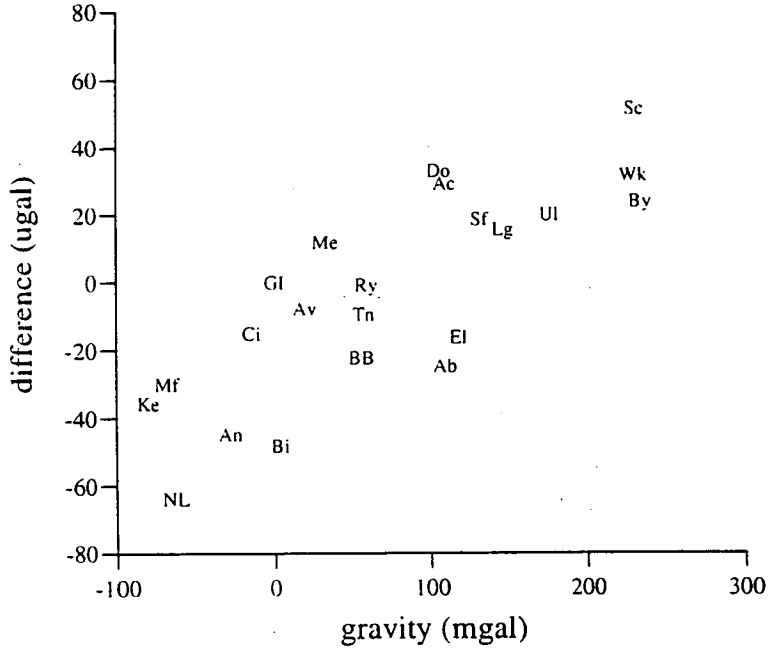

Figure 6.6 The difference between the gravity solutions with a drift line fitted to each day (59 traverses) and a drift line fitted to the whole sequence (3 traverses).

Zero drift

This was achieved by overwriting all the non-diagonal elements of the normal equation matrix (section 3.7) which had row or column indices between M+K and M+2K, with zero, and the diagonal elements with one.

Applying the zero-drift model to the single-instrument nets indicates a discrepancy between the G275 and D meter results. The effect on the G275 net is shown in Figure 6.7a. A large step of about 40 μgal occurs at the Scottish border, between Wooler(Wo)-Edinburgh(GI) and Moffat(Mf)-Talkin(Tk). For the D145 and D154 nets, the only effect is to change the overall scaling factor. The D145 result is shown in Figure 6.7b. The D154 result is not shown, but is similar to D145.

When the data from the three instruments are combined and the scaling factor C_f fitted as a free parameter, only the D145 factor changes significantly (Table 6.6).

	χ^2	rmseadj (μgal)	rmse G275	rmse D145	rmse D154	C_f D145	C_f D154
linear drift	10.4	7.86	5.06	12.14	17.72	1.0004230± 0.0000240	1.0006751± 0.0000334
zero drift	15.6	10.27	6.40	15.39	27.79	1.0003255± 0.0000244	1.0006551± 0.0000379

Table 6.6 Effect of applying the zero-drift model to the complete network adjustment.

Figure 6.7c shows the change in the station gravity values for the combined network. It shows characteristics of both Figure 6.7a (G275 only) and Figure 6.7b (D145 only). The step (Wo-GI) is still present, but now Talkin (Tk) retains a smaller separation from Moffat (Mf). The large step occurs between Moffat and Wylam (Wy) instead. Examination of the respective locations of these sites (Figure 6.1) shows how the 'break' has changed its position. This sort of analysis helps to define which sites are strongly related (for example the group Wick(Wk)-Scourie(Sc)-Bettyhill(By) always seem to move together when the network parameters are changed).

The slope effect of D145 (Figure 6.7b), particularly for the Scottish sites (Kelton (Ke) to Wick (Wk)) is evident in the combined net, and corresponds to the effect shown in Figure 6.6 which was the result of applying the 'single traverse' model to the Scotland data. A similar change of slope is seen when applying these alternative drift models to other

sections of the net. It is apparent that different scaling factors result from adjusting the different regions of the net independently, which if they were real would mean that the scaling factor for the micrometer screw calibration (section 2.2.4) is not linear. It is more likely that this result means that the factor C_f and the drift rates b_k are not independent in the network adjustment.

The separation of Lanivet (La) and Ashburton (As) seen in the D145 result (Figure 6.7b), but not in the G275 result (Figure 6.7a) is also present in the combined adjustment (Figure 6.7c).

Other drift models

Some drift models, for example those used in the IGSN71 (section 3.5) included quadratic and cubic terms in the drift function. Although this may be appropriate for fitting a curve to many observations closely spaced in time (readings at least every 15 minutes), it is not appropriate for the majority of BPGN traverses, which include only about 7 observations which may be more than 1 hour apart in time. For the vertical gradient and ex-centre sequences (section 5.2) and for the calibration experiments described in section 2.4, where readings are made more frequently than every 10 minutes, it would be possible to fit a non-linear drift curve. The method of fitting a spline curve to the calibration data is described in section 2.4.4. It was found that allowing a more complicated drift curve did not affect the shape of the apparent calibration curve, but only increased its amplitude. In addition, the choice of the number of nodes of the spline would have to be made arbitrarily and it was concluded that a simple linear drift model should be maintained. There may be a case for using a non-linear drift curve if it is one that is known to be a reproducible characteristic of a particular instrument (section 6.4.4).

Conclusions

All the investigations of fitting different drift models have shown that the b_k values can vary considerably. The gravity solutions of the complete network rarely change by more than about 20 μgal. The drift rates b_k and the scaling factors C_f both act as 'soaks' for observational data that was 'too high' or 'too low', i.e. extreme values can be absorbed by these scaling parameters. The discussion of singular value decomposition (section 6.5.4) also confirms that the most poorly determined parts of the solution are the b_k values. The examination of the daily drift plots (section 6.4.1) before and after discrepant observations have been deleted (section 6.5.6) demonstrates how the slope of the drift line varies dramatically in order to accommodate large residuals.

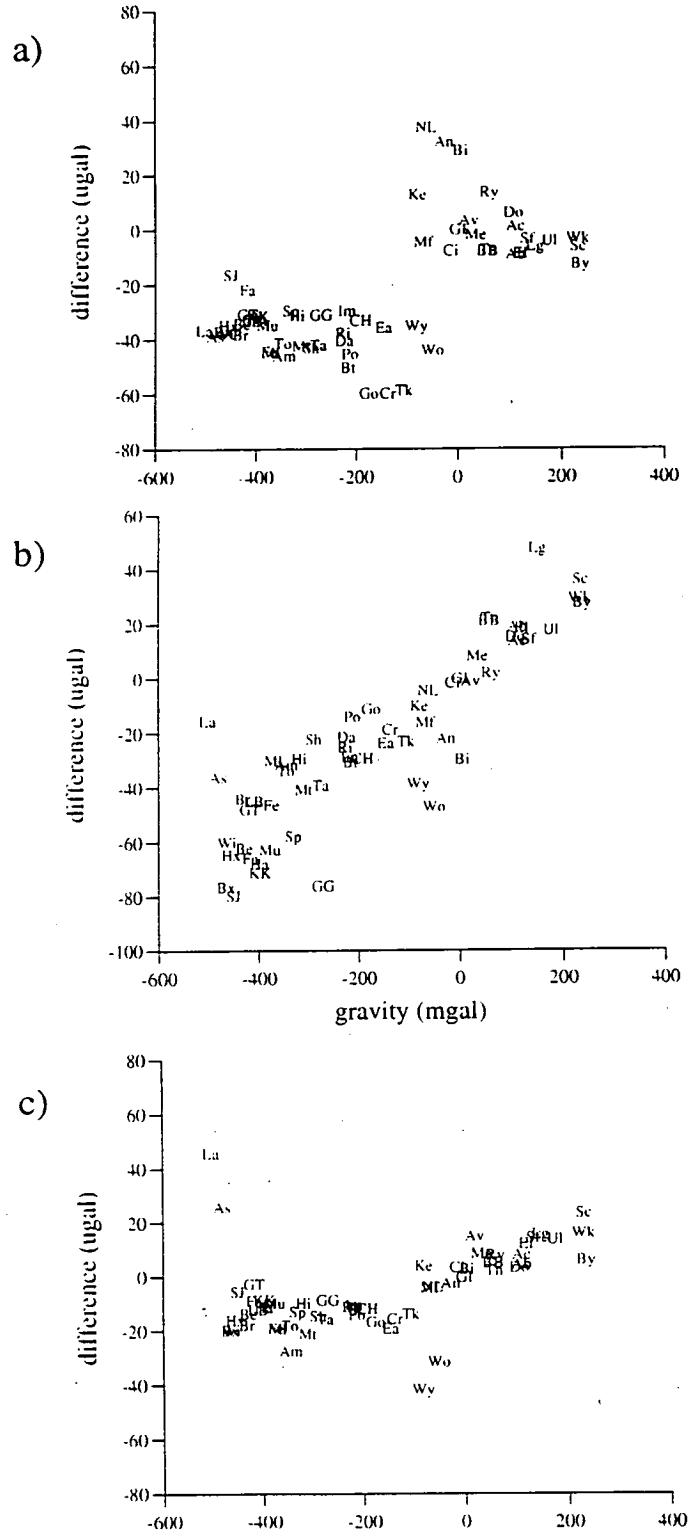

Figure 6.7 Applying the zero-drift model to the single-instrument nets a) G275 only, b) D145 only and c) the combined G275, D145 and D154 net. a) shows a large step of about 40 µgal at the Scottish border. The comparison of a) and b) indicates a discrepancy between the G275 and D meter results. c) has characteristics of both a) and b) and shows the change in the station gravity values for the combined network.

6.4.4 Characteristic Drift

Hipkin *et al.* (1988) describe a non-linear characteristic instrumental drift for G275 observed during 28 sequences measured in 1981. Their result (Figure 6.8a) shows that there is a constant linear drift for the first 30 - 40 minutes, then almost zero drift for the next hour. They note, however, that this response, which was also detected during 1978, was absent between 1982 and publication. During the BPGN fieldwork (1992 -1993), the same behaviour was occasionally observed. However, because of the large (one hour) time interval between readings at field sites, it was more easily identified in some of the vertical gradient sequences where the time between readings is less than ten minutes. A similar response was noted less frequently in D145. Of three tests made by the author to observe this meter continuously for an hour after unclamping, only one showed the steep initial drift (Figure 6.8b).

Hipkin (1978) observed part of a network using an 'equilibrium technique' which meant that the meter was read by two observers alternately over a two hour period at each site. It was concluded that the results obtained by allowing the drift to reach equilibrium at each occupation were not any more consistent than those available with less effort by a conventional sequence (Hipkin *et al.* 1988).

It is certainly the case that the largest drifts are observed after the meters have been unused for some months, so care has been taken to read the meter in the laboratory during the two days before field campaigns to allow this rapid drift to dissipate before starting the field readings. The response of the spring to unclamping (the 'spring hysteresis model') was discussed in section 2.4.4.

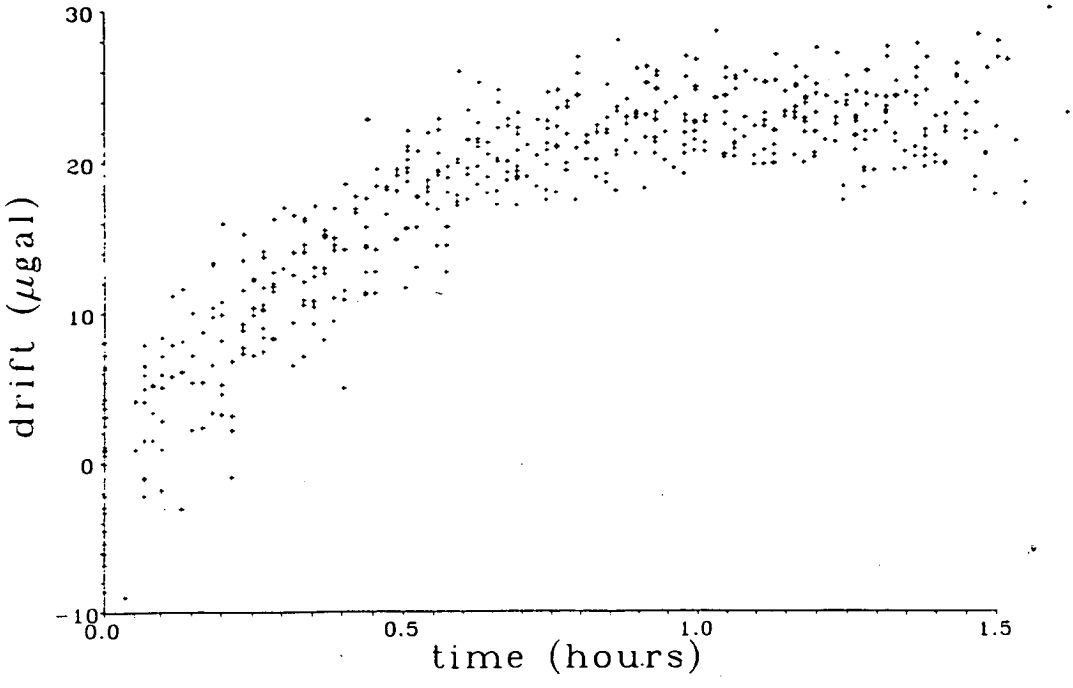

Figure 6.8a The characteristic non-linear instrumental drift for G275 observed during 28 sequences measured in 1981 (from Hipkin *et al.* (1988)).

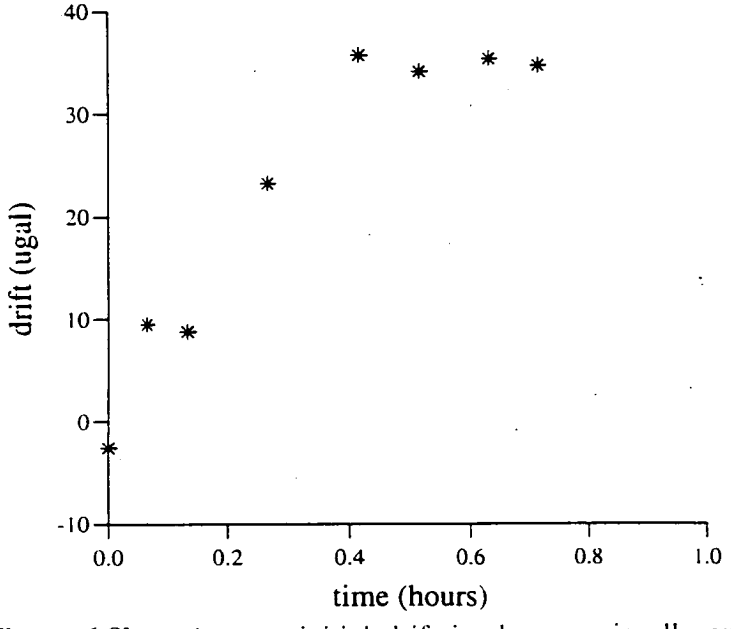

Figure 6.8b A steep initial drift is also occasionally exhibited by D145. The author observed this response during the hour following unclamping, but on only one of three similar tests.

6.5 Error Trapping

6.5.1 Introduction

As with any large dataset and particularly one based on field observations, there are many opportunities for generating errors. The data for the BPGN were collected in the field over a two year period using precise but delicate instruments. Five scientists contributed to the program and observed three different instruments under a variety of physical and mental stresses. These have led to inevitable mistakes in recording the time, date, dial reading and atmospheric pressure. The author has typed in all the field data and is doubtless responsible for further transcription errors amongst the 2500 readings.

Various techniques have been used to identify problem data. The weighting procedure (section 3.7.3) enables individual observations with large residuals to be identified. Singular value decomposition (section 6.5.4) has been useful for identifying whole traverses for which the linear drift value b_K is poorly determined because of bad data. The gravity values obtained by adjusting isolated loops have been compared with the values from the complete network (section 6.5.3). This has shown up weak regions by identifying particular stations or pairs of adjacent stations for which the values are inconsistent. The stability of the network has been tested by checking the resilience of the solution when particular links are broken.

6.5.2 Residuals Larger than 2 standard errors

The program NETWORK produces a list of residuals greater than twice the instrument-weighted standard error for the appropriate instrument (Table 6.3). These are shown as blunders on the Drift Plots (Figures 6.3). An early stage of analysis involves the visual examination of these plots and the individual observations with large residuals can be immediately identified from the list.

6.5.3 Network Loops

An important test of the reliability of the network is whether the gravity differences between stations calculated using a small portion of the net agree with those calculated using the complete net. The net was broken into six 'loops' of similar size with significant overlap, as shown in Figures 6.9 and 6.10. The Edinburgh loop (Edloop), POL loop and NPL loop are centred on absolute stations. The North loop (Nloop) includes POL, Edinburgh and the stations in between. South loop (Sloop) covers most of NPL loop and includes the south-west England stations. The Scotland loop (Scotloop) includes all the stations north of Edinburgh. The aim was to identify weak areas of the network and hopefully to track down the observations which were causing problems. The method both helps to identify problem data, and once these are eliminated it gives a measure of the reliability of the final adjustment.

Examples

The Edinburgh loop (Edloop) and the Southern loop (Sloop) will be illustrated as examples. Some of the observation sequences shown in Figures 6.2a (for Edloop) and 6.2b (for Sloop), have been edited to make the loops complete. For example the beginning or end of a sequence is not included if it leaves sites 'hanging' off the loop. This happens for sites that were visited only once at the beginning or end of one of the daily sequences. This editing is done carefully to ensure adequate drift control of the truncated sequences.

The *Edloop* dataset consisted of a total of 494 observations made with three instruments on 32 traverses which included 14 sites. It includes stations in southern Scotland and northern England which were mostly observed during the July 1993 and September 1992 campaigns. The links between Edinburgh, Moffat and Bishopton have been observed at various times between 1992 and 1994 (Table 6.2). The differences between the values from the adjustment of this dataset and the corresponding values from the whole net adjustment (both adjustments with fixed scaling factor) are plotted in Figure 6.11a. The differences are calculated by the program LOOPDIF (section 6.1.1), and the standard deviation of these is given in the figure captions. When the problem observations were later identified (using all the methods described here), nine observations were deleted. The corrected version of the loop data, *Edloop1*, is now much more consistent with the complete net (Figure 6.11b). The Figures 6.11a and 6.11b illustrate the value of loop adjustments, both for identifying bad data, and for displaying the effect of correcting it. Table 6.7 shows the difference between

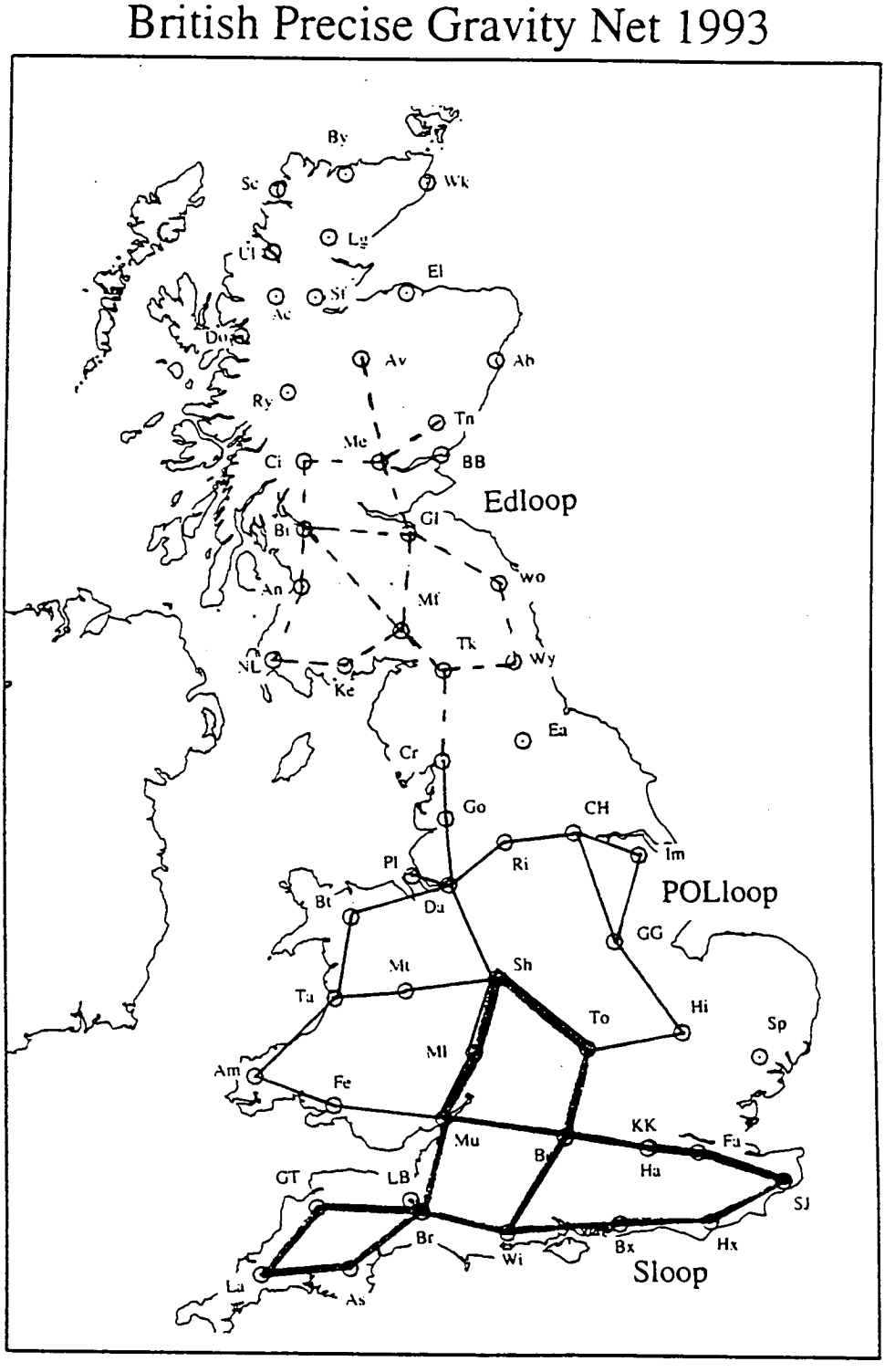

Figure 6.9 Edinburgh (Edloop), POL (POLloop) and South (Sloop) network loops. These sections of the network were adjusted independently to check the consistency of their solutions with that of the complete net.

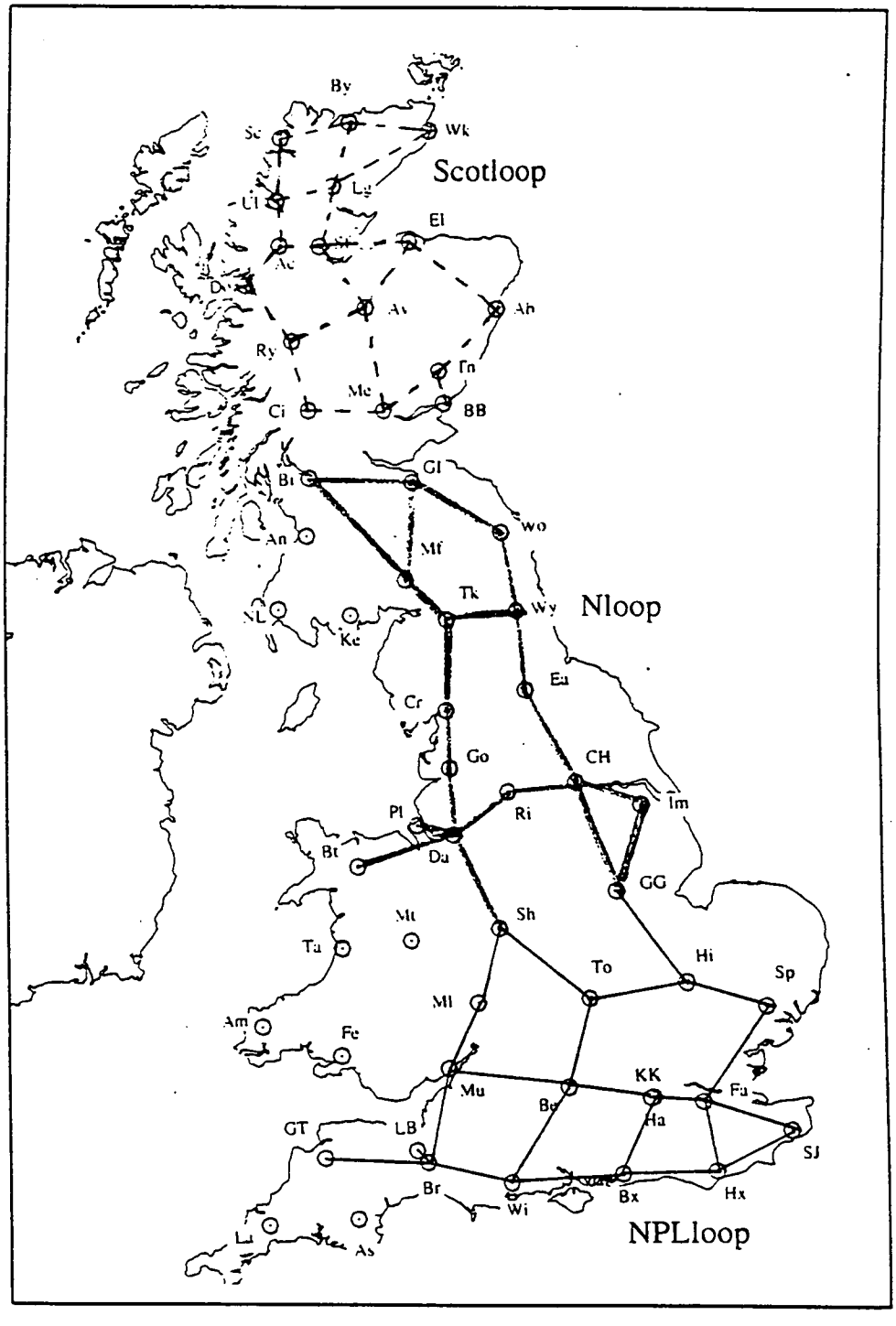

Figure 6.10 Scotland (Scotloop), North (Nloop) and NPL (NPLloop) network loops. These sections of the network were adjusted independently to check the consistency of their solutions with that of the complete net.

the uncorrected and corrected loop values, rather than the difference between the loop and the whole network, which is shown in the figures.

ref	name	edloop1 (mgal)	edloop (mgal)	diff (μgal)	± s.e (μgal)	
140	GI 140 Floor	0.0000	0.0000	0.0	6.9	GI
13	Bishopton	3.7814	3.7777	3.7	8.2	Bi
15	Moffat TH	-68.3061	-68.3083	2.2	7.7	Mf
17	Crooklands	-137.4063	-137.4097	3.4	12.9	Cr
201	Wooler	-50.3558	-50.3568	1.0	10.0	Wo
202	Wylam	-82.6943	-82.6963	2.0	10.7	Wy
226	Talkin	-106.3125	-106.3165	4.0	10.1	Tk
240	Methven	32.5570	32.5598	-2.8	7.4	Me
241	Tannadice	56.9795	56.9797	-0.2	11.9	Tn
253	Alvie	19.2603	19.2609	-0.6	12.3	Av
254	Crianlarich FBM	-14.9702	-14.9653	-4.9	9.0	Ci
255	Annbank	-27.9874	-27.9914	4.0	10.6	An
256	New Luce	-62.8824	-62.8987	16.3	11.3	NL
257	Kelton	-80.4214	-80.4298	8.4	10.0	Ke

Standard deviation of difference 4.9 μgal

Table 6.7 Difference between the original *Edloop* solution and the corrected *Edloop1* solutions. The standard error on the difference is calculated from the standard errors on the gravity values, which are not shown in the table.

Sloop consists of 516 observations made on 38 traverses at 17 sites, and is important because it includes two absolute stations at NPL and Taunton. It also includes the stations Ashburton and Lanivet in the extreme south-west which appear to be particularly unstable, and change their values by up to about 20 μgal in some of these tests. Figure 6.12a shows the difference between the original *Sloop* data and the whole network. The investigation of *Sloop* and the NPL loop, which covers a very similar area, led to the rejection of one whole traverse comprising 18 readings (D154 Loading Bay - Broadway) and also three readings made after a battery failure. The comparison of the corrected (*Sloop1*) data and the whole network is shown in Figure 6.12b, and is much improved. The change in the gravity values due to the 21 deletions are given in Table 6.8.

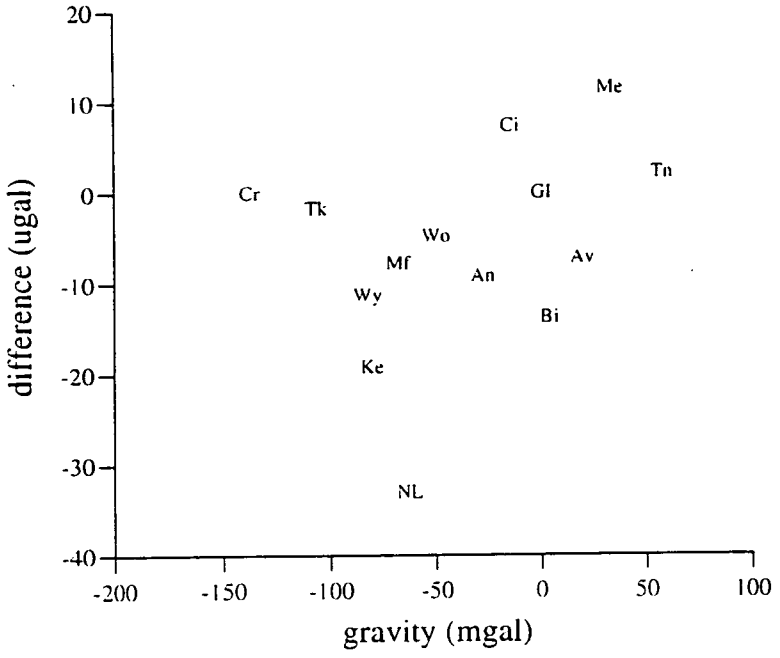

Figure 6.11a The difference between the values from the independent adjustment of the uncorrected Edloop dataset and the corresponding values from the whole net adjustment (both adjustments with fixed scaling factor). The s.d of the differences is 10.9 μgal

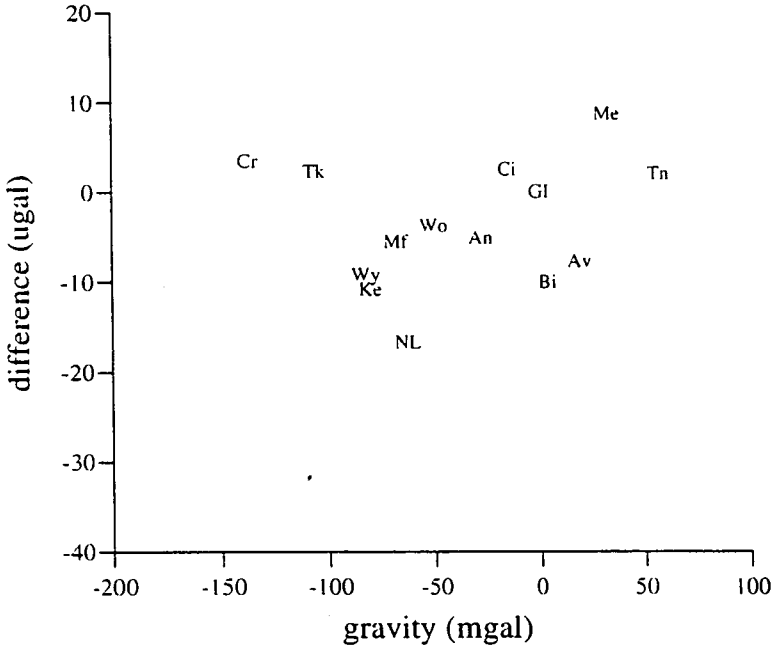

Figure 6.11b Difference between the independent adjustment of the corrected Edloop1 (Edloop with nine observations deleted) and the complete net. The s.d of the differences has been reduced to 6.7 μgal.

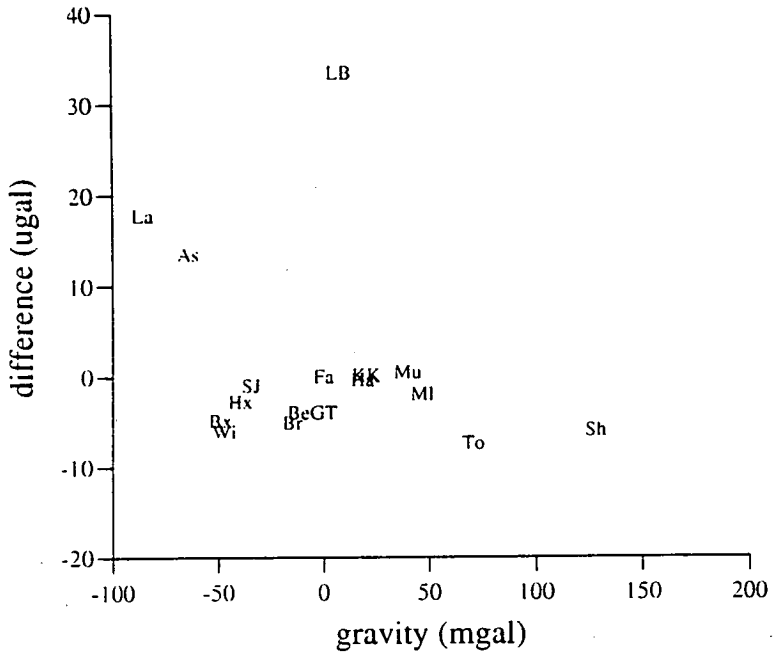

Figure 6.12a The difference between the values from the independent adjustment of the uncorrected Sloop dataset and the corresponding values from the whole net adjustment (both adjustments with fixed scaling factor). The standard deviation of the differences is 10.3 μgal.

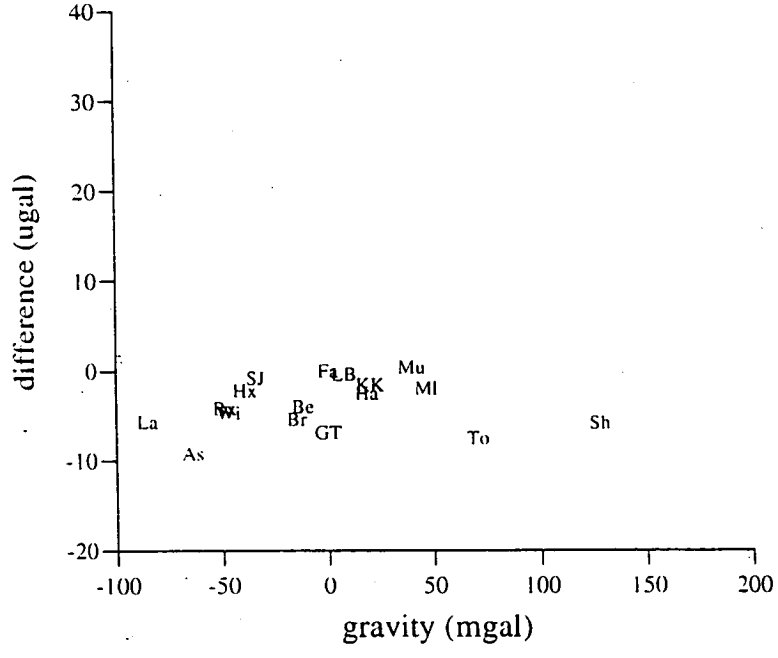

Figure 6.12b Difference between the independent adjustment of the corrected Sloop1 and the complete net. One whole traverse (D154 Loading Bay - Broadway) and three readings made after a battery failure have been deleted from Sloop to make Sloop1. The standard deviation of the differences is now 2.8 μgal.

ref	name	sloop1 (mgal)	sloop (mgal)	diff (μgal)	± s.e (μgal)	
208	Farningham	0.0000	0.0000	0.0	4.3	Fa
209	St John Commdry	-34.3290	-34.3292	0.2	3.5	SJ
210	Herstmonceux	-39.4282	-39.4288	0.6	5.5	Hx
211	Boxgrove	-49.0223	-49.0230	0.7	6.2	Bx
212	Wimborne	-46.9614	-46.9628	1.4	6.4	Wi
213	Broadway	-14.8428	-14.8425	-0.3	6.8	Br
52	Loading Bay	7.6264	7.6603	-33.9	8.1	LB
214	Ashburton	-64.0928	-64.070	-22.7	9.2	As
215	Lanivet	-85.4459	-85.422	-23.5	9.8	La
216	Gt Torrington	-0.0870	-0.0841	-2.9	7.9	GT
217	Mounton	39.4736	39.4737	-0.1	6.8	Mu
218	Malvern	46.5543	46.5543	0.0	7.4	Ml
219	Shareshill	127.8888	127.8886	0.2	7.3	Sh
220	Beedon	-11.9478	-11.9478	0.0	6.2	Be
222	Hampton Church	18.2868	18.2889	-2.1	5.7	Ha
33	KKitchen1 BH NPL1	19.8742	19.8759	-1.7	6.5	KK
223	Towcester	70.4471	70.4472	-0.1	6.9	To

Standard deviation of difference 10.3 μgal

Table 6.8 Difference between the original *Sloop* solution and the corrected *Sloop1* solutions. The standard error on the difference is calculated from the standard errors on the gravity values, which are not shown in the table.

6.5.4 Singular Value Decomposition

A set of equations, where one or more of them is a linear combination of the others (degeneracy), is called *singular*. Singularity can occur when independent equations are so close to being linearly dependent that roundoff errors during computation can cause them to become dependent. A zero pivot (a pivot is any element of the matrix which you divide by) gives no solution at all. A very small pivot typically results in fitted parameters with very large magnitudes that are delicately (and unstably) balanced to cancel out almost precisely when the fitted function is evaluated (Press *et al.* 1988). Least-squares problems are often overdetermined (number of equations greater than number of unknowns) *and* underdetermined (ambiguous combinations of parameters exist). The BPGN network adjustment is certainly overdetermined, with over 2000 observations for about 370 unknowns, and the current tests show that there are a number of statistically valid but significantly different solutions possible. Singular value decomposition (SVD) works by defining the reciprocal of zero or very small pivots as zero, not infinity. The definition of 'very small' can be made small enough so that not too many values are zeroed by the process, but big enough to identify the troublesome small elements.

The routine used is from Press *et al.* (1988), from which the following description is taken:

Any M × N matrix **A** (with M ≥ N) can be written as the product of an M × N column-orthogonal matrix **U**, an N × N diagonal matrix **W** with positive or zero elements, and the transpose of an N × N orthogonal matrix **V**.

$$\begin{pmatrix} & A & \end{pmatrix} = \begin{pmatrix} & U & \end{pmatrix} \begin{pmatrix} w_1 & & \\ & \ddots & \\ & & w_N \end{pmatrix} \begin{pmatrix} & V & \end{pmatrix} \tag{2}$$

$U^T \cdot U = V^T \cdot V = I$, and the ratio of the largest to the smallest elements of W (the w_j) influences the definition of 'very small' in deciding which elements to zero. When the decomposition has been performed, the largest w (w_{max}) is found, and the limit below which w_j are zeroed (w_{min}) are set so that

$$w_{min} = w_{max} \times L \tag{3}$$

On the first iteration, L was chosen so that no eigenvalues were zeroed, to allow the weighting procedure to work as usual. On all subsequent iterations, L was chosen to zero only one eigenvalue.

The solution (the vector x) of the equation

$$\mathbf{A}.\mathbf{x} = \mathbf{B} \tag{4}$$

(see section 3.7 for notation), is found by is calculating the inverse of **A** :

$$\mathbf{A}^{-1} = V \cdot \left[\mathrm{diag}(1/w_j)\right] \cdot U^T \tag{5}$$

and then x can be found by computing

$$\mathbf{x} = V \cdot \left[\mathrm{diag}(1/w_j)\right] \cdot (U^T \cdot \mathbf{B}) \tag{6}$$

SVD on whole network

Doing SVD on the whole network is extremely slow - it takes 4 hours to do 10 iterations on one of Edinburgh's faster processors, 'waverley'. It is not very helpful either because there are so many eigenvalues that even with a very small value of L it is not possible to zero only one or two of them at a time. When more than about ten values are zeroed, the solution rapidly becomes meaningless.

Loop examples

At each iteration, the smallest 1 % of the eigenvalues were written to the screen so that the appropriate value of L could be chosen. After about 3 iterations, this list of eigenvalues consistently showed that one was 3 or 4 orders of magnitude smaller than the others. This single poorly determined eigenvalue showed up in the results as an anomalously large b_k value, resulting in the whole traverse being downweighted. By ensuring that only one eigenvalue was zeroed each time, the solution converged. The effect of this procedure is illustrated with the Sloop and Edloop data.

i) Sloop

Sloop includes the absolute ex-centre stations at Taunton and NPL1. Setting L equal to the value such that a single eigenvalue was zeroed on each of iterations 2 to 11, the solution converged and assigned an unrealistic b_k value for the D154 Broadway-Loading Bay traverse, and the whole of that traverse was severely downweighted. The adjustment statistics between the normal and SVD solutions are compared in Table 6.9. The scaling factor was held fixed in both cases.

SLOOP	χ^2	$rmse_{adj}$ (μgal)	rmse G275	rmse D145	rmse D154	C_f D145	C_f D154
normal	14.0	6.56	4.40	9.19	15.28	1.000 4230	1.000 6751
SVD	20.8	6.07	4.12	6.41	19.14	1.000 4230	1.000 6751

Table 6.9 Effect of doing singular value decomposition on the *Sloop* adjustment.

The change in gravity values between the normal and SVD solutions of *Sloop* are given in Table 6.10. Most of the sites in southern England are lower by 10 to 20 μgal in the SVD solution. Loading Bay is 29.7 ± 8.6 μgal lower.

		test(svd) (mgal)	normal (mgal)	diff ± s.e (ugal)		
208	Farningham	0.0000	0.0000	0.0	5.8	Fa
209	St John Comdry	-34.3471	-34.3292	-17.9	3.3	SJ
210	Herstmonceux	-39.4489	-39.4288	-20.1	5.4	Hx
211	Boxgrove	-49.0422	-49.0230	-19.2	6.2	Bx
212	Wimborne	-46.9742	-46.9628	-11.4	6.7	Wi
213	Broadway	-14.8527	-14.8425	-10.2	7.2	Br
52	Loading Bay	7.6311	7.6603	-29.2	8.6	LB
214	Ashburton	-64.0810	-64.0701	-10.9	8.8	As
215	Lanivet	-85.4326	-85.4224	-10.2	10.1	La
216	Gt Torrington	-0.0970	-0.0841	-12.9	8.6	GT
217	Mounton	39.4652	39.4737	-8.5	7.2	Mu
218	Malvern	46.5388	46.5543	-15.5	7.9	Ml
219	Shareshill	127.8869	127.8886	-1.7	7.9	Sh
220	Beedon	-11.9545	-11.9478	-6.7	6.8	Be
222	Hampton Church	18.2798	18.2889	-9.1	6.4	Ha
33	KKitchen1 NPL1	19.8795	19.8759	3.6	7.1	KK
223	Towcester	70.4457	70.4472	-1.5	7.4	To

Standard deviation of difference 8.0 ugal

Table 6.10 SLOOP differences between the svd solution and the normal solution (solution values in mgal), and the s.e on the difference (μgal).

ii) Edloop

When SVD was applied to *Edloop*, a stable solution resulted from zeroing one eigenvalue on the first iteration, and one thereafter. The adjustment statistics are shown in Table 6.11.

EDLOOP	χ^2	$rmse_{adj}$ (μgal)	rmse G275	rmse D145	rmse D154	C_f D145	C_f D154
normal	9.9	13.11	9.81	14.31	23.54	1.000 4230	1.000 6751
SVD	8.9	12.65	9.67	12.98	21.77	1.000 4230	1.000 6751

Table 6.11 Effect of doing singular value decomposition on the *Edloop* adjustment.

The changes in the gravity values between the normal and SVD solutions for *Edloop* are given in Table 6.12.

		test(svd) (mgal)	normal (mgal)	diff ± s.e (ugal)		
140	GI 140 Floor	0.0000	0.0000	0.0	6.7	GI
13	Bishopton	3.7796	3.7777	1.9	8.1	Bi
15	Moffat TH	-68.3058	-68.3083	2.5	7.6	Mf
17	Crooklands	-137.4075	-137.4097	2.2	12.4	Cr
201	Wooler	-50.3570	-50.3568	-0.2	9.6	Wo
202	Wylam	-82.6966	-82.6963	-0.3	10.3	Wy
226	Talkin	-106.3127	-106.3165	3.8	9.8	Tk
240	Methven	32.5556	32.5598	-4.2	7.2	Me
241	Tannadice	56.9751	56.9797	-4.6	11.5	Tn
253	Alvie	19.2592	19.2609	-1.7	11.9	Av
254	Crianlarich FBM	-14.9743	-14.9653	-9.0	8.8	Ci
255	Annbank	-27.9852	-27.9914	6.2	11.8	An
256	New Luce	-62.8880	-62.8987	10.7	16.2	NL
257	Kelton	-80.4274	-80.4298	2.4	13.7	Ke

Standard deviation of difference 4.7 ugal

Table 6.12 EDLOOP differences between the svd solution and the normal solution (solution values in mgal), and the s.e on the difference (μgal).

Only Crianlarich changes its gravity value significantly. The SVD value is lower by 9.0 ± 8.8 μgal, and the SVD value at New Luce is higher by 10.7 ± 16.2 μgal, than the normal solution. There are large errors are on the 'spur' sites : Wylam, Tannadice, Alvie and Crianlarich (Figure 6.9).

Conclusions SVD

When SVD is used with care, it can improve the solution. The method particularly helps to identify poor traverses and shows up weaknesses in the design of the network. For example, the Edloop dataset includes observations from the September '92, and July '93 field campaigns, and isolated sequences between Edinburgh and Moffat (August '93) and Moffat and Bishopton (June '94) (Table 6.2). The adjustment requires that all these observations are consistent, which they would be in an ideal world. However, our experience shows that the first day of a field campaign usually produces worse results than the last, because both the instruments and the observers take some time to 'warm up' (but see section 6.4.4).

If the adjustment is allowed to proceed with more than two eigenvalues zeroed at each iteration, it shows that the most poorly determined parameter is the linear drift term (b_k). If the process is allowed to continue so that about 40 eigenvalues are zeroed, the gravity values at adjacent stations can no longer be distinguished, and two or three are assigned identical values. This extreme case is only useful for finding weak regions in the network as the

numerical values of such an altered solution are meaningless. SVD proved to be a more severe method of dealing with inconsistent observations than the blunderweighting scheme, and in general it identifies the same troublesome data as the other methods.

6.5.5 Legbreaking

The network can be thought of as a two dimensional 'Meccano' structure, with all the links in tension. If one of these links is broken, then all the rest have to move to take up a new stable structure. The breaking of particular links could have significant consequences if that link was one of only two joining large sections of the network together. For example breaking the link between Wooler (Wo) and Wylam (Wy) leaves the whole of the Scottish section connected to the rest of the country via the single link between Talkin (Tk) and Moffat (Mf) (Figure 6.1). Breaking other links for example Elgin (El)-Aberdeen (Ab) would leave isolated 'spurs' i.e. sections of the network 'floating' (because they only attached at one end), in this case Methven (Me)-Tannadice (Tn)-Aberdeen (Ab).

The sum of the gravity differences around the links which form the 3 to 7 -sided polygons making up the net must be zero, and this is the principle on which the adjustment program works. In the real net, the gravity values at each site *do* have some dependence on the neighbouring links and on the sequence in which they were observed. The effect of this dependence has been investigated by breaking some of the links one by one. An example is the Shareshill-Daresbury link (Figures 6.1 and 6.2b), which is important as it splits an otherwise 10-sided polygon into two smaller polygons of 5 and 7 sides (North Wales and Central England, respectively). It is also close to the absolute site at POL, and is part of the connection between POL and other absolute sites at Taunton and NPL.

Method

Daresbury (Da) and Shareshill (Sh) are connected by the sequence observed on September 24 1993. Shareshill is also connected to Montgomery (Mt), Malvern (Ml) and Towcester (To) (Figure 6.13a). The program NETWORK uses the site reference numbers 19 and 219 for Daresbury and Shareshill respectively. The reference number and site code for Shareshill are changed to 919 and S9 when Shareshill is connected to Daresbury, and there is no link between 919 (S9) and 219 (Sh). This arrangement is illustrated in Figure 6.13b. The rest of the data file is unchanged. The site S9 is added to the location file for the

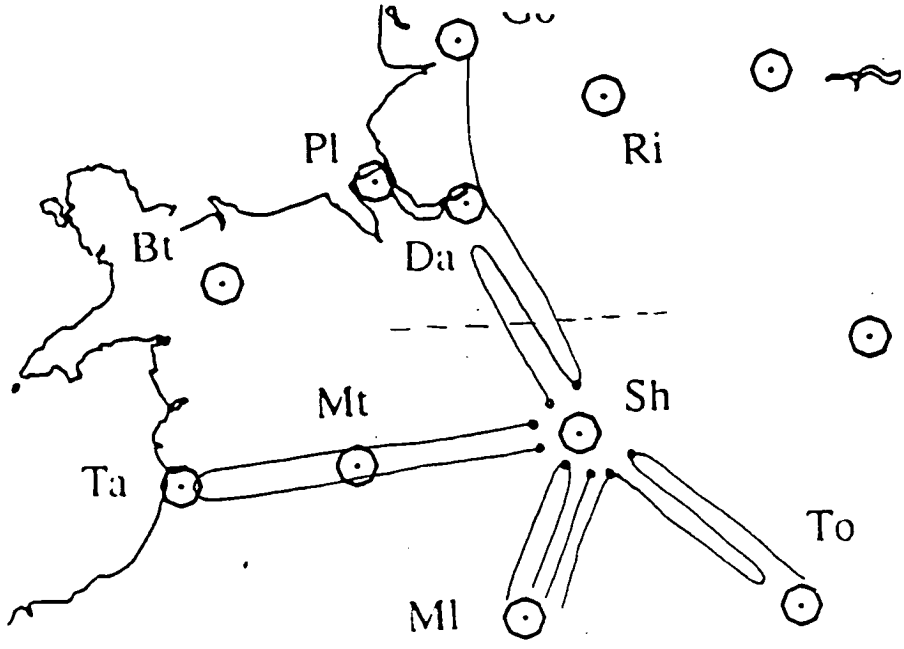

Figure 6.13a Extract of Figure 6.2b, showing the links to Shareshill (Sh) from Daresbury (Da), Montgomery (Mt), Malvern (Ml) and Towcester (To).

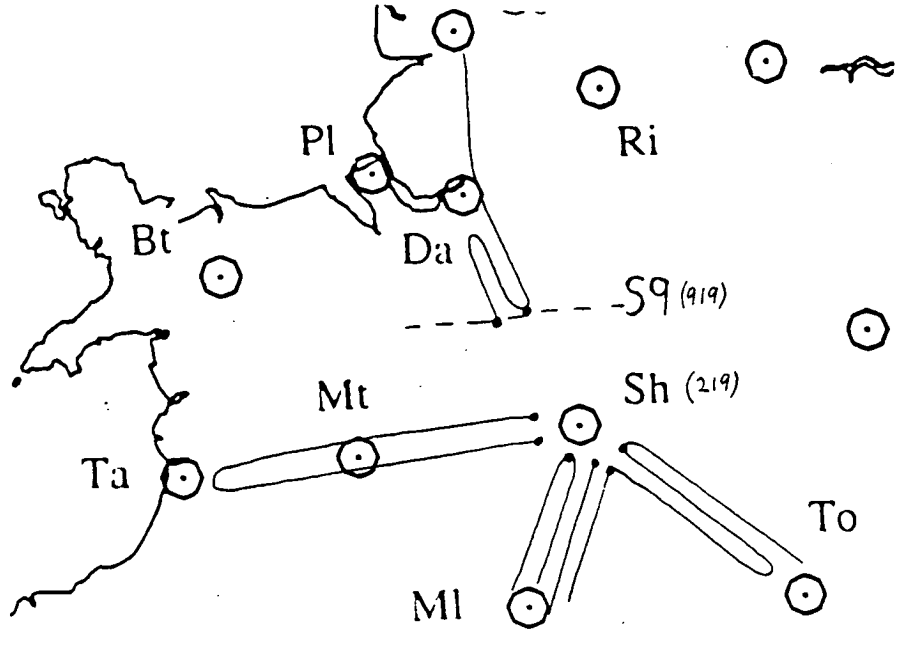

Figure 6.13b Diagram showing how the breaking of the Shareshill-Daresbury link is simulated in the data. The reference number 919 is used for the imaginary station 'S9' which is attached only to Daresbury. The original station Sh retains the code 219, and is still 'attached' to the rest of the net through its other links.

program REDUCE (section 3.4), and there is an extra row and column added to the normal equation matrix (section 3.7).

Results

The comparison between broken and unbroken 'single-instrument' nets showed different behaviour for each instrument (Figures 6.14 a, b and c). Figure 6.14a (G275 net only) shows S9 about 19 μgal above Sh. (S9 is attached only to the station to the north (Da), but Sh is attached to the west (Mt), south (Ml) and east (To)). Most other sites move by less than 5 μgal. The result for D145 (Figure 6.14b) is much less encouraging, showing a 40 μgal difference between S9 and Sh, and, more significantly, an approximately linear change of values between -40 and -5 μgal for sites with gravity values different from Edinburgh (GI) by -400 to 0 mgal. Sites north of Edinburgh are not affected. The D154 result (Figure 6.14c) is rather surprising, showing changes of up to 18 μgal in sites along the south coast of England (SJ, Hx) which are far from Shareshill. S9 and Sh are separated by 16 μgal.

If the three, broken 'single-instrument' nets are combined, and compared with an unbroken three-instrument net, it is seen (Figure 6.15) that the 'combined' network is much 'stronger' than any of the single nets, with sites south of Shareshill moving by +6 or 7 μgal, and sites north by about -4 μgal. Sh is about 10 μgal higher than S9. Although they are far from Shareshill, the extreme south-western sites Ashburton (As) and Lanivet (La) have moved by 42 and 25 μgal respectively. This apparently anomalous effect results from the different instrument weighting between the 'complete' and 'broken' adjustments. For example, if the D154 observations at Lanivet were very discrepant, they may be severely downweighted as a consequence of the instrument weighting scheme (section 3.7.3) in one solution, and so not contribute to the final gravity value assigned to the station.

It is highly improbable that all three instruments would fail at the same time, but breaking the Shareshill-Daresbury link with one instrument while leaving the other two nets intact demonstrates the consequences of a more realistic situation where only one instrument fails. Figure 6.16 is the difference between a three instrument net with broken G275 leg (i.e. only one failure) and an unbroken three instrument net. The stations south of Shareshill have all moved by about +5 μgal, and the stations north have moved by -3 to 6 μgal. S9 is about 14 μgal higher than Sh. The corresponding plot for D145 shows less than 2 μgal change for all the stations except Lanivet (La), Great Torrington (GT) and S9, which are higher by 14, 4 and 10 μgal respectively in the unbroken network. The D154 plot is similar to the D145 plot, but now Lanivet (La), Ashburton (As) and S9 are higher by 3, 13 and

8 μgal in the unbroken net. The different behaviour of G275 is because it has more weight than the other instruments and also that the result may demonstrate a weakness in the G275 net.

Conclusions - Leg Breaking

The (unfortunately) realistic situation where one instrument performs very badly during the whole of a particular day, or repeatedly badly at a particular site can be simulated by detaching portions of the network. The sometimes non-intuitive results (where stations geographically far from the break are significantly affected) demonstrate the influence of the sophisticated weighting scheme. The total weight is a combination of an observation weight (blunderweight) and an instrument weight (section 3.7.3). At stations where many of the observations were 'marginal blunders', in the sense that a small change in the solution results in a large number of these observations being severely downweighted, the gravity value may change significantly. The breaking of other the links has been investigated, in particular between Wooler and Wylam, and between Alvie and Roybridge. These configurations have caused similar behaviour in their respective regions of the net. It is seen that certain groups of stations always move together, and that particular sites, which jump between one group and another, are critical in determining the conformity of the network.

6.5.6 Deletions

A total of 63 observations (of which 18 were on the same traverse) were deleted from the 2234 BPGN observations. The choice of which to delete was made after all the tests of sections 6.4 and 6.5, and checking the field notes for transcription errors and remarks on the conditions under which the observation was made. A note of a battery failure during the occupation either before or after the suspect observations was felt to be sufficient grounds for discounting them. A recorded impact sometimes coincided with bad observation and sometimes didn't. A tare in a D154 traverse linking Wimborne, Broadway, Ashburton and Lanivet led to the deletion of the first part of the traverse. This reduces the instability of the Ashburton value (shown, for example, in Figures 6.15 and 6.16). A list of the data which have been eliminated from the final network adjustment is given in Appendix 2.

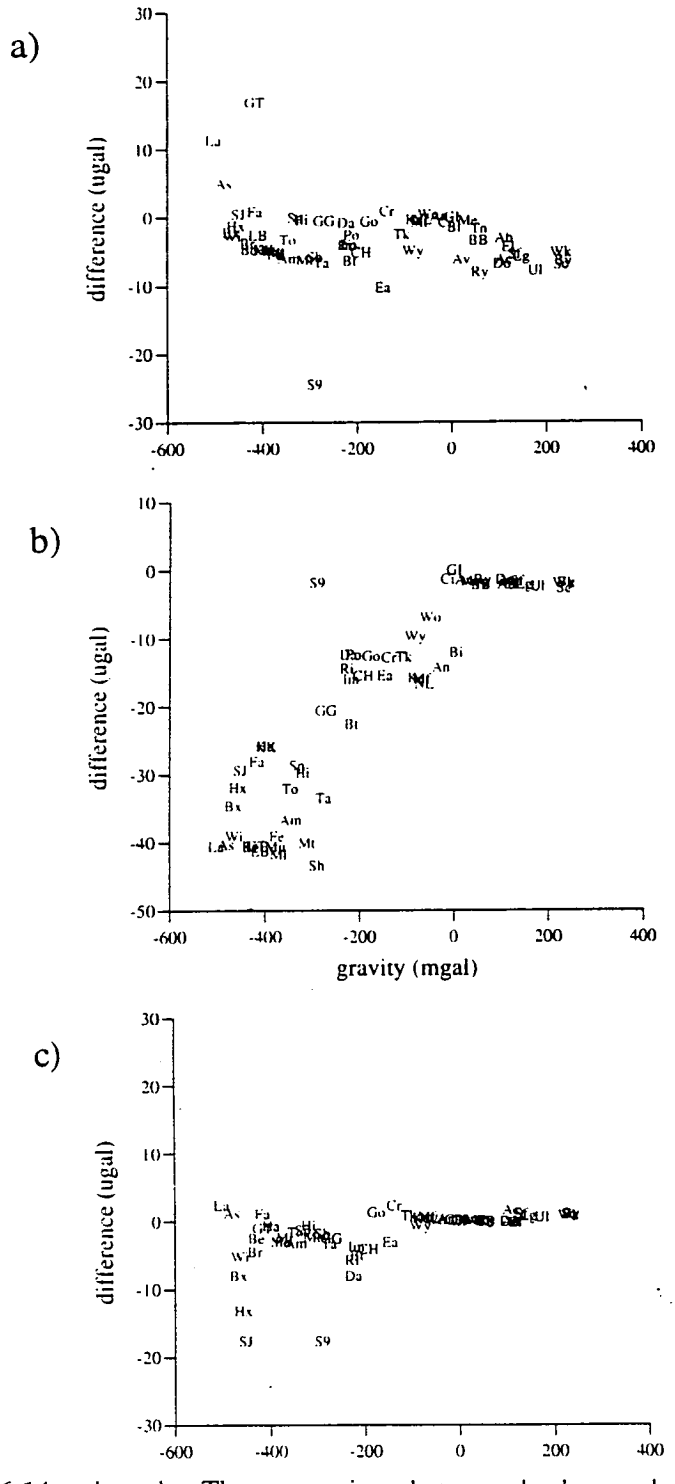

Figure 6.14 a, b and c The comparison between broken and unbroken 'single-instrument' nets for G275, D145 and D154 respectively. a) (G275 net only) shows S9 (unattached) about 19 µgal above Sh (attached). b) (D145 only) shows about 40 µgal difference between S9 and Sh, and a linear change of values for sites with gravity values different from Edinburgh (GI) by -400 to 0 mgal. c) (D154) shows changes in the values at sites along the south coast of England (SJ, Hx) and a separation of 16 µgal between S9 and Sh.

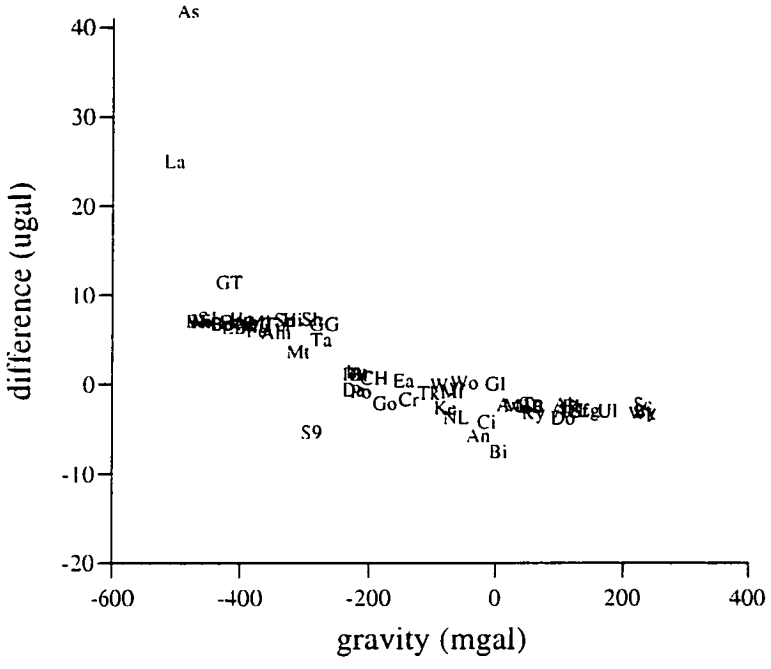

Figure 6.15 The combined net, including a break in all three of the single instrument nets, compared with an unbroken net. Sh is about 10 μgal higher than S9. The combined net is much 'stronger' than any of the three single instrument nets.

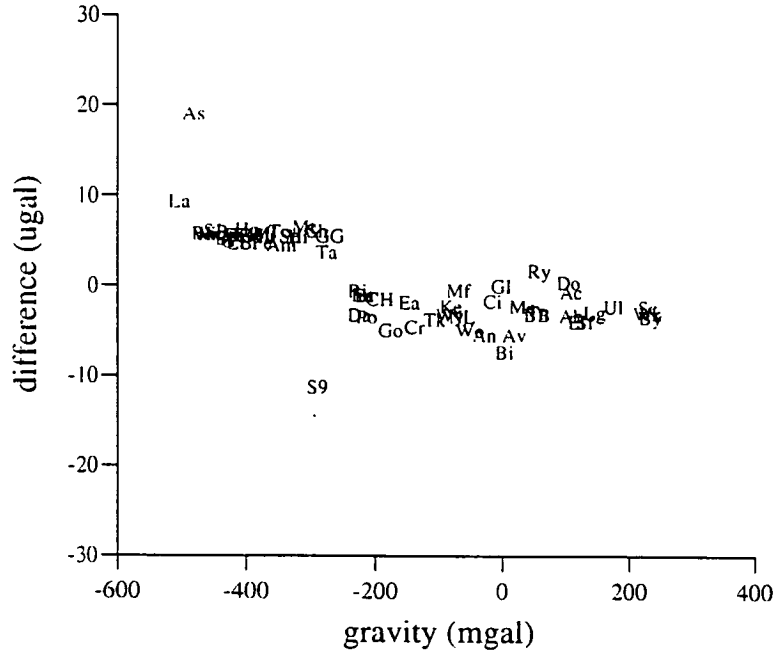

Figure 6.16 Effect of only one instrument failing. Plot of the difference of the solution from a three instrument net with broken G275 leg (i.e only one failure) and an unbroken three instrument net.

6.6 Final Net and Results

6.6.1 Effect of Fixing the Scaling Factor C_f

For most of the methods of testing the network described above, the scaling factor (the term C_f in equation (1)) was held fixed so that the result of the test was not influenced by variations in it. The scaling factors for D145 and D154 with respect to G275 (which is the primary instrument) were determined from a free adjustment of the complete (corrected) dataset using the program NETWORK (section 3.7). When the scaling factors are held fixed at the level determined by the free adjustment, and the same data is adjusted again, the gravity values at most sites change by less than ± 10 μgal. Table 6.14 shows the adjustment statistics for the free and fixed adjustments

BPGN	χ^2	rmse$_{adj}$ (μgal)	rmse G275	rmse D145	rmse D154	C_f D145	C_f D154
free	14.0	7.18	4.41	12.44	17.08	1.000 412 ± 0.000 024	1.000 729 ± 0.000 032
fixed	12.9	7.90	5.15	12.01	17.86	1.000 412	1.000 729

Table 6.14 Effect of fixing the scaling factors for the BPGN adjustment.

Figure 6.17 shows these differences plotted against the adjusted values of the sites from the free adjustment. The points are labelled with the site codes which are listed in Table 6.1. The instability of Lanivet (La) and Ashburton (As) evident in the previous tests is also evident here, and the sites around the Scottish border are most affected (NL, Mf etc.). The Lanivet and Ashburton observations were plagued with battery failure, as well as being on a peripheral loop which is only connected to the rest of the network through the Broadway site.

There are many causes of 'bad' readings, for example poor site conditions (unstable foundations, water table effects); instrumental effects (large drift, 'sticking beam') or observer effects (careless handling of instrument, poor lighting, rain) etc. These events are equally likely to affect any of the network observations. It is therefore more probable that the combination of bad readings with a weak observational sequence is the cause of the instabilities mentioned. Examples of a 'weak' sequence would be when a forward loop is not completed, or when a particular station is observed only once, during a day

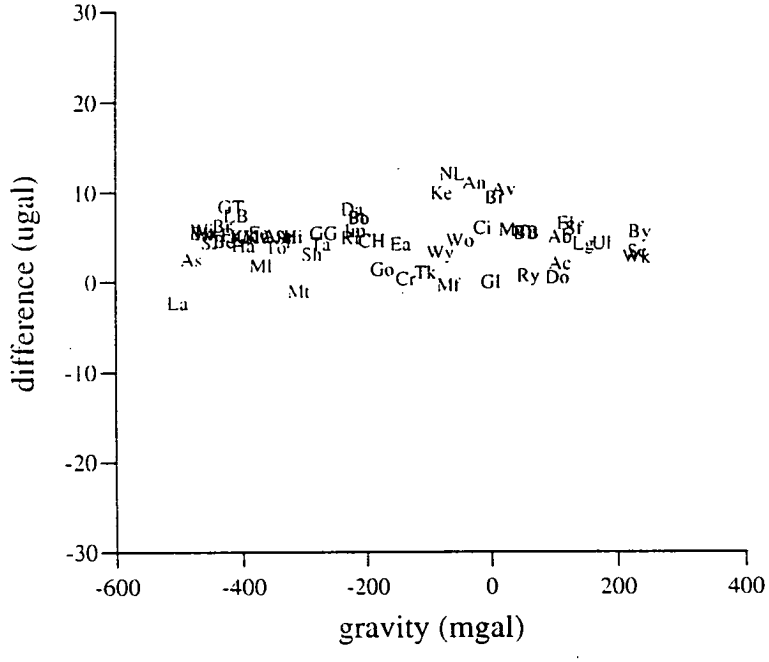

Figure 6.17 Effect of fixing the scaling factor for the whole BPGN adjustment. Most of the gravity values have changed by less than 10 μgal

6.6.2 Single Instrument versus Combined Net

Because the complete net was measured with each of three instruments, the individual nets form three independent 'single-instrument' nets. The relative effect of each instrument on the complete net is shown by the comparison of the relative gravity values from each 'single-instrument' net with the complete net. The program NETWORK operates on the basis of having a pre-selected 'primary' instrument. This was always chosen to be G275 because of its greater reliability (section 6.1.3). The 'primary' instrument always has a scaling factor of one. Figures 6.18 a, b and c show the comparison of the independent G275, D145 and D154 nets respectively with the combined free adjustment. The D145 and D154 values have been multiplied by the scaling factors 1.0004119 and 1.0007291 respectively (Table 6.14) to enable the comparison to be made with the whole net, which is adjusted on the scale of G275. The vertical scale is ± 80 μgal, which is larger than previous plots, in order that the three instruments can be shown on the same scale. The higher quality of G275 is immediately apparent when the Figures 6.18 are compared. The D145 and D154 results are fairly randomly scattered.

6.6.3 BPGN Free Adjustment Results

The 'free' adjustment of BPGN93 consists of 2171 observations made on 157 traverses with 3 LCR instruments. It includes the absolute sites at Edinburgh and NPL1, and the ex-centres at Loading Bay and South Porch for the Taunton and POL absolute sites respectively. The observations have been pre-processed with the program REDUCE (section 3.4) and corrected for the earth tide, ocean load tide and atmospheric pressure. The earth tide correction includes the static term. Of the original 2234 field observations, 63 have been rejected (Appendix 2) on the basis of thorough testing as described in sections 6.4 and 6.5. The 374 unknowns (58 gravity values, 314 drift parameters and 2 scaling factors) were solved for using the program NETWORK. The results of the BPGN93 adjustment on the scale of G275 are given in Table 6.15 (next page). The factor 1.000622 ± 0.000027 converts these values to the scale of IGSN71 (Hipkin et al. 1988). The FG5 constrained adjustment (next section) provides a new scaling factor the the'FG5 absolute' scale.

ref	Name	gravity (ugal)	s.e (ugal)	weight	code	n
140	GI 140 Floor	00 000.0	2.3	71.080	GI	91
11	Aberdn St.M	109 198.5	4.4	26.977	Ab	29
13	Bishopton	3 781.9	3.2	41.203	Bi	59
15	Moffat TH	-68 301.9	2.7	48.653	Mf	71
17	Crooklands	-137 413.5	5.5	25.637	Cr	30
18	Goosnargh	-175 793.8	5.8	12.555	Go	14
19	Daresbury	-224 898.1	6.1	60.677	Da	55
24	POL S Porch	-213 033.2	6.8	13.339	Po	12
201	Wooler	-50 357.1	3.9	24.425	Wo	24
202	Wylam	-82 689.9	4.4	22.326	Wy	26
203	Easby	-146 445.9	5.4	18.404	Ea	22
204	Chapl Had	-191 855.8	5.8	70 095	CH	73
205	Gt Gonerby	-270 096.0	6.3	30.886	GG	37
206	Histon	-319 125.3	6.5	45.714	Hi	44
207	Sproughton	-331 537.6	6.8	17.173	Sp	20
208	Farningham	-417 458.5	6.9	29.906	Fa	32
209	St.J Comdry	-451 786.6	7.3	26.880	SJ	26
210	Hstmnceux	-456 886.9	7.4	23.889	Hx	28
211	Boxgrove	-466 479.8	7.3	20.898	Bx	25
212	Wimborne	-464 419.3	7.1	45.269	Wi	45
213	Broadway	-432 301.6	7.0	86.007	Br	87
52	Loading Bay	-409 838.7	7.1	39.247	LB	37
214	Ashburton	-481 506.1	7.6	15.145	As	19
215	Lanivet	-502 847.3	8.2	10.516	La	24
216	Gt Torngtn	-417 538.6	7.4	25.668	GT	29
217	Mounton	-377 984.1	6.6	58.202	Mu	59
218	Malvern	-370 897.5	6.7	20.028	Ml	25
219	Shareshill	-289 559.5	6.3	43.176	Sh	54
220	Beedon	-429 401.9	6.7	42.976	Be	50
222	Hampton Ch	-399 167.9	6.9	38.507	Ha	34
33	KK1 NPL1	-397 582.8	7.3	20.481	KK	19
223	Towcester	-347 001.7	6.5	35.587	To	35
224	Montgomery	-310 569.1	7.0	9.563	Mt	15
225	Talybont	-275 516.4	6.6	35.758	Ta	34
226	Talkin	-106 318.0	5.0	14.932	Tk	31
230	Immingham	-218 714.5	6.0	32.939	Im	38
231	Rishworth	-226 603.2	6.1	18.531	Ri	21
232	Felindre	-374 742.9	6.9	17.567	Fe	22
233	Ambleston	-345 535.5	7.0	25.380	Am	26
234	Betws	-216 727.9	6.5	21.769	Bt	29
240	Methven	32 544.3	2.6	32.025	Me	43
241	Tannadice	56 974.2	4.0	34.066	Tn	43
242	Bry Budn VLBI	55 311.7	4.7	12.586	BB	20
243	Elgin South	117 742.4	4.2	37.762	El	45
244	Strathpeffer	130 997.3	4.3	50.516	Sf	71
245	Lairg	145 931.2	4.6	66.463	Lg	64
246	Wick	229 522.7	5.2	30.116	Wk	34
247	Betyhil FBM	234 226.9	5.2	27.840	By	43
248	Scourie	230 334.4	5.8	22.102	Sc	29
249	Ullapool Mus	175 694.2	4.6	29.594	Ul	42
250	Achnashn FBM	108 717.6	4.4	26.798	Ac	37
251	Dornie	105 293.0	4.6	26.459	Do	29
252	Roybridge	58 380.7	4.1	28.194	Ry	41
253	Alvie	19 262.3	4.1	29.406	Av	53
254	Crinlrch FBM	-14 977.4	3.3	29.009	Ci	41
255	Annbank	-27 994.5	4.0	27.110	An	33
256	New Luce	-62 879.9	4.5	28.836	NL	25
257	Kelton	-80 422.8	3.9	25.412	Ke	27
					Total	2171

Chi squared = 13.973 with 14 degrees of freedom

RMS weighted error of the adjustment = 7.18 ugal

RMS unweighted error for meter 1 = 4.41 ugal
RMS unweighted error for meter 2 = 12.44 ugal
RMS unweighted error for meter 3 = 17.08 ugal

Corr'n to scale factor = 1.0004119 +/- 0.0000238
Corr'n to scale factor = 1.0007291 +/- 0.0000321

Table 6.15 BPGN Free adjustment

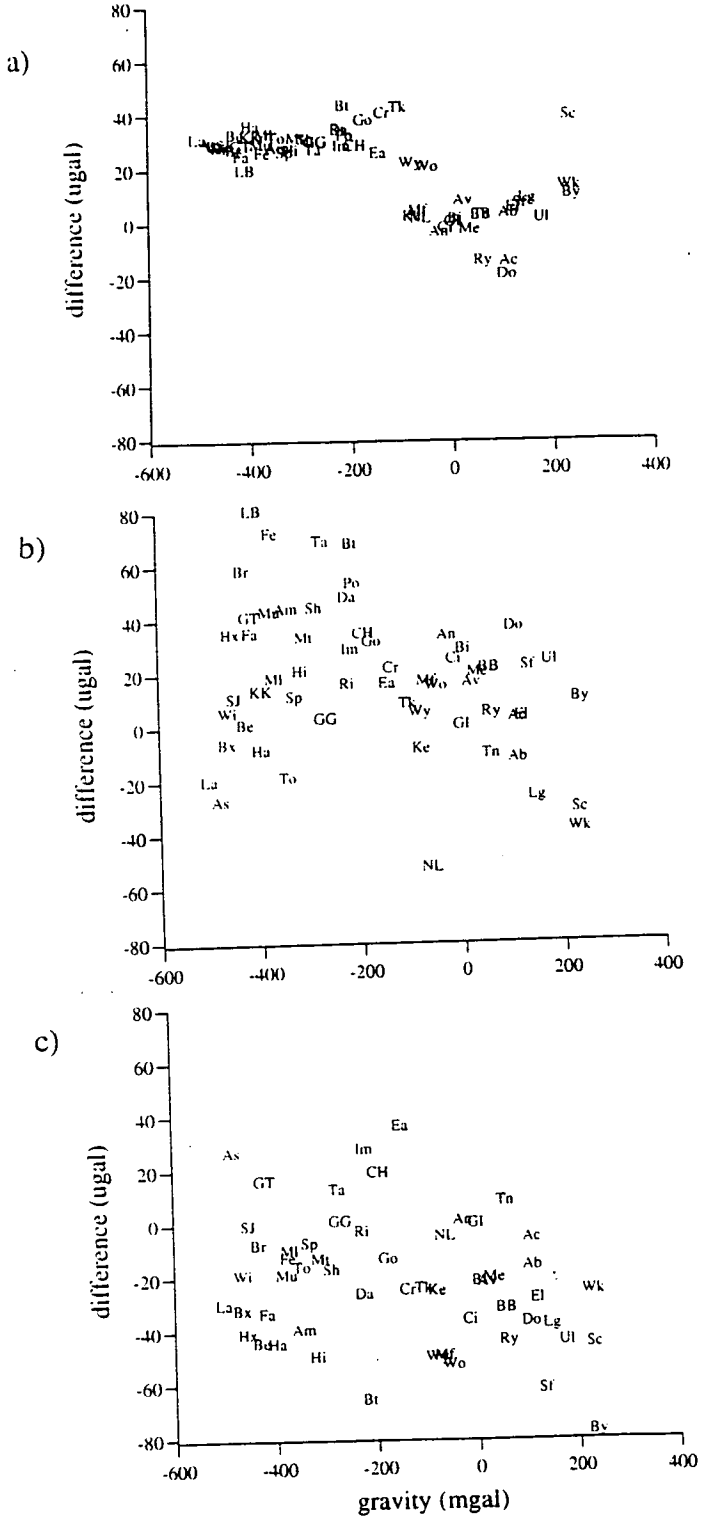

Figure 6.18 Showing the different influence of the independent G275 (a), D145 (b) and D154 (c) nets on the combined free adjustment. The D145 and D154 values have been multiplied by the scaling factors 1.0004119 and 1.0007291 respectively. The standard deviation of the differences is 15.7, 27.3 and 23.9 μgal for a, b and c respectively.

6.6.4 BPGN FG5-Constrained Adjustment Results

By constraining the absolute gravity values at four sites in the network adjustment, a test of the consistency of the BPGN relative observations with absolute FG5 observations has been made. A new scaling factor for G275 to the FG5 absolute scale can be found. The absolute values at 12 cm above the floor at Edinburgh, POL, NPL1 and Taunton from Chapter 5 are summarised in Table 6.16.

	gravity at 120 mm (μgal)	difference from Edin.GI (μgal)
Edinburgh GI	981 579 544.8 ± 2.3	000 000.0 ± 2.3
POL1	981 367 644.3 ± 4.3	-211 900.5 ± 4.9
NPL1	981 181 710.5 ± 7.4	-397 834.3 ± 7.7
Taunton	981 169 188.4 ± 3.2	-410 356.4 ± 3.9

Table 6.16 FG5 absolute values at 120 mm above the floor for the absolute sites. The values include the system response corrections from section 5.3.5.

To compare the effect of constraining the FG5 stations, the absolute ex-centre links (section 6.2.2) needed to be added to the BPGN observations. The triangular sequence at Taunton (Loading Bay-Challenger Absolute-Water Tank) and the POL (South Porch-POL1) are included. The adjustment of these 2256 observations is called BPGNA.

The four FG5 values (differences from Edinburgh in Table 6.16) are included in the data as 'traverse zero' (section 3.7.5), and FG5 is the primary instrument for this adjustment. There is no drift for traverse zero, and no blunderweighting for the FG5 observations. FG5 is assigned an rms weight of 3 μgal. The program NETWORKA incorporates the necessary modifications. The adjustments with and without the FG5 observations are compared in Figure 6.19a.

The figure shows that the POL (Pl at -200 mgal) and Taunton (Tu) absolute sites have negative residuals, but that NPL1 (KK) has a large positive residual. The standard deviation of the residual values is 9.0 μgal. The absolute and relative observations should only differ by a constant scaling factor, but the figure shows that this hypothesis cannot be sustained.

If the apparently anomalous absolute observation at NPL1 is excluded, then the agreement between the relative and absolute values is much improved (Figure 6.19b). The standard

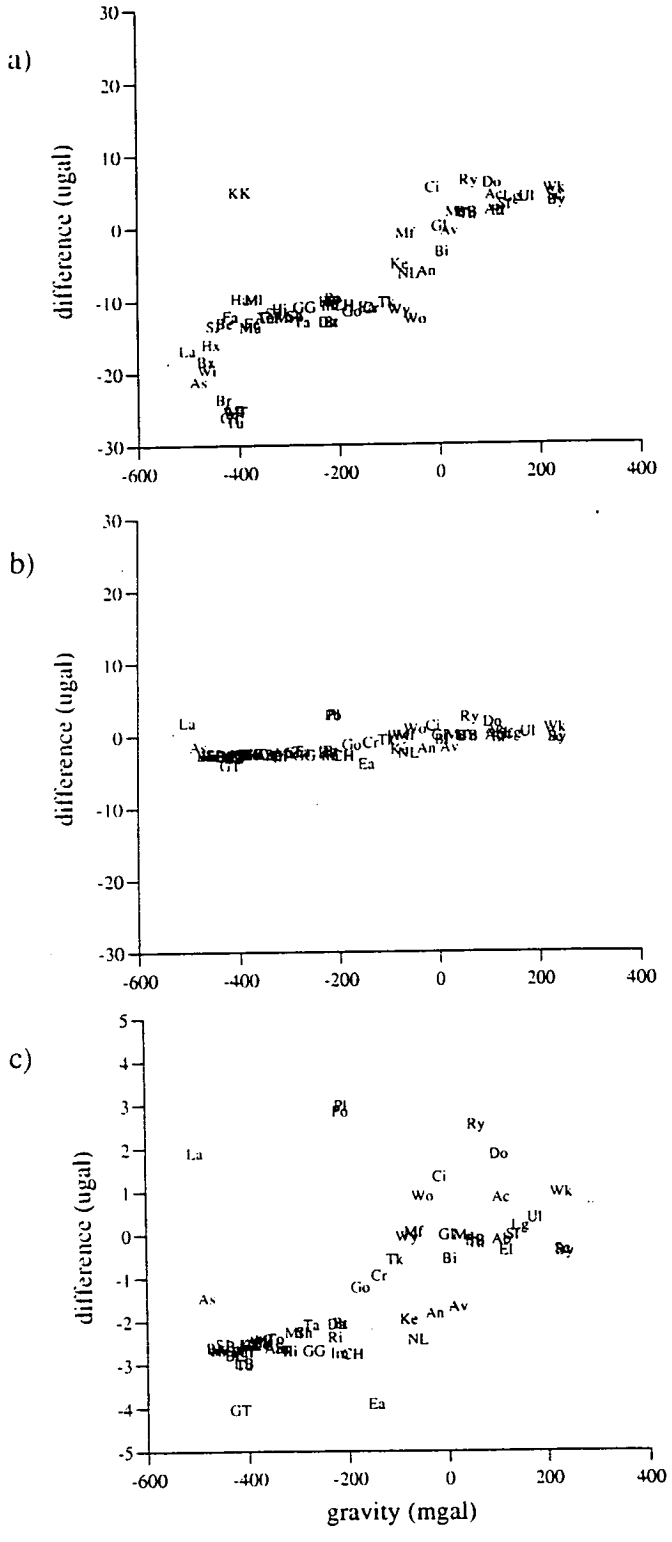

Figure 6.19 a) Comparison of the adjustment solutions with and without constraint by the FG5 observations. b) As (a), but without the absolute observation at NPL1, showing an improvement in the agreement between the relative and absolute values. c) is the same as Figure 6.19b, but at an expanded scale to show the detail. The standard deviation on the differences is 9.0 and 1.7 μgal respectively for (a) and (b). The values plotted are the result of the 'FG5 constrained' minus the 'free' adjustment.

deviation of the scatter is reduced to 1.7 μgal. Figure 6.19c is the same as Figure 6.19b, but at an expanded scale to show the detail. Table 6.17 shows the adjustment statistics for the BPGNA adjustment (relative values only, including links to the absolute sites) and the FG5 constrained adjustments with and without the NPL1 absolute observation. The original BPGN adjustment without the links to the absolute sites is included for comparison. The scaling factors C_f are with respect to the primary instrument (FG5 or G275). The gravity values for the 'BPGNA+FG5 (no NPL1)' solution are given in Table 6.18

	BPGN (free)	BPGNA (inc links to abs)	BPGNA+FG 5 (with NPL1)	**BPGNA+FG5 (no NPL1)**
total observations	2171	2256	2260	**2259**
χ^2	14.0	19.0	14.64	**14.3**
rmse adjustment (μgal)	7.18	7.26	7.08	**7.27**
rmse for FG5 (μgal)	-	-	3.00	**3.00**
rmse for G275 (μgal)	4.41	4.60	4.42	**4.56**
rmse for D145 (μgal)	12.44	11.94	12.05	**12.11**
rmse for D154 (μgal)	17.08	17.81	18.26	**18.07**
C_f for G275	1.000 0000	1.000 0000	1.000 689± 0.000 018	**1.000 757± 0.000 021**
C_f for D145	1.000 420± 0.000 024	1.000 389± 0.000 023	1.001 100± 0.000 027	**1.001 154± 0.000 029**
C_f for D154	1.000 729± 0.000 032	1.000 743± 0.000 033	1.001 409± 0.000 037	**1.001 489± 0.000 037**

Table 6.17 Comparison of the BPGN adjustments.

The values obtained by dividing the D145 and D154 scaling factors (1.001 154 and 1.001 489 respectively) by the 'G275 scaling factor to FG5' (1.000 757) are 1.000 397 for D145 and 1.000 731 for D154, which are consistent with those obtained from the unconstrained adjustments. The scaling factor of 1.000 757 ± 0.000 021 for G275 from the FG5 constrained adjustment (no NPL1) is a new conversion for G275 to the absolute scale. The previous scale factor for G275 to IGSN71 was 1.000 622 ± 0.000 027, which was found by measuring the interval between IGSN71 sites at Edinburgh and Rome in 1986 (Hipkin *et al.* 1988) with G275. These two values are inconsistent but the FG5 value is more likely to be closer to the true scaling factor for the portion of the measuring screw of G275 used for

ref	Name	gravity (ugal)	s.e (ugal)	weight	code	n
140	GI 140 Floor	00 000.0	2.9	76.175	GI	92
11	Aberdn St.M	109 281.3	6.0	27.243	Ab	29
13	Bishopton	3 785.3	3.9	38.615	Bi	59
15	Moffat TH	-68 352.9	3.0	48.234	Mf	71
17	Crooklands	-137 509.3	4.4	25.250	Cr	30
18	Goosnargh	-175 918.5	4.5	12.357	Go	14
19	Daresbury	-225 059.8	3.4	59.701	Da	55
20	POL Abs1	-211 901.0	2.7	26.938	Pl	13
50	Taunton Abs	-410 356.3	2.9	36.469	Tu	23
53	Water Tank	-410 235.1	3.5	24.472	WT	19
24	POL S Porch	-213 182.4	3.1	32.770	Po	24
201	Wooler	-50 382.1	4.0	25.792	Wo	24
202	Wylam	-82 742.1	4.0	22.140	Wy	26
203	Easby	-146 551.3	4.5	15.955	Ea	22
204	Chapl Had	-191 995.1	4.1	73.128	CH	73
205	Gt Gonerby	-270 288.6	4.3	30.566	GG	37
206	Histon	-319 355.8	4.3	44.791	Hi	44
207	Sproughton	-331 777.4	4.7	16.824	Sp	20
208	Farningham	-417 762.9	5.4	29.225	Fa	32
209	St.J Comdry	-452 116.7	6.0	26.433	SJ	26
210	Hstmnceux	-457 220.0	5.9	23.495	Hx	28
211	Boxgrove	-466 819.6	5.6	20.488	Bx	25
212	Wimborne	-464 757.3	5.1	44.536	Wi	45
213	Broadway	-432 614.0	4.0	84.852	Br	87
52	Loading Bay	-410 133.9	3.4	64.822	LB	57
214	Ashburton	-481 855.7	5.5	14.973	As	19
215	Lanivet	-503 212.0	6.2	13.042	La	24
216	Gt Torngtn	-417 839.4	4.8	25.054	GT	29
217	Mounton	-378 261.1	4.3	52.755	Mu	59
218	Malvern	-371 171.3	4.4	23.072	Ml	25
219	Shareshill	-289 769.9	3.7	42.405	Sh	54
220	Beedon	-429 716.2	5.1	42.274	Be	50
222	Hampton Ch	-399 459.2	5.1	38.013	Ha	34
33	KK1 NPL1	-397 872.6	5.7	20.303	KK	19
223	Towcester	-347 254.3	4.2	34.951	To	35
224	Montgomery	-310 795.0	4.9	9.817	Mt	15
225	Talybont	-275 715.6	4.2	35.044	Ta	34
226	Talkin	-106 390.7	4.3	14.868	Tk	31
230	Immingham	-218 873.1	4.3	32.462	Im	38
231	Rishworth	-226 768.2	4.0	18.329	Ri	21
232	Felindre	-375 018.2	4.9	17.120	Fe	22
233	Ambleston	-345 789.6	5.0	22.167	Am	26
234	Betws	-216 883.1	4.1	21.401	Bt	29
240	Methven	32 570.1	4.2	31.501	Me	43
241	Tannadice	57 018.4	5.1	33.806	Tn	43
242	Bry Budn VLBI	55 354.3	5.8	12.323	BB	20
243	Elgin South	117 832.2	6.0	37.280	El	45
244	Strathpeffer	131 097.0	6.2	49.542	Sf	71
245	Lairg	146 041.3	6.6	65.864	Lg	64
246	Wick	229 695.7	8.1	29.797	Wk	34
247	Betyhil FBM	234 403.8	8.2	27.187	By	43
248	Scourie	230 507.6	8.6	21.726	Sc	29
249	Ullapool Mus	175 827.3	7.0	28.943	Ul	42
250	Achnashn FBM	108 799.9	6.1	26.571	Ac	37
251	Dornie	105 372.8	6.2	26.214	Do	29
252	Roybridge	58 425.2	5.3	27.985	Ry	41
253	Alvie	19 278.9	5.1	29.255	Av	53
254	Crinlrch FBM	-14 987.1	4.2	28.535	Ci	41
255	Annbank	-28 014.5	4.5	26.517	An	33
256	New Luce	-62 925.8	4.8	28.316	NL	25
257	Kelton	-80 482.1	4.3	24.679	Ke	27
					Total	2259

Chi squared = 14.325 with 14 degrees of freedom

RMS weighted error of the adjustment = 7.27 ugal

RMS unweighted error for meter 1 = 3.00 ugal

RMS unweighted error for meter 2 = 4.56 ugal

RMS unweighted error for meter 3 = 12.11 ugal

RMS unweighted error for meter 4 = 18.07 ugal

Corr'n to scale factor = 1.0007565 +/- 0.0000210

Corr'n to scale factor = 1.0011542 +/- 0.0000286

Corr'n to scale factor = 1.0014893 +/- 0.0000371

Table 6.18 BPGNA+FG5 :BPGN including links to absolute sites, adjustment constrained by FG5 observations (except NPL1).

the BPGN. Hipkin *et al.* (1988) make the following comments on the accuracy of their result:

'It is legitimate to question whether (the) formal error estimates are realistic, especially when the largest source of error in the whole international gravity connection....actually comes in the 15 km link between Edinburgh and Penicuik!'

Their connection relies on only one double link between Edinburgh A and Athens Airport.

Comments on the exclusion of the NPL1 result

It is unfortunate to have to exclude the NPL1 result from the already rather small number of absolute values available for the BPGN-FG5 adjustment. Figure 6.19a shows that NPL1 is inconsistent with POL and Taunton by about 13 and 30 μgal respectively, i.e. it is higher than the scaled relative result by these amounts.

The NPL1 value is a weighted mean of two sets from FG5-103 and two sets from FG5-105 obtained during the simultaneous occupation of NPL in July 1993 (section 5.6). It includes an estimate of the system response correction of +10.8 ± 6.3 μgal, calculated from the FG5-103 dataset NPL0307A. The discussions of section 5.3 showed that the structure in the fringe residuals had a particularly large amplitude, and very little decay compared to data from other sites. This correction at NPL1 is larger than those for Edinburgh, POL and Taunton, which were 5.4 ± 2.2, 3.8 ± 2.6 and -1.4 ± 2.8 μgal respectively (section 5.3.5). If the methods of 5.3 have not been successful, then the NPL1 value may be incorrect. The FG5-105 values were almost the very first taken with it after its delivery. It has a shorter drop than FG5-103, so a drop length correction of -3.2 ± 2.4 has been applied. The NPL1 absolute value is the only one which includes data from an instrument other than FG5-103. The weighted mean of the FG5-105 sets was 7.9 ± 8.0 μgal higher than the FG5-103 weighted mean (section 5.6.3).

In spite of all these caveats, the apparent consistency of the remaining three FG5 values is encouraging, and it is suggested that the NPL1 absolute value is wrong for other reasons. One possibility is the effect of groundwater at NPL, which is sited on aquiferous sediments. The effects of groundwater on gravity were described in section 3.3.3, and variations of potentially more than 10 μgal could be caused by the fluctuating water table. Without permanent hydrological monitoring, the actual effect is very difficult to predict. It is hoped that NPL will continue their absolute gravity measurements in the near future, and the author eagerly awaits their results.

6.7 Summary and Conclusions

The BPGN was established to provide a baseline from which to measure vertical crustal movements. Current rates of uplift in Britain are about 5 mm per year over a 1000 km baseline. A 10 mm change in absolute height causes a gravity change of about 2 μgal. The precision of between 2 and 8 μgal on the gravity values of BPGN sites should enable current rates of uplift to be measured in a period of less than 10 years. The observation of the net took place between 1992 and 1993 and the 58 specially chosen sites were measured in a carefully designed sequence with three LCR relative gravity meters.

The BPGN dataset and the adjustment model have been thoroughly tested, and in doing so, some discrepant observations have been identified. Where the cause of the discrepancies can be attributed to a definite event, such as a battery failure, the observations have been deleted. The appropriateness of fitting a different linear drift line to each daily traverse has been confirmed for many samples of BPGN data. Alternative models have also been tried, and the relative importance of the drift parameters to the general solution has been determined. The influence of the characteristic instrumental drift of G275 and D145 on the adjustment of datasets with long (1 hour) and short (10 minute) time intervals between readings has been noted.

The investigations of the drift model and the results of the SVD tests have shown that the gravity values are much more strongly determined than the linear drift parameter b_k. (The parameter a_k is simply a constant related to the gravity at the first site of each traverse). It is noted that the adjustment model of NETWORK allows outlying observations (which resulted in gravity values much higher or lower than the mean) to be absorbed into the free parameters b_k and C_f (the scaling factor).

The investigations of loops and legbreaking have shown the consistency of the various regions of the network and identified a small number of weak areas. These are the sections Wooler-Wylam-Easby-Chapel Haddlesey in north-east England; Crooklands-Goosnargh in north-west England; Lanivet and Ashburton in the extreme south-west of England; New Luce in south-west Scotland, and Wick-Bettyhill-Scourie in the far north of Scotland. These are the 12 stations (from the total of 58) which should be reobserved at the earliest opportunity.

Although not mentioned specifically in the examples given, the links to two of the absolute sites have also demonstrated some instability. The Taunton (Loading Bay) to Broadway link and the NPL to Hampton Church link need to be reobserved. The author strongly suggests that all the absolute ex-centres should be linked to three or four other network sites in the same way as the main BPGN stations. The property that the gravity differences around a loop must sum to zero is the main advantage of observing in a networked sequence, and it should be used to the full. The gravity differences and geographical distances between the absolute ex-centres and the linking BPGN sites are small, so it was felt that such effort was not necessary. However, because of the prime importance of these links in the relative-absolute comparison (section 6.6), the effort *is* justified. It is unfortunate that many of the absolute sites are located within secure compounds (for example the Hydrographic Office at Taunton) so the logistics of access and the bureaucratic procedures are an additional hindrance to the effective observation of these links.

The free adjustment of the links between the 58 BPGN sites has an rms of 7.18 μgal. The absolute gravity meter FG5-103 has measured at four sites, and these have been linked to the BPGN. Unfortunately, the links between the BPGN and some absolute sites are found to be weak, and it is recommended that they be re-observed. The absolute values measured by FG5-103 (Chapter 5) are introduced with a fixed nominal standard error of 3 μgal, and are used to constrain the adjustment. The combined 'BPGNA+FG5' solution shows up a discrepancy of about 30 μgal in the NPL1 absolute value. When this value is excluded, the relative and absolute results are consistent to about 7 μgal. A new scaling factor of 1.000 757 ± 0.000 021 converts G275 results to the absolute scale of FG5-103.

CHAPTER 7. Conclusions and Further Work

7.1 Conclusions

Measuring vertical crustal movements in Britain

Tide gauge data and geomorphological indicators suggest that Scotland is rising and the south east of England is subsiding with respect to an axis oriented approximately SW-NE crossing the north of England. Consequently, the maximum differential rates of uplift is about 5 mm per year over a 1000 km baseline. Assuming that 10 mm of uplift causes a change in gravity of about 2 μgal, the precision obtained for the British Precise Gravity Network 1993 (BPGN93) should enable crustal motions to be detected in less than a decade. The BPGN has a range of 900 mgal and standard errors of 2 - 8 μgal. It was measured simultaneously with three LaCoste & Romberg gravity meters, and includes absolute gravity observations from FG5-103. It has two sites near to primary position fixing centres.

Calibration of relative gravity meters

The calibration of the relative gravity meters is of utmost importance for precise surveys. The linear scaling factors for these instruments were previously determined on the IGSN71, but by constraining the BPGN adjustment with FG5, a new scale factor has been determined. A search for periodic errors in the unique double-dial instrument D145 found an apparent period of 404 coarse dial turns which is unexpected from the known gear ratios. The amplitudes and frequencies of other CD periodic errors were determined but when the calibration function of D145 was corrected, apparent periodic errors appeared for G275. The phase of the correction term for G275 was found to correspond with that for D145 suggesting a dependence between the two results. It was concluded that the apparent periodic errors were spurious. The spring hysteresis model explains well the behaviour observed in many of the sequences. Importantly, the discussion of the model has shown the limitations of using least squares for adjusting sequences which are symmetrical about the central time.

Tidal corrections

The oceanic tides cause periodic loading of the crust, which has an effect which is regionally variable with an amplitude range of 1 to 12 μgal in Britain. For the duration of the BPGN fieldwork, the solid earth tide and ocean load corrections had typical amplitudes

of 90 and 6 μgal respectively. A comparison of the elastic tidal corrections from a full Cartwright-Tayler-Edden expansion with a closed calculation for 24 hour periods on three different dates show that they differ by less than 0.5 μgal. Inconsistent treatment of the static tide leads to confusion and error, and the various approximations of the I.G.C formula, commonly used to estimate it, give answers different by up to 2.4 μgal.

The correct treatment of tidal and atmospheric pressure disturbances and the use of appropriate statistical models is important when very high precision is sought. The procedure used for the adjustment of gravity datasets must succeed even when the dataset is very small and/or it is of poor quality. Appropriate modifications to a standard least squares adjustment have been described.

The 'effective measurement height' for free-fall absolute gravity meters

The intercomparison of absolute gravity meter data requires that all observations be corrected to the same datum. When the vertical gradient of gravity is not included in the equation of motion for free-fall observations, the gravity estimate is some average value over the drop length, and is assigned to the 'effective measurement height' (h_{eff}). When this simple equation of motion is used, h_{eff} has been estimated to be about 1/3 of the way down the drop. Both the least-squares (LSS) and continuous least-squares (CLS) estimates of Niebauer (1989) predict a value for the ratio $h_{eff}/\Delta z$ (Δz is the drop length) lower than that which is observed, which for FG5 is found to be consistently about 0.43. The failure of the observed value of the ratio $h_{eff}/\Delta z$ to agree with the theoretical predictions is due to missed fringes. For FG5-103, it is found that although 150 fringes are fitted, and time and distance are always correctly associated, an average of 16 fringes are missed, which is about 10 % of the total number. This increases the actual length (Δz) by 10 % and then the agreement between the observed fraction and the CLS estimate of Niebauer is improved. However, the 'effective measurement height' remains poorly determined, and the equation of motion used must include the vertical gradient terms. Observations made with the simple equation cannot be compared with those using the full equation unless the original time-distance data is still available.

Non-linear vertical gradients

For the purposes of the Vertical Gradient (correction to the 'top of the drop') and Datum Corrections (transfer to a datum height, for example to 1 metre above floor level) to absolute gravity measurements, the vertical gradient must be known. Gradients at British absolute sites have been carefully observed by the author and techniques for optimising the accuracy of these corrections have been developed. It is important to use the value of the gradient averaged over the drop length for fitting the full equation of motion which gives an estimate of gravity at the top of the drop. For the Datum Correction, it is not sufficiently accurate to multiply the height difference by the same average vertical gradient. The actual gravity difference between the two heights must be used. If this gravity difference between the two heights has not been measured directly, then the variation of gravity with height may be determined by fitting the available gravity-height data with low order polynomials.

Variation in gravity estimate with drop length

Before a comparison of different instruments at different sites can be made, the individual gravity estimates have to be made equivalent. The unique characteristics of each FG5 instrument may cause the estimate of gravity to vary with the length of its drop. Because the drop length of FG5-103 was changed from 90 to 150 fringes during its first upgrade, a correction of about 23 μgal is needed to reconcile pre and post upgrade observations. Most FG5s have a drop length of between 130 and 160 fringes, so the 'drop length correction' is reduced to less than 4 μgal. It would be much more satisfactory if all FG5s counted exactly the same number of fringes all of the time.

The variation in gravity estimate with drop length is related to structure in the fringe residuals, which has an amplitude of up to 0.6 nm for FG5. If the fringe positions are corrected with the average residuals, the gravity estimate becomes constant. When the residuals are stacked over a large number of drops, the structure is seen to depend on the particular instrument and the site. The structure is caused by imperfections in the drop and catch of the falling mass, and by vibrations of the instrument-floor system. Although different in origin, both effects can be modelled by damped sinusoids.

Modelling the structure in the fringe residuals with damped sinusoids

The frequency and decay rate of the sinusoids were found from the stacked residuals in two ways : a Chebychev interpolation followed by a Fourier transformation; and a least squares search. In order to rid the gravity estimate of the influence of the sinusoids, they have to

fitted at the same time as gravity. The amplitude and phase vary with each drop, so simply correcting with two or three sinusoids having an average, but fixed, amplitude and phase is not successful. The amplitude and phase have to be included as unknowns in the observation equation. Because the fit to the distance time pairs is parabolic, it is the lower frequency sinusoids which have the greatest influence on the estimate of gravity.

The largest sinusoidal component in FG5-103 residuals typically has a frequency of about 8 Hz and an amplitude of about 0.6 nm. This sinusoid causes a change of between 2 and 6 μgal in the estimate of gravity, depending on the instrument and site. The remaining residuals have smaller sinusoids at about 50 and 30 Hz, but these have only a barely significant effect on the estimate.

By including the damped sinusoids in the equation of motion, the variation in drop length is reduced, and the 'system-response correction' can be estimated. For FG5-103 at POL, Edinburgh, NPL and Taunton, the system-response correction has been estimated as 3.8 ± 2.6, 5.4 ± 2.2, 10.8 ± 6.3 and -1.4 ± 2.8 μgal, respectively. (For the comparison of FG5-103 with FG5-105 at NPL, and with FG5-107 at Taunton, the system response correction was not included, because it has only been determined for FG5-103.)

Comparison of FG5 values at British absolute sites

Between August 1992 to August 1994, FG5-103 was upgraded three times, and the data taken at POL for this period is wide-ranging in quality and repeatability. During this period, the estimate of gravity from FG5-103 varied by up to 40 μgal. It is possible to correct for some of the different configurations of FG5-103 between upgrades, but comparisons with JILA4 and other FG5 instruments demonstrate that FG5-103 did not perform according to its specification until November 1993. However, observations made at NPL in June 1993 agreed with FG5-105 to within one standard deviation, and observations made in July 1994 at Edinburgh give a good agreement with a JILA4 observation made there in 1989. The estimate for gravity at the top of the drop (at 1309 mm) at POL1 from two sample sets taken in June and August 1994 is 981 367 361.1 ± 0.2 μgal.

In 1992, FG5-103 measured in Edinburgh at both BGS and GI, but the 're-occupation' tests of 1992 show that there is an inconsistency of 22 μgal in the difference in gravity between the 1309 mm datum at BGS and GI, as measured by FG5-103 and relative gravity instruments. The comparison of the JILA4 observation made in 1989 at BGS with the FG5-103 observation made in 1994 at GI shows that JILA4 89 is lower than FG5 94 by

2.5 ± 8.8 μgal when compared at 1309 mm at BGS. The weighted mean of the July 1994 occupation is 981 579 187.1 ± 0.7 μgal at 1309 mm in GI.

The success of the FG5 (1994) and JILA (1989) comparison shows that the transfer by relative observations of 527.9 ± 5.7 μgal has been made with adequate precision and accuracy for a good comparison of absolute instruments which observed at different sites. Transfers of similar magnitude are a vital part of the international comparisons, where relative observations are needed to transfer the absolute values to a common site and to measure the vertical gradients. Boulanger *et al.* (1991) find that relative and absolute observations made during the ICAG in Sèvres also give generally consistent results.

A new British Fundamental Gravity Station (BFGS93) has been established at the National Physical Laboratory (NPL), to replace Teddington A which will shortly be lost due to building reconstruction. The vertical gradients measured at Teddington A, NPL1 and NPL2 were found to be very similar, which suggests that they are also likely to be linear at these sites. FG5-103 and FG5-105 observed simultaneously at the BFGS93 in July 1993. The difference between the weighted means of the FG5-103 and FG5-105 results at 120 mm at the BFGS93 is just insignificant at 7.9 ± 8.0 μgal, although the individual occupation means at the respective measurement heights at NPL1 and NPL2 suggest that there may be a systematic difference between the instruments. A drop length correction of -3.2 ± 2.4 μgal has been applied to the gravity estimate of FG5-105 because of its shorter drop length (130 fringes compared to 150 for FG5-103). The weighted mean of the July 1993 occupations of FG5-103 at NPL2 is 981 181 343.1 ± 1.5 μgal at 1312 mm.

A comparison of absolute observations made at NPL since 1939 shows that determinations by Cook (1967), Hammond-Faller (1971) and IMGC (1987) agree with the FG5 value within their stated errors, but the value assigned to Teddington A in the IGSN71 adjustment is too low by about 30 μgal. The pendulum observation made by Clark in 1939 is different from FG5 by only 70 μgal. The FG5 value (a combined estimate from FG5s 103 and 105) is higher than the BPGN93 value by about 15 μgal. At the time of these observations, FG5-105 had only been operating for a few weeks, and at the end of the occupation, the laser on FG5-103 failed. These reasons, and the lack of knowledge of the gravity effect of groundwater in the aquiferous rocks underlying the site, suggest that FG5 should reobserve at NPL soon, and that absolute gravity should be monitored regularly, if not continuously, using the NPL's FG5-105.

FG5-107 observed at the Hydrographic Office in Taunton in September 1993, and FG5-103 observed there in July 1994. The instruments have slightly different operating heights, so the FG5-107 value has been corrected to the FG5-103 height for comparison. The occupation means are compared in at 1315 mm above the stone plinth at the Challenger site. The FG5-103 value of 981 168 833.0 ± 1.3 μgal and the FG5-107 value of 981 167 848.1 ± 3.4 μgal differ by 15.1 ± 3.6 μgal, which is incompatible with the 1-2 μgal precision specified for FG5 instruments. However, it is believed that the height of the top of the drop for FG5-107 has been mechanically adjusted, so that FG5-107 now gives values 'about 17 μgal' higher than other FG5 instruments (*pers. comm.* R.J. Edge 17 January 1995 and T.M Niebauer 15 September 1994).

The British Precise Gravity Network 1993

The observation of the BPGN93 took place between 1992 and 1993, and the 58 specially chosen sites were measured in a carefully designed sequence with three LCR relative gravity meters.

A variety of novel techniques have demonstrated the reliability of the net, and have helped to identify a small number of errors in the data. Adjusting parts of the net in isolation and comparing the solution with that from the complete net shows which sites have poorly determined gravity values. Breaking particular links demonstrates which groups of sites are closely associated, and singular value decomposition identifies the traverses for which the linear drift term b_k is poorly determined because of bad data.

The drift model which fits a different linear drift line to each daily traverse has been found to be appropriate for many samples of BPGN data. Alternative drift models have also been tried, and the relative importance of the drift parameters to the general solution has been determined. The ability of the drift parameter b_k and scaling factor C_f to absorb outlying observations has been noted. These investigations and the results of the singular value decomposition tests have shown that the gravity values are much more reliably determined than the linear drift parameter b_k.

Characteristic instrumental drift

The influence of the characteristic instrumental drift of G275 and D145, which is central to the 'spring hysteresis model' developed for the periodic error experiments, has been noted for the adjustment of datasets with long (1 hour) and short (10 minute) time intervals

between observations. Only with the latter sequences can the characteristic behaviour be seen, but for the longer time intervals, the scatter of the observations is too large for it to have a significant effect. The drift signature is strongest when the instrument has not been used for a period, so it is recommended that instruments are unclamped and read for an hour in the laboratory sometime during the two days prior to going into the field.

The adjustment of the BPGN93

The free adjustment of the links between the 58 BPGN sites has an rms of 7.2 μgal. The mean standard error on the gravity values at the sites is 4.9 ± 1.2 μgal, in the range 3 to 8 μgal. The absolute gravity meter FG5-103 has measured at four sites, and these have been linked to the BPGN. Unfortunately, the links between the BPGN and the absolute sites are found to be weak, and it is recommended that they be re-observed in the manner described in section 7.2. The absolute values measured by FG5-103 are introduced with a fixed nominal standard error of 3 μgal, and are used to constrain the adjustment. The combined 'BPGNA+FG5' solution shows up a discrepancy of up to 30 μgal in the NPL1 absolute value. When this value is excluded, the relative and absolute results are consistent to about 7 μgal. A factor of 1.000 757 ± 0.000 021 converts G275 to the FG5-103 scale, compared with the value of 1.000 622 ± 0.000 027 previously determined for G275 on the IGSN71.

7.2 Further Work

Periodic error determination

Further work is necessary to verify the periodic errors for D145. The risk of aliassing known periods could be reduced by re-designing the CD-FD experiments, or by using electrostatic feedback. A shorter sampling interval which was not an integer multiple of a known period, for example 75 instead of 200 FD turns, should be used. This would require many more observations to include the necessary range of the coarse screw. To look for the 25 CD period, samples at less than 10 CD turns (100 FD turns) would be necessary, although the total range could be reduced to 3 or 4 whole periods (100 CD turns).

Reobservation of parts of the BPGN93

The investigations of loops and legbreaking have shown the consistency of the various regions of the network and identified a small number of weak areas. These are the sections Wooler-Wylam-Easby-Chapel Haddlesey in north-east England; Crooklands-Goosnargh in north-west England; Lanivet and Ashburton in the extreme south-west of England; New Luce in south-west Scotland, and Wick-Bettyhill-Scourie in the far north of Scotland. These are the 12 stations (from the total of 58) which should be reobserved at the earliest opportunity.

Some links have demonstrated instabilities which are apparently due to a weak linking sequence. For example a 'double-forward-looping' sequence ABABCBC is found to be more reliable then a sequence ABCBCD. Visiting the 'end' sites (A, D) only once during a day's sequence relies more on the previous and following day's observations giving entirely consistent results. Particular care is needed to avoid batteries failing. It was found that batteries of the type supplied by LCR sometimes ran down towards the end of long field days. A system of using of a larger battery during transport and the smaller ones for reading worked well.

The links to two of the absolute sites have also demonstrated some instability. The Taunton (Loading Bay) to Broadway link and the NPL to Hampton Church link need to be reobserved. Because of the prime importance of these links in the relative-absolute comparison, the author suggests that all the absolute ex-centres should be linked to three or four other network sites in the same way that the main BPGN stations.

Absolute gravity program

More absolute gravity sites are needed to constrain BPGN93, especially in Scotland. A new site has been established in Aberdeen (May 1995), and sites in west and central Scotland should be installed so that the secular gravity variations at the centre of the postglacial rebound can be well constrained. Further observations by FG5-105 at NPL are expected to begin shortly, and a continuous monitoring program there could help to determine the effect ground water variations. Groundwater remains a problem for relative and absolute gravity, and the limited availability of boreholes, and the increasing confidentiality of the data compounds the difficulties.

Only a few of the FG5s are operating at the specification of 1 μgal precision and 2 μgal accuracy (Axis Instruments 1992). Many instrumental improvements have taken place to FG5-103 over the last three years, resulting in a more reliable gravity meter, and it is now approaching a repeatability of better than 5 μgal in the field. However, only by comparing it with other FG5s and in particular, other types of absolute gravity meters, can its accuracy be determined. It is recommended that FG5-103 contribute to the International Intercomparisons at Sèvres as soon as is possible. The variation of the FG5 gravity estimate with drop length needs further investigation, in order to determine the system response correction more precisely.

Appendix 1.

Manufacturers Calibration Tables for G275, D145 and D154

Milligal Values for LaCoste & Romberg, Inc. Model G Gravity Meter #275

COUNTER READING*	VALUE IN MILLIGAL	FACTOR FOR INTERVAL	COUNTER READING*	VALUE IN MILLIGAL	FACTOR FOR INTERVAL
000	000.00	1.05115			
100	105.12	1.05108	3600	3786.12	1.05337
200	210.22	1.05104	3700	3891.46	1.05347
300	315.33	1.05100	3800	3996.81	1.05356
400	420.43	1.05095	3900	4102.16	1.05365
500	525.52	1.05093	4000	4207.53	1.05374
600	630.62	1.05090	4100	4312.90	1.05380
700	735.71	1.05090	4200	4418.28	1.05385
800	840.80	1.05090	4300	4523.67	1.05392
900	945.89	1.05090	4400	4629.06	1.05399
1000	1050.98	1.05094	4500	4734.46	1.05405
1100	1156.07	1.05097	4600	4839.86	1.05411
1200	1261.17	1.05103	4700	4945.27	1.05415
1300	1366.27	1.05107	4800	5050.69	1.05417
1400	1471.38	1.05115	4900	5156.11	1.05416
1500	1576.49	1.05124	5000	5261.52	1.05415
1600	1681.62	1.05133	5100	5366.94	1.05412
1700	1786.75	1.05140	5200	5472.35	1.05407
1800	1891.89	1.05150	5300	5577.76	1.05402
1900	1997.04	1.05160	5400	5683.16	1.05395
2000	2102.20	1.05170	5500	5788.55	1.05388
2100	2207.37	1.05180	5600	5893.94	1.05380
2200	2312.55	1.05187	5700	5999.32	1.05372
2300	2417.74	1.05198	5800	6104.69	1.05364
2400	2522.93	1.05207	5900	6210.06	1.05355
2500	2628.14	1.05216	6000	6315.41	1.05344
2600	2733.36	1.05226	6100	6420.76	1.05330
2700	2838.58	1.05237	6200	6526.09	1.05315
2800	2943.82	1.05248	6300	6631.40	1.05297
2900	3049.07	1.05260	6400	6736.70	1.05275
3000	3154.33	1.05270	6500	6841.97	1.05253
3100	3259.60	1.05283	6600	6947.23	1.05227
3200	3364.88	1.05295	6700	7052.45	1.05200
3300	3470.18	1.05305	6800	7157.65	1.05163
3400	3575.48	1.05316	6900	7262.82	1.05115
3500	3680.80	1.05326	7000	7367.93	

*** Note: Right hand wheel on counter indicates approximately 0.1 milligals.**

10-14-71
AWS

Table A1.1 Manufacturer's calibration table for G275, taken from the Instruction Manual for LaCoste & Romberg Inc., Model G Geodetic Gravity Meter N. 275., 1971.

CALIBRATION TABLE FOR D-145
COARSE SCREW

MILLIGAL VALUES FOR LACOSTE & ROMBERG, INC. MODEL D GRAVITY METER

COUNTER READING*	VALUE IN MILLIGALS	FACTOR FOR INTERVAL	COUNTER READING*	VALUE IN MILLIGALS	FACTOR FOR INTERVAL
000	000.000	0.74757			
100	74.757	0.74756	5100	3816.997	0.75011
200	149.513	0.74754	5200	3892.007	0.75015
300	224.267	0.74753	5300	3967.022	0.75018
400	299.020	0.74753	5400	4042.039	0.75020
500	373.774	0.74753	5500	4117.060	0.75015
600	448.527	0.74754	5600	4192.075	0.75023
700	523.281	0.74755	5700	4267.097	0.75024
800	598.036	0.74756	5800	4342.121	0.75025
900	672.792	0.74756	5900	4417.146	0.75026
1000	747.548	0.74757	6000	4492.172	0.75026
1100	822.306	0.74758	6100	4567.198	0.75027
1200	897.063	0.74759	6200	4642.225	0.75028
1300	971.822	0.74760	6300	4717.253	0.75029
1400	1046.582	0.74762	6400	4792.282	0.75029
1500	1121.344	0.74764	6500	4867.311	0.75029
1600	1196.109	0.74767	6600	4942.340	0.75029
1700	1270.876	0.74772	6700	5017.369	0.75029
1800	1345.648	0.74776	6800	5092.398	0.75028
1900	1420.424	0.74780	6900	5167.426	0.75027
2000	1495.204	0.74785	7000	5242.453	0.75026
2100	1569.989	0.74790	7100	5317.479	0.75023
2200	1644.780	0.74795	7200	5392.502	0.75023
2300	1719.575	0.74802	7300	5467.525	0.75020
2400	1794.377	0.74808	7400	5542.546	0.75018
2500	1869.185	0.74814	7500	5617.564	0.75015
2600	1943.999	0.74822	7600	5692.578	0.75011
2700	2018.821	0.74829	7700	5767.589	0.75007
2800	2093.650	0.74837	7800	5842.597	0.75002
2900	2168.488	0.74845	7900	5917.599	0.74998
3000	2243.333	0.74853	8000	5992.596	0.74993
3100	2318.186	0.74862	8100	6067.589	0.74986
3200	2393.047	0.74871	8200	6142.575	0.74979
3300	2467.919	0.74881	8300	6217.554	0.74973
3400	2542.800	0.74890	8400	6292.527	0.74965
3500	2617.690	0.74898	8500	6367.491	0.74959
3600	2692.588	0.74906	8600	6442.450	0.74950
3700	2767.494	0.74915	8700	6517.400	0.74942
3800	2842.410	0.74923	8800	6592.341	0.74932
3900	2917.332	0.74931	8900	6667.273	0.74923
4000	2992.264	0.74940	9000	6742.196	0.74912
4100	3067.203	0.74948	9100	6817.108	0.74903
4200	3142.152	0.74956	9200	6892.012	0.74893
4300	3217.107	0.74963	9300	6966.905	0.74883
4400	3292.070	0.74970	9400	7041.788	0.74873
4500	3367.041	0.74977	9500	7116.661	0.74862
4600	3442.018	0.74984	9600	7191.522	0.74851
4700	3517.002	0.74991	9700	7266.373	0.74839
4800	3591.993	0.74996	9800	7341.212	0.74827
4900	3666.989	0.75001	9900	7416.039	0.74814
5000	3741.990	0.75006	10000	7490.852	

*Note: Right-hand wheel on counter indicates approximately 0.07 milligal

05-18-1989

JRA

Table A1.2 Manufacturer's calibration table for the coarse screw of D145, taken from the Instruction Manual for LaCoste & Romberg Inc., Model G & D Gravity Meter, 1989.

CALIBRATION TABLE

FINE SCREW D-145

COUNTER READING*	VALUE IN MILLIGALS	FACTOR FOR INTERVAL
00	00.000	0.07282
100	7.282	0.07281
200	14.563	0.07281
300	21.844	0.07281
400	29.124	0.07281
500	36.405	0.07281
600	43.686	0.07281
700	50.966	0.07281
800	58.247	0.07281
900	65.529	0.07281
1000	72.809	0.07280
1100	80.089	0.07279
1200	87.368	0.07277
1300	94.645	0.07275
1400	101.920	0.07274
1500	109.194	0.07273
1600	116.468	0.07273
1700	123.740	0.07271
1800	131.012	0.07270
1900	138.282	0.07269
2000	145.551	0.07268
2100	152.818	0.07266
2200	160.085	0.07264
2300	167.349	0.07263
2400	174.612	0.07261
2500	181.873	0.07261
2600	189.134	0.07259
2700	196.393	0.07258
2800	203.651	0.07256
2900	210.907	0.07254
3000	218.161	

One unit of right-hand wheel on counter indicates approximately 0.007 milligal

05-18-1989 JRA

Table A1.3 Manufacturer's calibration table for the fine screw of D145, taken from the Instruction Manual for LaCoste & Romberg Inc., Model G & D Gravity Meter, 1989.

CALIBRATION TABLE FOR D-154
COARSE SCREW

MILLIGAL VALUES FOR LACOSTE & ROMBERG, INC. MODEL D GRAVITY METER

COUNTER READING*	VALUE IN MILLIGALS	FACTOR FOR INTERVAL	COUNTER READING*	VALUE IN MILLIGALS	FACTOR FOR INTERVAL
000	000.000	1.12014			
100	112.014	1.12009	5100	5711.423	1.12140
200	224.023	1.11994	5200	5823.563	1.12155
300	336.018	1.11987	5300	5935.718	1.12165
400	448.004	1.11978	5400	6047.883	1.12174
500	559.982	1.11971	5500	6160.057	1.12184
600	671.954	1.11965	5600	6272.241	1.12193
700	783.918	1.11957	5700	6384.433	1.12201
800	895.876	1.11953	5800	6496.635	1.12209
900	1007.828	1.11946	5900	6608.844	1.12219
1000	1119.774	1.11945	6000	6721.063	1.12228
1100	1231.719	1.11935	6100	6833.291	1.12236
1200	1343.654	1.11931	6200	6945.526	1.12244
1300	1455.585	1.11930	6300	7057.771	1.12251
1400	1567.514	1.11927	6400	7170.022	1.12260
1500	1679.442	1.11927	6500	7282.282	1.12265
1600	1791.369	1.11927	6600	7394.547	1.12271
1700	1903.296	1.11928	6700	7506.818	1.12276
1800	2015.225	1.11930	6800	7619.094	1.12283
1900	2127.154	1.11931	6900	7731.377	1.12287
2000	2239.085	1.11932	7000	7843.664	1.12292
2100	2351.017	1.11933	7100	7955.956	1.12295
2200	2462.950	1.11937	7200	8068.251	1.12298
2300	2574.887	1.11941	7300	8180.549	1.12301
2400	2686.827	1.11943	7400	8292.850	1.12303
2500	2798.770	1.11944	7500	8405.153	1.12303
2600	2910.714	1.11948	7600	8517.455	1.12302
2700	3022.662	1.11953	7700	8629.757	1.12301
2800	3134.615	1.11956	7800	8742.058	1.12297
2900	3246.571	1.11961	7900	8854.355	1.12292
3000	3358.532	1.11967	8000	8966.647	1.12285
3100	3470.499	1.11974	8100	9078.932	1.12277
3200	3582.473	1.11978	8200	9191.209	1.12270
3300	3694.451	1.11985	8300	9303.479	1.12260
3400	3806.435	1.11990	8400	9415.739	1.12249
3500	3918.425	1.11997	8500	9527.987	1.12237
3600	4030.422	1.12003	8600	9640.224	1.12222
3700	4142.425	1.12011	8700	9752.446	1.12209
3800	4254.436	1.12020	8800	9864.656	1.12196
3900	4366.456	1.12030	8900	9976.852	1.12183
4000	4478.486	1.12039	9000	10089.034	1.12165
4100	4590.525	1.12047	9100	10201.199	1.12149
4200	4702.572	1.12057	9200	10313.348	1.12129
4300	4814.629	1.12067	9300	10425.477	1.12109
4400	4926.696	1.12076	9400	10537.586	1.12088
4500	5038.772	1.12085	9500	10649.674	1.12065
4600	5150.857	1.12095	9600	10761.739	1.12039
4700	5262.952	1.12105	9700	10873.777	1.12008
4800	5375.056	1.12113	9800	10985.785	1.11980
4900	5487.170	1.12119	9900	11097.765	1.11936
5000	5599.288	1.12134	10000	11209.701	

*Note: Right-hand wheel on counter indicates approximately 0.07 milligal

05-18-1989

JRA

Table A1.4 Manufacturer's calibration table for the coarse screw of D154, taken from the Instruction Manual for LaCoste & Romberg Inc., Model G & D Gravity Meter, 1989. This table is clearly not the right one for D154, since the interval factors are all about 1.122, not 0.7 as stated in the caption. LaCoste & Romberg did not respond to a request for a corrected table, so it has been assumed that the one supplied has the correct shape, but that a different gearbox was used for the calibration procedure (section 2.2.2) to the one fitted on purchase. A provisional multiplying factor of 0.663838 was determined from local intercomparisons with G275 and D145. Corrections to it are found from network adjustments (section 2.2.4).

CALIBRATION TABLE

FINE SCREW D-154

COUNTER READING*	VALUE IN MILLIGALS	FACTOR FOR INTERVAL
	00.000	0.06499
100	6.499	0.06499
200	12.998	0.06500
300	19.497	0.06500
400	25.998	0.06501
500	32.499	0.06502
600	39.000	0.06503
700	45.503	0.06504
800	52.008	0.06506
900	58.513	0.06507
1000	65.020	0.06509
1100	71.529	0.06510
1200	78.039	0.06512
1300	84.551	0.06514
1400	91.065	0.06515
1500	97.580	0.06516
1600	104.096	0.06518
1700	110.613	0.06519
1800	117.132	0.06519
1900	123.651	0.06520
2000	130.171	0.06520
2100	136.691	0.06520
2200	143.211	0.06519
2300	149.730	0.06518
2400	156.248	0.06516
2500	162.764	0.06515
2600	169.279	0.06513
2700	175.791	0.06511
2800	182.303	0.06509
2900	188.811	0.06507
3000	195.318	

One unit of right-hand wheel on counter indicates approximately 0.007 milligal

05-18-1989 JRA

Table A1.5 Manufacturer's calibration table for the fine screw of D154, taken from the Instruction Manual for LaCoste & Romberg Inc., Model G & D Gravity Meter, 1989.

Appendix 2.

Deletions from BPGN dataset

Date	Time	Station	CD	FD	Meter	Reason if known
scotloop	(11)					
03.07.93	0748	140 GI	6757.533	1500.00	154	steep initial drift
03.07.93	0753	140 GI	6757.519	1500.00	154	steep initial drift
06.07.93	2031	244 Sf	6933.243	1500.00	154	
09.07.93	1355	248 Sc	7066.344	1500.00	154	
09.07.93	1355	248 Sc	7066.327	1500.00	154	
11.07.93	1210	250 Ac	7150.287	1500.00	145	rain in electronics
11.07.93	1243	250 Ac	7150.260	1500.00	145	rain in electronics
11.07.93	1247	250 Ac	7150.394	1500.00	145	rain in electronics
11.07.93	1253	250 Ac	7150.361	1500.00	145	rain in electronics
14.07.93	1700	250 Ac	6903.531	1500.00	154	
14.07.93	1703	250 Ac	6903.516	1500.00	154	
edloop	(9)					
05.08.92	1118	154 Bi	6742.487	1693.00	154	
05.08.92	1120	154 Bi	6742.487	1693.20	154	
25.09.92	1708	226 Tk	6556.200	1668.21	154	
25.09.92	1710	226 Tk	6556.200	1668.26	154	
21.07.93	1203	256 NL	6921.620	1500.00	145	
21.07.93	1205	256 NL	6921.619	1500.00	145	
22.07.93	0752	256 NL	6673.506	1500.00	154	
22.07.93	0755	256 NL	6673.498	1500.00	154	
23.08.93	1221	140 Gi	6758.400	1500.00	154	
pol/nloop	(14)					
06.09.92	1411	203 Ea	6766.900	1913.79	145	battery unplugged
06.09.92	1414	203 Ea	6766.900	1914.14	145	battery unplugged
06.09.92	1605	202Wy	6852.361	1912.28	145	battery unplugged
06.09.92	1607	202Wy	6852.361	1912.25	145	battery unplugged
07.09.92	1110	203 Ea	6540.270	1702.54	154	
07.09.92	1114	203 Ea	6540.270	1702.35	154	
07.09.92	1824	204 CH	6707.181	1910.50	145	
07.09.92	1826	204 CH	6707.181	1910.51	145	
07.09.92	2041	205 GG	6374.620	1701.14	154	battery low ?
07.09.92	2046	205 GG	6374.620	1701.14	154	battery low ?
15.03.93	1416	204 CH	6501.168	1500.00	154	
20.03.93	1718	234 Bt	6467.968	1500.00	154	
24.03.93	1315	223 To	6542.865	1499.00	145	FD wrong
23.08.93	2049	140 GI	6758.274	1500.00	154	

Table A2.1 Observations deleted from the BPGN dataset (63 in total) as a result of the tests described in section 6.5.

.....continued over

Date	Time	Station	CD	FD	Meter	Reason if known
npl/sloop	(11)					
14.09.92	0808	212 Wi	6114.630	1696.94	154	tare
14.09.92	0811	212 Wi	6114.630	1696.90	154	tare
14.09.92	0946	213 Br	6157.700	1697.65	154	tare
14.09.92	0949	213 Br	6157.700	1697.55	154	tare
14.09.92	1906	215 La	4454.254	-	275	battery failure
14.09.92	1909	215 La	4454.251	-	275	battery failure
14.09.92	1912	215 La	4454.253	-	275	battery failure
17.09.92	1459	219 Sh	4656.665	-	275	knock
17.09.92	1503	219 Sh	4656.656	-	275	knock
17.09.92	1505	219 Sh	4656.656	-	275	knock
17.09.92	1535	219 Sh	4656.647	-	275	knock
30.09.93	whole	traverse	LB / Br	18 readings	154	

Table A2.1 continued... Observations deleted from the BPGN dataset (63 in total) as a result of the tests described in section 6.5.

Appendix 3.

Gravity Station Information Sheets

BPGN93 sites

Absolute sites and ex-centres

Edinburgh University - Gravity Station Information

Reference# 11

Country:	SCOTLAND	
Region/County:	GRAMPIAN	
Nearest Town:	Aberdeen	
Name:	**Cathedral of St Machar**	
Latitude:	+ 57.16974°	Grid Reference:
Longitude:	- 02.10138°	393870 808750

Station Description

Leave the Aberdeen ring road NW of the city centre, SP University, Old Aberdeen. Go down the hill to the roundabout where turn half-left at Strathdee Bakery SP Fraserburgh, Peterhead A92. At traffic lights, straight on SP Fraserburgh A978. At next roundabout, straight on then left into narrow road (The Chanonry) SP St Machar's Cathedral. Continue to the cathedral.
The site is roughly in the centre of the porch, on the centre of the middle slab of the row of seven slabs, which is two rows further in than the row with the iron gate stops (see below).

For access contact The Minister, The Cathedral Manse, 18 The Chanonry, Old Aberdeen, Grampian.

Location Diagram

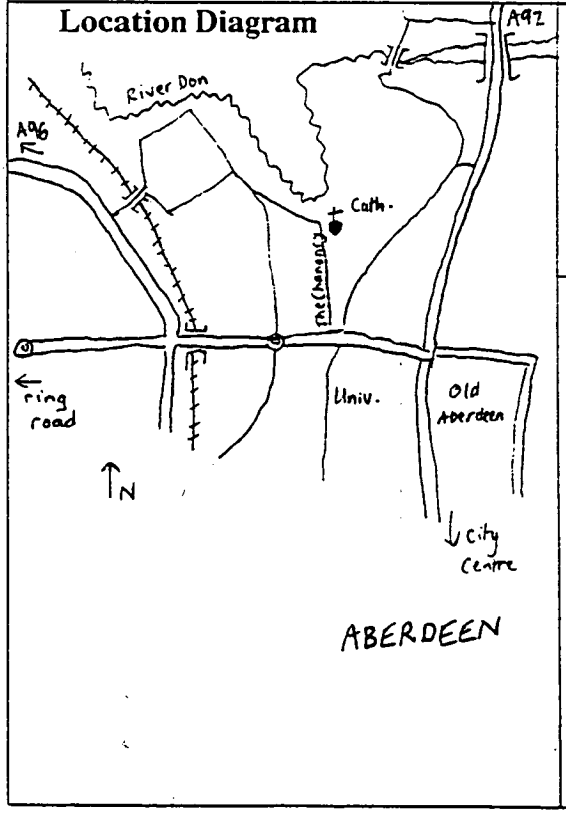

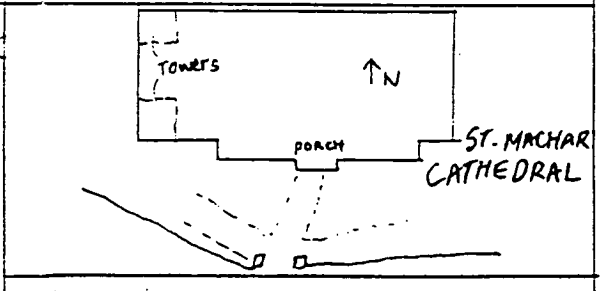

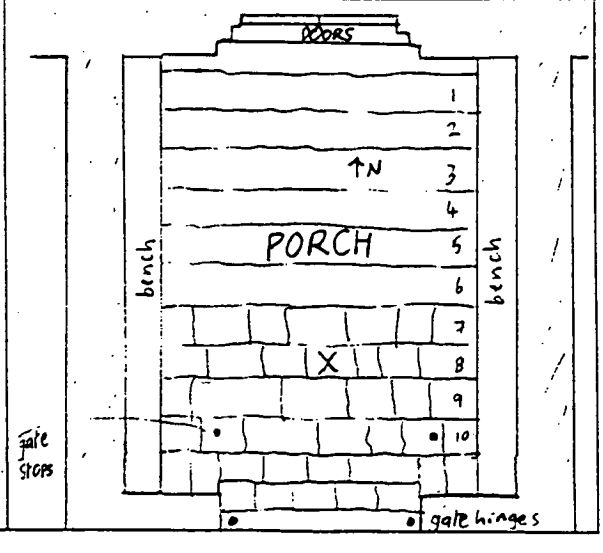

24.05.95 Department of Geology & Geophysics, University of Edinburgh.

Edinburgh University - Gravity Station Information

Reference# 13

Country:	SCOTLAND	
Region/County:	STRATHCLYDE	
Nearest Town:	Paisley	
Name:	**Bishopton, Church of Scotland Church Centre**	
Latitude:	+ 55.90460°	Grid Reference:
Longitude:	- 04.51979°	242493 670808

Station Description

Leave M8 at Junction 30 (SP M898 Erskine Bridge). At Junction 1 leave motorway and take B815 SP Bishopton. Continue to village and to T junction where R, SP Greenock A8. Turn L after the Bishopton Inn into Newton Road (No Through Road). The church centre is the white building on the left.
The site is in the centre of the first step (which is the step with metal bars attached to it), at the front of the building (on the roadside).

For access contact Church Centre c/o 14 Anderson Road. Telephone: Bishopton 863051.

Location Diagram

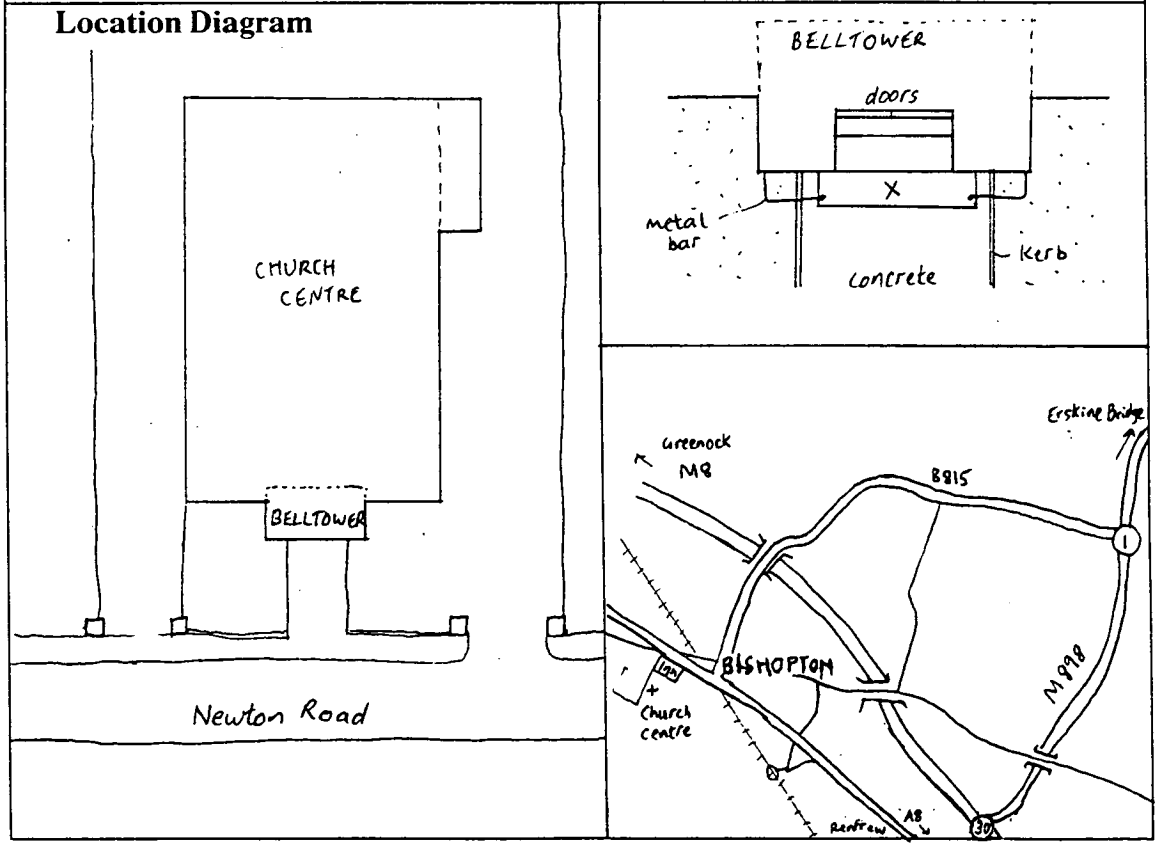

24.05.95 Department of Geology & Geophysics, University of Edinburgh.

Edinburgh University - Gravity Station Information
Reference# 15 Moffat

Country:	SCOTLAND	
Region/County:	DUMFRIES & GALLOWAY	
Nearest Town:	Moffat	
Name:	**Moffat Town Hall**	
Latitude:	+ 55.33336°	Grid Reference:
Longitude:	- 03.44367°	NT 0843 0532

Station Description

The Town Hall is in the centre of Moffat, opposite the Moffat Ram monument. The A701 road to Edinburgh passes the door. The site is the large concrete front step at the NE corner of the building. The station is near the middle of the large flat step, 85 cm in front of the top step.

Location Diagram

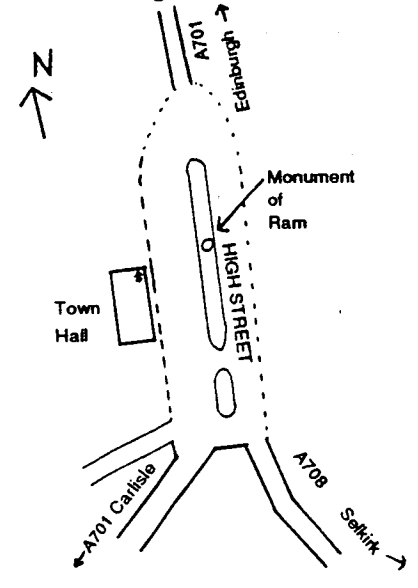

MOFFAT TOWN CENTRE

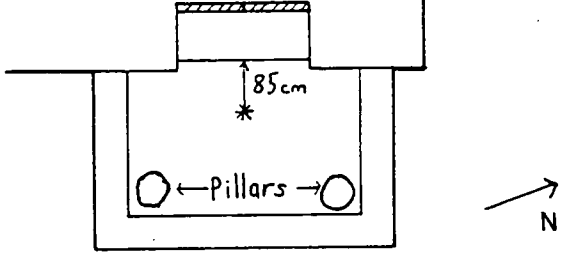

NE CORNER OF TOWN HALL

25.03.92

Department of Geology & Geophysics, University of Edinburgh.

Edinburgh University - Gravity Station Information

Reference# 17 Crooklands

Country:	ENGLAND	
Region/County:	CUMBRIA	
Nearest Town:	Kendal	
Name:	**Preston Patrick Church, Crooklands**	
Latitude:	+ 54.24502°	Grid Reference:
Longitude:	- 02.71059°	SD 5370 8351

Station Description

Leave the M6 at junction 36, taking the A65 towards Kirkby Lonsdale. Shortly at the next roundabout turn left (SP Crooklands). Continue towards the village,under the motorway and past the garage on the right. Opposite a fenced yard on the left, take sharp right into a narrow track (SP Preston Patrick Church). Follow the track up the hill to the church. The site is in the middle of the higher step, against the outer church door.

Location Diagram

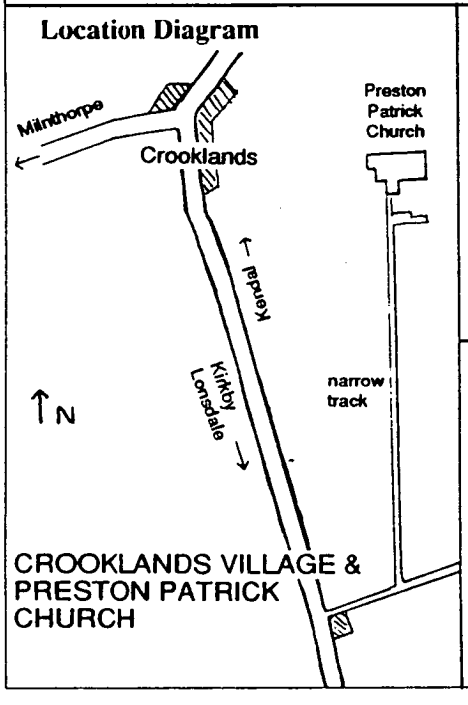

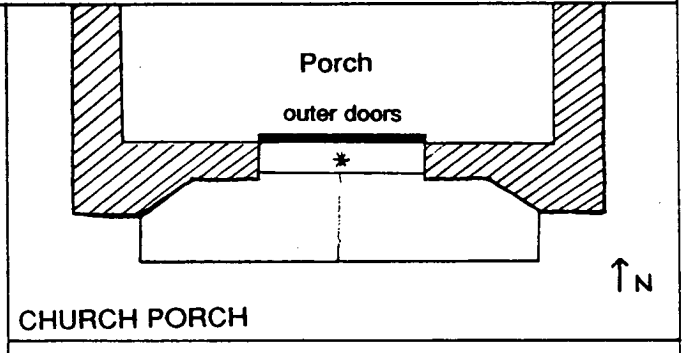

25.03.92

Department of Geology & Geophysics, University of Edinburgh.

Edinburgh University - Gravity Station Information
Reference# 18 Goosnargh

Country:	ENGLAND	
Region/County:	LANCASHIRE	
Nearest Town:	Preston	
Name:	Goosnargh Church	
Latitude:	+ 53.82638°	Grid Reference:
Longitude:	- 02.66960°	SD 5593 3691

Station Description
From Broughton, take the B5269 East (Whittingham Lane) towards Longridge. Pass under the motorway and continue for approximately 2 miles to Whittingham and Goosnargh. Turn left opposite the Post Office into Church Lane. Follow Church Lane for 300m to the village green. The church is straight ahead, beyond the 'Grapes Inn'. The station is in the doorway of the tower at the West end of the church, in the middle of the sandstone step.

Location Diagram

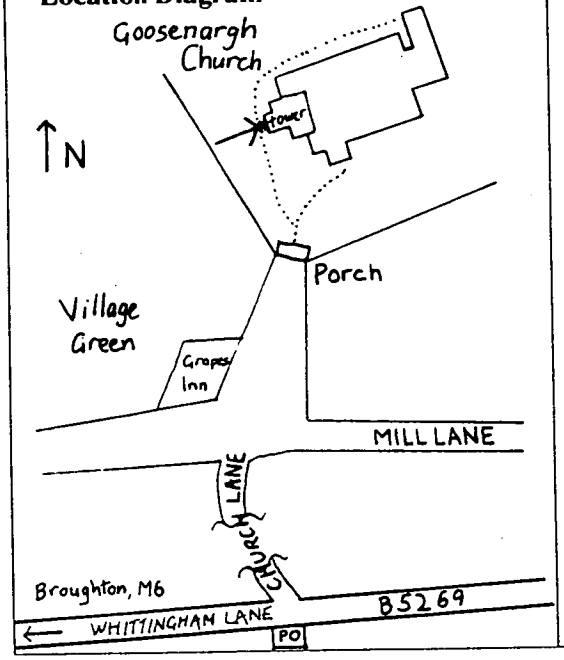

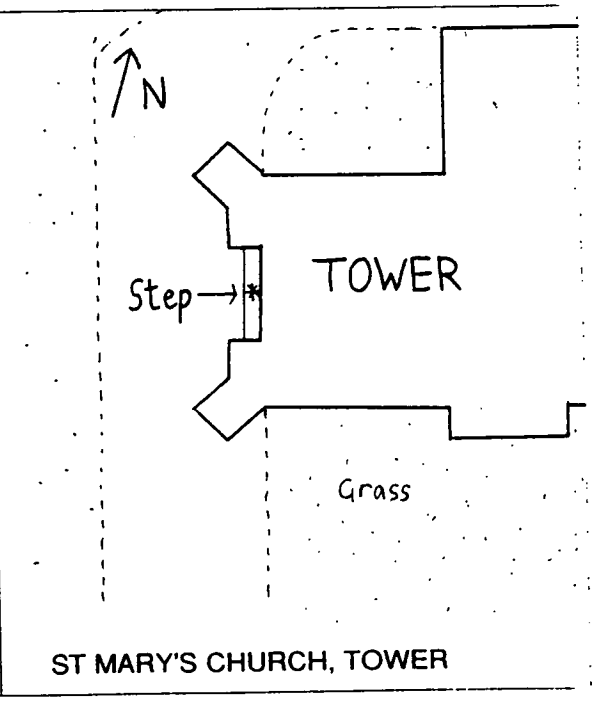

25.03.92

Department of Geology & Geophysics, University of Edinburgh.

Edinburgh University - Gravity Station Information

Reference# 19

Country:	ENGLAND	
Region/County:	CHESHIRE	
Nearest Town:	Warrington	
Name:	**All Saints Parish Church, Daresbury**	
Latitude:	+ 53.34017°	Grid Reference:
Longitude:	- 02.62997°	358058 382781

Station Description

From the M6 Junction 10, take B5356 to Stretton, where turn R then L to cross the'A' road. Continue through Hatton to Daresbury. The church is in the R on entering village.
From M56 Junction 11, take A56 (SP Warrington). Soon take 1st R to Daresbury village. Turn R in village onto B5356 just before the road rejoins A56.
The station is in the front porch, centrally against the main outer door

For access contact The Vicarage, Daresbury, Cheshire WA4 4AB. Telephone 01925 740 348

Location Diagram

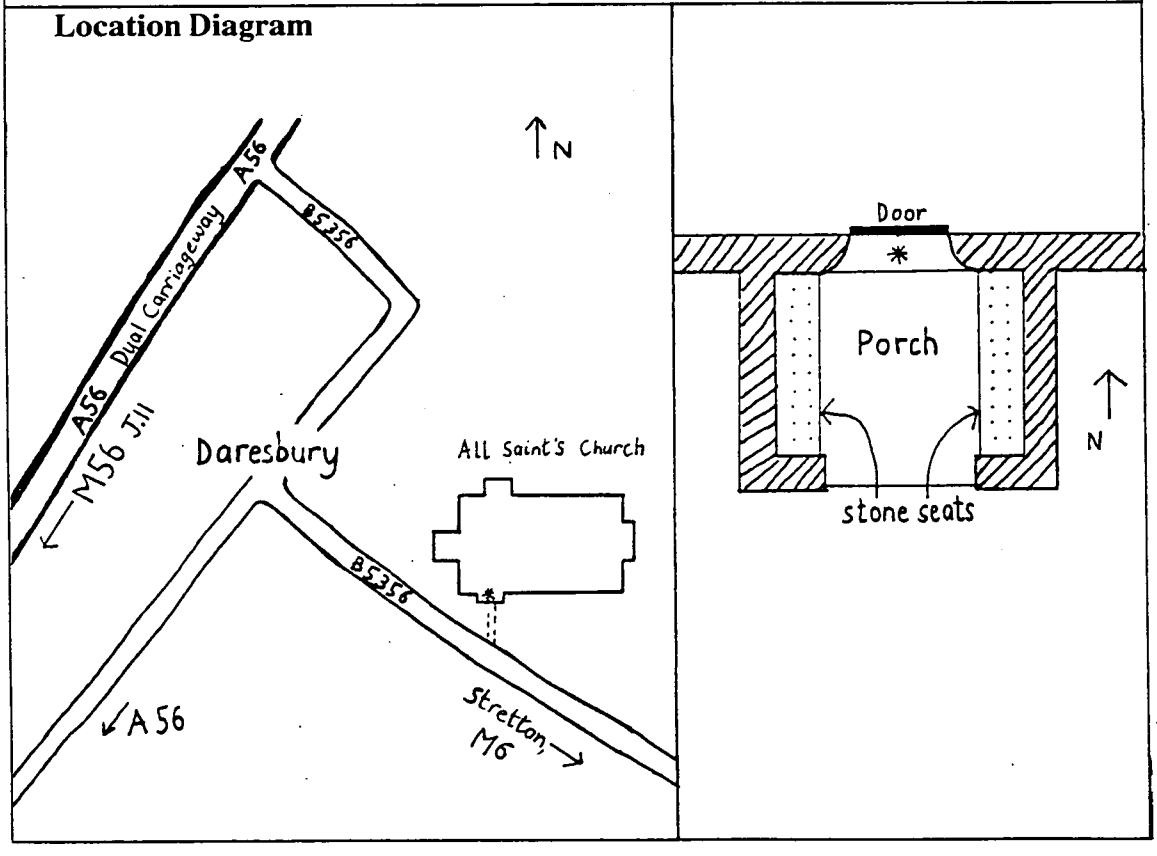

24.05.95 Department of Geology & Geophysics, University of Edinburgh.

Edinburgh University - Gravity Station Information

Reference# 201

Country:	ENGLAND	
Region/County:	NORTHUMBERLAND	
Nearest Town:	Alnwick	
Name:	**Parish Church of St Mary, Wooler**	
Latitude:	+ 55.54600°	Grid Reference:
Longitude:	- 02.01100°	399306 628033

Station Description

Wooler is on the A697 between Morpeth and Coldstream.
The church lies just downhill from the village centre (Market Place), on Church St.
The site is in the centre of the large grey stone slab in front of the main door at the foot of the tower.

Location Diagram

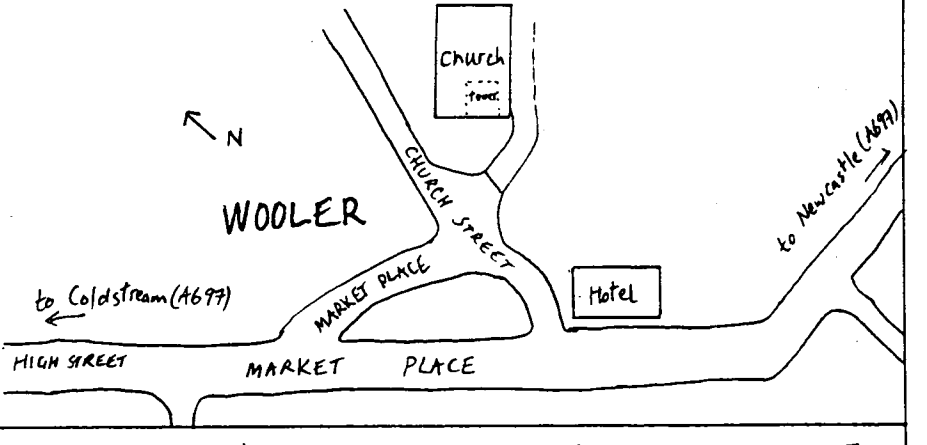

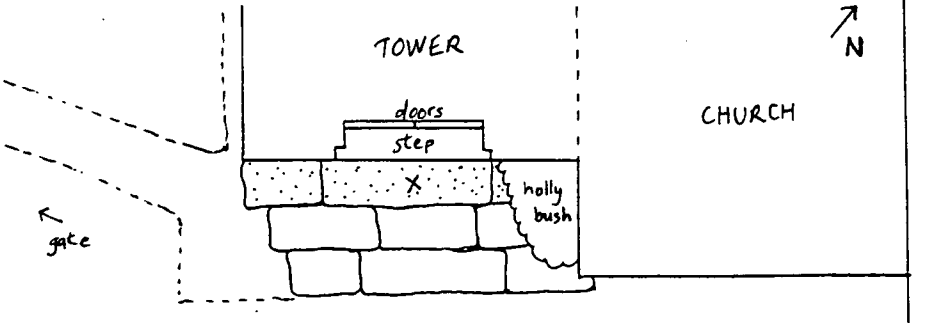

24.05.95 Department of Geology & Geophysics, University of Edinburgh.

Edinburgh University - Gravity Station Information

Reference# 202

Country:	ENGLAND	
Region/County:	TYNE & WEAR	
Nearest Town:	Newcastle upon Tyne	
Name:	**Church of St Oswin, Wylam**	
Latitude:	+ 54.97700°	Grid Reference:
Longitude:	- 01.82200°	411392 564733

Station Description

From the Newcastle ring road, take the A69 (SP Hexham). Continue westwards for about 6 miles. Exit left SP Horsley, Wylam, Ovingham (B6528). At T-junction, turn L and at crossroads go straight on over the main road (SP Wylam).
From A69 west, take B6528 (SP Horsley, Wylam, Ovingham). Continue through Horsley to crossroads, where turn R (SP Wylam).
Continue into village. St Oswin's church is on the left. The station is in the main porch, in the centre of the step against the wooden church doors.

Location Diagram

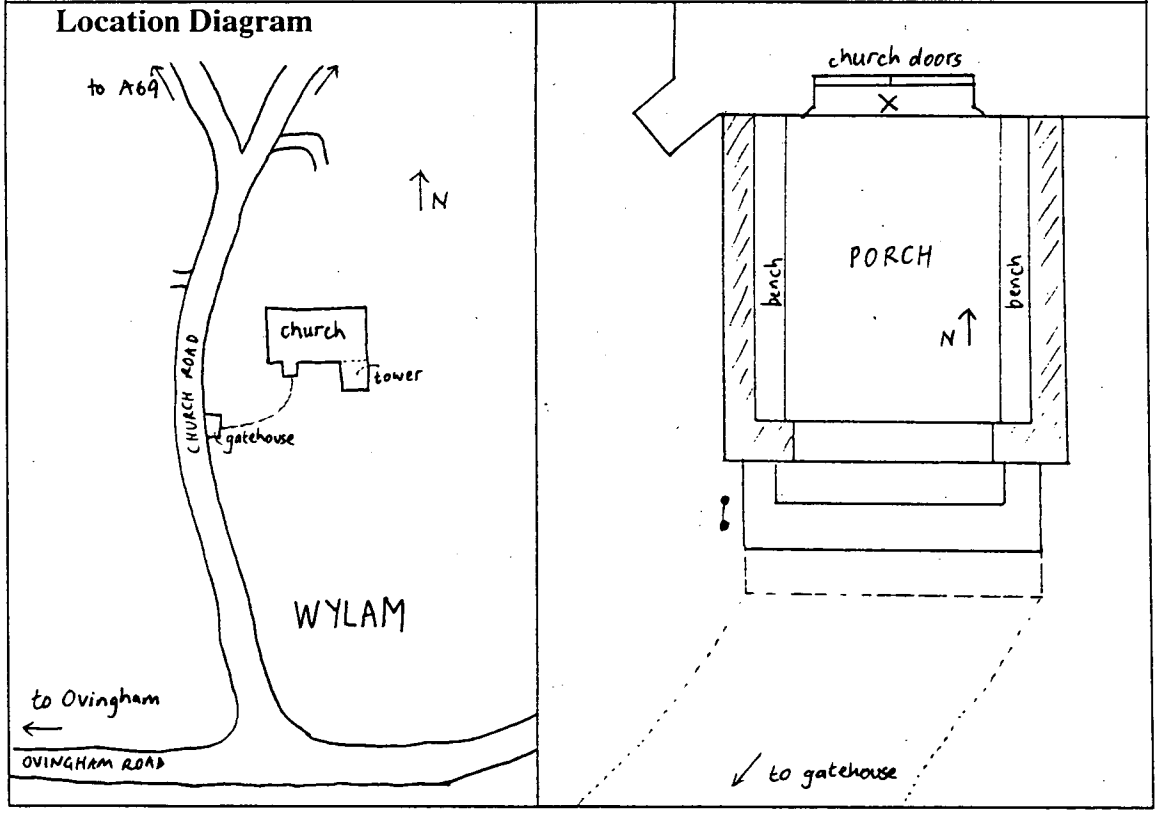

25.05.95 Department of Geology & Geophysics, University of Edinburgh.

Edinburgh University - Gravity Station Information

Reference# 203

Country:	ENGLAND	
Region/County:	NORTH YORKSHIRE	
Nearest Town:	Richmond	
Name:	**Parish Church of St Agatha, Easby**	
Latitude:	+ 54.39800°	Grid Reference:
Longitude:	- 01.71400°	418566 500335

Station Description

From A1 north, leave at Scotch Corner and take the A6108 (SP Richmond). Continue through Skeeby to Richmond, where go straight on over roundabout towards town centre, then acute left turn onto B6271 (Maison Dieu). Continue for 1/2 mile, taking 1st R (SP Easby Abbey).
From A1 south, leave at Catterick (SP Catterick Garrison). Continue through Catterick to Catterick Bridge where cross river and take 2nd L (SP Brompton). Follow B6271 for about 2 miles then turn L (SP Easby Abbey).
Follow signs to Abbey. The site is roughly in the middle of the main porch, in the centre of the stone flag wich is 3.04 metres in front of the wooden church door.

Location Diagram

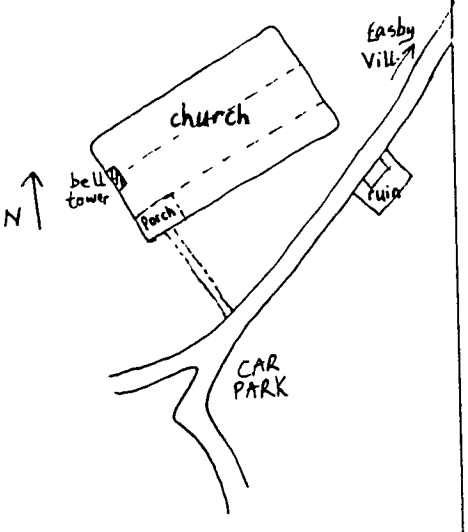

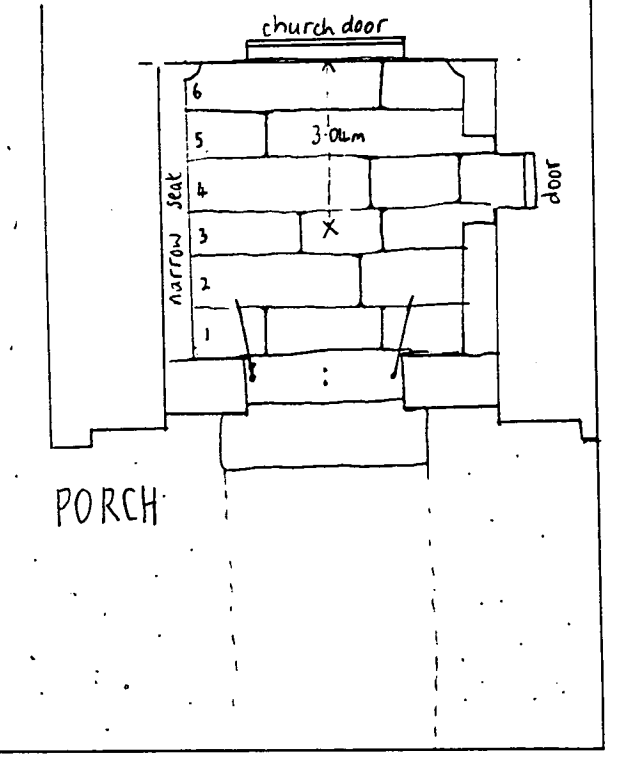

25.05.95 Department of Geology & Geophysics, University of Edinburgh.

Edinburgh University - Gravity Station Information
Reference# 204

Country:	ENGLAND	
Region/County:	NORTH YORKSHIRE	
Nearest Town:	Selby	
Name:	**Chapel Haddlesey**	
Latitude:	+ 53.72737°	Grid Reference:
Longitude:	- 1.11733°	458230 426050

Station Description

Leave A1/M1 1 mile south of Knottingley (SP M62). Leave M62 at next junction (J34, SP Selby). At roundabout take 2nd exit (SP A19 Selby). Continue for 3 miles to Chapel Haddlesey. Immediately after the humpback bridge, turn right at the crossroads by the Burmah garage. The church is about 350 yards on the right. The site is in the centre of the stone slab directly under the arch at the front of the porch.

For access contact: J. L. Bromyard, Westfield House, Chapel Haddlesey, Nr. Selby Y08 8QF

Location Diagram

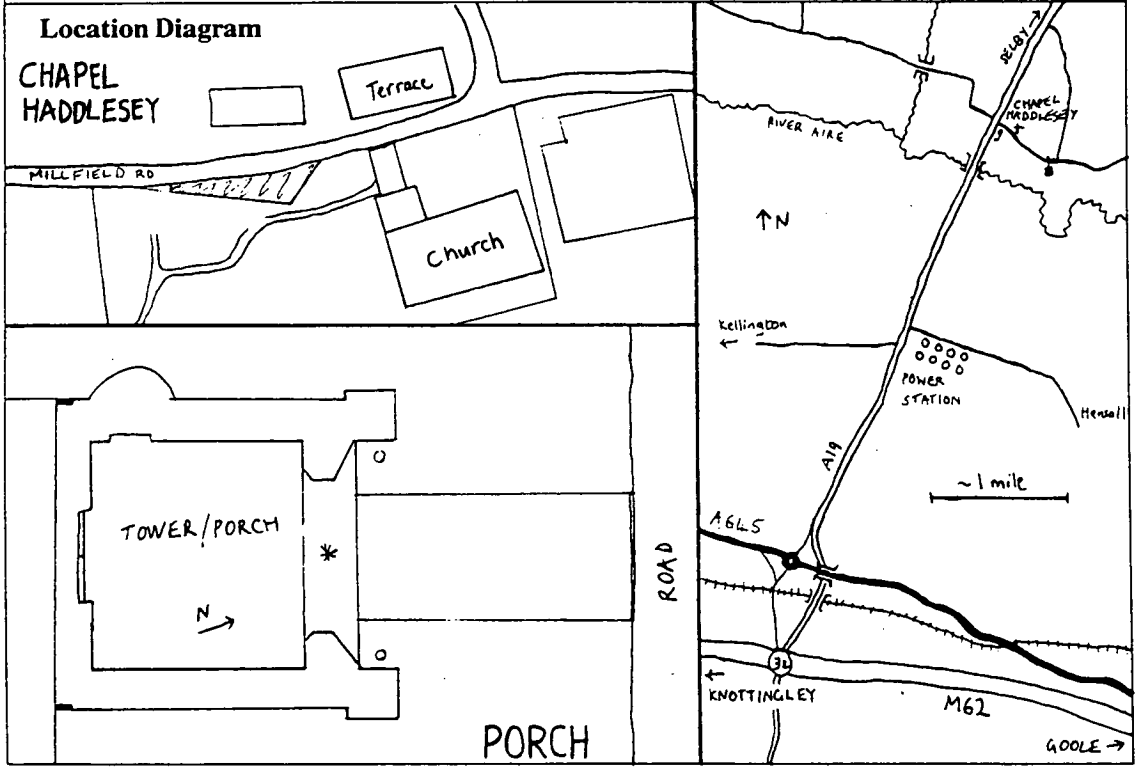

5.1.94 Department of Geology & Geophysics, University of Edinburgh.

Edinburgh University - Gravity Station Information

Reference# 205

Country:	ENGLAND	
Region/County:	LINCOLNSHIRE	
Nearest Town:	Grantham	
Name:	**St.Sebastian's Church, Great Gonerby**	
Latitude:	+ 52.93200°	Grid Reference:
Longitude:	- 0.66400°	489800 338100

Station Description

Leave the A1 at the services 1 mile north of Grantham. Take the B1174 into Great Gonerby. The church is at the south end of the village on the east side of the road, next to the primary school. The site is on the outer step of the porch which is on the south side of the building.

For access contact: Rev. Peter Hopkins, The Rectory, Long Street. Tel. Grantham 65737

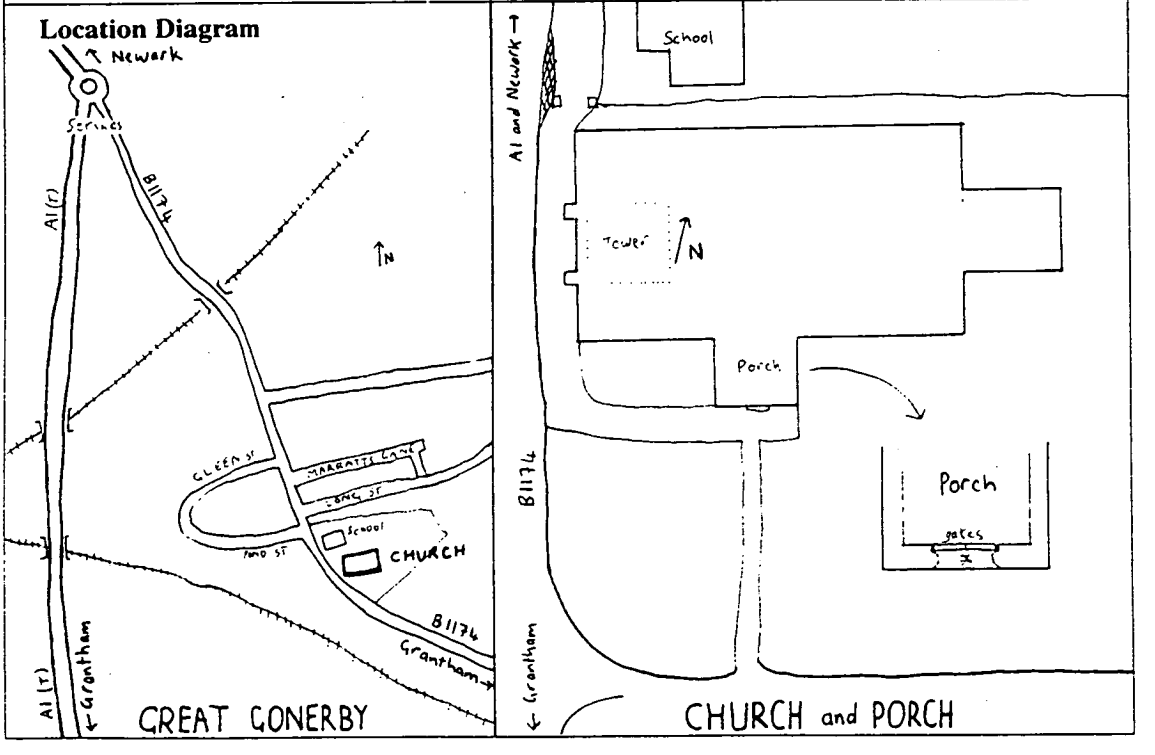

21.12.93

Department of Geology & Geophysics. University of Edinburgh.

Edinburgh University - Gravity Station Information
Reference# 206

Country:	ENGLAND	
Region/County:	CAMBRIDGESHIRE	
Nearest Town:	Cambridge	
Name:	**St.Andrew's Church, Histon**	
Latitude:	+ 52.25500°	Grid Reference:
Longitude:	+ 0.10400°	543600 264000

Station Description

From the A45 2 miles north of Cambridge, take the B1049 northwards (SP Histon). From the roundabout continue into village. At crossroads with traffic lights turn left past the pond (SP Histon, Gorton). Follow the Cottenham road past the shops, bearing right into Windmill Lane and then left into Church St. Continue to a small green with a lamp post (St. Andrews Park). Turn left and follow to church.

For access contact: Rev. Hugh McCurdy, Church House, Histon, Cambridgeshire CB4 4ED

Location Diagram

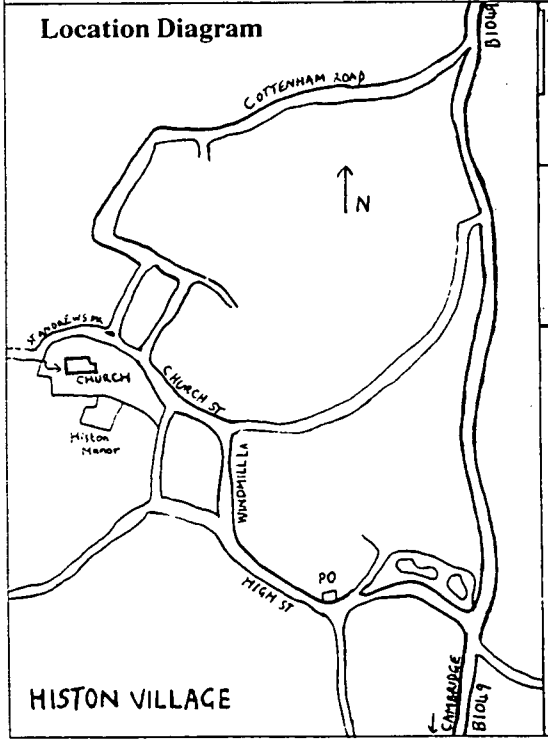

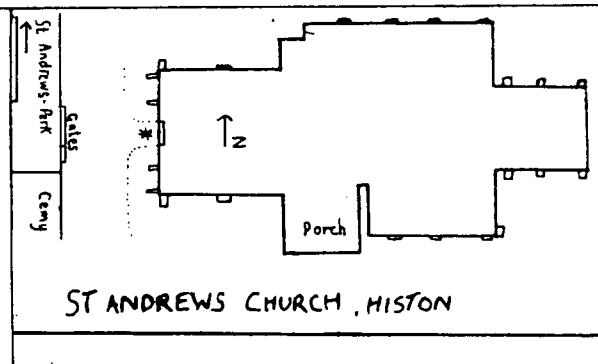

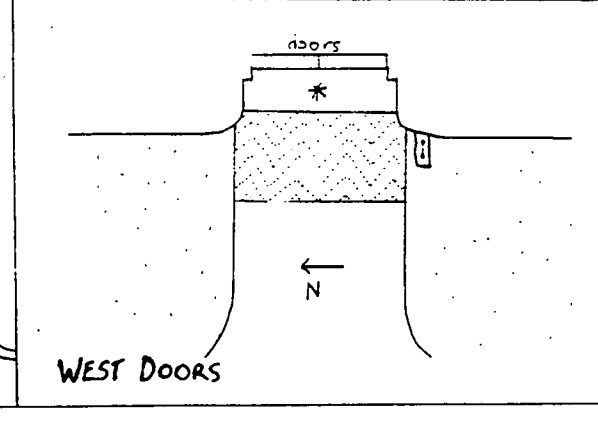

21.12.93 Department of Geology & Geophysics, University of Edinburgh.

Edinburgh University - Gravity Station Information

Reference# 207

Country:	ENGLAND	
Region/County:	SUFFOLK	
Nearest Town:	Ipswich	
Name:	**Sproughton Church**	
Latitude:	+ 52.06300°	Grid Reference:
Longitude:	+ 01.00000°	605620 244808

Station Description

From north, leave A45 at exit south of Ipswich turnoff, but north of A45/A12 interchange, SP Sproughton Industrial Estate, Sproughton. On entering village, cross over the millpond and turn L to church (No through road except for access).
The site is in the middle of the stone slab against the porch door, under the sundial.

Location Diagram

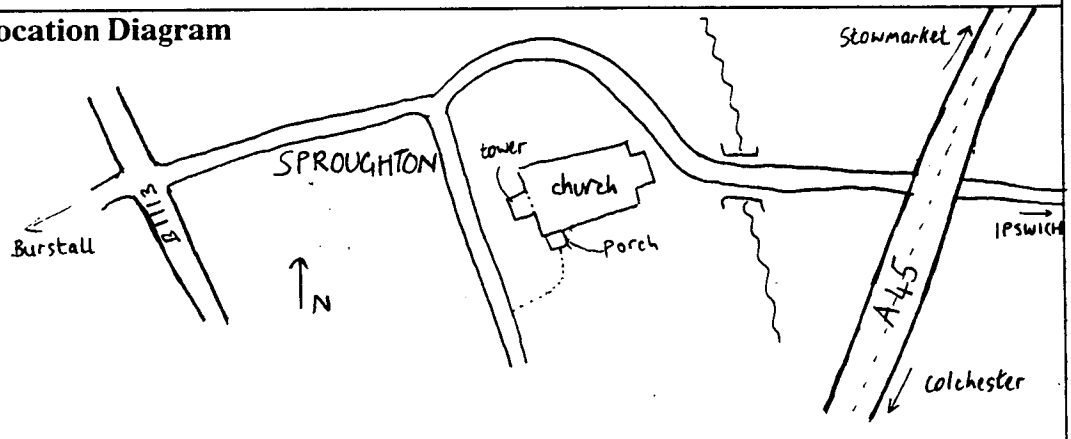

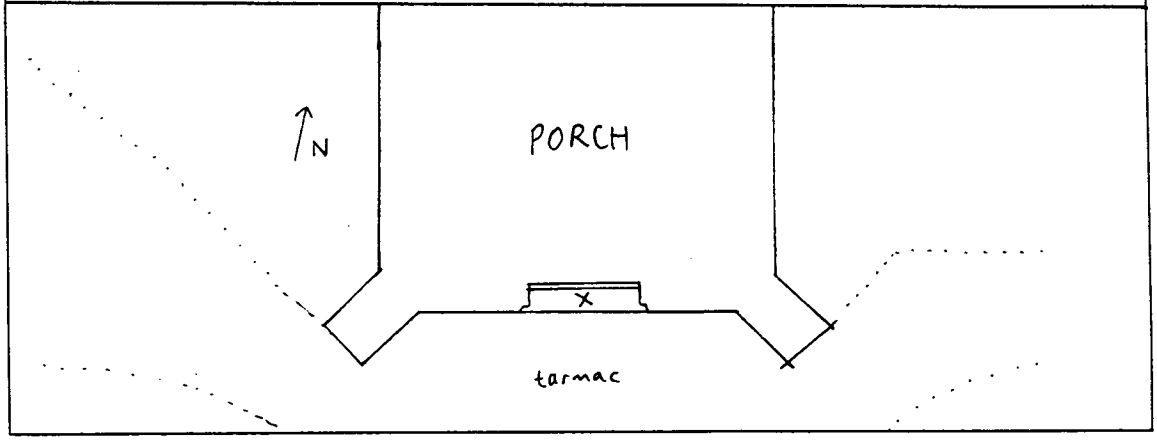

25.05.95 Department of Geology & Geophysics, University of Edinburgh.

Edinburgh University - Gravity Station Information

Reference# 208

Country:	ENGLAND	
Region/County:	KENT	
Nearest Town:	Orpington	
Name:	**Parish Church of St Peter and St Paul, Farningham**	
Latitude:	+ 51.37900°	Grid Reference:
Longitude:	+ 00.22300°	554689 166839

Station Description

Leave the M25 at Juction 3 (SP Swanley A20, Brands Hatch). At the big roundabout, follow Farningham/Brands Hatch. Continue over small roundabout and down hill towards Farningham. At roundabout, turn R (SP Farningham) into village. At T-junction turn L. The church is a few hundred yards on the right.
The site is in the centre of the stone slab in front of the step up to the porch doors.

Location Diagram

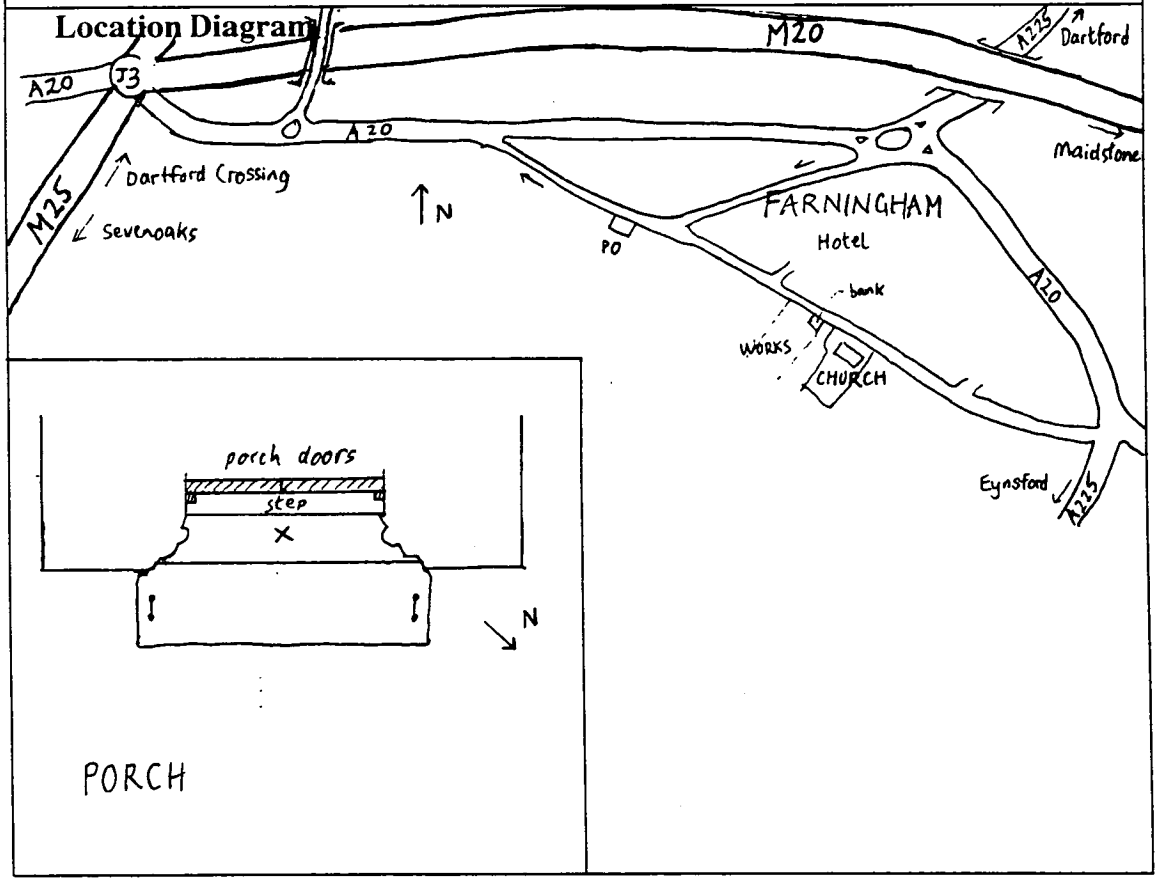

25.05.95 Department of Geology & Geophysics, University of Edinburgh.

Edinburgh University - Gravity Station Information

Reference# 209

Country:	ENGLAND	
Region/County:	KENT	
Nearest Town:	Folkestone	
Name:	**St John Commandery, Swingfield**	
Latitude:	+ 51.15100°	Grid Reference:
Longitude:	+ 01.19200°	623208 143985

Station Description

Stay on the M20 until its end at Folkestone, then follow A20 (SP Dover). Straight on at roundabout (SP A260 Canterbury). At large roundabout turn L (SP A260 Canterbury). Continue up the hill for about 3.5 miles through Hawkinge and Densole to Swingfield Minnis. At pub on L, turn R. Straight on at small crossroads (SP Swingfield, Lydden), to T-junction between farmyards where turn L (SP Lydden). The Commandery is shortly on R on outside of LH bend in road.
The porch faces the road and is accessed by a small gate on the bend in the road. The site is on the centre of the weathered stone slab at the front of the porch, between the flint chippings and the brick-like tiles which form the floor of the porch.

For access contact English Heritage.

Location Diagram

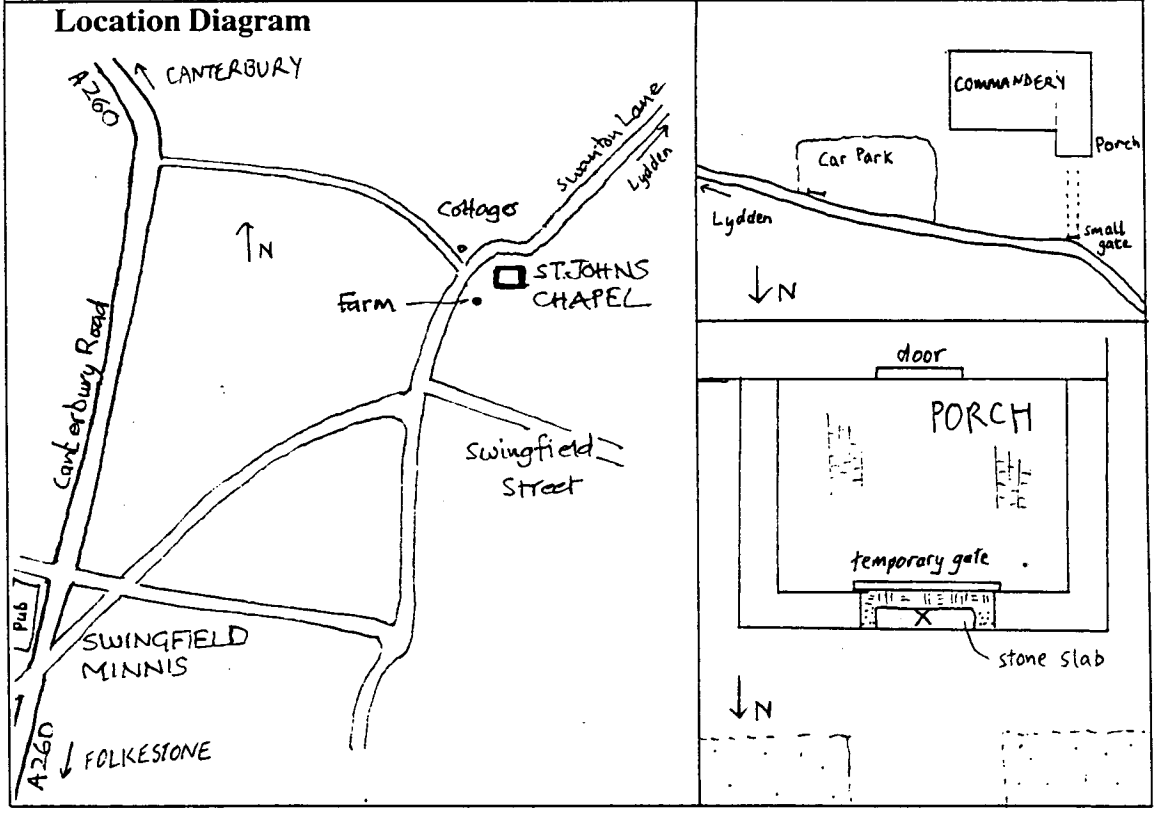

25.05.95 Department of Geology & Geophysics, University of Edinburgh.

Edinburgh University - Gravity Station Information

Reference# 210

Country:	ENGLAND	
Region/County:	EAST SUSSEX	
Nearest Town:	Hastings	
Name:	**All Saints Church, Herstmonceux**	
Latitude:	+ 50.86700°	Grid Reference:
Longitude:	+ 00.33400°	564219 110157

Station Description

Herstmonceux lies on the A271 between Hailsham and Bexhill. At the east end of the village take the small lane south, SP Flowers Green. Continue for about 1.5 miles to the end of the lane. The church is on the right, and the old Greenwich Observatory and Herstmonceux Castle are on the left. The site is NOT in the main front porch, but on the centre of the step to the door on the opposite (south) side of the church.

Location Diagram

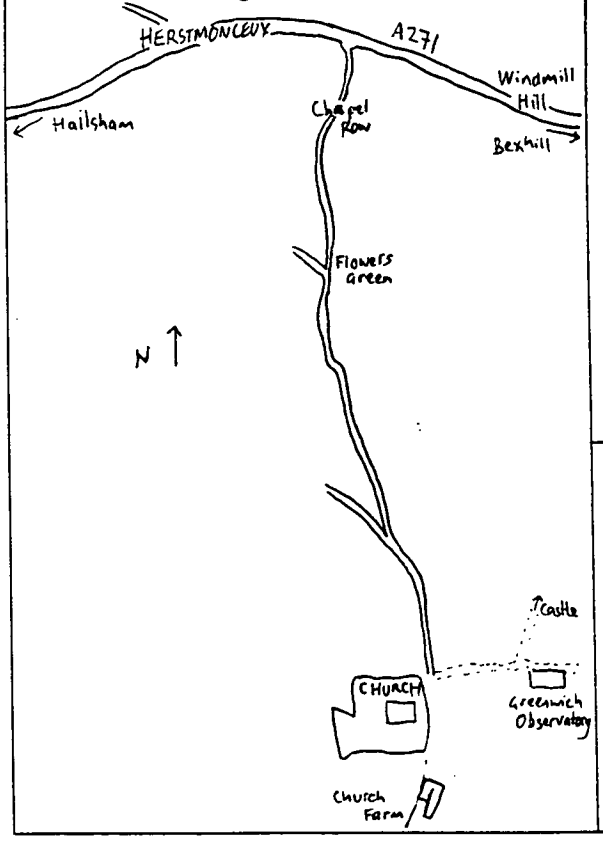

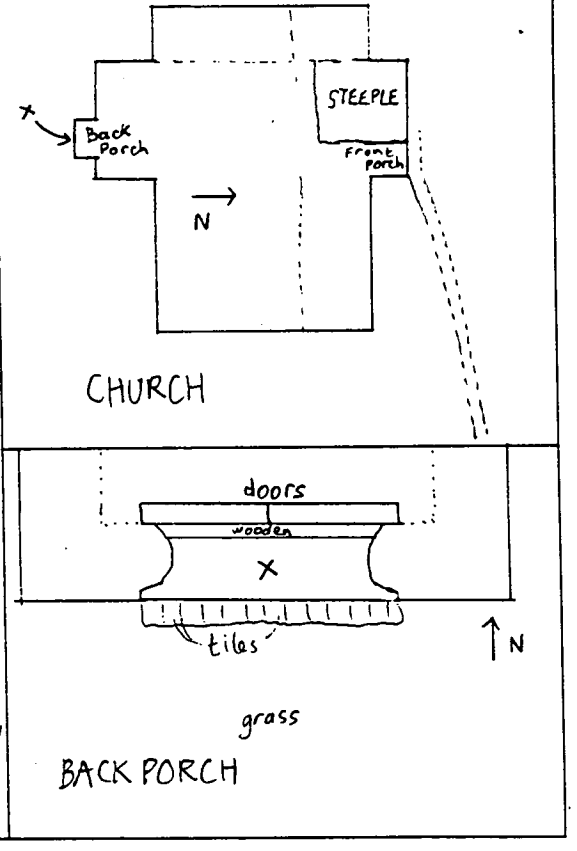

25.05.95 Department of Geology & Geophysics, University of Edinburgh.

Edinburgh University - Gravity Station Information

Reference# 211

Country:	ENGLAND	
Region/County:	WEST SUSSEX	
Nearest Town:	Chicester	
Name:	**Boxgrove Priory**	
Latitude:	+ 50.86000°	Grid Reference:
Longitude:	- 00.71000°	490781 107576

Station Description

Boxgrove lies on the A27 about 2 miles north-east of Chichester. From the east, follow A27 (dual carriageway) SP Chichester. At the end of the section with 'No Racing of Horse Drawn Vehicles' signs, turn R at roundabout (SP Boxgrove & Priory). In the village, turn R immediately after the Post Office (Church Lane). The site is at the entrance to the main porch at the west end of the church, centrally against the wooden doors.

Location Diagram

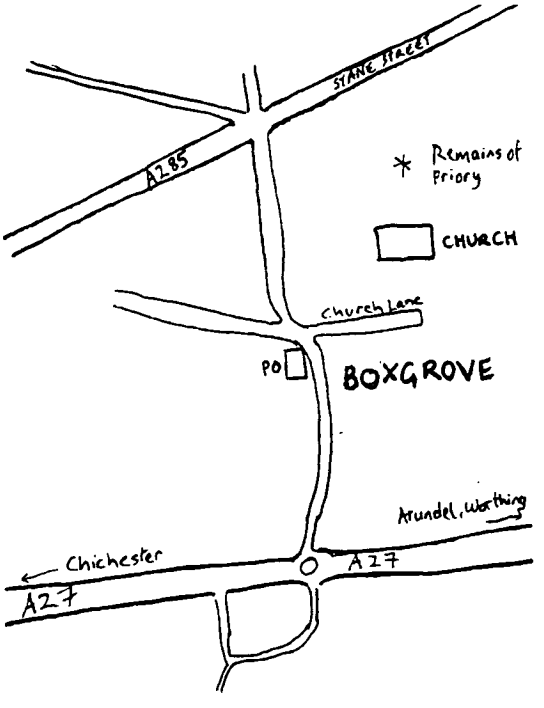

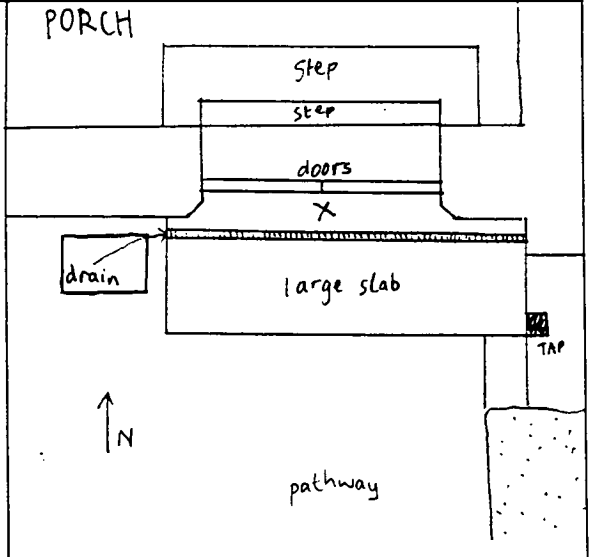

26.05.95 Department of Geology & Geophysics, University of Edinburgh.

Edinburgh University - Gravity Station Information
Reference# 212

Country:	ENGLAND	
Region/County:	DORSET	
Nearest Town:	Wimborne Minster	
Name:	**Wimborne Minster**	
Latitude:	+ 50.79855°	Grid Reference:
Longitude:	- 01.98723°	400900 099950

Station Description

Wimborne Minster lies off the A31, about 5 miles north of Poole. Follow the one-way system to the car park behind the Minster. The site is in the centre of the large stone slab directly in front of the doors at the west end of the Minster, which are only opened during processions. The main entrance is on the north side.

Location Diagram

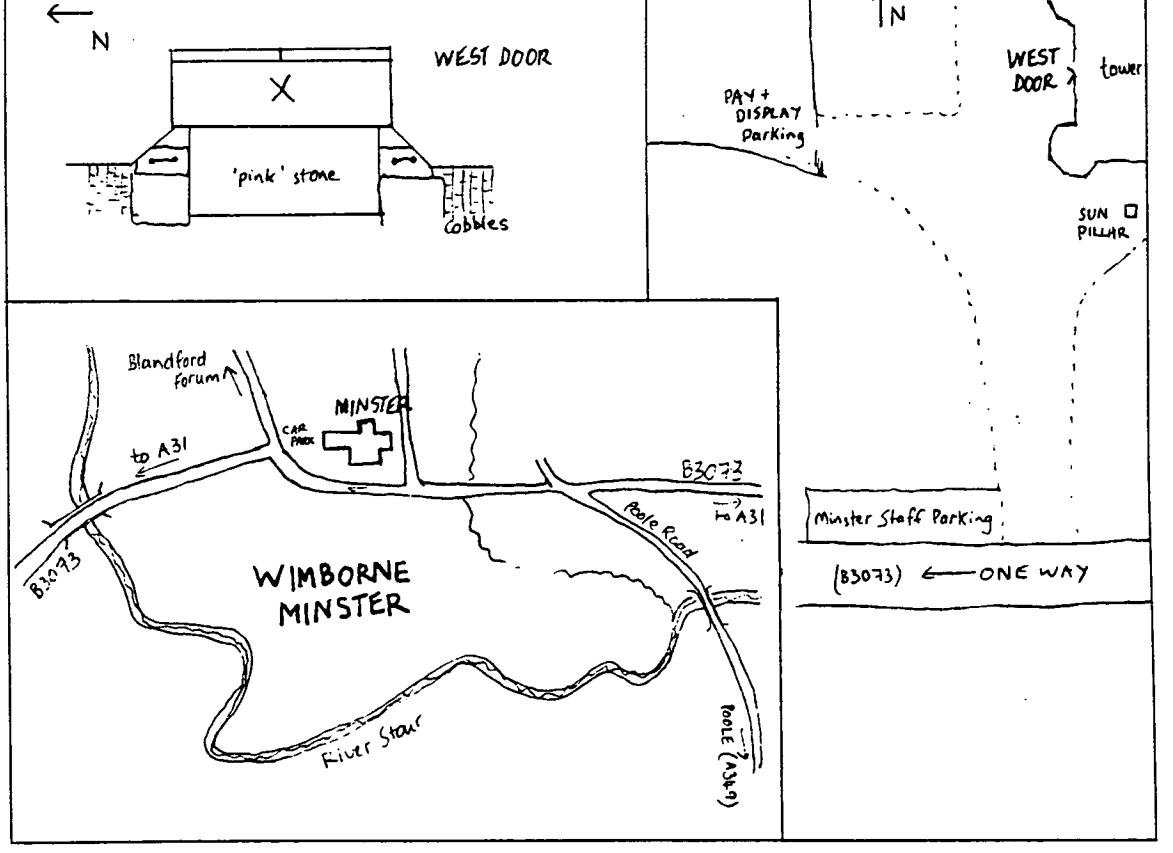

26.05.95 Department of Geology & Geophysics, University of Edinburgh.

Edinburgh University - Gravity Station Information
Reference# 213

Country:	ENGLAND	
Region/County:	SOMERSET	
Nearest Town:	Ilminster	
Name:	**Broadway Church**	
Latitude:	+ 50.93854°	Grid Reference:
Longitude:	- 02.95438°	332950 115950

Station Description

From East (A303): At roundabout in front of Happy Eater take A358 (3rd exit) SP Taunton, Motorway. After 1 mile take 1st left SP Broadway.
From North (M5): leave at J25 (Taunton). Take A358 SP Ilminster, Chard for about 8 miles. After passing through Ashill take 2nd left SP Broadway.
The Church of St Aldhelm & St Eadberga is on the left after 300 yards. The site is on the centre of the step to the door of the tower. There is an OS benchmark symbol on the right of the door.

For access, contact the Churchwarden, Miss H.C.I. Bolitho, Woodcote, Broadway, Ilminster, Somerset TA19 9QY.

Location Diagram

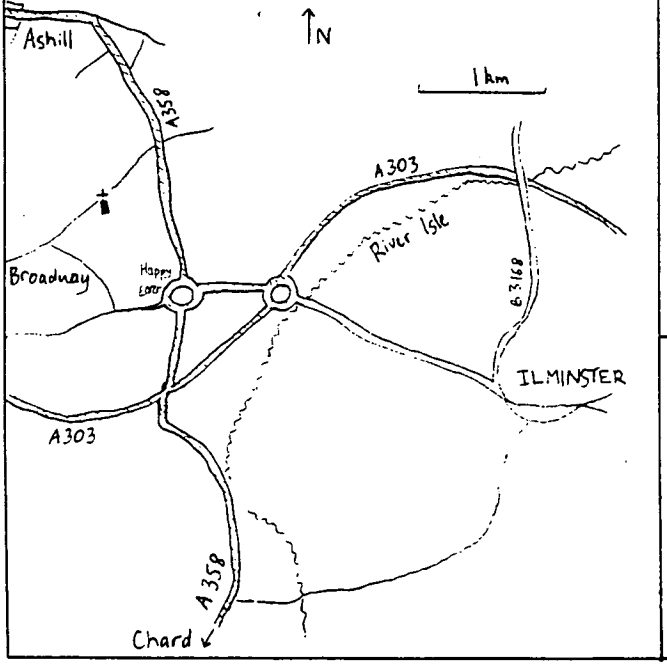

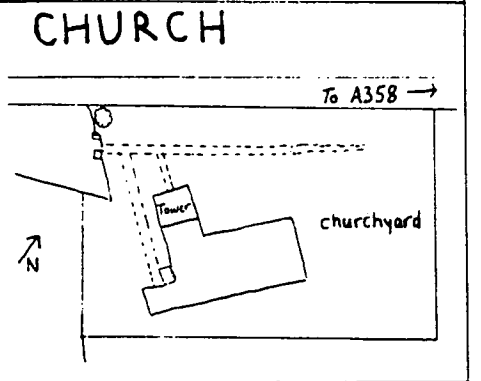

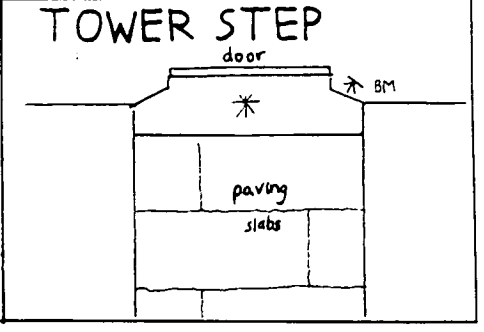

10.03.93 Department of Geology & Geophysics, University of Edinburgh.

Edinburgh University - Gravity Station Information
Reference# 214

Country:	ENGLAND	
Region/County:	DEVON	
Nearest Town:	Ashburton	
Name:	**Parish Church of St Andrew, Ashburton**	
Latitude:	+ 50.51369°	Grid Reference:
Longitude:	- 03.75620°	275500 069750

Station Description

From A38 leave at southern Ashburton exit (SP Services). Opposite the Motel and Garage turn right into Western Rd (B3352). Follow 3/4 mile into Ashburton. The church is on the right, before reaching the town centre proper.
The site is in the middle of the large worn step of the porch, in front of the iron/glass gates. The base plate was placed directly over the relict brass gate fitting.

For access contact Rev. Peter Gregson, The Vicarage, West St, Ashburton, Devon.

Location Diagram

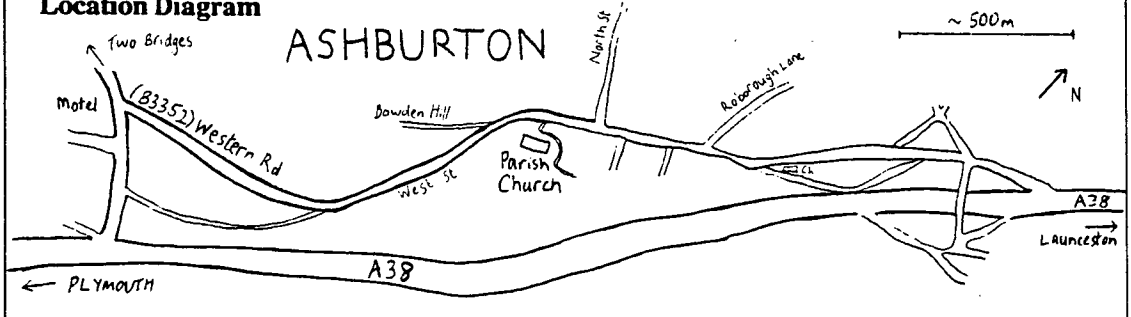

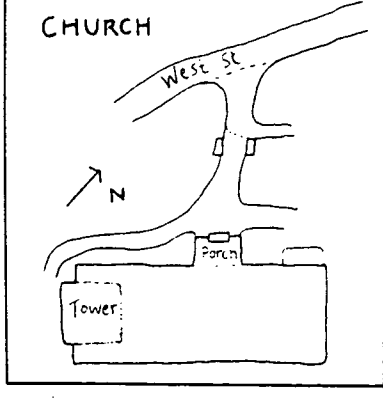

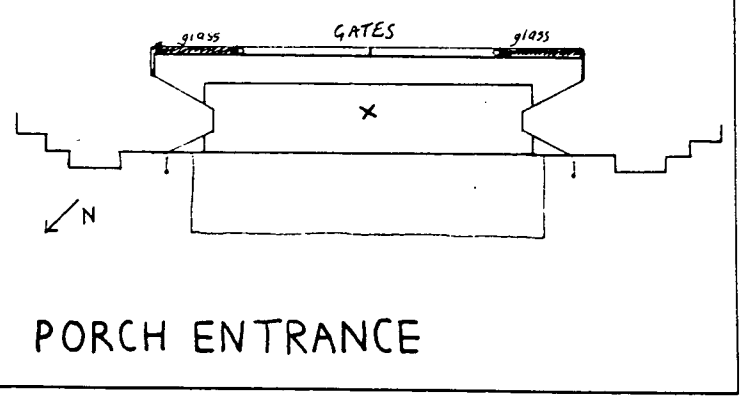

10.03.93

Department of Geology & Geophysics, University of Edinburgh.

Edinburgh University - Gravity Station Information
Reference# 215

Country:	ENGLAND	
Region/County:	CORNWALL	
Nearest Town:	Bodmin	
Name:	**Lanivet Parish Church**	
Latitude:	+ 50.44423°	Grid Reference:
Longitude:	- 04.76226°	203900 064200

Station Description

From East (A303) Bodmin bypass: At roundabout and end of dual carriageway section of A303, take 3rd exit SP Lanivet, Bodmin. Follow for 1.5 miles to the village centre. Turn right just after the garage on the right (Church Road). The church is 300 yards on the left.
The site is in the centre of the narrow granite slab immediately in front of the closed gate.

For access contact Rev. Fr. S.R.F. Drakeley, The Rectory, Lanivet, Bodmin, Cornwall.

Location Diagram

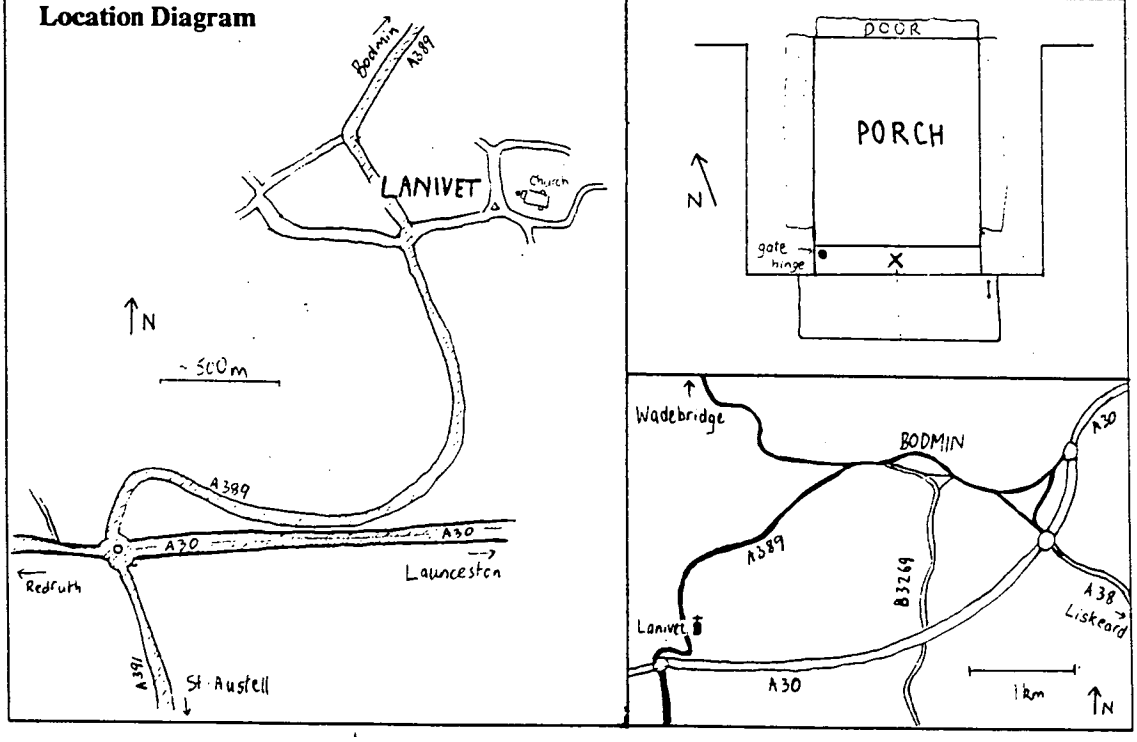

10.03.93

Department of Geology & Geophysics, University of Edinburgh.

Edinburgh University - Gravity Station Information

Reference# 216

Country:	ENGLAND	
Region/County:	DEVON	
Nearest Town:	Bideford	
Name:	**Great Torrington**	
Latitude:	+ 50.95200°	Grid Reference:
Longitude:	- 04.14300°	249493 119199

Station Description

Great Torrington is about 7 miles south of Bideford on the A386 to Okehampton. On entering the village from the A386 north, the church is on the right, opposite the sign for Dartington Crystal. The porch is on the opposite side of the church from the main road. It may be approched on foot from the town centre via cobbled streets.
The site is in the centre of the slab at the front of the porch, in front of the gates.

Location Diagram

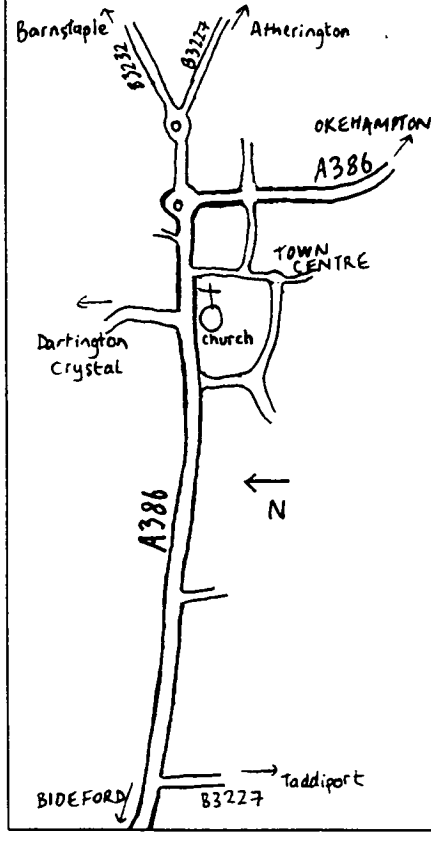

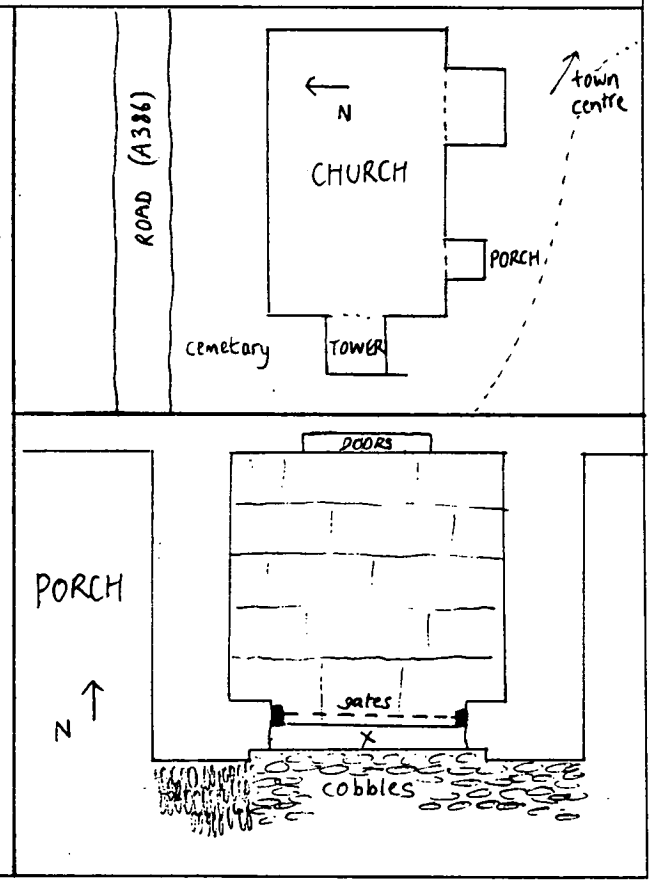

26.05.95 Department of Geology & Geophysics, University of Edinburgh.

Edinburgh University - Gravity Station Information

Reference# 217

Country:	WALES	
Region/County:	GWENT	
Nearest Town:	Chepstow	
Name:	**Mounton Parish Church**	
Latitude:	+ 51.63300°	Grid Reference:
Longitude:	- 02.70400°	351281 192974

Station Description

From Monmouth (north) via A466: at roundabout at outskirts of Chepstow, go straight on (SP M4). Shortly after hospital buildings on R, turn R (SP Mounton, Hospital Stores).
From Severn Bridge (south), leave M4 at 1st roundabout after bridge (Junction 22) (SP Chepstow, A48). At next roundabout go straight on (SP Monmouth, A466). Take 1st L before hospital (SP Mounton, Hospital Stores).
Follow the road to a small roundabout on a green and turn L (SP Newport).
The church is a few hundred yards on L, and the site is in the middle of the step on the roadside, under the bell tower.

For access contact Rev A.R. Willie. Telephone: Chepstow 2317.

Location Diagram

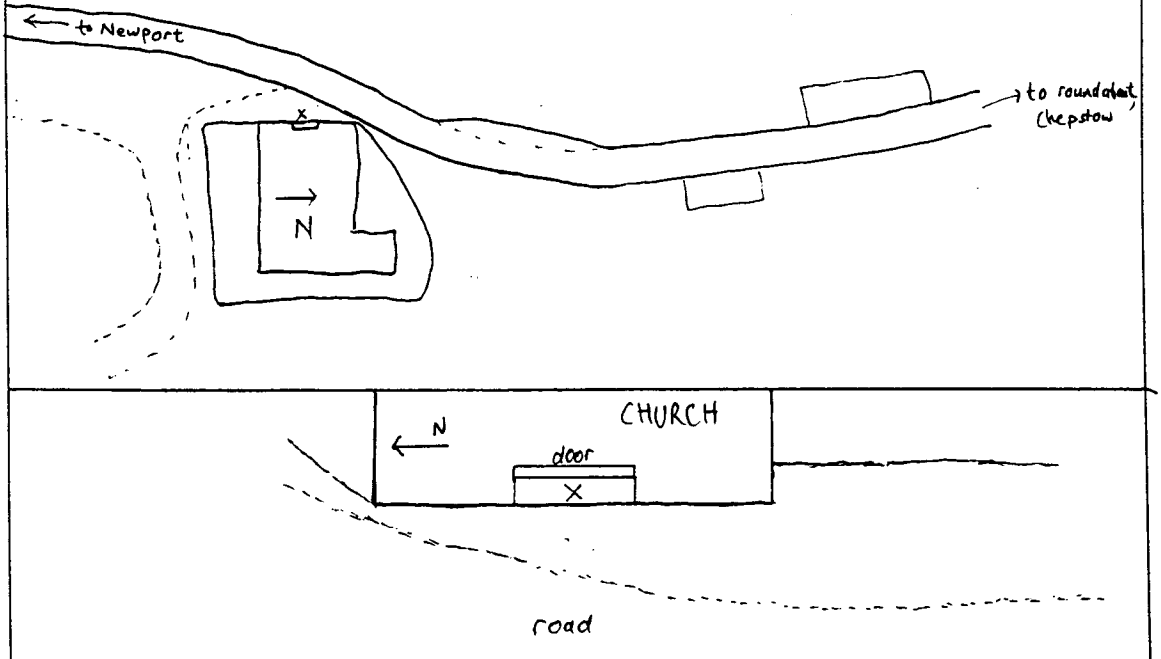

26.05.95 Department of Geology & Geophysics, University of Edinburgh.

Edinburgh University - Gravity Station Information

Reference# 218

Country:	ENGLAND	
Region/County:	HEREFORD & WORCESTER	
Nearest Town:	Great Malvern	
Name:	**St James Church, West Malvern**	
Latitude:	+ 52.11200°	Grid Reference:
Longitude:	- 02.34600°	376309 246066

Station Description

Leave the M5 at Junction 7, and take the A44 (SP Worcester). At 1st roundabout turn L. Pass under the railway, and straight on at the next roundabout. At the A38 go straight on over the roundabout, crossing the river Severn. At the next roundabout, turn L (SP Malvern, A449). Continue towards the hill through Malvern Link, and immediately after a left hand bend, turn acute R (SP West Malvern). Continue along the top road to the church, which is below the road.
The main porch is on the north side of the building, reached by a path from the gate at the cattlegrid. The site is in the middle of the slab which forms the front of the 'top step', underneath the lamp.

For access contact The Vicarage, 2 North Malvern Road. Telephone 574 380.

Location Diagram

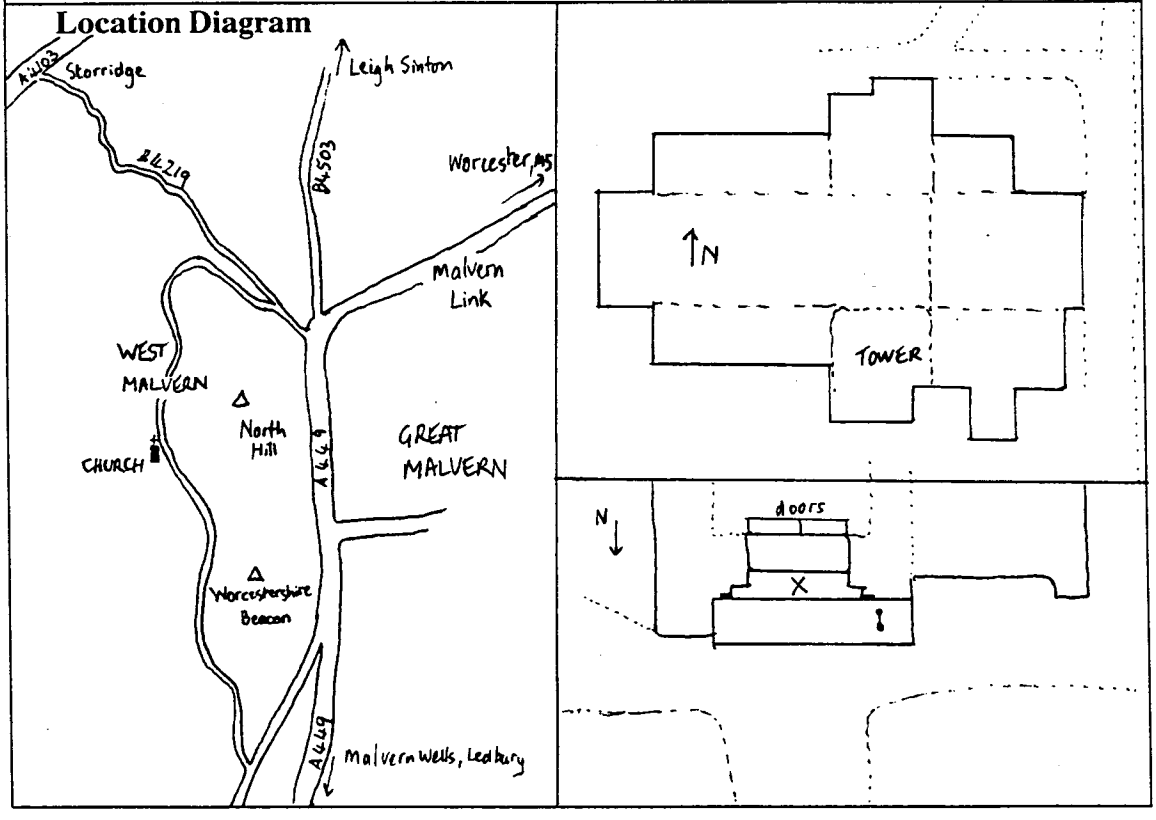

27.05.95 Department of Geology & Geophysics, University of Edinburgh.

Edinburgh University - Gravity Station Information

Reference# 219

Country:	ENGLAND	
Region/County:	STAFFORD	
Nearest Town:	Wolverhampton	
Name:	**Parish Church of St Mary & St Luke, Shareshill**	
Latitude:	+ 52.65700°	Grid Reference:
Longitude:	- 02.08300°	394386 306628

Station Description

Shareshill is between the M54 (Junction 1) and M6 (Junction 11). From the M54, take A460 (SP Cannock). Continue through Featherstone to Shareshill. Just before BP garage, turn L into village. On bend in road, turn L (Church Road). Church is on R.

The site is approximately in the middle of the porch, centrally on a line just behind the widest-apart white pillars.

For access contact Rev. G.F. Smith, 11 Brookhouse Lane, Featherstone. Telephone 01902 727579.

Location Diagram

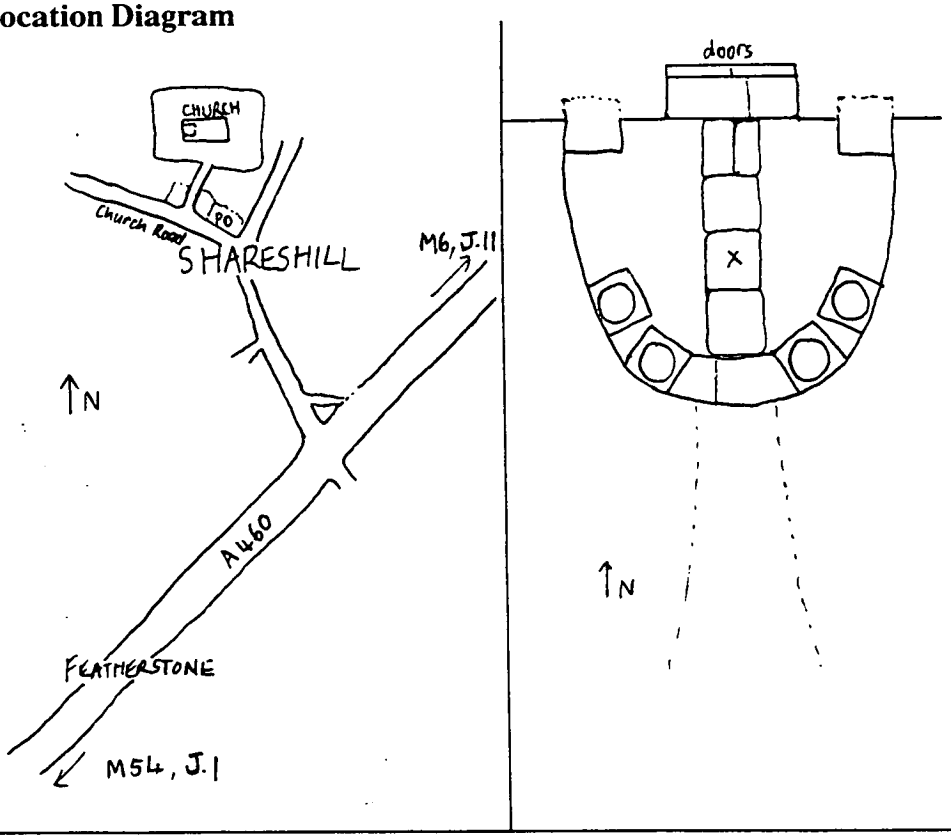

27.05.95 Department of Geology & Geophysics, University of Edinburgh.

Edinburgh University - Gravity Station Information

Reference# 220

Country:	ENGLAND	
Region/County:	BERKSHIRE	
Nearest Town:	Newbury	
Name:	**Beedon Church**	
Latitude:	+ 51.49900°	Grid Reference:
Longitude:	- 01.30500°	448238 178067

Station Description

Beedon is about 7 miles north of Newbury, off the A34. Leave the M4 at Junction 13 (SP Oxford, A34). At roundabout follow Oxford, A34. At T-junction turn L then immediately R onto old A34 (SP Chieveley). Continue for about 2 miles through Chieveley and World's End to Beedon. Take L fork in village (SP Stanmore). Continue about 1/2 mile to Beedon Manor farmyard, turn L immediately after yard into No Through Road. The church is on the L, and the cockerel on top of the spire is visible from afar.

The site is at the back of the porch, in the middle of the stone slab against the door.

For access contact Rev. Peter Renouf, The Vicarage, Beedon.

Location Diagram

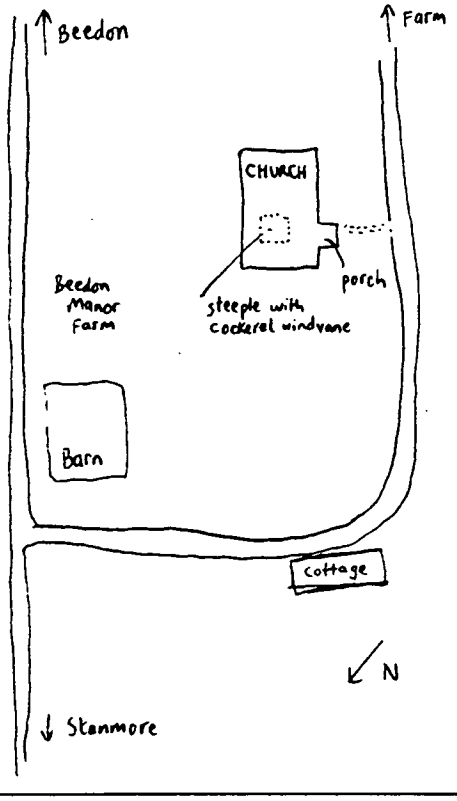

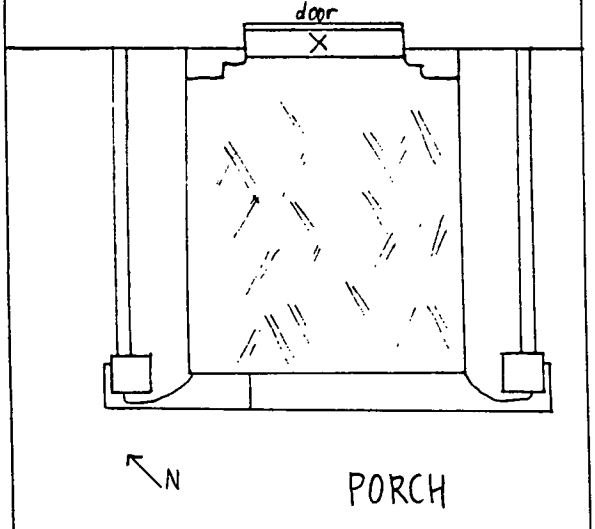

26.05.95 Department of Geology & Geophysics, University of Edinburgh.

Edinburgh University - Gravity Station Information
Reference# 222

Country:	ENGLAND	
Region/County:	MIDDLESEX	
Nearest Town:	Hampton	
Name:	**Hampton Parish Church**	
Latitude:	+ 51.41254°	Grid Reference:
Longitude:	- 0.35986°	514050 169500

Station Description
From the A308 (Hampton Court Road) turn into Church Road. Parking is usually possible on the left by the church. The site is at the North side-door near the tower, opposite a pyramid shaped tomb in the churchyard. The site is in the centre of the stone slab at ground level against the closed doors.

Location Diagram

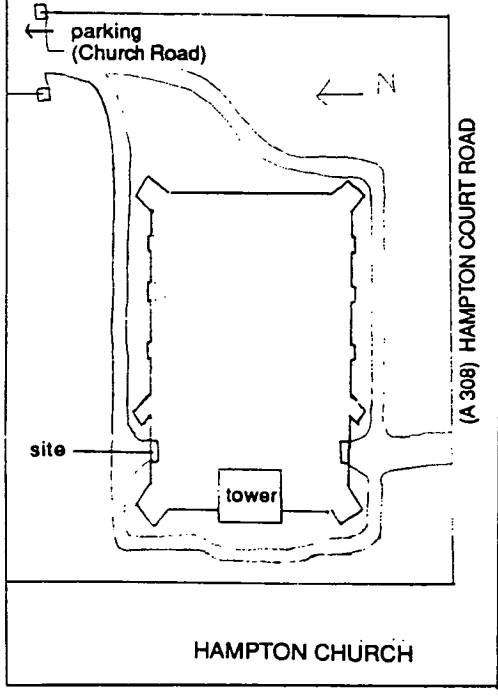

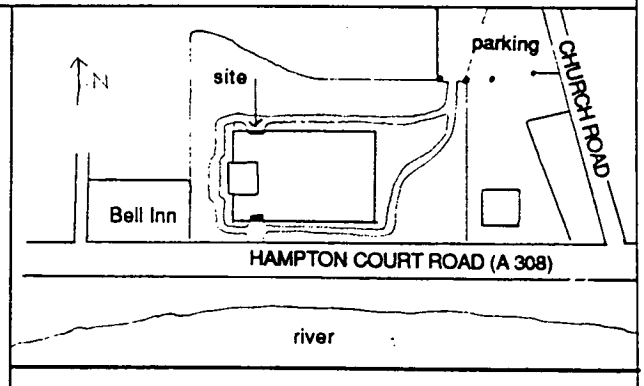

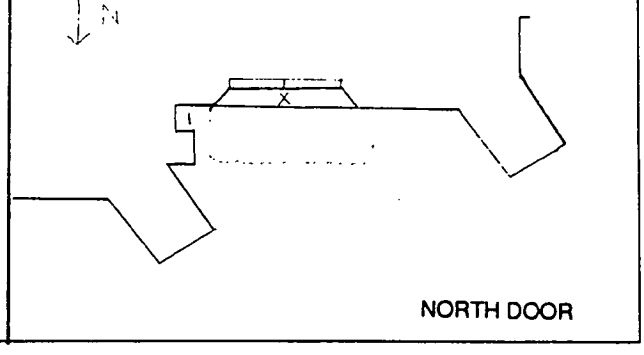

24.02.93 Department of Geology & Geophysics, University of Edinburgh.

Edinburgh University - Gravity Station Information

Reference# 223

Country:	ENGLAND	
Region/County:	NORTHAMPTONSHIRE	
Nearest Town:	Towcester	
Name:	**Church of St Bartholomew, Greens Norton**	
Latitude:	+ 52.41300°	Grid Reference:
Longitude:	- 01.02200°	466919 249908

Station Description

Greens Norton is about 10 miles SW of Northampton. From M1, leave at Junction 15a (SP Northampton). Take A43 towards Towcester, Brackley. At junction of A43 with A5, take local exit (SP Greens Norton). Continue to village, church is on R before village centre.
The site is in the centre of the slab at the front of the porch, between the red tiled floor and the metal grille.

For access contact Rev. John Evans, The Rectory, Greens Norton. Telephone 359508.

Location Diagram

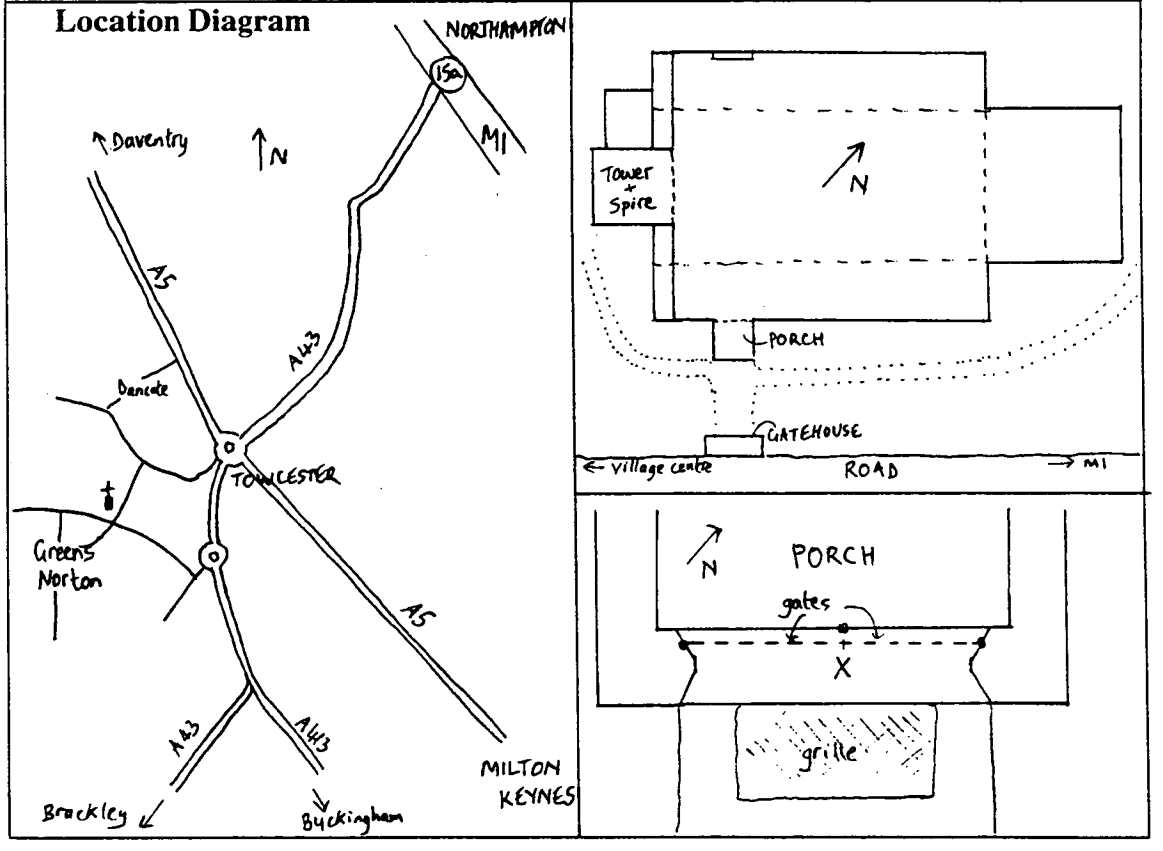

26.05.95 Department of Geology & Geophysics, University of Edinburgh.

Edinburgh University - Gravity Station Information

Reference# 224

Country:	WALES	
Region/County:	POWYS	
Nearest Town:	Montgomery	
Name:	**Parish Church of St Nicholas, Montgomery**	
Latitude:	+ 52.56000°	Grid Reference:
Longitude:	- 03.14600°	322321 296453

Station Description

Montgomery is on the Welsh border between Bishop's Castle and Welshpool. The church is close to the town centre. Turn off the main street opposite the clock tower onto Church Bank. The site is NOT in the main porch, but on the other side of the church, at the foot of the tower. The site is in the centre of the stone slab, against the doors.

For access contact Rev. Barry Letson, The Rectory, Montgomery. Telephone 668243.

Location Diagram

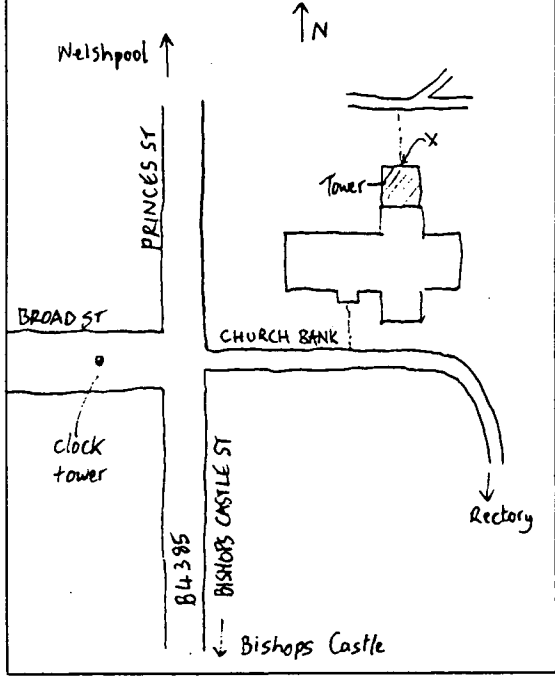

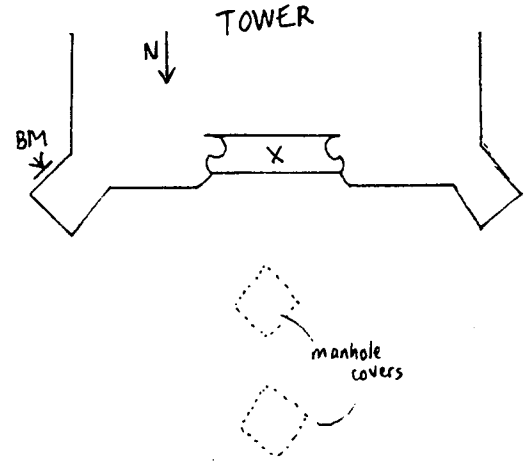

26.05.95 Department of Geology & Geophysics, University of Edinburgh.

Edinburgh University - Gravity Station Information

Reference# 225

Country:	WALES	
Region/County:	DYFED	
Nearest Town:	Aberystwyth	
Name:	**Church of St David, Talybont**	
Latitude:	+ 52.48900°	Grid Reference:
Longitude:	- 03.97900°	265646 289780

Station Description

Talybont is about 8 miles north of Aberystwyth on the A487. At the crossroads at the north end of the village, turn east (inland). The church is about 200 yards on the left. The site is in the centre of the porch step in front of the door.

Location Diagram

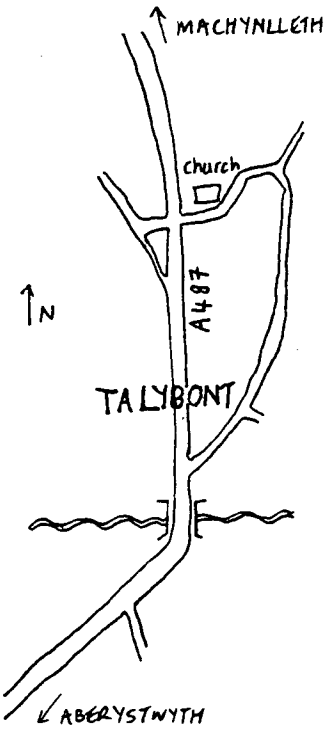

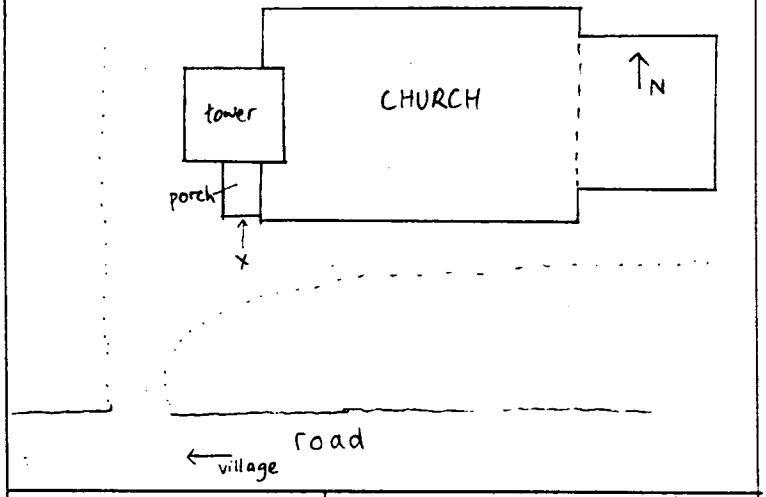

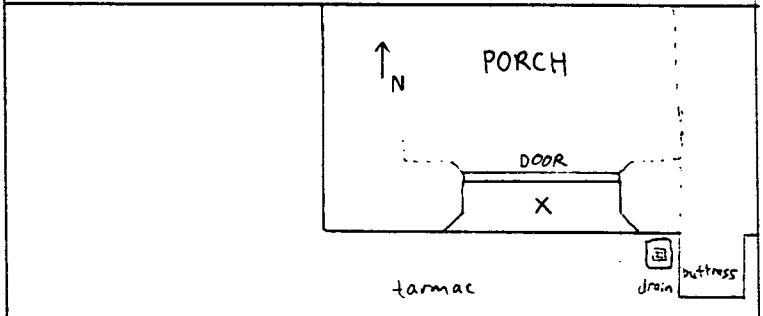

26.05.95 Department of Geology & Geophysics, University of Edinburgh.

Edinburgh University - Gravity Station Information

Reference# 226

Country:	ENGLAND	
Region/County:	CUMBRIA	
Nearest Town:	Carlisle	
Name:	**Talkin Church**	
Latitude:	+ 54.90800°	Grid Reference:
Longitude:	- 02.70300°	354932 557267

Station Description

Leave M6 at Junction 43 and take A69 east (SP Hexham). Continue for 7 miles to roundabout at Brompton and follow signs for town centre. Keep right at end of main street to follow B6413 towards Castle Carrock. Continue for about 2 miles, passing under the A69, and over a level crossing. Turn L after the small lake on L and follow into the village. At the crossroads in the village centre, go straight on. The church is about 100 yards on R.

The site is in the centre of the top step at the entrance to the porch, in front of the outer door.

Location Diagram

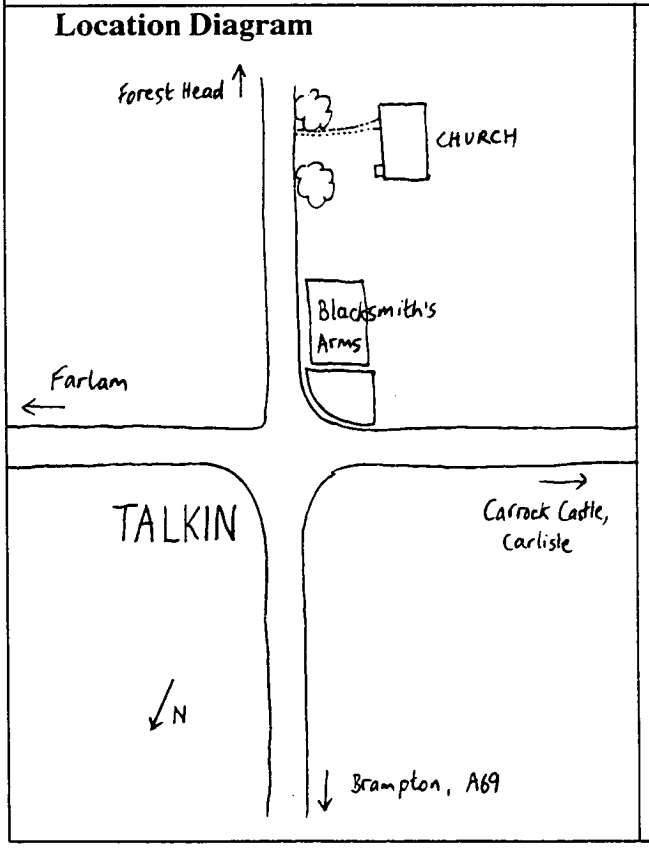

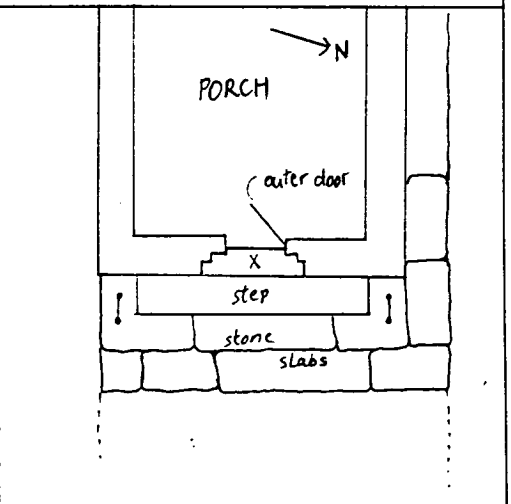

25.05.95 Department of Geology & Geophysics, University of Edinburgh.

Edinburgh University - Gravity Station Information

Reference# 230

Country:	ENGLAND	
Region/County:	HUMBERSIDE	
Nearest Town:	Immingham	
Name:	**Church of St Peter, Great Limber**	
Latitude:	+ 53.56000°	Grid Reference:
Longitude:	- 00.33200°	510471 408363

Station Description

Leave the M180 at Junction 5 and take the A18 (SP Humberside Airport). Continue past the airport to the village of Great Limber. Turn right on a bend in the road by the New Inn. The church is behind the pub and the village pond. The porch is on the south side of the church, and the site is in the centre of the front step of the porch, directly under the archway, on the same level as the stone-tiled floor.

For access contact Rev. S.Phillips, The Vicarage, Great Limber.

Location Diagram

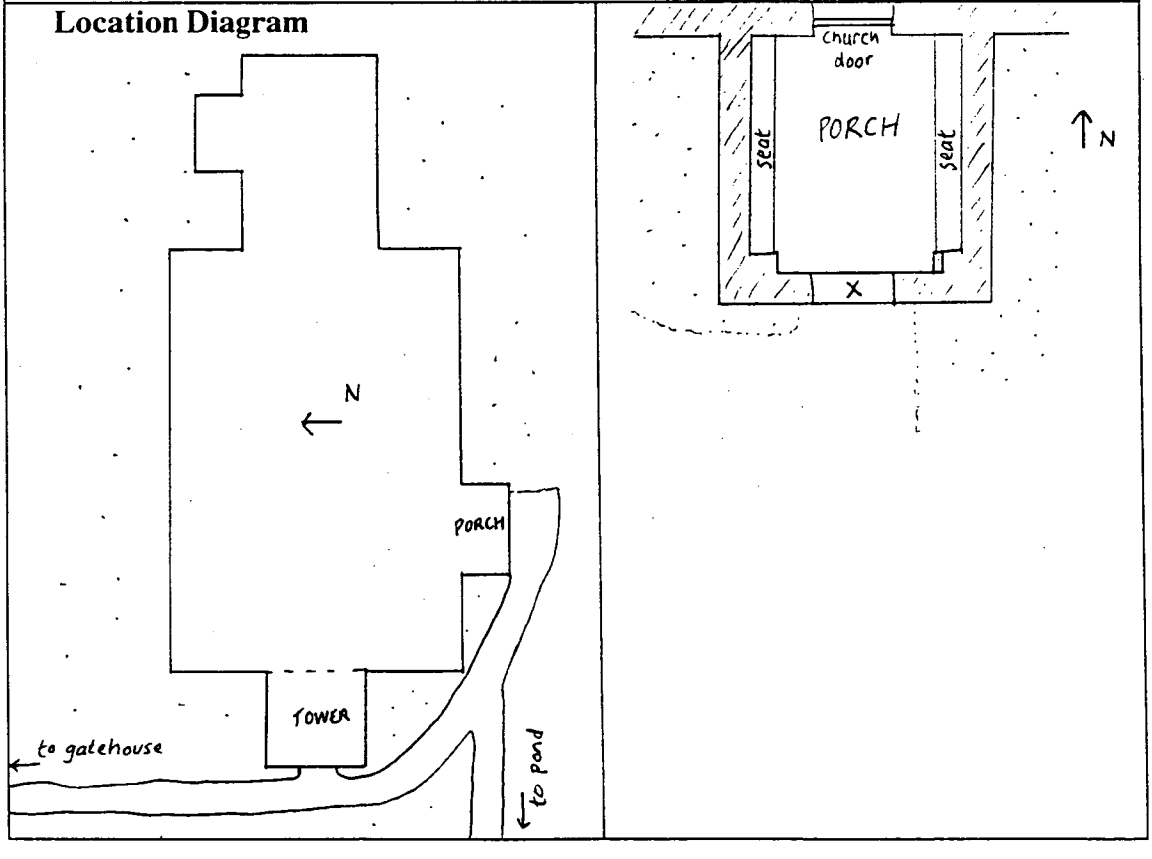

24.05.95 Department of Geology & Geophysics, University of Edinburgh.

Edinburgh University - Gravity Station Information

Reference# 231

Country:	ENGLAND	
Region/County:	WEST YORKSHIRE	
Nearest Town:	Halifax	
Name:	**St John the Divine Church, Rishworth**	
Latitude:	+ 53.65800°	Grid Reference:
Longitude:	- 01.95200°	403172 417972

Station Description

Leave the M62 at Junction 22. Take the A672 SP Halifax. Continue 4 miles past Boothwood Reservoir to the village of Rishworth. Continue through the village past the Cunning Corner pub then take the very small road on R (Godly Lane), on a righthand bend in the road, just after old garages on L and just before terrace on R. The church is at the top of the hill on the L.
The site is in the small (southern-most) porch which is the second entrance as approached from the main gateway below the building, in the centre of the top step against the wooden doors.

For access contact Rev. C.Dixon. Telephone 822239.

Location Diagram

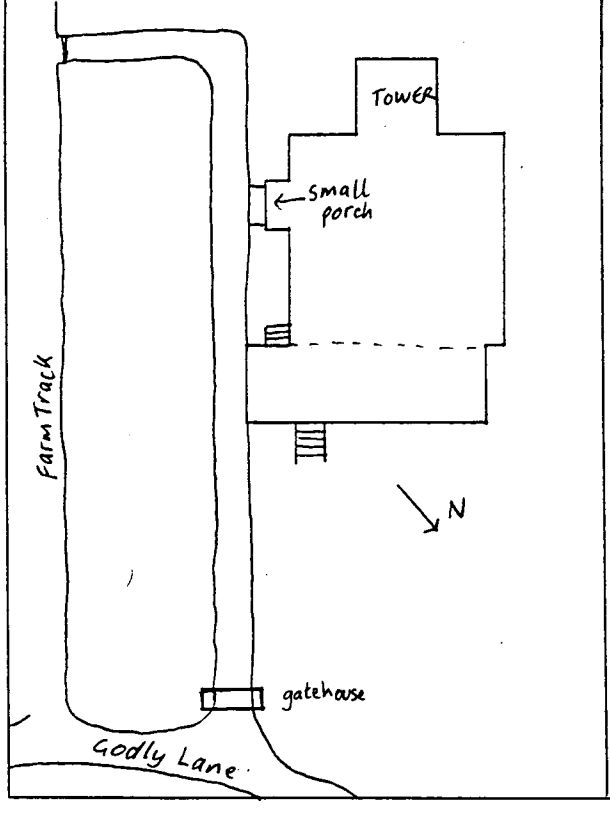

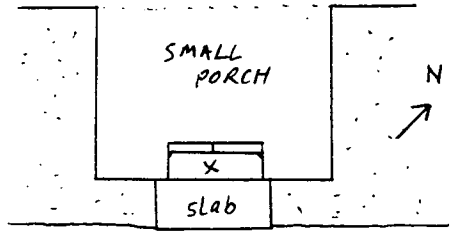

10.03.93 Department of Geology & Geophysics, University of Edinburgh.

Edinburgh University - Gravity Station Information

Reference# 232

Country:	WALES	
Region/County:	WEST GLAMORGAN	
Nearest Town:	Swansea	
Name:	**Capel yr Anymddybynwyr, Felindre**	
Latitude:	+ 51.70600°	Grid Reference:
Longitude:	- 03.97100°	263824 202696

Station Description

From M4 (east), leave at Junction 46 (limited interchange) SP B4489. At the roundabout take 3rd exit SP A48 Llanelli, and after 200 yards turn R SP Felindre. Continue past the steel works along a narrow winding lane for 2.5 miles to Felindre. After the tennis court and PO on R, turn R on lefthand bend up a steep hill ('Unsuitable for long vehicles' sign). The chapel is above the road on the way up the hill.

The site is in the centre of the step against the main doors, on the east side of the building.

Location Diagram

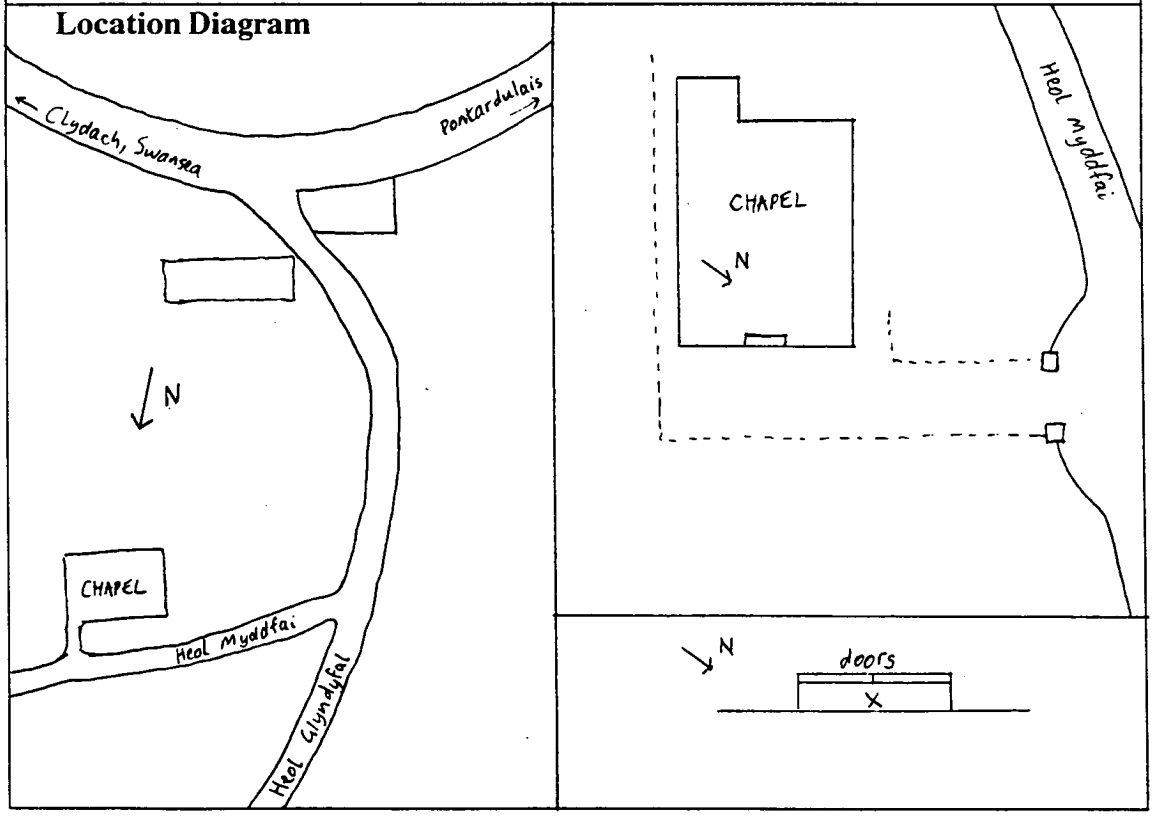

10.03.93 Department of Geology & Geophysics, University of Edinburgh.

Edinburgh University - Gravity Station Information

Reference# 233

Country:	WALES	
Region/County:	DYFED	
Nearest Town:	Haverfordwest	
Name:	**Ambleston Church**	
Latitude:	+ 51.89400°	Grid Reference:
Longitude:	- 04.90600°	200070 225756

Station Description

From the junction of the B4329 and B4313 near Rosebush, take the B4329 south towards Haverfordwest. Continue for about 3 miles through Tufton to Woodstock, where take 3rd R SP Letterston, Ambleston. Turn L at T-junction, cross a stream and turn R at crossroads SP Ambleston. The church is in the centre of the village, and the site is in the porch at the foot of the tower, in the centre of the stone slab against the wooden doors.

For access contact Roger White. Telephone Trefcan 505.

Location Diagram

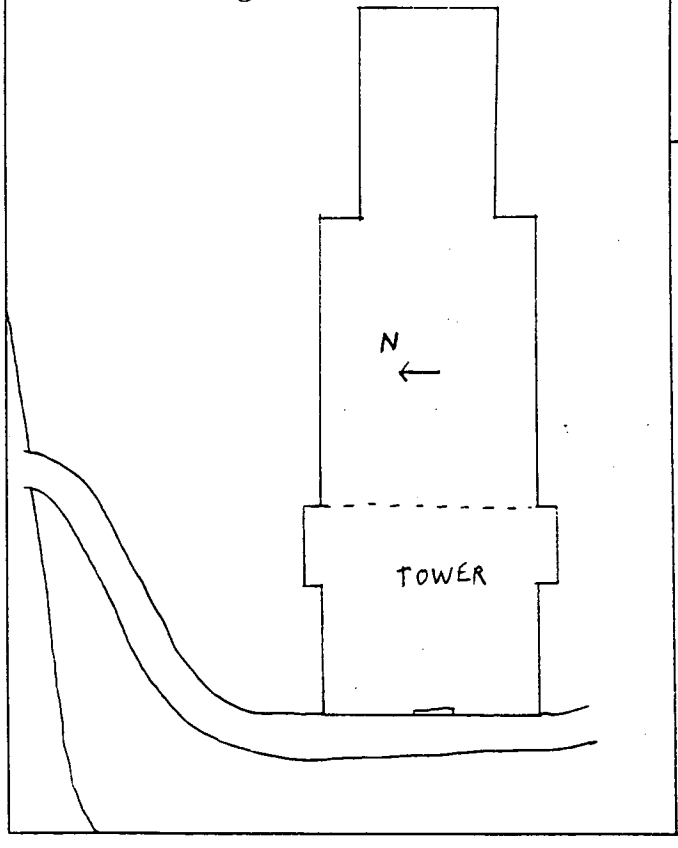

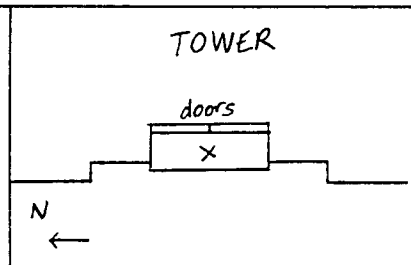

10.03.93 Department of Geology & Geophysics, University of Edinburgh.

Edinburgh University - Gravity Station Information

Reference# 234

Country:	WALES	
Region/County:	GWYNEDD	
Nearest Town:	Betws-y-Coed	
Name:	**St Mary's Church, Betws y Coed**	
Latitude:	+ 53.09100°	Grid Reference:
Longitude:	- 03.80200°	279339 356416

Station Description

The church is on the main street (the A5) in Betws y Coed, on the opposite side of the road from the playing field which is in front of the railway station.
The site is at the front of the main entrance porch on the NW side of the building, in the middle of the stone slab under the decorated wooden doorframe

For access contact Rev. John Barden Davies. Telephone Betws y Coed 313.

Location Diagram

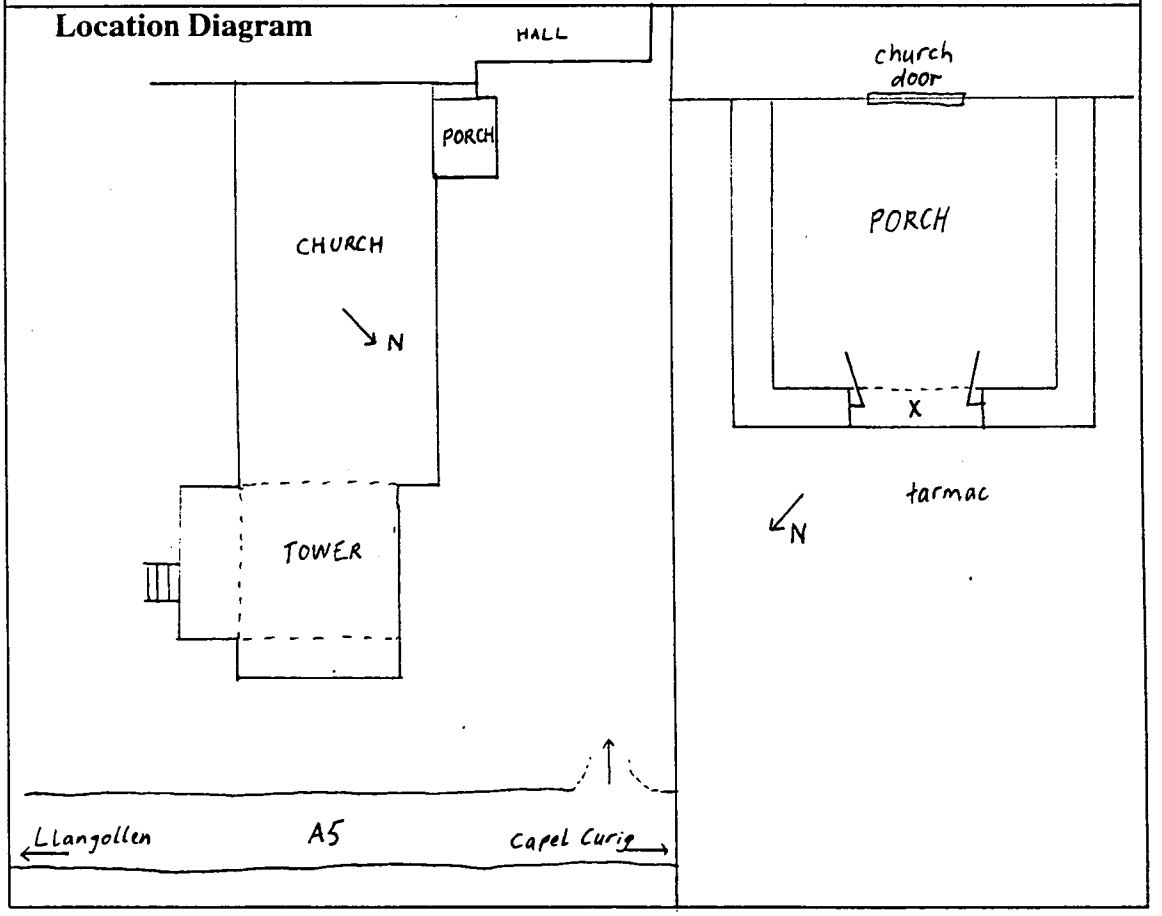

24.05.95 Department of Geology & Geophysics, University of Edinburgh.

Edinburgh University - Gravity Station Information

Reference# 240

Country:	SCOTLAND	
Region/County:	TAYSIDE	
Nearest Town:	Perth	
Name:	**Methven Mausoleum**	
Latitude:	+ 56.41670°	Grid Reference:
Longitude:	- 03.57945°	302570 726050

Station Description

Methven is on the A85 between Perth and Crieff. Leave the A9 at the junction NW of Perth (SP Crieff, Crianlarich, A85). Continue for about 4 miles to Methven, where turn R at Bell Inn (Church Road). The entrance and parking are on the far side (N) of the church. The mausoleum is behind the church, and the site is in the middle of the doorway of the mausoleum, which faces the church.

For access contact Rev. B. Bain, 5 Sauchob Road, Methven.

Location Diagram

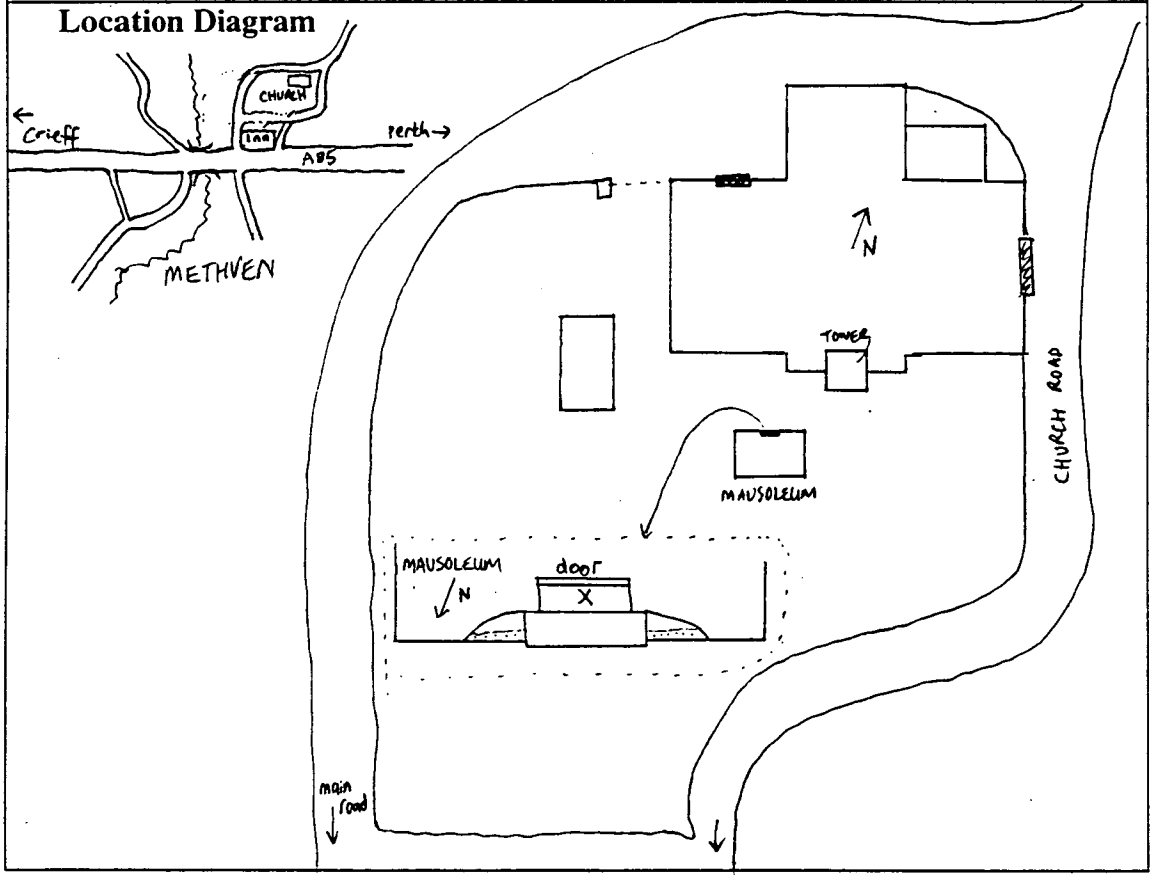

27.05.95 Department of Geology & Geophysics, University of Edinburgh.

Edinburgh University - Gravity Station Information

Reference# 241

Country:	SCOTLAND	
Region/County:	TAYSIDE	
Nearest Town:	Forfar	
Name:	**Church of Scotland, Tannadice**	
Latitude:	+ 56.71177°	Grid Reference:
Longitude:	- 02.85770°	347500 758100

Station Description

Tannadice is about 5 miles north of Forfar. Leave the A94 (dual carriageway) at Finavon (Garage and Cafe) (SP Tannadice, B957). Continue for about 2 miles to Tannadice. The church is on the L on entering village. The site is in the centre of the large step of the front door. (The dustmat was removed).

For access contact Rev. A. Jolly, The Manse, Tannadice, By Forfar. Telephone: Finavon 376.

Location Diagram

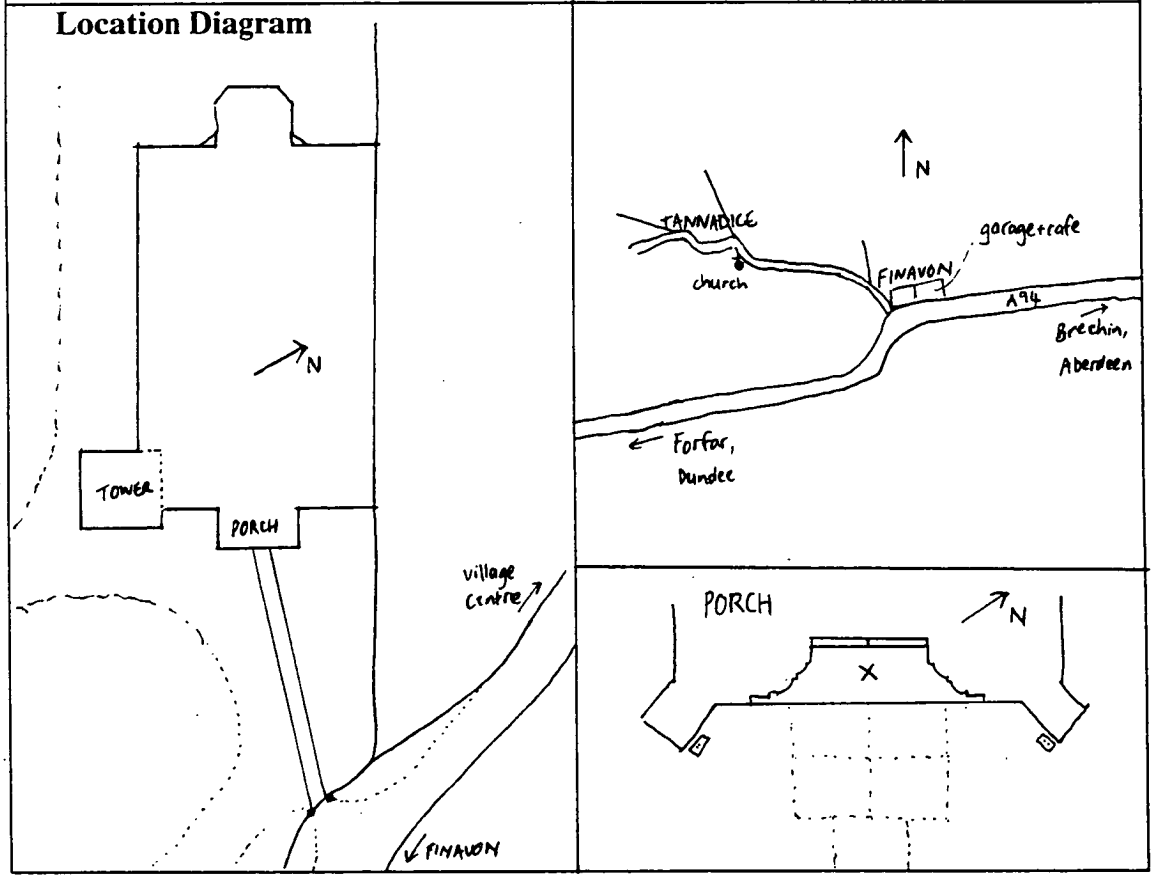

27.05.95 Department of Geology & Geophysics, University of Edinburgh.

Edinburgh University - Gravity Station Information

Reference# 242

Country:	SCOTLAND	
Region/County:	TAYSIDE	
Nearest Town:	Monifieth	
Name:	**MOD Barry Buddon, VLBI site**	
Latitude:	+ 56.47800°	Grid Reference:
Longitude:	- 02.78100°	351900 732050

Station Description

From the A930 west, turn R in Monifieth town centre, just after the (Wm Low) supermarket. Turn L then R under railway bridge (narrow road), then sharp left and continue to the camp. The Ordnance Survey installed witness marks (WM) and bolts at the VLBI site in 1989. Gravity was measured about 2 m north of the manhole cover which marks the OSBM (this was covered in turf).

For access contact The Range Commandant, Barry Buddon Camp, Monifieth, Tayside. Telephone: 01382 533025.

Location Diagram

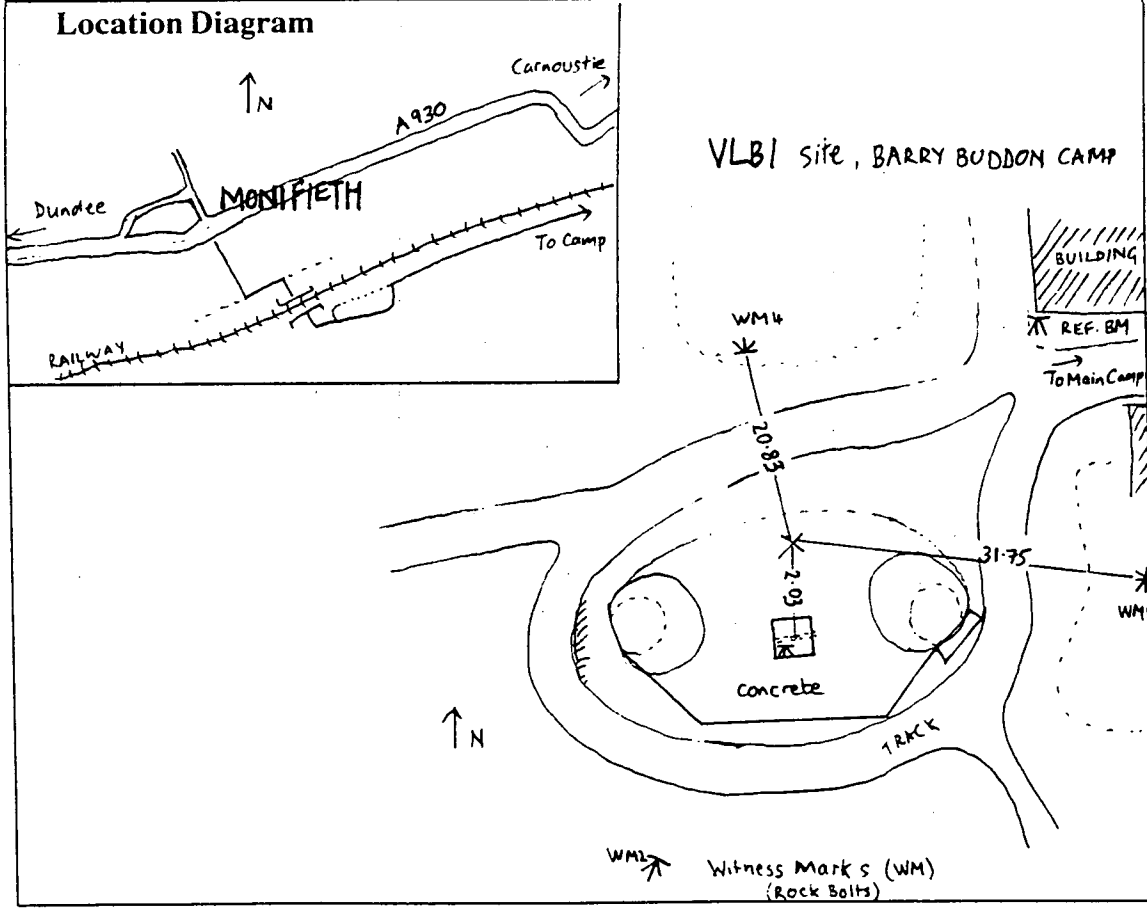

27.05.95 Department of Geology & Geophysics, University of Edinburgh.

Edinburgh University - Gravity Station Information

Reference# 243

Country:	SCOTLAND	
Region/County:	GRAMPIAN	
Nearest Town:	Elgin	
Name:	**Church of Scotland, Elgin South**	
Latitude:	+ 57.64601°	Grid Reference:
Longitude:	- 03.31360°	321600 862520

Station Description

From Inverness (west) A96: At roundabout by Post Office, turn right (SP Perth). At mini roundabout by garage, straight on. Take 1st L (Morray St) (SP Police). The church is on the R, past the police station.
The site is in the main entrance, facing N. Guildry St, in the middle of the front of the top step.

For access contact The Session Clerk, Mr R.J. Burns., Telephone 544582.

Location Diagram

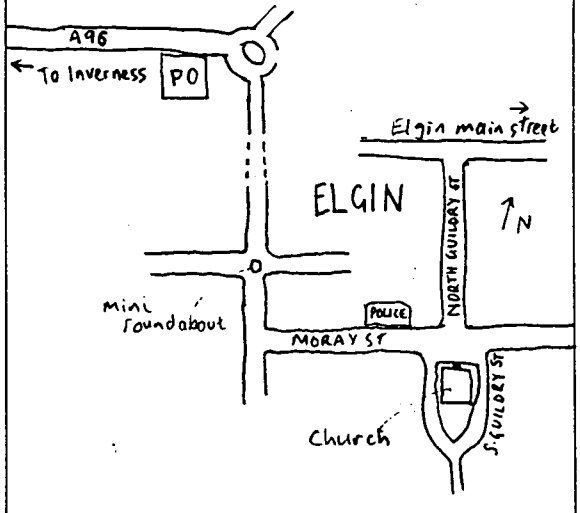

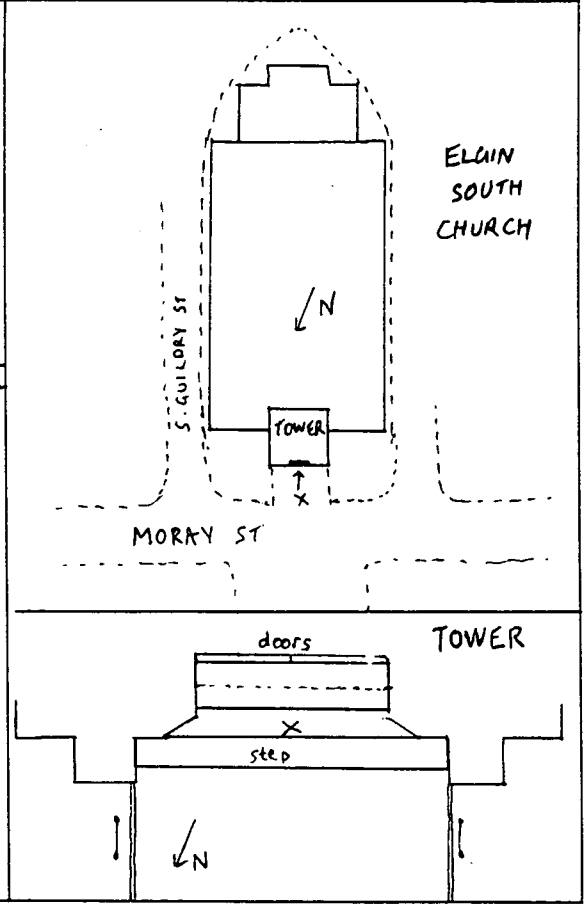

27.05.95 Department of Geology & Geophysics, University of Edinburgh.

Edinburgh University - Gravity Station Information

Reference# 244

Country:	SCOTLAND	
Region/County:	HIGHLAND	
Nearest Town:	Dingwall	
Name:	**St Annes Scottish Episcopal Church, Strathpeffer**	
Latitude:	+ 57.58855°	Grid Reference:
Longitude:	- 04.53766°	248320 858200

Station Description

From the A835 at Contin, turn R (SP Strathpeffer A834). Continue for about 2 miles to Strathpeffer, follow road down hill, passing garage on left. Church is on R after lefthand bend in road, just before the town centre.
The site is on the front (outermost section) of the curved step to the main entrance, at the base of the tower.

For access contact Rev. S. Hotchen. Telephone: Dingwall 62204.

Location Diagram

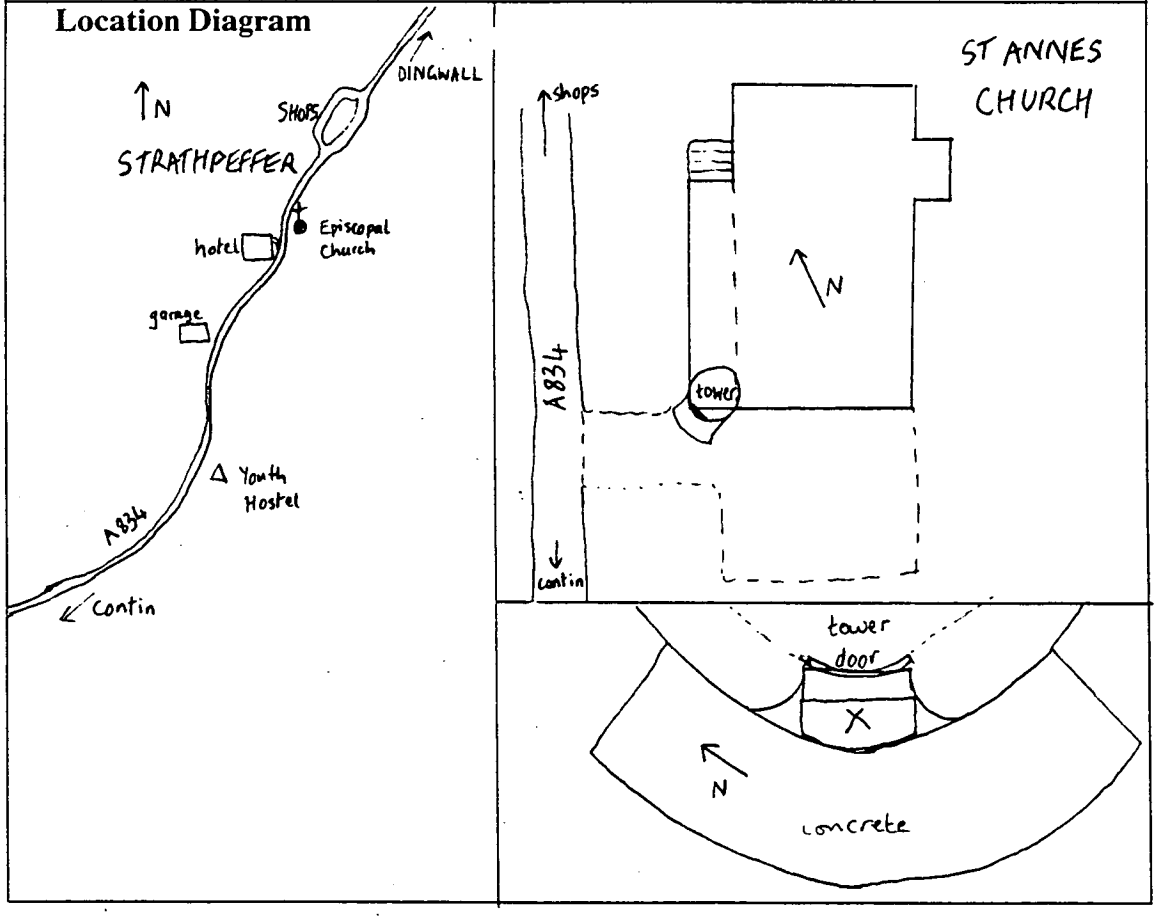

27.05.95 Department of Geology & Geophysics, University of Edinburgh.

Edinburgh University - Gravity Station Information

Reference# 245

Country:	SCOTLAND	
Region/County:	HIGHLAND	
Nearest Town:	Dornoch	
Name:	**Church of Scotland, Lairg**	
Latitude:	+ 58.02512°	Grid Reference:
Longitude:	- 04.39948°	258300 906480

Station Description

From the A836 (south) from Bonar Bridge, turn R in Lairg, between the garage and the hotel (SP Rogart, A839). Turn L after the Bank of Scotland (Church Road). Follow road round to L to the church. The site is in the middle of the bottom step to the main door, on the west side of the building.

Location Diagram

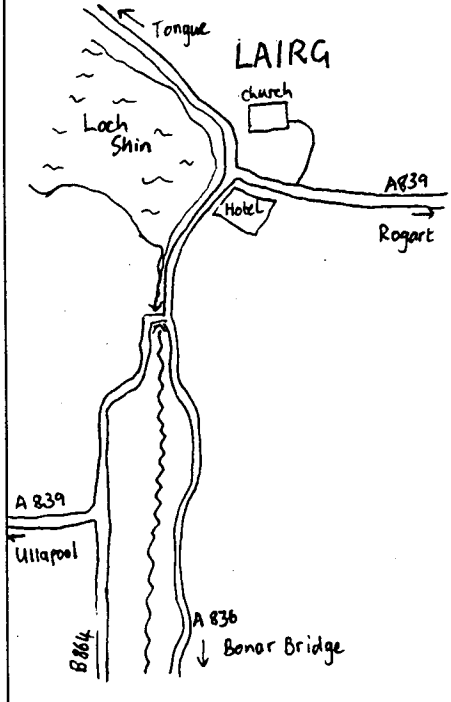

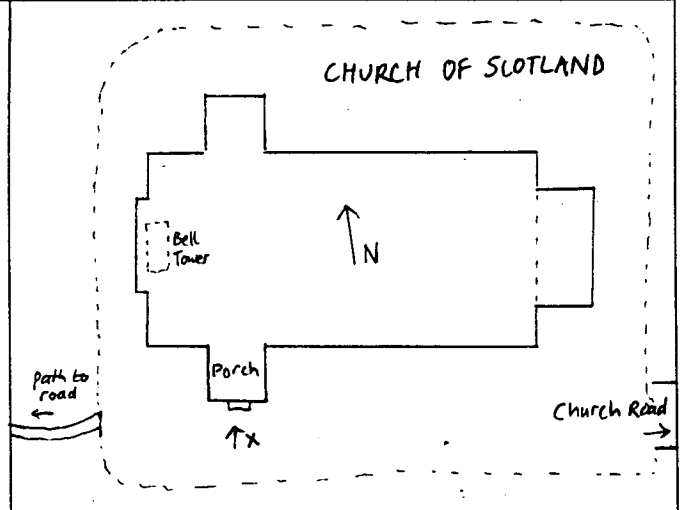

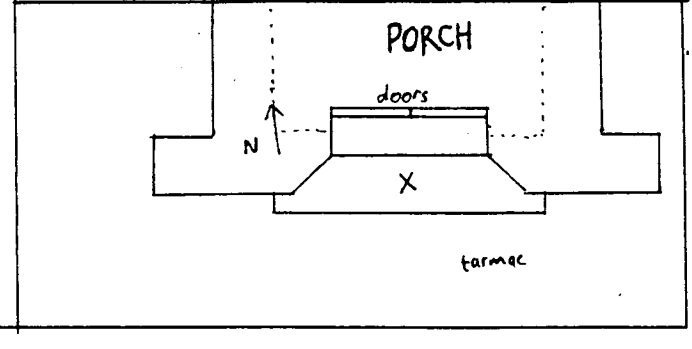

28.05.95 Department of Geology & Geophysics, University of Edinburgh.

Edinburgh University - Gravity Station Information

Reference# 246

Country:	SCOTLAND	
Region/County:	HIGHLAND	
Nearest Town:	Wick	
Name:	**Church of Scotland, Wick**	
Latitude:	+ 58.44386°	Grid Reference:
Longitude:	- 03.09408°	336140 951100

Station Description

The church lies on the A9 in Wick, above the River Wick on the north bank. From the A9 (south), cross the bridge at the mini roundabout. At the traffic lights, turn L (SP John o' Groats, Airport). The church is about 200 yards on the L.
The site is in the LEFT-hand doorway, NOT the centre (main) doorway, in the middle of the outer stone slab.

Location Diagram

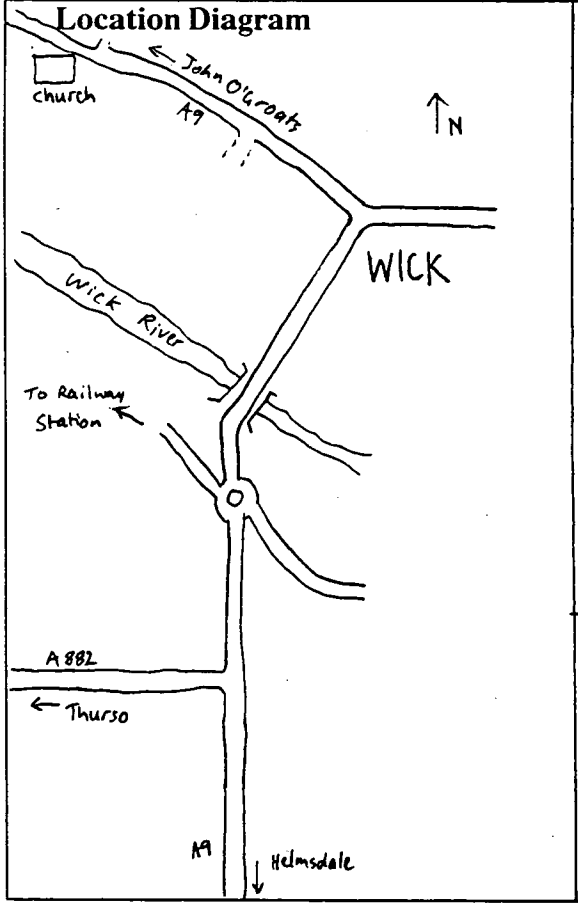

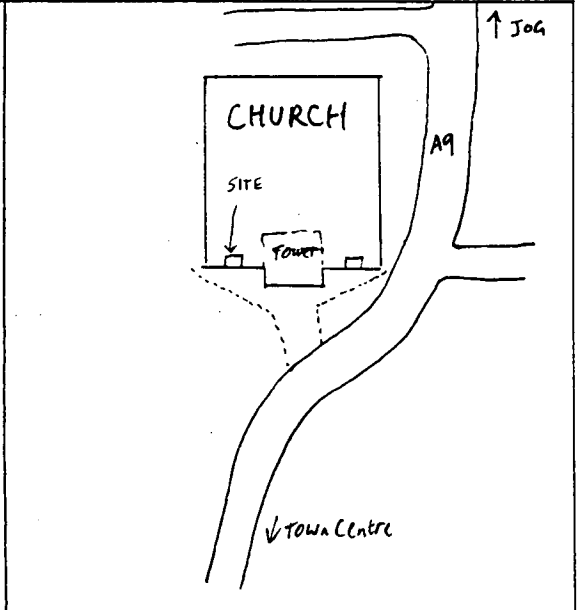

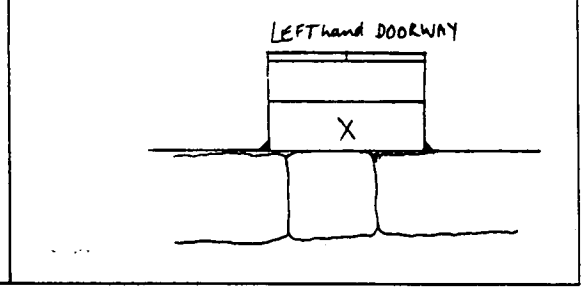

28.05.95 Department of Geology & Geophysics, University of Edinburgh.

Edinburgh University - Gravity Station Information

Reference# 247

Country:	SCOTLAND	
Region/County:	HIGHLAND	
Nearest Town:	Tongue	
Name:	**Bettyhill FBM**	
Latitude:	+ 58.48639°	Grid Reference:
Longitude:	- 04.21363°	270960 957440

Station Description

Bettyhill FBM is on the A836 north coast road between Bettyhill and Tongue, close to the junction with the B871 (Strathnaver road). From the south (Strathnaver) trun L at the junction and continue up the hill, until about 200 yards past the warning sign for a T-junction on the other side of the road. The FBM is behind a knoll on the left hand side of the road, opposite some bushes on the right, about 15 yards from the roadside. In the summer it is totally hidden by the bracken.

Location Diagram

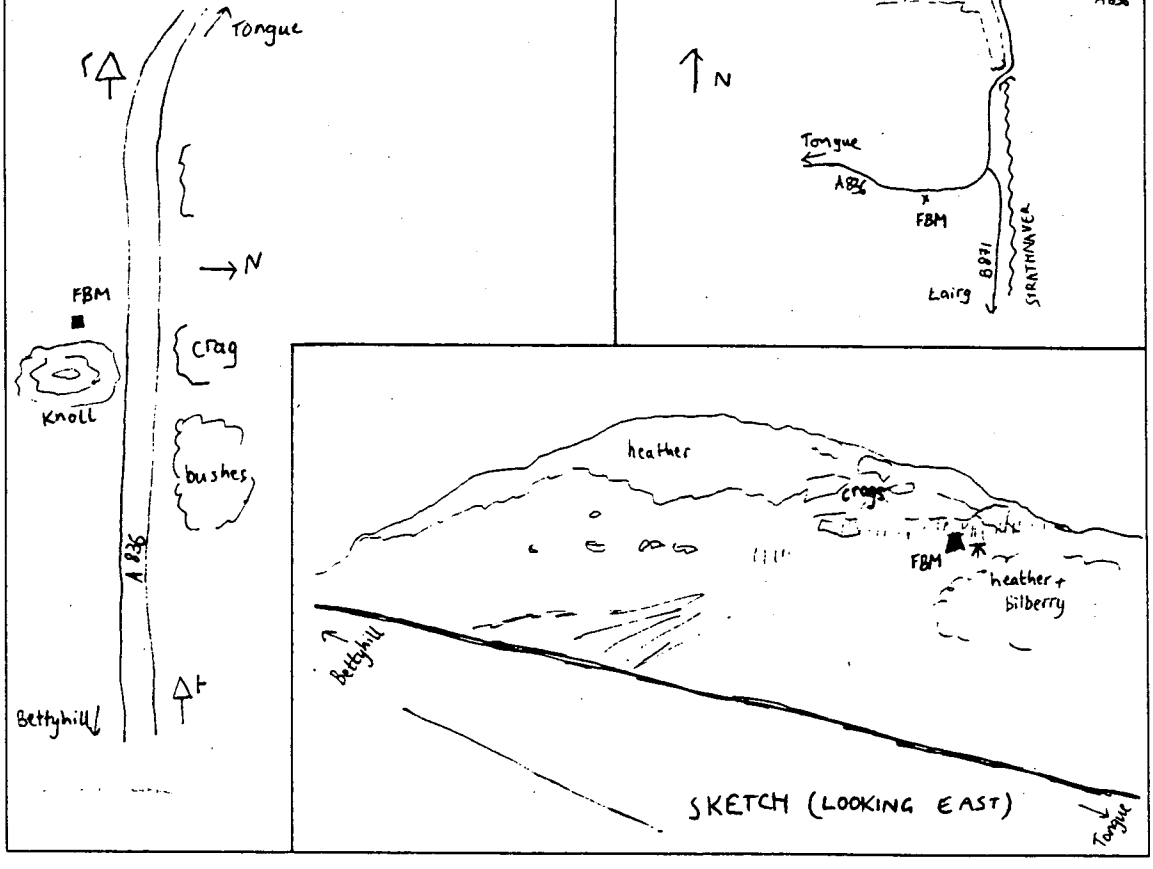

28.05.95 Department of Geology & Geophysics, University of Edinburgh.

Edinburgh University - Gravity Station Information

Reference# 248

Country:	SCOTLAND	
Region/County:	HIGHLAND	
Nearest Town:	Scourie	
Name:	**Church of Scotland, Scourie**	
Latitude:	+ 58.34848°	Grid Reference:
Longitude:	- 05.15852°	215180 944300

Station Description

The church is south of the village centre on the west side of the road. From the north, continue through the village and past the caravan site. The church is on the R shortly after a small road to the bay.
The site is in the centre of the square step to the back door.

Location Diagram

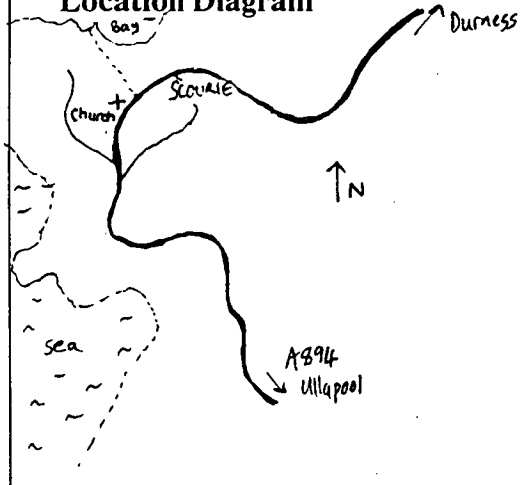

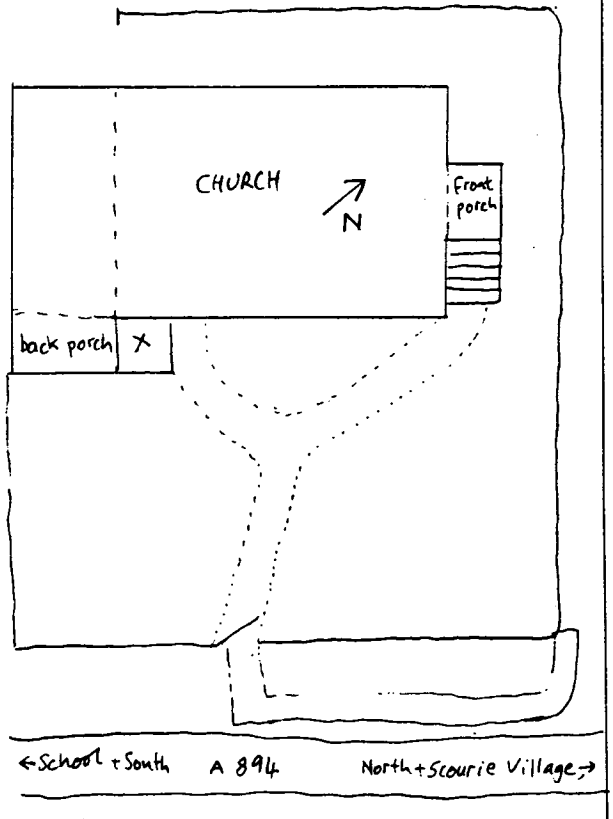

28.05.95 Department of Geology & Geophysics, University of Edinburgh.

Edinburgh University - Gravity Station Information

Reference# 249

Country:	SCOTLAND	
Region/County:	HIGHLAND	
Nearest Town:	Ullapool	
Name:	**Ullapool Museum**	
Latitude:	+ 57.89628°	Grid Reference:
Longitude:	- 05.16143°	212650 894000

Station Description

The Museum in Ullapool is a converted church, two buildings along from the Post Office in Ullapool. The site is in the doorway to the left of the gate, in the middle of the step. The other doorway is used as the entrance.

Location Diagram

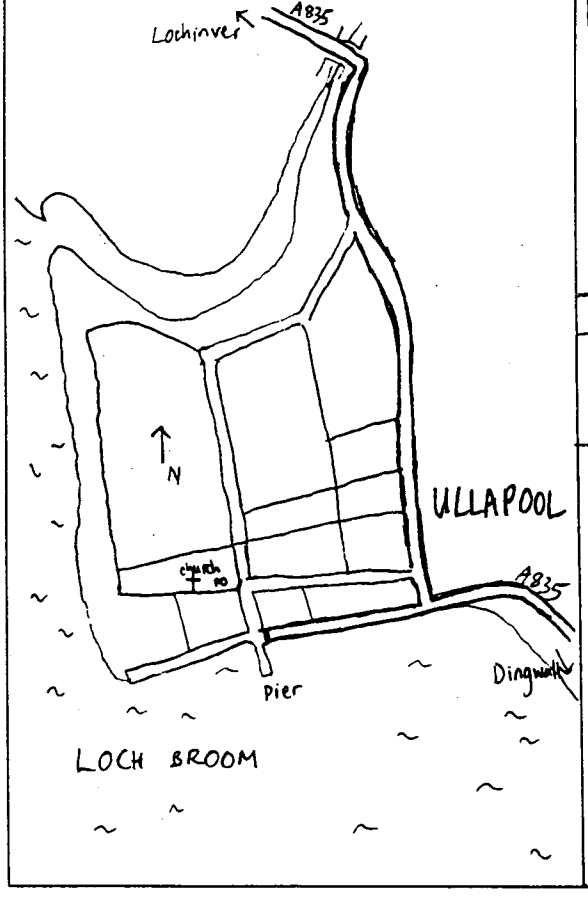

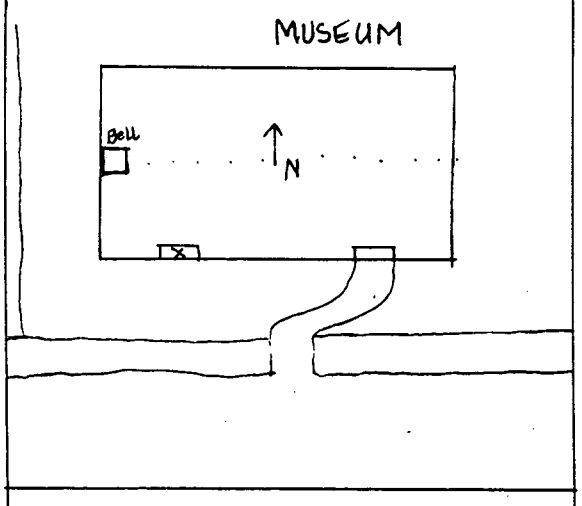

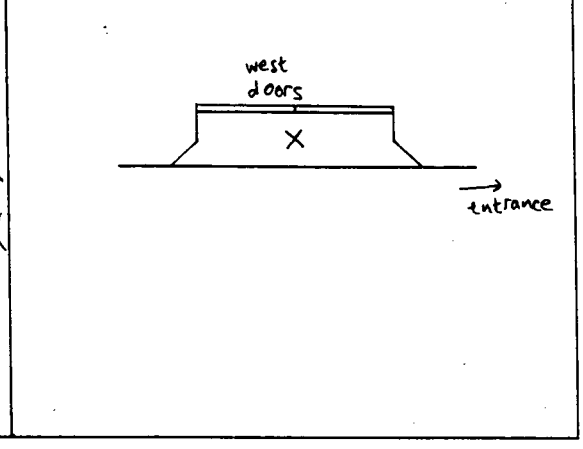

28.05.95 Department of Geology & Geophysics, University of Edinburgh.

Edinburgh University - Gravity Station Information

Reference# 250

Country:	SCOTLAND	
Region/County:	HIGHLAND	
Nearest Town:	Ullapool	
Name:	**Achnasheen FBM**	
Latitude:	+ 57.57872°	Grid Reference:
Longitude:	- 05.08027°	215850 858450

Station Description

Achnasheen is at the junction of the A832 Gairloch-Garve road and the A890 Strathcarron road. The FBM is in a field about 200 yards NNW of the road junction.

Location Diagram

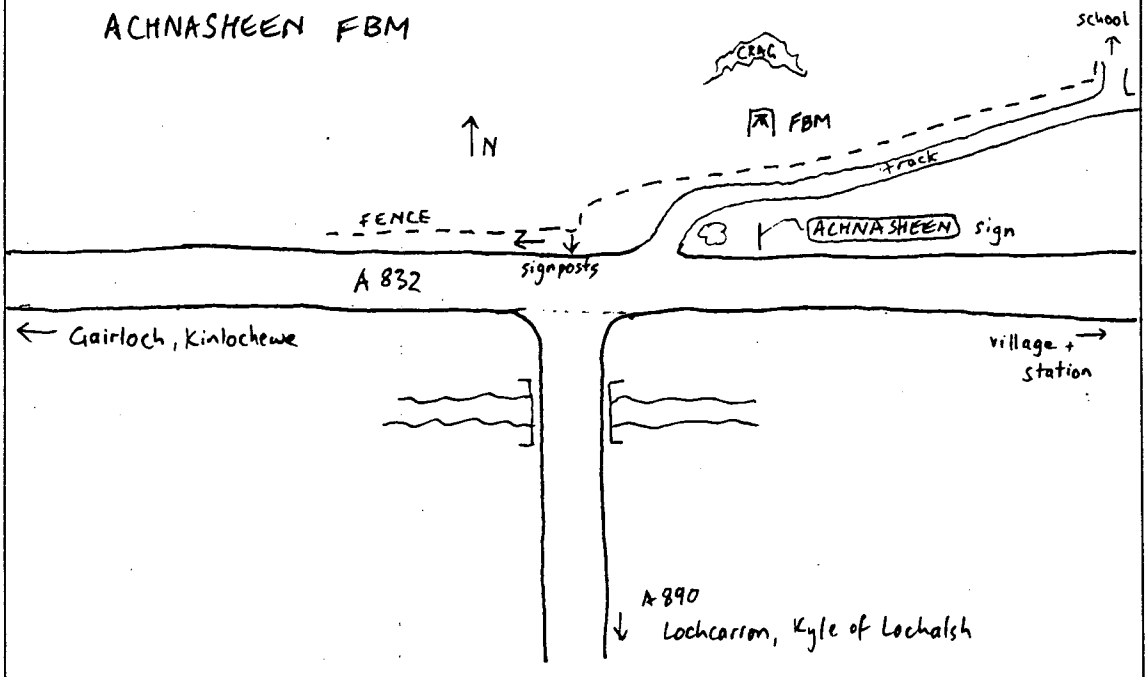

28.05.95 Department of Geology & Geophysics, University of Edinburgh.

Edinburgh University - Gravity Station Information

Reference# 251

Country:	SCOTLAND	
Region/County:	HIGHLAND	
Nearest Town:	Kyle of Lochalsh	
Name:	**St Duthacs Catholic Church, Dornie**	
Latitude:	+ 57.27826°	Grid Reference:
Longitude:	- 05.51041°	215850 858450

Station Description

Turn off the A87 (Kyle of Lochalsh-Shiel Bridge) road on east side of bridge over Loch Long, opposite the castle. Follow the road to through the village centre and continue past the museum towards Bundalloch. The Catholic church is on the R opposite a lay-by.
The site is in the back of the porch, in the middle of the stone step against the wooden door.

Location Diagram

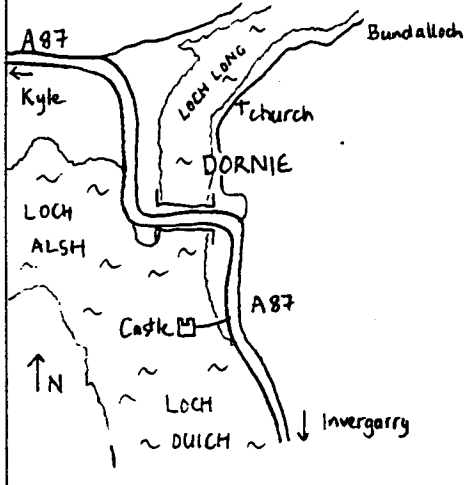

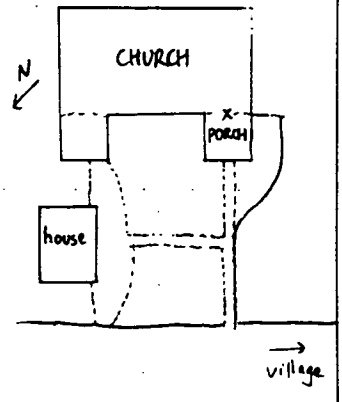

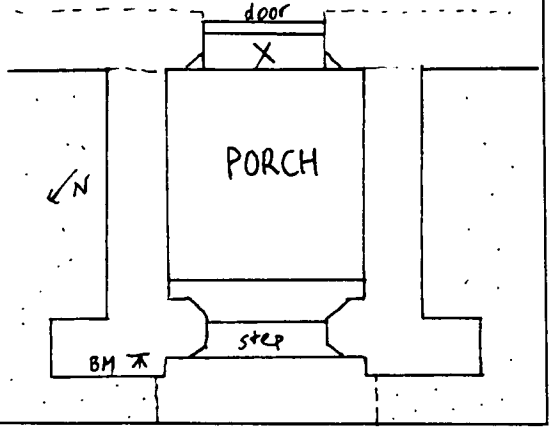

28.05.95 Department of Geology & Geophysics, University of Edinburgh.

Edinburgh University - Gravity Station Information

Reference# 252

Country:	SCOTLAND	
Region/County:	HIGHLAND	
Nearest Town:	Fort William	
Name:	**St Margaret's Catholic Church, Roybridge**	
Latitude:	+ 56.89216°	Grid Reference:
Longitude:	- 04.83939°	227060 781440

Station Description

From A82 (Fort William-Inverness), turn off at Spean Bridge (SP Newtonmore, A86). Continue for about 3 miles to Roybridge. The Catholic church is on the left just before the bridge, behind the shop and the village hall, on the road to Glenroy. The site is in the middle of the 2nd step to the outer doors of the porch.

Location Diagram

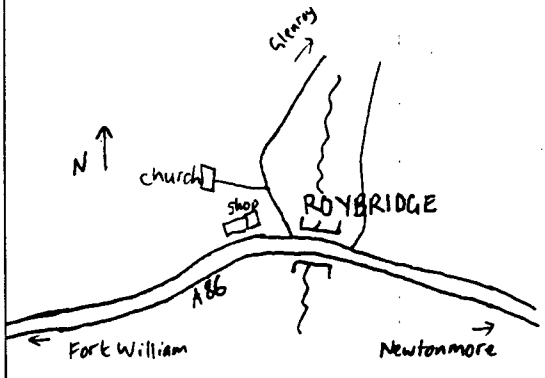

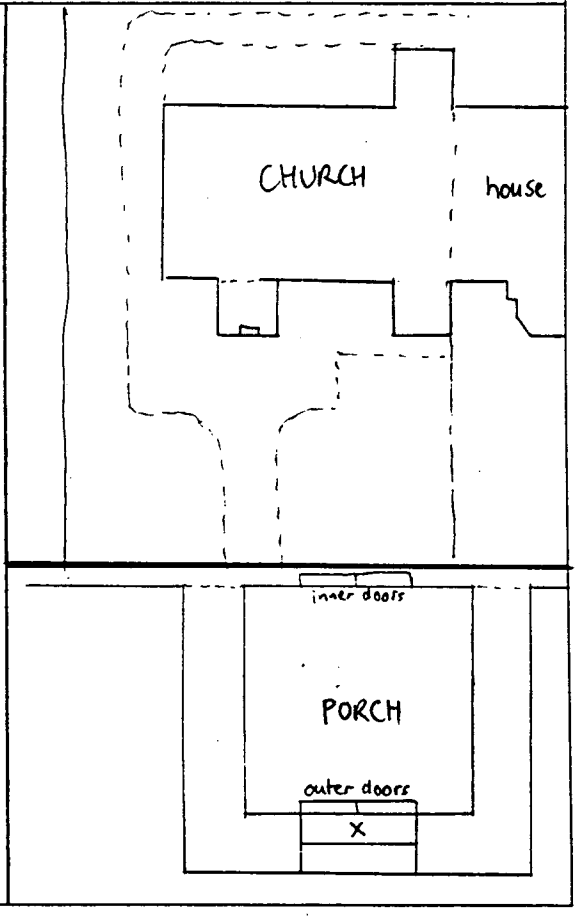

28.05.95 Department of Geology & Geophysics, University of Edinburgh.

Edinburgh University - Gravity Station Information

Reference# 253

Country:	SCOTLAND	
Region/County:	HIGHLAND	
Nearest Town:	Aviemore	
Name:	**Church of Scotland, Alvie**	
Latitude:	+ 57.16076°	Grid Reference:
Longitude:	- 03.87779°	286440 809310

Station Description

Leave A9 at the junction 1 mile south of Aviemore (SP Aviemore, Coylumbridge). Turn R at the junction (SP Loch Insh Watersports, B9152). Continue for about 2.5 miles to Alvie. At end of Alvie Loch, turn R after cottage on R, and follow narrow lane to the church.
The site is in the middle of the BACK doorway.

Location Diagram

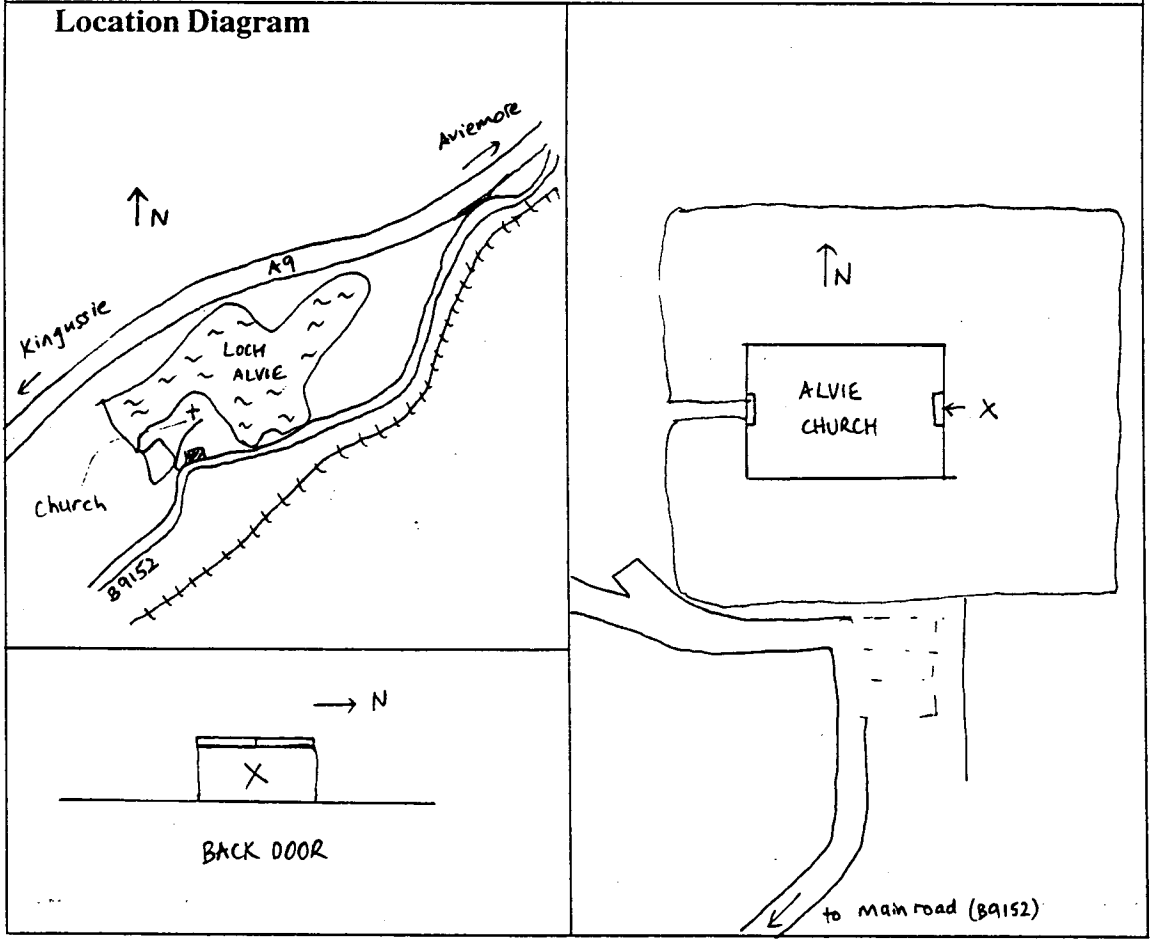

28.05.95 Department of Geology & Geophysics, University of Edinburgh.

Edinburgh University - Gravity Station Information

Reference# 254

Country:	SCOTLAND	
Region/County:	CENTRAL	
Nearest Town:	Crieff	
Name:	**Crianlarich FBM**	
Latitude:	+ 56.39732°	Grid Reference:
Longitude:	- 04.57128°	241320 725740

Station Description

The Crianlarich FBM is about 2 miles east of the village, at Benmore Farm on the A85. Leave the village in the direction of Callander and continue past Benmore Lodges on the left. At the SP for Portnellan Lodges, turn R just after the bridge into a farm track (Benmore Farm) beside a big barn. The FBM is behind the house, above the track, near the corner of the fence.

Location Diagram

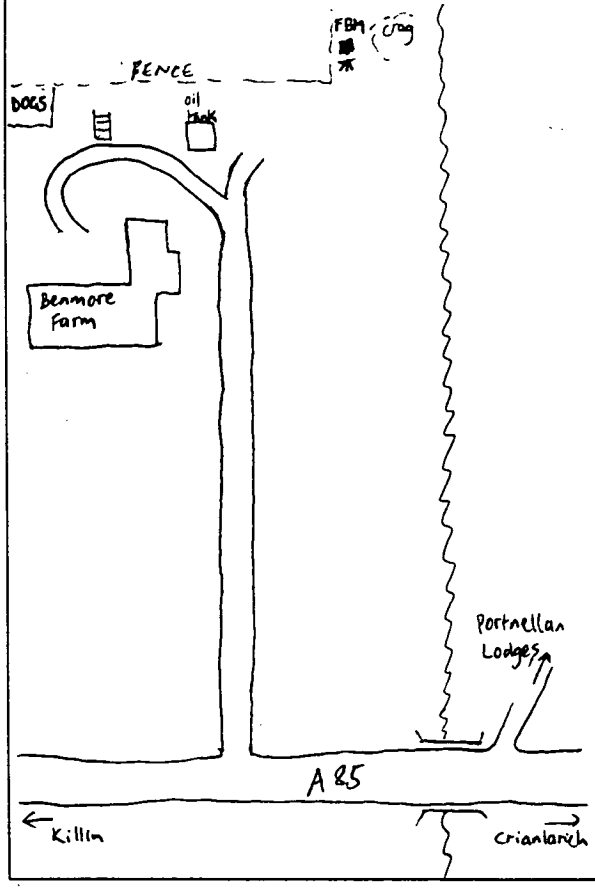

28.05.95 Department of Geology & Geophysics, University of Edinburgh.

Edinburgh University - Gravity Station Information

Reference# 255

Country:	SCOTLAND	
Region/County:	STRATHCLYDE	
Nearest Town:	Ayr	
Name:	**Church of Scotland, Annbank**	
Latitude:	+ 55.48600°	Grid Reference:
Longitude:	- 04.52100°	241320 725740

Station Description

Annbank is about 6 miles east of Ayr. From A77 (north), turn L at junction with A719 (SP Galston), then immediately R (SP Mossblown, B742). Straight on at Mossblown towards Annbank. Continue past the houses to the church on L, in a dip. From the A70 (south), turn L in Belston (SP Annbank, B744). Continue through the village of Annbank and turn left at the bridge. The church is a few hundred yards on the R.

The site is in the middle of the bottom step to the main entrance, which faces the road.

For access contact Rev. Kenneth Johnston, 9 Annbank Road, Mossblown.

Location Diagram

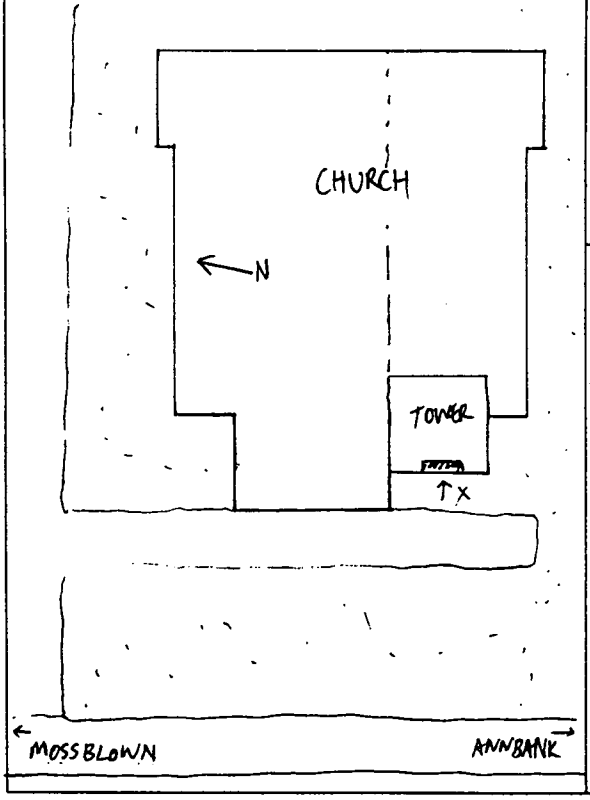

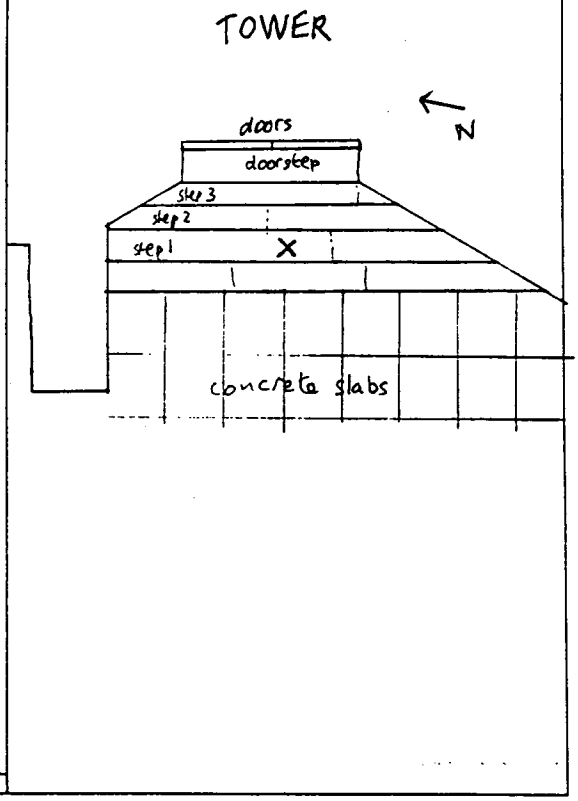

28.05.95 Department of Geology & Geophysics, University of Edinburgh.

Edinburgh University - Gravity Station Information

Reference# 256

Country:	SCOTLAND	
Region/County:	DUMFRIES & GALLOWAY	
Nearest Town:	Stranraer	
Name:	**Church of Scotland, New Luce**	
Latitude:	+ 54.94200°	Grid Reference:
Longitude:	- 04.85000°	217450 564500

Station Description

New Luce is about 6 miles off the A75 (Ayr-Stranraer), and can be reached from Castle Kennedy or Glenluce.
From Castle Kennedy, turn L and follow for about 6 miles to Glen Luce. At the T-junction in the village, turn R. Continue past the hotel and over the brideg. The church is on the left.
From Glenluce, follow signs for Abbey, and continue to New Luce. Church is on R on entering village.
The site is in the BACK doorway, on the concrete between the slabs and the door.

For access contact Rev. Graham Dickson, Ladyburn Manse, Glenluce.

Location Diagram

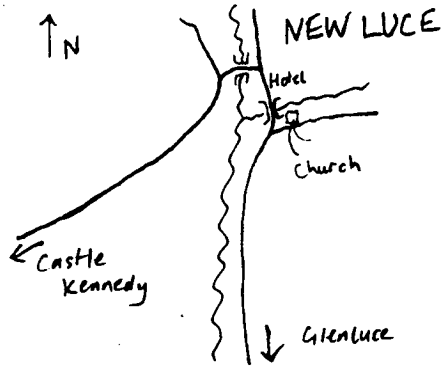

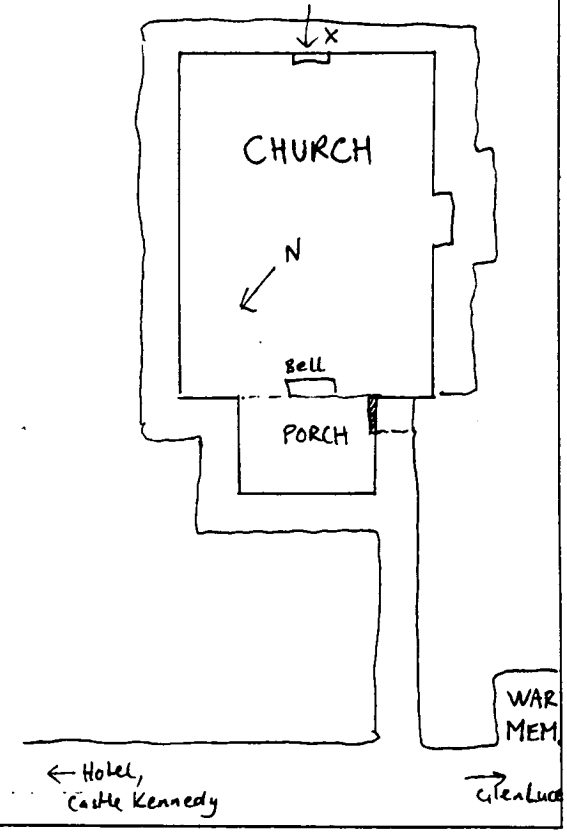

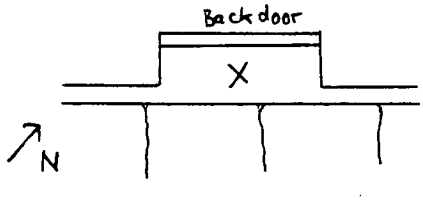

28.05.95 Department of Geology & Geophysics, University of Edinburgh.

Edinburgh University - Gravity Station Information

Reference# 257

Country:	SCOTLAND	
Region/County:	DUMFRIES & GALLOWAY	
Nearest Town:	Castle Douglas	
Name:	**Church of Scotland, Kelton**	
Latitude:	+ 54.92100°	Grid Reference:
Longitude:	- 03.93700°	275900 560250

Station Description

Kelton is about 3 miles south of Castle Douglas. Leave the A75 at the roundabout south of the town (SP Threave Gardens, Castle Douglas). After 1/2 mile turn R (SP Threave Gardens, Kelton Church). Continue past the entrance to the gardens. The church is on R, before righthand bend in road by a white house.
The site is in the middle of the large slab in front of the main entrance on the south side of the church.

Location Diagram

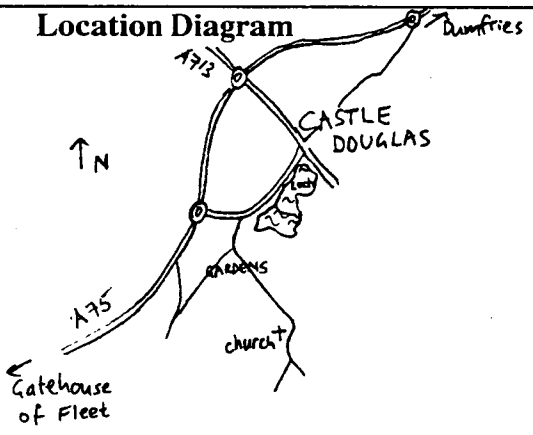

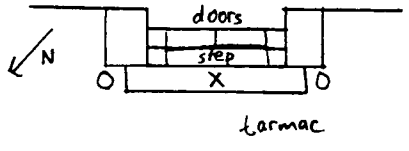

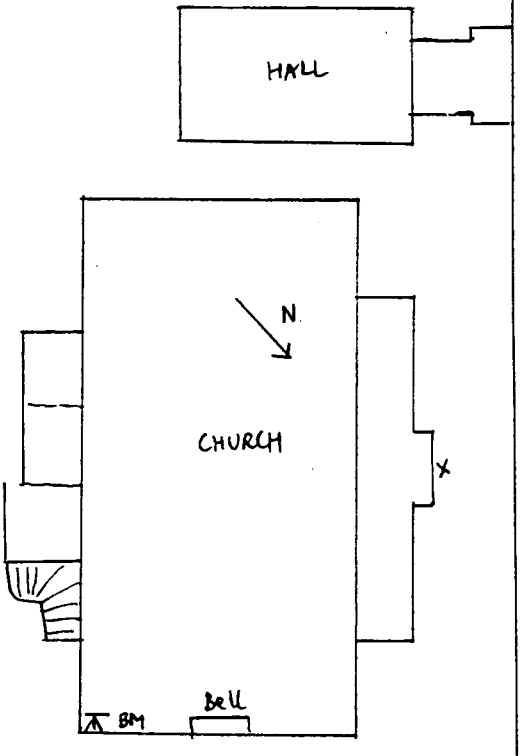

28.05.95 Department of Geology & Geophysics, University of Edinburgh.

Edinburgh University - Gravity Station Information

Reference# 20 POL Absolute 1

Country:	ENGLAND
Region/County:	MERSEYSIDE
Nearest Town:	Birkenhead
Name:	**POL, Observatory, Absolute 1**
Latitude:	+ 53.40039°
Longitude:	- 03.07280°
Grid Reference:	328680 389850

Station Description

Enter the Proudman Oceanographic Laboratory (POL) site at the large gateposts and continue straight on up the hill past the new building on the right. Follow the drive to the original Observatory and Lighthouse at the top of the hill. Enter the Observatory building by the door on the West side. Turn right and then descend the flight of stairs through the door on the left. Turn left at the bottom and descend another flight of stairs through a door into the basement. The 'Absolute 1' site is at the right (East) end of the basement, in the centre of a 1 m^2 concrete block set into the floor.

For access contact Dr. R.J. Edge or Dr. T. Baker, POL, Bidston Observatory, Birkenhead, Merseyside, L43 7RA. (Tel. 051 653 8633)

Location Diagram

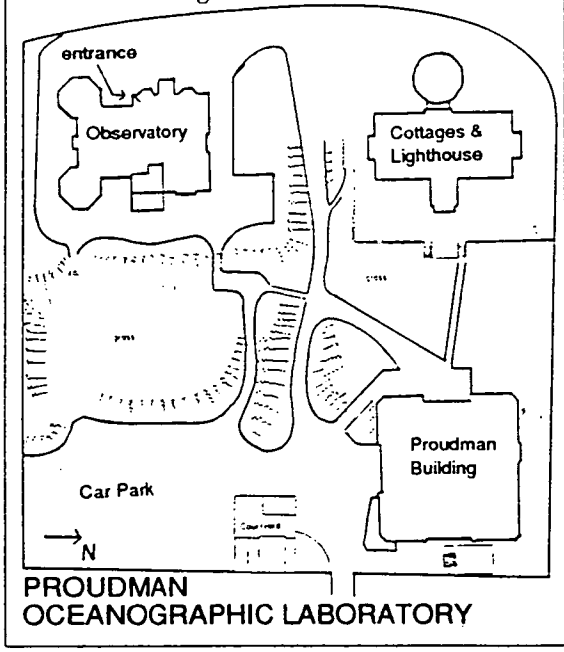

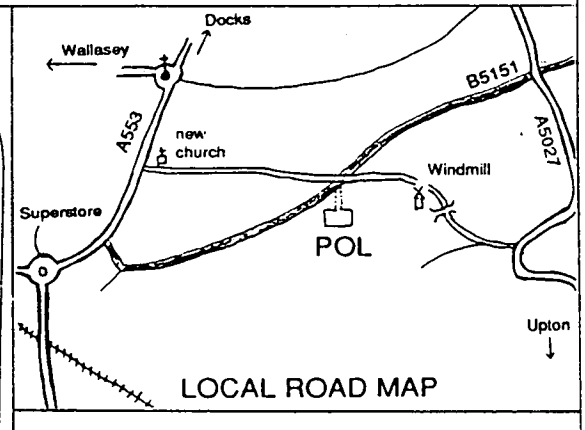

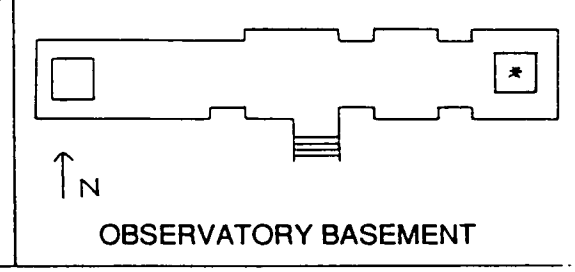

25.03.92 Department of Geology & Geophysics, University of Edinburgh.

Edinburgh University - Gravity Station Information
Reference# 24 POL S.Porch

Country:	ENGLAND
Region/County:	MERSEYSIDE
Nearest Town:	Birkenhead
Name:	**POL, Observatory, South Porch**
Latitude:	+ 53.40021°
Longitude:	- 03.07294°

Grid Reference:
328670 389830

Station Description

Enter the Proudman Oceanographic Laboratory (POL) site at the large gateposts and continue straight on up the hill past the new building on the right. Follow the drive to the original Observatory and Lighthouse at the top of the hill. Turn left and continue round to the 'back' of the building (South side). The station is in the middle of the step to the back door.

For access contact Dr. R.J. Edge or Dr. T. Baker, POL, Bidston Observatory, Birkenhead, Merseyside, L43 7RA. (Tel. 051 653 8633)

Location Diagram

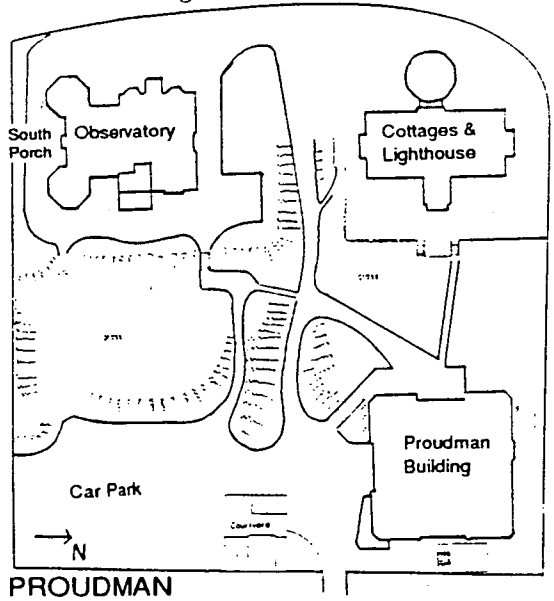

PROUDMAN OCEANOGRAPHIC LABORATORY

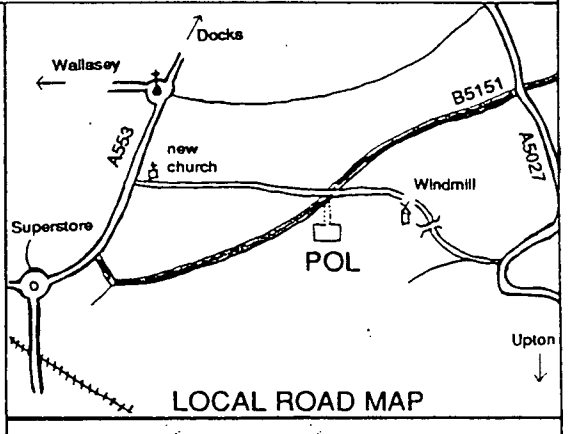

LOCAL ROAD MAP

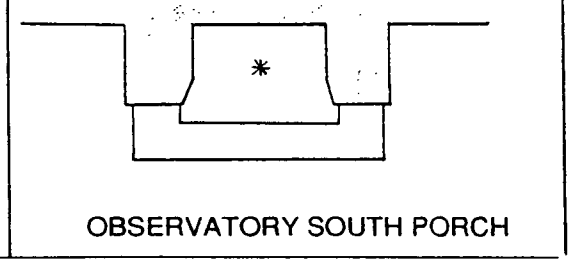

OBSERVATORY SOUTH PORCH

25.03.92

Department of Geology & Geophysics, University of Edinburgh.

Edinburgh University - Gravity Station Information
Reference# 25 POL Current Meter

Country:	ENGLAND	
Region/County:	MERSEYSIDE	
Nearest Town:	Birkenhead	
Name:	**POL, Current Meter Site**	
Latitude:	+ 53.40093°	Grid Reference:
Longitude:	- 03.07236°	328710 389910

Station Description

Enter the Proudman Oceanographic Laboratory (POL) site at the large gateposts. The current meter site is a concrete platform (approx. 40cm across) set into the lawn in front of the Proudman Building. The site is about 7m beyond the path which links the Cottages and the Proudman Building, and about 11m NE of the bottom of the steps at the end of the path.

For access contact Dr. R.J. Edge or Dr. T. Baker, POL, Bidston Observatory, Birkenhead, Merseyside, L43 7RA. (Tel. 051 653 8633).

Location Diagram

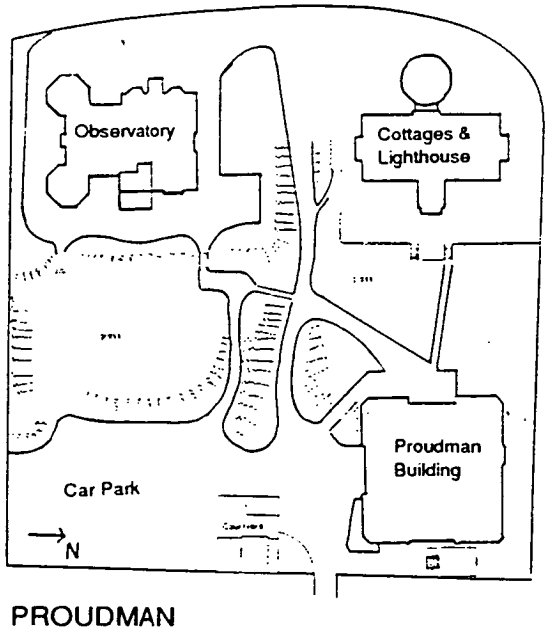

PROUDMAN OCEANOGRAPHIC LABORATORY

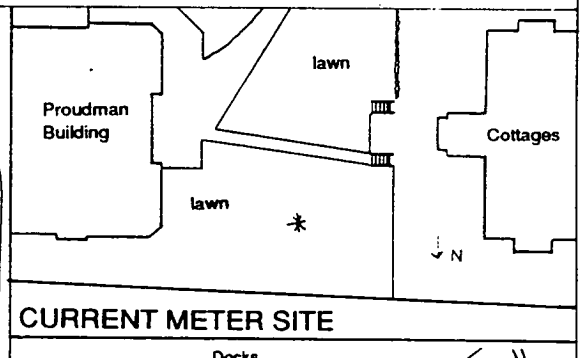

CURRENT METER SITE

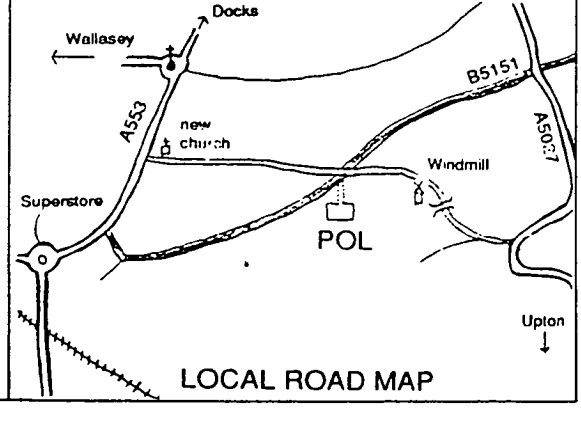

LOCAL ROAD MAP

25.03.92

Department of Geology & Geophysics, University of Edinburgh.

Edinburgh University - Gravity Station Information
Reference# 30

Country:	ENGLAND	
Region/County:	MIDDLESEX	
Nearest Town:	Teddington	
Name:	**NPL Teddington A (Bldg 3, Room 11)**	
Latitude:	+ 51.42043°	Grid Reference:
Longitude:	- 0.33915°	515470 170410

Station Description

From Queens Road (B358), enter the National Physical Laboratory site by the Main Gate. Follow Bushy Road round to the left towards Bushy House (Bldg 1). In front of Bushy House, turn right, passing behind the Darwin Building (Bldg 2). Enter Bldg 3 by Newton's Apple Tree. Room 11 is about 2/3 of the way down the corridor, on the left. The station is marked by a brass knob on a pillar set in the floor at the SE corner of the room.

For access contact Dr. B. Kibble, National Physical Laboratory, Queens Road, Teddington, Middlesex TW11 0LW.

Location Diagram

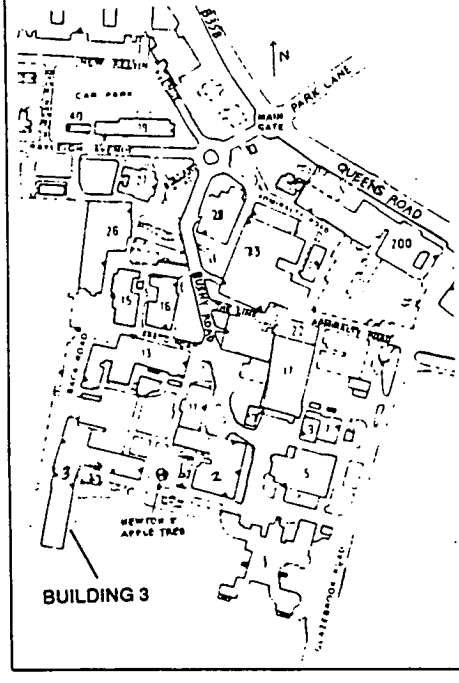

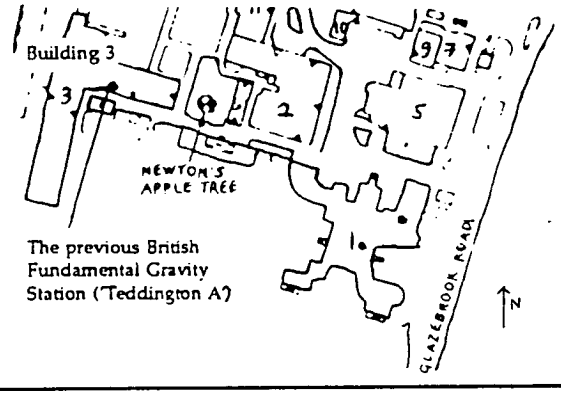

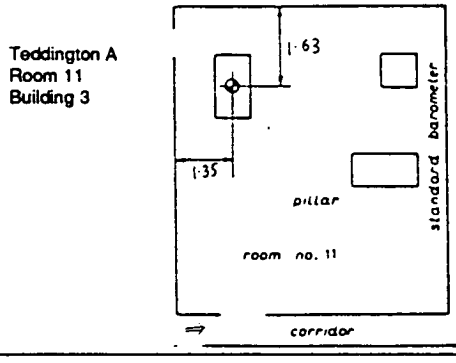

04.02.93 Department of Geology & Geophysics, University of Edinburgh.

Edinburgh University - Gravity Station Information
Reference# 33

Country:	ENGLAND	
Region/County:	MIDDLESEX	
Nearest Town:	Teddington	
Name:	**NPL Kitchen 1 (Bldg 1, Site B)**	
Latitude:	+ 51.41970°	Grid Reference:
Longitude:	- 0.33774°	515570 170330

Station Description

From Queens Road (B358), enter the National Physical Laboratory site by the Main Gate. Follow Bushy Road round to the left to Bushy House (Bldg 1). Room 16 can be accessed via Room 12 and the door on the North side of the building. The British Fundamental Gravity Site (1993) is monumented by a stainless steel plaque on the floor.

For access contact Dr B. Kibble, National Physical Laboratory, Queens Road, Teddington, Middlesex TW11 0LW.

Location Diagram

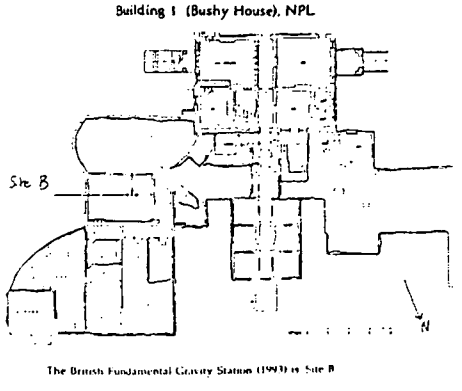

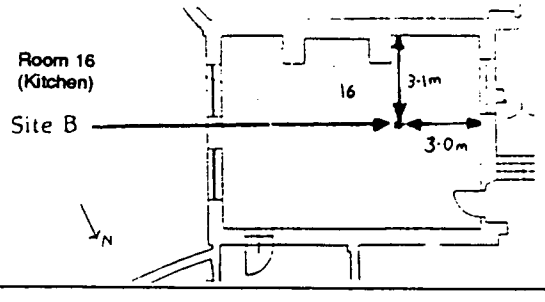

NATIONAL PHYSICAL LABORATORY

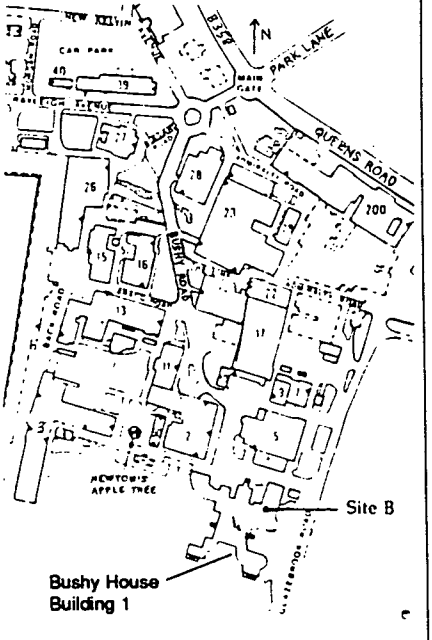

04.02.93

Department of Geology & Geophysics, University of Edinburgh.

Edinburgh University - Gravity Station Information
Reference# 37

Country:	ENGLAND	
Region/County:	MIDDLESEX	
Nearest Town:	Teddington	
Name:	**NPL Entrance Hall, Bushy House (Bldg 1, Site C)**	
Latitude:	+ 51.41970°	Grid Reference:
Longitude:	- 0.33774°	515570 170330

Station Description

From Queens Road (B358), enter the National Physical Laboratory site by the Main Gate. Follow Bushy Road round to the left to Bushy House (Bldg 1). Continue towards the Sports Field and turn right (Glazebrook Road), following to the front of the building and up the steps to the Entance Hall of Bushy House. The station is against the right hand wall, opposite the fireplace, and is monumented by a brass knob.

For access contact Dr B. Kibble, National Physical Laboratory, Queens Road, Teddington, Middlesex TW11 0LW.

Location Diagram

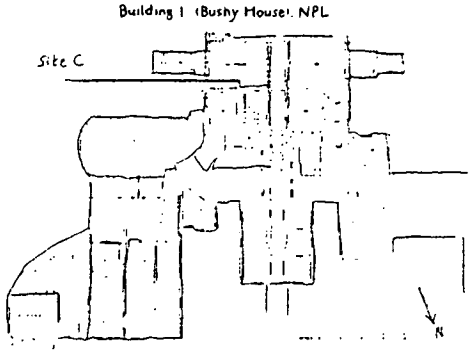

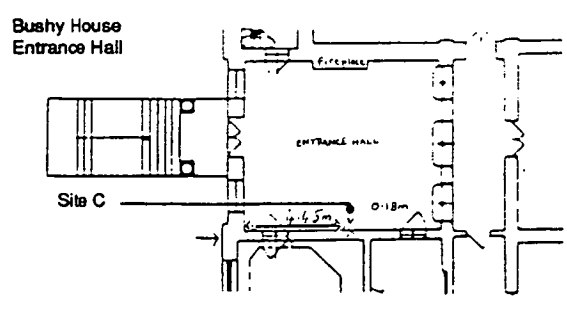

NATIONAL PHYSICAL LABORATORY

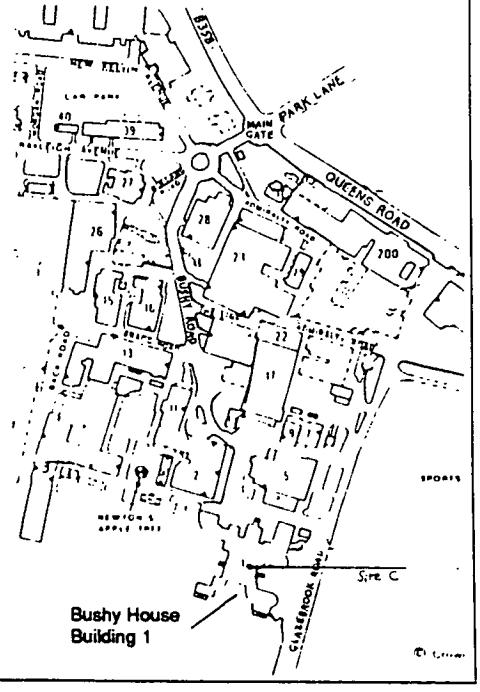

04.02.93

Department of Geology & Geophysics, University of Edinburgh.

Edinburgh University - Gravity Station Information
Reference# 38

Country:	ENGLAND	
Region/County:	MIDDLESEX	
Nearest Town:	Teddington	
Name:	**NPL Force Balance (Bldg 17, Site A)**	
Latitude:	+ 51.42131°	Grid Reference:
Longitude:	- 0.33754°	515580 170510

Station Description

From Queens Road (B358), enter the National Physical Laboratory site by the Main Gate. Follow Bushy Road past Bldg 28 to Bldg 17 which is on the left. Enter the building, passing straight through the lobby into the experiment hall. The Force Balance machine is housed in an enclosed 'clean room' on the left towards the back of the hall. Descend the few steps which lead into the clean room. The station is on the floor in the far left hand corner of the room.

For access contact Dr. B. Kibble, National Physical Laboratory, Queens Road, Teddington, Middlesex TW11 0LW.

Location Diagram

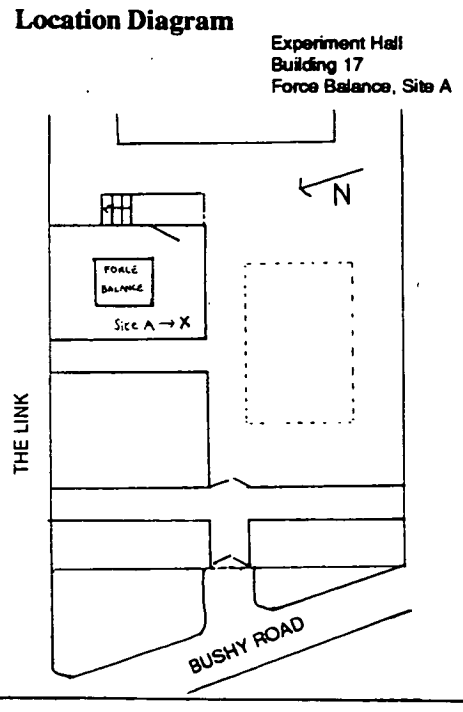

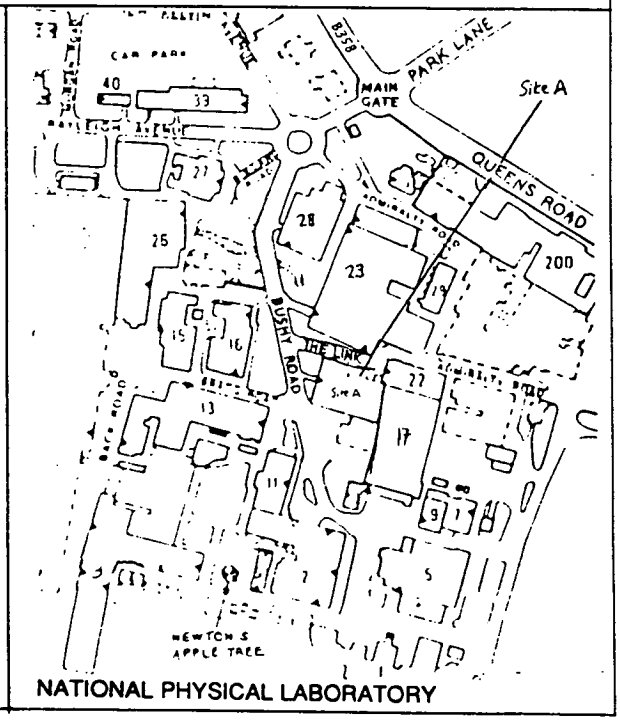

25.03.92

Department of Geology & Geophysics, University of Edinburgh.

Edinburgh University - Gravity Station Information
Reference# 39

Country:	ENGLAND	
Region/County:	MIDDLESEX	
Nearest Town:	Teddington	
Name:	**NPL Visitors Reception Porch (Bldg 31, Site D)**	
Latitude:	+ 51.42221°	Grid Reference:
Longitude:	- 0.33736°	515590 170610

Station Description
From Queens Road (B358), enter the National Physical Laboratory site by the Main Gate. Turn L immediately past the Security building and enter the Visitors Car Park on L. The station is in the porch of the NPL Visitors Reception (Bldg 31), on the stainless steel plaque between the inner and outer pillars on the right hand side.

For access contact Dr. B. Kibble, National Physical Laboratory, Queens Road, Teddington, Middlesex TW11 0LW.

Location Diagram

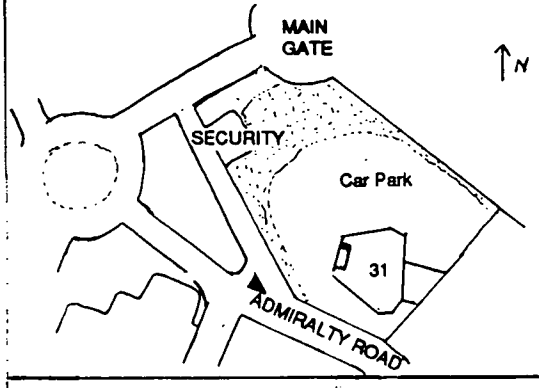

NPL VISITORS RECEPTION

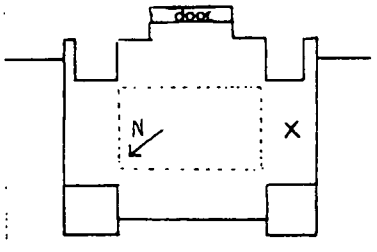

NATIONAL PHYSICAL LABORATORY

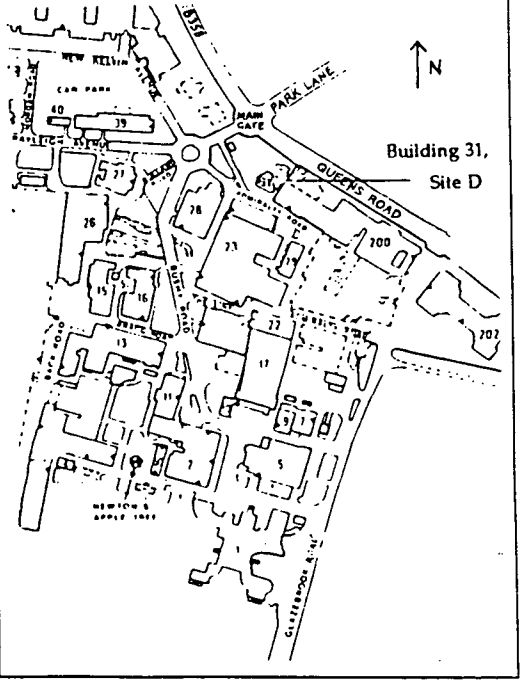

25.03.92 Department of Geology & Geophysics, University of Edinburgh.

Edinburgh University - Gravity Station Information

Reference# 50

Country:	ENGLAND	
Region/County:	SOMERSET	
Nearest Town:	Taunton	
Name:	**Challenger Absolute**	
Latitude:	+ 51.02194°	Grid Reference:
Longitude:	- 03.07499°	324612 125340

Station Description

From the entrance gate of the Hydrographic Office, continue through the site towards the car park. Challenger Block is on the right just before the car park. The site is in Room E2c in the centre of the stone plinth to the right of the corridor doors.

For access contact: SMCO (Geophysics), Marine Science Branch 6, Hydrographic Office, Taunton, Somerset TA1 2DN (0823 337900 x3264).

Location Diagram

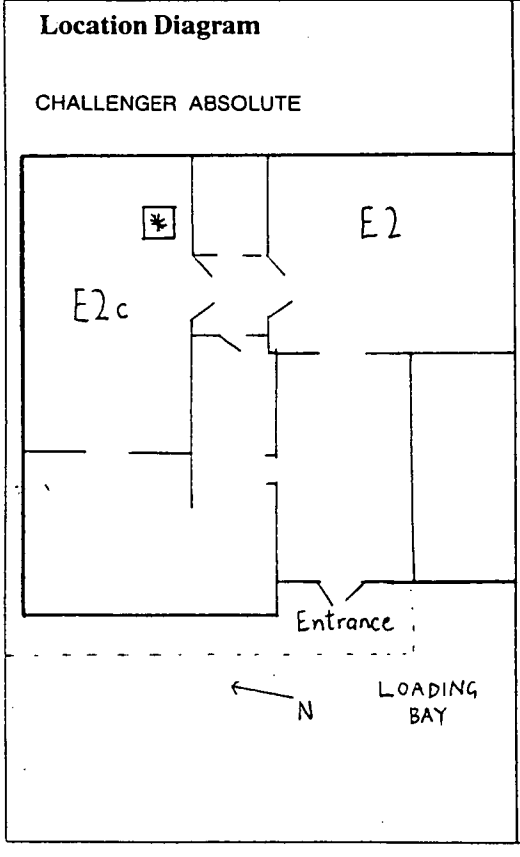

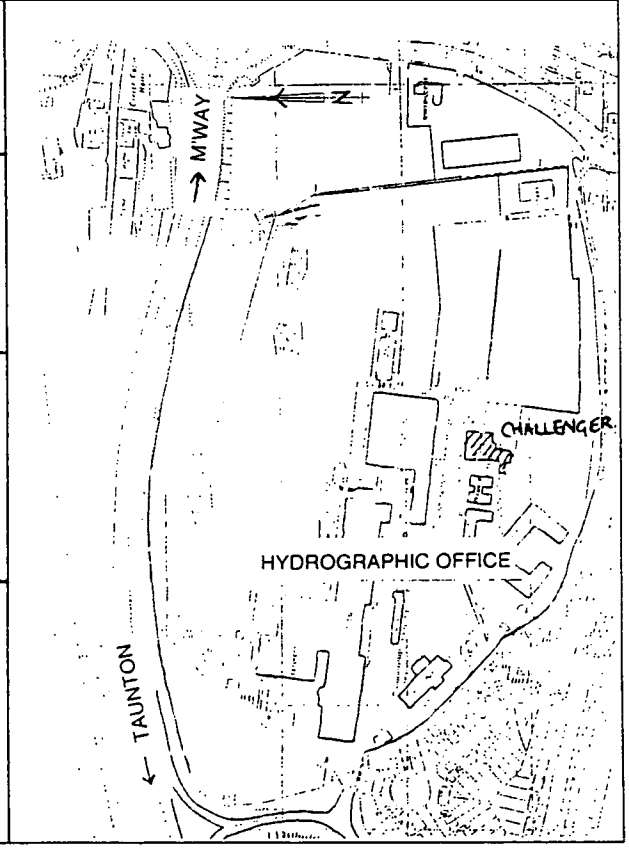

27.04.94

Department of Geology & Geophysics, University of Edinburgh.

Edinburgh University - Gravity Station Information

Reference# 52

Country:	ENGLAND	
Region/County:	SOMERSET	
Nearest Town:	Taunton	
Name:	**Challenger Loading Bay**	
Latitude:	+ 51.02185°	Grid Reference:
Longitude:	- 03.07530°	324590 125330

Station Description

From the entrance gate of the Hydrographic Office, continue through the site towards the car park. Challenger Block is on the right just before the car park. The Loading Bay is obvious from the building entrance and the site is in the middle of the concrete section closest to the ramp. It is 1.6 m away from (west of) the ramp edge and 3.5 m in from (south of) the front edge of the concrete.

For access contact: SMCO (Geophysics), Marine Science Branch 6, Hydrographic Office, Taunton, Somerset TA1 2DN (0823 337900 x3264).

Location Diagram

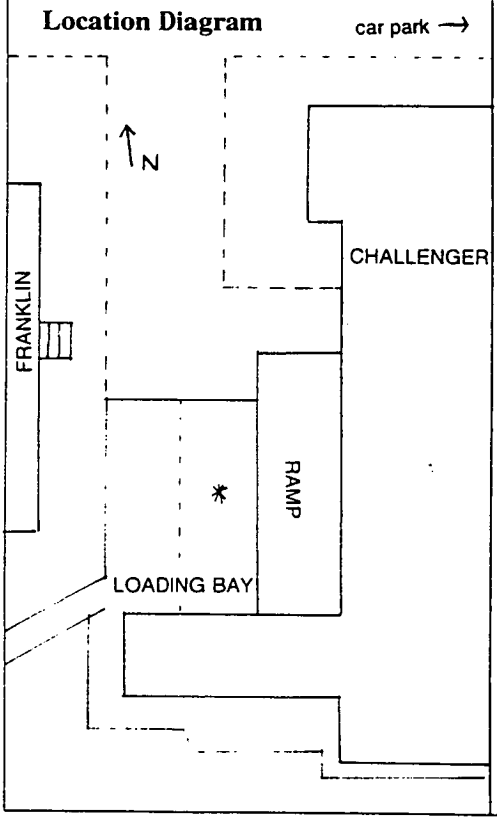

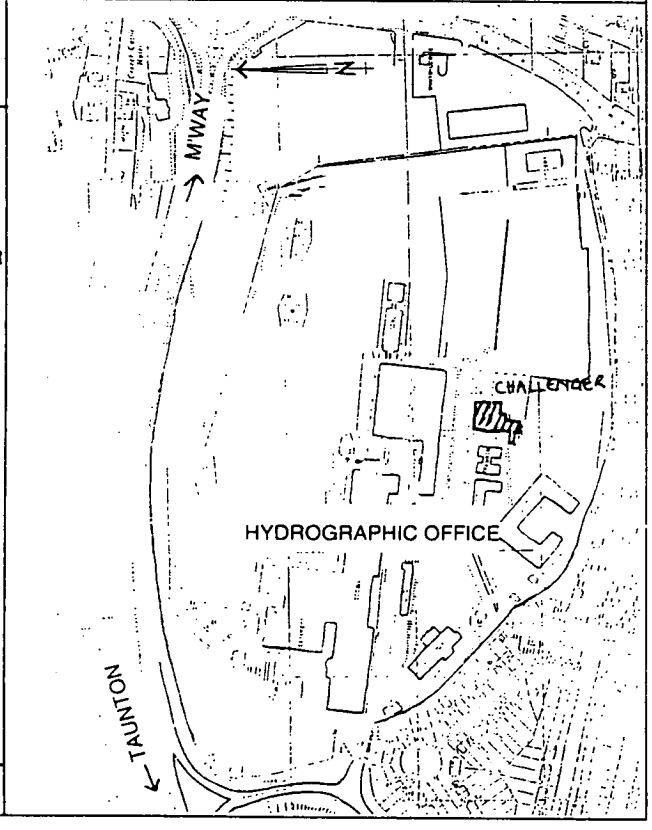

27.04.94

Department of Geology & Geophysics, University of Edinburgh.

Edinburgh University - Gravity Station Information

Reference# 53

Country:	ENGLAND	
Region/County:	SOMERSET	
Nearest Town:	Taunton	
Name:	**Challenger Water Tank**	
Latitude:	+ 51.02194°	Grid Reference:
Longitude:	- 03.07498°	324613 125340

Station Description

From the entrance gate of the Hydrographic Office, continue through the site towards the car park. Challenger Block is on the right just before the car park. The Water Tank site is on the west side of the building, between the crane and the large cylindrical water tank. There is a brass disc set in a square of pink concrete adjacent to the tarmac surround of the tank. The brass disc is not quite in the centre of the square, but measurements were made at the centre, rather than over the disc.

For access contact: SMCO (Geophysics), Marine Science Branch 6, Hydrographic Office, Taunton, Somerset TA1 2DN (0823 337900 x3264).

Location Diagram

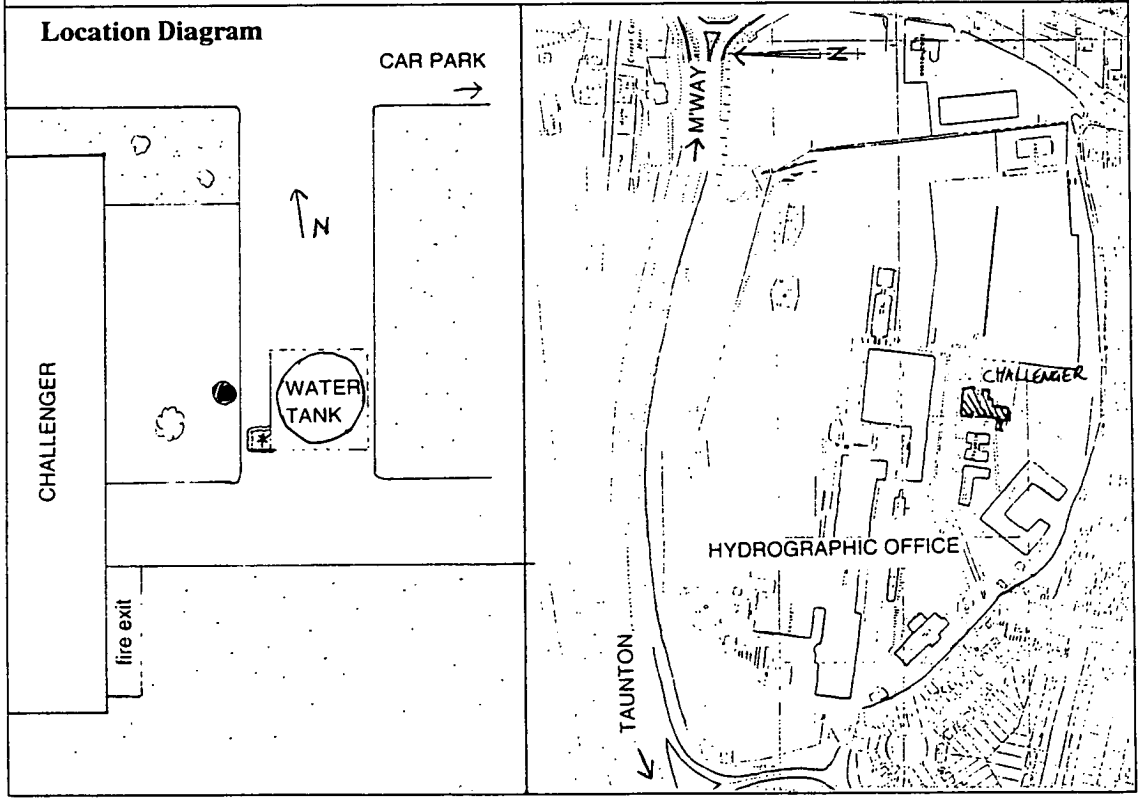

27.04.94

Department of Geology & Geophysics, University of Edinburgh.

Edinburgh University - Gravity Station Information
Reference# 1 JCMB

Country:	SCOTLAND	
Region/County:	LOTHIAN	
Nearest Town:	Edinburgh	
Name:	JCMB	
Latitude:	+ 55.92185°	Grid Reference:
Longitude:	- 03.17290°	NT 2671 7048

Station Description

The station is in the James Clerk Maxwell Building at the King's Buildings site of the University of Edinburgh. Enter the site and follow signs to the JCMB. Enter the building and the Entrance Hall by the main front doors. The site is immediately left of the doors, near the 'phonecard' telephone. There is a 15 cm diameter marker disk attached to the wall at ground level 10 cm South of the window. The station is on the floor, 30 cm in front of the disk.
Access hours are 0700 - 1945 on weekdays, 0830 - 1845 at weekends.
Contact R.G. Hipkin, Grant Institute, West Mains Road, Edinburgh EH9 3JZ. (Tel. 031 650 4910).

Location Diagram

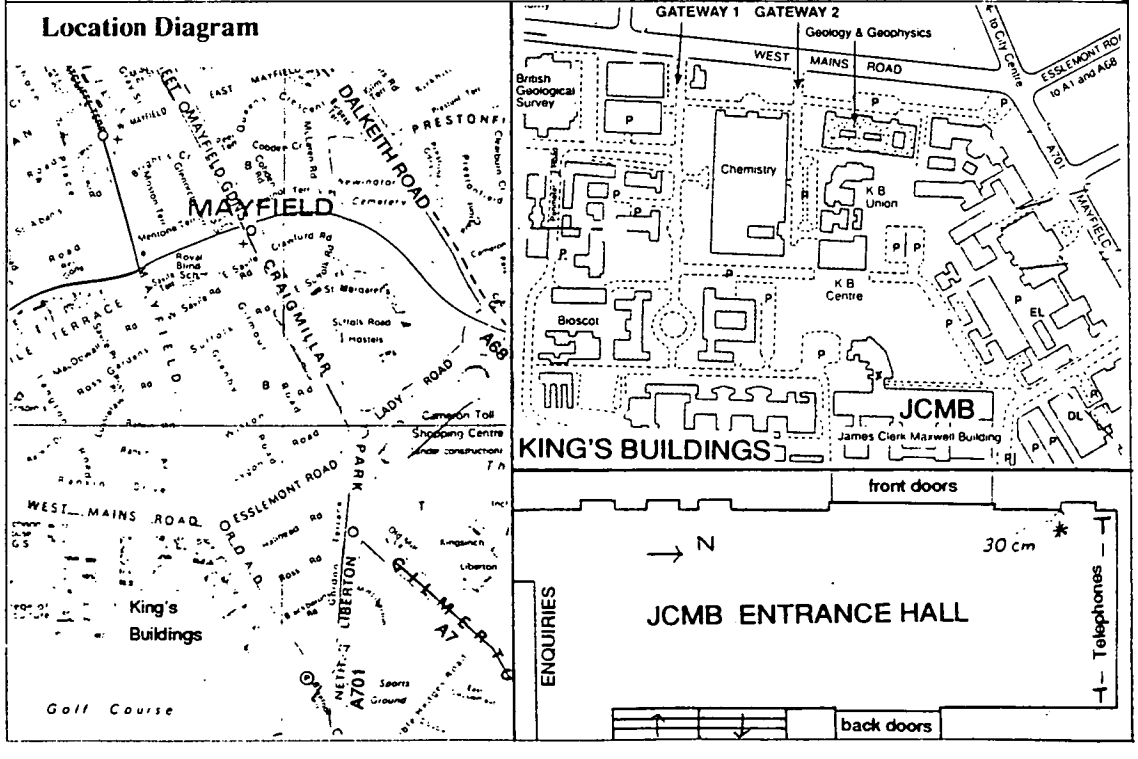

25.03.92 Department of Geology & Geophysics, University of Edinburgh.

Edinburgh University - Gravity Station Information

Reference# 100 BGS Absolute

Country:	SCOTLAND	
Region/County:	LOTHIAN	
Nearest Town:	Edinburgh	
Name:	**Room 44, British Geological Survey, Murchison House**	
Latitude:	+ 55.92440°	Grid Reference:
Longitude:	- 03.17826°	NT 2638 7077

Station Description

The station is situated in Room 44 of the north-west wing of BGS Murchison House, which is on the King's Buildings Site of the University of Edinburgh. Enter the site from West Mains Road (Gateway 1). Turn R after the car park to the BGS. From the reception area, turn R through the doors immediately after the reception desk, and go down the stairs to the next floor. Turn R and R again to reach Room 39 which is up a short ramp on the R. Room 44 is accessed through room 39. The site is at the 3/4 " brass disk set in the floor, in the middle of the triangularly shaped space to the left of the double doors.

For access contact Dr. Chris Browitt, British Geological Suvey, Murchison House, West Mains Road, Edinburgh EH9 3JZ. (Tel. 031 650 1000).

Location Diagram

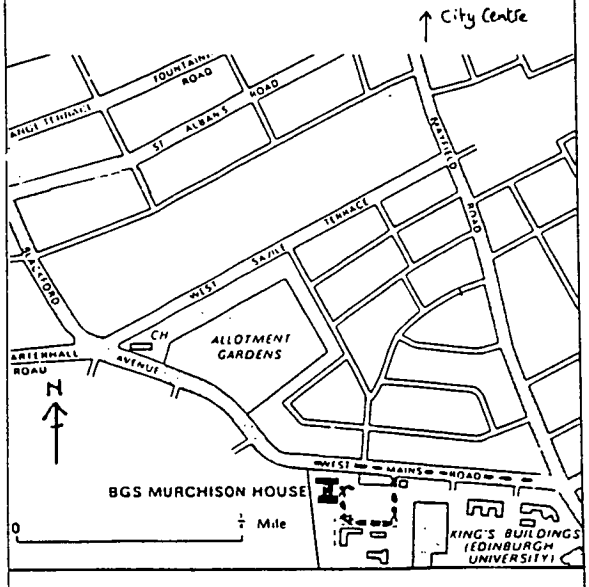

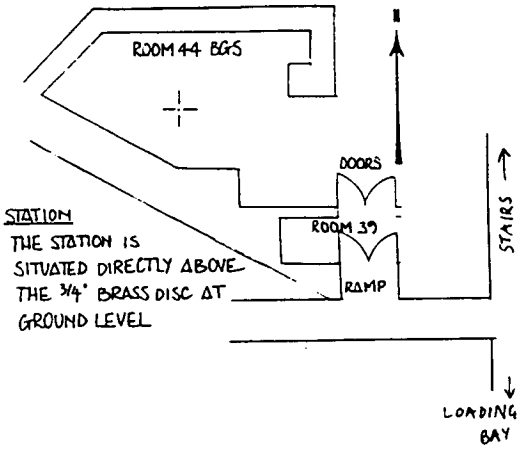

25.03.92 Department of Geology & Geophysics, University of Edinburgh.

Edinburgh University - Gravity Station Information
Reference# 101 Car Park

Country:	SCOTLAND	
Region/County:	LOTHIAN	
Nearest Town:	Edinburgh	
Name:	Car Park	
Latitude:	+ 55.92400°	Grid Reference:
Longitude:	- 03.17617°	NT 2651 7072

Station Description

The station is situated in the stairwell at the SE corner of the multi storey car park at the King's Buildings Site of the University of Edinburgh. Enter the site from West Mains Road (Gateway 1). The Car Park is on the right, and the stairwell faces the road.
The station is level with the bottom of the staircase, midway between the South wall and the first step.

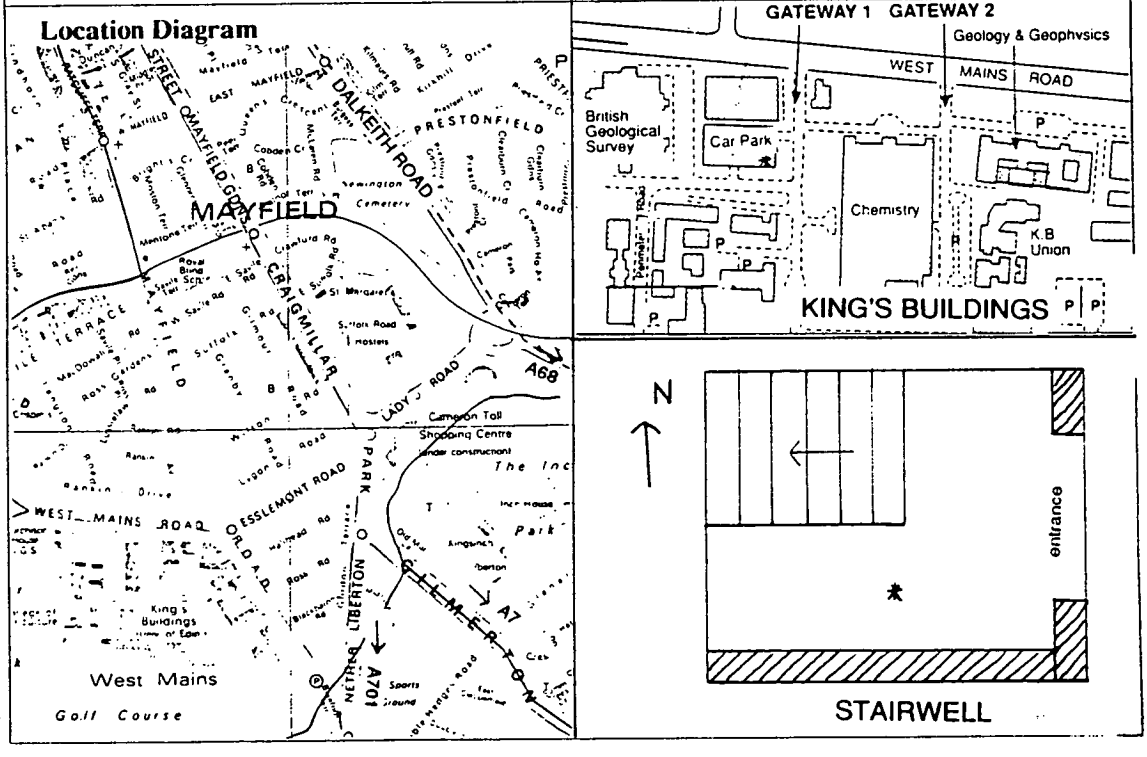

25.03.92

Department of Geology & Geophysics, University of Edinburgh.

Edinburgh University - Gravity Station Information
Reference# 140 Grant Institute

Country:	SCOTLAND	
Region/County:	LOTHIAN	
Nearest Town:	Edinburgh	
Name:	**Grant Institute R140**	
Latitude:	+ 55.92382°	Grid Reference:
Longitude:	- 03.17296°	NT 2671 7070

Station Description

The station is in the new basement of the Grant Institute (Dept. of Geology & Geophysics) at the King's Buildings site of the University of Edinburgh. Enter the Grant Institute by the main front doors on the North side of the building. Turn left and proceed along the corridor towards the main lecture theatre. After the corridor bends to the right, descend one flight of the stairs which are just beyond the lift, and go through the double doors facing you. Turn left past the Cold Store, and Room 140 is the next door on the left.

The station is behind the door, midway between the long walls, and 2 metres from the short wall at the South end of the room.

For access, contact R. G. Hipkin, Grant Institute, West Mains Road, Edinburgh EH9 3JZ. (Tel. 031 650 4910).

Location Diagram

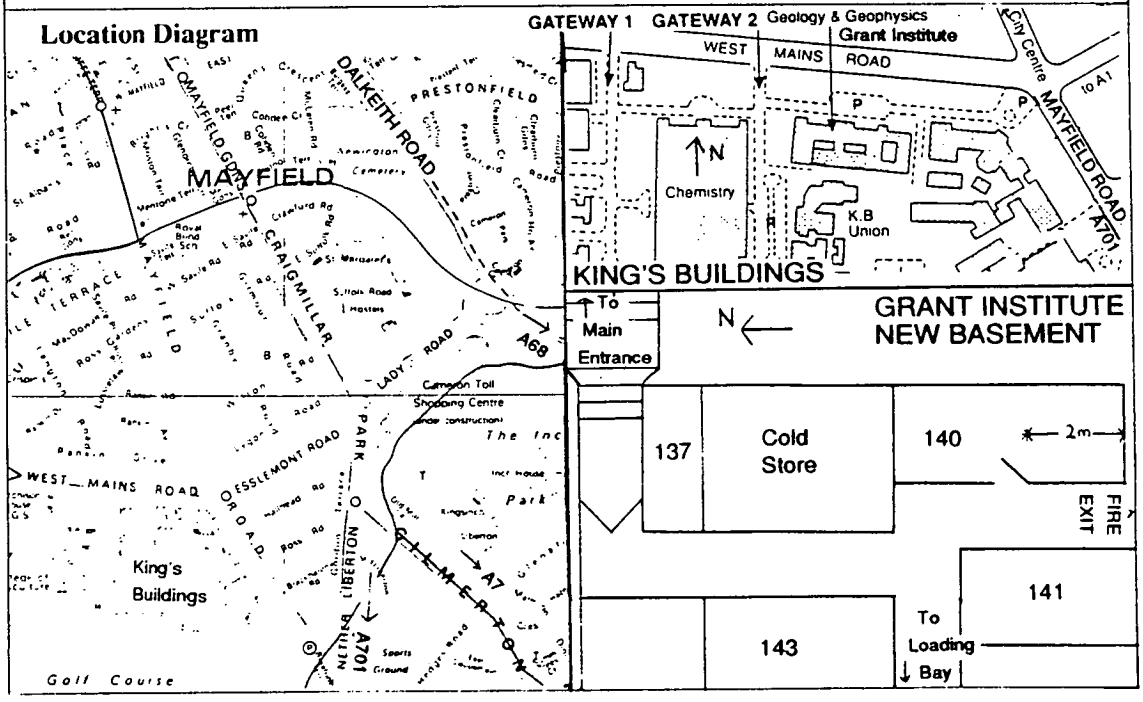

25.03.92

Department of Geology & Geophysics, University of Edinburgh.

References

Alasia, F., Cannizzo, L., Cerutti, G. & Marson, I,. 1982. Absolute Gravity Acceleration Measurements : Experiences with a Transportable Gravimeter, *Metrologia,* **18,** 221-229.

Anon, 1954. The British Fundamental Gravity Station, *Nature,* **173,** 794-795.

Ashkenazi, V. & Ffoulkes-Jones, G., 1990. Millimeters over hundreds of kilometres by GPS, *GPS World,* Nov/Dec 1990.

Ashkenazi, V., Bingley, R. M., Whitmore, G. M. & Baker, T.F. 1993. Monitoring changes in mean-sea-level to millimetres using GPS, *Geoph. Res. Lett.,* **20,** 1951-1954.

Axis Instruments Company, 1992. Operating Manual for the FG5 Absolute Gravimeter, Axis Instruments, Boulder, Colorado.

Baker, T. F., 1980. Tidal gravity in Britain: tidal loading and the spatial distribution of the marine tide, *Geophys. J. R. astr. Soc.*, **62,** 249-267.

Baker, T. F., Edge, R. J. & Jeffries, G., 1991. Tidal gravity and ocean tide loading in Europe, *Geophys. J. Int.,* **107,** 1-11

Balhorn, R., Kunzmann, H. & Lebowsky, F., 1972. Frequency Stabilization of Internal-Mirror Helium-Neon Lasers, *Applied Optics,* **11,** No. 4, 742-744.

Becker, M., Groten, E., Lambert, A., Liard, J. O. & Nakai, S., 1987. An intercomparison of LaCoste & Romberg Model-D gravimeters : results of the International D-meter Campaign 1983, *Geophys. J. R. astr. Soc.*, **89,** 499-526.

Becker, M., 1989. Adjustment of microgravimetric measurements for detecting local and regional vertical displacements. *In* Rummel, R. & Hipkin, R.G. (eds) *Gravity, Gradiometry and Gravimetry* : International Association of Geodesy Symposium 103, Edinburgh, Scotland, 8-10 August 1989. Springer-Verlag, New York.

Becker, M. 1994. Relative Gravity Measurements during the 4th International Intercomparison of Absolute Gravimeters. Paper presented at the meeting of the International Gravity Commission / International Commission on the Geoid at Graz, Austria, 11-17 September 1994.

Boedecker, G., 1981. Instrumental Capabilities of LaCoste & Romberg gravity meters for detection of small gravity variations with time, *Bureau Gravimetrique International, Bull. d'Information,* **49,** 72-94.

Boedecker, G., Marson, I. & Wenzel, H-G., 1994. The Adjustment of the Unified European Gravity Network 1994 (UEGN94). Paper presented at the meeting of the International Gravity Commission / International Commission on the Geoid at Graz, Austria, 11-17 September 1994.

Boedecker, G. & Richter, B., 1981. The new gravity base net 1976 of the Federal Republic of Germany (DSGN76), *Bull. Geod.,* **3,** 250-266.

Boulanger, Y,. Faller, J., Groten, E. *et al.*, 1986. Results of the 2nd International Comparison of Absolute Gravimeters in Sèvres 1985, *Bureau Gravimetrique International, Bull. d'Information,* **59,** 89-103.

Boulanger, Y,. Faller, J., Groten, E. *et al.*, 1991. Results of the 3rd International Comparison of Absolute Gravimeters in Sèvres 1989, *Bureau Gravimetrique International, Bull. d'Information,* **68,** 24-44.

Boulton, G. S., 1992. Quaternary. *In* Duff, P. McL. D. & Smith, A. J. (eds) *Geology of England and Wales,* pp 413-439. The Geological Society, London.

Cannizzo, L., Cerutti, G. & Marson, I., 1978. Absolute Gravity Measurements in Eurpoe, *Il Nuovo Cimento,* **1C,** No. 1, 39-85.

Carter, W. E., Peter, G., Sasagawa, G. *et al.* 1994. New Gravity Meter Improves Measurements, *Eos, Trans. Amer. Geoph. Union,* **75,** 22 Feb 1994, 90-92.

Carter, W. E., Aubrey, D. G., Baker, T. F. *et al.* 1989. Geodetic Fixing of tide gauge bench marks. Woods Hole Oceanog. Inst. Tech. Rep. WHOI-89-31/CRC-89-5.

Cartwright, D.E. & Edden, A. C., 1973. Corrected tables of harmonics, *Geophys. J. R. astr. Soc.*, **33,** 253-264.

Cartwright, D. E. & Tayler, R. J., 1971. New Computations of the Tide-generating Potential, *Geophys. J. R. astr. Soc.*, **23,** 45-74.

Charles, K., 1994. Noise Survey of the Edinburgh Absolute Gravity Site. Unpublished manuscript, Dept. of Geology and Geophysics, University of Edinburgh.

Chartier, J-M., Labot, J., Sasagawa, G., Niebauer, T. M. & Hollander, W., 1993. A Portable Iodine Stabilized He-Ne Laser and its use in an Absolute Gravimeter, *IEEE Trans. Instrum. Meas.*, **42,** No. 2, 420-422.

Chave, A.D., Thomson, D. J. & Ander, M.E, 1987. On the Robust Estimation of Power Spectra, Coherences and Transfer Functions, *J. Geoph. Res.*, **92,** No. B1, 633-648.

Clark, J. S., 1939. An absolute determination of the Acceleration due to Gravity, *Phil. Trans. R.. Soc. Lond.*, **A 238,** 65-123 & 549.

CollierJackson, T. K., 1990. *Report on Edinburgh Absolute Gravity Station by No. 2 Doppler Section 512 Specialist Team of the Royal Engineers. Ref. 512/G6103,* Ministry of Defence, Middlesex.

Cook, A. H., 1967. A new absolute determination of the acceleration due to gravity at the National Physical Laboratory, England, *Phil. Trans. R.. Soc. Lond.*, **A 261,** 211-252.

Cook, A. H. & Hammond, J. A., 1969. The Absolute Determination of Gravity at the National Physical Laboratory, *Metrologia,* **5,** 141-142.

Coron, S. & Monnet, F., 1959. *Reseau Gravimetrique International de Premiere Ordre (Système de Potsdam),* Publ. du Bureau Gravimétrique International, Paris.

Davidson, N. C., 1992. The Analysis of Geomagnetic Storm-Time Variations. PhD Thesis, University of Edinburgh.

Delcourt-Honorez, M., 1990a. Water-level fluctuations in a borehole at the Royal Observatory of Belgium : effects on local gravity, earth tidal and barometric responses, Proc. 11th Int. Sympos. on Earth Tides, Helsinki, 1989. E.Schweizerbart'sche Verlagsbuchhandlung, Stuttgart 1991.

Delcourt-Honorez, M., 1990b. Land Surface Displacement Induced by Water-Level Variations, Cahiers du Centre Europeen de Geodynamique et de Seismologie, Vol. 2. Luxembourg.

Doodson, A. T., 1954. Harmonic Development of the tide-generating potential, *Proc. R. Soc.*, A **100**, 305-329.

Ducarme, B., Mäkinen, J., Röder, R. & Poitevin, C., 1991. Intercomparison of the absolute gravimeters JILAG-3 and JILAG-5 at Brussels with reference to the superconducting gravimeter TT30. Proc. Workshop : Non Tidal Gravity Changes : Intercomparisons between absolute and superconducting gravimeters, Walferdange, Luxembourg, Sept 5-7, 1990.

Dunham, K. C., 1972. The evidence for subsidence, *Phil. Trans. R. Soc. Lond.*, A **272,** 81-86.

Dziewonski, A. M. & Anderson, D. L., 1981. Preliminary reference Earth model (PREM), *Phys. E. planet. Inter.*, **25,** 297-356.

Ekman, M., & Mäkinen, J., 1994. Postglacial Uplift, Gravity Change and Mass Flow in Fennoscandia. Poster presented at the meeting of the International Gravity Commission / International Commission on the Geoid at Graz, Austria, 11-17 September 1994.

Emery, K. O. & Aubrey, D. G., 1985. Glacial Rebound and relative sea levels in Europe from tide-gauge records, *Tectonophysics,* **120,** 239-255.

Faller, J. E. & Marson, I., 1988. Ballistic Methods of measuring g - the Direct Free-Fall and Symmetrical Rise-and-Fall Methods Compared, *Metrologia,* **25,** 49-55.

Farrell, W. E., 1972a. Global calculations of tidal loading, *Nature,* **238,** 43-44.

Farrell, W. E., 1972b. Deformation of the Earth by surface loads, *Rev. Geoph. Space Phys.*, **10,** 761-797.

Fisher, J., 1954. *Statistical Methods for Research Workers.* Oliver & Boyd, Edinburgh & London. 12th ed.

Garland, G. D., 1971. *Introduction to Geophysics - Mantle, Core and Crust,* W. B. Saunders Company, Philadelphia.

Gibbings, D. L. H., Patterson, J. B. & Bell, G. A., 1971. The Absolute Determination of the Gravitational Acceleration at Sydney, Australia, *Bull. Geod.*, **100,** 147-157.

Goodkind, J. M., 1986. Continuous Measurement of Non-tidal Variations of Gravity, *J. Geoph. Res.*, **91,** B9, 9125-9134.

Hammond, J. A. & Faller, J. E., 1967. Laser-interferometer system for the determination of the acceleration of gravity, *IEEE J. Quant. Elec.* **QE-3,** No. 11, 597-602.

Hammond, J.A., & Faller, J. E., 1971. Results of Absolute Gravity Determinations at a Number of Different Sites, *J. Geoph. Res.*, 76, No. 32, 7850-7854.

Harrison, J. C. & Sato, T., 1984. Implementation of Electrostatic Feedback with a LaCoste-Romberg Model G Gravity Meter, *J. Geoph. Res.*, **89,** B9, 7957-7961.

Hipkin, R. G., 1978. A microgravimetric network for secular gravity studies in Scotland, *Geophys. J. R. astr. Soc.*, **52,** 385-396.

Hipkin, R. G., 1993a. Software Investigation (notes on FG5 processing software). Unpublished manuscript, Dept. of Geology and Geophysics, University of Edinburgh.

Hipkin, R. G., 1993b. A Note on Tidal Corrections and The Honkasalo Correction. Unpublished manuscript, Dept. of Geology and Geophysics, University of Edinburgh.

Hipkin, R.G. & Charles, K., 1993. Relative Gravity Observations made at the National Physical Laboratory, Teddington. Unpublished manuscript, Dept. of Geology and Geophysics, University of Edinburgh.

Hipkin, R. G. & Lagios, E., 1986. The Adjustment of Microgravimetric Observations on the Aegean Island of Santorini. Unpublished manuscript, Dept. of Geology and Geophysics, University of Edinburgh.

Hipkin, R.G., Lagios, E., Lyness, D. & Jones, P., 1988. Reference gravity stations on the IGSN71 standard in Britain and Greece, *Geoph. J.*, **92,** 143-148.

Houtse, H., 1991. Detection of Non-tidal gravity variation in China. Proc. Workshop : Non Tidal Gravity Changes : Intercomparisons between absolute and superconducting gravimeters, Walferdange, Luxembourg, Sept 5-7, 1990.

International Association of Geodesy, 1971. The Geodetic Reference System 1967, *Bull. Geod., Publ. Spec. No. 3,* Paris.

International Earth Rotation Service 1988. Information booklet assembled by the National Geodetic Survey and U. S. Naval Observatory.

Keary, P. & Vine, F. J., 1990. *Global Tectonics.* Blackwell Scientific Publications, Oxford.

Kelsey, J., 1972. Geodetic aspects concerning possible subsidence in southeastern England, *Phil. Trans. R. Soc. Lond.*, **A 272,** 141-149.

Klopping, F. J., Peter, G., Robertson, D. S., Berstis, K.A., Moose, R. E. & Carter, W.E., 1991. Improvements in Absolute Gravity Observations, *J. Geoph. Res.*, **96,** No. B5, 8295-8303.

Kuroda, K. & Mio, N., 1991. The correction due to the finiteness of the speed of light in interferometric absolute gravity measurement, *Metrologia.*

LaCoste, L., 1991. A new calibration method for gravity meters, *Geophysics,* 56, No. 5, 701-704.

LaCoste, L. & Romberg, A., 1942. *Force Measuring Device,* U.S Patent 2,293,437, United States Patent Office.

LaCoste, L. & Romberg, A., 1945. *Force Measuring Instrument,* U.S Patent 2,377,889, United States Patent Office.

LaCoste & Romberg Gravity Meters Inc., 1989. Instruction manual - Model G & D Gravity Meter, ed J. Fett. Spicewood Springs, Texas.

Lagios, E., Drakopoulos, J., Hipkin, R.G. & Gizeli, K., 1988. Microgravity in Greece : applications to Earthquake and volcano eruption prediction, *Tectonophysics,* **152,** 197-207.

Lambeck, K., 1990. Glacial rebound, sea-level change and mantle viscosity, *Q. J. R. astr. Soc.*, **31,** 1-30.

Lambeck, K., Johnston, P., Purcell, A., Kondilis, C. & Nakada, M., 1990. Mantle Viscosity, Glacial Rebound and Sea-level Change. *In* The Australian National University Research School of Earth Sciences Annual Report 1990, pp 116-119.

Lambert, A., 1993. Absolute Gravity : Applications to Global Sea Level Studies. Paper presented to IAPSO *ad hoc* Geodetic Committee, IOS Wormley, England, Dec. 1993.

Lambert, A., Liard, J. O., Courtier, N. & McConnell, R. K., 1987. The Importance of absolute gravimetry for gravity standards and geodynamics in Canada. Paper presented at IUGG, Vancouver, August 1987.

Larson, J. V., Dewhurst, W.T. & Moose, R. E., 1984. Use of Electrostatice Feedback for determining Calibration Errors in LaCoste & Romberg G and D meters. *Eos, Trans. AGU,* **65,** 860.

Liard, J., 1989. Laboratory method of calibrating LaCoste & Romberg model D Gracity meters. *In* Rummel, R. & Hipkin, R.G. (eds) *Gravity, Gradiometry and Gravimetry* : International Association of Geodesy Symposium 103, Edinburgh, Scotland, 8-10 August 1989. Springer-Verlag, New York.

Liard, J. & Courtier, N., 1991. Canada's contribution to the Absolute Gravity Program, *Bureau Gravimetrique International, Bull. d'Information,* **68,** 45-61.

Longman, I. M., 1959. Formulas for Computing the Tidal Accelerations Due to the Moon and the Sun, *J. Geoph. Res.,* **64,** No.12, 2351-2355.

Lyness, D., 1984. A study of High Precision Gravimetry. PhD Thesis, University of Edinburgh.

Mäkinen, J. & Tattari, S., 1989. The influence of variation in subsurface water storage on observed gravity. Draft of paper presented at 11th Int. Sympos. on Earth Tides, Helsinki, 1989.

Marson, I., 1994. National Report on Gravimetry in Italy 1990/1994. Paper presented at the meeting of the International Gravity Commission / International Commission on the Geoid at Graz, Austria, 11-17 September 1994.

Masson Smith, D., Howell, P. M., Abernethy-Clark, A. B. D. E. & Proctor, D. W., 1974. The National Gravity Reference Net 1973 (NGRN73), *Ord. Surv. prof. Pap, New Ser.,* **26.**

Merriam, J. B., 1992. Atmospheric pressure and gravity, *Geoph. J. Int.,* **109,** 488-500.

Moore, R. D. & Farrell, W. E., 1970. Linearization and calibration of electrostatically fed back gravimeters, *J. Geoph. Res.,* **75,** No. 5, 928-932.

Morelli, C., Gantar, C., Honakasalo, T. *et al.* 1974. The International Gravity Standardisation Net 1971 (IGSN71), *Publ. Spec. No. 4,* Int. Assoc. Geodesy, Paris.

Mörner, N-A., 1990. Glacial Isostasy and long-term crustal movements in Fennoscandia with respect to lithospheric and asthenospheric processes and properties, *Tectonophysics,* **176,** 13-24.

National Geodetic Survey, 1990. NGS Absolute Gravity Network as of May 25,1990. *On* Gravity Earth System Data CD-Rom Alpha Release, U.S Dept. of Commerce. NOAA.

Niebauer, T. M., 1987. New absolute gravity instruments for physics and geophysics, PhD Thesis, University of Colorado, Boulder.

Niebauer, T. M., 1988. Correcting gravity for the effects of local air pressure, *J. Geoph. Res.,* **93,** 7989-7991.

Niebauer, T. M., 1989. The Effective Measurement Height of Free-fall Absolute Gravimeters, *Metrologia,* **26,** 115-118.

Niebauer, T. M. & Faller, J. E., 1992. Continuous Gravity Observations Using Joint Institute for Laboratory Astrophysics Absolute Gravimeter, *J. Geoph. Res.*, **97,** B9, 12,427-12,435.

Okubo, S. & Fukuda, Y., (1994). Report on the Gravimetry in Japan during the period from April 1990 to March 1994. Paper presented at the meeting of the International Gravity Commission / International Commission on the Geoid at Graz, Austria, 11-17 September 1994.

Press, W. H., Flannery, B. P., Teukolsky, S. A. and Vetterling, W. T., 1988. *Numerical Recipes : the art of scientific computing.* Cambridge University Press, Cambridge.

Röder, R. H., Schnüll, M. & Wenzel, H-G., 1987. SRW Feedback for LaCoste-Romberg gravimeter with extended range. Paper presented at IUGG Vancouver, Aug 9-22, 1987.

Röder, R. H. & Wenzel, H-G., 1986. Relative Gravity Observations at BIPM, Sèvres in 1985 and 1986, *Bureau Gravimetrique International, Bull. d'Information,* **59,** 177-183.

Sakuma, A., 1983. An industrial Absolute Gravimeter: Type GA60 and its trial use on the French Gravity Net. Paper presented at the meeting of the IUGG, Hamburg, August 1983.

Sasagawa, G., Klopping, F., Niebauer, T. M., Faller, J. E. & Hilt, R. L., 1994. Intracomparison Tests of Precision of the FG5 Absolute Gravity meters. Abstract submitted to the meeting of the International Gravity Commission / International Commission on the Geoid at Graz, Austria, 11-17 September 1994.

Schnüll, M., Rehren, F., Timmen, L. & Torge, W., 1994. SRW Feedback systems for LCR-gravimeters with 1400 $\mu m/s^2$ range to determine periodical errors. Paper presented at the meeting of the International Gravity Commission / International Commission on the Geoid at Graz, Austria, 11-17 September 1994.

Schwiderski, E. W., 1980. Ocean tides, Part I : global ocean tidal equations; Part II : a hydrodynamical interpolation model, *Mar. Geod.,* **3,** 161-255.

Shennan, I., 1989. Holocene crustal movements and sea-level changes in Great Britain, *J. Quaternary Sci.,* **4,** 77-89.

Stacey, F. D., 1992. *Physics of the Earth* (3rd ed). Brookfield Press, Brisbane, Australia.

Thompson, K. R., 1980. An analysis of British monthly mean sea level, *Geoph J. R. astr. Soc.,* **63,** 57-73.

Timmen, L., Röder, R. H. & Schnüll, M., 1993. Absolute gravity determination with JILAG-3, improved data evaluation and instrumental techniques, *Bull. Geod.,* **67,** 71-80.

Topping, J., 1972. *Errors of Observation and Their Treatment.* Chapman & Hall, London & New York.

Torge, W., 1989. *Gravimetry.* de Gruyter, Berlin & New York.

Tsubokawa, T., 1991. Absolute and Superconducting Gravimetry in Japan. Proc. Workshop : Non Tidal Gravity Changes : Intercomparisons between absolute and superconducting gravimeters, Walferdange, Luxembourg, Sept 5-7, 1990.

Turnbull, G., 1987. The gravity reference net in the Highlands of Scotland, *Rep. reg. Geoph. Res. Group, Brit. geol. Surv., RGRG 87/1,* 19pp.

Valliant, H. D., 1991. Gravity Meter Calibration at LaCoste & Romberg, *Geophysics,* **56,** No. 5, 705-711.

VanDam, T. M. & Wahr, J. M., 1987. Displacements of the Earth's surface due to atmospheric loading : Effects on gravity and baseline measurements, *J. Geoph. Res.,* **92,** 1281-1286.

West, R. G., 1972. Relative land-sea level changes in southeastern England during the Pleistocene, *Phil. Trans. R. Soc. Lond.,* **A272,** 87-98.

Woodworth, P. L., 1987. Trends in UK Mean Sea Level, *Mar. Geod.,* **11,** 57-87.

Woodworth, P. L., Shaw, S. M. & Blackman, D. T., 1991. Trends in mean tidal range around the British Isles and along the adjacent European Coastline, *Geoph. J. Int.,* **104,** 593-609.

Zumberge, M.A., 1981. PhD Thesis, University of Colorado, Boulder.

Zumberge, M. A., Sasagawa, G. & Kappus, M., 1986. Absolute Gravity Measurements in California, *J. Geoph. Res.,* **91,** 9135-9144.